Hirohiko Tsujii · Tadashi Kamada
Toshiyuki Shirai · Koji Noda
Hiroshi Tsuji · Kumiko Karasawa
Editors

Carbon-Ion Radiotherapy

Principles, Practices, and Treatment Planning

Springer

Carbon-Ion Radiotherapy

Hirohiko Tsujii • Tadashi Kamada
Toshiyuki Shirai • Koji Noda
Hiroshi Tsuji • Kumiko Karasawa
Editors

Carbon-Ion Radiotherapy

Principles, Practices, and Treatment Planning

Springer

Editors
Hirohiko Tsujii
National Institute of Radiological Sciences
Chiba, Japan

Tadashi Kamada
National Institute of Radiological Sciences
Chiba, Japan

Toshiyuki Shirai
National Institute of Radiological Sciences
Chiba, Japan

Koji Noda
National Institute of Radiological Sciences
Chiba, Japan

Hiroshi Tsuji
National Institute of Radiological Sciences
Chiba, Japan

Kumiko Karasawa
National Institute of Radiological Sciences
Chiba, Japan

ISBN 978-4-431-54456-2 ISBN 978-4-431-54457-9 (eBook)
DOI 10.1007/978-4-431-54457-9
Springer Tokyo Heidelberg New York Dordrecht London

Library of Congress Control Number: 2013956974

Preface

This book is based on approximately 20 years of clinical experience with carbon-ion radiotherapy at the National Institute of Radiological Sciences (NIRS) and a review of literature worldwide on particle beam radiotherapy. It describes the rationale of applying carbon-ion radiotherapy in our efforts to develop the optimal treatment planning and irradiation techniques for various types of tumors and provides, as well, a description of treatments that unfortunately resulted in severe toxicities or tumor control failure. Accordingly, readers can learn about successful techniques for applying charged particle radiotherapy to prevent potential adverse effects and can also learn how to overcome or treat such effects if they develop.

In recent years, increasing evidence has been accumulated demonstrating the potential efficacy of charged particle radiotherapy in terms of increasing both the local control and survival rates in many types of tumors. Among various kinds of ion beams, carbon ion beams are used in cancer therapy worldwide because they are considered to have the most balanced, optimal properties, exhibiting both physically and biologically superior dose localization in tumors. This is due to the fact that, compared with photon beams, carbon ion beams exhibit a Bragg peak around the tumor at a fixed depth, and their radiobiological effectiveness increases with depth, reaching a maximum at the end of the beam's range. Therefore, with carbon ions, a physiobiologically sufficient dose can be precisely localized in the tumor at a fixed depth while delivering a physiobiologically lower dose to the surrounding normal tissue.

From the standpoint of cancer radiotherapy, however, carbon ions with such unique properties could become a double-edged sword depending on their application. This is because they are seen to deliver selective irradiation to the tumor while having at the same time a risk of inducing unwanted severe side effects in the normal tissue or critical organs and potentially causing local tumor failure unless properly employed. In fact, in initial phase I or I/II studies at the NIRS, severe late complications were encountered in the rectosigmoid colon or cutaneous and connective tissues in selected patients who received higher dose levels in a series of dose-escalation studies for head and neck tumors or pelvic tumors. In subsequent treatment, however, such adverse effects have not been observed as a result of determining the safe dose levels and of improving irradiation techniques. Also included in this book is a description of cases in which patients developed adverse effects that were satisfactorily managed with salvage treatment. This feature of the book makes it unique among other books in the field.

Carbon-ion radiotherapy provides improved outcomes for entities such as locally advanced tumors arising from various sites, in particular, those with pathologically non-squamous cell types, including adenocarcinoma, adenoid cystic carcinoma, melanoma and bone and soft tissue sarcomas, and those not suited for surgical resection. Furthermore, there is a rationale for the use of short-course radiotherapy regimens due to the superior dose localization and unique biological properties of high-LET carbon ion beams. The efficacy of this approach has been proven in the treatment of many different tumor sites, where the number of fractions per patient has been successfully reduced to a range between a single fraction in 1 day to 16 fractions in 4 weeks. How this has been achieved is also introduced here.

History is said to repeat itself. The negative aspects of radiotherapy, which are due to the use of immature techniques or poor knowledge of the nature of ion beams or the tumor itself, should not be repeated. In this regard, we have attempted to present information in this book

with the hope that it will serve as an introduction for those new to the field and as a useful resource for those currently involved in the use of charged particle radiotherapy, including protons and carbon ions in a clinical setting.

In closing, I wish to acknowledge our patients, who placed their trust in us as they received treatment with carbon ions at the NIRS. I wish to thank the current and past staff of the NIRS who contributed to the chapters of this book, as well as the many other individuals who provided their support and expertise for its publication.

I hope that our published work will prove to be a useful resource for the entire radiotherapy community to enhance the field of radiation oncology.

Chiba, Japan Hirohiko Tsujii

Contents

Contributors

Yutaka Ando National Institute of Radiological Sciences, Chiba, Japan

Satoshi Endo National Institute of Radiological Sciences, Chiba, Japan

Shigekazu Fukuda National Institute of Radiological Sciences, Chiba, Japan

Akifumi Fukumura National Institute of Radiological Sciences, Chiba, Japan

Takuji Furukawa National Institute of Radiological Sciences, Chiba, Japan

Yoshiya Furusawa National Institute of Radiological Sciences, Chiba, Japan

Azusa Hasegawa National Institute of Radiological Sciences, Chiba, Japan

Reiko Imai National Institute of Radiological Sciences, Chiba, Japan

Taku Inaniwa National Institute of Radiological Sciences, Chiba, Japan

Hitoshi Ishikawa Proton Medical Research Center, Tsukuba University, Tsukuba, Japan

Tetsuro Isozaki National Institute of Radiological Sciences, Chiba, Japan

Yoshiyuki Iwata National Institute of Radiological Sciences, Chiba, Japan

Tadashi Kamada National Institute of Radiological Sciences, Chiba, Japan

Nobuyuki Kanematsu National Institute of Radiological Sciences, Chiba, Japan

Kumiko Karasawa National Institute of Radiological Sciences, Chiba, Japan

Masashi Koto National Institute of Radiological Sciences, Chiba, Japan

Naruhiro Matsufuji National Institute of Radiological Sciences, Chiba, Japan

Nobutaka Mizoguchi National Institute of Radiological Sciences, Chiba, Japan
Department of Radiation Oncology, Kanagawa Cancer Center, Kanagawa, Japan

Manabu Mizota National Institute of Radiological Sciences, Chiba, Japan

Shinichiro Mori National Institute of Radiological Sciences, Chiba, Japan

Mio Nakajima National Institute of Radiological Sciences, Chiba, Japan

Koji Noda National Institute of Radiological Sciences, Chiba, Japan

Takuma Nomiya National Institute of Radiological Sciences, Chiba, Japan

Makoto Shinoto National Institute of Radiological Sciences, Chiba, Japan
Graduate School of Medical Sciences, Kyushu University, Fukuoka, Japan

Miho Shiomi National Institute of Radiological Sciences, Chiba, Japan

Toshiyuki Shirai National Institute of Radiological Sciences, Chiba, Japan

Ryo Takagi National Institute of Radiological Sciences, Chiba, Japan

Yuka Takei National Institute of Radiological Sciences, Chiba, Japan

Kohtaro Terashima National Institute of Radiological Sciences, Chiba, Japan
Graduate School of Medical Sciences, Kyushu University, Fukuoka, Japan

Shingo Toyama National Institute of Radiological Sciences, Chiba, Japan
Department of Heavy Particle Therapy and Radiation Oncology, Saga University, Saga, Japan

Hiroshi Tsuji National Institute of Radiological Sciences, Chiba, Japan

Hirohiko Tsujii National Institute of Radiological Sciences, Chiba, Japan

Masaru Wakatsuki National Institute of Radiological Sciences, Chiba, Japan

Shigeu Yamada National Institute of Radiological Sciences, Chiba, Japan

Naoyoshi Yamamoto National Institute of Radiological Sciences, Chiba, Japan

Shigeo Yasuda National Institute of Radiological Sciences, Chiba, Japan

Part I

The History of Carbon-Ion Radiotherapy

History of Charged Particle Radiotherapy

1

Hirohiko Tsujii

Abstract

Among various types of charged particles, protons and carbon ions have been most extensively used for cancer therapy around the world. In 1954, clinical application of proton beams was started for the first time in the world at Lawrence Berkeley National Laboratory (LBNL), which was shortly followed by Uppsala, Boston, Russia (three facilities), and Chiba. It is only after 1973, when computerized tomography (CT) was invented, that accurate calculation of dose distributions became feasible in clinical practice. In 1990, the world's first hospital-based proton facility with a rotating gantry was built in Loma Linda. Since then, proton therapy has been applied to cancer treatment in an increasing number of facilities. Currently, there are about 36 facilities for proton beam therapy in operation, with still more facilities under construction or being planned in the world. As for the clinical application of heavier ions, the first patient was treated with helium ions in 1957 and with neon ions in 1975 at LBNL. Until it was closed in 1992, 2,054 patients were treated with helium ions and 433 patients with neon ions and other heavy ions. In 1994, the National Institute of Radiological Sciences (NIRS) in Japan started clinical application of carbon ions generated by Heavy Ion Medical Accelerator (HIMAC) in Chiba, which was the world's first medically dedicated facility. Among various types of ion species, carbon ions were chosen for therapy because the biologically expressed dose distribution was assumed to be superior to other ions and the amount of high-LET components would be sufficient to ensure biological benefit in controlling photon-resistant tumors. By March 2013, more than 7,300 patients were treated at NIRS. In 1997, carbon-ion therapy was also initiated at Gesellschaft für Schwerionenforschung (GSI) in Germany to treat 440 patients until 2005, when it was closed and succeeded by Heidelberg University. Currently, there are six carbon therapy facilities in operation and several other facilities under construction in the world.

Keywords

Carbon ion • Charged particle • Dose distribution • High-LET • Proton

H. Tsujii (✉)
National Institute of Radiological Sciences, Chiba, Japan
e-mail: h-tsujii@bj9.so-net.ne.jp

H. Tsujii et al. (eds.), *Carbon-Ion Radiotherapy: Principles, Practices, and Treatment Planning*,
DOI 10.1007/978-4-431-54457-9_1, © Springer Japan 2014

1.1 Introduction

Within 2 months of the discovery of X-rays by Wilhelm Conrad Röntgen in 1895, X-rays were used to take pictures for diagnostic purposes as well as to treat a wide variety of diseases including malignant tumors. Since then, the primary principle of radiotherapy (RT) has been extensively pursued, which lies in precise dose localization in the target lesion and minimal damage to the surrounding normal tissues. In this sense, the era of the 1950s, when high-energy accelerators such as the tele-cobalt machine and linear accelerator were developed and employed in clinical practice, marked the beginning of modern RT.

In the late twentieth century, high-technology approaches including the development of intensity-modulated RT (IMRT) and three-dimensional stereotactic RT (SBRT) became available and contributed to the improvement of treatment results as well as extended their applicability to a wider range of tumors. IMRT delivers photon beams aimed at the target from many different directions, thereby permitting high dose concentration in the target while diluting unwanted doses outside the treatment volume [1, 2]. Currently, these photon treatments are widely available and are often called "conventional" RT to distinguish them from the new charged particle RT such as proton and carbon-ion RT.

Particle RT has a history of 60 years or more, and it has enhanced the clinical possibilities of RT. Among a wide variety of particles, particular attention has been focused on protons and carbon ions, which have been the front-runners around the world. This is based on the fact that, when compared to photons, they provide beneficial dose distribution and, in the case of carbon ions being heavier than protons, larger relative biological effectiveness (RBE), leading to a higher probability of tumor control while sparing surrounding normal tissues [3, 4].

In this chapter, the history of charged particle radiotherapy with special emphasis on carbon-ion RT is presented.

1.2 The Dawning of Particle Beam Radiotherapy

1.2.1 Invention of Accelerators for Particle Beam Radiotherapy

The success of radiation therapy largely depends on the performance of accelerators, beam delivery system, treatment planning system, and many other related devices. This becomes particularly clear when we take note of the evidence of the higher energy of photons reaching the order of MV in the 1950s contributing significantly to the improvement of therapeutic outcomes (Table. 1.1) [5].

Table 1.1 Improved survival of several types of cancers with the advent of megavoltage therapy

	5-year survival (%)	
Type of cancer	kV X-rays	MV X-rays
Hodgkin's disease	30–35	70–75
Ca. of the cervix	35–45	55–65
Ca. of the prostate	5–15	55–60
Ca. of the nasopharynx	20–25	45–50
Ca. of the bladder	0–5	25–35
Ca. of the ovary	15–20	50–60
Retinoblastoma	30–40	80–85
Seminoma of the testis	65–70	90–95
Embryonal ca. of the testis	20–25	55–70
Ca. of the tonsil	25–30	40–50

From Report of the Panel of Consultants on the Conquest of Cancer Washington, D.C., U.S. Government Printing Office, 1970

Then, extrapolating from this, if charged particles were to be used for cancer therapy, treatment results could be expected to be improved even more.

Among various types of charged particles, protons and carbon ions have been most widely employed for cancer therapy in the world. The energetic ion beam deposits much of its energy at the end of its range, resulting in what is called the Bragg peak (Fig. 1.1), so-named after Sir William Henry Bragg, a British physicist. He reported this phenomenon in 1904 [6]. Realizing the advantage of the Bragg peak, Robert R. Wilson (1914–2000) published his seminal paper on the rationale of using accelerated protons and heavier ions for human cancers in 1946 [7]. This was the first proposal to apply charged particles for medical use. He participated in the development of the atomic bomb in Los Alamos during World War II. After the war, he returned to Berkeley to look for peaceful atomic-energy projects, and he wrote a historic paper on the potential benefit of high-energy protons in cancer therapy. He later became the first director of the Fermi Laboratory, where clinical research of fast neutron therapy was conducted on more than 3,100 patients. Compared to conventional photon treatment, charged particle beams appeared to promise higher cure rates with smaller complications as they could deliver sufficient doses precisely, while lowering unwanted doses to normal tissues adjacent to the tumor. Wilson also hypothesized that carbon ions might be superior to proton beams.

Prior to Wilson's proposal, Ernest Orlando Lawrence (1901–1958) discovered a method of accelerating particles to very high energy without the use of high voltage, which was actually the development of the cyclotron in 1929. The first model of Lawrence's cyclotron was made of brass, wire, and sealing wax and was only 4 in. in diameter—it could literally be held in one hand. A photograph of Lawrence holding the first cyclotron in his hand appeared on the front cover of "Time" newsmagazine. Subsequently, higher-energy

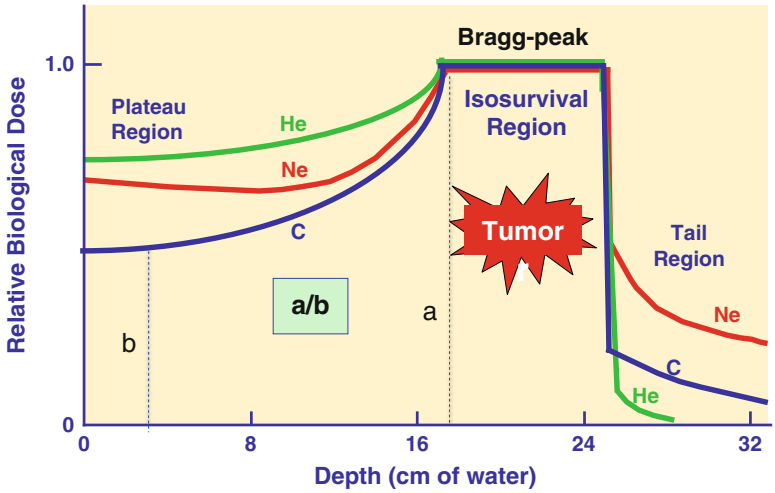

Fig. 1.1 Depth dose distributions of various ion beams. When the same biological endpoint is used, carbon-ion beams have the largest peak to plateau ratio (a/b) in biological effect as compared to other ion beams

cyclotrons 11, 27, and 37 in. in diameter were constructed at Berkeley.

In 1938, the world's first particle therapy was conducted on 24 patients with a single fraction of fast neutrons generated by the historic 37-inch cyclotron. This treatment was judged as successful, and then from 1938 to 1943 a total of 226 patients were treated with fractionated fast neutrons generated by a 60-inch cyclotron. Together with the clinical effects of fast neutron therapy, however, long-term side effects on normal tissues deemed were too high, and in 1948 Dr. Stone concluded that fast neutrons should not be used for cancer therapy [8].

A British group, however, evaluated fast neutron therapy again, and in 1965 Mary Catterall at Hammersmith Hospital in London once more began this therapy. By 1969, it was shown that for certain tumors, better local control could be achieved with neutron irradiation. Encouraged by these results, many other institutes in Europe, the USA, and Japan began neutron therapy research in the 1970s. However, the demand for fast neutron therapy decreased thereafter, and most of the institutions abandoned this therapy. Fast neutron therapy is currently conducted at only a few facilities for the treatment of selected tumors.

Incidentally, in the same year (1938) of the start of fast neutron therapy, Gerald Kruger, a physicist at the University of Illinois, came up with a new idea for cancer therapy using alpha particles emitted from boron when it captured neutrons. He proposed to saturate the tumor with a boron compound and then exposed it to a neutron beam. The boron capture cross section for thermal neutrons was about 100 times higher than that of other tissue compounds. This method came to be known as "neutron capture therapy."

1.2.1.1 First Phase of Proton Beam Radiotherapy

In 1947, E. Lawrence completed construction of the 184-inch synchrocyclotron at the University of California (UC) Berkeley, making it possible to accelerate protons, deuterons, and helium nuclei to energies of several hundred MeV/u. Protons and heavier ions, being much more massive than electrons, require bigger accelerators to accelerate them to produce enough kinetic energy to treat deep-seated tumors. For example, a proton is 1,836 times heavier than an electron. E. Lawrence suggested that Cornelius A. Tobias and John H. Lawrence at UC Berkeley jointly use the 184-inch cyclotron to test the scientific validity of Wilson's ideas [9].

Prior to irradiation of human patients, they decided to deliver deuteron beams to the pituitary of a dog patient with breast cancer in 1954 [10]. The dog's tumor was ulcerated, bleeding and oozing milk continuously. Within a few days, pituitary irradiation caused a noticeable effect and the bleeding stopped. Within 2 weeks, the secretion of milk dried up completely and the animal had regained some strength. The dog was well and her tumor remained in remission for several months before death due to tumor relapse.

In 1954, encouraged by this favorable effect on the animal tumor, the world's first human patient with disseminated breast cancer had pituitary irradiation with protons generated from the 184-inch synchrocyclotron [11]. Therapeutic exposure was performed with ion beams for a total of 50 human patients (deuterons, protons, and helium ions). The first human patient with widespread breast cancer was given pituitary proton irradiation, about half of what they actually expected to be an effective dose. She showed almost immediate improvement but eventually died several months later. Although it was impossible to determine who might benefit from the treatment, the earliest optimistic sign was the reduction of both skin temperature and swelling. After pituitary irradiation, more than half of the patients treated exhibited some beneficial effects, although in some there was no effect at all. As for toxicities, the most prominent side effect was the development of diplopia. It was thought that protons and helium ions were most likely spread too wide inside the

head due to multiple scattering, and such effect could be minimized if carbon or oxygen beams could be used.

The second series of pituitary irradiation were for patients with acromegaly. Eventually about 700 patients were treated. Unlike with other treatments, acromegaly remained in regression and the growth hormone levels stayed within normal limits for many years [12]. In 1957, the 184-inch synchrocyclotron was modified to accelerate helium nuclei. By the time of the closure of the facility in 1992, a total of 2,054 patients had been treated with helium ions. These initial treatments with protons in the 1950s and 1970s had been mainly aimed at pituitary tumors, as they could be localized by orthogonal plane X-ray films and rigid immobilization of the skull. This was the manner of proton therapy before the invention of computed tomography (CT).

1.2.1.2 Second Phase of Proton Beam Radiotherapy

Soon after the initiation of clinical studies at UC Berkeley, programs of proton therapy also began at other proton facilities. They were originally constructed for nuclear physics research, including Uppsala, Sweden (1957), Cambridge, Massachusetts (1961), Dubna (1967), Moscow (1969), St Petersburg (1975), Chiba (1979), Tsukuba (1983), and Villigen (1984) [13].

Charged particle therapy was only made practical for cancer therapy with the advent of CT scanning in 1973, which could accurately determine the beam path in a patient. In 1974, Suit et al. initiated studies of fractionated RT with protons [14]. In the 1970s and 1980s, however, throughout the world the tumors treated with protons were mostly choroidal melanoma, skull base tumors, and intracranial tumors (Table 1.2). Among them, the largest number of patients treated with proton beams had choroidal melanomas, the first tumor treated safely with a large dose of 60–70 GyE in 4 to 5 fractionations in 1 week. At that time, only at Tsukuba University were deep-seated tumors such as lung, esophagus, liver, uterine cervix, prostate, and head and neck malignancies extensively treated by Tsujii et al. [15].

In 1990, a hospital-based proton facility was commissioned by James Slater at the Loma Linda University Medical Center in California [16], the historic world's first facility to employ a 250 MeV proton accelerator dedicated to medical service and research. It had passive beam nozzles and four treatment rooms with three rotating gantries and one fixed beam line. Since then, an increasing number of facilities have begun proton therapy throughout the world (Fig. 1.2). As of April 2013, around 35 industry-built proton therapy facilities are operational and about 30 more facilities are under construction or being planned around the world.

1.3 Carbon-Ion Radiotherapy

1.3.1 Initiation of Carbon-Ion Radiotherapy

High-energy heavy-ion beams were obtained at the Berkeley Bevatron, a synchrotron-based facility, which was constructed in 1954. The injector was designed to obtain carbon, oxygen, and neon particles. During the almost 40 years since its commissioning, the venerable Bevatron made major contributions to four distinct areas of research: high-energy particle physics, nuclear heavy-ion physics, medical research and therapy, and space-related studies of radiation damage and heavy particles in space. The Bevatron was later given a productive new lease on life through the invention of the Bevalac, in which the Bevatron was linked to the SuperHILAC linear accelerator in 1974.

The Berkeley research teams embarked on helium-ion therapy in 1957 and then neon-ion RT in 1975. During the 1970s and 1980s, the use of Bevalac beams in medical and biological research became an important part of the program. In 1977, the first carbon-ion patient was treated in Phase I trials at LBNL [17–19]. At that time, however, only a small number of patients were treated with carbon ions, with the majority being treated with neon ions together with helium ions. Unfortunately, after 17 years and more than 2,000 patients treated, Berkeley terminated all radiotherapy programs in 1992.

Encouraged by the clinical studies at LBNL, other facilities sprang up around the world. As if a baton had been passed from the West Coast across the Pacific Ocean (Fig. 1.3), the National Institute of Radiological Sciences

Table 1.2 Distribution of tumors treated with proton beams in the early phase of its clinical application in the world. This was summarized in May 1993

Tumor sites	USA	Europe	Russia	Japan	Total (%)
Ocular melanoma	1,698	2,196	355	44	4,293 (35.1)
Skull base and upper spine	3,132	15	1,678	58	4,883 (39.9)
Head and neck	79	20	0	21	120 (1.0)
Thoraco-abdominal	2	0	0	127	129 (1.1)
Pelvis (prostate, uterus, etc.)	469	41	242	61	813 (6.6)
Others	18	12	77	128	235 (1.9)
Unknown	709	27	1,025	0	1,761 (14.4)
Total (%)	6,107 (49.9)	2,311 (18.9)	3,377 (27.6)	439 (3.6)	12,234 (100.0)

Fig. 1.2 Photos taken at the PTCOG meeting held at NIRS in 1992. From left to right: Wambersie A, Fujimoto K, Castro J, Blakeley E, Jones D, Kraft G, Schabel M, Slater J, Tsujii H, and Kawachi K

(NIRS), Japan, built the first heavy-ion accelerator in the world, called HIMAC in Chiba (Fig. 1.4), and started the clinical application of carbon ions in 1994 [20, 21]. Many of the Berkeley experiences with ion beam therapy were transferred to NIRS (Fig. 1.3). Following NIRS, the Gesellschaft für Schwerionenforschung (GSI), Germany, also started clinical studies with carbon-ion RT in 1997 [22], but then clinical usage was terminated and succeeded by Heidelberg Ion-Beam Therapy Center (HIT) in 2009 [23, 24]. HIT is the world's first particle therapy facility for treatment using protons and carbon ions with a scanning beam delivery system.

At this writing, there are six facilities in operation for carbon-ion RT in the world: three in Japan, one in Germany, one in Italy, and one in China. The four facilities besides NIRS and HIT are Hyogo Ion Beam Medical Center, Hyogo, Japan (2002); Institute of Modern Physics (IMP), Lanzhou, China (2006); Gunma University Heavy Ion Medical Center, Gunma, Japan (2010); National Center of Oncological Hadrontherapy (CNAO), Pavia, Italy (2011). At present, two facilities in Japan, one in Germany, one in Austria, and two in China are under construction. In the USA, only proton facilities are in operation or under construction, but increasing interest in C-ion RT has recently emerged.

1.3.2 Clinical Experiences of Carbon-Ion RT

1.3.2.1 Clinical Experiences at LBNL

At LBNL, a total of 433 patients were treated with neon ions by the end of 1988. Among them, 239 patients received a minimum neon physical dose of 10 Gy (median follow-up for survivors, 32 months). According to Castro et al. and Linstadt et al. [25, 26], as compared with historical results, favorable results of neon-ion therapy were observed in several types of tumors, including advanced or recurrent macroscopic salivary gland carcinomas, paranasal sinus tumors, advanced soft tissue sarcomas, macroscopic sarcomas of the bone, locally advanced prostate carcinomas, and biliary tract carcinomas. However, the treatment results of malignant gliomas, pancreatic cancer, gastric cancer, esophageal cancer, lung cancer, and advanced or recurrent head and neck cancer appeared no better than those achieved with conventional X-ray therapy. Unfortunately, clinical research at LBNL was terminated in 1992 because of budget constraints and aging of the machine.

1.3.2.2 Clinical Experiences at NIRS, GSI, and Other Facilities

The number of patients treated with proton beams and C-ion beams in the world is shown in Figs. 1.5 and 1.6. The largest numbers of patients were treated by proton therapy in the USA (47 %) and by carbon-ion RT in Japan (91 %).

At NIRS, clinical trials were initiated in June 1994 with Phase I/II dose-escalation studies on various types of tumors, aiming to confirm the safety of carbon-ion RT and to evaluate its antitumor effects. Carbon-ion RT has been given at 4 times per week while keeping both the fraction number and treatment period fixed in all tumor-specific protocols. For the initial clinical study, locally advanced head and neck tumors were chosen, after which the range of application was expanded to many other tumors. As of March 2013, more than 7,300 patients with various types of tumors had been

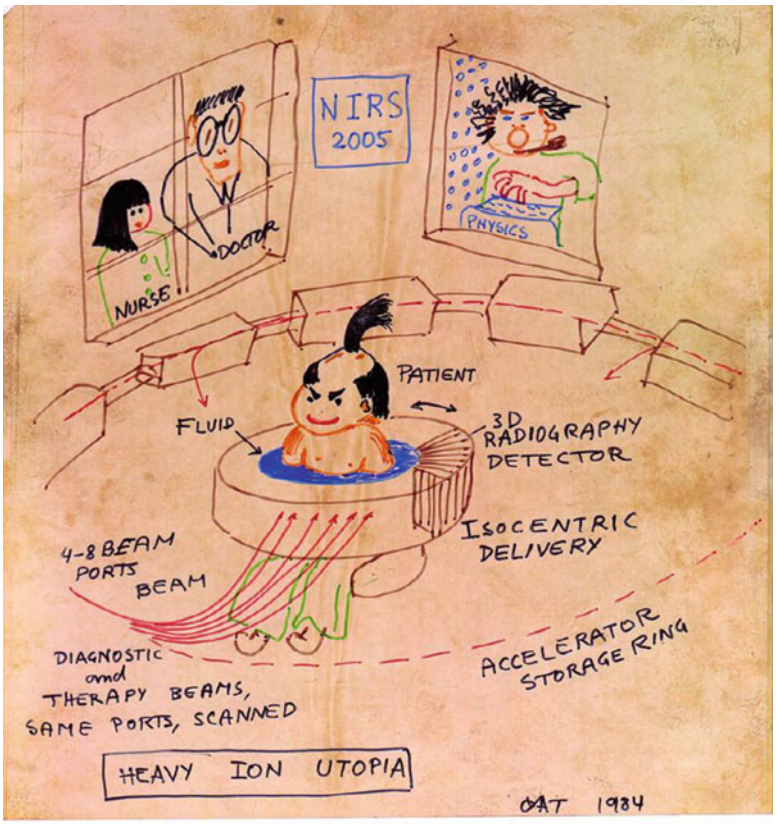

Fig. 1.3 Heavy Ion UTOPIA drawn by Tobias CA, LBNL, and presented to NIRS (1984). His idea was to perform radiotherapy and image diagnosis simultaneously with the same accelerator. HIMAC was successfully built in cooperation with LBNL (courtesy of Dr Umegaki, Y)

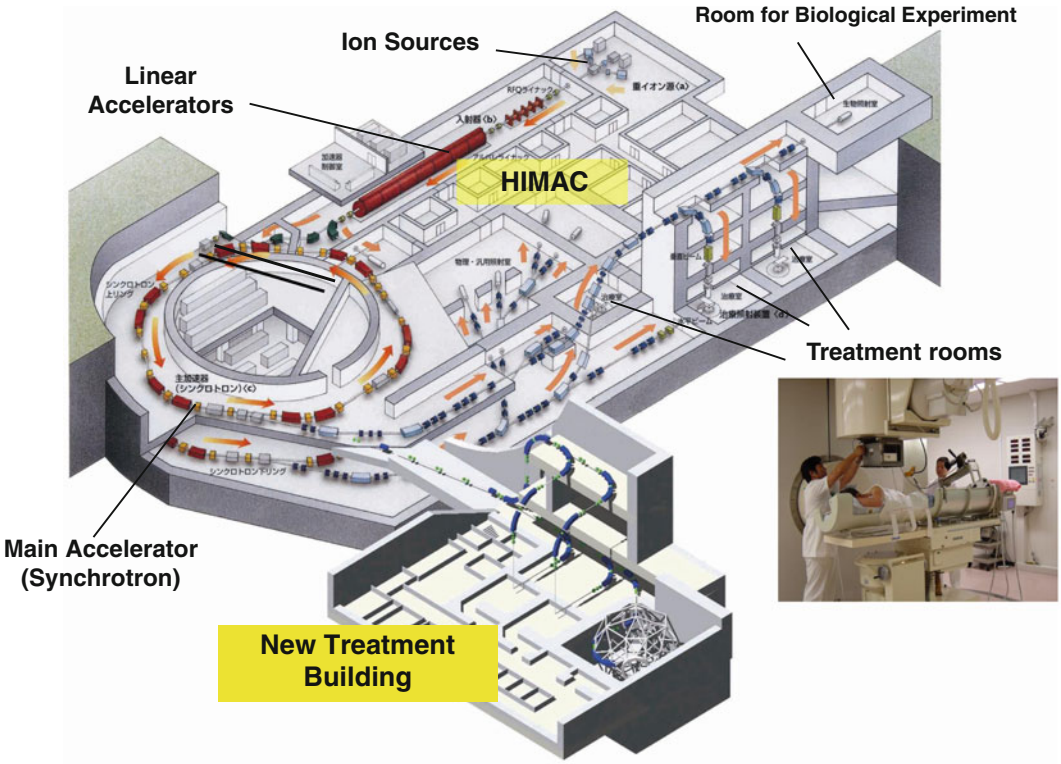

Fig. 1.4 Overview of HIMAC in Chiba, the world's first accelerator complex dedicated to cancer therapy. It was built in 1993 at NIRS

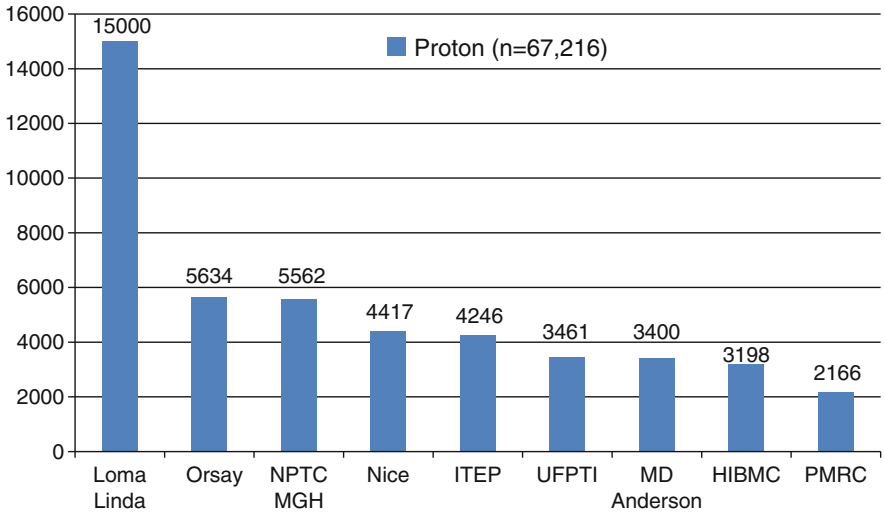

Fig. 1.5 Number of patients treated at proton facilities in the world according to PTCOG web site (as of June 2012)

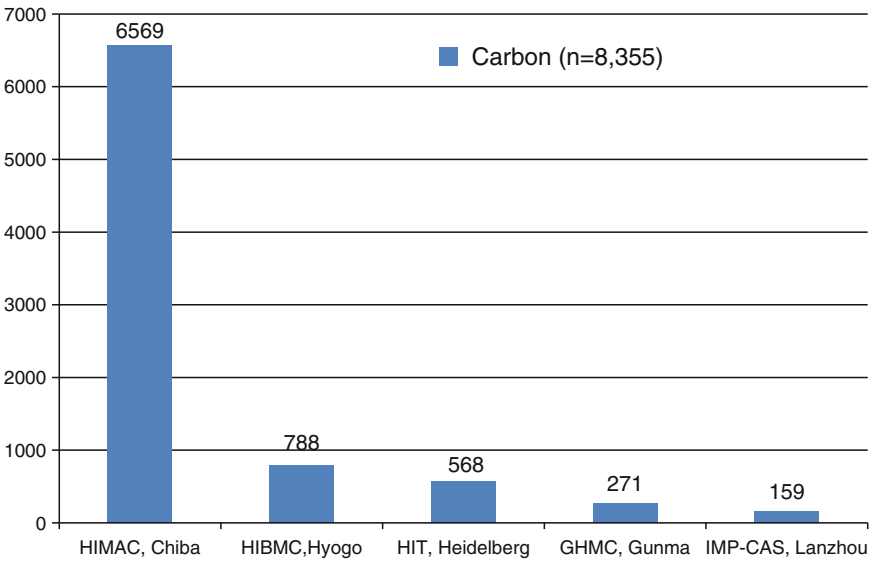

Fig. 1.6 Number of patients treated at carbon-ion facilities in the world according to PTCOG web site (as of June 2012)

treated with carbon ions based on more than 50 protocols at NIRS [3, 27].

Experiments with high-LET radiations including carbon ions and fast neutrons demonstrated that increasing their fraction dose tended to lower the RBE for both tumor and normal tissues, but the RBE for tumor did not decrease as rapidly as the RBE for normal tissues. These results substantiated that the therapeutic ratio could increase rather than decrease even though the fraction dose was increased. In carbon-ion RT at NIRS, it has been possible to complete a treatment course with an average of 13 fractions over approximately 3 weeks. This means that the carbon therapy facility can be operated more efficiently, offering treatment for a larger number of patients than is possible with other modalities over the same period of time.

At GSI, the raster-scan method (active beam scanning) was developed by Haberer et al. [22], allowing the narrow carbon beam to precisely and selectively scan the tumor volume.

By this method, the speed of ions and consequently their penetration depth is controlled by varying the energy levels of the accelerator, and the whole tumor is scanned layer by layer. Scanning is performed by deflecting the beam horizontally and vertically within each layer using magnets, similar to electron beams in a cathode ray tube. Even an irregular shape of tumors within the body can thus be uniformly irradiated to the nearest millimeter, with the damage to healthy tissue being minimized.

Until termination of its clinical study, more than 450 patients were treated at GSI using active beam scanning. Main indications treated at GSI were patients with chordomas and chondrosarcomas of the skull case, locally advanced adenoid cystic carcinomas (ACC), as well as chordomas and chondrosarcomas of the sacrum and prostate cancer [23]. Carbon-ion RT offered an effective treatment option for these tumors with acceptable toxicity. Based on these experiences at GSI and the overall need for particle therapy in Germany, the Heidelberg Ion-Beam Therapy Center (HIT) was constructed as a university hospital-based center.

Facilities other than NIRS and GSI/HIT are also accumulating experiences of C-ion RT for various types of cancers.

1.4 Conclusions

The principle of RT is to concentrate a sufficient dose to the target while minimizing radiation to the surrounding normal tissues. Historically, there have been technological developments for improving the spatial dose distribution, and in the late twentieth century, high-precision 3D conformal RT was developed, including SBRT, IMRT, and charged particle radiotherapy, by which dose concentrations have become significantly improved. Among them, C-ion RT has been employed for almost 20 years in Japan and Europe. It has demonstrated a clinical advantage in terms of high physical dose concentration with a narrow penumbra and, as high-LET radiations, clinical gain from high radiobiological effectiveness. Additionally, it has been confirmed that hypofractionation is feasible in treatment of almost all types of tumors. Hopefully, the next generation will be so advanced in this specialty that our present high technology of treatment planning and delivery can be considered obsolete. Our expectation is that within three decades, a very large proportion of definitive radiation treatment will be based on particle beams and feature 4D image-guided radiation therapy to maintain the target correctly positioned in the beam throughout each pencil beam scanning treatment session. A responsibility for the present generation should be to further develop radiotherapeutic techniques and deepen radiation oncology expertise.

Acknowledgements The author is thankful for the support of the Chang Yung-Fa Foundation and the NIRS International Open Laboratory (IOL).

References

1. Hall EJ, Wuu CS. Radiation-induced second cancers: the impact of 3D-CRT and IMRT. Int J Rad Oncol Biol Phys. 2003;56:83–8.
2. Hall EJ. Intensity-modulated radiation therapy, protons, and the risk of second cancers. Int J Rad Oncol Biol Phys. 2006;65:1–7.
3. Tsujii H, Kamada T. A review of update clinical results of carbon ion radiotherapy. Jpn J Clin Oncol. 2012;42:670–85.
4. Schulz-Ertner D, Tsujii H. Particle radiation therapy using proton and heavier ion beams. J Clin Oncol. 2007;25:853–64.
5. Conquest of Cancer. Report of the National Panel of Consultants of the Committee on Labor and Public Welfare United States Senate; 1970. p. 51.
6. Bragg WH, Kleeman R. On the ionization curves of radium. Philos Mag. 1904;8:726–38.
7. Wilson RR. Radiological use of fast protons. Radiol. 1946;47:487–91.
8. Stone RS. Neutron therapy and specific ionization. Am J Roentgenol. 1948;59:771–81.
9. Tobias CA, Anger HO, Lawrence JH. Radiological use of high-energy deuterons and alpha particles. Am J Roentgenol. 1952;67:1–27.
10. Cornelius, Ida Tobias. People and particles. San Francisco Press, Inc. CA; 1997. p. 121.
11. Tobaias CA, et al. Pituitary irradiation with high-energy proton beams. Cancer Res. 1958;18:121.
12. Laramore JH, et al. Heavy-particle therapy in acromegaly and Cushing's disease. J A Med Assoc. 1976;235:2306.
13. Raju MR. The history of ion beam therapy. In: Ute Lintz, editor. Ion beams in tumor therapy. Chapman & Hall; 1995. p. 3–9.
14. Suit HD, Goitein M, Munzenrider J, et al. Definitive radiation therapy for chordoma and chondrosarcoma of the base of the skull and cervical spine. J Neurosurg. 1982;56:377.
15. Tsujii H, Tsuji H, Inada T, et al. Clinical results of fractionated proton therapy. Int J Radiat Oncol Biol Phys. 1993;25:49–60.
16. Slater JM, Daniel W, Archambeau JO, et al. Development of a hospital-based proton beam treatment center. Int J Radiat Oncol Biol Phys. 1988;14:761–75.
17. Castro JR, Quivey JM, Lyman JT, et al. Radiotherapy with heavy charged particles at Lawrence Berkeley Laboratory. J Can Assoc Radiol. 1980;31:30–4.
18. Chen GTY, Castro JR, Quivey JM, et al. Heavy charged particle radiotherapy. Ann Rev Biophys Bioeng. 1981;10:499–529.
19. Chatterjee A, Alpen EL, Tobias CA, et al. High energy beams of radioactive nuclei and their biomedical applications. Int J Radiat Oncol Biol Phys. 1981;7:503–7.
20. Tsujii H, Minohara S, Noda K. Heavy-particle radiotherapy: system design and application. In: Chao AW, editor. Reviews of accelerator science and technology, vol. 2. UK: Imperial College Press; 2009. p. 1–19.
21. Tsujii H, Mizoe J, Kamada T, et al. Overview of experiences on carbon ion radiotherapy at NIRS. Radiother Oncol. 2004;73 Suppl 2:S41–9.
22. Kraft G. Tumor therapy with heavy charged particles. Prog Part Nucl Phys. 2000;45:S473–544.
23. Haberer T, Becher W, Schardt D, Kraft G. Magnetic scanning system for heavy ion therapy. Nucl Instrum Methods. 1993;A330:296–305.
24. Combs SE, Jaekel O, Heberer T, Debus J. Particle therapy at the Heidelberg Ion Therapy Center (HIT) – integrated research-driven university-hospital-based radiation oncology service in Heidelberg, Germany. Radiother Oncol. 2010;95:41–4.
25. Castro JR, Saunders WM, Tobias CA, et al. Treatment of cancer with heavy charged particles. Int J Radiat Oncol Biol Phys. 1982;8:2191–8.
26. Linstadt DE, Castro JR, et al. Neon ion radiotherapy: results of the phase I/II clinical trial. Int J Radiat Oncol Biol Phys. 1991;20:761–9.
27. Tsujii H, Kamada T, Baba M, et al. Clinical advantages of carbon-ion radiotherapy. New J Phys. 2008;10:1367–2630.

Part II

An Overview of Carbon-Ion Radiotherapy

The Characteristics of Carbon-Ion Radiotherapy

2

Tadashi Kamada

Abstract

The fundamental principle of radiotherapy lies in precise dose delivery to the target, while minimizing damage to the surrounding normal organs. Carbon ion beams have a definite range and sharp high-dose Bragg peak. At the carbon ion Bragg peak, the ionization is enormous and shows high biological effects. Hence, among the various ion species, carbon ions were selected for cancer therapy because they were thought to have the optimal properties in terms of biologically effective dose-localization to realize this principle of radiotherapy.

The Bragg peak of the carbon ion beam is sharp and narrow. To cover various sizes of tumors with carbon ion beams, two different beam delivery techniques, a passive beam delivery using a fixed spread out of the Bragg peak (SOBP) and active beam scanning, were developed.

Keywords

Beam scanning • High LET • OER (oxygen enhancement ratio) • Passive beam delivery • Spread out of the Bragg peak (SOBP)

2.1 Introduction

Radiation has been used in the treatment of various diseases, including cancer, since soon after the discovery of X-rays [1]. Since then, extensive studies have been carried out to improve radiotherapy outcomes, in which the radiation is precisely targeted at tumors to enable a higher uniform dose while reducing damage to surrounding normal tissues and organs. In this regard, the carbon ion beam is a relatively new type of radiation introduced to the field of radiotherapy, and it is unique and has several physical and biological advantages compared to other types of radiation used for cancer therapy.

T. Kamada, M.D., Ph.D. (✉)
Research Center for Charged Particle Therapy,
National Institute of Radiological Sciences,
Anagawa 4-9-1, Inage-Ku, Chiba 263-8555, Japan
e-mail: t_kamada@nirs.go.jp

2.2 Physical Advantages of Carbon Ion Beams

Charged particle beams, such as the carbon ion beam, that travel in the body deposit energy along their paths. The depth of penetration of the particles into the body is determined by their acceleration energy, and charged heavy particles like carbon ions deposit more energy as they go deeper into the body, increasing to a high peak at the end of their range (where the remaining energy is lost over a very short distance). This results in a steep rise in the absorbed dose, known as the Bragg peak [2]. Beyond the Bragg peak, there is a rapid falloff of the dose to nearly zero for the carbon ion beam (Fig. 2.1).

Multiple focused beams are usually required to selectively irradiated deep-seated tumors with external X-rays. Intensity-modulated radiotherapy (IMRT) is the most recent development to provide a better dose distribution of such multiple beam radiotherapies [3]. This makes it possible to realize a highly conformal dose distribution and steep dose

H. Tsujii et al. (eds.), *Carbon-Ion Radiotherapy: Principles, Practices, and Treatment Planning*,
DOI 10.1007/978-4-431-54457-9_2, © Springer Japan 2014

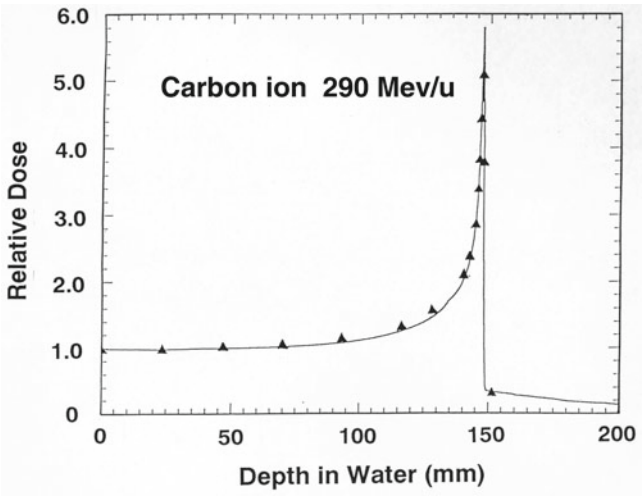

Fig. 2.1 The depth-dose profile of carbon ion beams (290 MeV/u)

gradients even with X-rays. However, there are concerns regarding the low-dose bath effect of multiple entry/exiting paths of X-rays, which lead to a larger proportion of the body receiving low-level radiation during IMRT. This is because a high-energy X-ray, which is a form of electromagnetic radiation with no mass or charge, passes through the body very easily and ionizes (deposits energy) its whole pathlength. As a consequence, the normal tissue integral dose (NTID) is higher when this new technique is used. On the other hand, radiotherapy using carbon ion beams can produce a more conformal dose distribution and steeper dose gradients without increasing the NTID, with a smaller number of beams compared with IMRT (Fig. 2.2).

In addition to the definite range, another advantage of the carbon ion is that it travels in almost a straight line, so that sharp and accurate collimation is possible. The lateral scattering is only 1.5 mm at a 20 cm depth in water for the carbon ion beam. This is much smaller than the 6.5 mm for protons. On the other hand, higher energies are required to reach deeply seated tumors for carbon ion beams compared to proton beams.

The magnetic rigidity fixes the bending radius of the particles and determines the size of the accelerator and beam delivery system. The energy and magnetic rigidity of carbon ions are 330 MeV and 5.67 Tm for the 20 cm range in water, while these values for protons are 175 MeV and 2.00 Tm, respectively. As a consequence, a larger accelerator and beam delivery system is required to make a carbon ion facility.

2.3 Biological Advantages and Hypofractionation in Carbon Ion Radiotherapy

As a particle (ion) of charge Z, speed v, passes a quasi-stationary electron in a medium, the impulse, the momentum transferred (force x time), is proportional to $Z\times(1/v)$. Therefore, the energy transferred is proportional to Z^2/v^2. Hence the ionization density increases as the speed of the particle slows down, until very close to end of the range, when the ionic charge is reduced by electron pickup and the ionization falls rapidly to zero. The high-dose Bragg peak is formed by this phenomenon. Thus, the position of the Bragg peak of the particle can be accurately controlled by its acceleration energy in a known medium. The Z^2 dependence is also very important for therapy. This means that, for equal velocities, the ionization density for the carbon ion ($Z=6$, $A=12$) is 36 times greater than that of the proton. However, a carbon ion has 12 times more total kinetic energy, so the range of the carbon ion is three times lower.

The larger mass of the carbon ion also makes it attractive for therapy. The extent of beam blurring (straggling) is inversely proportional to the square of the mass number. This means that, even when the range is same, the Bragg peak is more narrowly concentrated with carbon ions at the end of the range. In other words, the rate of energy loss along the track (linear energy transfer (LET): KeV/μm) of carbon ions is higher than that of protons. Usually, accelerated atomic nuclei with an atomic number greater than 2 are classified as high LET beams, because different biological effects are more clearly observed for these beams. Hence, carbon (atomic number 6) ion beams are defined as high LET beams showing higher biological effects.

Fractionation in external beam radiotherapy is based on the "four Rs": the repair of sublethal damage, redistribution of the cell cycle, reoxygenation of tumor cells, and repopulation of cancer cells. However, this is not the complete story regarding the biological properties of high LET carbon beams. The radiation-induced damage to cells is the result of DNA strand breaks. If cells are irradiated with different fractions, much higher doses are required to obtain a similar effect with low LET radiation with larger fraction numbers. The sublethal damage and repair of DNA can be exploited by changing the fraction number and dose. Normal cells generally have better DNA damage repair capability compared with tumor cells. Small recovery differences following each treatment between normal cells and tumors cells can lead to a significant gain after multiple treatment sessions. However, in the case of high LET beams, the repair of sublethal damage is not so obvious. The stage of the cell cycle is one of the factors that affect the radiosensitivity of cells. Cancer cells have varying sensitivities to radiation depending on their phase in the cell cycle. Between treatments with conventional radiation, some proportion of the cells will cycle into a more sensitive phase, rendering them more susceptible to radiation damage. On the other hand, high LET radiation shows uniform effects irrespective of the cell cycle.

The majority of low LET radiation damage to the DNA of cancer cells occurs through a free radical mechanism that is enhanced by oxygen. The existing oxygen also hinders radiation damage from being repaired, in other words, repair is

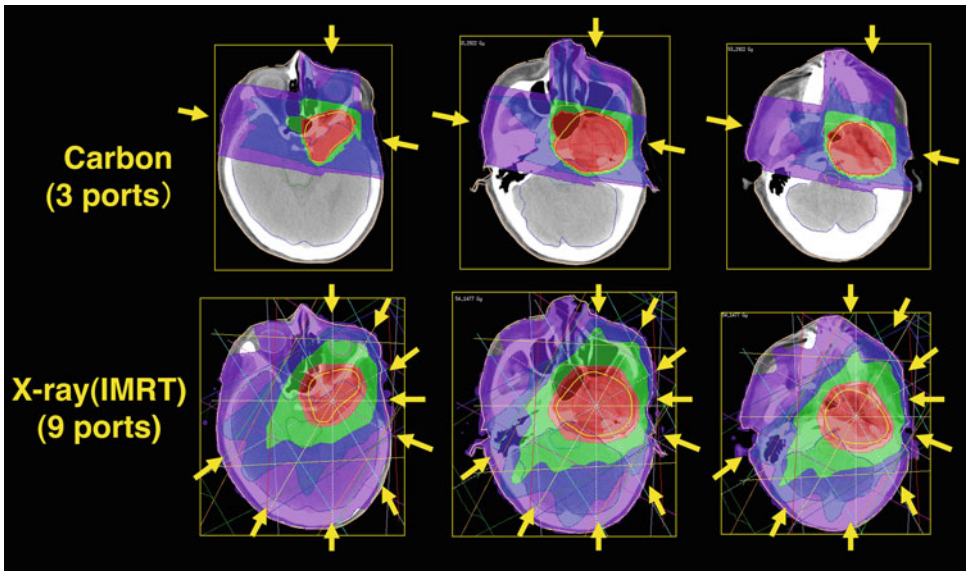

Fig. 2.2 The dose distribution of IMRT using X-rays (*left*) and carbon ion beams (*right*). Carbon ion beams could produce a more conformal dose distribution and steeper dose gradients without an increase in the normal tissue integral dose and with a smaller number of beams compared with IMRT

more promoted under hypoxic conditions. Hence, existing hypoxic cancer cells have been considered to be a major cause of radioresistance in tumors. The time interval between fractions allows additional perfusion of oxygen into areas of the tumor that tend to have low levels of oxygen (that is, hypoxic regions), leading to an enhanced effect of radiation on the tumor. On the contrary, high LET radiation has more direct effects on the DNA and causes extensive damage which is less influenced by the oxygen level. As a consequence, the advantages of fractionation are not as remarkable in radiotherapy using high LET beams. Thus, the high LET carbon beams are associated with less DNA repair, are cell cycle nonspecific, have a low OER (oxygen enhancement ratio), and have low repopulation. In addition to these biological properties, the conformality of the carbon ion beam has enabled us to realize less fractionated or hypofractionated regimens.

2.4 Beam Delivery

The Bragg peak of the carbon ion beam is sharp and narrow, only a few millimeters thick. To cover various sizes of tumors with carbon ion beams, two different beam delivery techniques, a passive beam delivery using a fixed spread out of the Bragg peak (SOBP) and active beam scanning, are employed at the National Institute of Radiological Sciences (NIRS) in Japan (Fig. 2.3). Since the details of each method will be described in Chaps. 4 and 5, the passive beam delivery and the active scanning are only briefly described here.

The passive beam delivery has been used from the beginning of carbon ion radiotherapy and has shown stable and reliable performance at the NIRS. The narrow carbon beam delivered from the accelerator is wobbled by a pair of dipole magnets placed in tandem. Controlling the amplitudes of the magnetic fields, the pencil beam moves on a circular orbit around the original beam axis. At the same time, the beam is broadened with a thin metal foil as a scatterer, which is placed just downstream from the wobbler magnets. With an appropriate combination of the amplitudes of wobbling and thickness of the scatterer, a uniform dose distribution can be obtained at the isocenter. A bar-ridge filter has been used in order to SOBP so as to match its size with the target thickness. Irrespective of the size of the SOBP, the clinical relative biological effectiveness (RBE) value was determined to be 3.0 at the distal part of SOBP. A ridge filter was designed to produce a physical dose gradient of the SOBP so that the biological effect along the SOBP became uniform. This was based on the biological response of human salivary gland (HSG) tumor cells at the 10 % survival level. The biological response flatness along the SOBP was confirmed by measuring the physical dose and dose-averaged LET, together with the biological cell survival experiments throughout the SOBP [4].

Using the beam-wobbling and ridge-filter methods, the maximum lateral field and the SOBP size were designed to be 22 cm in diameter at the isocenter and 15 cm in thickness, respectively, at the NIRS. A multi-leaf collimator (MLC) and a patient collimator are utilized in order to match the lateral dose distribution precisely with a lateral target shape. On the other hand, a bolus compensator is utilized to

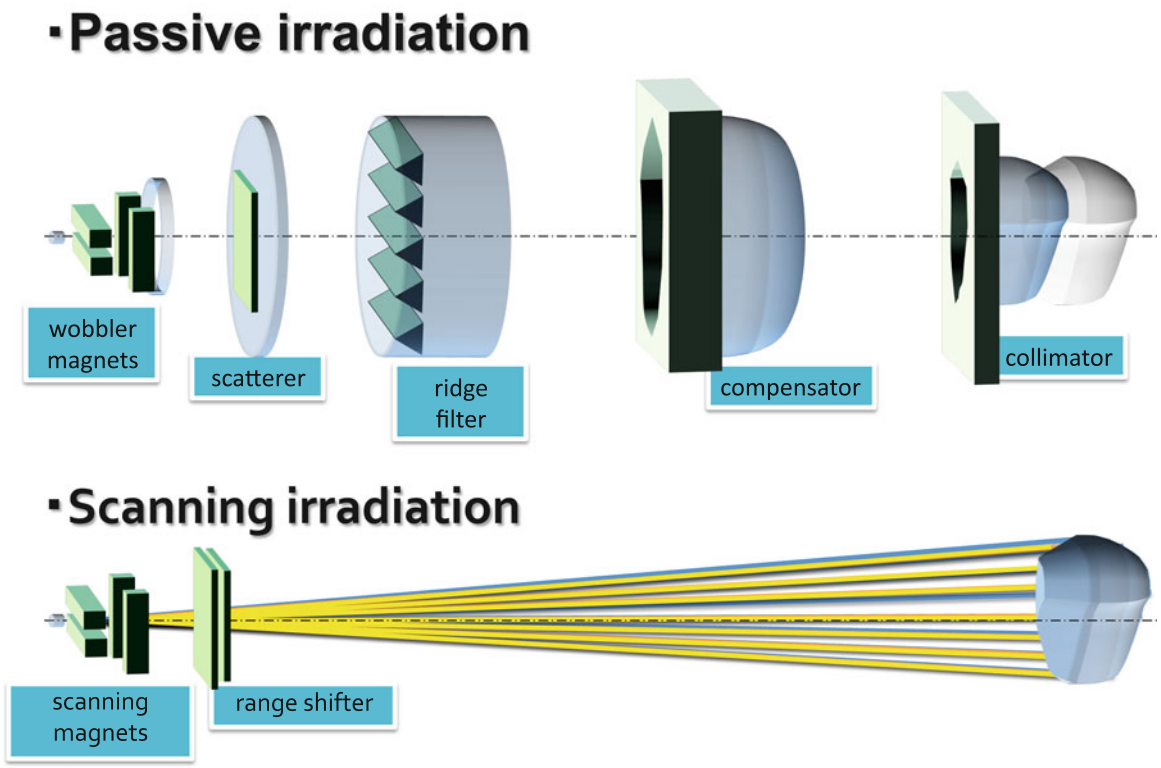

Fig. 2.3 A schematic diagram of passive beam delivery and active beam scanning. An unnecessary high dose at the proximal region of the target was unavoidable, and a collimator and compensation bolus should be used during passive beam delivery. On the other hand, scanning using a narrow beam is more flexible in field shaping and provides a better dose distribution at the proximal region without the collimator and compensation bolus

precisely match the SOBP with a distal target shape. For targets that move with respiration, we have developed a respiratory gating system for passive beam delivery.

The active pencil beam scanning, a type of three-dimensional (3-D) scanning with a pencil beam, is much simpler and more versatile compared to the passive technique. It does not use the wobbling magnets, the scatterer, a bolus, or collimators. Alternatively, just a pair of dipole scanning magnets is used, together with a highly sophisticated beam control technique. We have recently completed the development of a 3D scanning method that can treat fixed targets, although this method has not yet been put into practice for the treatment of a moving target with respiration (as of June 2013). Active scanning for moving targets and a compact rotating gantry using superconducting magnets have been under development, and these techniques will be implemented in the near future. Used in combination with the rotating gantry, the 3D active scanning method can achieve a higher accuracy for treatment even for a target close to critical organs and/or when it is moving.

References

1. Grubbe EH. Priority in the therapeutic use of X-rays. Radiology. 1933;21:156–62.
2. Bragg WH, Kleeman R. On the ionization curve of radium. Phyl Mag A. 1904;8:726–38.
3. Brahme A, Roos JE, Lax I. Solution of integral equation in rotation therapy. Phys Med Biol. 1982;27:1221–9.
4. Kanai T, Furusawa Y, Ohara H, et al. Irradiation of mixed beam design of spread-out Bragg peak for heavy-ion radiotherapy. Radiat Res. 1997;147:78–85.

Overview of the Heavy-Ion Medical Accelerator in Chiba (HIMAC) Practices

3

Tadashi Kamada

Abstract

In 1994, carbon ion radiotherapy was begun at the National Institute of Radiological Sciences (NIRS) using the Heavy-Ion Medical Accelerator in Chiba (HIMAC), which was the world's first heavy-ion accelerator complex dedicated to medical use. In the past 19 years, more than 7,000 patients have been treated with carbon ion beams at the NIRS. A total of 70 protocol studies (Phase I/II and Phase II) have been conducted to investigate the optimal indications and irradiation techniques. Hypo-fractionated carbon ion radiotherapy protocols (average: 13 fractions per patient) with acceptable morbidities have been established for various types of tumors. Carbon ion therapy is associated with improved local control and survival in radioresistant advanced tumors such as sarcomas, melanomas, and other non-squamous cancers. The next-generation carbon ion therapy system has been under development to realize more advanced techniques, such as respiration-gated 3-D active beam scanning with a compact rotating gantry with superconducting magnets.

Keywords

HIMAC • Hypo-fractionated • Protocol studies

3.1 Introduction

In Japan, the decision to implement the medical use of heavy ions was made in 1984 as one of the main projects of the first comprehensive 10-year strategy for cancer control. The Heavy-Ion Medical Accelerator in Chiba (HIMAC) was the world's first heavy-ion accelerator complex dedicated to clinical research. The accelerator complex took almost 10 years to design and construct and was completed at the end of 1993. After 6 months of commissioning of the facility, clinical trials using carbon ion beams generated from the HIMAC were initiated in June 1994. This chapter will provide an overview of carbon ion radiotherapy over the last 19 years at the National Institute of Radiological Sciences (NIRS).

T. Kamada, M.D., Ph.D. (✉)
Research Center for Charged Particle Therapy, National Institute of Radiological Sciences, Chiba, Japan
e-mail: t_kamada@nirs.go.jp

3.2 The HIMAC

The design parameters of the HIMAC were based on the estimated radiological requirements. Ion species ranging from He to Ar can be accelerated to the desired energies. The beam energy was designed to vary from 100 to 800 MeV/u for efficient treatment. The HIMAC consists of an injector linear accelerator (linac) cascade, dual synchrotron rings with independent vertical and horizontal beam lines, and three treatment rooms equipped with passive beam delivery systems.

For carbon ion radiotherapy, a C^{2+} beam produced by the 10 GHz-ECR ion is injected into the linac cascade consisting of RFQ and Alvaretz linacs and is accelerated up to 6 MeV/n. After the carbon beam is fully stripped with a carbon-foil stripper, the beam is then injected into the synchrotron rings by a multiturn-injection scheme and is slowly extracted after acceleration to a desired energy. Finally, the carbon beam extracted from the synchrotron is delivered via the beam

H. Tsujii et al. (eds.), *Carbon-Ion Radiotherapy: Principles, Practices, and Treatment Planning*,
DOI 10.1007/978-4-431-54457-9_3,

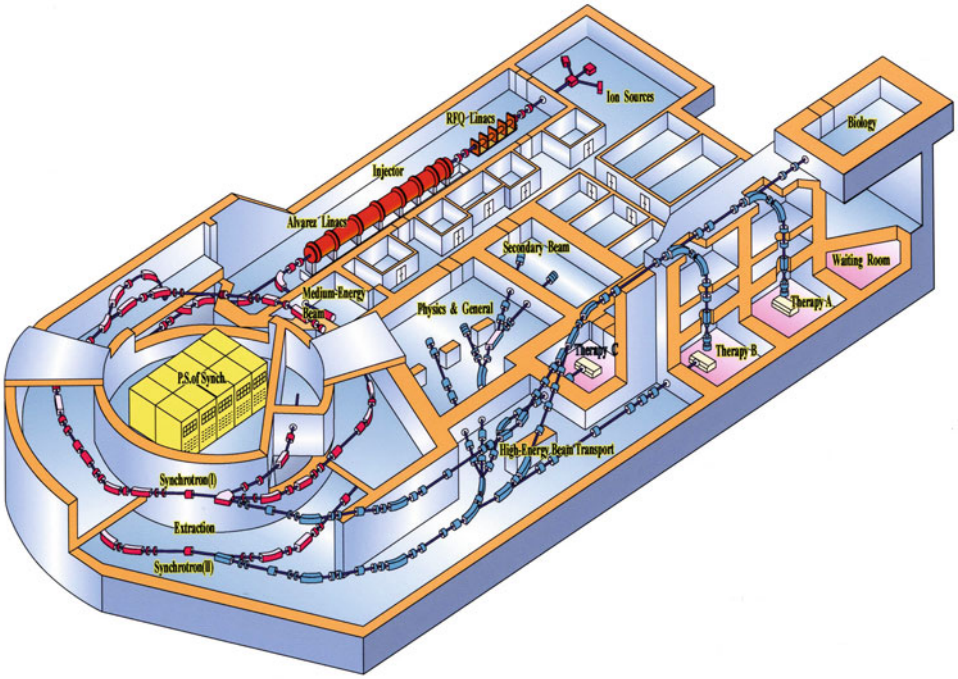

Fig. 3.1 A bird's-eye view of the HIMAC facility A unique double-synchrotron ring heavy-ion accelerator system dedicated for medical use was designed and constructed. It consists of two ion sources, an RFQ (radio frequency quadrupole) linear accelerator (linac), an Alvarez linear accelerator (linac), two synchrotron rings, a high-energy beam transport system, and an irradiation system

delivery system [1, 2]. A bird's-eye view of the HIMAC facility is shown in Fig. 3.1, and the specifications of the HIMAC are listed in Table 3.1. The footprint of the HIMAC was 120×65 m, and its construction cost reached to 32,600,000,000 JPY.

In order to conform the dose to a specific target, a passive beam delivery technique has been employed. The beam lines in the treatment room are equipped with a pair of wobbler magnets, beam scatterers, ridge filters, multi-leaf collimators, and the ability to administer a compensation bolus. An appropriately designed ridge filter, which corresponds to and determines the size of the spread out of Bragg peak (SOBP), is chosen to avoid unnecessary dosing of normal tissues along the beam path in each port. Twelve different size ridge filters were made to cover thicknesses of 2–15 cm.

The patients are positioned in customized cradles and immobilized with a low-temperature thermoplastic cast. A set of CT images are taken for treatment planning with the immobilization devices in place. Respiratory gating for both the CT acquisition and therapy is performed when indicated [3]. A three-dimensional treatment planning is performed using our original HIPLAN software program, which was developed for carbon ion radiotherapy CIRT [4]. A margin of 5 mm is usually added to the clinical target volume to create the planning target volume. The dose is calculated for the target volume and any nearby critical structures and expressed in Gray-equivalents (GyE = carbon physical dose in Gray × Relative Biological Effectiveness {RBE}).

Radiobiological studies were carried out in mice and in five human cell lines cultured in vitro to estimate RBE values relative to megavoltage photons. Irrespective of the size of the SOBP, the RBE value of carbon ions was estimated to be 3.0 at the distal part of the SOBP, and ridge filters were designed to produce a physical dose gradient of the SOBP so that the biological effect along the SOBP became uniform. This was based on the biologic response of human salivary gland tumor cells at a 10 % survival level. The biological response flatness along the SOBP was checked by measuring the physical dose distributions and dose-averaged LET, which were in satisfactory agreement with the calculated results [5].

Carbon ion radiotherapy (C-ion RT) is given once daily, 4 day/week (Tuesday to Friday). During every treatment session, the patient's position is verified with a computer-aided online positioning system.

A new beam delivery with active scanning was started in May 2011, and we have since treated more than 200 patients with fixed targets.

Table 3.1 Specifications of the HIMAC

Ion: H–Ar	
Max energy	100–800 MeV/u
Treatment room [3]	
Fixed vertical	Room A
Fixed horizontal	Room C
Fixed vertical and horizontal	Room B
Accelerated energy	
Vertical beam	140 or 290 or 350 or 400 MeV/u
Horizontal beam	140 or 290 or 400 or 430 MeV/u
Range of carbon ion beam in water	
140 MeV/u	5 cm
290 MeV/u	15 cm
350 MeV/u	20 cm
400 MeV/u	25 cm
430 MeV/u	30 cm
Maximum field size	15 cm by 15 cm

3.3 Clinical Trials at the NIRS

From June 1994 until March 2013, a total of 70 protocols were conducted in an attempt to determine the optimal dose-fractionation and irradiation method for the treatment of specific diseases. The HIMAC passive beam delivery system has been showing reliable and stable performance for the last 19 years, and a total of more than 7,000 patients had been registered for treatment, and the C-ion RT was approved as a clinical practice in 2003. The number of patients treated as part of clinical practice as of June 2013 has been more than 4,000 at the NIRS (Fig. 3.2). The categories of disease that can be treated in routine clinical practice include lung cancer, prostate cancer, head and neck cancer, skull base tumors, ocular melanoma, bone and soft tissue sarcoma, liver cancer, pelvic recurrences of rectal cancer, pancreatic cancer, uterine cervical cancer, and re-irradiation after conventional radiotherapy, among others. The number of patients has increased every year, and the facility has reached a capacity permitting more than 800 patients to be treated each year (Fig. 3.3).

The clinical trials began with a small dose per fraction. At first, the average number of fractions was around 18. All these early trials were carried out as dose-escalation studies. It was found that a very high dose per fraction could be administered because of the better dose distribution of carbon ion beams. In addition to the high physical selectivity of carbon ion beam, the biological properties associated with the high-LET carbon beam, low DNA repair, cell cycle non-specific activity, and low OER are well-known effects that facilitate cancer eradication. Hence, a protracted fractionated regimen is not advantageous in carbon therapy. Therefore, we started performing less fractionated or hypo-fractionated radiotherapy. When using such treatments, the overall treatment time should be shorter, and the effect of repopulation is limited. The average number of fractions could subsequently be reduced from 18 to 12–13. Over the last several years, this reduction of fraction number has led to remarkable improvements in patient throughput at the NIRS (Fig. 3.4).

The clinical results in the most common sites of cancer at the NIRS are briefly summarized below:

1. Head and Neck Cancers
   Carbon ion radiotherapy was first applied for the treatment of patients with unresectable locally advanced head and neck tumors. A dose-escalation study using 18 fixed fractions delivered over 6 weeks was conducted and then shortened to 16 fractions over 4 weeks' schedule. More than 800 locally advanced tumors were treated in head and neck protocols with this protocol, with the total dose being either 57.6 or 64 GyE. The treatment results obtained so far can be summed up by stating that a very favorable local control rate of around 80 % has been achieved, mainly for adenocarcinoma, adenoid cystic carcinoma, and mucosal malignant melanoma. With regard to malignant melanoma, however, a combined regimen of carbon ion radiotherapy and chemotherapy was initiated in order to better control or prevent distant metastasis. For sarcomas arising from head and neck region, a total dose of 70.4 GyE was required to achieve a similar local control rate.
2. Lung Cancer
   Patients with medically inoperable stage I non-small cell lung cancer were treated under several protocols. We started with fixed 18 fractions over 6 weeks' dose-escalation study and then shortened the overall treatment time to 3 weeks in two protocols. The results of these studies were better than those of conventional radiotherapy and almost the same as those of surgery. We have beeen conducting a fixed four fractions over 1 week protocol since 2000. We are able to give a very high dose in 1 week without unacceptable side effects. A single fraction dose-escalating study was started in 2003, and the dose was increased from 28 to 50 GyE in more than 200 patients. A total of more than 400 patients with stage I non-small cell lung cancer have been enrolled in these protocols. The results are quite promising, including those of the single fraction study that have been reported so far. To clarify the best regimen for stage I non-small cell lung cancer, a randomized controlled clinical trial comparing different fractionations could be conducted.
3. Liver Cancer
   For primary liver cancer, 15 fractions over 5 weeks' irradiation schedule were employed initially. The overall treatment time of 5 weeks then was shortened to 3, 2, and 1 week and then to 2 days in the subsequent studies. The shortest irradiation schedule of two fractions/2 days has been showing encouraging results in terms of a favorable local control rate and the absence of any particular serious

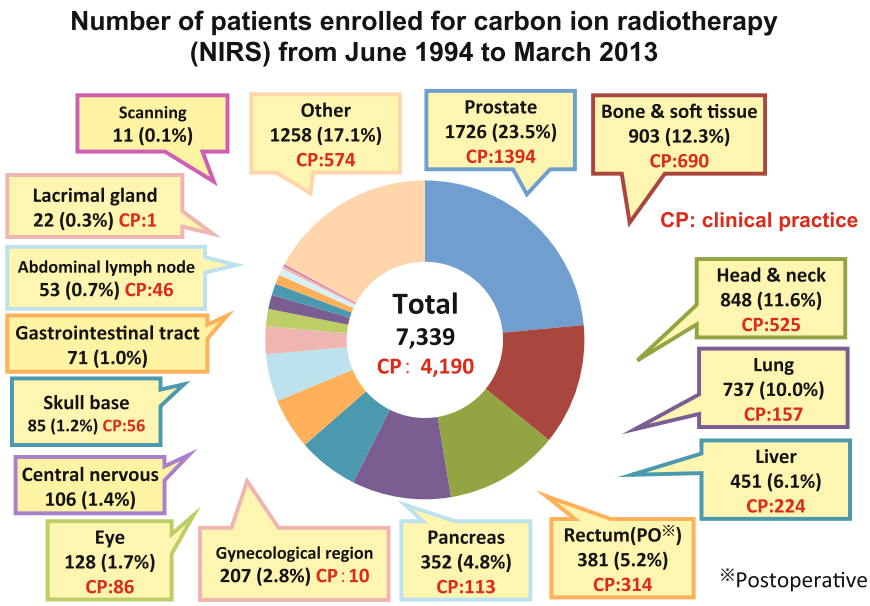

Fig. 3.2 The number of patients treated using carbon ion radiotherapy from June 1994 to March 2013 at the NIRS. A total of 7,349 patients had received carbon therapy at the NIRS as of March 2013. Prostate cancer, sarcoma, head and neck cancer, lung cancer, liver cancer, postoperative local recurrence of rectal cancer, and pancreatic cancer were the most frequently treated tumors at the NIRS. More than 4,000 patients have received carbon ion radiotherapy as part of clinical practice

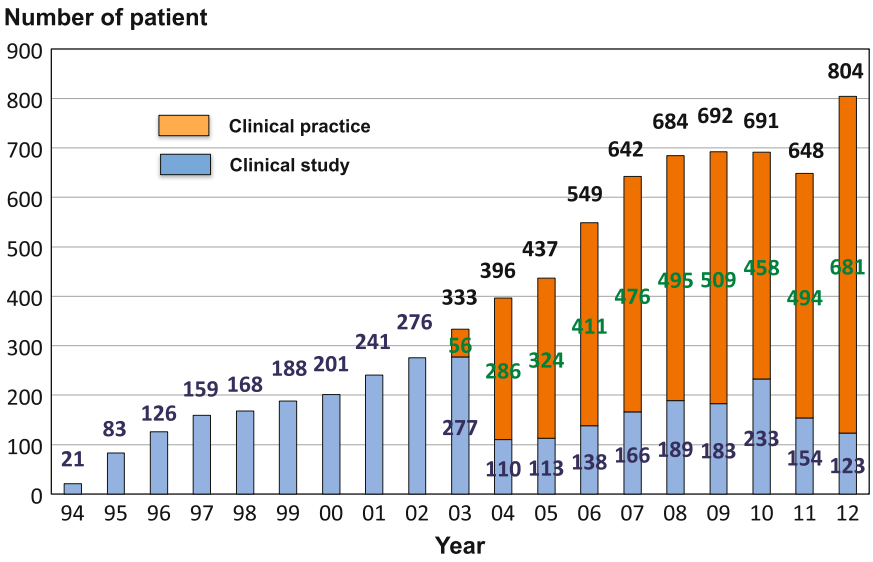

Fig. 3.3 The annual patient accrual at the NIRS. Carbon ion radiotherapy has been performed as part of clinical practice with government approval since 2003. The cost of carbon ion treatment as part of clinical practice is 3,140,000 JPY per case, irrespective of the fraction number. However, the number of patients has been increasing every year, and in 2012, 804 patients were registered for treatment at the NIRS

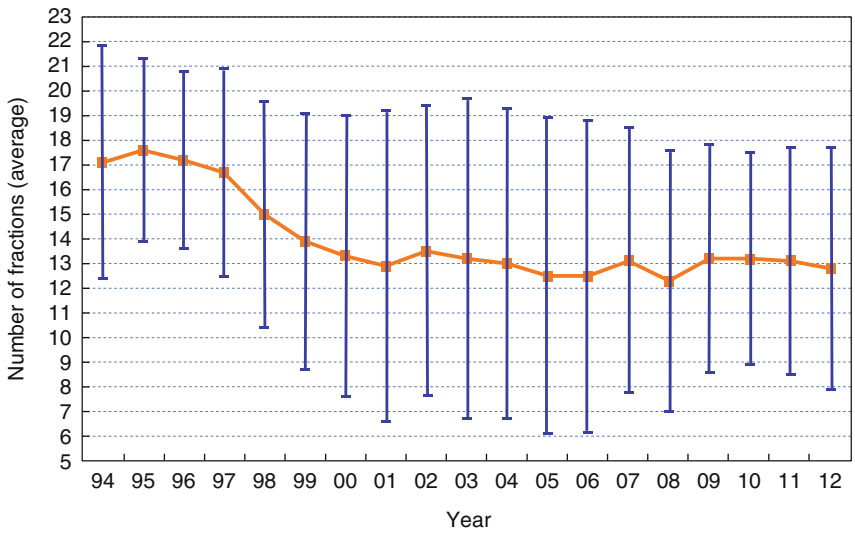

Fig. 3.4 The average fraction number per case. The average number of fractions administered at the beginning was almost 18 and has since then been reduced to 13. The reduction has mainly been achieved by implementing hypo-fractionation protocols. This reduction of the fraction number per patient not only improves the outcome for patients, but also increases the number of treatment slots at the NIRS

toxic reactions even in patients with a large (5 cm or more in diameter) tumor. Nearly 450 patients were treated with carbon beams. A single fraction dose-escalation study for metastatic liver cancer, which is associated with a better liver function compared to primary liver cancer, is currently ongoing.

4. Pancreatic Cancer
   Pancreatic cancer is rarely curable, and because of its location, it causes significant symptoms such as intractable back pain and gastrointestinal obstruction. The 5-year survival rate achieved with surgical resection is generally unfavorable, at less than 20 %. In the case of locally advanced unresectable cancer of the pancreas, the 2-year survival rate is even lower. In order to improve the treatment results for cancer of the pancreas, the critical factor is how effectively liver metastasis and retroperitoneal recurrence are controlled, since these account for 50 % of all recurrences. Attempts have been made to improve the local efficacy first and to establish therapeutic strategies involving the concomitant use of chemotherapy with C-ion RT. At present, a clinical trial of short-course preoperative carbon beam irradiation is in progress.

   For locally advanced unresectable pancreatic cancer, a dose-escalation clinical trial of 3 weeks of concurrent chemo-carbon ion irradiation was conducted, and a dramatic improvement of the 2-year overall survival rate was observed, without severe morbidities, in the high-dose group.
5. Rectal Cancer (Postoperative Pelvic Recurrence)
   Although the incidence of postoperative rectal cancer recurrence in the pelvis has decreased as a result of improvements in surgical procedures, the incidence of recurrence after surgery is still almost 20 %. Many of the patients with local recurrence are not eligible for surgical resection and are frequently referred for radiotherapy. However, the results are far from adequate. Many of the previous reports have documented a 50 % survival period of 12 months and a 3-year survival rate of around 10 %, and the role of radiotherapy is often described as palliative. Almost 400 patients have so far been treated with carbon ion radiotherapy, and no serious toxic reactions have been observed. The results, in terms of the local control and survival rates, have been favorable in comparison with conventional radiotherapy and are comparable to those achieved with surgery.
6. Prostate Cancer
   A total of three clinical trials have so far been carried out in patients with prostate cancer. The first carbon ion radiotherapy trial (20 fixed fractions over 5 weeks) with concomitant endocrine therapy was conducted for B2-C stage patients. The second trial had a wider scope of eligibility and consisted of carbon ion monotherapy for stage A2-B1 prostate cancer and C-ion RT combined with endocrine therapy for stage B2-C. In the first clinical trial, the most serious toxicities in the rectum were recorded among the patients exposed to the highest dose. As a result, a safe dose for the digestive tract was established, and no serious toxic reactions were subsequently encountered in the later clinical trials. A total dose of 63 GyE was found to be the optimal dose for the 20 fractions over 5 weeks' protocol. The overall treatment time was then shortened to 4 weeks and showed better outcomes. After that we conducted a study of 12 fractions over 3 weeks in 2010. There were no severe side effects, and since April 2013, all prostate cancers were treated with the 3 weeks regimen. The total number of prostate cancers treated with carbon ion is now nearly 1,800.
7. Bone and Soft Tissue Sarcomas
   Bone and soft tissue sarcomas are generally considered to be radioresistant. Advanced tumors originating in the trunk, in particular, are often not resectable and have a poor prognosis. The use of carbon ion beams offers a favorable prospect of improved local control in view of its superior biological dose distribution. The patients enrolled in our initial dose-escalation trial were primarily subjects who had not successfully responded to surgery or were totally inoperable. This trial has produced favorable local control, and it showed that chordoma and osteosarcoma are prime candidates for C-ion RT. Some 10 % of the patients whose lesions are close to the body surface, making it impossible to avoid exposure of the skin to high radiation doses, developed severe reactions, such as skin ulceration. As more experience has been gained and significant improvements in irradiation techniques have been achieved, such severe reactions no longer occur. Bone and soft tissue tumors in the trunk are the most typical lesions qualifying for carbon ion radiotherapy, and 900 such patients have been treated so far.

3.4 Future Prospects of Carbon Ion Radiotherapy at the NIRS

Our clinical experience has demonstrated the superiority of carbon ion beams over other types of irradiation for the treatment of various tumors. The current facilities and devices may be termed the "first-generation" equipment for carbon ion radiotherapy. It is important to develop advanced second- and third-generation equipment to bolster international competitiveness, because many countries are starting to establish new medical facilities for carbon ion radiotherapy. Mere downsizing of the treatment equipment will be far from satisfactory.

One new technique that deserves particular attention is the 3-D scanning beam delivery method, which uses "narrow" pencil beams of carbon ions to cover an entire target volume. The NIRS has been conducting extensive research

and development projects for the clinical application of the 3-D scanning. We have successfully developed a 3-D active scanning method that can treat fixed targets, although this method has not yet been put into practice for the treatment of a moving target with respiration (as of June 2013).

Active 3-D beam delivery is appropriate for the treatment of complex-shaped lesions that cannot be adequately irradiated by the passive beam delivery. It will also adapt treatment to time-course changes in the target shape. The current treatment procedure for prostate cancer requires 12 fractions over 3 weeks. The number of fractions can possibly be reduced by applying the 3-D scanning technique, since it can reduce the dose to the urethra, which is the most serious organ at risk, because it runs through the middle of the prostate gland. The use of a rotating gantry will minimize the time required for patient positioning and the patient's physical burden during irradiation. For example, in the case of a patient with lung cancer, the current system using fixed beam lines requires 1.0–1.5 h per session with four different angle irradiations for single fraction treatment. The new system will reduce this to 30 min, because the session will not require repositioning of the patient. In addition, the new system may be applicable for patients with a poor general condition, owing to its simplified treatment setup procedures and reduced treatment time.

We anticipate that the introduction of the 3-D scanning technique and the rotating gantry will not only improve the therapeutic outcome but also dramatically increase the number of patients who can be treated (due to expanded indications and a higher treatment efficiency, as well as the shorter duration of treatments).

References

1. Sato K, Yamada H, Ogawa K, et al. Performance of HIMAC. Nucl Phys A. 1995;588:229–34.
2. Kanai T, Endo M, Minohara S, et al. Biophysical characteristics of HIMAC clinical irradiation system for heavy-ion radiation therapy. Int J Radiat Oncol Biol Phys. 1999;44:201–10.
3. Minohara S, Kanai T, Endo M, et al. Respiratory gated irradiation system for heavy-ion radiotherapy. Int J Radiat Oncol Biol Phys. 2000;47:1097–103.
4. Endo M, Koyama-Ito H, Minohara S, et al. HIPLAN: a heavy ion treatment planning system at HIMAC. J Jpn Soc Ther Radiol Oncol. 1996;8:231–8.
5. Kanai T, Furusawa Y, Ohara H, et al. Irradiation of mixed beam design of spread-out Bragg peak for heavy-ion radiotherapy. Radiat Res. 1997;147:78–85.

Part III

Radiobiology of Carbon-Ion Radiotherapy

Heavy-Ion Radiobiology

4

Yoshiya Furusawa

Abstract

In biological processes after energy deposition of radiation in cells, DNA damage occurs at first to produce chromosomal breaks and then appear many cell responses. Reproductive and interphase cell death causes inactivation of cancer tissue. Traditional target theory and linear quadratic model are used to explain mechanism and treatment prediction. There are many factors to modify the efficiency of radiobiological effects such as oxygen and other chemical substances as well as physical distribution of radiation. For high-LET radiations, relative biological effectiveness is the most important factor to explain the radiobiological effects on cancer therapy as well as oxygen enhancement ratio.

Keywords

4R's • Dose response • LET • OER • RBE

4.1 Physical, Chemical, and Biological Processes

4.1.1 Processes of Radiobiological Effects

Biological effects after exposure to ionizing radiations proceed in the time sequence as follows: physical processes such as energy absorption by the atoms and molecules proceed before 10^{-15} s after the irradiation, chemical process; reaction drives direct or indirect molecular changes including free-radical production in the order of 10^{-6} s and thereby biological process; and biological effects bring on initial damages to biomolecules in the cell components (e.g., DNAs, proteins) in the order of 10^{-3} s. A part of those damages will be repaired through the biological processes to be a healthy cell, or fixed through the processes to kill the cells leading to the death of individual cells. Or the cells will live but produce a genetic change to produce a mutant or a tumor. A conceptual time sequence of the various processes initiated by radiation is shown in Fig. 4.1. The initial changes that include ionization and excitation occurring at the atomic level and DNA damage occurring at the molecular level lead to changes at a cellular level, organ level, and then total body level, eventually resulting in changes in the whole individual.

4.1.2 Direct and Indirect Actions of Radiation

Biological effects after exposure of radiation are divided into two categories, direct action and indirect action of radiation by the very early process of the energy deposition (Fig. 4.2). DNA molecules can receive energy directly from the secondary electrons produced by the incident radiation, resulting in their ionization, and are damaged by cleavage of the chemical bonds. This direct action of radiation accounts for approximately 1/3 of all biological effects after radiation. DNA molecules can also be damaged by active group of molecules (free radicals) produced by ionization of the surrounding water molecules. This is an indirect action of radiation and accounts for the remaining approximately 2/3 of the biological effects.

Y. Furusawa (✉)
National Institute of Radiological Sciences, 9-1, Anagawa-4, Inage-ku, Chiba 263-8555, Japan
e-mail: furusawa@nirs.go.jp

H. Tsujii et al. (eds.), *Carbon-Ion Radiotherapy: Principles, Practices, and Treatment Planning*,
DOI 10.1007/978-4-431-54457-9_4, © Springer Japan 2014

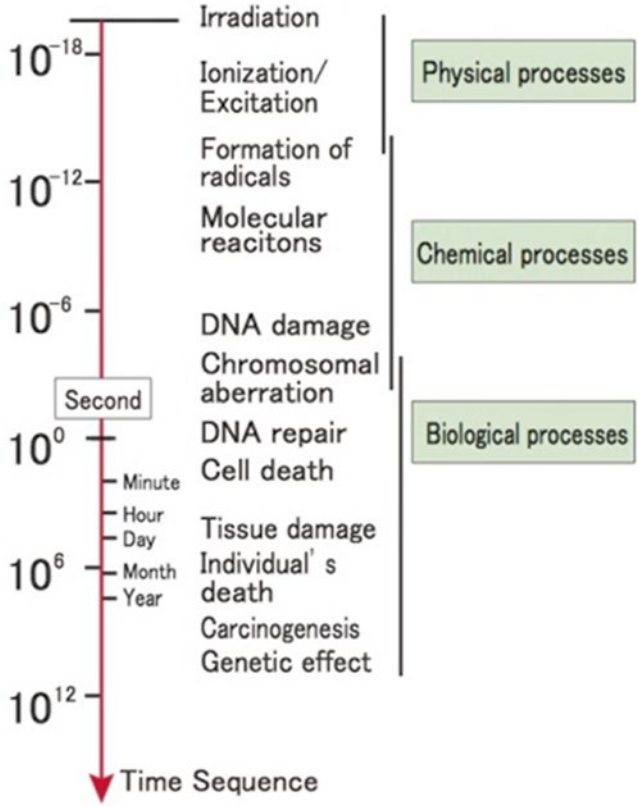

Fig. 4.1 Time sequence of radiobiological process after ionization radiation

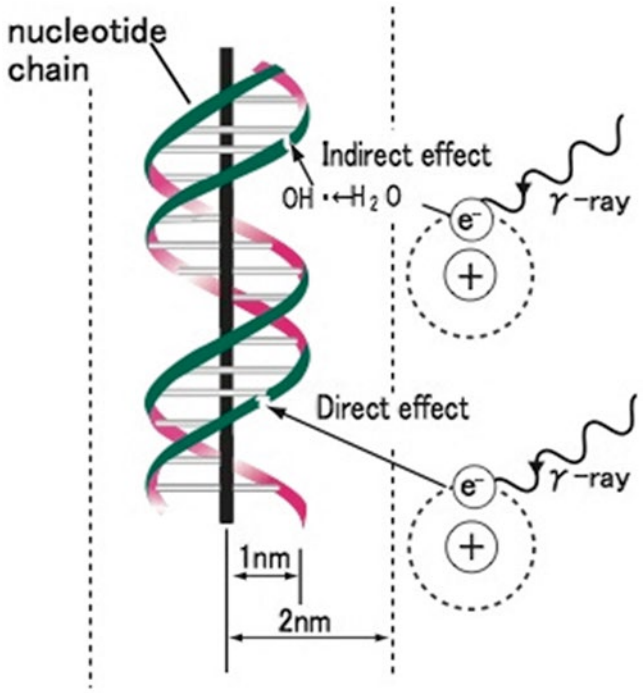

Fig. 4.2 Direct and indirect actions of radiation. Indirect action (*upper*), the secondary electron interacts with, for example, a water molecule to produce a hydroxyl radical (OH·), which produces a damage to the DNA. Direct action (*lower*), a secondary electron resulting from absorption of a photon interacts with the DNA to produce damages. Modified from [1]

The efficiency of free-radical production is expressed as a *G*-value, which is defined as the number of free-radical molecules produced per 100 eV of absorbed energy. The values are obtained as the final result of chain reactions. This process mainly consists of the chemical reactions of water molecules with the body constituents and can be affected by the surrounding various free-radical scavengers. These active species deprive a biomacromolecule (R) of a hydrogen atom (dehydrogenation) to make a radical R; the radical R binds with a hydroxyl radical (OH·) or reacts with another radical biomolecule to compose a new molecule. Consequently, the active species cause various reactions (Fig. 4.3).

4.1.3 Direct and Indirect Actions of Radiation

Low-LET radiations (photon) show a uniform, sparse spatial distribution of ionization in cells. High-LET particles bring about a dense ionization along their track through energy deposit to the medium, showing distributions called track structures (Fig. 4.4). Charged-particle beams that form the Bragg's peak in matter change the ionization density along the traveling direction, showing complexities.

Various physical and chemical processes are involved in the biological effects as direct and indirect effects of radiations and details of these processes can be found in other materials [2]. Particle beams have more different characteristics than photon beams that originate from the differences in their ionization-density distributions. Unlike low-LET photon beams, for example, high-LET particle beams show an ionization density higher than necessary for cell killing in some area in matter and also produce concentrated damages such as multiple DSBs or complex lesions. Thus, particle beams have different and severe biological effects from those of low-LET radiations.

4.2 Biological Elementary Processes

The organs comprising a human body are composed of tissue, which is a collection of cells with various functions to achieve specific objectives. The impact of ionizing radiations on a human body is initiated in the cells. Ionizing radiations delivered to a human body have the most serious impact on the genes that contained cell nucleus or DNA molecule. DNA damage causes the transmission of erroneous information,

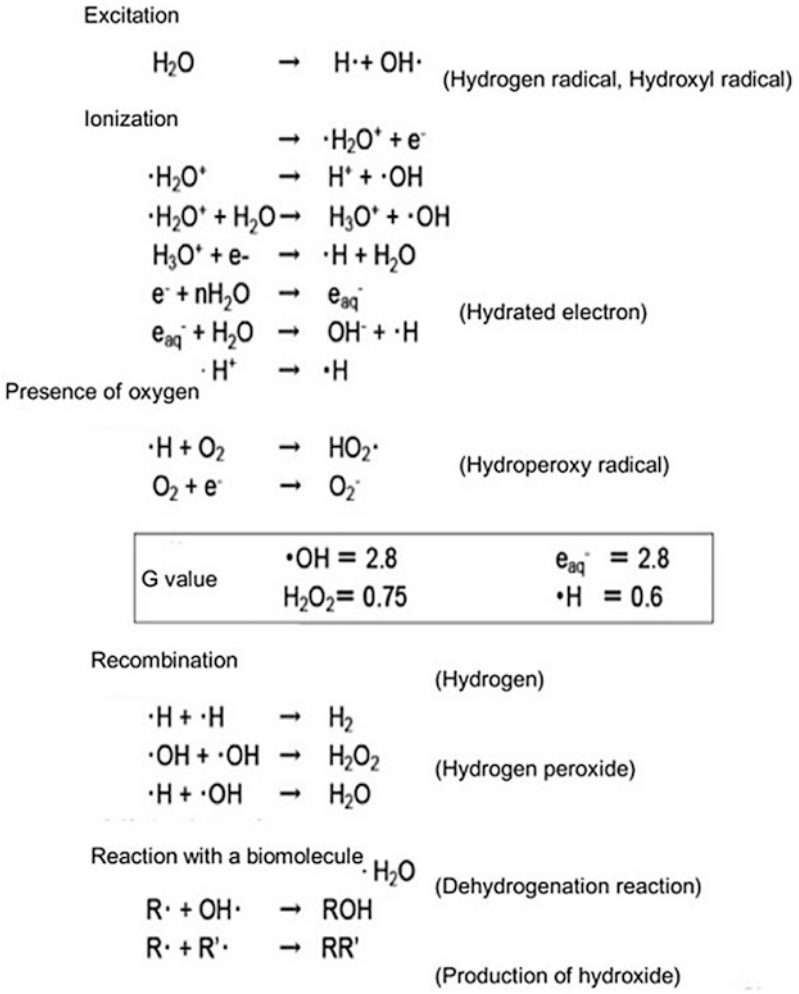

Fig. 4.3 Radiation chemical processes of water molecules after ionization radiation and the efficiency, G-value of major products

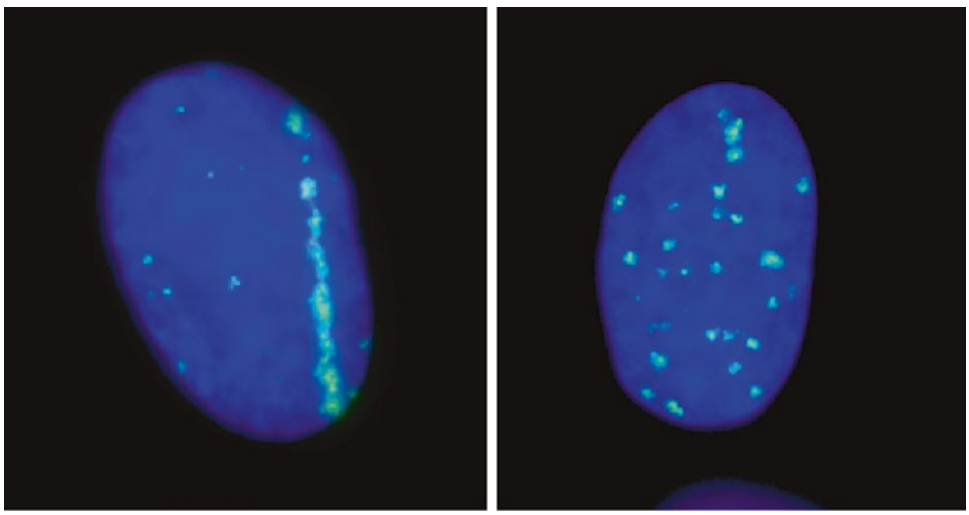

Fig. 4.4 Biological track structure of heavy-ion traversal in cell nuclei. DNA double-strand breaks were visualized after very high-LET horizontal iron-ion beam (*left*) and X-rays (*right*). Clear structure after iron beam traversal was observed, but no such structure for X-rays

makes cell growth difficult unless repaired, and produces abnormal conditions such as mutations or carcinogenesis. This damage in a cell impairs functions of the organ as damage to the tissue, eventually influencing the individual. A DNA molecule consists of a pair of backbone chains with the four (ATGC) nucleobases, which are involved in the encoding of genetic information. DNA is a long molecule encoding a huge amount of genetic information. The DNA contained in one human cell weighs approximately 6 pg, and the human genetic information is written as 4-bit data in approximately 32 hundred million base pairs.

A process of cell proliferation is carried out through a "cell cycle" sequence consisting of the four ($M/G_1/S/G_2$) phases. Certain types of cells are usually proliferating by repeatedly dividing to supply functional cells. In contrast, many somatic cells (nonreproductive cells) usually stay in another G1-like interphase (G_0 phase) without proceeding to the S phase, performing their own functions.

4.2.1 DNA Damages

The most important biological damage of cells after exposure of ionizing radiation is believed to be DNA damage. Many kinds of DNA damages will generate in a cell [3]. Damages or losses of nucleotide bases and DNA single-strand breaks (SSBs) are potentially to be repaired without errors of genetic information because of the existing right genetic information in the complementary DNA strand. Numbers of double-strand breaks (DSBs) are also rejoined to reconstruct DNA strand by the nonhomologous end joining (NHEJ) and homologous recombination (HR) systems. Damaged site is reconstructed by using the genetic information in complementary strand of sister chromatid by the HR system and shows error-free repair. Some nucleotide bases near the damage site are removed to clean up the damaged end, rejoin the strands without correct genetic information in the NHEJ process; thus it will be an error-prone rejoining. In addition, productions of complex lesion of DNA breaks are expected for heavy-ion exposure, because the density of ionization must be very high at around the traversal of the ion.

When cells are exposed to ionizing radiation, DNA damages in the form of SSBs, DSBs, base damage, or their combinations are frequent events. It is known that the complexity and severity of DNA damage depend on the quality of radiation and the microscopic dose deposited in small segments of DNA, which is often related to the linear transfer energy (LET) of the radiation. Experimental studies have suggested that under the same dose, high-LET radiation induces more small DNA fragments than low-LET radiation, which affects Ku binding with DNA end efficiently and might be a main reason for high-LET radiation-induced RBE since DNA DSB is a major cause for radiation-induced cell death. In this work, we proposed a mathematical model of DNA fragments rejoining according to NHEJ mechanism.

4.2.2 Chromosome Aberrations

One set of chromosomes in a human individual consists of 22 pairs of autosomes (any of the chromosomes in a cell other than the sex chromosomes) and two sex chromosomes, all of which are inherited from one's parents. In the DNA synthetic phase of the cell cycle, one copy of the genetic information is created and associated with the original one as a pair of sister chromatids, bound at the centromere, in order that the same genetic information may be distributed to two daughter cells in the coming mitotic phase. In the metaphase of the mitotic phase, DNA, distributed homogeneously within a cell nucleus in other phases, condenses to form 46 structures that can be microscopically observed as chromosomes. In the anaphase, 46 pairs of sister chromatids are pulled apart to transmit the genetic information to the two daughter cells.

In the cells of which DNA has been damaged by radiation exposure, abnormality can be observed as a chromosomal aberration which is effective as an indicator of radiation exposure as it is easy to quantify and correlates well with radiation-caused cell death. Various types of chromosomal aberration (Fig. 4.5) are caused by radiations, depending on the phase of the cell when its DNA is damaged. If it occurs during the period from the first pause (G1 phase) to the early DNA synthetic phase (early S phase), the so-called chromosomal aberration can be observed, which appears to be caused by simultaneous cleavage of both of the sister chromatids. If a cleaved chromosome is not reunited, "terminal deletion" and "fragment formation" are observed. After a chromosome is cleaved at the two sites, the center section turns over and is then reunited with the remaining fragments. This phenomenon is called "inversion." If the termini of this center section rejoin with one another, a "circular chromosome" is formed, with the fragments left over. After two chromosomes are cleaved, they can rejoin with each other to form a dicentric chromosome, which has two kinetochores (structures of protein associated with DNA located at the centromere region). This phenomenon is called "mutual translocation." On the other hand, if DNA damage occurs late in the DNA synthetic phase (late S phase) or the second pause (G2 phase), chromatid aberration is observed, with damage showing on either of the sister chromatids (Fig. 4.5).

4.2.3 Cellular Effects

Many of the multiplied human cells undergo cell cycle about once a day, with one parent cell dividing into two daughter cells; the number of the cells doubles again and again.

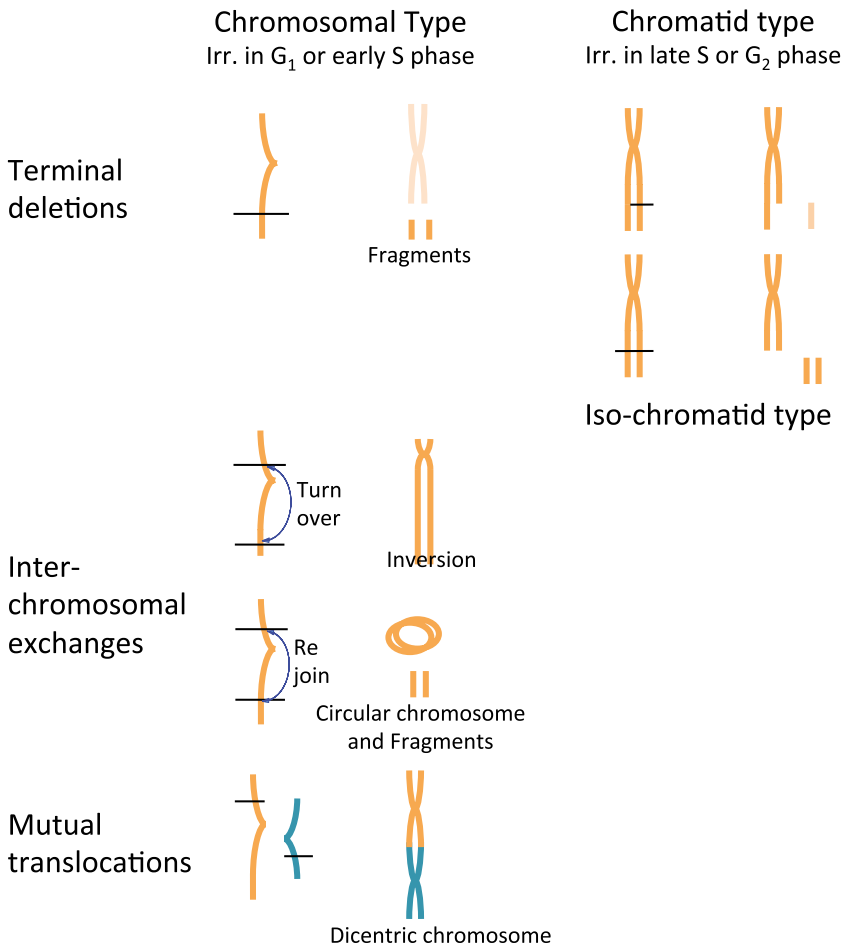

Fig. 4.5 Types of chromosomal aberrations. Many iso-chromatid-type aberration can be seen after high-LET radiation

A tens-of-micron single cell proliferates into a macroscopic colony with a diameter of several millimeters after a dozen days or so. When these cells are irradiated, some of them die owing to the resulting damage, while others survive. The surviving cells can form a colony, but the colonies show different morphology from those made by unirradiated cells, and the number of colonies they form is usually smaller. There are several cell death modes, but they are generally classified into reproductive death and interphase death.

4.2.3.1 Reproductive Death

Even after irradiation, the surviving cells can continue proliferating; cells have the ability to repair damage to their DNA or chromosomes and many cells can remove these damage. After repair, the cell cycle goes into a temporary pause, which is called G_1 block or G_2 block. These additional pauses in the cell cycle result in mitotic delay, which is often observed for the first division after irradiation. Approximately 1-Gy irradiation often causes a 1-hour mitotic delay.

Reproductive death is the mode of death of the irradiated cells that have lost reproductive ability after several cell divisions. These cells may still retain ability to synthesize DNA and proteins. These cells, however, have various functional aberrations; for example, the nucleus divides but fail in cytokinesis (the last stage of cell division following the nuclear division, division of cytoplasm) and the cell grows but cannot divide or shows abnormal morphology. In radiobiological observations after irradiation, which aim at counting the reproductive cell deaths, a colony consisting of 50 or more cells (after 5 to 6 divisions) is regarded as a colony originating from a surviving cell. The cell survival rate is determined from the ratio of the number of colonies formed in a plate to the number of irradiated cells seeded in the plate.

4.2.3.2 Interphase Death

With this mode, irradiated cells die without dividing. Interphase death, therefore, cannot be determined by the

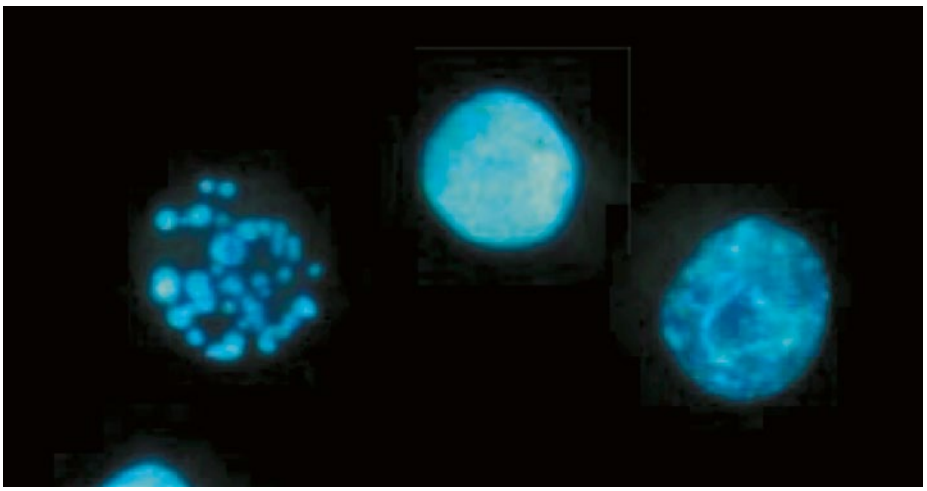

Fig. 4.6 Apoptotic cells. A finely fragmented (*left*), condensed (*middle*), and being fragmented (*right*) DNA

colony formation method. The cells are usually observed by morphological methods such as the dye exclusion method and fluorescence staining. Apoptosis and necrosis are mostly known as active and passive interphase death.

Apoptosis is an interphase death occurring even at very low doses, often observed in lymphoid stem cells. It is an active programmed cell death and a mode to exclude unnecessary cells. Cells with irreparable damage to their genetic information are identified and actively excluded to make spaces into which the surrounding normal cells can proliferate, resulting in maintenance of the entire function they are involved in. Cells undergoing apoptosis become round and are divided into units called "apoptotic vesicles." The nuclei are condensed, with DNA being cleaved into nucleosomes. The fundamental units of chromatin, the material of which eukaryotic chromosomes are made, consisting of cores of histone proteins around which are coiled about 160 bp of DNA. The divided cells are then scavenged by phagocytes such as macrophages, so that spaces for proliferation are created.

Necrosis is often observed in cells exposed to very high doses of radiations where the cells lose their functions, melt or break, and die. Necrosis is observed in nerve, muscle, and other cells, but unlike programmed cell death such as apoptosis, necrosis is not accurately controlled and means the passive death of nonfunctional cells (Fig. 4.6).

4.3 Models for Radiobiological Effects

In many cases, the biological effects of ionizing radiations are determined from the exposure dose. These effects can be expressed as a function of the dose, with the dose-effect relationship shown graphically, which enables these effects to analyze quantitatively. Plotting the rate of surviving cells against the irradiation dose can draw survival curves, and models to analyze these curves have been proposed with which the effects of ionizing radiations can be quantitatively studied.

4.3.1 Target Theory

In order to quantitatively describe the properties of radiobiological effects using survival curves, models to explain the shapes of these curves have been proposed. The target theory is the most classical model. This model assumes "parts of a cell are sensitive to ionizing radiations and regarded as targets for radiations"; "the targets are much smaller than the entire cell, but essential for survival of the cell"; and "when these targets are hit by radiations, the cell can lose its functions to become inactivated (killed)." This is the idea of "all or nothing"; cells can survive, unless they are hit. The linear quadratic model takes the place of this theory now especially in the field of radiotherapy.

4.3.2 Linear Quadratic Model

Although a DNA single-strand break leads to neither chromosomal aberration nor cell death, a DNA double-strand break could cause lethal damage. Taking this into account, in addition to the classical model described above, another model has been devised through analysis based on microscopic dose distributions. Probability of a single event that an electron track originating from one ionizing particle

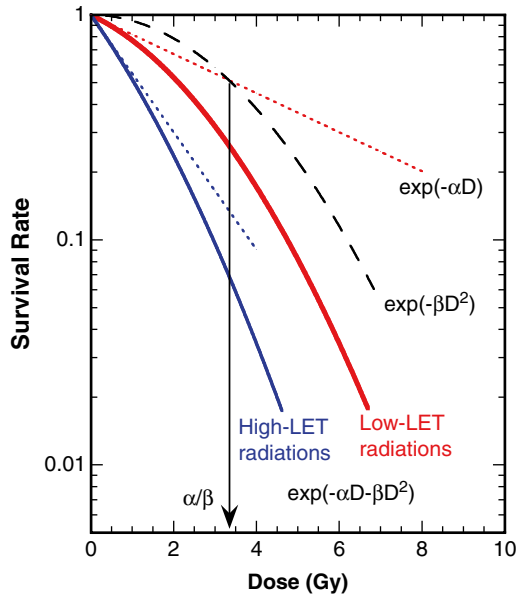

Fig. 4.7 Survival curves and parameters in the linear quadratic model. Overall cell survival curves (*solid lines*) for low- and high-LET radiations are plotted with each component in the LQ equations as the linear components (*dotted lines*) and quadratic components (*broken line*). The dose of the crossing points indicates the α-/β-value. Survival curve for high-LET radiation is drawn under the assumption of 3 times higher α-value with the same β-value to the low-LET radiation

passing near DNA cleaves both strand is proportional to the first-order term of the dose. Although the first ionizing event breaks one strand of DNA but does not lead to inactivation of the cell, the second event cleaves another strand leading to inactivation. The probability of this composite event is proportional to square of the dose. Considering these two causes, the radiation effect on a cell population can be expressed as the survival probability $S = \exp(-\alpha D - \beta D^2)$, where two constants α and β have been introduced. According to this model, the survival curves look like as shown in Fig. 4.7. Although the third and fourth events may also be taken into consideration, they are ignored for simplicity because of their small contribution. This model is called "LQ model (linear quadratic model)." In addition, there are different theories expressed with the same formula: one that a composite event consisting of the first and second radiation doses causes lethal damage and another considering damage due to one event, its repair, and the primary factors. Some theories different from the original have been proposed for interpretation and opinion is divided as to whether they accurately explain the radiobiological effects. Presently, however, the LQ model is often used for analysis of experimental data because of its greater consistency with experimental data, compared with the classical model.

4.4 Modifying Factors of Cell Sensitivity

Radiosensitivities of cells are modified by physical (radiation quality; LET, dose rate, etc.), chemical (oxygen, scavengers, protectors, etc.), and biological (metabolism, cell cycle, repair, etc.) conditions.

4.4.1 Biological Factors

The cell damage caused by ionizing radiations is classified into irreparable damage, or lethal damage (LD), and reparable damage. The reparable damage is divided into sublethal damage (SLD) and potentially lethal damage (PLD). SLD can be repaired within several hours under normal circumstances, but additional SLD before repair is completed leads to LD owing to interaction. PLD is lethal under normal circumstances, depending on the postirradiation condition of cell circumstances. There are two main ways to repair the DNA damage by which damaged DNA segments are resynthesized after being removed. One is SLD repair/recovery (SLDR), which is also known as Elkind recovery; and the other is PLD repair/recovery (PLDR).

4.4.1.1 Sublethal Damage

SLD is considered slight nonlethal damage. When fractionated irradiation is performed, damage caused by the first irradiation becomes lethal owing to the second irradiation. Because of the first irradiation to cells, some cells are lethally damaged so as to die, and others undergo SLDs and survive. Damaged cells with SLD surviving the first irradiation can recover to become exactly like they were as original normal cells with no damage, when they have sufficient time to repair the damage to themselves before the second irradiation. Cells undergoing fractionated irradiation twice with a certain dose show a higher survival rate than those undergoing sequential irradiation with the same dose. A survival curve for the second irradiation after sufficient time has passed is similar to that for the first irradiation from dose zero. When the SLDR occurs, the slope of the lineal part of the survival curve is reproduced universally, and the "shoulder" of the survival curve appears again to various extents depending on the time allowed to pass. Cells undergoing more instances of fractionated irradiation show a higher survival rate, under the condition that the given dose is constant (Fig. 4.8). When high-LET radiation is applied, the cell survival curve will be a straighter line and shows a small shoulder, because repair efficiency is small and shows a larger α-value and a smaller β-value of LQ model. SLDR is also small for high-LET radiations.

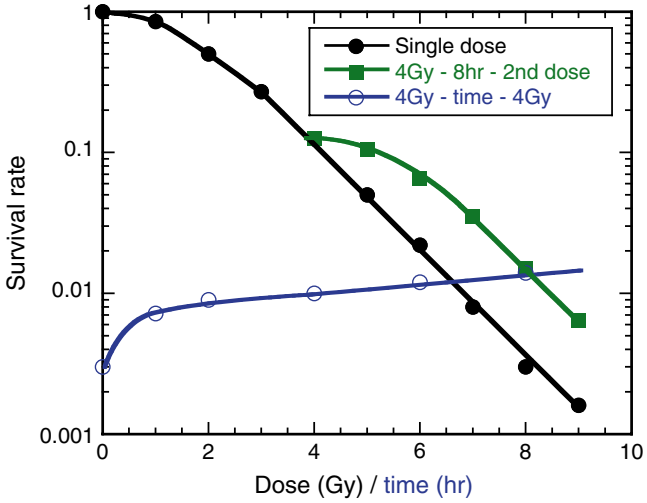

Fig. 4.8 Sublethal damage repair and survival rate. Fresh cells were irradiated with different single doses (*closed circle*), cells irradiated with 2nd challenging doses following 4-Gy priming doses and 6-h incubation (*closed square*), or survival after different interval time between 4-Gy priming dose and 4-Gy challenging dose

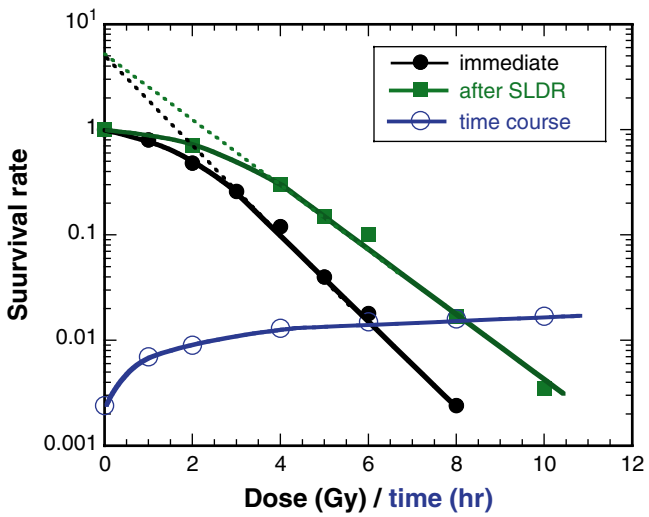

Fig. 4.9 Potentially lethal damage repair and survival rate. Cells were irradiated with different single doses plated immediately after irradiation (*closed circle*) or after 24-h incubation (*closed square*). Cell survival after 8-Gy irradiation and different incubation time (*open circle*)

4.4.1.2 Potentially Lethal Damage

PLD is essentially lethal. Recovery from PLD can be observed in cells placed in special circumstances, though the mechanism for this is little understood. Probably a difference occurs in the survival rate, if sufficient time can be provided for damage repair, with cell growth arrested, or if the conformation of DNA or a cell nucleus can be changed. This recovery can be observed in irradiated cells placed in special circumstances, especially inadequate conditions for cell growth. For example, recovery can be markedly observed in cells that are placed in poor nutritional conditions such as saline rather than in a growth medium containing sufficient nutrition. Recovery can also be observed in a population of steady-state cells that are too crowded to proliferate.

The potentially lethal damage repair/recovery (PLDR) after irradiation can occur with poor nutrition, low pH, and hypoxic conditions that arrest the cell cycle (proliferation) and in an extracellular environment that inhibits cell proliferation. According to the repair time, a fast type (<1 h), a slow type (2–6 h), and a very slow type (>8 h) have been observed. Fixation of PLD where PLD is converted into lethal damages and then the damage type is fixed has also been observed after treatment with an isotonic sodium chloride solution, caffeine, or some anticancer drugs. In these cases the slope of the survival curve changes in regard to the linear part (Fig. 4.9) or decreases the α-value. PLDR becomes smaller as well as SLDR and less prominent for high-LET radiations.

4.4.1.3 Cell Cycle

Tissues are classified into two groups according to their activity for multiplication. One group comprises cells that repeat proliferation vigorously in the proliferative tissue, including the bone marrow, skin, intestinal crypt, and genital gland. The other group comprises nonproliferative tissues including the cranial nerve, bone, muscle, and lung. Importantly, tissues that are proliferating vigorously have high radiosensitivity in general, and cells that are not proliferating have radiation resistance.

Cells are also known to change their radiosensitivity during the cell division process with the cell cycle consisting of G_1 (G_0), S, G_2, and M phases. Cells in the early S and M phases undergo DNA synthesis and cell division, respectively, and radiosensitivity of the cells in these active periods is higher. Cells in the G_1 and G_2 phases are less active and have less sensitivity to X-rays. However, high-LET radiation increases the sensitivity and decreases the variation through the cell cycle (Fig. 4.10). It gives an advantage on high-LET heavy-ion radiotherapy, because there are little resistant cells in target.

4.4.2 Chemical Factors

Among processes through which radiations produce biological effects, the indirect effect causes damage through chemical reactions, including reactions of DNA with active free radicals of water molecules, which accounts for about 2/3 of

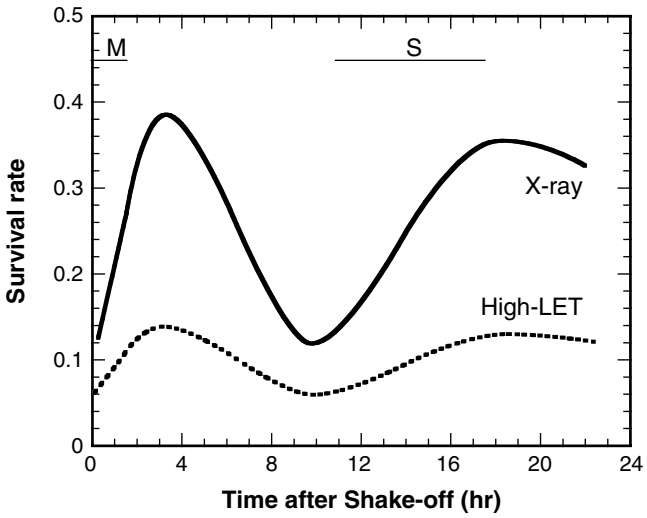

Fig. 4.10 Cell cycle and radiosensitivity. Cells exposed to three X-rays or high-LET radiations after shake-off (synchronization at M phase). M and S with bars correspond to the cell cycle at M phase and S phase after shake-off. Modified and reproduced from [4]

a cell. The radiation effect can be chemically augmented or attenuated by modifying substances participating in the reaction paths. In order to describe the change of radiosensitivity by these chemical substances, the dose reduction factor (DRF, mainly protectors) and the dose-modifying factor (DMF, mainly sensitizers) are used as well as the oxygen enhancement ratio (OER). The OER, DRF, and DMF are expressed as the ratio of isoeffective doses. Usually, a combination of the denominator and numerator of these fractional expressions is determined so that the quotient can exceed one.

$$DRF = D_{(with\ protectors)} / D_{(radiation\ alone)}$$

$$DMF = D_{(radiation\ alone)} / D_{(with\ sensitizers)}$$

$$OER = D_{(under\ hypoxic)} / D_{(under\ oxic)}$$

It is thought that those chemical modifiers are less effective on high-LET radiations. Since serious DNA damages are produced prominently by the direct action of radiation and the complexity of the damages after irradiation of high-LET radiations.

4.4.2.1 Oxygen

Oxygen produces the maximal radiosensitization effect in many parts of the mechanism. The presence of oxygen produces more free radicals to increase its chemical yield in a water solution. However, because the chemical yield is approximately doubled, the fact that the oxygen effect triples the biological effect cannot be explained. Thus, it is necessary to consider the contribution of other factors as well as the chemical yield. In a living body, glutathione with a thiol (SH) group, which participates in oxidation-reduction reactions, contributes to both the protection and oxygen effect for radiations. Some of the damage caused in the early stage of irradiation can be repaired chemically; the reduction reaction of glutathione with some of the free radicals produced by radiations leads to chemical repairs and elimination of the damages. However, the presence of oxygen causes competition between the oxygen and glutathione, resulting in establishing the damages before chemical repairs.

4.4.2.2 Other Chemical Substances

Some chemical substances are known as radiosensitizers or radioprotectors. Radiosensitizers are sensitizing agents of radiation that can be incorporated into cells and mainly augment the radiation effect in radiotherapy are typified by halogenated pyrimidines and hypoxic cell sensitizers. The halogenated pyrimidines are analogues to nucleobases comprising DNA and incorporated into DNA to increase the efficiency of cleavage of the DNA by radiations. Bromodeoxyuridine (BUdR) is incorporated into DNA as a substitute for thymidine, and it was used for BAR therapy for approximately 10 years from 1965; however, BUdR went out of favor because there were no significant differences in the 5-year survival rate between it and radiation therapy, although the short-term survival rate was favorable. Radioprotectors attenuating the radiation effect during irradiation have been known for a long time. Such attenuation is observed during exposure to radiations when drugs with antagonistic activity against subcellular radiation-produced active agents or drugs with repairing activity that brings produced active agents back into its original state are administered. Both types of the drugs are included in the radioprotective agents. Some drugs containing -SH groups and S–S bonds are well known as radical scavengers, including cysteine and cysteamine. In addition to these compounds with SH, serotonin, WR-2721, and AET are representative compounds. Alcohols, glycerins, and other coexisting substances that have high reactivity with free radicals such as·OH and·H can also scavenge and remove the free radicals, competing with oxygen to chemically repair the targeted molecules, attenuating the radiation effect.

4.4.3 Physical Factors

The magnitude of the radiation effect depends on the physical properties of the radiations as well as the radiation quality represented typically as LET, temporal (dose rate) and spatial (irradiation field) distributions of irradiation.

The dose-rate dependence of the radiation effect is known [5]. As the dose rate decreases from 1 Gy/min, radiosensitivity, which is high with high dose rates (acute irradiation,

short interval), reduces, with the survival curve becoming straighter with a decrease in the parameter β of the survival curve. For chronic irradiation of 0.2 Gy/h or less, radiation resistance increases, with the survival curve being straight ($\beta = 0$) and similar to that for fractionated irradiation. This is because the rate at which DNA damage is repaired is sufficiently higher than the rate at which the radiations cause the damage. The effect in much higher dose-rate region is not clear, because many have interest in radiation protection field and the difficulty of radiation sources. Dose rate from a high-LET particle must be extremely high when we consider single particle traversal in a cell. We confirmed the dose-rate effect on cell killing with a carbon ion beam at 70 keV/μm between 0.008 and 10 Gy/min (0.5 and 600 Gy/h) and found no significant change in those survival curves.

The radiosensitivity depends on the dose distribution in a body and becomes higher as the volume dose (g×Gy) increases. As this gets higher, the burden on the whole body becomes much greater, with recovery of the irradiated site being retarded, even though the influence of radiations on the cells in the irradiated site has not changed. If organs at risk (hematopoietic tissue, intestine) are included in the irradiated region, functions of these organs can be impaired so as to kill the individual. The treatment is associated with the idea of volume dose distribution (DVH, dose volume histogram) for treatment planning. As a DVH curve of normal tissue appears at the lower left, the risk is lower.

4.5 Characteristics of High-LET Radiations

4.5.1 Relative Biological Effectiveness: RBE

The biological effect depends on the quality of the delivered radiations. According to the LET, quality of radiation, X-rays, or γ-rays with several keV/μm or less can be classified into low-LET radiations, and particle beams with tens of keV/μm or more are classified into high-LET radiations. The biological effects of high-LET radiations are usually larger than that of low-LET radiations, where the difference between these biological effects is expressed as the relative biological effectiveness (RBE). RBE is described as dose ratio of test and reference radiations having the same biological effect:

$$RBE = D_{reference} / D_{test}$$

The RBE changes little in the low-LET region up to several keV/μm that correspond the LET region for γ-rays or X-rays, starts clear increasing after 10 keV/μm or more, and shows a peak in the LET at 100–200 keV/μm. However, the peak of the RBE depends on the particles accelerated and radiobiological end points. The RBE decreases in much higher-LET region and shows similar values to the low-LET radiations, and it goes to show less effect than one in the region above thousands of keV/μm. This is supposedly due to the fact that as LET increases, the number of particles to give the same absorbed dose decreases and the probability of hit cells also decreases (Fig. 4.11). Huge previous RBE data are summarized [8–10].

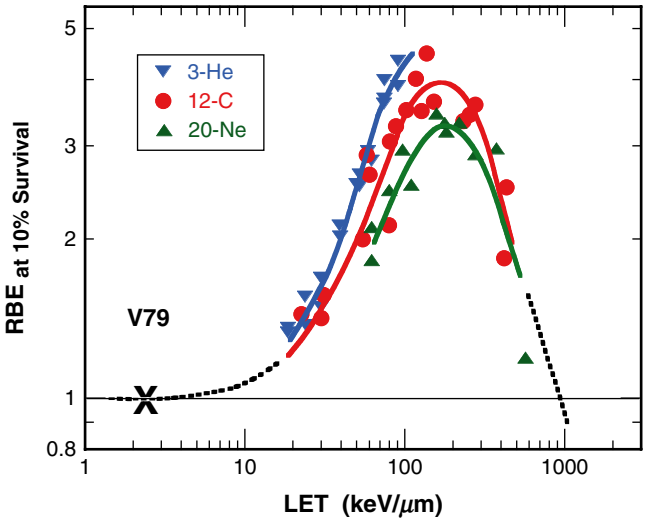

Fig. 4.11 RBE to different LETs for different ion species for cell killing of V79 Chinese hamster cells. Reproduced from [6, 7]

This all depends on cell types and nature of the biological effect observed (cell death, chromosome aberration, DNA strand breaks, mutation, carcinogenesis, and so on) and depends on the types of ionizing particles even though they have the same LET. The reason for this fact has not yet been properly explained. However, because the potential distribution of damage occurring is different owing to the difference in track structure specific to particle beams and geometrical structures of biomolecules in a cell, the types and complexity of this damage may be different. In addition, because this damage may influence the efficiency of biological repair system, geometrical distribution of damages, etc., the final influence may be different. Moreover, the dose-effect relationship of low-LET radiations is usually expressed with a straight line connecting to a quadratic curve with a nonlinear "shoulder" and that of high-LET radiations is expressed with a simple straight line. Considering the definition of RBE, or the ratio of two radiation doses to give the same biological effect, RBE depends on the level of the biological effect when the two radiation doses are compared.

It is recommended to use special X-rays showing a LET of 3 keV/μm and a dose rate of 0.1 Gy/min as a defined reference radiation from the viewpoint of radiation protection. Actually, ^{60}Co γ-rays or generated X-rays by a tube operated with several hundreds kVp are often employed as the reference radiations, since they have widely been used.

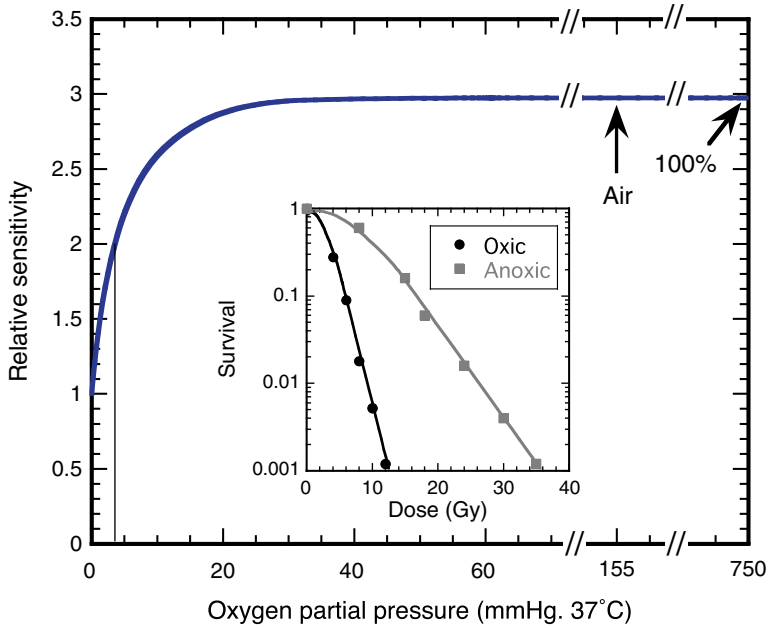

Fig. 4.12 OER for photons to oxygen concentration. Superimposed small figure shows cell survival curve at normoxic and anoxic conditions

In comparison with these X-rays, RBE of γ-rays and high-energy X-rays generated by linacs is clearly small. As radiobiological papers often show no clear definition of the reference radiation, attention should be paid to these facts.

4.5.2 Oxygen Enhancement Ratio: OER

In normal tissue, blood vascular systems are often substantial, with the oxygen partial pressure (pO_2) ranging from 10 to 80 mmHg. In the microenvironments of tumor tissue with blood vessels incompletely constructed, the oxygen concentration is low, and there are often regions with a pressure less than 5 mmHg. The oxygen effect can reduce radiation dose 3 times in normal cells to obtain the same effect (killing) or 2 at a pO_2 of 3 mmHg, for example (Fig. 4.12). Thus, cells at this site survive as radiation therapy-resistant cells, causing a repopulation of cancer cells in the treated site. In order to solve the problem of recurrence in the irradiated region, hypoxic cell sensitizers, which show a similar activity to oxygen and establish damage, were developed. Nitroimidazole agents have been the main ones developed, though at first misonidazole and etanidazole were developed but not put to practical use because tests revealed some adverse side effects. Today, however, to reduce these side effects, study into drug design is being vigorously performed.

In different oxygen conditions, such as normal internal body, compared with oxygen-free conditions, radiations are strong enough to have the same biological effect at an about one-third dose. Relative radiosensitivity under oxygen-rich condition is almost constant for the concentration above 30 mmHg, decreased with decreasing the concentration, and reached to be 1/3 at 0 mmHg. In order to describe the magnitude of the oxygen effect, the OER is used, defined as the ratio of a dose under testing oxygen conditions, D_{hypoxic}, to a dose having the same biological effect under oxygen-rich conditions, D_{normoxic}:

$$OER = D_{hypoxic} / D_{normoxic}$$

This maximum oxygen effect is observed as OER = 3 for low-LET radiations such as γ-rays or X-rays under oxygen-free anoxic condition and causes both a decrease in the sensitivity of intratumoral hypoxic cells and a recurrence of cancer in treated sites. Healthy cells in the normal tissues or cancer tissues having enough blood vessels are rich in oxygen and undergo the ultimate oxygen effect when exposed to radiations.

When high-LET ion beams are delivered, the hypoxic sites in tumors are unlikely to be affected by oxygen, showing similar radiosensitivity; the radiation effect on the hypoxic regions is larger. The OER decreases over tens of keV/μm for carbon beam, reaches to 2 at 100 keV/μm, and further decreases in higher-LET region (Fig. 4.13 also see [11]). We could see the difference in particles at the same LET region, and lighter ion can reduce the OER at lower LET. However, proton beams with an LET of several keV/μm may not be expected to produce this effect, because the LET is too low to reduce the OER. A combination of a high RBE and low OER is expected to have the effect of suppressing the proliferation of cancer cells during cancer treatment.

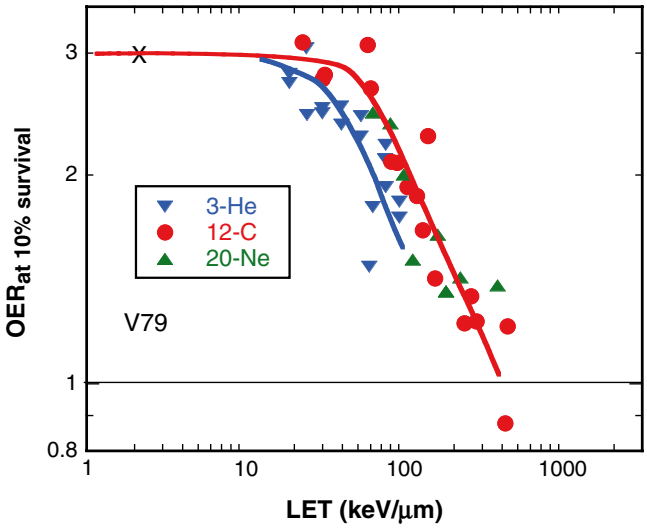

Fig. 4.13 OER to different LETs for different species for cell killing of V79 Chinese hamster cells reproduced from [6, 7]

This oxygen effect may also show a difference among ion spices accelerated. The oxygen effect is believed to cause fixation of radiation damage. The reason for decreasing the oxygen effect to high-LET radiations has different interpretations: oxygen may be produced during the recombination of ionized water molecules because of the extremely high ionization density and the radiation damage may be severe enough and thus established as local compound damage even without oxygen. However, the oxygen effect is not well understood in detail.

4.5.3 Fractionated Irradiation and 4R

Fractionated irradiation is typically performed during radiation treatment since the therapeutic ratio may be improved through various biological effects of the fractionated irradiation. This is known as the "4Rs" which consist of (1) repair, (2) repopulation, (3) redistribution, and (4) reoxygenation. The 4Rs are important issue especially for photon therapy, but they are usually a little for high-LET radiations. Those factors depend on the LET and the LET of therapeutic carbon beams are still smaller to neglect the factors. However, it is more important for carbon ion therapy that normal healthy cells that stay both at shallower part and deeper part from the target area in a patient will receive low dose of low-LET radiation and those cells will escape from radiation damage. Because there are small dose rate and lower LETs at the upper stream of the target and very small dose rate and the lowest LET from fragments behind the target. Only a less repair could be possible in target volume by irradiation with high-dose and high-LET radiation and possibly better repair in normal tissues by the ion beam with lower LET and lower dose at carbon ion radiotherapy (see [12]).

Repair is an important issue in radiotherapy. It is expected that the survival rate for normal cells is a little larger than that for cancer cells in lower irradiation doses, even though these survival rates are the same with higher irradiation doses. Thus, it is expected that this difference will increase logarithmically by SLDR to become large at total treatment dose when fractionated irradiation is performed using a dose range in which the survival rate for normal cells is larger than that for cancer cells. This is a reason why fractionated irradiation is performed during radiation treatment. The difference of survival level between normal and cancer cells at low-dose region is unfortunately not analyzed well for heavy-ion beams yet. A small fractionation treatment is applied in carbon ion therapy and obtains successful results.

Repopulation means new cell proliferation during treatment, which suppresses the entire cell growth inhibitory effect of irradiation. Repopulation is markedly observed in rapidly proliferating cancer cells, the effect of repopulation being small in cells proliferating slowly in the late-response tissue. During the final period of treatment, repopulation is promoted by growth stimulation, which becomes stronger because the number of dying cells has increased. The total dose required for treatment is constant because of non-prominent repopulation, if the total treatment period is not more than 30 days. The total dose that is required for the equivalent biological effect increases because of strong proliferation, if the total treatment period exceeds a certain value. In this point, it is difficult to find an analysis for heavy-ion therapy.

Redistribution means change in cell cycle distribution in tumor population. During irradiation to cells, cells in the highly sensitive periods such as the G2/M phase are likely to be killed, and cells in the resistant periods such as the late S phase of the cell cycle can specifically survive. After a cell suffers damage, a checkpoint at G_2 or other phases temporarily arrests the cell cycle, probably in order that the damage can be repaired. Less sensitive normal cells in the G_0 resting phase enter the cell cycle to become highly sensitive. In a cell population, the general sensitivity depends on the cell cycle distribution.

Reoxygenation is attributed to the decrease of oxygen consumption through the death of the surrounding cells, removal of killed cells, changes in the bloodstream, and other factors. Cells in the hypoxic regions of tumors are radioresistant and very likely to survive the first irradiation. However, if radiations kill the surrounding cells in oxic region or other factors change the microenvironment, the hypoxic regions are oxygenated to become sensitive to the subsequently coming radiation doses. Reoxygenation in different extent and at various times has been observed in almost all tumors. Some studies with high-LET carbon beams showed that the reoxygenation occurs earlier and is also stronger than reoxygenation caused by photon beams.

References

1. Hall EJ, Giaccia AJ. Radiobiology for the radiologist. 7th ed. Philadelphia: Lippincott; 2012.
2. Meesungnoen J, Jay-Gerin JP. Radiation chemistry of liquid water with heavy ions: Monte Carlo simulation studies. In: Hatano H et al., editors. Charged particle and photon interactions with matter. Boca Raton: CRC Press; 2013.
3. Kiefer J. Biological radiation effect. Heidelberg: Springer; 1990.
4. Terashima T, Tolmach LJ. X-ray sensitivity and DNA synthesis in synchronous populations of HeLa cells. Biophys J. 1963;3:11–33.
5. Leenhouts HP, Chadwick KH. The influence of dose rate on the dose-effect relationship. J Radiol Pårot. 1990;10:95–102.
6. Furusawa Y, Fukutsu K, Aoki M, Itsukaichi H, Eguchi-Kasai K, Ohara H, Yatagai F, Kanai T, Ando K. Inactivation of aerobic and hypoxic cells from three different cell lines by accelerated 3He-, 12C- and 20Ne-ion beams. Radiat Res. 2000;154:485–96.
7. Furusawa Y. Corrections: in the article "Inactivation of Aerobic and Hypoxic Cells from Three Different Cell Lines by Accelerated 3He-, 12C- and 20Ne-Ion Beams". Radiat Res. 2012;177:129–31.
8. Ando K, Kase Y. Biological characteristics of carbon-ion therapy. Int J Radiat Biol. 2009;85:715–28.
9. Ando K, Aoki M, Furusawa Y. Annex III; Measurement of RBE of carbon ions for cells, tumor response and tissue reactions in experimental systems. In: Relative biological effectiveness in ion beam therapy, IAEA Technical Report Series 461, Vienna: IAEA; 2008. p. 120–134.
10. Friedrich T, Scholz U, Elsässer T, Durante M, Scoltz M. Systematic analysis of RBE and related quantities using a database of cell survival experiments with ion beam irradiation. J Radiat Res. 2013;54(3):494–514.
11. Wenzl T, Wilkens JJ. Modelling of the oxygen enhancement ratio for ion beam radiation therapy. Phys Med Biol. 2011;56:3251–68.
12. Steel GG. Basic clinical radiobiology. 3rd ed. New York: Oxford University Press; 2002.

Biophysical Models and RBE

5

Naruhiro Matsufuji

Abstract

A primary goal for treatment delivery is to achieve a homogenous effect throughout the target volume. In contrast to conventional photon therapy, this cannot be achieved by applying a uniform distribution of absorbed dose within the target volume due to the drastic change in the biological effectiveness of ion beam as shown in the previous section. In this section, biophysical models used in carbon-ion radiotherapy (C-ion RT) at HIMAC are explained.

Keywords

Linear quadratic model • Microdosimetric kinetic model • RBE

5.1 Usage of RBE in Carbon-Ion Radiotherapy

As introduced in Sect. 5.1, the term relative biological effectiveness (RBE) is defined as a concept in radiobiology as the ratio of absorbed dose required to evoke the same biological effect (endpoint) by two different radiations. If this RBE is introduced in clinical situation, the clinical effect (tumor control) is expected to be the same if the RBE-weighted dose is the same. In case of proton therapy, generic RBE of 1.1 has been recommended [1] irrespective of dose-modifying factors of radiation effects such as fractionation, overall time, and tissue type or radiation quality of the therapeutic beams.

C-ion RT is on the same line with this proton RBE usage. There are little evidences for the comparison on the clinical outcomes between X-ray and C-ion RT due to vast difference in target selection, fraction size, schedule, and so on. In this sense that the clinical RBE has not yet been proven in C-ion RT, however, the term RBE is used in this textbook as a dose modification factor from the viewpoint of consistency in notation between proton and C-ion RT.

N. Matsufuji (✉)
National Institute of Radiological Sciences, 9-1, Anagawa-4, Inage-ku, Chiba 263-8555, Japan
e-mail: matufuji@nirs.go.jp

RBE-weighted absorbed dose, designated by D_{RBE}, represents the product of the ion absorbed dose, D, and the RBE with respect to photons delivered under the same conditions.

$$D_{RBE} = RBE \times D \tag{5.1}$$

where D represents the ion absorbed dose, expressed in gray (Gy). D_{RBE} is the RBE-weighted carbon ion absorbed dose and is the dose of photons that would produce the same therapeutic effect as an ion absorbed dose, D, given under identical circumstances; it is also expressed in gray (Gy). To avoid this confusion the quantity D_{RBE} is expressed in units of Gy, followed by a space and the parenthetical descriptor "(RBE)." The RBE-weighted absorbed dose specification would read "$D_{\mathrm{RBE}} = 70$ Gy (RBE)." This notation will be used throughout the remainder of this textbook. RBE of therapeutic carbon-ion beams can be affected by many factors complexly such as dose level, linear energy transfer (LET), biological endpoint, fractionation, oxygen status, and so on. The role of the biophysical model is to take into account the changeable biological effect appropriately in treatment planning. However, full simulation of the underlying biological processes is not yet feasible the physical properties of the different radiation types can be described in great detail and thus form the basis of different theoretical approaches/models to predict the increased effectiveness of particle beams in experimental and therapeutic situations.

H. Tsujii et al. (eds.), *Carbon-Ion Radiotherapy: Principles, Practices, and Treatment Planning*,
DOI 10.1007/978-4-431-54457-9_5, © Springer Japan 2014

5.2 Biophysical Model in Carbon-Ion Radiotherapy

When starting C-ion RT at HIMAC in 1994, little was known on the clinical effectiveness of ion beams. In order to design the dose distribution under the situation, an experimentally oriented pragmatic approach has been developed [2], referring to the clinical experience with neutron beams and combined with a dose-escalation strategy. Therefore, the estimation of the clinically relevant RBE values is implemented as a two-step procedure in this case, where a "biological RBE" is distinguished from the "clinical RBE."

The first step includes the shaping of the spread-out Bragg peak (SOBP) and thus the ridge filter design. It is based on similar procedures developed for the pioneering study at LBL, but slightly differs with respect to the endpoints chosen as representative for the typical treatments performed at HIMAC, i.e., a human salivary gland (HSG) tumor cell line was selected as in vitro model system because the initial patients to receive carbon-ion radiotherapy were forecasted to have salivary gland tumors, which were known to respond well to fast neutron therapy.

5.2.1 Shaping of the SOBP

Treatment fields for application in tumor therapy are typically characterized by a superposition of Bragg peaks with different energies and even different ion species. The field is characterized by a distribution of LET values. Therefore, it is of particular interest to determine the RBE as a function of depth in such a typical mixed field treatment configuration. In general, dose-averaged LET value, determined by weighting the individual components of the field by their contribution to the total dose, is regarded as an adequate index for the biological effectiveness of mixed fields. Due to fragmentation of the primary carbon ions, a small dose contribution originating from the lighter particles is observed in the beam and more prominent beyond the distal falloff of the dose distribution. Though the RBE values might differ even in the case of similar dose-averaged LET values if different ion species are contaminated, the influence was regarded limited and therefore negligible in this model.

For the HSG cells, cell survival measurements were performed for different monoenergetic beams and mixed beams [3] covering a broad LET range, from which the linear-quadratic coefficients $\alpha(x)$ and $\beta(x)$ as a function of the depth x in a monoenergetic, pristine Bragg peak can be derived according to the LET at the depth x as shown as Eq. (5.2). Based on these values, dose-effect curves for mixed fields composed of k Bragg peaks were calculated from the linear-quadratic coefficients $\alpha_{\mathrm{RM}}(x)$ and $\beta_{\mathrm{RM}}(x)$ at the depth x in a range-modulated Bragg peak by using Eqs. (5.3) and (5.4):

$$S = \exp\{-[\alpha_{RM}(x)d + \beta_{RM}(x)d^2]\} \tag{5.2}$$

$$\alpha_{RM}(x) = \frac{\sum_1^k r_j d(x+s_j)\alpha(x+s_j)}{\sum_1^k r_j d(x+s_j)} \tag{5.3}$$

$$\sqrt{\beta_{RM}(x)} = \frac{\sum_1^k r_j d(x+s_j)\sqrt{\beta(x+s_j)}}{\sum_1^k r_j d(x+s_j)} \tag{5.4}$$

Here, r_j denotes the weight, i.e., the relative fluence contribution, of the jth pristine Bragg peak to the total SOBP, $d(x)$ denotes the dose deposition in depth x of a pristine Bragg peak, and s_j denotes the distance between the position x and the depth of the jth Bragg peak. Using $\alpha_{\mathrm{RM}}(x)$ and $\beta_{\mathrm{RM}}(x)$, survival at depth x can be determined for the given total dose at that depth, and finally the corresponding biological RBE can be determined.

The 10 % surviving fraction level for HSG cells was chosen as the relevant endpoint for biological RBE determination of carbon ions. This allowed the design of a ridge filter required to achieve a homogenous cell killing of HSG cells throughout the extension of the SOBP. The design has been checked experimentally by irradiation of HSG cells with carbon ions at various positions of a 6-cm SOBP. Figure 5.1 shows the biological RBE-weighted dose distribution of 290 MeV/n carbon-ion beams with a 6-cm SOBP [3]. The biological RBE-weighted doses range from 1.6 to 2.1 Gy (RBE) within the SOBP, depending on cell lines and positions. HT1080 cells show slightly higher RBE-weighted doses than HSG cells at proximal positions while the reverse is true at distal positions. In general, however, the biological dose distributions are sufficiently flat. Because they were derived from in vitro cell survival data, the corresponding RBE values were designated "biological RBE."

5.2.2 Determination of Neutron Equivalent Point

In a second step, the link to previous experience with neutron therapy was made. Biological RBE values of neutrons for cultured cells and in vivo systems are experimentally obtainable and can be compared with RBE values of carbon ions. A position in the SOBP was determined which exhibited the same biological RBE as the neutron radiation used for the

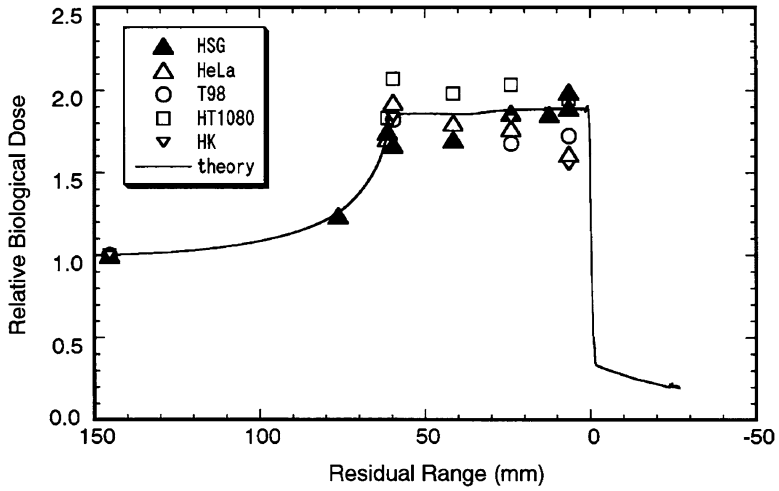

Fig. 5.1 Biological dose distribution of a therapeutic carbon beam. The Bragg peak of a monoenergetic carbon beam of 290 MeV/n was spread out to 6 cm. Image from published paper [3]

clinical trials at NIRS. This position is designated the "neutron equivalent point" in the SOBP. Measurements of the biological RBE for 10 % cell survival of HSG cells revealed that after irradiation within a 6-cm SOBP the RBE increased with an increase of dose-averaged LET of carbon ions and was 2.05 at 85 keV/μm (see Fig. 5.2 [3]). This RBE was identical to the neutron RBE for the same endpoint. Similar measurements were performed for normal tissue effects in an in vivo system, where RBE for the induction of early skin reaction was determined at a scoring level of 2.5 (dry desquamation) as endpoint. Here, the RBE of 3.1—corresponding to the neutron RBE—was achieved at a dose-averaged LET of 75 keV/μm for carbon ions. Combining the results for in vitro and in vivo systems, it was thus decided to use the point with an LET of 80 keV/μm as the neutron equivalent point; this corresponds to a position approximately 8 mm upstream of the distal falloff in case of the 6-cm SOBP with 290 MeV/n beam.

Therefore, it was assumed that the RBE at this position of a carbon-ion SOBP should be the same as that of fast neutrons used for patient therapy. The NIRS experience of fast neutron therapy in the past was thus used to determine the corresponding "clinical RBE" of carbon-ion therapy at one point in the SOBP.

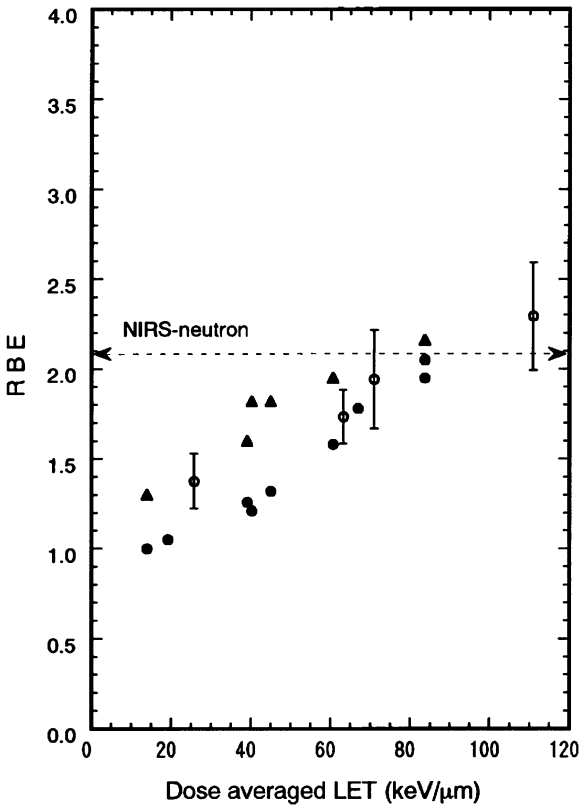

Fig. 5.2 LET dependency of the RBE for colony formation of HSG cells at the 10 % survival level. The data of the RBE were obtained by exposures of a HIMAC carbon beam of 290 MeV/n. The *dashed line* shows the RBE for the NIRS neutron beam for the HSG cells. Image from published paper [3]

5.2.3 Estimation of Clinically Applicable RBE-Weighted Dose Profile

Tsunemoto [4] published clinical results of fast neutron therapy at NIRS. He summarized clinical results after various fractionation schedules for fast neutron therapy. Kutsutani-Nakamura [5] published a treatment planning method of fast neutron therapy and calculated RBE values of fast neutrons for tolerance of acute skin reaction. Based on the formula $\mathrm{RBE}(N) = 1.8 \times N^{0.2}$, he calculated clinical RBE values of neutron vs. number of fraction (N). Depending on the number of fractions the clinical RBE of neutrons increased such that it was 2.5, 2.9, and 3.3 as the number of fractions increased from 5, 10, and 20. Because it was intended to use an 18-fraction scheme over 6 weeks for C-ion RT, which is

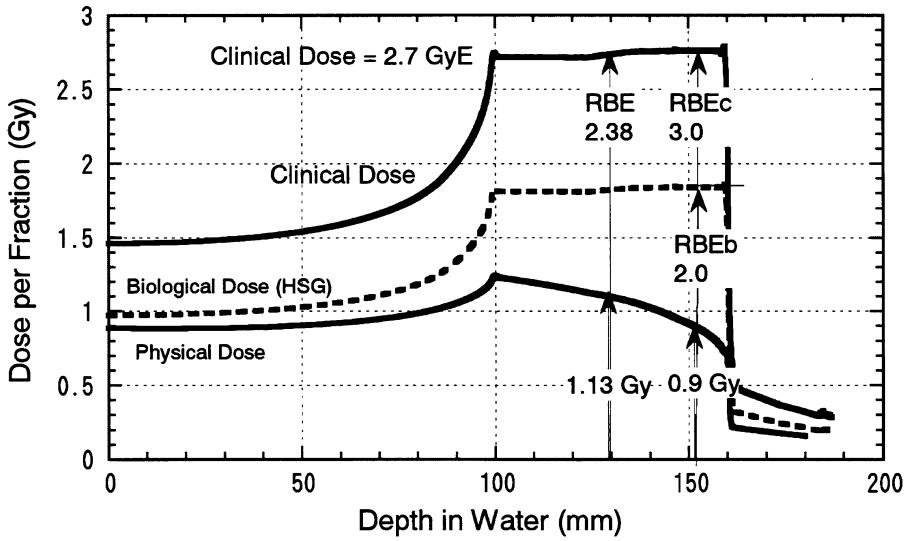

Fig. 5.3 Schematic method used to determine the RBE at the center of the SOBP for the clinical situation. Image from published paper [3]

slightly different from the schemes used for neutron irradiation, a value of 3.0 was selected for the neutron RBE.

In order to move from a biological endpoint to a clinical endpoint it was assumed that a flat RBE-weighted dose distribution for one endpoint can be transformed into a flat RBE-weighted dose distribution of a different endpoint by appropriate scaling with a single value. According to this approximation, the so-called clinical dose distribution can be obtained by scaling the RBE-weighted dose distribution for in vitro cell survival by the conversion factor between the clinically observed RBE values for neutron radiation and the RBE for HSG cell survival at the neutron equivalent point.

In the example given in Fig. 5.3 [3], a clinical RBE-weighted dose of 2.7 Gy (RBE) would be given at any position within the SOBP. According to the assumed neutron RBE of 3, this requires an absorbed dose of 0.9 Gy at the neutron equivalent point 8 mm upstream of the distal end of the carbon SOBP. The biological RBE for 10 % HSG cell survival at this position is 2.0. The assumed RBE for the clinically applicable RBE-weighted dose distribution is then obtained by scaling the RBE-weighted dose profile for the HSG cell survival by a common scaling factor of 3.0/2.0 = 1.5 at each position in the field. The resulting RBE values for any position are then obtained by comparing this scaled profile with the absorbed dose profile; for example, at the middle of SOBP, based on an absorbed dose of 1.13 Gy, an RBE of 2.7/1.13 = 2.4 is estimated.

5.2.4 Validity of the Model

The clinical validation of the underlying RBE model needs to be performed systematically using the clinical data derived from the dose-escalation studies. We present here the tumor control probability (TCP) analysis for non-small cell lung cancer (NSCLC) as an example for the validation of the clinical results in terms of the abovementioned clinical RBE prescription scheme.

Miyamoto et al. [6] analyzed the clinical results of NSCLC treated by HIMAC beams. They depicted a very conspicuous dose dependency of the local control rate. A dose-escalation study was performed with a treatment schedule of 18 fractions in 6 weeks. Hayakawa et al. reported the local control rate for NSCLC using photons. In order to compare the two results, dose dependency of TCP with the photon beam was fitted by the following formula [7]:

$$TCP = \sum \frac{1}{\sqrt{2\pi\sigma}} \exp\left[-\frac{(\alpha_i - \alpha)^2}{2\sigma^2}\right] \cdot TCP(\alpha_i) \qquad (5.5)$$

$$TCP(\alpha_i) = \exp\left\{-N \exp\left[-n\alpha_i d\left(1 + \frac{d}{\alpha_i/\beta}\right) + \frac{0.693(T - T_K)}{T_d}\right]\right\} \qquad (5.6)$$

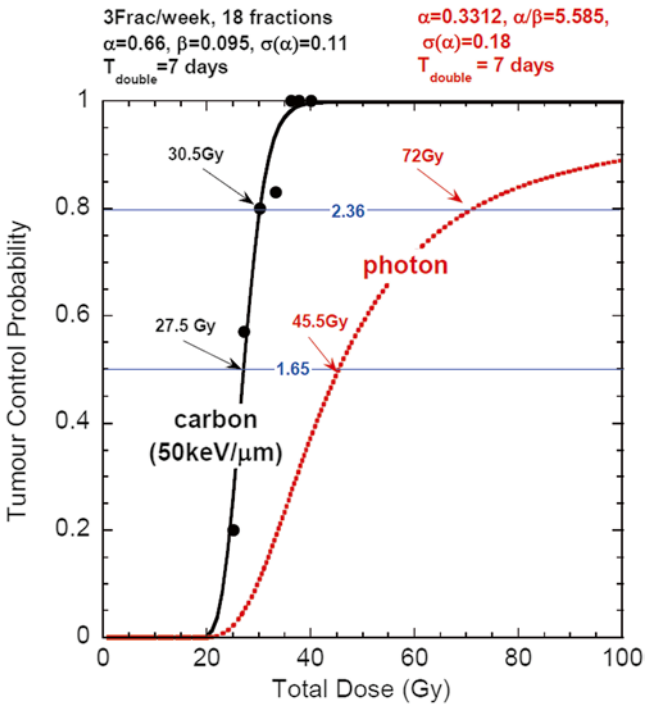

Fig. 5.4 TCP of NSCLC with photon (*dashed*, *red line*) and carbon (*black line*) beams. *Circles* show clinical results at HIMAC. For carbon TCP, the width of SOBP and LET were fixed at 60 mm and 50 keV/μm, respectively. Image from published paper [8]

α and β are coefficients of the linear-quadratic (LQ) model of the cell survival curve. In the analysis, α and β values of HSG cells were used. σ is a standard deviation of the coefficient α, which reflects patient-to-patient variation of radiosensitivity. N is the number of clonogens in tumor (fixed value of 10^9 was used). n and d are total fraction number and the fractionated dose, respectively. T (42 days), T_k (0 day), and T_p (7 days) are overall time for treatment, kick-off time, and average doubling time of tumor cells, respectively. Values used in the analysis are shown in brackets. The result is shown in Fig. 5.4 [8].

The same analysis was carried out to determine the TCP using carbon-ion RT [9]. Here, the width of SOBP and dose-averaged LET in the SOBP region were both fixed at 60 mm and 50 keV/μm, respectively, for simplicity. The result is also shown in Fig. 5.4. It is clear from the figure that the TCP curve of the carbon beam is much steeper than that of the photon beam. The value of σ in Eq. (5.5) was 0.18 for the photon beam, while that for the carbon beam was reduced to 0.11. The result implies that carbon beam provides equally excellent local tumor control regardless of the individual radiosensitivity.

Taking into account the difference between the TCP slopes shown in Fig. 5.4 when TCP is regarded as an end-point, the RBE value is found to be dependent on the TCP level. Furthermore, the biological RBE value coincided with the RBE at 50 % TCP, whereas the clinical RBE value corresponded to that at 80 % TCP [8]. This agreement of the designed clinical RBE at higher TCP level is considered to be justified from the therapeutic point of view.

5.2.5 Characteristics of NIRS RBE

In the clinical trial of hypo-fractionation and dose-escalation studies of ion beam therapy, the number of fractions was decreased and the dose per fraction increased. The biological RBE of the treatment beam increases according to the dose level treated. However at NIRS a constant dose-weighting factor is assumed, independent of dose per fraction. From the definition of RBE, which is biological effectiveness relative to 250 KV X-ray, this is apparently a contradictory usage of the term "RBE." Nevertheless this framework is worth for treatments restricted to the use of ion beams only. Here, RBE in NIRS approach is not the one referring equivalency to photon therapy but the one used to express the weighting factor.

The principle of depth-clinical dose profile used at NIRS can be summarized as Eq. (5.7).

$$D_{CRx}(z) = 1.45 \times \frac{d_x^{HSG}(0.1)}{d_{SOBP}^{HSG}(0.1;z)} \times D(z;SOBP;E) = CRx(z;SOBP;E) \times D(z;SOBP;E) \tag{5.7}$$

$$D_{CRx}(z;SOBP;E) = 1.45 \times \frac{d_x^{HSG}(0.1)}{d_{SOBP}^{HSG}(0.1;center)} \times \frac{d_x^{HSG}(0.1;center)}{d_{SOBP}^{HSG}(0.1;z)} \tag{5.8}$$

where the number 1.45 is the ratio of clinical RBE used in the NIRS neutron therapy and the biological RBE of HSG for the neutron beam. $D(z;$ SOBP,$E)$ is the physical dose of SOBP beam at depth of z for the initial energy of E. $d_x^{HSG}(0.1)$ and $d_{SOBP}^{HSG}(0.1;z)$ are a physical dose of photon and SOBP carbon beam at depth of z which are required to achieve the survival fraction of 10 % for HSG cells, respectively. In the NIRS approximation, the shapes of the physical dose

distribution of the SOBP are assumed to be fixed regardless of the dose level.

$$\frac{d_{SOBP}^{HSG}(0.1;center)}{d_{SOBP}^{HSG}(0.1;z)} \approx \frac{d_{x}^{HSG}(s;center)}{d_{SOBP}^{HSG}(s;z)} \tag{5.9}$$

From the above approximation, RBE is not dependent on the dose level to be treated. The optimized dose of carbon therapy has been clinically obtained through dose-escalation studies of clinical trial of carbon therapy at NIRS.

5.3 Improvement of the Biophysical Model

For a given ion species and cell type, as the first approximation LET or dose-averaged LET is a good predictor for the RBE. However, when comparing different ion species, LET is not flawless in a strict sense to uniquely describe the RBE. This can be attributed to the fact that LET is a simplified one-dimensional representation of the particle track, which does not take into account the three-dimensional distribution of energy deposition around the particle trajectory. Since for a given LET value the corresponding energy is lower for a light particle as compared to a heavier particle, the track radius is smaller for the lighter particle because of the lower energy transferred to the secondary electrons. As a consequence, the average energy density is higher in the track of the light particle, finally leading to the higher effectiveness. This problem made it necessary in the original model to tabulate α and β parameters in the LQ model as functions of ion species and energy. Pragmatically this works fairly well in most conditions; however, it is inevitable to introduce a kind of assumption or interpolation at a condition out of the table. Eventually it could not only introduce a possible error in the estimation of therapeutic effectiveness of carbon ions, but also it makes it difficult to make a prospective, reliable, or mechanistic estimation of the beam. In order to account for that, upon the accumulated knowledge in the first decade, we aimed at updating the biophysical model in more mechanistic approach for the biological effect of ion beams which leads to thorough understanding of the clinical effectiveness of the ion beams designed with the original pragmatic approach.

Methods based on microdosimetric characterization of the radiation field focus on a detailed description of the stochastic energy deposition distributions. Experimental microdosimetry is based on measurements or calculation of energy deposition events typically in spherical volumes of simulated micrometer dimensions. Microdosimetric kinetic model (MKM) has been developed by Hawkins [10] as a model to predict biological effectiveness of radiations based on the microscopic spatial energy distribution. MKM realizes prospective estimation of biological effectiveness of various ion species based on their physical properties. This is expected to provide more precise estimation of the biological effectiveness of the therapeutic carbon beam; therefore, MKM has been introduced as the updated biophysical model implemented in the new treatment planning system for scanning irradiation.

MKM extended the microdosimetric concept of the theory of dual radiation action (TDRA) [11], which gives estimation of biological effect based on the energy deposited in a site in the order of micrometer. In TDRA, the number of lesion L is proportional to the square of the specific energy z given in the site while MKM incorporates additional component in lesion formation which is linearly proportional to the specific energy as

$$L = Az + Bz^2 \tag{5.10}$$

The units for y are the same as for the LET, namely keV/μm. Similar to the LET, also for the lineal energy, the dose-weighted average value y_D is expected to be representative for the biological effectiveness:

$$-\ln S = N\bar{L} = N\left(A\bar{z} + B\bar{z}\right)^2 = (\alpha_0 + \beta \cdot z_{1D}) + \beta D^2 \tag{5.11}$$

where α_0 denotes the initial slope of the survival curve in the limit LET $\to 0$ and β is assumed to be independent on radiation quality. Since z_{1D} rises with LET, Eq. (5.9) would lead to a steady increase of RBE with LET. However, RBE is known to decrease with LET after reaching a maximum at approximately 100 keV/μm. Therefore, saturation correction on specific energy was introduced [12].

$$z_{1D}{}^{*} = \frac{l}{m} y_0^2 \cdot \frac{\int\left[1 - \exp\left(-y^2/y_0^2\right)\right] f(y)\,dy}{\int y f(y)\,dy} \tag{5.12}$$

By replacing z_{1D} in Eq. (5.9) with z_{1D}*, the modified MKM is shown to allow a good representation of the experimental data. Figure 5.5 [12] shows the experimental α value of HSG cells for various incident beams as a function of its saturation-corrected lineal energy. As demonstrated in the figure, this saturation-corrected modified MKM is useful in estimating the biological effectiveness of various ion species. The modified MKM has been installed in the treatment planning both for scanning irradiation [13] and broad-beam irradiation.

Figure 5.6 shows the cell survival distribution of HSG cells for the beam of C-290 MeV/n with 60 mm SOBP. As shown in the figure, MKM can predict the HSG cell response in excellent precision. Figure 5.7 shows the comparison of depth-biological dose profile for the beam in Fig. 5.6 with the original model (labeled as KANAI1999 in the figure) and MKM. Both models agreed to each other in general. This proves that the original approach is

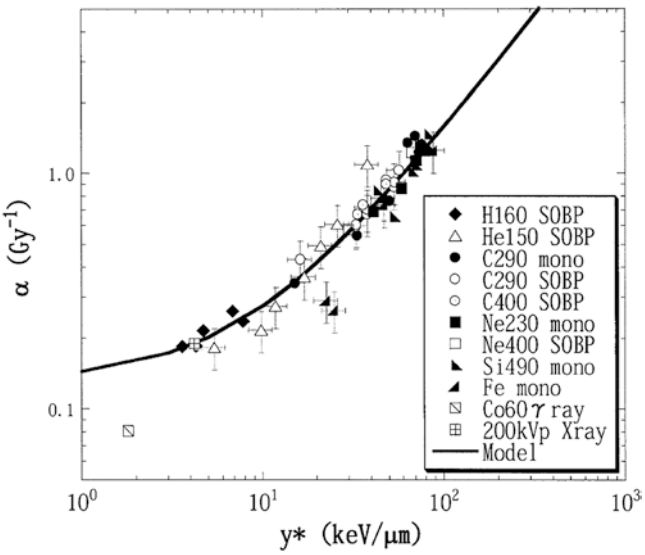

Fig. 5.5 Experimental α value with $\beta = 0.05$ Gy^{-2} fixed for HSG cells as a function of the saturation-corrected dose mean lineal energy, y^*. The values of y^* were measured by the TEPC with a simulated diameter of 1.0 μm and with a saturation parameter of $y_0 = 150$ keV/μm. The solid line indicates the curve calculated using saturation-corrected modified MKM. Image from published paper [12]

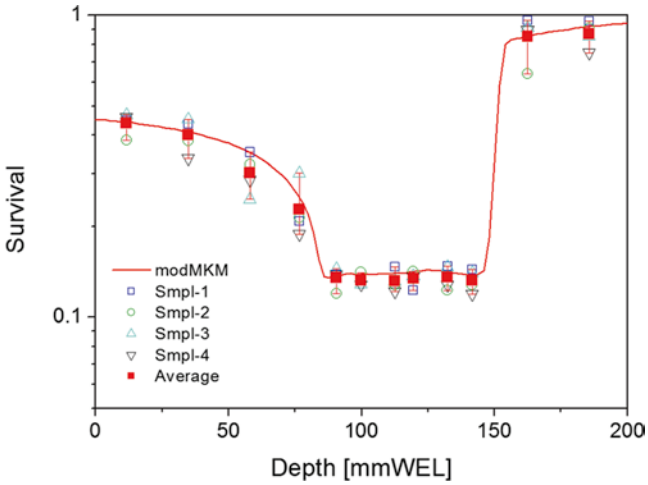

Fig. 5.6 Cell survival distribution of HSG cells for the beam of C-290 MeV/n with 60 mm SOBP. The beam is delivered by scanning method at HIMAC. Line in the figure shows the estimation of MKM

pragmatically adequate enough for the therapeutic purpose. Slight difference found at the distal part of the SOBP can be attributed to the improved estimation of the MKM on the biological effect of the beam where the fragment particles are relatively abundant.

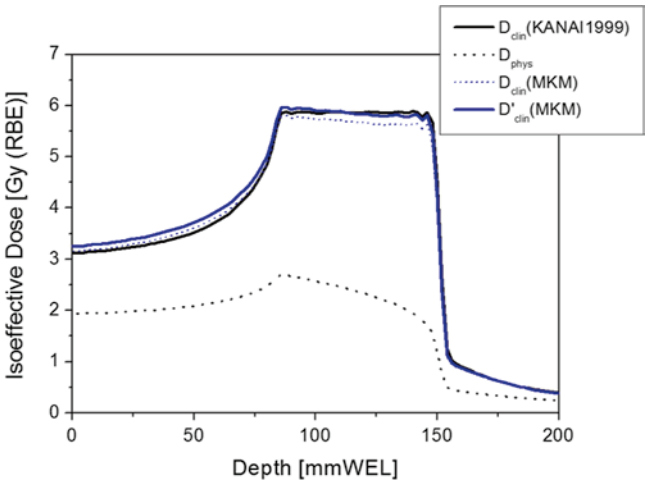

Fig. 5.7 Depth-biological dose profile corresponding to Fig. 5.6

References

1. International Commission on Radiation Units & Measurements. Prescribing, recording, and reporting proton-beam therapy (ICRU Report 78). Maryland: Bethesda; 2009.
2. Kanai T, Endo M, Minohara S, et al. Biophysical characteristics of HIMAC clinical irradiation system for heavy-ion radiation therapy. Int J Radiat Oncol. 1999;44:201–10.
3. Kanai T, Furusawa T, Fukutsu K, et al. Irradiation of mixed beam and design of spread-out Bragg peak for heavy-ion radiotherapy. Radiat Res. 1997;147:78–85.
4. Tsunemoto H. Clinical evaluation of fast neutron therapy. Nippon Igaku Hoshasen Gakkai Zasshi. 1982;42:823–47.
5. Kutsutani-Nakamura Y. Treatment planning method in the use of the TDF biological equivalent concept in fast neutron therapy. Nippon Igaku Hoshasen Gakkai Zasshi. 1978;38:950–60.
6. Miyamoto T, Yamamoto N, Nishimura H, et al. Carbon ion radiotherapy for stage I non-small cell lung cancer. Radiother Oncol. 2003;66:127–40.
7. Webb S, Nahum AE. A model for calculating tumour control probability in radiotherapy including the effects of inhomogeneous distributions of dose and clonogenic cell density. Phys Med Biol. 1993;38:653–66.
8. Matsufuji N, Kanai T, Kanematsu N, et al. Specification of carbon ion dose at the National Institute of Radiological Sciences (NIRS). J Radiat Res. 2007;48:A81–6.
9. Kanai T, Matsufuji N, Miyamoto T, et al. Examination of GyE system for HIMAC carbon therapy. Int J Radiat Oncol. 2006;64:650–6.
10. Hawkins RB. A statistical theory of cell killing by radiation of varying linear energy transfer. Radiat Res. 1994;140:346–67.
11. Kellerer AM, Rossi HH. A generalized formation of dual radiation action. Radiat Res. 1978;75:471–88.
12. Kase Y, Kanai T, Matsumoto M, et al. Microdosimetric measurements and estimation of human cell survival for heavy-ion beams. Radiat Res. 2006;166:629–38.
13. Inaniwa T, Furukawa T, Kase Y, Matsufuji N, Toshito T, Matsumoto Y, Furusawa Y, Noda K. Treatment planning for a scanned carbon beam with a modified microdosimetric kinetic model. Phys Med Biol. 2010;55:6721–37.

Part IV

Carbon-Ion Radiotherapy System

Workflow of Carbon-Ion Radiotherapy

6

Toshiyuki Shirai and Yuka Takei

Abstract

The carbon-ion radiotherapy system consists of oncology information system (OIS), radiotherapy treatment planning system (RTPS), and beam delivery system (BDS), which is similar to the standard radiotherapy system. However, there are some differences, such as a big accelerator system, no gantry system (except HIT), and an efficient workflow system. The outline of the carbon-ion radiotherapy (C-ion RT) system and the workflow system is introduced.

Keywords

OIS • Schedule • Workflow

6.1 Overview of Carbon-Ion Radiotherapy System

Particle therapy using carbon-ion beams is a desirable cancer therapy method due to the high-dose localization and the high biological effect around the Bragg peak. On the other hand, the system of C-ion RT is expensive and the number of the facility is very limited. Therefore, the efficient system is required. In HIMAC, there are two treatment facilities: one is inside the HIMAC building (room A/B/C) and the other is in the new treatment facility (room E/F/G) (see Fig. 6.1). The former has a broad beam irradiation system and the latter has a scanning irradiation system. There are three treatment rooms and one or two CT-simulation rooms in each facility. In the new facility, there are six preparation rooms for patients (two preparation rooms per one treatment room) to shorten the occupation time of the treatment room (see Fig. 6.2).

One important feature of the carbon-ion radiotherapy is an absence of the rotating gantry. The treatment room has a fixed horizontal and vertical irradiation ports. The port layouts of the HIMAC are the following:

Room A: Vertical port

Room B: Horizontal and vertical ports

Room C: Horizontal port

The construction cost of the irradiation ports and the beam line can be reduced by the nonidentical irradiation port layout. But the patients are treated in the different rooms day by day. The capable scheduling system is necessary to make best use of the nonidentical rooms.

Recently, the rotating gantry for carbon-ion radiotherapy has been developed in Heidelberg University (HIT) and NIRS. The world's first carbon-ion gantry was designed and constructed at HIT (total weight of over 600 t). The clinical operation of the gantry was started in 2012. A lightweight rotating gantry using superconducting magnets (~3T) has been constructed at the new treatment facility (room G) in NIRS (see Fig. 6.3). The adoption of the gantry will be an important point for the future carbon-ion radiotherapy facility.

The carbon-ion radiotherapy system supports the workflow not only accurately but also efficiently. It consists of a radiotherapy treatment planning system (RTPS), a patient handling system (PTH), a beam delivery system (BDS), a quality assurance (QA) system, and an oncology information system (OIS) in Fig. 6.4. The PTH covers a wide range of

T. Shirai (✉) • Y. Takei
National Institute of Radiological Sciences
9-1, Anagawa-4, Inage-ku, Chiba 263-8555, Japan
e-mail: t_shirai@nirs.go.jp; yukakoba@nirs.go.jp

H. Tsujii et al. (eds.), *Carbon-Ion Radiotherapy: Principles, Practices, and Treatment Planning*,
DOI 10.1007/978-4-431-54457-9_6, © Springer Japan 2014

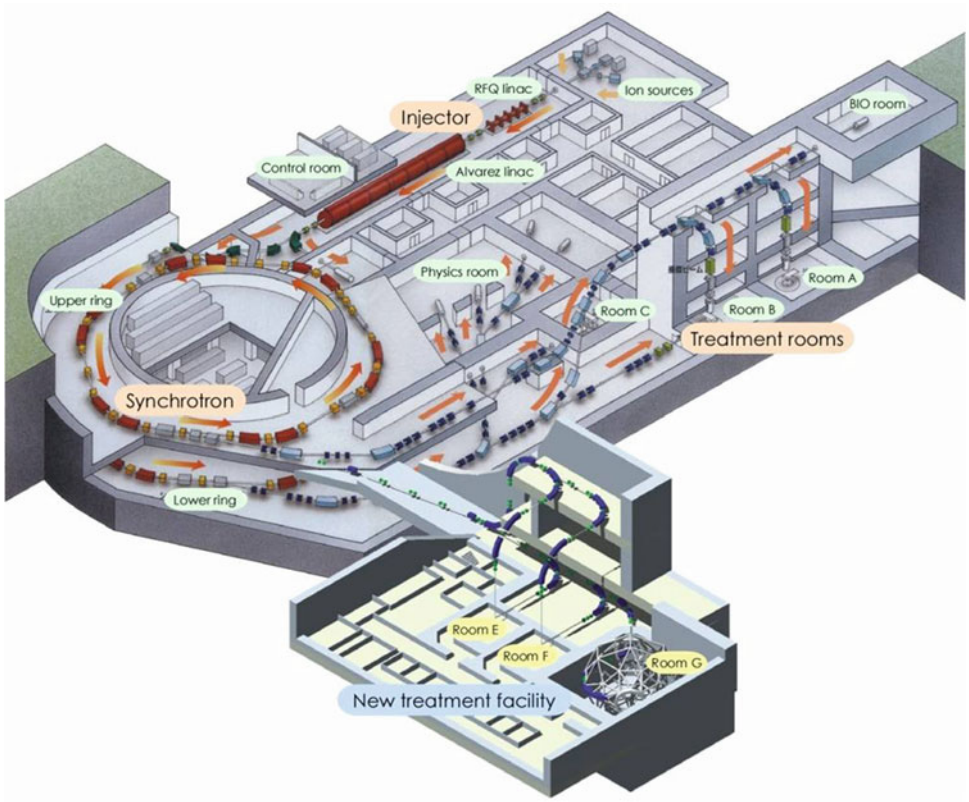

Fig. 6.1 Bird's-eye view of the HIMAC

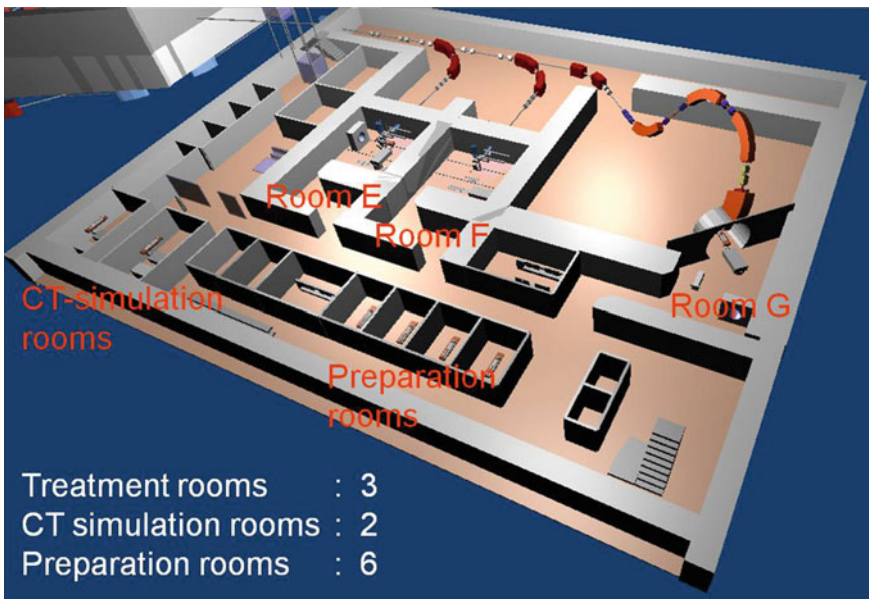

Fig. 6.2 Layout of the treatment floor in the new facility

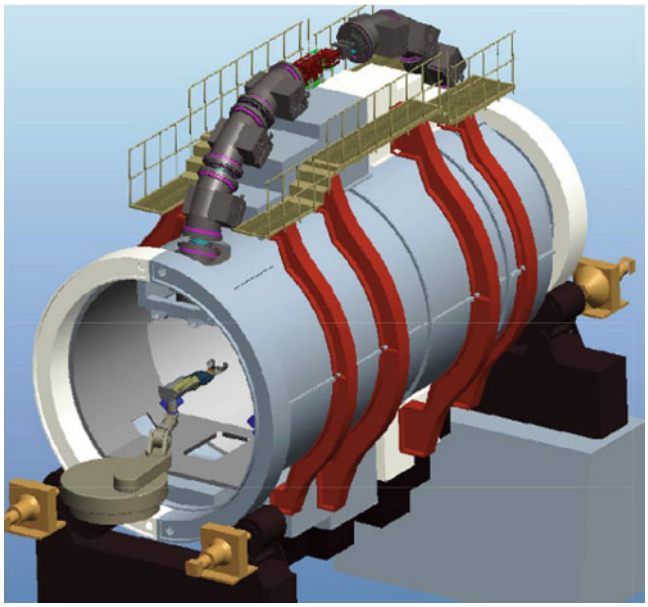

Fig. 6.3 Bird's-eye view of the rotating gantry for carbon-ion radiotherapy using superconducting magnets at HIMAC

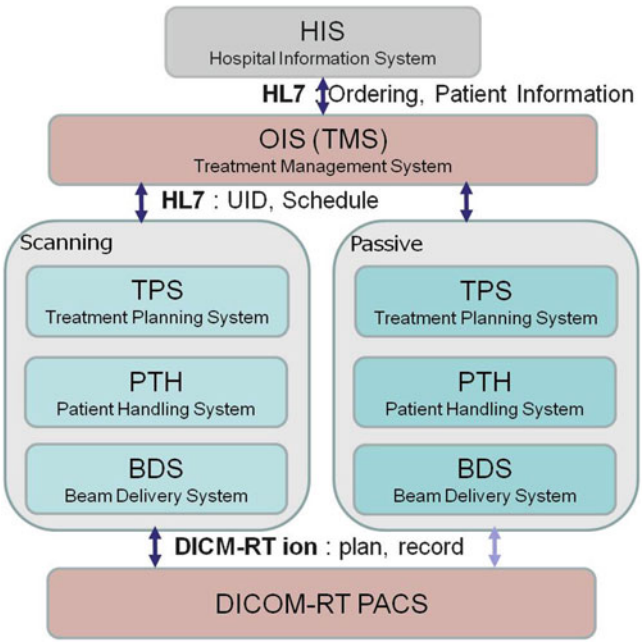

Fig. 6.4 The block diagram of the carbon-ion radiotherapy system in HIMAC

patient data management, and the treatment scheduling functions. Especially the scheduling system is important to enhance the efficiency of the facility. The OIS also transfers the patient and order information from the hospital information system (HIS) to subsystems. The patient data for the treatment is stored in the database. The database of digital imaging and communications in medicine—ion radiation therapy (DICOM RT ion)—is used as a multi-vendor one at HIMAC. The industry standards, such as Health Level 7 (HL7), are also used as a message format between subsystems

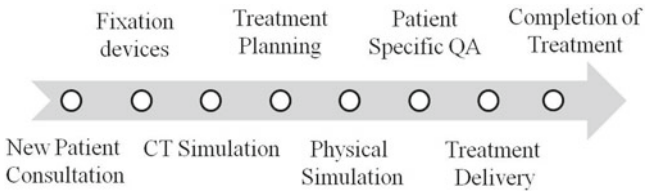

Fig. 6.5 Workflow of the carbon-ion radiotherapy

6.2 Workflow of Carbon-Ion Radiotherapy

Figure 6.5 shows the typical workflow of the carbon-ion radiotherapy at HIMAC. Because of the lack of the gantry, the treatment table is rolled for substantive multifield irradiation. Therefore, the preparation of the fixation devices is an important process and the rolling angle is decided at this time. In many cases, there are multiple setup positions and rolling angles for one patient. The fixation devices and the treatment planning CT are required for each setup. The physical simulation is performed in the simulation room to reduce the occupation time of the treatment room, especially for patients with large rolling angle of the bed. Digitally reconstructed radiography (DRR) images are replaced by flat panel display (FPD) images in the physical simulations. When the physical simulation is omitted, DRR images are used in the treatment. The patient-specific QA is optional at HIMAC. It is carried out for the selected treatment plan in the passive delivery system and all plans for the scanning delivery system at this moment.

6.3 Scheduling of Carbon-Ion Radiotherapy

The patient number at HIMAC is close to 1,000 per year and the efficient scheduling method has been developed for years because of the limited number of the medical staff. There are three steps in the scheduling process at HIMAC, a patient scheduling, a beam scheduling, and a treatment room scheduling. The OIS scheduling system at HIMAC supports all three steps of the scheduling.

The patient scheduling uses the idea of "treatment frame." The treatment frame is a set of the schedule for one patient such as a preparation of the fixation device, a CT simulation, and irradiations (see Fig. 6.6). The treatment

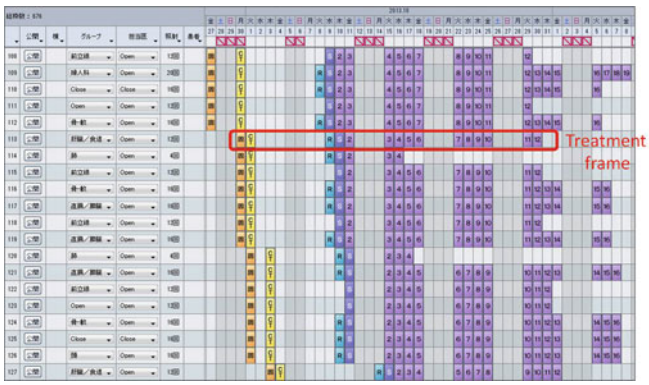

Fig. 6.6 OIS screenshot of the treatment frame table

Fig. 6.8 OIS screenshot of the treatment room schedule

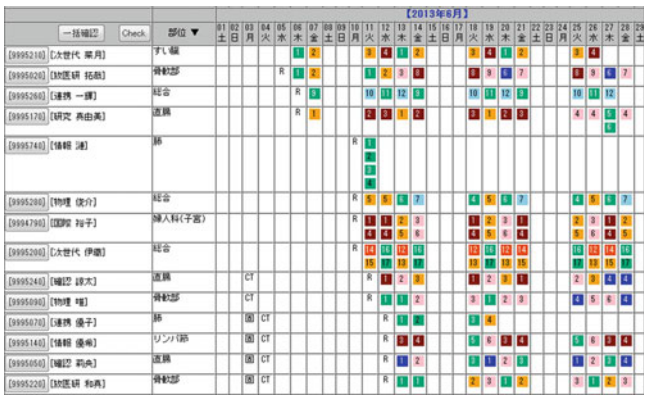

Fig. 6.7 OIS screenshot of the beam schedule

frame is created regularly (e.g., every half year) according to the predicted patient number and the capacity of the facility. Figure 6.6 shows an example of the screenshot of the OIS. The schedule of the new patient is fixed by the assignment to the treatment frame and at the same time, the ordering of the CT and the irradiation is completed. Using the idea of the treatment frame, the number of the patient in the treatment workflow can be equalized.

The second step of the schedule is a beam scheduling. Figure 6.7 shows the screen of the beam schedule for patients. The fraction scheme is determined by the treatment planning process, but when the imbalance for the irradiation system is too large, the beam schedule can be changed by OIS scheduling system within the acceptable range.

The third step of the scheduling is the treatment room scheduling. Figure 6.8 shows the screen of the treatment room schedule for room A/B/C in 1 day. According to the beam scheduling, the treatment room schedule is determined automatically by OIS scheduling system in order to equalize the patient number among three rooms. The medical staffs can also change not only the patient order in the room but also the room of the patient, if the beam port is compatible between treatment rooms. The compatibility of the irradiation port is an important feature in the nonidentical treatment room design.

Beam-Delivery Systems

7

Shigekazu Fukuda, Takuji Furukawa, and Yoshiyuki Iwata

Abstract

A particle therapy facility consists of three main equipment components: an accelerator, a beam transport system, and a treatment delivery system. In the beam-delivery system the narrow beam from the accelerator is tailored to suit the lesion being treated. The requirements of beam depend on details of the beam-delivery system used. Both passive and active beam-delivery systems are employed to deliver the required dose to the target. In this chapter, both delivery system and the accelerator for heavy ions are introduced.

Keywords

Beam delivery • Dose conformation

7.1 Passive Delivery System

7.1.1 Basic Principles of Passive Delivery

A high-energy beam accelerated by an accelerator is delivered through a beam transport system to a treatment delivery system. The narrow pristine beam extracted from the accelerator, and sometimes called a "pencil beam," is not suitable for use in treatment except for the beam-scanning method. The passive irradiation system expands "the pencil beam" and tailors the expanded beam to meet clinical requirements of a higher-dose delivery in a target tumor within a patient with lower-dose irradiation to normal tissue. This method is called "passive beam delivery," sometimes classified as "broad-beam method." We describe the details of the passive beam delivery with the beam-delivery systems of HIMAC.

S. Fukuda (✉) • T. Furukawa • Y. Iwata
National Institute of Radiological Sciences, 9-1, Anagawa-4, Inage-ku, Chiba 263-8555, Japan
e-mail: sfukuda@nirs.go.jp; t_furu@nirs.go.jp; iwata@nirs.go.jp

7.1.2 Passive Beam-Delivery Systems of HIMAC

HIMAC has three treatment rooms which have the passive beam-delivery systems. Treatment rooms A, B, and C are equipped with vertical, vertical and horizontal, and horizontal beam courses, respectively. Figure 7.1 shows the beam-delivery systems of treatment room B of the HIMAC [1, 2]. Both beam ports have the almost same structure, but the horizontal beam course is slightly longer than the vertical one. Beam transport lines deliver the pencil beam and focus the beam on the isocenter without momentum dispersion.

The method mainly used to widening the pencil carbon beam uniformly in the lateral direction is a wobbler-scattering method. The wobbler-scatterer method generates a uniform irradiation field using a combination of a wobbler magnet system and a scatterer system. The wobbler magnet system is a pair of bending magnets which are installed so that the directions of their magnetic fields are mutually orthogonal. By applying alternating currents to the two magnets which are out of phase with each other by 90°, the pencil beam delivered from the accelerator is rotated in a circular pattern as shown in Fig. 7.2b. The radius of the circle can be changed by varying the effective current supplied to the wobbler magnet system. The wobbler magnets of HIMAC beam-delivery systems are located 11.7 m upstream from the isocenter of

H. Tsujii et al. (eds.), *Carbon-Ion Radiotherapy: Principles, Practices, and Treatment Planning*,
DOI 10.1007/978-4-431-54457-9_7, © Springer Japan 2014

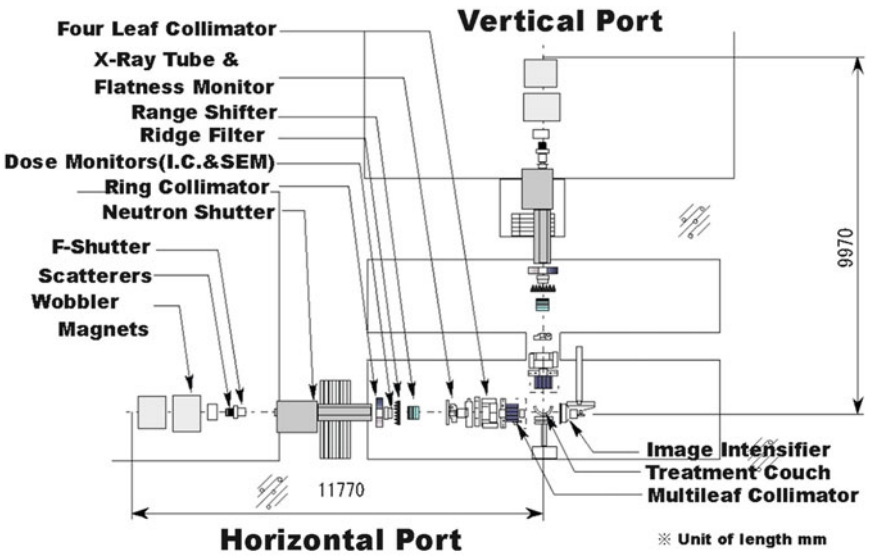

Fig. 7.1 Beam-delivery systems of treatment room B of HIMAC. The horizontal beam port and vertical beam port which have a common isocenter are shown. Both beam ports have the same configuration

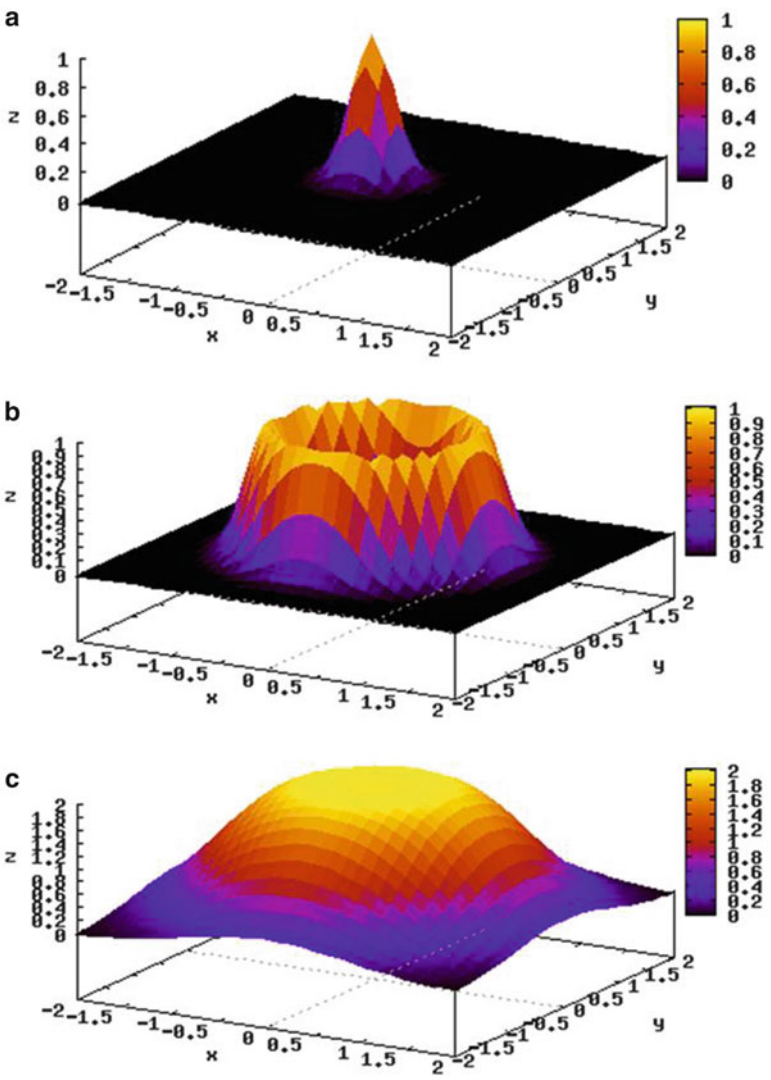

Fig. 7.2 Uniform broad beam generated by the wobbler-scattering method. (**a**) A pencil beam delivered from an accelerator source, (**b**) a beam rotated by wobbler magnets, and (**c**) a beam broadened by a scattering system placed downstream from the wobbler magnet system

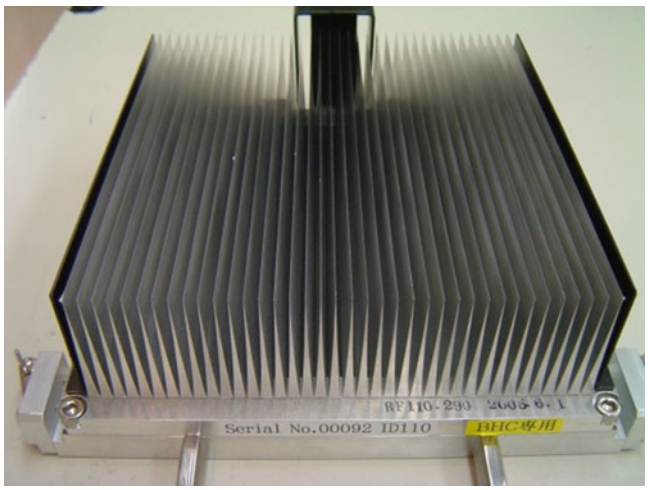

Fig. 7.3 Ridge filter

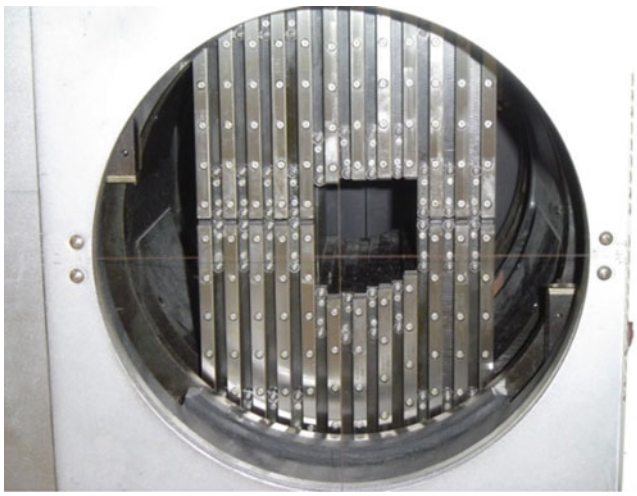

Fig. 7.4 Multi-leaf collimator (MLC)

the horizontal beam course and 9.9 m from the isocenter of the vertical beam course. Each magnet has an effective magnetic length of 660.1 mm and its pole gap is 110 mm. Both magnets can be excited at 1,200 A at the maximum.

The annular beam is broadened by the scatterer system placed downstream from the wobbler magnet system (Fig. 7.2c). As the scatter system, a binary scatter system is often used. It has several scatterer boards and each differs in thickness from the neighbor board by a factor of two. The total thickness can be changed by selecting a binary combination of scatterer boards. The scatterer system of HIMAC contains seven metal sheets, each of which is plunged into the beam course by an actuator.

By tuning the currents to the wobbler magnets and the thickness of the scatterer it is relatively easy to make different uniform irradiation fields with different sizes. The irradiation field made by the wobbler-scatterer method is not susceptible to the variation in the beam position at the entrance of the irradiation system. Meanwhile, it has a periodic time structure corresponding to the frequency of the alternating current.

Uniform broadening of a beam in the depth direction corresponds to producing a spread-out Bragg peak (SOBP). An SOBP is formed by superposing many monoenergetic Bragg peaks. In other words, the SOBP is made to respond to the energy modulation of a monoenergetic beam. There are two main ways of modulating the beam energy and superimposing Bragg peaks: one uses a ridge filter device and the other a rotating range modulator. The ridge filter device is used for the beam-delivery system using the wobbler-scatterer method.

The ridge filter device is composed of many uniform bar-ridges, manufactured with highly precise processing technology, which are set parallel to each other on one plane as shown in Fig. 7.3. Ridge filter devices, corresponding to different SOBP widths, are often prepared for a high-energy beam and a low-energy beam. Since the cross-sectional shape for the bar-ridge determines the change of thickness, appropriate design of the bar-ridge allows delivery of a homogeneous biological dose to the target region. In the case of a carbon beam, the SOBP is composed of a range of LET components with different weighting factors at each depth. The survival rate under a mixed LET radiation field was experimentally proved to be described by a formalism proposed in the theory of dual radiation action on the basis of the linear-quadratic (LQ) model [3].

After broadening of a beam in the lateral and depth directions, the beam is cut to the shape of the target tumor projected in the beam's eye view. A patient collimator, a multi-leaf collimator (MLC) device or their combination is used for the two-dimensional cutting of a uniform beam. The patient collimator is a block that has a tumor projection-shaped aperture. The block is thicker than the maximum range of the beam and is often made of brass, which is easy to cut by a wire-electrical discharge machine. Although the patient collimator needs to be manufactured for each irradiation direction, it reduces blurring of the lateral dose distribution because the patient collimator can be placed near the body surface of the patient.

The MLC is a device that has many pairs of thin leaves. These leaves are shifted to suitable positions to make a tumor projection-shaped aperture. Use of an MLC device has the advantages of increased speed and reduced costs for treatment preparation because no individual patient collimators need to be manufactured. In some situations the MLC device cannot be moved close to the body surface of a patient due to its size and blurring of the lateral dose; then distribution is not necessarily small.

Figure 7.4 shows the MLC used at the horizontal beam port of HIMAC beam-delivery systems. The MLC consists of 23 pairs of 6.5 mm thick iron plates with 0.25 mm spacing. The leaf with thickness of 140 mm in the beam direction

Fig. 7.5 Manufacture of patient compensators by machining center

has a tongue-and-groove structure except the central leaf to reduce the interleaf dose-leakage. The central leaf has the tongue structure on both sides. The leaf moves at a maximum speed of 80 mm/s and stops at a position with less than ±0.5 mm precision.

The final step in the broad-beam method is the adjustment and conformation to the target in the depth direction using a range shifter (RSF) device and a patient compensator (bolus).

The RSF is composed of several energy absorbers having different thicknesses and the total thickness of the system can be changed by selecting suitable absorbers. The RSF of HIMAC systems consists of ten polymethyl methacrylate (PMMA) plates of various thicknesses. Combinations of plates result in thicknesses from 0.25 to 255.75 mm in a binary manner.

A patient compensator is a block that has an engraved depression in the shape of the depth direction of the target tumor volume. The block is often made of high-density polyethylene which is easy to engrave and is a low-atomic-number material for reduced scattering of the beam. Patient compensators, like patient collimators, also need to be manufactured for each irradiation direction. Figure 7.5 shows the manufacture of patient compensators by a machining center.

The dose control of irradiation with the passive beam method is performed by each individual irradiation. As well as a conventional X-ray irradiation system, the treatment delivery system with carbon beams requires two independent monitor systems to ensure safe and reliable irradiation.

Each treatment delivery system of HIMAC has two identical parallel-plate ionization chambers (IC; aperture diameter about 20 cm). They are filled with atmospheric air and operated by applying +2,000 V. Each IC consists of three cathodes and two anodes that are staggered with the gap of 5 mm. There used to be other monitors, an ionization chamber and a secondary emission monitor (SEM), to have redundancy by using different types of monitors. They were, however, replaced with the present ICs after the high reliability of ICs in practical use was confirmed [3]. One of the ICs works as the main monitor and the other works as the auxiliary monitor. A beam shutter is interlocked to the beam monitors and is closed when the measured dose value reaches the prescribed value. The auxiliary monitor also closes the beam shutter when the measured dose value reaches the value that is larger than the prescribed value by 5 %.

7.1.3 Layer-Stacking Method

In the broad-beam method, with arrange modulator, a constant SOBP over the field area results in an undesirable dose to the normal tissue proximal to the target [3, 4]). Therefore, in order to avoid unwanted doses, a layer-stacking method was developed. The layer-stacking method is a way of stacking many mini SOBPs along the depth direction and changing apertures of the MLC as if drawing the lineation of the cross-sectional surface of the target tumor volume as shown in Fig. 7.6.

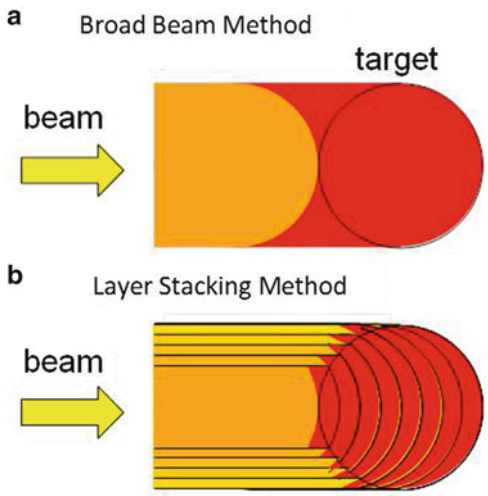

Fig. 7.6 Layer-stacking method. (**a**) Because the broad-beam method makes the fixed SOBP irradiation field, the high-dose region exists outside the tumor target. (**b**) The layer-stacking method can change SOBP according to the shape of the target and reduce the high-dose region outside the tumor target

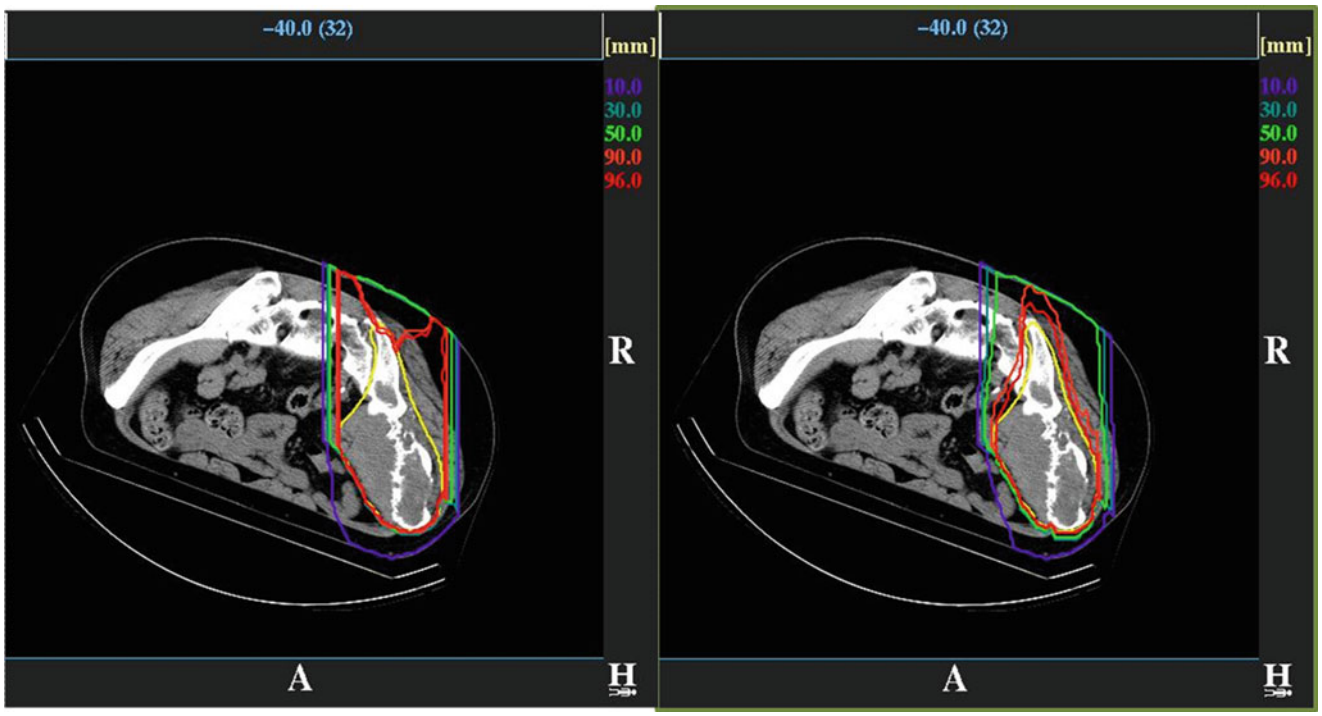

Fig. 7.7 Example of dose distribution planed to the tumor in the bone and soft tissue region by the broad-beam method (*left*) and the layer-stacking method (*right*)

At HIMAC the layer-stacking method has been used for carbon-ion radiotherapy (C-ion RT) since 2005. A thin-layer irradiation field with a mini SOBP (about 10 mm) is longitudinally swept step by step with changing thickness of a range shifter from the distal end of the target volume to the shallowest end. The mini SOBP is produced with a thin ridge filter. At each step, the radiation field shaped by the MLC changes to conform the contour of the target at each slice. Once the described dose is delivered to the slice volume, beam extraction is quickly cut off and the MLC and the range shifter are set to the next slice, and this sequence is repeated to the last slice. To accomplish the irradiation in clinically acceptable time, quick responses of the MLC motion, of the range shifter motion, and of the beam on/off are essential. Figure 7.7 shows an example of dose distributions of tissues during treatment planning. The left one is of tissues by the ordinary broad-beam

method, and the right one by the layer-stacking method. The dose to the normal tissue proximal to the target is remarkably reduced by the layer-stacking method. Among the merits of this method are not only the improved dose distributions, but also that they are achieved with the same devices as the passive treatment delivery system.

7.2 Scanning Delivery System

7.2.1 Overview and Basic Principles of Scanning Delivery

In order to achieve the required dose distribution, the treatment planning system (TPS) for the scanning delivery optimizes and outputs the particles numbers (weight) for each irradiation point (spot) in the target volume. Figure 7.8 shows an example of the optimized weight maps. It is required to the scanning delivery system to realize required particle distribution safely. Thus, the scanning delivery system controls the beam position three-dimensionally by magnetic deflection for transverse and by changing energy for longitudinal. The schematic of the scanning delivery is shown in Fig. 7.9. To realize desired field as calculated by the TPS, we must control the fluence of each spot to keep it as close as possible to the prescribed fluence in the TPS, because errors in the irradiation disturb the uniformity. There are several kinds of errors in the irradiation that commonly occur, such as size and position of the pencil beam and resolution of the monitor, making the uniformity of the irradiated dose distribution worse than that in the TPS.

7.2.2 Transverse Beam-Scanning Methods

There are several scanning methods to deliver the required fluence maps, while it is common to scan the beam by the magnetic deflection. Three scanning methods, as schematically shown in Fig. 7.10 and summarized in Table 7.1, are well known as follows: (1) spot scanning, (2) raster scanning, and (3) continuous raster scanning. (1) Spot scanning and (2) raster scanning are sometimes called “discrete spot scanning” and “continuous spot scanning,” because both of them employ the spot by spot control of the magnet. In spot scanning irradiation, the beam supply is turned off just after the counter reaches the preset value of each spot. Thus, exposure during the transition between spots is zero, although leakage after the beam is turned off is unavoidable. In raster-scanning irradiation, when the preset count is delivered to a raster point, the beam position is shifted to the next raster point without turning the beam off, within each iso-energy slice. Meanwhile, when the slice needs to be shifted or all irradiation is finished, it is necessary to turn off the beam. Continuous raster scanning is similar to raster scanning as far as beam-on/beam-off operations are concerned. The scanning magnets are operated according to the preset current pattern for each iso-energy slice. In this method, it is

Fig. 7.8 Example of optimized weight map

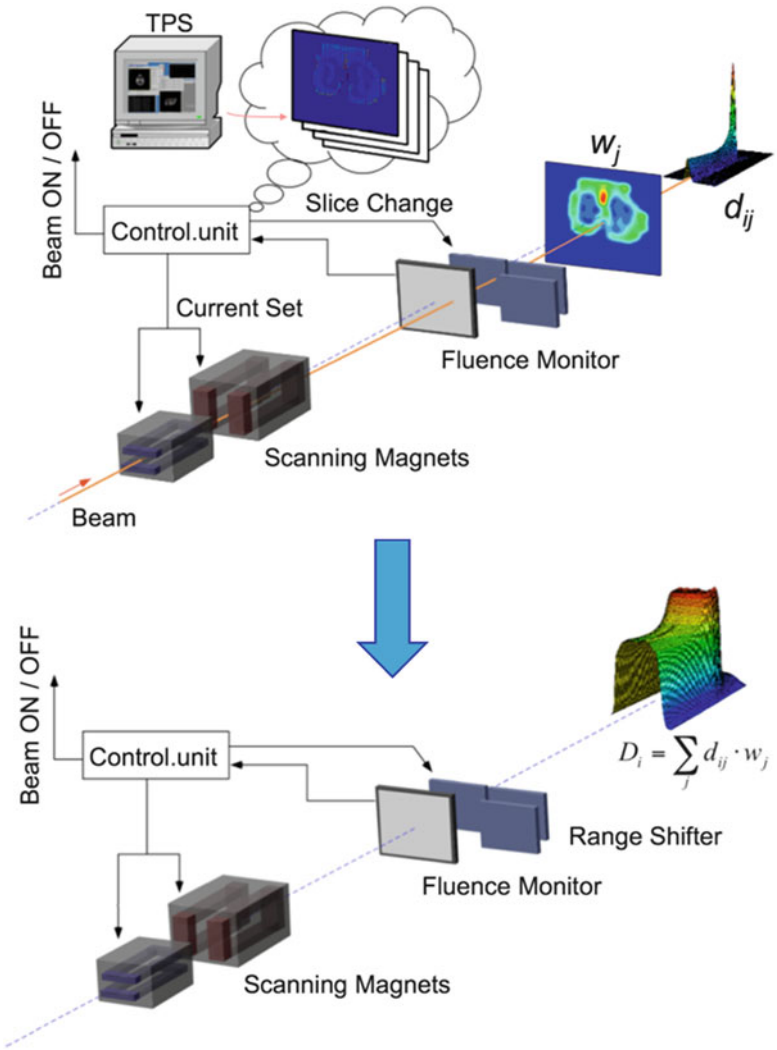

Fig. 7.9 Schematic of dose conformation by scanning delivery

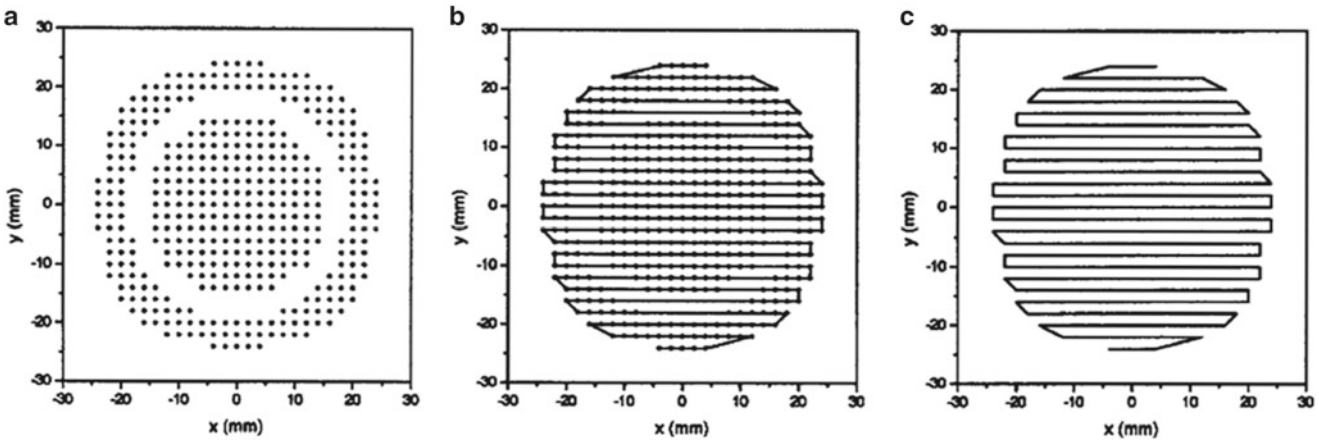

Fig. 7.10 Comparison of transverse beam-scanning methods

Table 7.1 Comparison of transverse scanning methods

	Spot scanning	Raster scanning	Continuous raster scanning
Magnet control	Stepwise	Stepwise	Continuous
Dose control	Spot by spot, discrete	Spot by spot, continuous	Continuous
Optimization	Discrete	Discrete	Continuous
Unavoidable exposure	Limited by beam-off time	Limited by scan speed	None

necessary to apply a different optimization procedure, in which a discrete weight map is interpolated and iteratively optimized to obtain a continuous weight map.

7.2.3 Depth-Scanning Methods

The depth scanning, i.e., shifting the Bragg-peak position in the target, can be realized by changing the beam energy. Two popular depth-scanning techniques are (1) range shifter scanning and (2) energy scanning. Recently, an alternative technique combining the range shifter scanning and the energy scanning, (3) hybrid depth scanning, is proposed. These three scanning methods are schematically shown in Fig. 7.11. In the range shifter scanning, the energy absorber, which consists of plastic plates, is used to shift the Bragg-peak depth. The commissioning and the control of this method are easier than others. Further, the irradiation time can be shortened compared with other method, because it takes only few hundred milliseconds to insert/remove the plates. However, the range shifter plates may broaden the spot size of the beam on a target and produce secondary fragments. On the other hand, in the energy scanning, the Bragg-peak depth can be controlled by directly changing the beam energy from the accelerator. Thus, this method does not employ the range shifter plates. However, this method needs relatively longer time for energy variation and for the commissioning. Further, the fine adjustment of the Bragg-peak position is required, because the energy step from the accelerator is usually discrete. In order to overcome these problems, the hybrid depth-scanning method was developed. In this method, coarse tuning of the beam range is provided by the accelerator, while fine tuning is provided by the range shifter plates. The hybrid depth scanning can provide dose distributions with steeper lateral dose falloffs and higher peak-to-plateau ratio compared to the range shifter scanning and comparable to the energy scanning. Thus, the hybrid depth-scanning method is routinely used at NIRS-HIMAC since 2012.

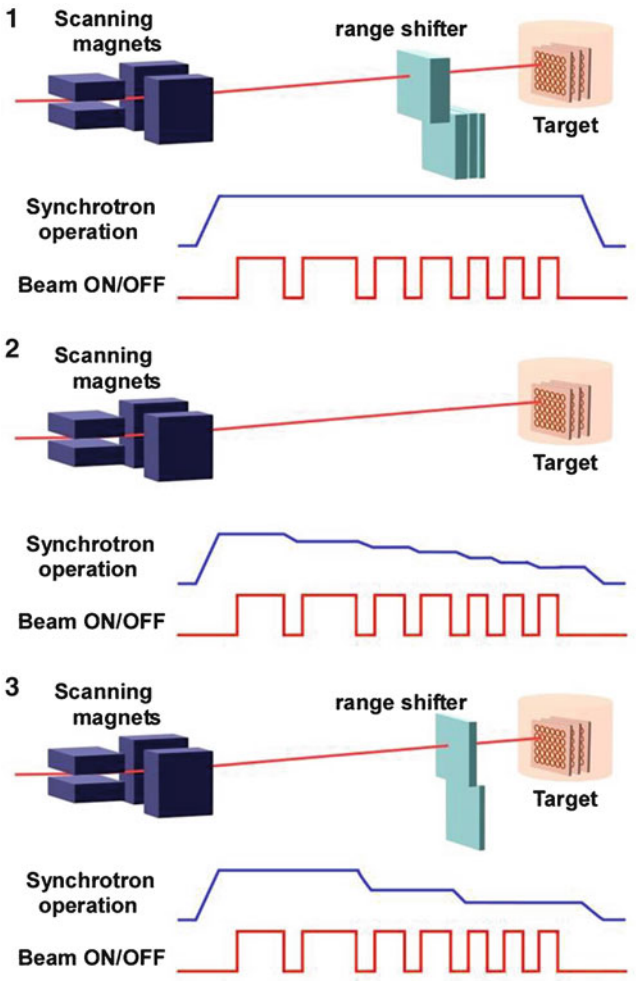

Fig. 7.11 Schematic of depth-scanning methods, from the upper (*1*) range shifter scanning, (*2*) energy scanning, and (*3*) hybrid depth scanning

7.2.4 Control System and Beam Monitoring

While the advantage of the scanning delivery is its flexibility for dose conformation, the implementation of quick and reliable beam control and monitoring are required because the beam properties from the accelerator directly affect the dose distribution compared to the passive delivery. Further, sufficient safety features should be implemented. For this purpose, two flux monitors and one or two beam position monitors are employed in the scanning delivery system. The safety interlock features for errors of the beam flux, position, and size should be implemented including the watchdog and the monitoring of each device. Since these undesirable errors deteriorate the dose distribution, the beam should be turned off as quickly as possible after their detection. Example of control system configuration is shown in Fig. 7.12.

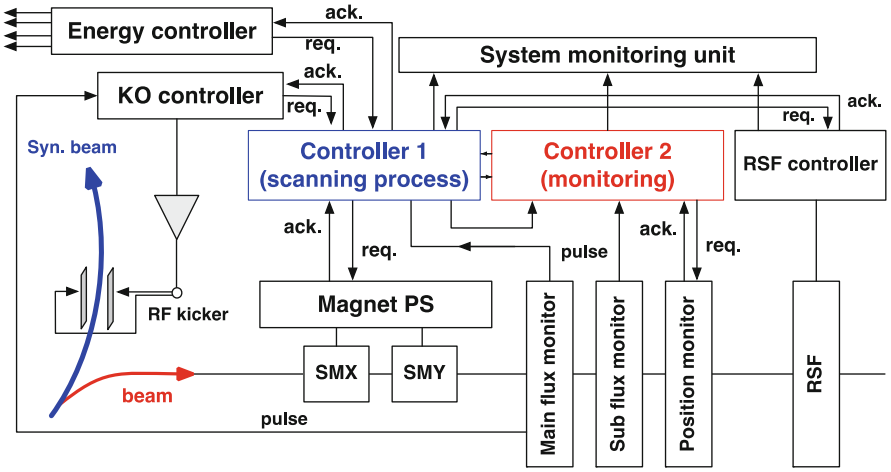

Fig. 7.12 Schematic of control system for NIRS scanning system

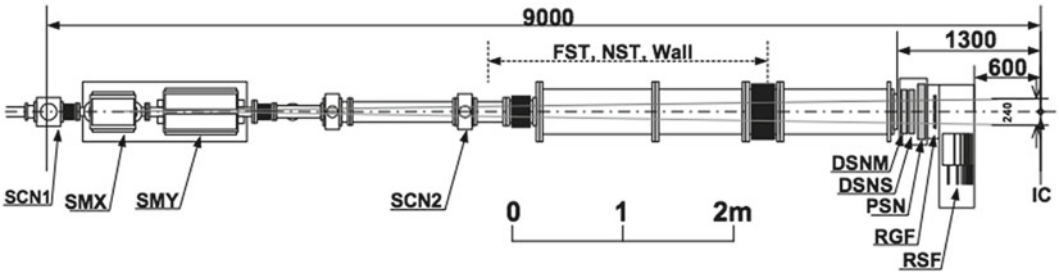

Fig. 7.13 Layout of NIRS scanning system

7.2.5 System Configuration Example: NIRS Scanning System

Layout of the fast scanning system is shown in Fig. 7.13. It consists of the scanning magnets (SMX and SMY), main and sub flux monitors (DSNM and DSNS), position monitor (PSN), mini ridge filter (RGF), and range shifter (RSF). To achieve the fast beam scanning at the isocenter, the distances from SMX and SMY to the isocenter are designed to be 8.4 and 7.6 m, respectively. The vacuum window is made of 0.1 mm thick Kapton and located 1.3 m upstream from the isocenter. Beam monitors, RGF, and RSF are installed downstream of the vacuum window. The primary beam shutter (FST) and the neutron shutter (NST) are placed in the middle of the irradiation port (indicated by the dotted arrow in Fig. 7.13).

The basic parameters of the NIRS scanning system are described as follows. To obtain the range of more than 300 mm, the maximum energy is chosen as 430 MeV/u. The required field size is 220×220 mm^2 for the transverse directions with a 150 mm length for the longitudinal direction. This covers most of the target that are treated by the existing passive irradiation system at the HIMAC. Under these conditions, the new system must be as fast as possible to treat the moving target with rescanning. Based on the conceptual design study, the system was designed so as to provide a modulated dose delivery with beam-scanning velocities of 100 and 50 mm/ms at the isocenter. These scanning velocities enable us to achieve the fastest irradiation time of around 40 ms for an example uniform 2D field having a 102×102 mm^2 size with spot spacing of 3 mm. To fulfill these requirements, we made strong efforts to develop (1) the fast scanning magnet and its power supply, (2) the high-speed control system, and (3) the beam monitoring. As a result of the development, the NIRS system took only 20 s to deliver the physical dose of 1 Gy to a spherical target having a diameter of 60 mm with eight rescans. In this irradiation, the average of the spot-staying time was considerably reduced to 154 μs, while the minimum staying time was 30 μs.

7.3 Heavy-Ion Accelerators

7.3.1 Overview of Heavy-Ion Accelerators

To treat a deeply seated tumor in a patient using carbon ions, ions have to be accelerated up to 430 MeV/u. A speed of carbon ions at this energy is roughly 73 % of the light speed,

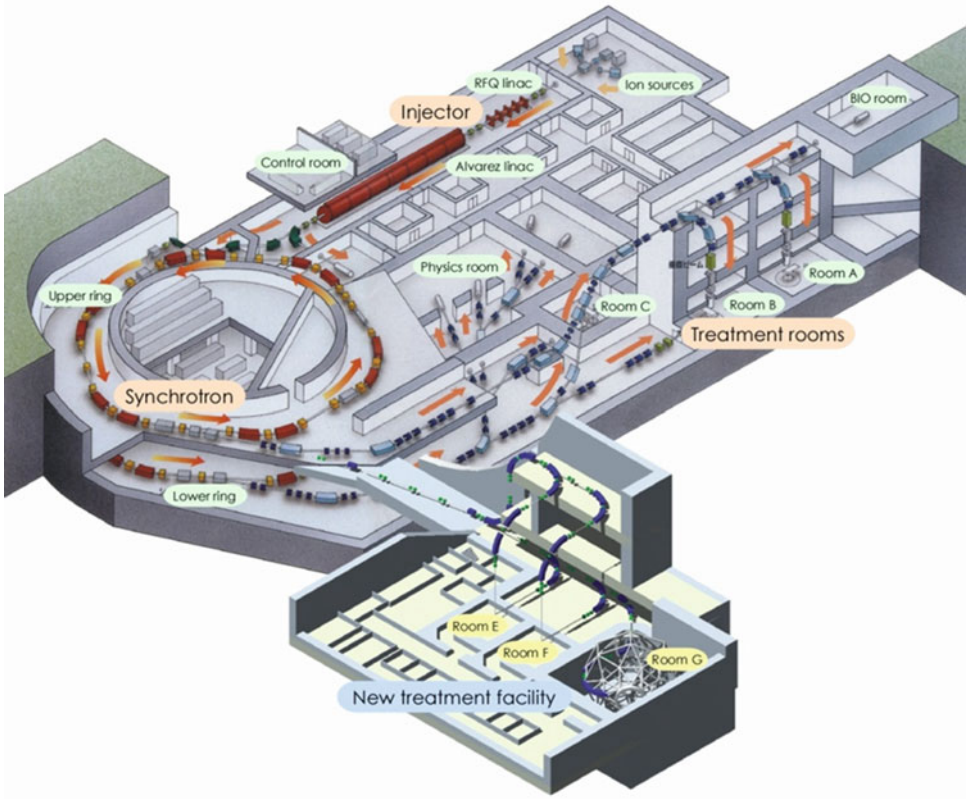

Fig. 7.14 Bird's-eye view of the HIMAC

and a corresponding residual range in a patient is approximately 30 cm, which may cover most of tumor sites. To accelerate carbon ions to the required energy, heavy-ion accelerators, such as synchrotrons or cyclotrons, are used. For proton radiotherapy, cyclotrons are commonly used, because cyclotrons can generally provide higher beam intensity, as compared with that of synchrotrons. However, only synchrotrons are presently employed for C-ion RT, because synchrotrons can change energy of output beams directly from accelerators, and control intensity of extracted beam. These features of synchrotrons are preferable for ion radiotherapy and further quite attractive for the scanning beam delivery, since a quality of treatment beam is quite important to control dose distributions.

A bird's-eye view of the HIMAC accelerator complex is shown in Fig. 7.14 [5]. The accelerator part of the HIMAC complex consists of three ion sources: a linear-accelerator cascade and two synchrotron rings. The ion source produces carbon ions of C^{2+}, and they are transported and injected to the linear-accelerator cascade. A linear accelerator, abbreviated as "linac," refers to a device that accelerates ions along a linear path. The linear-accelerator cascade of the HIMAC complex consists of a radio-frequency-quadrupole (RFQ) linac and an Alvarez drift-tube linac (DTL) and can accelerate ions up to 6 MeV/u having a charge-to-mass ratio of A/Z = 7.

The ions, as accelerated with the linear-accelerator cascade, are then injected and accelerated with the synchrotron rings. When energy of ions reaches to those, required for treatment beams, the circulating beam in the ring is slowly extracted from the ring by using an RF-knockout (RF-KO) slow-extraction method [6] and is delivered to a beam-delivery system, as described in the preceding sections. For a reliable and stable dose management in ion radiotherapy, the extracted beam should have characteristics, such as a sufficiently long duration, low fluctuation in the time structure, and quick beam on/off for gated irradiation to moving targets, such as lung or liver tumor, which is called "respiratory-gated irradiation"; the heavy-ion accelerators for ion radiotherapy must be designed so as to satisfy those requirements.

7.3.2 Multiple-Energy Operation

In raster-scanning irradiation, a target is directly irradiated with high-energy heavy ions. The position of the focused beam on a target is controlled by the fast horizontal and vertical scanning magnets. To control the depth dose distribution, energy degraders, such as range shifters, consisting of PMMA plates having various thicknesses, are used in the

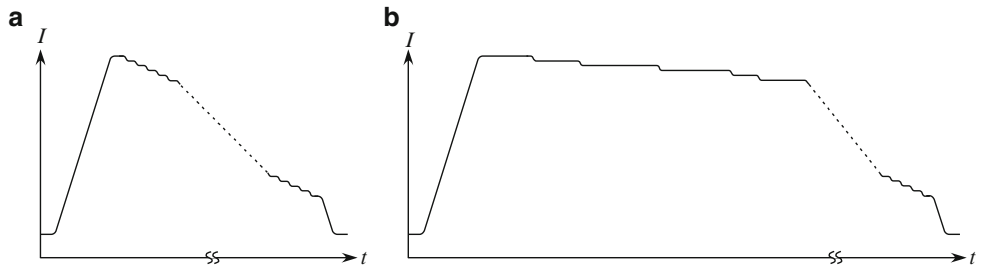

Fig. 7.15 Schematic drawing of synchrotron pattern for multiple-energy operation. (**b**) The same pattern as (**a**), but with the extended flattops. The beam is extracted from the synchrotron ring during these extended flattops

present irradiation system with broad-beam irradiation. However, these range shifters may broaden the spot size of the beam on a target and concurrently produce secondary fragments, which could adversely affect the depth dose distribution. Since focused beams are used to irradiate a target in the raster-scanning irradiation method, it is preferable to change the beam energy directly by the accelerators, instead of using such energy degraders.

To change the energy of the beam, as provided by the synchrotron ring, a multiple-energy operation with extended flattops is developed [7]. The proposed operation enables us to provide heavy ions having various energies in a single synchrotron cycle, namely, the beam energy would be successively changed within a single synchrotron pulse by an energy step, corresponding to a water range of 2 mm. With this operation, the beam range could be controlled without using any energy degraders, such as the range shifters, and hence an excellent depth dose distribution could be obtained.

The multiple-energy operation employs operation patterns having a stepwise flattop, as schematically shown in Fig. 7.15a. With these operation patterns, the heavy ions injected in the ring are initially accelerated to the maximum energy and then successively decelerated to lower energies. Although the stepwise pattern only has short flattops, where the beam can be extracted from the ring, we can extend the flattop and extract the beam during the extended flattop. Having consecutively extended the flattops, as illustrated in Fig. 7.15b, the beams having various energies can be extracted from the ring within a single synchrotron cycle, and hence the total irradiation time can be considerably reduced.

To prove the principle of multiple-energy operation with extended flattops, beam acceleration and extraction using the stepwise operation pattern was performed. The pattern has 11 short flattops, corresponding to beam energies of 430, 400, 380, 350, 320, 290, 260, 230, 200, 170, and 140 MeV/u. A similar pattern was prepared for other devices, such as the main quadrupole and sextupole magnets, the RF-acceleration cavity, and the beam-extraction devices in the extraction channel. By using the prepared operation pattern, the beam will be first accelerated to 430 MeV/u and then consecutively decelerated down to 140 MeV/u at an energy step of 20 or 30 MeV/u. Results of the beam test are shown in Fig. 7.16. Beams having 11 different energies were successively extracted from the synchrotron ring. The multiple-energy operation using this pattern was successfully commissioned and has been used for scanning treatments since FY 2012 [8].

7.3.3 Intensity Control

In ion radiotherapy, intensity control of treatment beams, as well as fast on/off switching and stability in position and intensity of beams, is quite important. Thus, the RF-KO slow-extraction method has been used to meet these requirements of treatment beams. In this method, the beam is diffused by the transverse RF field. When the frequency of which has frequency modulation (FM) that is matched with betatron motion, the beam is excited by the third-order resonance and hence extracted from a synchrotron ring. The control of the transverse RF field is responsible for beam-on/beam-off switching.

Since beam intensity has to be controlled during irradiation a slice by a slice for a 3D-scanning irradiation method gated with patient's respiration, beam intensity has to be dynamically changed and precisely controlled. To satisfy these requirements, an intensity-modulation system was developed [9]. In the system, beam intensity is monitored with a flux monitor, installed at exit of a beam nozzle. Information on the beam intensity is fed into a feedback control system and used to control RF amplitude for the RF-KO beam-extraction system.

An example of intensity-modulation tests is shown in Fig. 7.17. In the tests, a beam having 350 MeV/u was used, and beam intensity, as extracted from the synchrotron ring, is modulated 1 to 30. As can be seen in the figure, beam intensity is well control as expected.

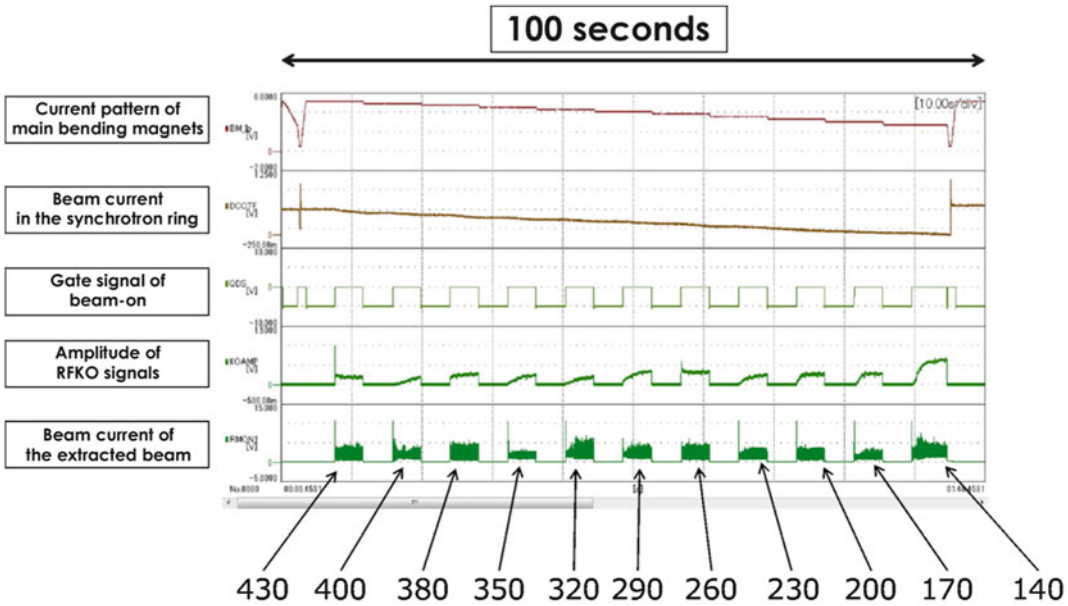

Fig. 7.16 Example of the beam acceleration test using the 11-flattop operation pattern. Beams having 11 different energies were successively extracted from the synchrotron ring

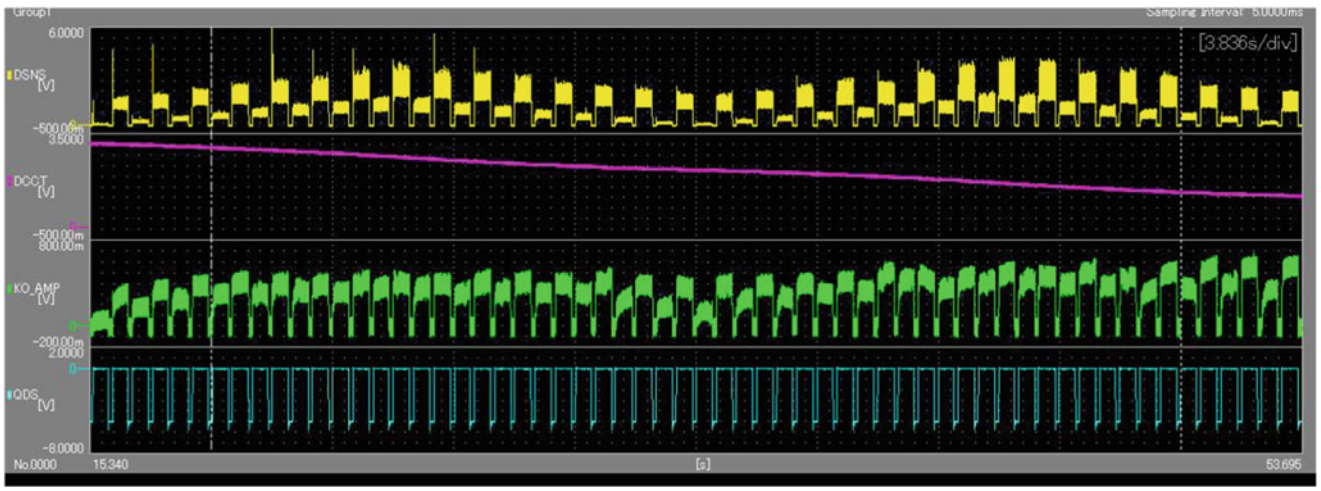

Fig. 7.17 Example of intensity-modulation tests using carbon beams of 350 MeV/u. Measured intensity of an extracted beam (*yellow*), beam current of a circulating beam (*pink*), an amplitude of RF-KO signal (*green*), and applied current for sextupole magnet in the ring (*blue*) are shown

References

1. Minohara S, Fukuda S, et al. Recent innovations in carbon-ion radiotherapy. J Radiat Res. 2010;51:385–92.
2. Torikoshi M, et al. Irradiation system for HIMAC. J Radiat Res. 2007;48(Suppl A):A15–25.
3. Kanai T, Sudo M, Matsufuji N, Futami Y. Initial recombination in a parallel-plate ionization chamber exposed to heavy ions. Phys Med Biol. 1998;43:3549–58.
4. Kanematsu N, Endo M, Futami Y, et al. Treatment planning for the layer-stacking irradiation system for three-dimensional conformal heavy-ion radiotherapy. Med Phys. 2002;29: 2823–9.
5. Hirao Y, et al. Annual report HIMAC. National Institute of Radiological Sciences:NIRS-M-89/HIMAC-001; 1992.
6. Tomizawa M, et al. Slow beam extraction at TARN II: Nucl Instr Method. 1993;A326:399.
7. Iwata Y, et al. Multiple–energy operation with extended flattops at HIMAC: Nucl Instr Method. 2010;A624:33.
8. Mizushima K, et al. Proceeding of particle accelerator society Japan FRUH09; 2012.
9. Mizushima K, et al. The HIMAC Beam-intensity control system for heavy-ion scanning: Proceeding of international particle accelerator conference (IPAC); 2011. pp. 3592–3594.

Dosimetry

8

Manabu Mizota and Akifumi Fukumura

Abstract

Absorbed-dose determination must be accurate and reproducible. Dose evaluated by a facility must be consistent with those by the other facilities. This chapter describes the dose evaluation in terms of absorbed dose to water with an ionization chamber for a carbon beam of an energy range of 100–450 MeV/n.

Keywords

Carbon-ion dosimetry • Dose calibration • Dose measurement

8.1 General

The goal of radiation therapy, including charged-particle radiotherapy, is to achieve tumor control with irradiation to a well-defined target volume of the patient, while as far as possible avoiding the exposure of surrounding healthy tissues. Since the beam delivery is generally characterized by absorbed dose at a reference point and relative dose distribution in a patient's body, radiation dosimetry is a major concern in radiation therapy.

One of the distinct physical characteristics of carbon-ion beams is the depth–dose distribution which shows the Bragg peak. Another important characteristic of the carbon-ion beam is that the relative biological effectiveness (RBE) varies with depth and with dose delivered to the tissue.

When heavy-ion beams pass the irradiation device or human body, fragmented particles are produced, and they reach deeper regions than the range of the primary particles. For an accurate determination of absorbed dose from heavy-ion beams using an ionization chamber, it is desirable to know the energy spectra of the incident heavy-ion beam, the projectile fragments, and also the target fragmented nuclei. About the dosimetry of carbon beams, however, very few data are available and simplified physical parameters are used instead.

8.2 Radiation Therapy and Doses

The absorbed dose to water, which is considered to be tissue equivalent, is often used in radiation therapy, including charged-particle radiotherapy. In principle, the absorbed dose can be a quantity directly measurable by observing the temperature increase upon the target substance during irradiation. However, in fact, this is extremely difficult to carry out. The practical instruments for absorbed-dose determination are ionization chambers, which are traceable to the primary standards of absorbed dose to water.

The following sections describe the dose evaluation mainly of passively modified carbon beam.

8.3 Carbon Beam Dosimetry in Practice

The absorbed dose to water for the charged-particle beam can be evaluated with an air cavity ionization chamber based on the Bragg–Gray cavity theory. However, in practice, there are various issues to be taken into account, such as selection of the ionization chamber, correction of the chamber wall

M. Mizota (✉) • A. Fukumura
National Institute of Radiological Sciences, 9-1, Anagawa-4, Inage-ku, Chiba 263-8555, Japan
e-mail: m_mizota@nirs.go.jp; fukumura@nirs.go.jp

H. Tsujii et al. (eds.), *Carbon-Ion Radiotherapy: Principles, Practices, and Treatment Planning*,
DOI 10.1007/978-4-431-54457-9_8,

and waterproofing sleeve effects, and evaluation of the effect of ion recombination. Further, the selection of various physical parameters, such as the mass stopping power ratio and *W*-value, and measurement conditions also need to be examined. For dosimetry in charged-particle radiotherapy, the Japan Society of Medical Physics recommends to use the dose evaluation protocol "JSMP standard dosimetry 12" [1], which is mostly based on IAEA TRS 398 [2]. This section outlines the dosimetry protocol. It is recommended to read both of them carefully before carrying out water absorbed-dose measurement in practice.

The absorbed dose to water with beam quality Q_0 is given by the following formula. Here, the ionization chamber is under the same environment as at the time of calibration:

$$D_{w,Q_0} = M_{Q_0} \cdot N_{D,W,Q_0}$$

where M_{Q_0} is the reading of the dosimeter at a reference condition and N_{D,w,Q_0} is the calibration coefficient in terms of absorbed dose to water for radiations of beam quality Q_0 (normally ^{60}Co γ beam). In the radiation field having beam quality Q which is different from Q_0, the absorbed dose can be obtained using the beam quality correction factor. That is, the dose at the standard depth of water can be obtained from the reading of the standard ionization chamber by

$$D_{w,Q} = M_Q \cdot N_{D,W,Q_0} \cdot k_{Q,Q_0}$$

where M_Q is the reading value of the standard dosimeter corrected for the influence quantities temperature and pressure, electrometer calibration, polarity effect, and ion recombination. In the case of scanned beams, the dose rate is very high and general recombination effects must be considered. k_{Q,Q_0} is a beam quality correction factor, which corrects the effect of difference between the reference beam quality Q_0 and the actual user quality and can be obtained theoretically by the following formula:

$$k_{Q,Q_0} = \frac{\left(S_{w,air}\right)_Q \left(W_{air}\right)_Q}{\left(S_{w,air}\right)_{Q_0} \left(W_{air}\right)_{Q_0}} \cdot \frac{P_Q}{P_{Q_0}}$$

which includes the ratios at the qualities Q and Q_0 of Spencer–Attix water/air stopping power ratios, $S_{w,\mathrm{air}}$, of the mean energy expended in air per ion pair formed, W_{air}, and of the perturbation factors P_Q.

When Q_0 is a ^{60}Co γ beam, it is recommended to use the following values:

$$\left(S_{w,air}\right)_{Q_0} = 1.133$$

$$\left(W_{air}\right)_{Q_0} = 33.97eV$$

Since not much progress has been made in the investigation of the perturbation factor to be used for carbon beams, it is assumed to be 1.0. Therefore, in the case of carbon beams,

$$\left(S_{w,air}\right)_Q = 1.130$$

$$\left(W_{air}\right)_Q = 34.50eV$$

$$P_Q = 1.0$$

$k_{Q,Q0}$ values for carbon beam are dominated by the ratio of W_{air} values and the chamber-specific perturbation factors at ^{60}Co. The values for various cylindrical and plane-parallel ionization chambers in common use are tabled [1, 2].

The following points should be noted regarding the ionization chamber to be used. Particle beams have Bragg peaks which change drastically throughout their depth–dose distributions. Therefore, when a depth–dose distribution is measured, a plane-parallel ionization chamber with high spatial resolution to the depth direction is often used. However, the plane-parallel ionization chamber has a greater uncertainty in P_{wall} than the cylindrical ionization chamber and has problems such as exhibiting a polarity effect and poor reproducibility. Thus the overall uncertainty of the plane-parallel ionization chamber is greater than that for the cylindrical type ionization chamber. Therefore, it is recommended to use the cylindrical type ionization chamber as the standard dosimeter for determining the absolute value of the absorbed dose to water. On the other hand, in the area near the Bragg peak, where the slope of the dose is large, it is appropriate to carry out measurements using the plane-parallel ionization chamber, which has a high spatial resolution. Therefore, it is recommended to calibrate the plane-parallel ionization chamber with the cylindrical type in the area where the dose distribution is flat and to use it for measuring the depth–dose distribution.

The following two cases are considered for standard conditions:

Case 1

A typical treatment beam having a spread-out Bragg peak (SOBP) is adopted as the standard condition. The reference point in this case is the center of the SOBP.

Case 2

The irradiation condition of the monochromatic energy is adopted as the standard condition. The reference point in this case is in an incident area where the dose distribution is flat.

The latter is recommended especially when the SOBP has a slope such as with the heavy-ion beam. In either case, the sensitivity of the dosimeter of the plane-parallel ionization chamber should be calibrated to the absolute value of the

absorbed dose per monitor unit at the reference point under the standard condition. The following cautions should also be taken into account in dose measurement:

- It is recommended to use an irradiation field size with a diameter of about 10 cm.
- Water is the standard substance used to determine the absorbed dose.
- The size of the water phantom is recommended to be longer than the range of the carbon beam by at least 5 cm and wider than the irradiation field by 5 cm.
- For the entrance window of the water phantom, use PMMA (polymethyl methacrylate) or a substitution of the minimum thickness that is not distorted by the water pressure.
- The waterproofing sleeve of the ionization chamber should be made of PMMA with a thickness of 1 mm or less and the air layer in between the ionization chamber is 0.1–0.3 mm or less.
- The effective point of measurement with a cylindrical chamber should be determined by comparing the built-up curve of the Bragg peak measured with the cylindrical chamber and that with a plane-parallel chamber.

Case 1

- It is desirable that the width of SOBP is sufficiently larger than the size of the standard ionization chamber.
- The reference point is at the center of the SOBP.

Case 2

- The reference point is in an incident area where the depth–dose distribution is not greatly changed.

Further, it is desirable to compare periodically dosimeters between different particle beam institutions.

8.4 Dosimetric Equipment

For clinical use, output factors, depth–dose distributions, transverse beam profiles, and penumbra size of the radiation fields for the various conditions of treatments should be measured.

There are few differences in principle between output-factor determination in scanned beams and passively modified beams. The output factor in scanned beams is calculated by the treatment planning system, while the one in passively modified case is based on measurements. The output factor is derived for each of the beam conditions (e.g., energy, SOBP, and range shifter) depending on the amount of radiation incident on a monitoring device.

Calibration of the device that monitors the dose delivered to the patient is necessary to ensure accurate determination of irradiation doses under a given set of equipment and beam conditions for each patient and irradiation port. Dose calibration is in principle performed using a calibrated ionization-chamber dosimeter with solid or liquid phantom, measuring radiation doses determined under a given set of equipment and beam conditions for each patient and irradiation port, and comparing the measurements obtained from the dose monitoring device installed in the beam-delivery device to the administered dose. In this manner, the calibration is currently performed using actual measurements, though attempts have been made to use highly precise calculations to give correction coefficients to simplify calibration.

It is very important to measure dose distribution for commissioning of beam lines and collecting data for treatment planning systems. Dose distribution can be determined by the water column method, where an ionization chamber is scanned in water. Accurate measurements are required to determine the range and penumbra characteristics. Plane-parallel chambers are recommended for depth–dose measurements in large fields, whereas small cylindrical chambers are recommended for depth–dose measurements in small fields and for all lateral dose-profile measurements. Ionization-chamber arrays are useful in daily measurements.

8.4.1 Reference Ionization Chamber for Absorbed Dose

There are some reference dosimetry techniques such as the faraday cup, calorimetry, and ionization chamber. However, the ionization-chamber dosimetry is widely adopted as a standard in the dosimetry for the particle therapy. The code of practice TRS-398 recommended procedures for ionization-chamber reference dosimetry. Thimble air-filled ionization chamber having the sensitive volume of 0.6cc is widely used and commercially available. Both cylindrical and plane-parallel ionization chambers are recommended for use as reference instruments. In the NIRS, Farmer chamber (PTW31013, PTW Freiburg, Germany) and Advanced Markus chamber (PTW34045, PTW Freiburg, Germany) are used as reference chamber in both passive and scanning delivery.

8.4.2 Large Plane-Parallel Ionization Chamber for Integral Depth–Dose Measurement

A plane-parallel ionization chamber having large sensitive area is used to measure the integral percentage depth–dose (PDD) of the pencil beam. By scanning the waterproof ionization chamber in the water tank, the measurement is usually performed. For proton beam, the Bragg peak chamber (PTW34070, PTW Freiburg, Germany) having the diameter of 84 mm is commercially available. In the NIRS, the

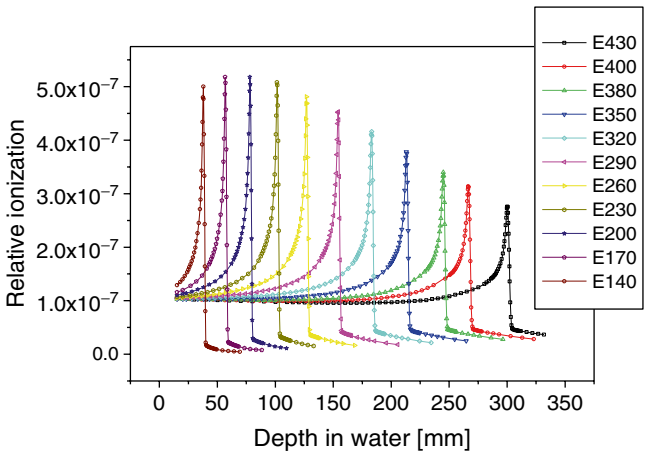

Fig. 8.1 Measured integral percentage depth dose as an example of large plane-parallel ionization-chamber dosimetry

ionization chamber having the diameter of 150 mm with 2 mm gap is developed considering the large scattered particles. The measured data, as typically shown in Fig. 8.1, is employed in the TPS for the scanning irradiation.

8.4.3 One-Dimensional Dosimetric Equipments

Multilayer ionization chamber (MLIC) is used for daily quality assurance (QA) measurements of passively modified beams at HIMAC [3]. The MLIC measures the depth–dose distribution of the irradiation field. The MLIC consists of 64 small cells that are aligned longitudinally. Each cell has a water-equivalent length of about 4.5 mm and forms a plane-parallel ionization chamber in which there is a 2 mm gap between an anode and a cathode [4]. The depth–dose distribution measurement provides information about the beam range as well as the calibration. So the overall QA of the patient-specific beam is done at the same time (Fig. 8.2).

Also, for measuring dose profiles (or field flatness), ionization-chamber arrays consisting of two-dimensional arrangements of small ionization chambers are used (Fig. 8.3). The pixel ionization chamber of each 64 cells with a 3.7×3.7 mm sensing area aligned in 4mm steps is arranged crosswise, which is put in perpendicular to the beam axis.

The typical dose distributions measured by the MLIC and the crosswise chamber arrays are shown in Figs. 8.4 and 8.5, respectively.

These ionization-chamber arrays are calibrated by an Advanced Markus chamber once a year in accordance with the IAEA TRS-398[2]. Farmer chamber, as well as the Markus chamber, is also calibrated once a year at a secondary standard dosimetry laboratory (SSDL).

Fig. 8.2 MLIC set on the couch to measure the depth–dose distribution of vertical beam

8.4.4 Two-Dimensional Dosimetric Equipments

Radiographic or radiochromic films are widely used for 2D dosimetry. Although the film dosimetry can easily obtain high spatial resolution, the film response depends on dose and LET. Therefore, the usual application of the film is evaluation of relative dose distribution in monoenergetic beam. For example, in the NIRS, the film dosimetry is used to evaluate the accuracy of the beam position and the fluence modulation in the scanning delivery as shown in Fig. 8.6. Since the film dosimetry needs relatively longer time to digitize the optical density, some institutions

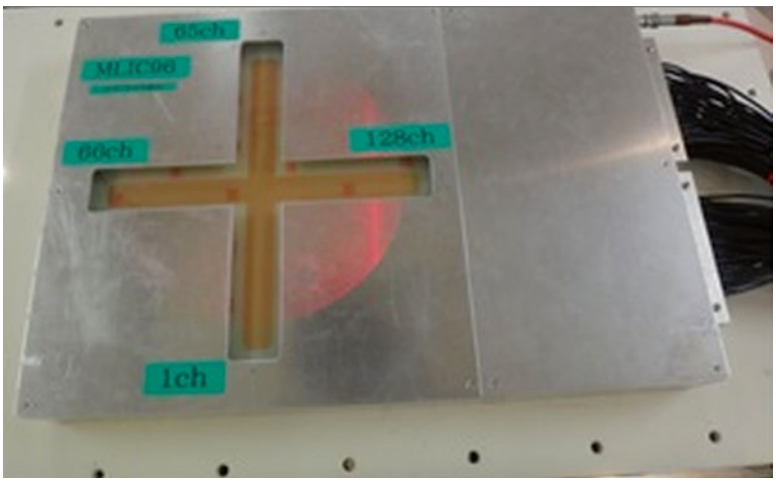

Fig. 8.3 Each 64 cells of the ionization chamber along the crisscross lines

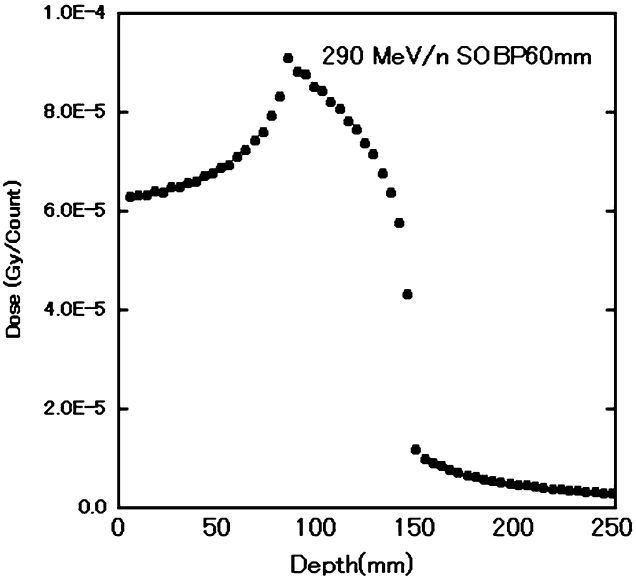

Fig. 8.4 Physical depth–dose distribution in a 290 MeV/n carbon beam (60 mm SOBP) measured by the MLIC

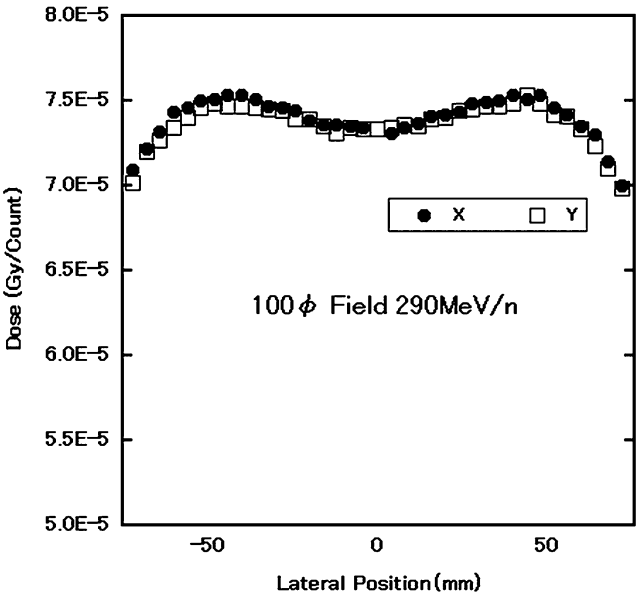

Fig. 8.5 Beam profiles of a 290 MeV/n carbon beam of which flattened area corresponds to 100 mm in diameter

develop the fluorescence screen with charge-coupled-device (CCD) camera system as an alternative of the film. Figure 8.7 shows the layout of the NIRS system and the typical result of the measurement in the QA of the scanned ion beam. Recently, on the other hand, a two-dimensional ionization-chamber array is commercially available. One is OCTAVIUS Detector 729 XDR (PTW Freiburg, Germany); another is MatriXX (IBA Dosimetry, Schwarzenbruck, Germany). Both detectors consist of two-dimensionally arrayed pixel ionization chambers. Such ionization-chamber array is widely used for the commissioning and the QA of the delivered field.

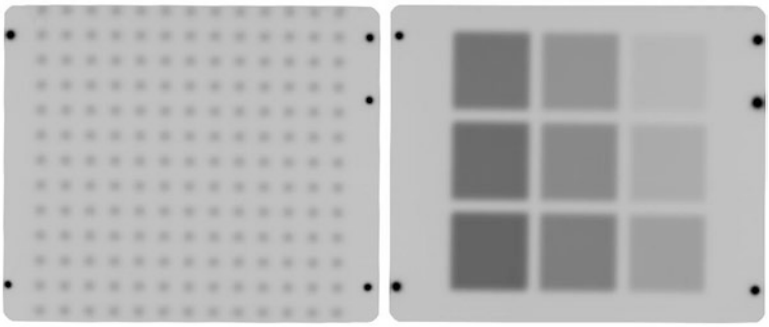

Fig. 8.6 Examples of film dosimetry

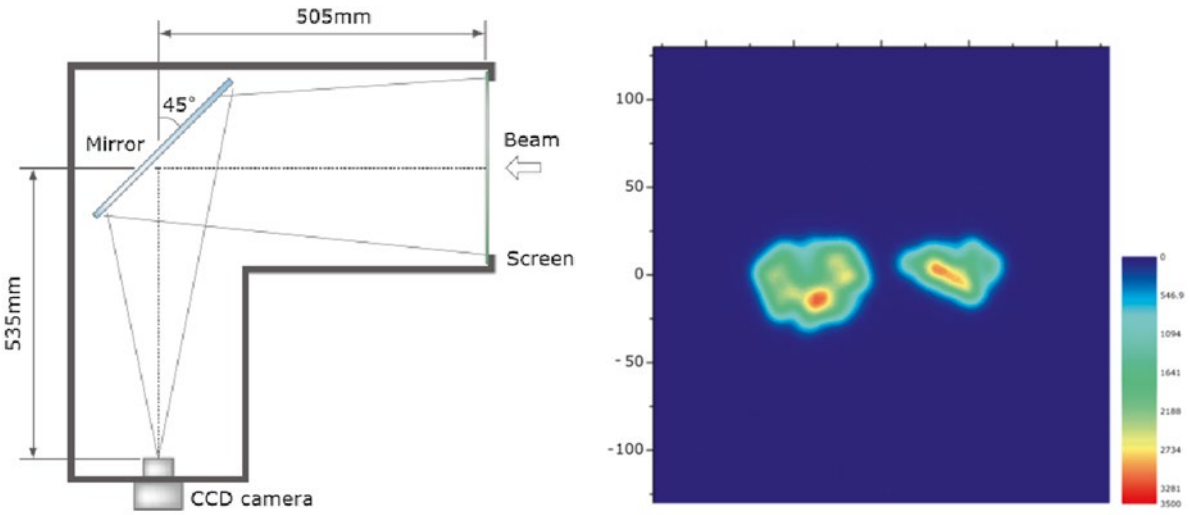

Fig. 8.7 Examples of fluorescent screen system and measurement

References

1. Japan Society of Medical Physics. Standard dosimetry of absorbed dose to water in external beam radiotherapy (Standard Dosimetry 12). Tokyo: Tsushosangyo Kenkyusha; 2012 (in Japanese). ISBN 4-86045-120-2 C3047.
2. IAEA. Absorbed dose determination in external beam radiotherapy. In: Technical Reports Series 398. Vienna: IAEA; 2000.
3. Torikoshi M, et al. Irradiation system for HIMAC. J Radiat Res. 2007;48:A15–25.
4. Shimbo M, et al. Development of a multi-layer ion chamber for measurement of depth dose distributions of heavy-ion therapeutic beam for individual patients. Nippon Acta Radiol. 2000;60:274–9 (in Japanese).

Motion Management

9

Shinichiro Mori

Abstract

Organ movement due to respiration may change the run of a charged particle beam that can result in degradation of dose conformation to the target. We introduced our approaches to quantitatively assessing potential problems in treatment planning and treatment beam irradiation processes due to organ movement.

Keywords

4D imaging • Gating • Intrafractional motion • Positioning • Registration

9.1 Intrafractional Motion

Rapid progress of radiotherapy treatment (RT) techniques has improved dose conformity compared to the conventional methods. A number of treatment centers have already delivered RT beams to targets in the thoracic and abdominal regions. The superiority of the advanced techniques lies in the fact that a sharp determination of the internal target volume (ITV) helps minimize dosing to the surrounding normal tissues and avoid an underdose being applied to the target volume. Even tumor movement is clearly recognizable on four-dimensional (4D) CT. Dose distribution variation due to organ motion has not been taken into consideration in the current treatment planning system. Generally, lung treatments are applied by the use of gating. Due to the imperfect reproducibility of the respiratory pattern and correlation between the skin surface and internal tumor motion across exhalations, the accuracy of gated radiotherapy could still be degraded and lead to possible irradiation of the tumor beyond the gating window, which, in turn, causes the position of the beam-on to be shifted relative to the actual target position (Fig. 9.1a). Cardiac motion, which is seen to perturb photon-beam treatment, could cause even greater perturbations in particle beam treatment. Figure 9.1b shows a single pencil beam that stops at the distal edge of the tumor when passing through the heart at diastole. However, it penetrated the tumor at systole due to beam range variation. One solution to minimizing range variation due to cardiac motion is to avoid tangential beam paths along the heart.

An understanding of motion characteristics in radiotherapy planning is useful for determining internal margins and optimizing beam parameters (beam angle, beam field and beam energy, etc.). Organ motion due to respiration has been investigated using a variety of methods, including fluoroscopy, ultrasound (US), MRI, CT, and PET, in the lung, liver, pancreas, kidney, and prostate sites.

We quantified organ motions due to respiration in thoracic, abdominal, and pelvic sites as a function of time using 4DCT. For pancreas, geometrical variation was greater around the pancreas tail than the pancreas body and head regions. The average pancreas head, body, and tail displacement in the inferior direction for the ungated phase was 8.3, 9.6, and 13.4 mm, respectively, which was minimized in the gated phase to 2.8, 2.8, and 3.6 mm, respectively. For all six patients with pancreatic cancer, the average pancreas center of mass (COM) displacement relative to that at peak exhalation was mainly in the inferior

S. Mori (✉)
National Institute of Radiological Sciences,
9-1, Anagawa-4, Inage-ku, Chiba 263-8555, Japan
e-mail: shinshin@nirs.go.jp

H. Tsujii et al. (eds.), *Carbon-Ion Radiotherapy: Principles, Practices, and Treatment Planning*,
DOI 10.1007/978-4-431-54457-9_9,

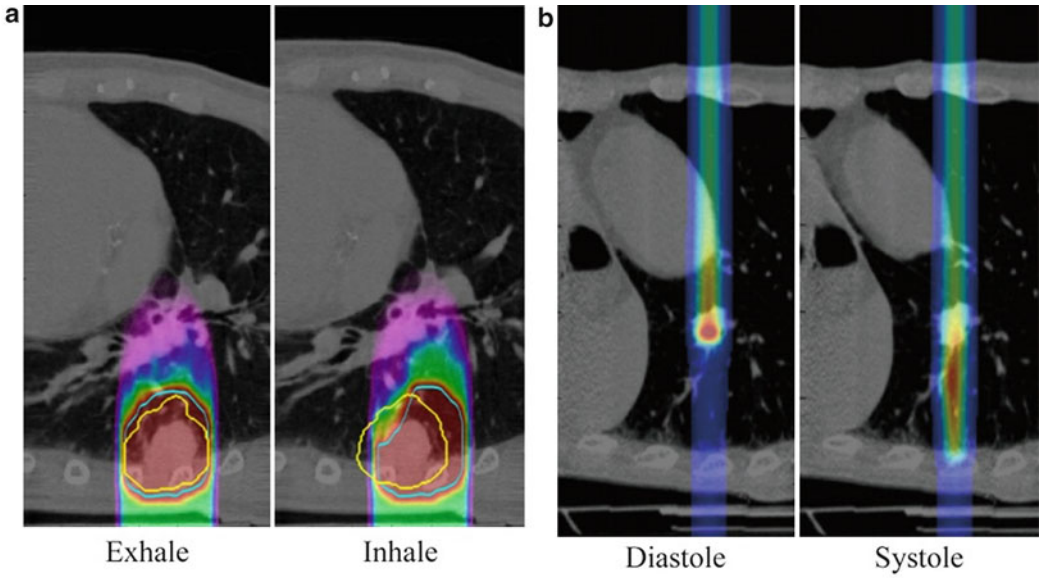

Fig. 9.1 (**a**) Carbon ion beam dose distribution in and out of the gating window. (**b**) A pencil beam stopped at the tumor at diastole, but caused overshoot at systole [1]

direction, at 9.6 mm for the ungated phase and 2.3 mm for the gated phase [2].

With regard to the liver site (irradiation administered with patients in the prone position), geometrical changes due to respiration were quantified by a deformable image registration between the reference and respective respiratory phases. The magnitude of the intrafractional displacement was increased close to the inhalation phase, with both AP and SI movement around the diaphragm. The GTV-COM displacement average in ten patients was 0.3 mm (max, 1.8 mm) in the left side, 2.2 mm (max, 5.3 mm) in the right side, 4.6 mm (max, 10.8 mm) in the anterior side, 0.1 mm (max, 0.3 mm) in the posterior side, and 11.6 mm (max, 17.4 mm) in the inferior side. No displacement was observed on the superior side.

For lung cases, a total of 14 lung cancer patients participated in the 4DCT immobilization study (supine position only). Although most tumors moved in a varying orbit during the respiratory cycle, showing hysteresis-like behavior, some moved in a closely similar orbit (Fig. 9.2). Therefore, it is important to evaluate tumor motion in 3D axis. The average GTV-COM displacement relative to that at peak exhalation was 1.4 mm (range 0.5–2.3 mm) in the left–right, 2.2 mm (range 0.8–4.7 mm) in the anterior–posterior, and 6.6 mm (range 1.6–21.8 mm) in the superior–inferior direction (3).

Twenty inpatients exhibited prostate displacement as a function of respiratory phase. Less than 1 mm of prostate COM moved in the superior, inferior, and posterior directions mainly due to intrafractional respiratory motion [3]. Therefore, we did not perform the gated prostate treatment. We have not yet compared prostate movements with and without immobilization, although these small displacements might be affected by immobilizing the patients as seen in the lung cases [4].

In clinical situations, it takes several minutes to complete treatment beam irradiation per fraction using the respiratory-gated strategy. Triple-phase dynamic enhancement CT acquisitions were routinely acquired for diagnostic purposes under inhalation breath-holding. The CT scan interval time of the venous phase and delayed phase from the arterial phase were 35 and 145 s, respectively. We defined the arterial phase CT data (scan interval time 0 s) as a treatment planning CT and calculated the compensating bolus, which was then applied to the CT data sets at the other two phases. Since the bolus was designed to cover the CTV at the planning CT, over 95 % of the dose was delivered to the CTV at 0 s. Although anatomical positions at each phase were similar, beam overshoot/undershoot was observed at 35 and 145 s due to extension/shortening of the radiological path length from the anterior and left directions against the planning CT. Since gas bubbles in the bowel may degrade dose conformation to the target, methods to appropriately deal with this issue are required (Fig. 9.3).

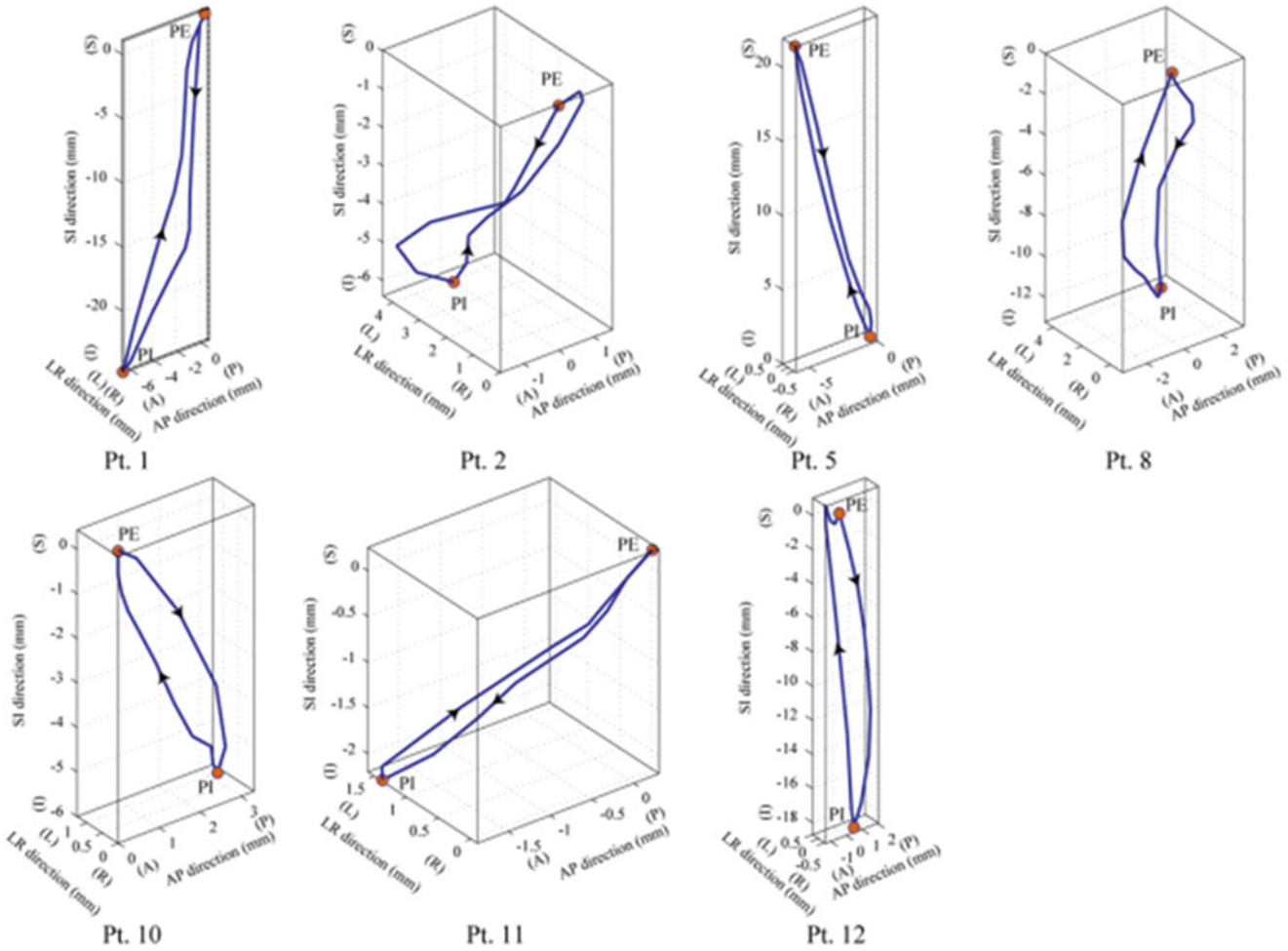

Fig. 9.2 3D visualization of tumor isocenter displacement for the right lung. Respiratory cycle and distance between PE and PI are shown in parentheses [5]. By permission of Elsevier

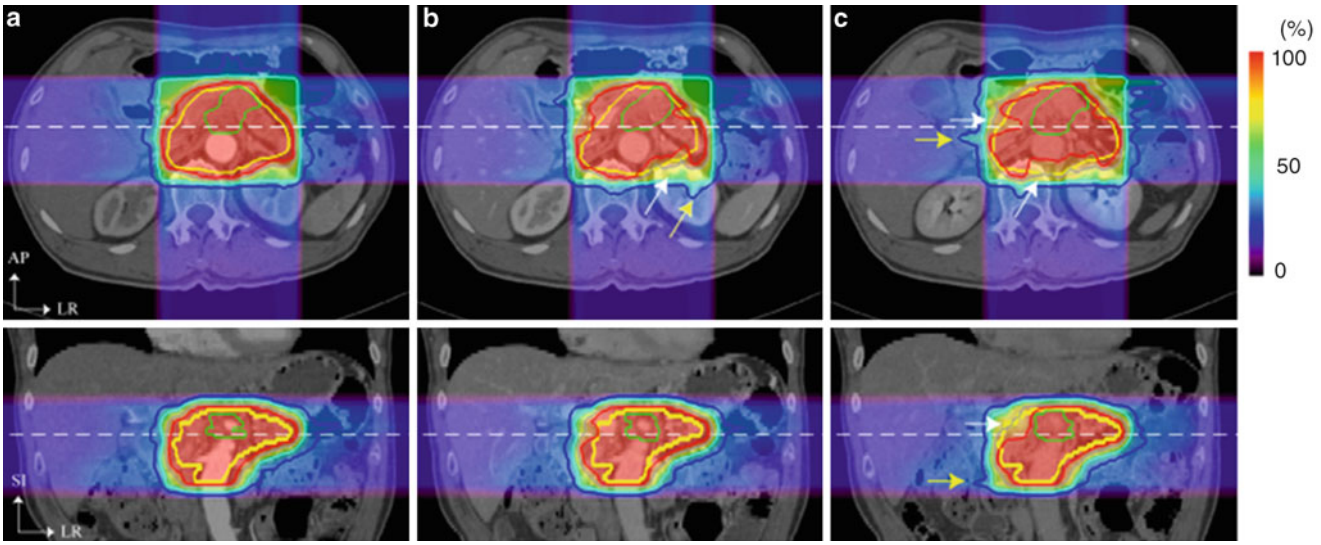

Fig. 9.3 Carbon ion beam distribution in axial and coronal sections (patient no. 1). Time of (**a**) 0 s (planning CT), (**b**) 35 s, and (**c**) 145 s. Beam overshoot (*yellow arrows*) and undershoot (*white arrows*) were observed at the scan interval time of 35 and 145 s. *Green* and *yellow lines* show GTV and CTV contours, respectively. *Red*, *pink*, *light-blue*, and *blue lines* show 95, 80, 50, and 30 % of doses, respectively [6]. By permission of Elsevier

9.2 Treatment Planning

A respiratory-gated CT scan was developed to minimize geometrical errors due to respiratory motion in the treatment planning stage. It acquires at the most reproducible respiratory phase only (in general, this is at peak exhalation) using respiratory monitoring system (details are described later) (Fig. 9.4a). When a quality of the gated-CT image was degraded due to irregular respiratory pattern at the couch position, gated CT was retried to acquire at the same couch position.

Routine with our lung treatment protocol, the prescribed dose is administered to the target via four different beam angles from the isolateral rather than the contralateral side of the tumor using orthogonal beam ports by rotating the treatment couch in ±20° (left and middle panels in Fig. 9.4b). Immobilization devices could minimize patient positional errors, albeit that, patient positions in +20° rotation and in −20° rotation were not same (right panel in Fig. 9.4b). Therefore, treatment planning was performed using two CT data sets, respectively; beam numbers 1/2 and 3/4 were using −20° and +20° rotation, respectively.

The treatment beam is on around exhalation in the gated Rx, but the temporal instant of the gated CT includes only peak exhalation. Gated CT and gated Rx, therefore, are not exactly the same temporal instant. A treatment planning system defines the optimum beam parameters for imported CT data, which is at peak exhalation in here. Even when gated Rx is applied, intrafractional motion may not be mitigated completely; therefore, it is questionable that these beam parameters can be adapted to the 30 % duty cycle ("gating window").

To solve this problem, an internal margin is added to the target in gated CT, and an ITV is defined. Now, 4DCT has become commercially available, which obtains 3D data at each respiratory phase and which allows the incorporation of organ motion. However, a 4DCT scan method was not yet available when gated Rx was started in the 1900s, so our group developed an algorithm for design bolus using gated-CT data to be compensating residual motion in gating window as the following.

Planning target volume (PTV) was calculated by a 5 mm shift of clinical target volume (CTV) on the superior and inferior sides (Fig. 9.5a). This shift value includes intrafractional respiratory motion within the gating window and interfractional change from our clinical experiences. PTV is

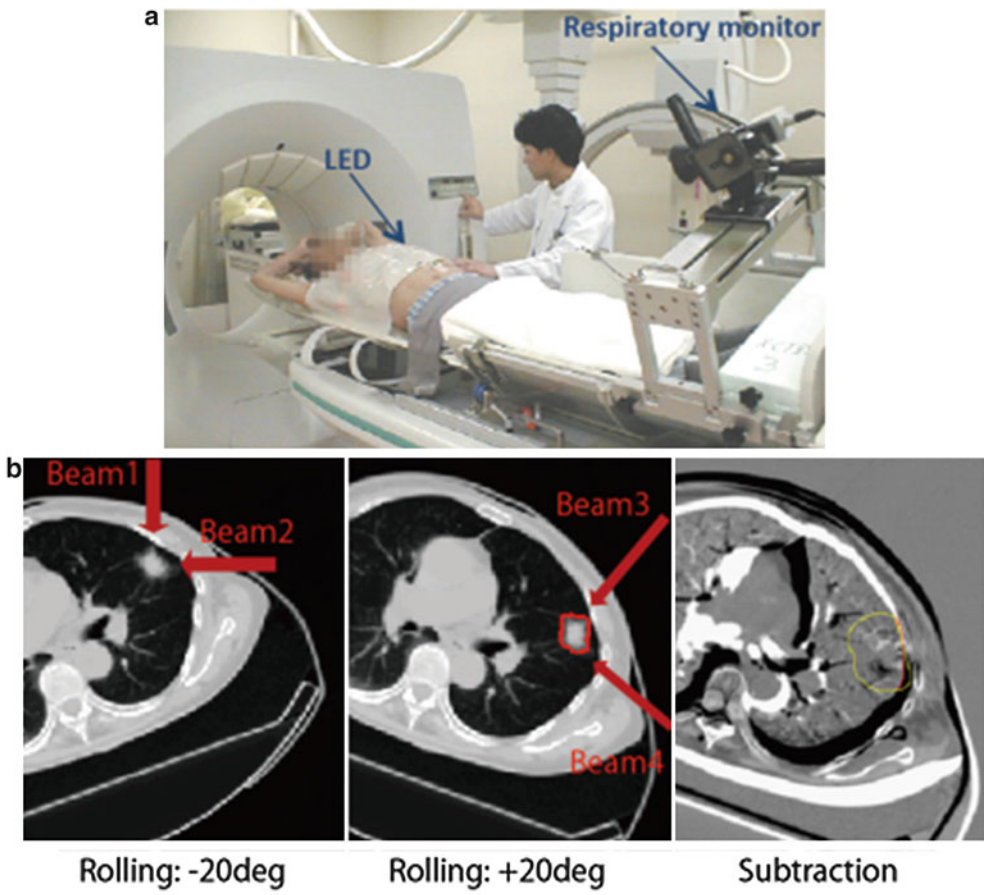

Fig. 9.4 (**a**) Respiratory correlated CT scan. (**b**) *Left* and *middle panels*: Axial CT images with the rotation of +20°/−20°. *Right panel*: Subtracted image using *left* and *middle panels* by registered by tumor position

calculated by maximum intensity projection by way of these three CTVs (Fig. 9.5b). Most treatment planning systems do not display any beam overshoot resulting from a moving target, even though the particle beam stopping position varies. Since our treatment planning strategy does not use the actual target, but rather an image-processed target, any beam overshoot resulting from the image-processed target is seen (Fig. 9.5d). We review dose distribution close to the actual situation by adapting the treatment planning parameters to the original CT (Fig. 9.5c).

9.3 Positioning and Verification

Precise patient positioning is an important aspect of treatment beam delivery since the potential benefits of high-precision particle therapy can only be achieved if the patient is precisely positioning in the treatment beam according to the coordinates determined by the treatment planning. By doing this, treatment beam can be delivered to the tumor and minimize excessive dose to the healthy tissue as little as possible. This challenge can be seen in both photon and particle therapies. Since charged particle beam relates to the finite penetration range and sensitivity to tissue density variations along a given ray rather than photon beam, positional changes in the particle beam therapy are strongly affected by variations in the radiological path length in the beam direction [7]. A positional change of 1.0 cm in water causes a 3 % dose difference in photon beams versus a 90 % difference on proton beams at the distal falloff position (Fig. 9.6).

To maintain the dose conformity over a treatment course, misalignment of the patient's body is typically constrained by immobilization equipment customized to the patient. Since our center uses orthogonal fixed irradiation ports, the

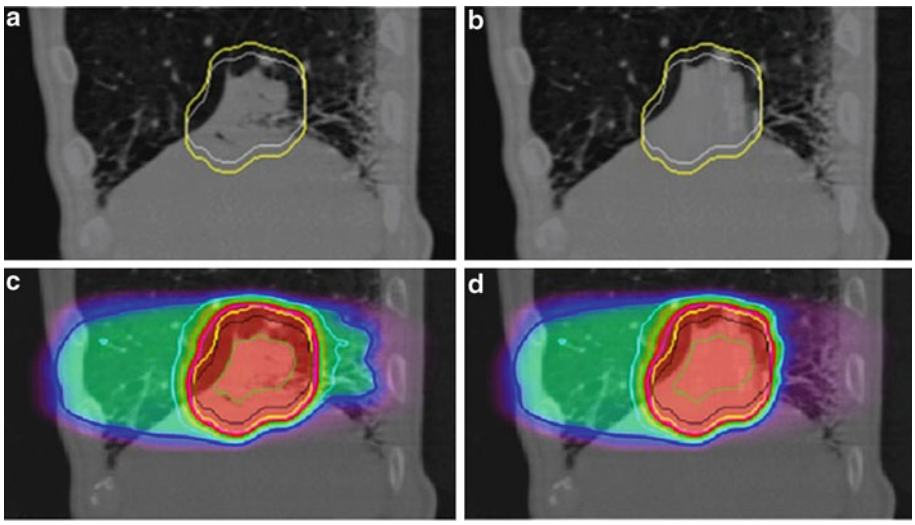

Fig. 9.5 (**a**) Original CT image at peak exhalation. (**b**) Image-processed CT image. *White* and *yellow lines* show CTV and PTV, respectively. (**c**) Dose distribution using original CT image. (**d**) Dose distribution using image-processed CT image

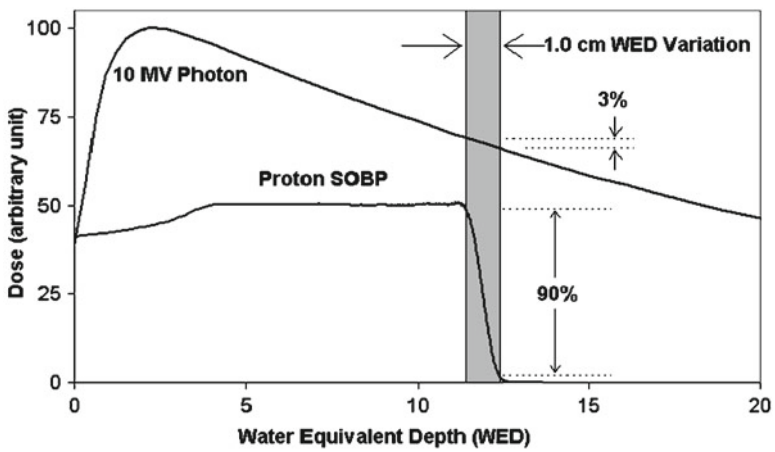

Fig. 9.6 Depth–dose curves for photon and proton beams (from Hsiao-Ming Lu, PhD, at MGH, the World Congress of Medical Physics in Seoul, 2006, with permission)

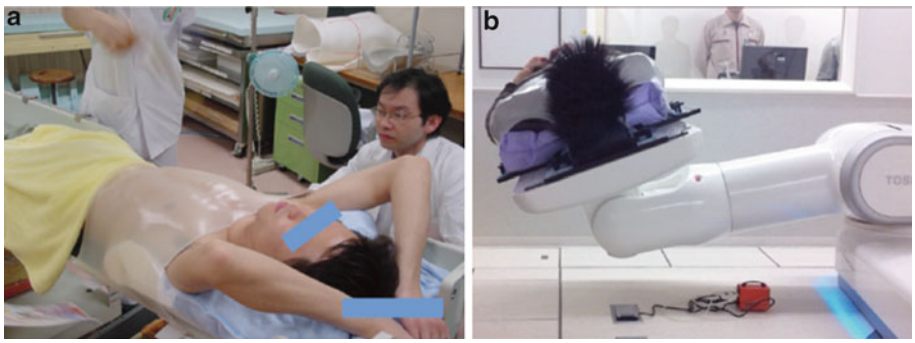

Fig. 9.7 (**a**) Example of immobilization for lung treatment using a hydraulic urethane resin cushion and low-temperature thermoplastic shell. (**b**) Rotational movement in lung treatment

treatment couch can be rotated to allow a greater range of beam angles (approximately ±20° roll at a maximum); immobilization is done with a relatively thicker shell (3 mm thickness) made of a low-temperature thermoplastic and hydraulic urethane resin (Fig. 9.7).

With regard to the patient positional verification, orthogonal (vertical and horizontal directions) X-ray imaging systems with 17 in. flat panel detectors (FPDs) were installed in the treatment room. The verification software (ITG: I-Ti-Gime) includes two functions, namely, 2D–2D manual registration and 2D–3D auto-registration. For 2D–2D registration function, a separate manual registration using point match strategy is not correctly registered because the respective image plane resulted in three parameters. The 2D–3D auto-registration is performed using orthogonal FPD images and the planning 3DCT data set. This algorithm registers digital reconstructed radiography (DRR) images projected by the 3DCT data to the acquired horizontal/vertical FPD images and derives 6° of freedom positional error values. The 2D–3D auto-registration uses graphics processing unit (GPU) computation as a parallel computational architecture to accelerate computation time while maintaining calculation accuracy.

After the patient entered the treatment room and was transferred to the isocenter automatically by the treatment bed, orthogonal FPD images were acquired and imported into the patient setup software. When respiratory gating treatment was selected, FPD images were acquired automatically by a signal around exhalation from respiratory monitoring system. Therapists started the 2D–3D auto-registration function and/or manual registration and obtained the corrected treatment bed position (three translations and three rotations) (Fig. 9.8). Orthogonal FPD images were again acquired and these FPD images and the reference FPD images were compared by visual inspection. These processes were repeated until the therapists and oncologists were satisfied with the patient positional accuracy compared with the reference images. Residual errors in translation and rotation were achieved less than 0.5 mm/0.2° in our clinical experiences [8].

9.4 Gated Irradiation

In our center, respiratory-gated irradiation is performed in 40–50 % of all patients: for lung, liver, bone and soft tissue sarcomas (partially), rectum, and pancreas. Gated irradiation in the treatment involves the synchronization of irradiation with a gating signal, generally obtained by observing the patient's respiration (Fig. 9.9). Synchronization means that the beam is only turned on if the motion is within a gating window. Depending on the duty cycle, gating significantly prolongs the treatment but minimizes the effect of residual organ motion during the irradiation to an acceptable level. In our center, the gating window is on average defined by a 30 % peri-exhalation duty cycle, since exhalation is the most reproducible respiratory state.

Gating irradiation faces several technical challenges, especially in the delay times between the actual motion and creation of the gating signal obtained by the respiratory monitoring system. There are two kinds of external respiratory monitoring systems: one uses tagging points with artificial marker that reflects and the other one that emits light. The first (light reflecting) type is called the "passive," and the latter (light emitting) type, the "active" version. The former type is widely used in treatment centers and consists of a charge-coupled-device (CCD) camera with an attached infrared illuminator. The process of generating software images results in a ~100 ms delay for output of gating signals, using ~30 Hz acquisition video image. This delay time might cause irradiating errors to the target in the respiratory-gated treatment mode. To achieve more accurate gate timing, we routinely use the "active" sensing system, which consists of a position-sensitive detector (PSD) sensor and an infrared-emitting light marker. For generating a 5 kHz sampling rate using

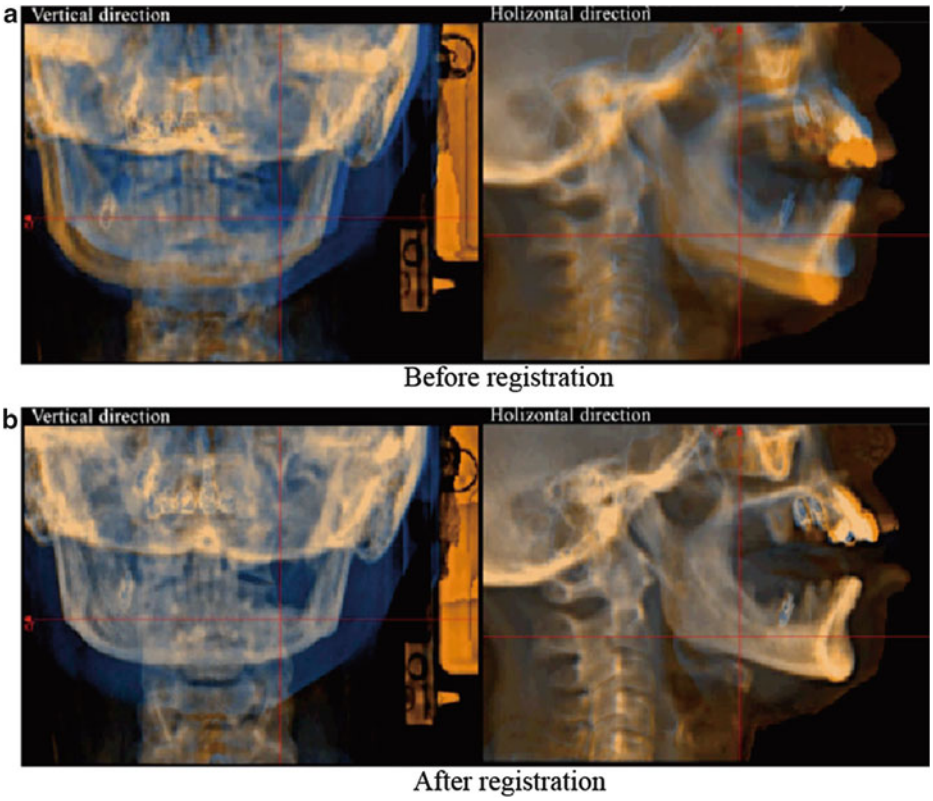

Fig. 9.8 FPD images (*blue layer*) overlaid on DRR images (*orange layer*) (**a**) before registration and (**b**) after registration

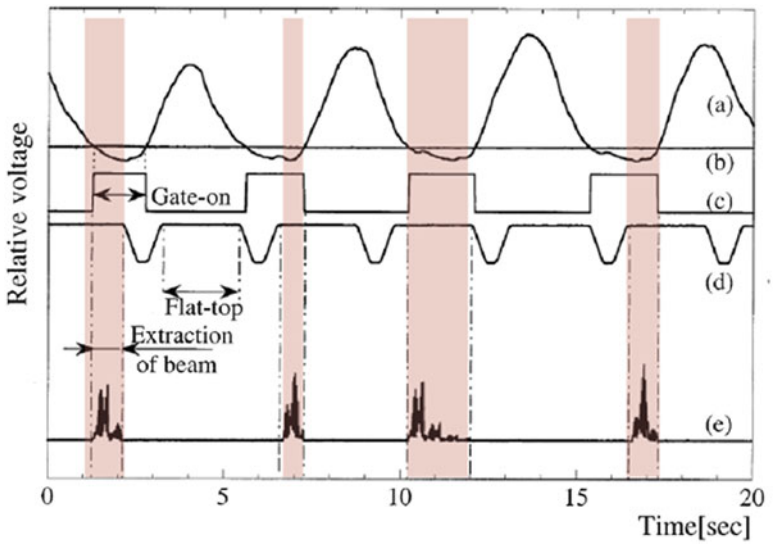

Fig. 9.9 Timing chart of gated irradiation, displayed as a function of relative voltage of the various data acquisition systems versus time in the passive beam treatment

field-programmable gate array (FPGA) processer, a ~30 ms delay is required to send the gating signals.

Only if the gating window and synchrotron pulse coincide, particles are extracted; however, since duty cycle of the beam extraction from the synchrotron is approximately 3.3 s, the treatment beam is not always giving in full gating window (Fig. 9.9). To apply the gating irradiation in the scanning irradiation with phase control rescannings, we have developed the synchrotron with a slow-extraction method [9].

While given that patient respiratory pattern is not always reproducible, when the respiratory curve varied during a treatment, the therapist manually adjusted the gating window to

maintain the original duty cycle. In this procedure, it is assumed that the discrepancy between the external surrogate motion and the internal tumor motion is small enough to be compensated for by the margin in the planning target volume.

References

1. Mori S, Zenklusen S, Knopf AC. Current status and future prospects of multi-dimensional image-guided particle therapy. Radiol Phys Technol. 2013;6(2):249–72.
2. Mori S, Hara R, Yanagi T, et al. Four-dimensional measurement of intrafractional respiratory motion of pancreatic tumors using a 256 multi-slice CT scanner. Radiother Oncol. 2009;92:231–7.
3. Kumagai M, Okada T, Mori S, et al. Evaluation of the dose variation for prostate heavy charged particle therapy using four-dimensional computed tomography. J Radiat Res. 2013;54(2):357–66.
4. Dobashi S, Sugane T, Mori S, et al. Intrafractional respiratory motion for charged particle lung therapy with immobilization assessed by four-dimensional computed tomography. J Radiat Res. 2011; 52:96–102.
5. Mori S, Endo M, Komatsu S, et al. Four-dimensional measurement of lung tumor displacement using 256-multi-slice CT-scanner. Lung Cancer. 2007;56:59–67.
6. Kumagai M, Hara R, Mori S, et al. Impact of intrafractional bowel gas movement on carbon ion beam dose distribution in pancreatic radiotherapy. Int J Radiat Oncol Biol Phys. 2009;73:1276–81.
7. Goitein M. What is difference about particle treatment planning? [Abst] Particle Therapy Co-Operative Group (PTCOG45); PTCOG45; 2006.
8. Mori S, Shibayama K, Tanimoto K, et al. First clinical experience in carbon ion scanning beam therapy: retrospective analysis of patient positional accuracy. J Radiat Res. 2012;53:760–8.
9. Mizushima K, Sato S, Shirai T, et al. Development of beam current control system in RF-knockout slow extraction. Nucl Instrum Meth B. 2011;269:2915–8.

Quality Assurance

10

Takuji Furukawa and Shinichiro Mori

Abstract

To ensure the quality of treatment, intensive quality assurance (QA) program should be performed. In this chapter, the QA for the ion therapy system with an example of HIMAC facility is briefly introduced.

Keywords

Dosimetry • Imaging system • Positional accuracy • Quality assurance

10.1 Beam Delivery System and Dosimetric QA

In order to ensure the quality of the therapeutic irradiation, periodic QA checks for the beam delivery system are required. Practical implementation of a QA program depends on the detail of the beam delivery. In both deliveries of passive and scanning, the monitor calibration is performed on a daily basis at many facilities. However, the recommended method defers between passive and scanning delivery, as shown in Fig. 10.1. An ionization chamber is set to the isocenter within a phantom. Instead of water, it is useful to use solid water. For monitor calibration, the reference field is irradiated and measured. For the passive delivery, it is recommended to measure in water in the center of an SOBP as the reference condition. On the other hand, for the scanning delivery, measurements in a plastic material in the entrance region of the depth-dose are recommended as a reference. Further, the verification of the beam range is performed on a daily basis at many facilities. Figure 10.2 shows the example of the daily QA for the NIRS scanning system. Additional check of depth and lateral dose profiles is also recommended. On the other hand, weekly and monthly QA should be programmed considering the constancy and configuration of the system.

The beam delivery system and its treatment planning system (TPS) require dosimetric patient-specific QA to check each individual plan and its delivery. The patient-specific QA is usually performed before therapeutic irradiation as the following steps. Schematic of patient-specific QA workflow is shown in Fig. 10.3. After the treatment planning, the dose distribution is measured using ionization chambers set in a water phantom. In the measurement, the irradiation sequence is performed using the same control-point sequence as for the patient treatment. The measured dose profiles are then compared with the dose distribution recalculated by the TPS using a homogeneous medium instead of the patient CT data. In this way, the quality of the field is checked. Such dosimetric verification is important especially for the scanning delivery, considering the fact that the dose conformation is performed by magnetically scanning the raw beam from the accelerator. Furthermore, each treatment plan is individual. Thus, the delivered field should be checked on the basis of the measured dose profiles. On the other hand, in the passive delivery, it is necessary to calibrate dose per monitor unit (Gy/MU) for each irradiation field. Further, the checks of patient-specific devices such as aperture and compensator/bolus are also required in the passive delivery. This check can be performed by measuring each device and comparing with the design.

The following describes the patient-specific QA program for the NIRS scanning delivery. In the patient-specific QA, a

T. Furukawa (✉) • S. Mori
National Institute of Radiological Sciences,
9-1, Anagawa-4, Inage-ku, Chiba 263-8555, Japan
e-mail: t_furu@nirs.go.jp; shinshin@nirs.go.jp

H. Tsujii et al. (eds.), *Carbon-Ion Radiotherapy: Principles, Practices, and Treatment Planning*,
DOI 10.1007/978-4-431-54457-9_10, © Springer Japan 2014

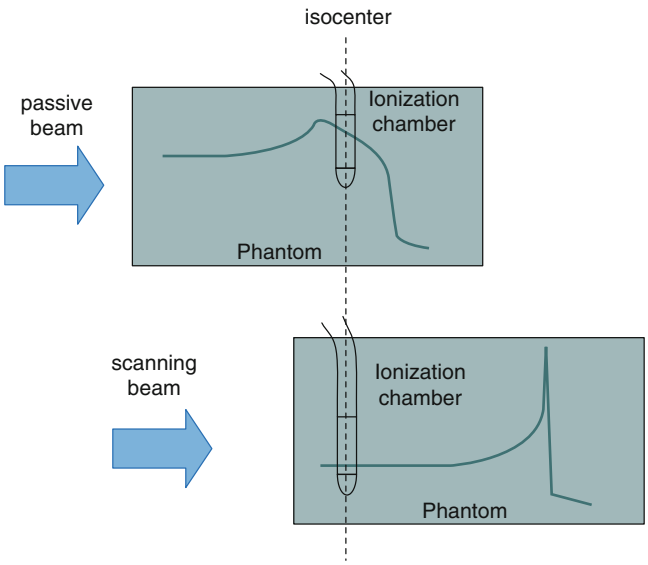

Fig. 10.1 Difference of reference condition for the monitor calibration between passive and scanning delivery

commercial 2D ionization chamber array (OCTAVIUS Detector 729 XDR, PTW Freiburg, Germany) is employed for the dose distribution measurement cooperating with an accordion-type water phantom. The water-equivalent depth can be changed from 30 to 300 mm. Owing to sealed water tank, this phantom can be used as both horizontal and vertical beams by rotating water tank. Before the QA measurement, the predose of around 5 Gy are applied for warm-up of the detector. In the measurement, the irradiation sequence is performed using the same control-point sequence as for the patient treatment. The measurements of each beam are performed for three different depths, which are predetermined in the treatment planning. The measured dose distributions are then compared with the dose distribution recalculated by the TPS using a homogeneous medium instead of the patient CT data. For the comparison, the gamma index analysis is performed by using the commercial software, Verisoft (PTW Freiburg, Germany). A typical result of comparison between the measured distribution and the recalculated one is shown in Fig. 10.4. In the analysis, distance to agreement of 3 mm and dose difference of 3 % are employed as accepted deviation. This tolerance is widely used at many facilities.

10.2 Patient Support System and Imaging System QA

Patient positioning (geometrical/position accuracy including motion management) is one of the major important factors to improve treatment accuracy as described in Chap. 9 (motion management). To quantify positional accuracy throughout the treatment course, we use an imaging system (X-ray flat panel detector (FPD) (CXDI55C, Canon, Tokyo, Japan, DAR8000f, Shimadzu Cop. Kyoto, Japan, and PaxScan 3030+, Varian Medical Systems, Palo Alto, CA) and computed tomography (CT) (LightSpeed 16-slice QX/i, General Electric Company, Waukesha, WI; Aquilion LB, Toshiba Medical Systems, Otawara, Japan; and Aquilion One Vision, Toshiba Medical Systems, Otawara, Japan) and patient support system (6° of freedom treatment bed (Escort, Toshiba, Tokyo, Japan)) and room laser (LSP-1170A, Takenaka Optonic Co., LTD, Kyoto, Japan)) (Fig. 10.5).

Positional accuracy for the orthogonal X-ray imaging system, CT scanner, treatment bed, and room lasers are confirmed using the QA phantom, which is an acrylic hollow box (220-mm square length, 10 mm thickness) with ten stainless steel beads (2-mm diameter) set on the phantom plane (Fig. 10.7a). Small bead positions are optimized to detect QA phantom pose (position and angle) correctly. Also 0.2-mm-diameter stainless steel wires are embedded in cross on every QA phantom plane. This QA phantom was used for the imaging system, patient support system, and beam delivery system (Fig. 10.6b). By doing so, all treatment systems can adjust their positions to the same reference position (room isocenter).

At the commissioning stage, the QA phantom was placed on the QA stand, and positional accuracy was adjusted to the room coordinate using two transits. Orthogonal FPD positions were also adjusted in the same way. And then, X-ray tube position was adjusted to overlap cross centerline wires on the QA phantom planes along the X-ray direction using FPD images. To do so, X-ray tube and FPDs positions are satisfactorily adjusted to the room coordinate within the 0.2-mm positional accuracy. After commissioning, orthogonal X-ray images for reference images were acquired (Fig. 10.6a).

The QA for the imaging system was done every month using the QA phantom on the QA stand. For the daily QA, in contrast, the QA phantom is placed on the treatment table (Fig. 10.7c), and orthogonal X-ray images are acquired. After these X-ray images are imported into the QA software, the QA phantom pose is calculated by analyzing small bead positions and comparing them to those of the reference images.

For the treatment bed QA, we used FPD imaging system instead of the laser tracker. The treatment bed was moved to predefined positions (monthly QA) and isocenter position only (daily QA) with the QA phantom, which was set on the treatment bed. Orthogonal FPD images are acquired and imported to the QA software; it calculated treatment bed pose. Acceptable level is absolute and relative positional accuracies are within the range of a sphere of 0.5- and 0.3-mm diameter, respectively. We also checked the safety

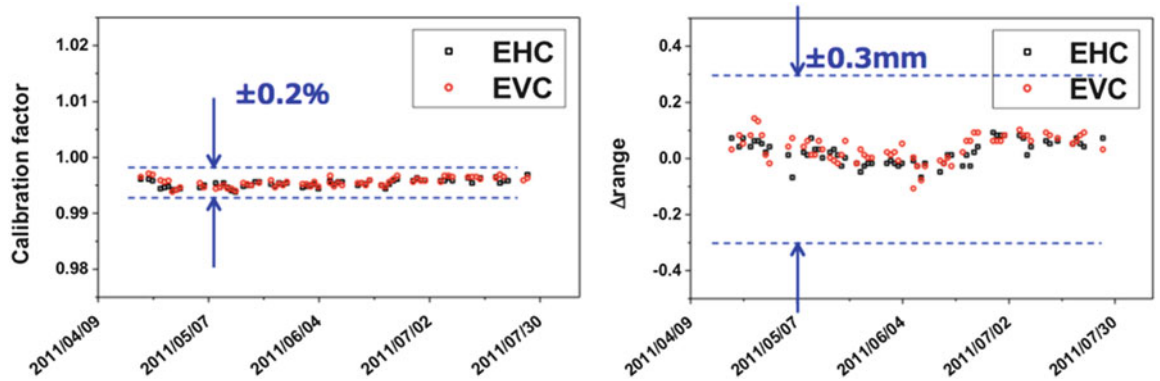

Fig. 10.2 Example of the daily QA for the NIRS scanning system

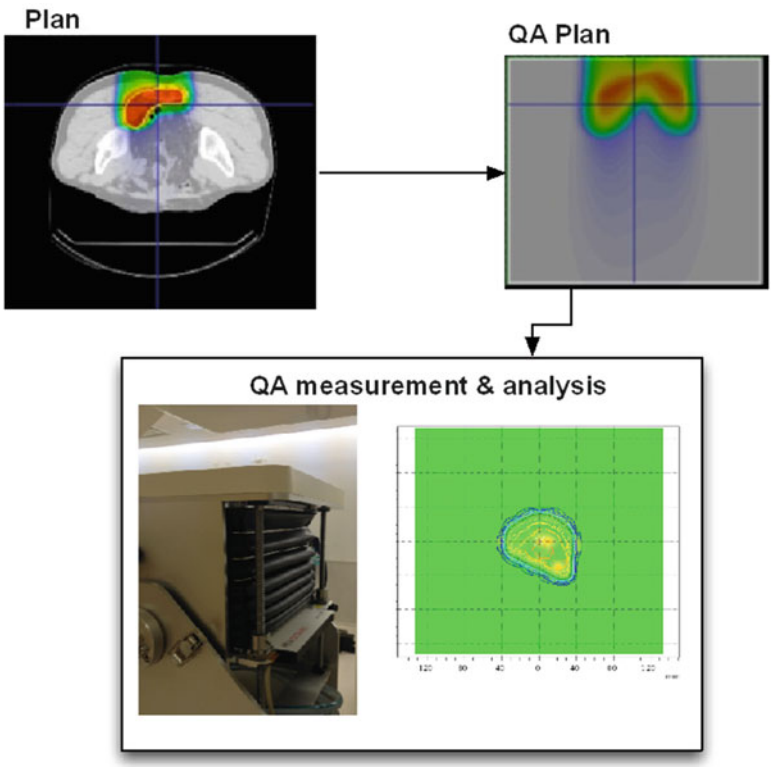

Fig. 10.3 Schematic of patient-specific QA workflow

function every month to void conflicting to the room wall or medical staff.

With regard to the CT, image quality and positional accuracy were evaluated. Image quality metrics were image noise, CT-number uniformity, and CT-number accuracy using the water phantom including several materials, which is provided from CT manufacture. Positional accuracy metric was scan position accuracy using the QA phantom, especially in the CT on rail that we used. All CT-QA items were analyzed by QA software automatically (Fig. 10.8).

For laser equipment (room laser and CT laser), several lasers are installed within the wall and provide lighting through laser slits. Positional accuracy is checked by observing the laser position and QA phantom cross centerlines on the phantom plates (Fig. 10.9).

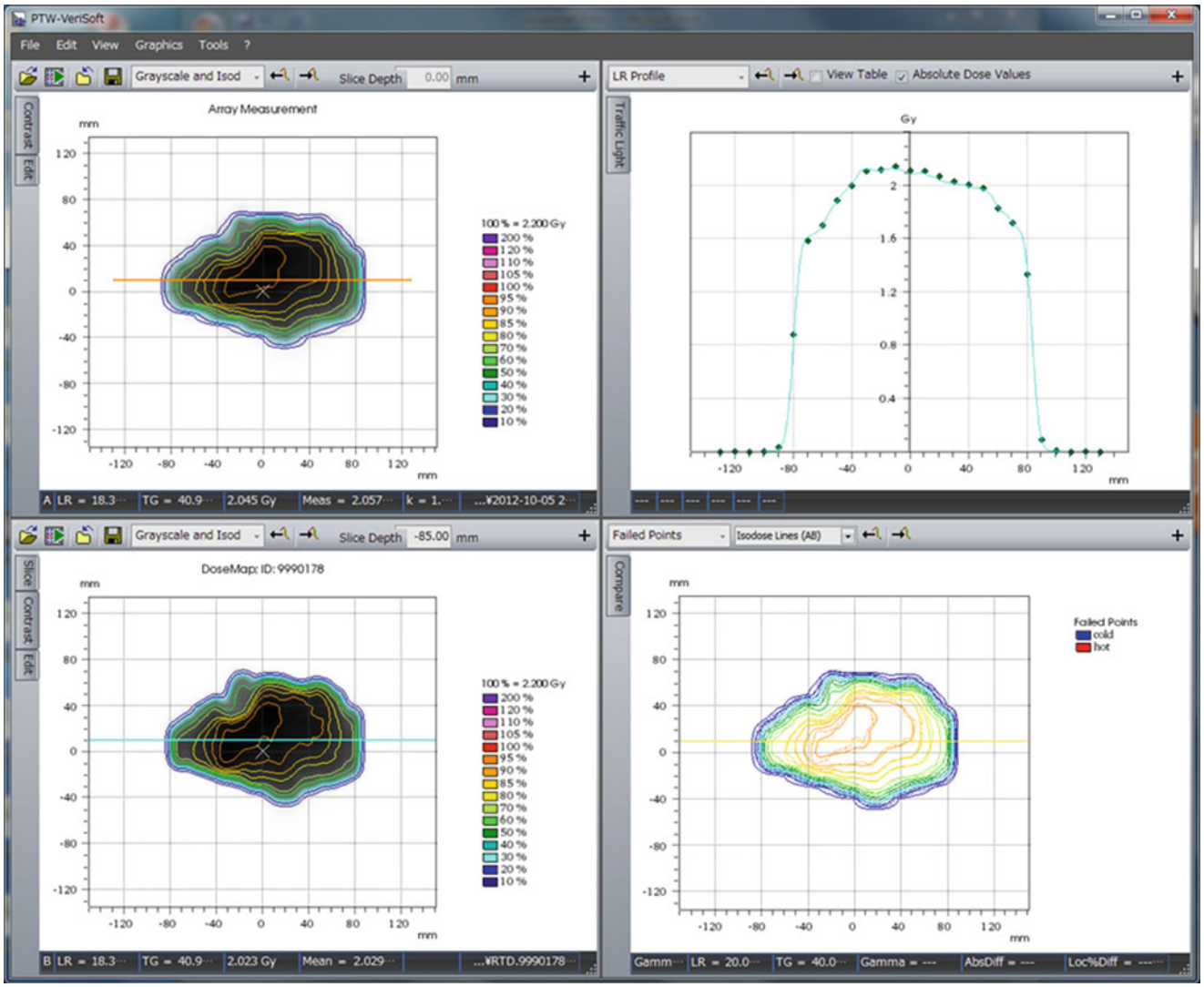

Fig. 10.4 Example of comparison between QA plan and measurement

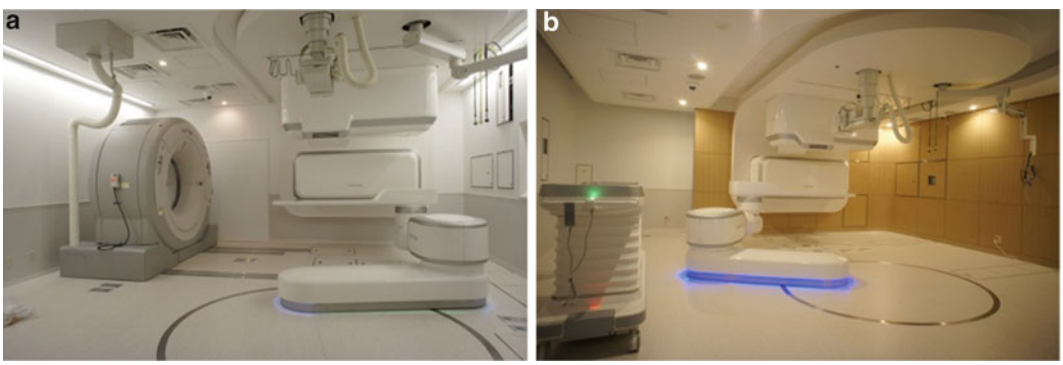

Fig. 10.5 (**a**) Simulation room. (**b**) Treatment room

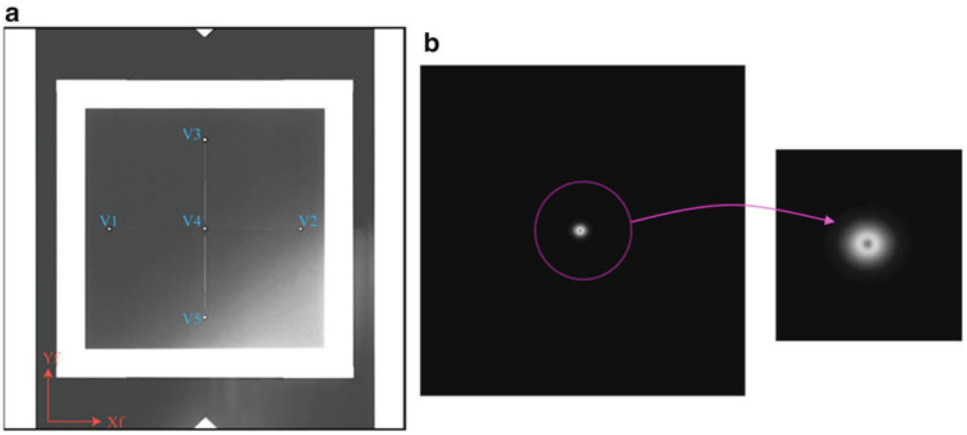

Fig. 10.6 (**a**) QA phantom X-ray image in the vertical direction. *Blue points* (V1–V5) are small beads positioned on the QA phantom vertical planes. (**b**) QA phantom image acquired bead number 4 by carbon-ion pencil beam

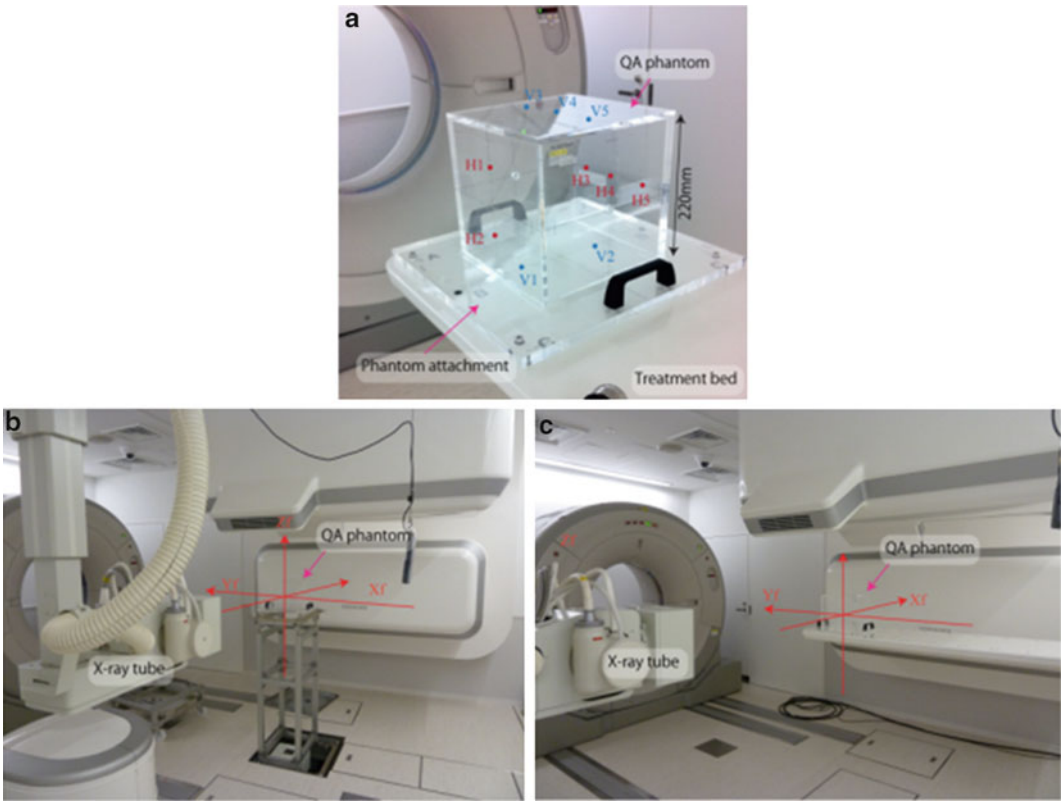

Fig. 10.7 (**a**) QA phantom and phantom attachment. The *blue* (V1–V5) and *red points* (H1–H5) are small beads on the vertical and horizontal planes. (**b**) QA phantom on the QA stand and (**c**) on the treatment bed

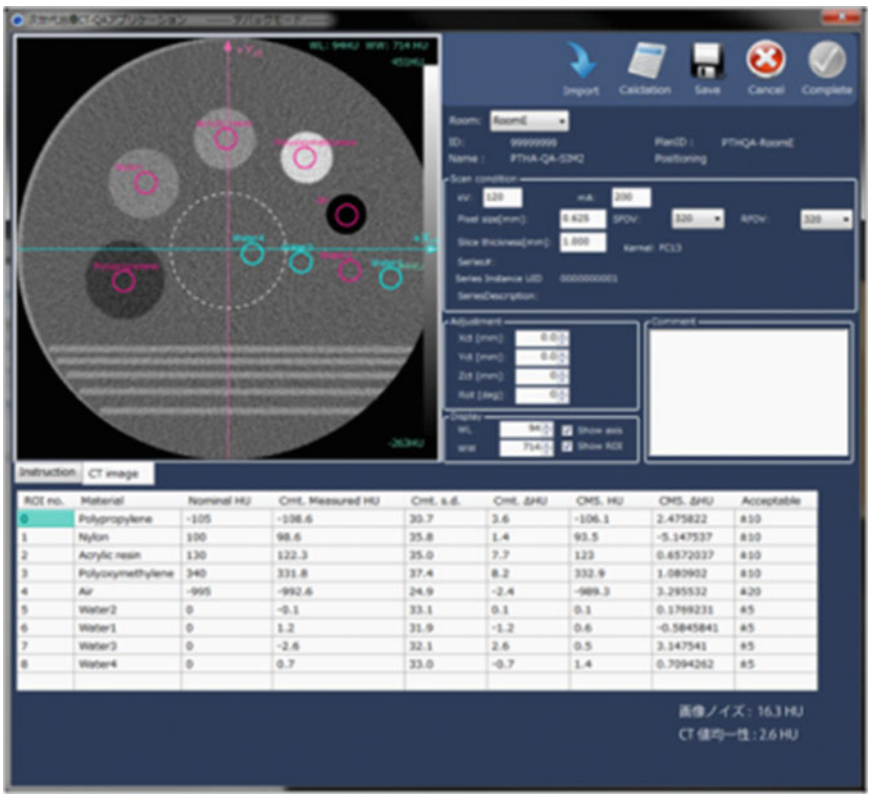

Fig. 10.8 QA software for CT image quality. After importing CT images, the CT-QA software automatically evaluates CT image quality

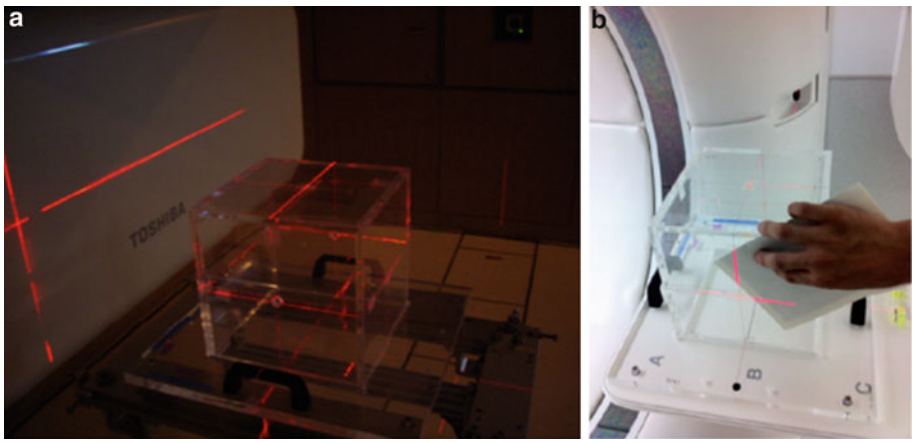

Fig. 10.9 (**a**) Room laser QA. The QA phantom was set on the QA stand. (**b**) CT laser QA. The QA phantom was set on the treatment bed

Part V

Treatment Planning of Carbon-Ion Radiotherapy

Treatment Planning of Carbon-Ion Radiotherapy

11

Nobuyuki Kanematsu and Taku Inaniwa

Abstract

Treatment planning of carbon-ion radiotherapy (C-ion RT) should best use the physical and biological advantages of the radiation, which is heavily coupled to the beam delivery system. In this section, overview of conventional system for broad-beam delivery, which has been used for many years, and a state-of-the-art system for pencil-beam scanning are described in addition to general aspects to plan a treatment of carbon-ion radiotherapy. Finally, we demonstrate the comparison between broad- and scanning-beam plans for a few cases.

Keywords

Broad beam • Dose calculation • Plan optimization • Scanning beam

11.1 Introduction

Treatment planning is a process to design radiation beams to achieve the optimum balance between dose conformation to a target and sparing of normal tissues and to evaluate the resultant dose to the patient. In this regard, treatment planning of C-ion RT is not at all different from treatment planning of other radiotherapy modalities. There are of course intrinsically distinctive features in carbon-ion radiotherapy, which must be best used for cancer treatment.

11.1.1 Physical Properties of Carbon Ions

Carbon ion and proton are heavy charged particles that are currently used for radiotherapy. A most favorable feature of these particles is formation of a Bragg peak dose at a certain depth of penetration, which can be placed to a tumor by adjusting the incident energy. A fully stripped carbon ion (or atomic nucleus) is a composite of six protons and six neutrons. Compared to a proton, its electric charge is a factor of 6 larger and its mass is approximately a factor of 12 larger. This makes differences to radiological properties between carbon-ion and proton beams:

- A carbon ion has 36 times higher LET for the same speed and 12 times more kinetic energy, resulting in reduced range to 1/3.
- Higher speed is thus required to achieve the same range, which makes carbon ion more rigid in addition to halved charge/mass ratio, resulting in reduced scattering to 28 % for the same range.
- Due to its larger size, loss of carbon ions by nuclear interactions is a few times larger than that of protons. About a half of carbon ions may be lost in 20 cm of penetration in water.
- The nuclear interactions may cause fragmentation of the nucleus into lighter nuclei, resulting unwanted fragmentation tail after the Bragg peak.

The reduced scattering, namely, sharper penumbra, is usually an advantage in radiation therapy, while increased nuclear interactions, namely, reduced Bragg peak, are clearly a disadvantage.

N. Kanematsu (✉) • T. Inaniwa
National Institute of Radiological Sciences, 9-1, Anagawa-4, Inage-ku, Chiba 263-8555, Japan
e-mail: nkanemat@nirs.go.jp; taku@nirs.go.jp

H. Tsujii et al. (eds.), *Carbon-Ion Radiotherapy: Principles, Practices, and Treatment Planning*,
DOI 10.1007/978-4-431-54457-9_11,

11.1.2 Radiobiological Modeling

In radiation biology, relative biological effectiveness (RBE) is defined as the ratio of a reference-radiation dose to an interest-radiation dose for the same biological endpoint under the same condition other than the radiation quality. For therapeutic applications, the RBE naturally depends on fraction dose size and clinical endpoint, which vary with tumor type, tumor site, and treatment intent. In addition, as the radiation quality of a carbon-ion beam varies with incident energy, range modulation, and penetration depth, the RBE varies in patient body within each single beam. Generally the RBE increases with depth in the spread-out Bragg peak (SOBP) region.

Because all these complex dependences of the RBE have not been accurately known, the RBE used in treatment planning (clinical RBE) may be only considered as assumption rather than estimation. Unlike estimation, to which uncertainty must always be associated, an unambiguously defined clinical RBE is used for the RBE-weighted absorbed dose to water to evaluate the clinically relevant dose. Unless otherwise specified, "dose" in treatment planning of C-ion RT refers to the RBE-weighted absorbed dose to water.

For photon beams, for example, absorbed dose to water in units of Gy is used for prescription although there is always variation in responsiveness of the tumor to the dose, which may vary significantly due to unknown or uncontrollable factors in clinical environment. In other words, the photon beam dose, against which the RBE is normally referenced, has intrinsic limitation for clinical relevance. It would be therefore a reasonable approach to consider the clinical dose as proper to carbon-ion beams and optimize its prescription in clinical studies systematically without relating to photon experiences. From a practical point of view, the precision of prescribed dose should be controlled within a few percent for clinical studies.

An important requirement for the clinical RBE is clarity in definition. NIRS chose to use 10 % cell survival of human salivary gland cells as the biological endpoint with rescaling for continuation of fast-neutron radiotherapy experiences. This clinical RBE has been mathematically defined and in fact has been used consistently in the NIRS, Hyogo Ion Beam Medical Center, and Gunma University for uniform dose prescription among these institutions. The clinical dose is the only quantity that the radiation oncologist may need to evaluate to treat patients with carbon ions while the complexity originated from radiation biology is normally hidden in the treatment planning system.

11.2 General Aspects of Treatment Planning for Carbon-Ion Radiotherapy

11.2.1 Patient Position and Beam Direction

Arrangement of beams is one of the most critical decisions in treatment planning. In the common practice of C-ion RT with fixed beam lines, the beam directions are severely limited. Consequently, multiple patient positions, typically supine and prone, are required for treatment of a tumor. In fact, treatment couches with large rolling capability, typically up to 20°, have been also used in the HIMAC treatment rooms. While a treatment with multiple patient positions and multiple patient rolls may be a reasonable approach to substitute for a rotating gantry, it substantially complicates the treatment process with multiple plans.

11.2.2 Immobilization and Planning CT

Volumetric X-ray computed tomography (CT) image of a patient is the basis of computerized treatment planning. For the planning CT, the patient must be immobilized exactly in the treatment condition. Figure 11.1 demonstrates a scene of planning CT, where a patient was immobilized in tilted position and the scanning timing was synchronized to breathing using the same respiratory gating system used for treatment beam delivery.

11.2.3 ROI Delineation

Anatomical determination of target volumes and organs at risk is a critical oncologic task and the resultant regions of interest (ROI) are used to design and evaluate a plan. Because contrast agents cannot be used for planning CT to secure correct interpretation of the CT number, ROI delineation is often difficult. Contrast-enhanced X-ray CT and magnetic resonance imaging (MRI) may give high-contrast image of patient anatomy. Positron emission tomography (PET) gives metabolic image of tumor as shown in clinical examples in this book. These imaging modalities are thus useful for identification of gross tumor volume (GTV) on the planning CT image, for which advancement of image-processing technologies has enabled computerized image registration and fused display even in the presence of body deformation.

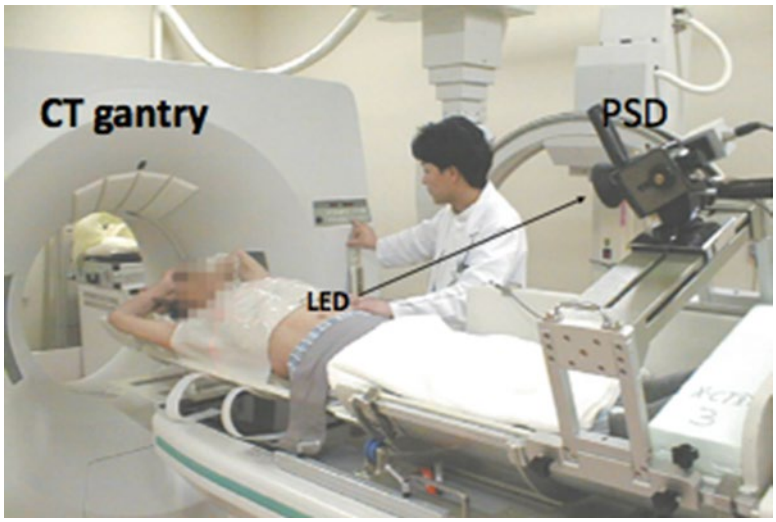

Fig. 11.1 Scene of planning CT for a patient in rolled treatment position with optical respiratory gating

To plan a beam for a tumor, a radiation oncologist first defines a clinical target volume (CTV) that includes the GTV and surrounding region of clinical margin for potential infiltration. The CTV is the volume to be treated in the planning CT. However, there are always differences between planning CT and treatment times due to physiological changes, organ motion, patient setup error, beam model error, etc. All these uncertainties must be considered at the time of planning. To treat the CTV with prescribed dose in reality, appropriate margins need to be added for a planning target volume (PTV), which is intended to receive the prescribed tumor dose in treatment planning. However, it is generally difficult to quantify these uncertainties. In the cases where the dominant uncertainties are expected in the clinical margins, the setup and internal margins may be disregarded. In such cases, the PTV may be defined as identical to the CTV.

Ideally, the margin against all uncertainties should be included in the PTV. Margin for setup error should expand the PTV in lateral direction while that for range error should expand the PTV in depth direction for each field. However, in common practice, the PTV is defined before the beams are set up, which makes it difficult to define field-specific PTV. Therefore, a common practice is to assign only minimum isotropic margin for PTV to account for the setup uncertainty, which is usually smaller than the range uncertainty. Therefore, the excess of the range uncertainty is usually considered by additional depth margin to cover the PTV with an SOBP of each beam.

11.2.4 Patient Modeling

As water is the reference material in radiation dosimetry, patients are modeled volumetrically as water of variable effective density (ED) to design beams and to calculate dose distributions. Precise beam-range control to cover the tumor site with SOBP is the essence of C-ion RT. For this purpose, the ED is defined by the stopping-power ratio of the tissue to water for carbon ions. In the planning CT, the CT number ideally represents the X-ray attenuation ratio of the body tissue to water. The conversion from CT number to ED is based on strong systematic correlation between X-ray attenuation and carbon-ion stopping power for human tissues as shown in Fig. 11.2. The CT-ED relation depends on tube voltage, X-ray filter, and hardening effects. Therefore, precise calibration of the conversion curve is necessary for each CT-scanning condition. The hardening effect is object-dependent and therefore considered to be dominant uncertainty for the conversion based on measurement with calibration phantom. Because the conversion uncertainty is generally assumed to be of the order of 1 %, the precision of conversion curves in the same calibration condition should naturally be below 1 %. As there are no available tissue-equivalent materials that are valid for carbon-ion beams, the construction of the CT-ED relationship requires knowledge of the X-ray energy spectrum and elemental composition of tissues, with which X-ray attenuation coefficient or CT number and stopping-power ratio or ED of body tissues can be associated.

In addition to energy loss of carbon ions, which is the major source of radiation dose, multiple Coulomb scattering and nuclear interactions also influence the dose distribution. The majority of body tissues are nearly equivalent to water, which is abundant in oxygen, while bone tissues are abundant in calcium and adipose tissues are abundant in carbon. These compositional differences are ignored in the ED-based patient model. Generally, this approximation may cause only marginal effects to dose distributions in clinical cases.

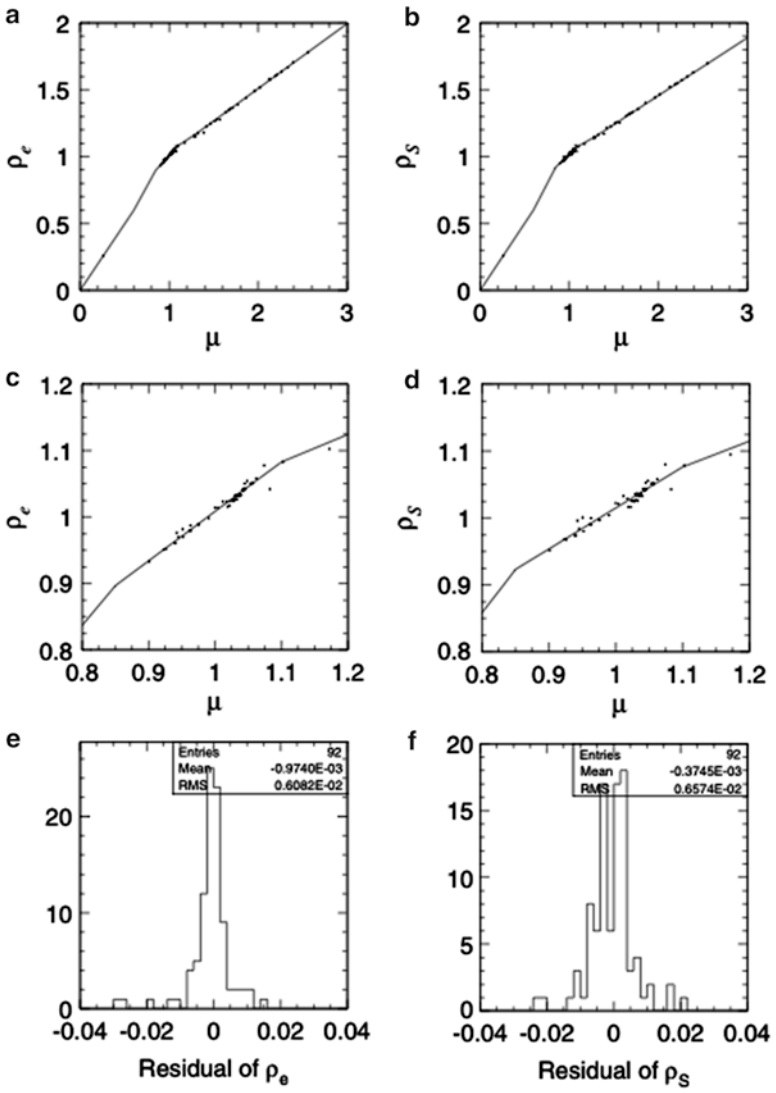

Fig. 11.2 Radiological properties of the body tissues in an example stoichiometric calibration; (**a**) and (**c**) are the correlation between linear attenuation coefficient ratio μ and relative electron density ρ_e, (**b**) and (**d**) correlation between μ and stopping-power ratio ρ_S and (**e**) and (**f**) residual histograms of ρ_e and ρ_S, respectively, with respect to the fitting polylines [1]

11.2.5 Plan Review

In general, common tools for treatment planning, such as isodose contours on a CT image and dose-volume histograms (DVHs), are useful also for C-ion RT, where the dose refers to the RBE-weighted dose for clinical evaluation.

For a treatment in multiple positions, one cannot simply sum individual dose distributions on different CT images using rigid image-registration techniques because the patient is usually deformed in different positions. Instead, deformable image-registration techniques may have to be used. Otherwise, for clinical dose evaluation purposes, a virtual plan is made for a virtual treatment machine that delivers equivalently oriented beams in one of the positions. The virtual plan may be useful for clinical review to assess the planned treatment of the patient.

During the review of treatment plans, uncertainties in the treatment planning and delivery process should be considered. The uncertainty in the dose distribution due to patient setup or range calculation may be assessed by calculating dose distributions for the hypothetic cases that include intentional perturbations for patient position and target depth by their estimated uncertainties. This procedure is often referred to as assessment of robustness.

In the scheme where the clinical RBE is an unambiguously formulated definition rather than estimation, no uncertainty is given to the RBE. In other words, the RBE-weighted dose is the basis of prescription as the most relevant quantity to clinical endpoints. Incidentally, the true RBE may be only derived from results of clinical studies. However, direct estimation of the RBE between carbon-ion and the reference X-ray radiations is often impossible due to differences of their standard treatment protocols in fractionation scheme.

11.3 Treatment Planning for Broad-Beam Delivery

11.3.1 Library of Standard Beams

In general, an ion beam should form a field of SOBP that covers a given target volume. In practice, the treatment planning and delivery systems have a common library of standard beams to cover a variety of possible target volumes in diameter, thickness, and depth. In the case of NIRS, there are a few energies, a few field diameters, and many different SOBP in steps of typically 1 cm. For each combination of the energy, the field diameter, and the SOBP, up to several different wobbling conditions are needed to achieve sufficiently uniform field with varied range shifter thickness for possible target depths. For each of these field-formation conditions, the beam properties such as field size, SOBP, range, and physical and clinical depth-dose curves are registered as the standard beams. There are as many as several hundred standard beams at NIRS that need to be defined and registered in the treatment planning system.

11.3.2 Field Customization

The broadened beam has to be collimated to conform to the projected target contour with an appropriate lateral margin to secure sufficiently high dose (normally 95 % of a prescribed dose) to a PTV. As the field is defined as the 50 % fluence contour, distance between 50 and 95 % may be a nominal lateral margin, which approximately coincides with the penumbra width (20–80 %).

There are several different beam-collimation devices whose setting parameters need to be determined in treatment planning. Jaw-type collimators are primarily for radiation-protection purposes and thus normally set to the minimum opening that does not affect the treatment field. A multileaf collimator is a cost- and labor-effective method for collimation. Alternatively, a patient collimator is placed close to the patient to obtain sharp lateral penumbra.

The most significant advantage of carbon-ion beams is the capability of beam-range control within the field. A range shifter is set to reduce the beam range to the maximum depth of the PTV with a depth margin that accounts for additional range uncertainty. A range compensator absorbs the excess of the beam range in the field so that the distal end of the SOBP coincides with the distal end of the PTV with the depth margin. Normally, the range compensation is designed with a simple ray-tracing calculation of the water-equivalent depth. Figure 11.3 shows the principle for range compensator design and ridge-filter selection, where w_1 and w_2 are proximal and distal water-equivalent depths of a target. The thickness of the range compensator should be the difference to the maximum of w_2. The ridge filter should have an SOBP larger than the maximum of $w_2 - w_1$.

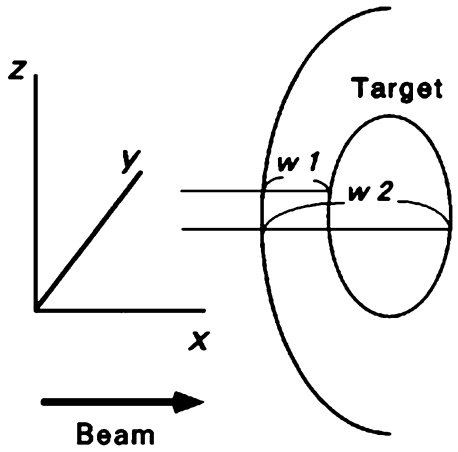

Fig. 11.3 Schematic of target analysis for range compensator design and ridge-filter selection [2]

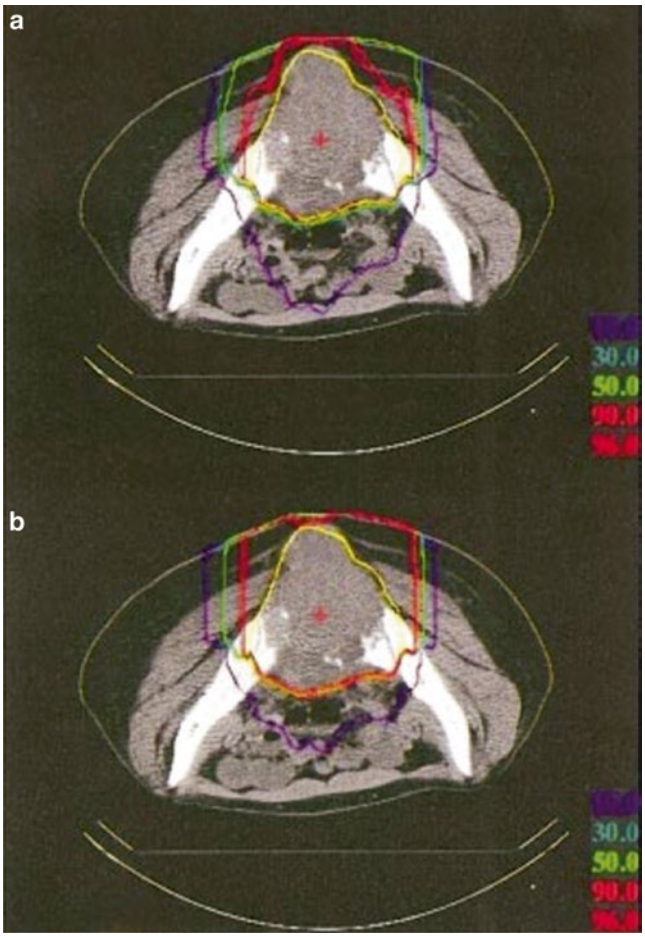

Fig. 11.4 Dose distributions of (**a**) layer-stacking and (**b**) conventional beams for osteosarcoma in pelvis (*yellow contour*) [3]

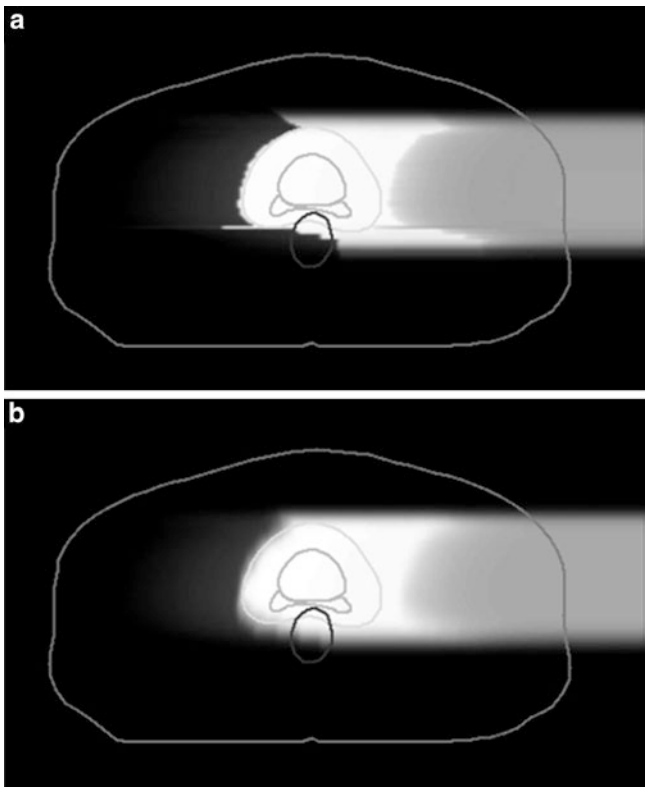

Fig. 11.5 Clinical dose distributions in grayscale from a carbon-ion beam for prostate treatment calculated with the (**a**) broad-beam and (**b**) pencil-beam algorithms [4]

In the conventional carbon-ion beam delivery, a ridge filter is used to form an SOBP to cover the PTV. However, since the SOBP has a fixed SOBP width, the SOBP in the proximal side cannot be conformal to the PTV. Therefore, the treated volume is normally conformal to the PTV by overlapping multiple fields.

In the layer-stacking delivery, a multileaf collimator field is dynamically conformed to the target in a layer-by-layer manner, which brings improved sparing to the organ at risk (OAR) proximal to the target, typically skin. Figure 11.4 shows an example of dose-distribution difference between the conventional and layer-stacking beams.

11.3.3 Dose Calculation Algorithms

Because the carbon-ion receives little scattering, the broad-beam algorithm is a reasonable approximation, in which variation of beam scattering effects are ignored and only common penumbra effects on the periphery of the field are simulated. This is simple and fast algorithm but lacks accuracy for highly heterogeneous systems. The pencil-beam algorithm models the field as comprised of two-dimensionally arranged pencil beams, which can reproduce realistic beam blurring of the field. Figure 11.5 shows an example of comparison between the two algorithms, where the broad-beam algorithm caused unrealistically sharp distal falloff except for the field penumbra region. Such artifacts due to algorithmic limitations must be carefully considered in dose-distribution analysis.

11.4 Treatment Planning for Scanning-Beam Delivery

In treatment planning for a passive beam delivery, the depth-dose profile is fixed by the ridge filter and no further optimization is necessary. In other words, in the system, there is no degree of freedom once a beam direction has been determined. On the other hand, the scanning-beam delivery system can produce nearly arbitrary shapes of the SOBP. To support this flexibility, two most relevant requirements on the treatment planning for the scanning system are:

- A physical beam model has to be established which describes the ion interaction with the matter, e.g., beam delivery devices and tissues, and the resultant dose distribution delivered in a patient with sufficient accuracy. Such a model should also provide the radiation quality of the beam requisite for the calculation of RBE in the patient.
- An algorithm has to be developed which is able to determine the particle number delivered to each Bragg peak position predetermined within or a small distance outside the target volume to achieve the prescribed dose distribution in the patient. This may include the optimization of the scan trajectory on each slice of equal radiological depth.

11.4.1 Beam Model

11.4.1.1 Beam Model for Calculating Absorbed Dose

In scanning-beam delivery, the prescribed dose distribution is realized by superimposing the dose of the individual pencil beams d according to their optimized weights w. The Bragg peak of the pristine beam is slightly broadened to produce a "mini peak" by the ridge filter [5]. The dose distribution at (x_i,y_i,z_i) delivered by the pencil beam stopped at (x_0,y_0,z_0) can be represented as follows:

$$d\left(x_i, y_i, z_i; x_0, y_0, z_0\right) = D_1\left(x_i; x_0, y_i; y_0, \sigma_1\left(z_i; z_0\right)\right) d_z\left(z_i; z_0\right). \quad (11.1)$$

Here, $d_z(z_i;z_0)$ is the planner-integrated dose at a depth of z_i, while $D_1(x_i;x_0,y_i;y_0,\sigma_1(z_i;z_0))$ is the two-dimensional normalized Gaussian functions with standard deviations $\sigma_1(z_i;z_0)$ representing the beam spread at a depth z_i.

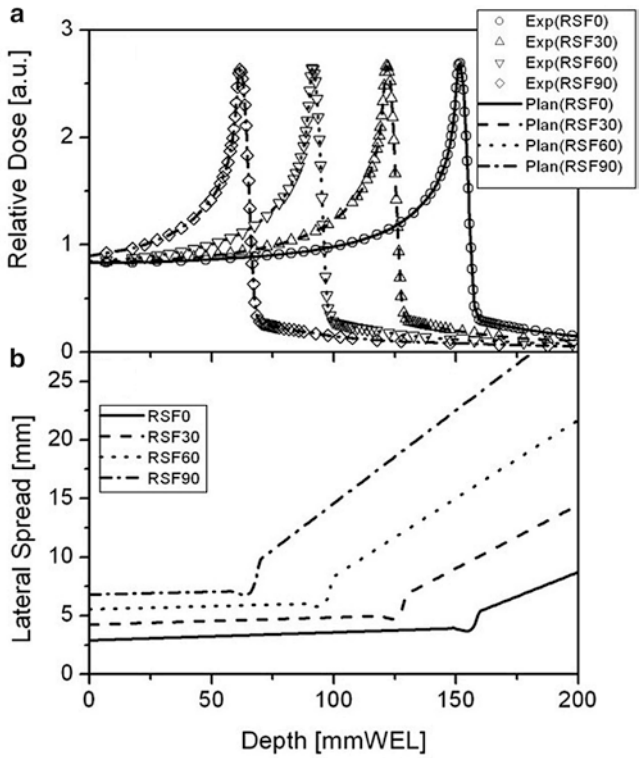

Fig. 11.6 Pencil-beam data for a 290 MeV/u carbon beam used by the treatment planning software. (**a**) Planner-integrated dose distribution d_z and (**b**) lateral beam spread σ_1 as a function of depth z_i for a range shifter of 0 (*solid line*), 30 (*dashed line*), 60 (*dotted line*), and 90 mm (*dash-dotted line*) water-equivalent thicknesses

The planner-integrated dose $d_z(z_i;z_0)$ and the lateral beam spread, i.e., $\sigma_1(z_i;z_0)$, were determined from the measured dose distribution with a large area parallel plate ionization chamber and a profile monitor, respectively. These data are fitted to simple formulae and incorporated into the planning software as shown in Fig. 11.6. With this algorithm, the effect of the beam spread due to multiple scattering in the range shifter can be incorporated, at least for the primary particles. However, our recent research revealed that the dose delivered to the target is reduced according to the field size in carbon-ion scanning with range shifter plates [6]. The observed dose reduction is referred to as the "field-size effect of dose" in this text. In order to account for this effect, we adopted three-Gaussian forms of lateral dose distributions. In this form, Eq. (11.1) can be rewritten as

$$d\left(x_i, y_i, z_i; x_0, y_0, z_0\right) = d_z\left(z_i;t\right) \times \left\{\left(1 - \sum_{j=2}^{3} f_j\left(z_i;t\right)\right) D_1\left(x_i; x_0, y_i; y_0, \sigma_1\left(z_i;t\right)\right)\right\}, + \sum_{j=2}^{3}\left(f_j\left(z_i;t\right) D_j\left(x_i; x_0, y_i; y_0, \sigma_j\left(z_i;t\right)\right)\right) \tag{11.2}$$

where $f_j(z_i;t)$ is the fraction of integrated dose assigned to the jth Gaussian component at a depth z_i delivered by the pencil beam with the range shifter plate of thickness t, and $D_j(x_i;x_0,y_i;y_0,\sigma_j(z_i;t))$ is a two-dimensional Gaussian function describing the lateral spread of the jth component at a depth of z_i with the standard deviation $\sigma_j(z_i;t)$. The parameters $\sigma_j(z_i;t)$ and $f_j(z_i;t)$ are experimentally determined and incorporated into the planning software. The lateral dose profile expressed with the three-Gaussian beam model is schematically shown in Fig. 11.7, along with that of the single-Gaussian beam model. The observed field-size effect of doses can be accounted for with this beam model. Figure 11.8 shows comparison of the measured- and planned-absorbed dose distribution with three-Gaussian beam model for a cylindrical target of 100 mm in diameter and 60 mm in SOBP. To shorten the planning time, a dose distribution calculated with the single-Gaussian beam model is simply scaled with the factor derived with the three-Gaussian beam model to account for the field-size effect of the doses [6].

11.4.1.2 Beam Model for Calculating RBE

The absorbed dose is not sufficient to predict the biological and clinical effects of a carbon-ion beam. To make optimal use of its characteristics, the clinically relevant dose, which is defined as the product of the absorbed dose and the RBE, has to be calculated in carbon-ion treatment planning. Since various kinds of ions with various kinetic energies coexist in therapeutic carbon-ion beams, the absorbed dose and the RBE should be evaluated carefully for the accurate calculation of the clinically relevant dose. In the past decades, two different biological models have been developed to predict the RBE in mixed radiation fields of therapeutic carbon-ion beams: an empirical model developed and has been used at the National Institute of Radiological Sciences (NIRS) [7] and the local effect model (LEM) [8, 9]. These models were integrated into the treatment planning systems and successfully used in patient treatments with passive beam delivery and scanning-beam delivery at the facilities in Japan and Germany, respectively. In the treatment planning of the scanning-beam delivery, a new biological model based on the microdosimetric kinetic model (MKM) [10–12] has been developed and adopted in clinical treatments to make the maximum advantage of the scanning method as well as the excellent clinical results achieved under the current passive beam delivery. The model parameters were determined to give the best fit to the data reported by Furusawa et al. [13] for HSG tumor cells which have been used to develop the empirical model [7]. With this procedure, we could keep the continuity from the clinical experiences with the passive beam delivery.

In the MKM, the cell nucleus is divided into many microscopic sub-volumes called domain. The cell survival fraction is predicted from the energy imparted to these domains, the

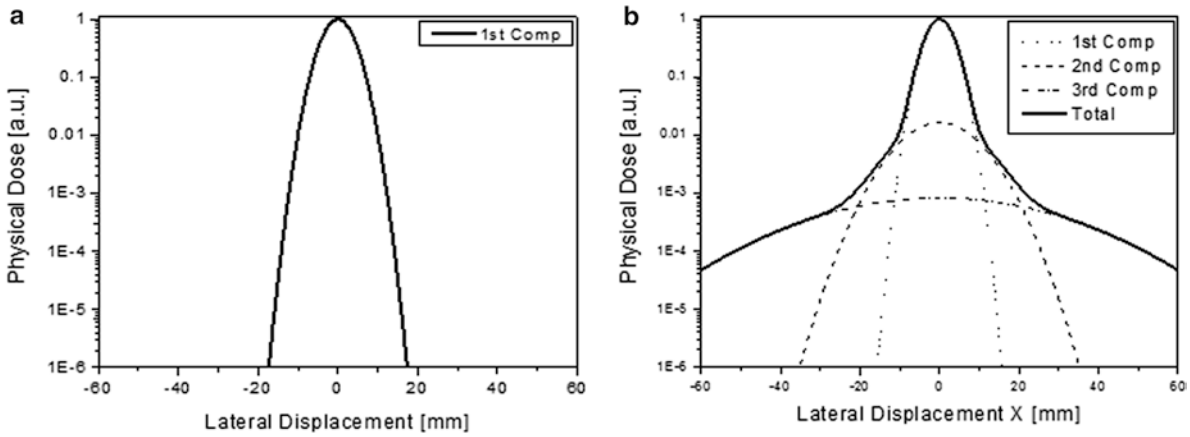

Fig. 11.7 Schematics of the lateral dose distribution expressed by (**a**) a single-Gaussian beam model and (**b**) a three-Gaussian beam model

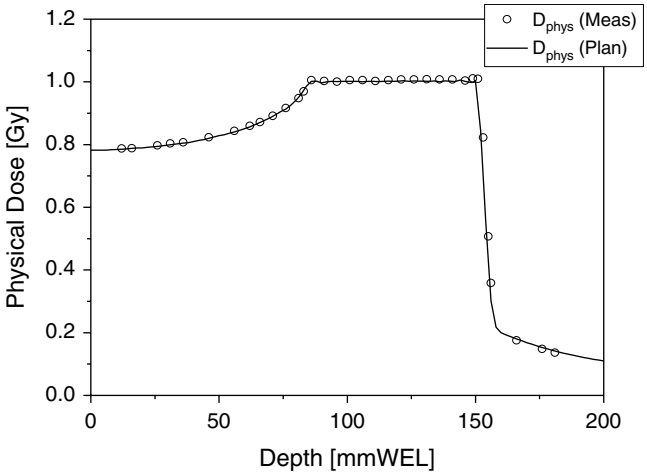

Fig. 11.8 A comparison of measured (*open circles*) and planned (a *solid curve*) absorbed dose distribution for a cylindrical target with 100 mm in diameter and 60 mm in SOBP. One Gy is prescribed to the target

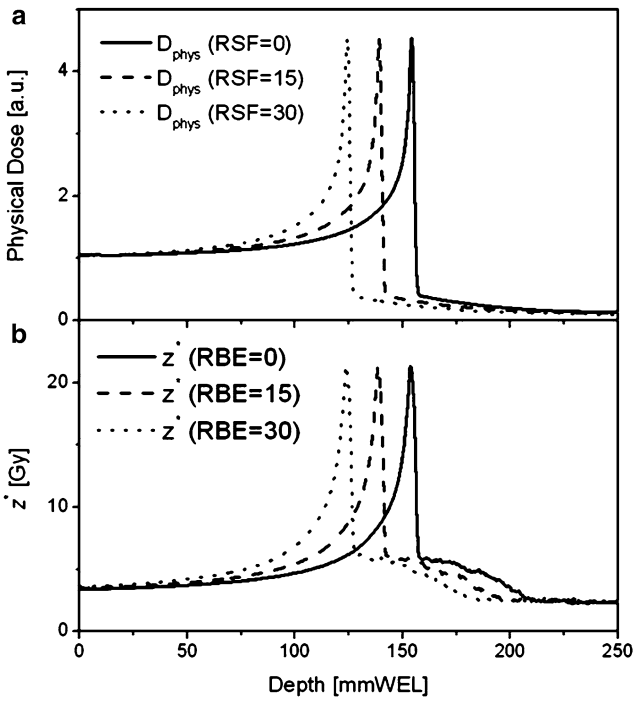

Fig. 11.9 (**a**) Depth-dose and (**b**) depth-z^* distribution for a scanned carbon-ion beam with 290 MeV/u

dose mean specific energy z^*, for any kinds of radiation. To simulate the radiation quality (ion species and their kinetic energies) of the therapeutic carbon-ion beam and to predict z^* of the beam, we use the Monte Carlo code Geant4. Figure 11.9 shows the depth-dose and depth-z^* distribution for a scanned carbon-ion beam with 290 MeV/u. The mathematical procedures to calculate the RBE of therapeutic carbon-ion beam in the treatment planning system are described in detail in [15] and omitted here. To confirm the reliability of the procedures, irradiation of HSG cells was performed with a scanned carbon beam at HIMAC. In Fig. 11.10, the measured depth-survival curve is compared with the prediction based on the MKM.

11.4.2 Dose Optimization

11.4.2.1 Optimization Algorithms

The goal of dose optimization in the treatment planning is to find the best particle numbers (weight) for each pencil beam, w, so that the resulting dose distribution is as close as possible to the prescribed dose distribution within the target volume and does not exceed the dose restrictions within the organs at risk. When determining w, the dose-based objective

function $f(w)$ is minimized through an iterative optimization process. The objective function can be described as

$$f(w) = \sum_{i\in T}\left(Q_P^o H'\left[D_{biol,i}(w) + U_i - D_P^{max}\right]_+^2\right) + Q_P^u H'\left[D_P^{min} + U_i - D_{biol,i}(w)\right]_+^2 + \sum_{i\in O} Q_O H'\left[D_{biol,i}(w) + U_i - D_O^{max}\right]_+^2 \quad (11.3)$$

where $D_{biol,i}(w)$, D_P^{max}, D_P^{min}, Q_P^o, Q_P^u, D_O^{max}, Q_O are the biological dose at a point i obtained with the matrix w, the maximum and minimum doses applied to the target T, the penalties for over- and underdosage specified for the target, the maximum dose allowed for the OAR, and the penalty for overdosage in OAR, respectively. $H'[r]$ is described as $H'[r] = rH[r]$ with the Heaviside step function, $H[r]$, defined so as to take the value of 1 only if r is greater than zero; otherwise, it takes the value of 0. In raster scanning irradiation, the beam delivery is not switched off during the transition time from one spot to the next. Therefore, in this scheme, the extra dose is inevitably delivered to the sites between two successive spots during the beam spot transition, along the scan trajectory. The contribution of the extra dose is included in the dose optimization by adding the term U_i to the objective function representing the amount of the extra dose delivered to a voxel i [6]. For the dose optimization, a number of mathematical algorithms have been proposed [14]. We used a gradient-based algorithm with the quasi-Newton method, because of its fast convergence.

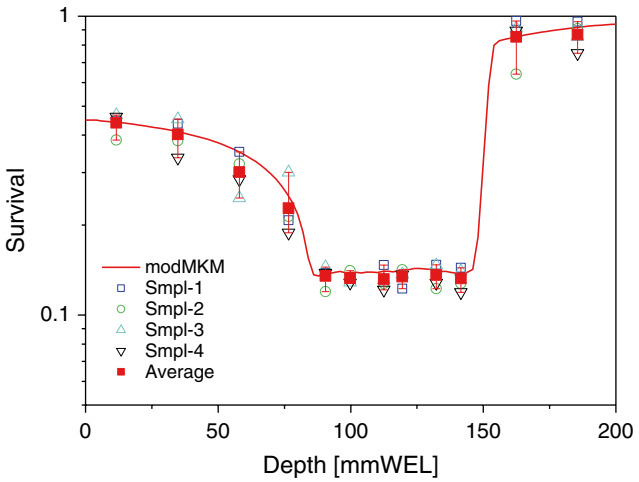

Fig. 11.10 Comparison between the measured and predicted depth-survival fraction for HSG tumor cells

11.4.2.2 Single-Field Uniform Dose (SFUD)

The separate optimization of single treatment fields is referred to as single-field uniform dose (SFUD) optimization. To obtain a homogeneous dose, SFUD includes an intensity modulation of individual fields.

11.4.2.3 Intensity-Modulated Particle Therapy (IMPT)

In intensity-modulated particle therapy (IMPT), the nonuniform dose distributions are delivered from several directions, and the desired dose distribution is obtained after superposing the dose contributions from all fields. IMPT has the ability to deliver highly conformal dose distributions to tumors of complex shapes, while preventing the undesired exposure to neighboring OARs. Figure 11.11a shows an example of IMPT plan for a cervical chordoma patient.

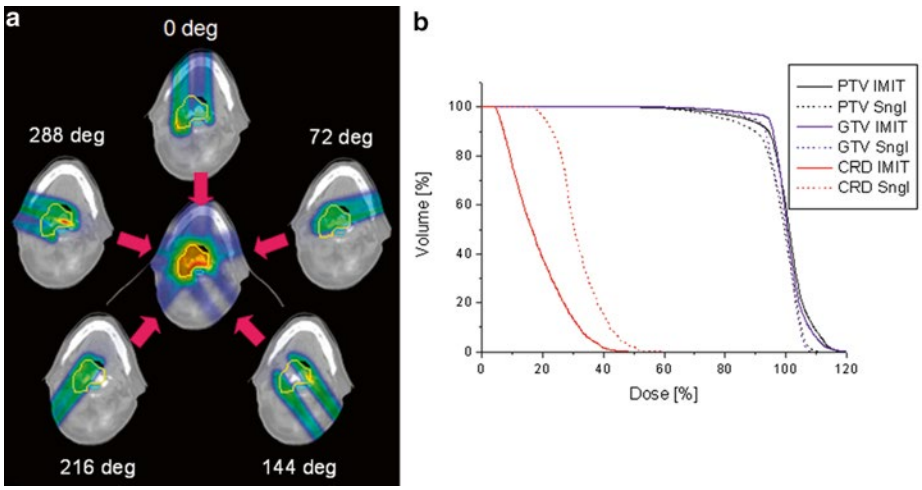

Fig. 11.11 (**a**) CT images of the cervical chordoma patient with color-wash biological dose display. The *yellow line* outlines the PTV and the *watery lines* delineate the OARs (spinal cord and brain stem). A five equidistant, coplanar beam setup was chosen during planning. (**b**) Dose-volume histogram of a five separate-beam plan (*dashed curves*) and a five-beam IMIT plan (*solid curves*) for the cervical chordoma patient

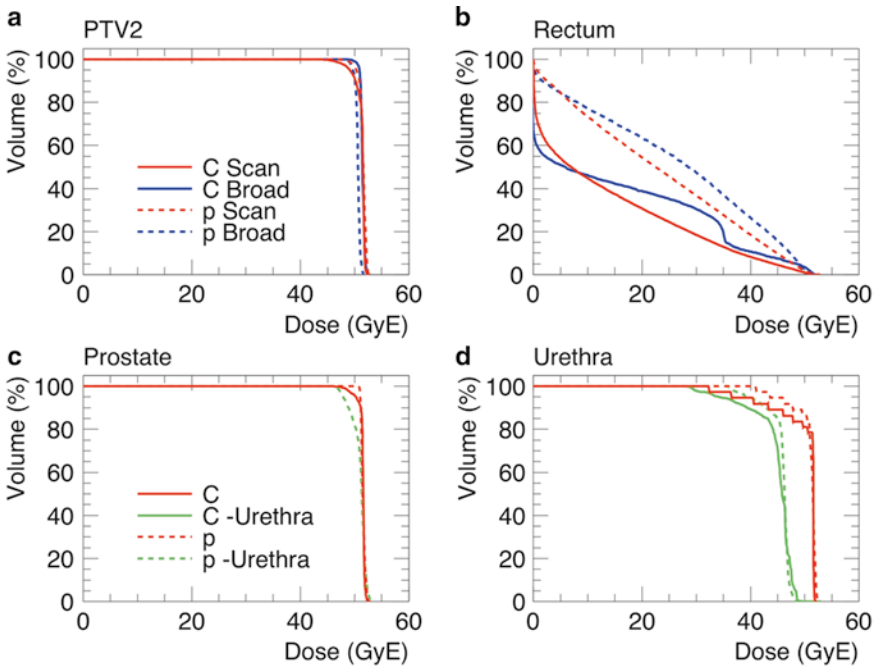

Fig. 11.12 DVHs of (**a**) reduced planning target (PTV2), (**b**) rectum (OAR), (**c**) prostate (GTV, CTV), and urethra (OAR) for a prostate treatment with carbon ion (C) or proton (p) and with broad-beam and scanning techniques

A five equidistant, coplanar beam setup was chosen for the treatment plan. Corresponding DVHs are shown with solid curves in Fig 11.11b. The dashed curves indicate the DVHs for SFUD plan with the same beam configuration. It can be seen that the dose delivered to the spinal cord could be reduced by a factor of 2.0 using the IMPT plan without any deterioration in dose conformation to the PTV as compared to the single-field plan.

11.5 Plan Comparison

Treatment planning is a dose optimization process and therefore there may be multiple plans for a treatment, one of which may be chosen for prescription. In such decisions, among many aspects to be considered, the dose distribution is the most essential information. Especially the curative dose coverage for the PTV and dose control below tolerance level for OAR are in most cases objectively evaluated with DVHs. However, as the PTV involves peripheral margin regions, which may be often compromised to spare OARs, DVH for various PTVs, CTVs, and GTV may possibly give supplemental information for plan evaluation.

For example, Fig. 11.12 compares DVHs for a prostate treatment planned with proton and carbon-ion beams with the broad-beam and scanning delivery techniques. For scanning-beam plans, optimization with and without urethra sparing were tested. In this case, the proton beams suffered from increased rectum dose due to larger lateral penumbra. The urethra-sparing optimization in fact resulted in reduced urethra dose for the scanning beams.

References

1. Kanematsu N, Matsufuji N, Kohno R, Minohara S, Kanai T. A CT calibration method based on the polybinary tissue model for radiotherapy treatment planning. Phys Med Biol. 2003;48:1023–64.
2. Endo M, Koyama-Ito H, Minohara S, Miyahara N, Tomura H, Kanai T, Kawachi K, Tsujii H, Morita K. HIPLAN–a heavy ion treatment planning system at HIMAC. J Jpn Soc Ther Radiol Oncol. 1996;8:231–8.
3. Kanematsu N, Endo M, Futami Y, Kanai T, Asakura H, Oka H, Yusa K. Treatment planning for the layer-stacking irradiation system for three-dimensional conformal heavy-ion radiotherapy. Med Phys. 2002;29:2823–9.
4. Kanematsu N, Yonai S, Ishizaki A. Grid-dose-spreading algorithm for dose distribution calculation in heavy charged particle radiotherapy. Med Phys. 2007;35:602–7.
5. Weber U, Kraft G. Design and construction of a ripple filter for a smoothed depth dose distribution in conformal particle therapy. Phys Med Biol. 1999;44:2765–75.
6. Inaniwa T, Furukawa T, Nagano A, Sato S, Saotome N, Noda K, Kanai T. Field-size effect of physical doses in carbon-ion scanning using range shifter plates. Med Phys. 2009;36:2889–97.
7. Kanai T, Endo M, Minohara S, Miyahara N, Koyama-Ito H, Tomura H, Matsufuji N, Futami Y, Fukumura A, Hiraoka T, Furusawa Y, Ando K, Suzuki M, Soga F, Kawachi K. Biophysical characteristics of HIMAC clinical irradiation system for heavy-ion radiation therapy. Int J Radiat Oncol Biol Phys. 1999;44:201–10.
8. Scholz M, Kraft G. Track structure and the calculation of biological effects of heavy ion beams for therapy. Adv Space Res. 1996;18:5–14.
9. Elsässer T, Weyrather WK, Friedrich T, Durante M, Iancu G, Krämer M, Kragl G, Brons S, Winter M, Weber KJ, Scholz M.

Quantification of the relative biological effectiveness for ion beam radiotherapy: direct experimental comparison of proton and carbon ion beams and a novel approach for treatment planning. Int J Radiat Oncol Biol Phys. 2010;78:1177–83.
10. Hawkins RB. A statistical theory of cell killing by radiation of varying linear energy transfer. Radiat Res. 1994;140:366–74.
11. Kase Y, Kanai T, Matsumoto Y, Furusawa Y, Okamoto H, Asaba T, Sakama M, Shinoda H. Microdosimetric measurements and estimation of human cell survival for heavy-ion beams. Radiat Res. 2006;166:629–38.
12. Inaniwa T, Furukawa T, Kase Y, Matsufuji N, Toshito T, Matsumoto Y, Furusawa Y, Noda K. Treatment planning for a scanned carbon ion beam with a modified microdosimetric kinetic model. Phys Med Biol. 2010;55:6721–37.
13. Furusawa Y, Fukutsu K, Aoki M, Itsukaichi H, Eguchi-Kasai K, Ohara H, Yatagai F, Kanai T, Ando K. Inactivation of aerobic and hypoxic cells from three different cell lines by accelerated ^{3}He-, ^{12}C- and ^{20}Ne-ion beams. Radiat Res. 2000;154:485–96.
14. Nocedal J, Wright SJ. Numerical optimization (Springer series in operations research). New York: Springer; 1996.

Part VI

Facility Design

Facility Design of Carbon-Ion Radiotherapy

12

Koji Noda

Abstract

This chapter describes design considerations of a carbon-ion radiotherapy (C-ion RT) facility, based on medical requirements. In addition, as examples of C-ion RT facilities, a pilot facility of a downsized version of the Heavy-Ion Medical Accelerator in Chiba (HIMAC) and the new treatment research facility with the HIMAC accelerator are introduced. The former facility employs the beam-wobbling method, which has been successfully operated in Gunma University Heavy Ion Medical Center (GHMC) since March 2010. The latter facility has three treatment rooms: Two of them are equipped with the horizontal and vertical beam-delivery systems and one room is prepared for a superconducting rotating gantry, which employs the pencil-beam 3D scanning for treatments of both the static and respiratory-moving tumors. The treatments in the new treatment research facility have been successfully carried out since May 2011, while a rotating gantry with superconducting magnet has been developed.

Keywords

Broad-beam method • Downsized carbon-ion accelerator • Pencil-beam scanning method • Rotating gantry

12.1 Medical Requirements for Facility

Carbon-ion radiotherapy (C-ion RT) utilizes complex and intelligent equipment to deliver therapeutic radiations for the maximum benefit of cancer patients. Thus, a C-ion RT facility should be designed considering the following:

1. Beam-delivery methods and irradiation parameters
   Depending on the kinds of tumors and tumor size, one should employ adequately beam-delivery methods and irradiation parameters such as field size and dose rate, which determine accelerator specifications.
2. The number of treatments

The number of annual treatments in a C-ion RT facility should be increased as high as possible due to an economical reason. For increasing the number of the annual treatments, one fractional treatment time, consisting of patient-positioning time, irradiation time, and setup time of irradiation devices and an immobilization tool, is one of the essential factors as well as the number of treatment rooms. In order to increase the daily treatment hours under constant working hours, the daily quality-assurance (QA) hours should be shortened as possible while keeping the treatment quality. Further, the facility requires rooms for the X-ray CT of treatment planning, those for the treatment rehearsal and those for the manufacturing of the immobilization tool. It is noted that the facility requires adequate staff number for medical work and radiotherapy information system (RIS) considering the workflow of C-ion RT.

K. Noda (✉)
National Institute of Radiological Sciences,
9-1, Anagawa-4, Inage-ku, Chiba 263-8555, Japan
e-mail: noda_k@nirs.go.jp

H. Tsujii et al. (eds.), *Carbon-Ion Radiotherapy: Principles, Practices, and Treatment Planning*,
DOI 10.1007/978-4-431-54457-9_12,

12.1.1 Beam-Delivery Methods and Irradiation Parameters

The kinds of tumors and tumor size treated by the C-ion RT have been shown as the clinical statistics in the C-ion RT facilities in the world. Among them, in particular, those of the eighteen-year treatment period with Heavy-Ion Medical Accelerator in Chiba (HIMAC) are very useful, because of the largest treatment experiences in the world. Considering such clinical experiences, the C-ion RT facility should be designed.

12.1.1.1 Irradiation and Beam-Delivery Methods

As beam-delivery methods [1], broad-beam methods such as the beam-wobbling and double-scattering methods have been applied for both the carbon-ion and proton RTs. The beam-wobbling method has been well utilized especially for the C-ion RT, because this method has an advantage over the double-scattering one in minimizing the range loss by scattering materials. The advantages of the beam-wobbling method are as follows:

1. Dose management is easy.
2. Dose distribution does not so much depend on beam qualities from accelerator.
3. It is relatively easy for respiratory-gated irradiation to be realized [2] owing to advantages 1 and 2.

Advantage 3 is the most important one, because both the carbon-ion and proton RTs have required not only treatments for static tumors but also those for respiratory-moving ones. According to recent statistics of the HIMAC treatment, around 40 % of treatments are provided to the respiratory-moving tumors. On the other hand, the disadvantages are as follows:

1. It is inevitable to give unwanted doses on normal tissue proximal to the tumor, because of a constant spread-out Bragg Peak (SOBP) over the field.
2. Beam-utilization efficiency is low as 10–30 %, which results in relatively large secondary neutrons and relatively high beam intensity from accelerator.
3. Compensator and patient collimator are required.

In order to reduce significantly the extra dose on the normal tissue, the layer-stacking method was proposed [3], which has been routinely applied [4, 5] especially for head and neck treatment in HIMAC.

A pencil-beam 3D scanning method has been required because of the following advantages compared with the broad-beam method:

1. Conformal irradiation is possible even under an irregularly shaped tumor.
2. Beam-utilization efficiency is almost 100 %, while it is 10–30 % in the broad-beam method. The radiation shielding of the facility, thus, can be easily compared with that in the broad-beam method. Secondary neutron, further, can be significantly suppressed.
3. Since both the patient collimator and the compensator are not required, it will be easy to realize "adaptive radiotherapy."

In the C-ion RT, therefore, the Gesellschaft für Schwerionenforschung (GSI) developed the hybrid scanning with a pencil beam [6], which results in the routine treatments in the Heidelberg Ion Therapy (HIT) facility [7] and Centro Nazionale di Adroterapia Oncologica (CNAO) facility [8]. However, the pencil-beam scanning is not robust against the position and profile errors of the beam from accelerator, and further a respiratory movement of the tumor considerably deteriorates the dose distribution. Up to today, thus, the pencil-beam scanning has not yet been applied to treatments for respiratory-moving tumors, which results in the limit of kinds of tumors treated. Recently, in order to apply the pencil-beam scanning to the respiratory-moving tumor, the phase-controlled rescanning method [9] was proposed and verified successfully its performance [10, 11].

A rotating-gantry system allows significantly wide choices of beam orientation, compared with a fixed beam-delivery system. In the clinical practice with HIMAC, since the beam can be delivered from either horizontal or vertical direction, the patient is fixed in supine, prone, and often rolled positions by typically 10–20° from the horizontal plane in order to achieve a better combination of beams. This situation often adds to the patient's load, complicates the treatment planning, and makes precise positioning difficult. A rotating-gantry system, which allows 360° rotation around the patient, will resolve many of these problems. Further, a combination between a rotating gantry and a pencil-beam scanning can realize an "Intensity Modulated Particle Therapy" (IMPT) [12], which can increase dose localization significantly. A rotating gantry for ion RT, on the other hand, is much larger, as its size is typically 10 m in diameter in the commercialized proton RT systems. For carbon-ion beam, the requirement for beam bending is a few times more severe. Only the HIT facility has a heavy-ion rotating-gantry system existing today. Applying the superconducting technology to the rotating gantry will be able to reduce its size and weight, which has been developed by NIRS [13].

12.1.1.2 Irradiation Parameters

Irradiation-Field Size

The HIMAC clinical statistics indicates the residual-range distribution for the therapeutic carbon-ion beams, as shown in Fig. 12.1. It is noted that the residual range is defined as the water-equivalent depth that the beam can penetrate after it has passed through the necessary beam-modifying devices. It is obviously found from the figure that a residual range of 250 mm covers most of the patients treated with HIMAC. The residual range depends not only on the beam energy but also on the beam-delivery method. In the broad-beam methods, range loss is caused mainly by the scatterer. In the pencil-beam scanning method, on the other hand,

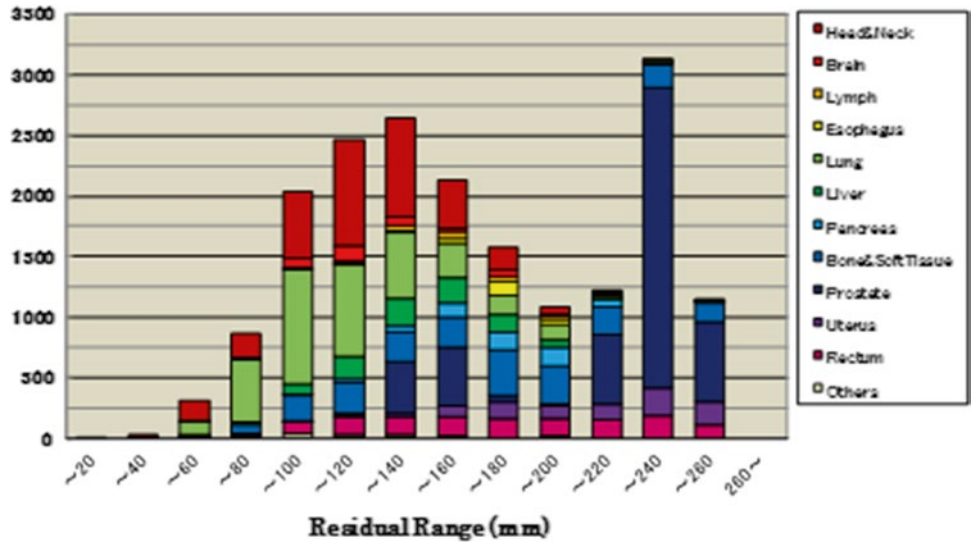

Fig. 12.1 Histogram of the number of irradiation shots as a function of the required residual range in mm

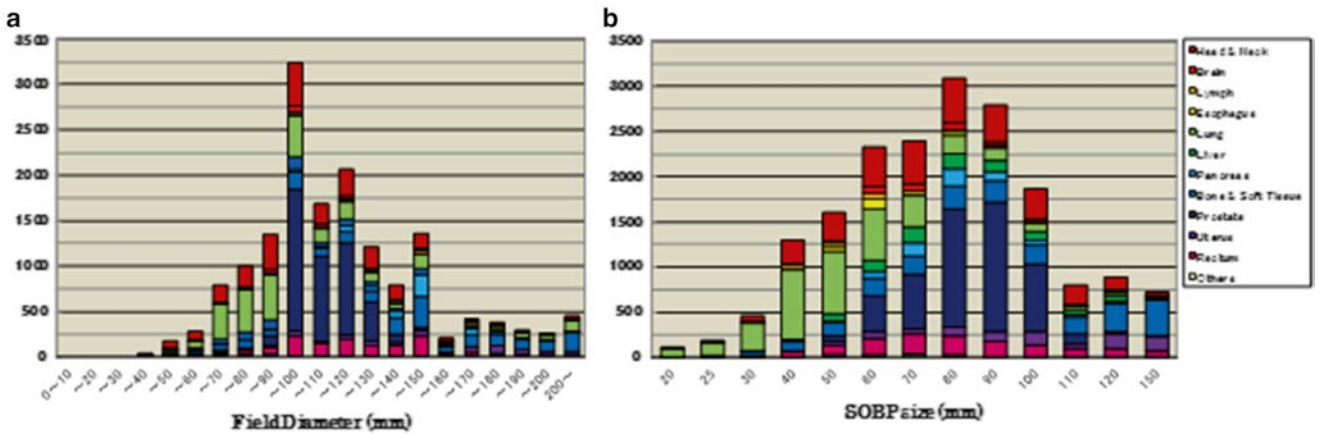

Fig. 12.2 Histograms of the session numbers as a function of the required field diameter in mm (**a**) and as a function of the required SOBP in mm (**b**)

range loss can be minimized. For HIMAC, the maximum residual range in the beam-wobbling method is typically estimated to be 250 mm for a 400 MeV/n carbon-ion beam, while 270 mm in the pencil-beam scanning.

Both the lateral field and SOBP size are also determined by the clinical statistics. As shown in Fig. 12.2, a lateral-field size of 220 mm in diameter and SOBP size of 150 mm can cover almost all types of patients treated with HIMAC. A larger field size of more than 200 mm is required mainly for the treatment of oblong tumors. In such cases, it is important to maintain the field length rather than the diameter. The field-patching method has been employed for a target size of more than 220mm in diameter. The SOBP size should range from 40 to 150 mm.

Dose Rate

For HIMAC, the dose rate is required to be 5 GyE/min so as to complete the fractional irradiation course within a tolerable time [14]. In carbon-ion RT using broad-beam methods, the dose rate of 5 GyE/min ($10 \times 10 \times 10$ cm) corresponds to around 10^9 particles per second (pps) of a beam intensity required at the entrance of a beam-delivery system, under a beam-utilization efficiency of around 20 % in the beam-delivery system. In the pencil-beam scanning method, beam-utilization efficiency increases to almost 100 %. The beam intensity, thus, can be decreased to 1/3–1/10, compared with the broad-beam methods in the carbon-ion RT. For the pencil-beam scanning, however, the dose-rate limitation is determined in order to decrease the extra dose: (1) the quantity of an extra dose due to the finite time to turn off the beam delivery in the spot-scanning method and (2) the amount of extra dose delivered when the beam is moving between positions in the raster-scanning method in which the beam is not turned off. In both cases, the extra dose is proportional to the beam intensity delivered.

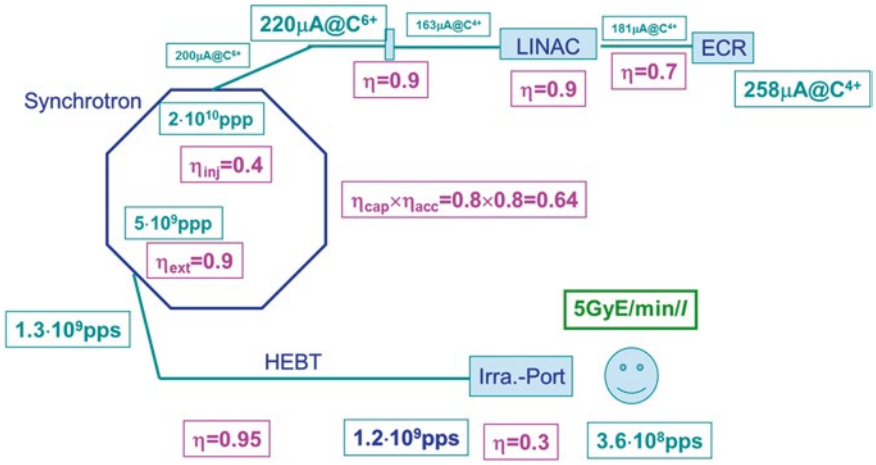

Fig. 12.3 Typical intensity schedule of a carbon-ion RT facility with the beam-wobbling method

An intensity schedule of accelerator is obtained by the dose rate required and penetration efficiencies. Figure 12.3 shows an intensity schedule under the beam-wobbling method with a beam-utilization efficiency of 30 %.

12.1.2 The Number of Annual Treatments

The number of annual treatments should be increased as high as possible, due to an economical reason. The number of annual treatments N_T is obtained as

$$N_T = \left(Ns \times N_{room}\right) / F, \tag{12.1}$$

where Ns is the number of annual sessions per room, N_{room} the number of treatment rooms, and F the average fraction number. The Ns, further, is given as

$$N_S = H_T \times D_W / T_{OCC}, \tag{12.2}$$

where H_T is the daily treatment hours, D_W the annual working days, and T_{OCC} one fractional treatment time corresponding to an occupancy time of a treatment room per patient. The H_T is given by subtracting the daily QA hours from the daily working hours. T_{OCC} consists of T_{pos} (positioning time), T_{irr} (irradiation time), and T_{setup} (setup time).

Assuming the D_W and the F are kept constant, the T_{OCC} should be reduced in order to increase the number of annual treatments N_T. For the purpose, the patient-positioning time T_{pos} should be reduced under keeping the treatment quality, because the T_{pos} is a major part of the T_{OCC}. The daily treatment hours H_T and the number of treatment rooms N_{room} should be determined considering the required number of annual treatments. However, the H_T is required to be increased as long as possible under constant working hours, which means the QA hours should be reduced under keeping the treatment quality. Further, the N_{room} should be optimized from the construction-cost point of view.

12.1.2.1 One Fractional Treatment Time

The patient-positioning time should be reduced in order to decrease the one fractional treatment time, because the patient-positioning time takes the longest time in one fractional treatment time. The poisoning time takes around 7–30 min, depending on kinds of tumors, patient age, and positioning method such as automatic and/or manual, while the irradiation time of 5 min at maximum and the setup time of beam-delivery devices and immobilization tools of around 5 min. It is noted that reduction of the patient-positioning time can decrease the patient's load.

The precision for the physical dose distribution and for the patient couch adjustment is required to be less than 1 mm. For example, the positioning accuracy of fixed targets such as skull-based tumor is around 1 mm and that of ocular melanoma treatment of the eyeball is at the submillimeter level. It is not easy, however, to keep the precision of patient positioning over the course of the treatment. Especially in case of organ motion during each delivery, positioning precision is much greater than the one-millimeter level. In clinical practice, accuracy of patient positioning depends on the skill of the radiotherapist, and its significance ultimately depends on target delineation by the radiation oncologist. At HIMAC, therefore, the patient-positioning time has not been reduced so much to keep the treatment quality, and the one fractional treatment time with the beam-wobbling method has been around 25 min on average. In order to shorten the one fractional treatment time, an automatic patient-positioning system has been developed [15]. Applying the automatic method in the new treatment research facility employing the pencil-beam scanning as described in Sect. 12.2, the one fractional treatment time is considerably reduced to less than 15 min on average while keeping the positioning accuracy. It is noted that the pencil-beam scanning never required the setup time for the beam-delivery tools such as patient collimator and compensator, unlike the broad-beam method.

12.1.2.2 Estimation of the Number of Annual Treatments

The number of the annual treatments is estimated under the following conditions:

1. Fixed parameters
   - The fraction number F of 12 on average obtained from the HIMAC clinical statistics.
   - The number of treatment rooms of 3, with the horizontal (H) and vertical (V) beam-delivery system, with the H and with the V, which are same with HIMAC and Gunma University Heavy Ion Medical Center (GHMC).
   - The daily treatment hours H_T of 6 h are same with HIMAC, while 2 h for the daily QA work, under 8 h of daily working hours.
   - The annual working day D_W of 240 days.
2. With the broad-beam method and without automatic patient positioning

   In this case, since the one fractional treatment time T_{OCC} is estimated to be 25 min, the number of annual sessions per room N_S is obtained from Eq. (12.2) as follows:

$$N_S = H_T \times D_W / T_{OCC} = 6\,(\mathrm{h}/day) \times (240\,days) / (25/60)(\mathrm{h}) = 3{,}456\,sessions.$$

   From Eq. (12.1), the number of annual treatments N_T is estimated to be

$$N_T = (N\mathrm{s} \times N_{room}) / \mathrm{F} = (3456 \times 3) / 12 = 864\,patients.$$

3. With the pencil-beam scanning and with automatic patient positioning

   In this case, using the one fractional treatment time T_{OCC} of 15 min, the N_S of 5,760 is obtained. Therefore, the number of annual treatments N_T is estimated to be 1,440 patients.

As the above estimation, the automatic patient-positioning system is a powerful tool to increase significantly the number of annual treatments.

12.1.3 Miscellaneous

12.1.3.1 Simulation Room

The treatment workflow has required to obtain CT images of each patient for treatment planning, to obtain the digital reconstructed radiographs (DRR) for patient positioning from the treatment planning CT images or from their approximate X-ray images, and to carry out the rehearsal before a treatment. The rehearsal can verify whether the patient can keep his/her configuration prescribed or not and/or whether a patient and a patient couch are interfered with beam-delivery devices such as a patient collimator, a compensator, and the irradiation port itself or not. This work is very important, in particular, in a facility without any rotating gantry, because of rotating the patient with 10–20°. When medical staffs carry out such works in a treatment room, the daily treatment hours is to be considerably reduced, which results in the large reduction of the number of annual treatments. One or two simulation rooms should be prepared, therefore, which are equipped with dummy irradiation devices, a patient-positioning system, a patient couch, and X-ray CT.

12.1.3.2 Safety

All systems in the medical facility should be designed with the safety of the patients and medical staff being of primary importance. One of the crucial considerations is radiation protection for the medical staff in the high-energy accelerator facilities [16]. For ensuring irradiation safety, each system needs to be designed to fail-safe standards. The system must be designed so that in any appropriate non-nominal situation, the instrumentation is designed to detect such situation quickly, and the interlock system can be activated with sufficient promptness to turn off the beam fast enough to ensure patient and personnel safety. If this occurs in one treatment room, it must be possible to allow clinical operation in the other treatment rooms, provided that it is safe to do so.

Radiation shielding should be designed considering safety not only for the people outside the facility building in general but also for the medical staff inside the treatment room when irradiating on a patient in the neighboring room. The pencil-beam scanning requires lower intensity than the broad-beam method, because of high beam-utilization efficiency. Thus the pencil-beam scanning can employ the thinner shielding wall, which results in lower construction cost of the facility building.

For curative treatments of young patients, risk of secondary cancer formation after radiotherapy has recently emerged as a matter of concern [17, 18]. Compared to photon beams, heavy-ion beams can minimize undesired exposure in normal tissues adjacent to the target volume because of their physical and/or biological advantages. It is also necessary to investigate the range of undesired exposure in normal tissues remote from the target, due mainly to secondary neutrons that are inevitably produced in patients and beamline devices [18, 19], although the risk of low-dose exposure is controversial [20]. Therefore, the pencil-beam scanning method should be employed in the treatment of young patient, but not the broad-beam method, because of small yield of secondary neutrons.

12.1.3.3 Quality Assurance

The QA is used to warrant the correct use of radiations for therapeutic purposes. QA activities primarily focus on detection of any possible abnormal behavior with the highest sensitivity practically achievable. In case of any failure, corrective action and estimation of the significance have to be carried out. The quality management of clinical systems demands great efforts in the endless sequence of plan, do,

check, and action, including routine (daily, weekly, monthly, annually) activities for inspection, measurement, recording, and reporting. Daily QA is usually performed prior to the first treatment of the day, typically within 30 min in the broad-beam method in HIMAC. In the pencil-beam scanning, however, not only the daily QA such as the range verification but also the patient-specific QA is required. The former takes around 15 min in one beam-delivery system, while the latter takes around 30 min in one patient. Therefore, it takes 2–3 h for the daily QA works.

In spite of the QA work, however, it is inevitable for subtle failures such as software and human errors to still occur, although safety is still assured. At HIMAC, information on the above failures has been qualitatively recorded since 1999. Analysis of the types of information, in particular, the number of events occurring due to hardware, has increased since 2005, around ten years since the HIMAC facility was put into operation. The total number of serious events that have occurred during around two years after a 15-year operation stands at 30, corresponding to less than 0.2 % of the serious-event rate. It should be noted that serious failure is defined as follows: Interruption of any treatment session must not exceed one hour until resumption.

12.2 Carbon-Ion Radiotherapy Facility

12.2.1 Overview

The operating and under-constructing C-ion RT facilities are summarized in Table 12.1. Until now, around 11,000 patients were already treated by the C-ion RT.

The HIMAC facility was constructed as the first medical heavy-ion RT facility in the world and has carried out the C-ion RT with the broad-beam method since 1994. As a result, more than 7,000 patients were already treated until 2012. The Hyogo Ion Beam Medical Center (HIBMC) was constructed as a low-energy version of HIMAC, and the treatments have been carried out by both protons and carbon ions. The Institute of Modern Physics (IMP) in China has carried out treatments not only by 100 MeV/n carbon-ion beams for superficially placed tumors since 2006 but also by 400 MeV/n ones for deeply seated tumors since March 2009. The GSI had successfully carried out cancer treatments for more than 400 patients with carbon-ion beam, applying the intensity-controlled raster-scanning method, since 1997. On the basis of the GSI development, the HIT facility was constructed, which is equipped with two horizontal beam-delivery systems and one rotating gantry. The CNAO facility employs the synchrotron based on the PIMMS design and the injector based on the HIT design [21], and the treatments have been carried out by both protons and carbon ions.

Among of the carbon-ion RT facilities in the world, this section introduces a pilot facility of a downsized version of carbon-ion RT facility constructed in GHMC and the new treatment research facility in NIRS.

12.2.2 Pilot Facility as a Downsized C-ion RT Facility

The HIMAC treatment has been applied to various types of malignant tumors since 1994. Owing to the good results and the accumulated number of protocols, the carbon-ion RT with HIMAC was approved in 2003 as a highly advanced medical technology by the Japanese government. Therefore, NIRS proposed a new C-ion RT facility in order to boost applications of carbon-ion RT, with emphasis being placed on a downsized version so as to reduce cost. After two-year design and R&D works, a pilot facility as the downsized carbon-ion RT facility was constructed in Gunma University. This facility consists of a compact 10 GHz ECR ion source

Table 12.1 Carbon-ion RT facility in the world

	Facility	Start	Patients	Until	Beam delivery
In operation	HIMAC	1994	7,207	March 13	Broad beam
		2011	132	March 13	3D scanning
	GSI	1997	440	July 08	3D scanning
	HIBMC[a]	2002	1,393	December 11	Broad beam
	IMP	2006	194	November 11	Broad beam
	HIT	2009	980	December 12	3D scanning
	GHMC (Gunma)	2010	537	December 12	Broad beam
	CNAO	2012	3	December 12	3D scanning
Under construction	PTC, Marburg	?			3D scanning
	Saga-HIMAT	2013			Broad beam
	MedAustron	2015			3D scanning
	U Fudan	2014			3D scanning
	i-Rock (Kanagawa)	2015			Broad beam 3D scanning

[a]Number of patients treated by only carbon-ion

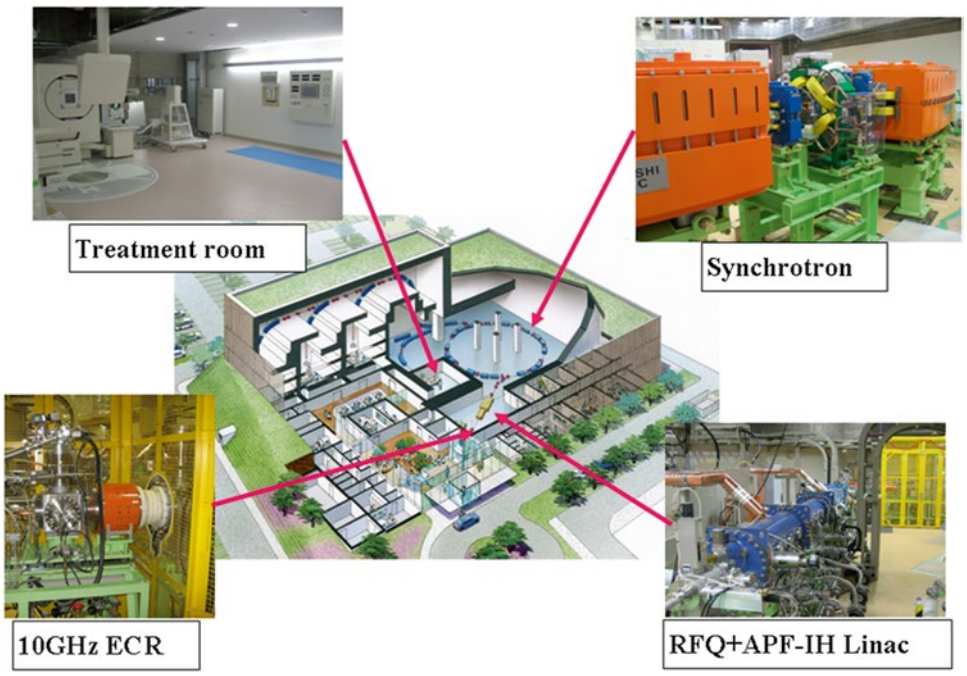

Fig. 12.4 Image view of the GHMC facility

with all permanent magnets [22], an RFQ and an APF-IH linac [23], a synchrotron ring, three treatment rooms, and one experimental room for basic research. In this facility, a C^{4+} beam, which is generated by a compact 10 GHz ERC ion source, is accelerated up to 4 MeV/u through the injector linac cascade. After fully stripped, the C^{6+} beam is injected into the synchrotron by a multi-turn injection scheme and is accelerated up to 400 MeV/n at maximum. All of the magnets in the beam transport lines are made of laminated steel in order to change the beam line quickly within 1 min. The beam-delivery system employs a spiral beam-wobbling method [24, 25] for forming a uniform lateral dose distribution with a relatively thin scatterer. The facility size was downsized to be one-third of the HIMAC facility. An image of this facility with installed devices is shown in Fig. 12.4 and the main specifications are summarized in Table 12.2.

Table 12.2 Specifications of the pilot facility of downsized carbon-ion RT facility

Ion species	Carbon
Energy	140–400 MeV/u
Maximum residual range	25 cm
SOBP	4–15 cm
Maximum lateral-field size	22 cm ϕ
Maximum dose rate	5 GyE/min/L
Beam intensity	1.2×10^9 pps in front of beam-delivery system
Beam-delivery method	Conventional and spiral beam wobbling
Irradiation method	Respiratory gating/layer-stacking method
Number of treatment rooms	3 rooms, equipped with H&V, H, V[a]
Number of treatments	>600 patients/year at plan

[a]H, horizontal beam-delivery system; V, vertical beam-delivery system

12.2.3 New Treatment Research Facility with HIMAC

The new treatment research project has been progressed for further development of HIMAC treatments [26]. One of the most important purposes in this project is to realize an "adaptive cancer radiotherapy," which can accurately treat tumors even in changing target size and shape during a treatment period. A pencil-beam scanning method has been well known to be very suitable for the adaptive cancer radiotherapy. Since HIMAC treats both fixed and moving tumors, it has proposed a fast 3D rescanning method with the gated irradiation to move toward the goal of adaptive cancer radiotherapy for treating both the moving and static tumors.

Figure 12.5 shows a schematic view of the new treatment research facility with the existing HIMAC facility. The new treatment facility is connected with the HIMAC accelerator. In the treatment hall, placed underground of the facility, three treatment rooms are prepared in order to treat more than 800 patients a year. Two of them are equipped with both horizontal and vertical beam-delivery systems, and the other is equipped with a rotating gantry. Two simulation rooms are also prepared for patient positioning as a rehearsal and for observing any change of the target size and shape during the

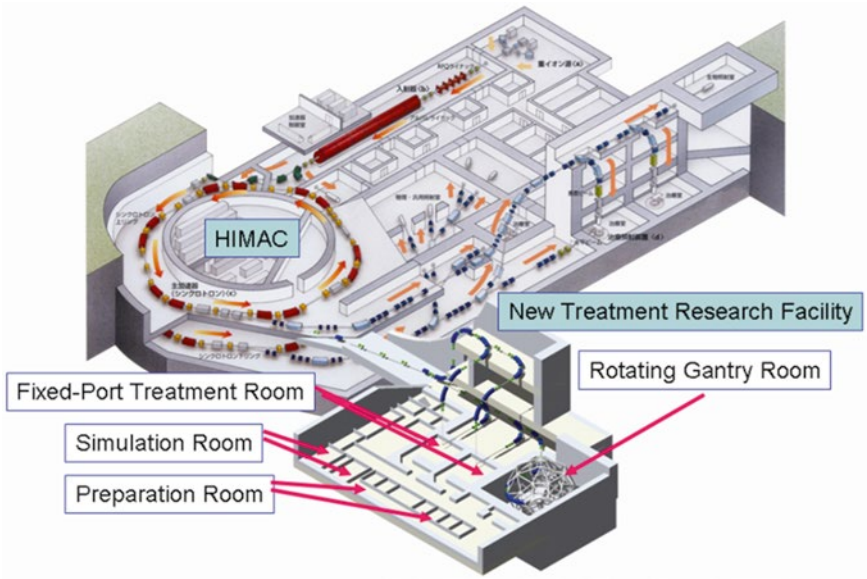

Fig. 12.5 Layout of the new treatment research facility connected with the HIMAC accelerator

Table 12.3 Main specifications of the new treatment research facility

Ion species	Carbon
Energy	140–430 MeV/u
Maximum residual range	30 cm
SOBP	4–15 cm
Maximum lateral-field size	22×22 cm for both H and V
	20×20 cm for R-Gantry
Maximum dose rate	5 GyE/min
Beam intensity	4×10^8 pps
Beam-delivery method	Pencil-beam 3D scanning
Irradiation method	Fast 3D rescanning with gating
Number of treatment rooms	3 rooms (2 H&V and R-Gantry)[a]
Number of treatments	>800 patients/year

[a]H, horizontal beam-delivery system; V, vertical beam-delivery system; R-Gantry, rotating gantry with superconducting

whole treatment period with an X-ray CT. Further, six rooms are devoted to patient preparation just before irradiation.

Specifications in the new treatment research facility are summarized in Table 12.3, which are determined considering the HIMAC clinical statistics. The maximum ion energy is designed to be 430 MeV/u in the fixed beam-delivery system, which gives the residual range of 30 cm in a ^{12}C beam and of 22 cm in an ^{16}O beam. Further, the rotating-gantry system under development employs the smaller lateral-field size of 20×20 cm in order to downsize the gantry size.

The new treatment research facility is designed to make energy scanning for slice change possible [27]. Thus all of the magnets in the beam transport line are manufactured with laminated iron plates. The beam optics is designed to realize a dispersion-free condition in the fixed beam-delivery system, and the beam size at the iso-center can be changed from 2 to 8 mm at one sigma by using the final Q-triplet. In 2011, one of the three treatment rooms, which is equipped with the horizontal and vertical beam-delivery systems with the pencil-beam scanning, treated 11 patients with the range shifter for depth scanning. However, the depth scanning with range shifter brings enlarging beam size due to multiple scattering and producing relatively large neutrons through the range shifter. Since 2012, the hybrid depth scanning [28] has been employed in two of the treatment rooms. A rotating-gantry system with superconducting magnets, further, has been under development and will be installed in the third room.

On the basis of the pilot facility in GHMC, Saga Heavy Ion Medical Accelerator in Tosu (Saga-HIMAT) was designed and constructed. This facility has three treatment rooms, but two of them, having the 45° and horizontal beam-delivery systems and the horizontal and vertical ones, will be operated with the beam-wobbling method in the first stage. After a preclinical study, the first treatment is scheduled in summer of 2013.

Ion-beam Radiation Oncology Center in Kanagawa (i-Rock) has been designed and constructed since 2012, based on the GHMC design for accelerator and the NIRS design for the pencil-beam scanning. The i-Rock facility has four treatment rooms: Two of the treatment rooms have a horizontal beam-delivery system, while the remaining two rooms both have the horizontal and vertical beam-delivery ones in each room. As the beam-delivery methods, both the pencil-beam scanning and broad-beam scanning are prepared. The first treatment is scheduled in 2015.

References

1. Chu WT, Ludewigt BA, Renner TR. Instrumentation for treatment of cancer using proton and light-ion beams. Rev Sci Instrum. 1993;64:2055–122.

2. Minohara S, Kanai T, Endo M, Noda K, Kanazawa M. Respiration gated irradiation system for heavy-ion radiotherapy. Int J Rad Oncol Bio Phys. 2000;47:1097–103.
3. Kanai T, Kawachi K, Matsuzawa H, Inada T. Broad beam three dimensional irradiation for proton radiotherapy. Med Phys. 1983; 10:344–6.
4. Kanai T, Kanematsu N, Minohara S, Komori M, Torikoshi M, Asakura H, Ikeda N, Uno T, Takei T. Commissioning of a conformal irradiation system for heavy-ion radiotherapy using a layer-stacking method. Med Phys. 2006;33:2989–97.
5. Kanematsu N, Endo M, Futami Y, Kanai T. Treatment planning for the layer-stacking irradiation system for three-dimensional conformal heavy-ion radiotherapy. Med Phys. 2002;29:2823–9.
6. Haberer T, Becher W, Shardt D, Kraft G. Magnetic scanning system for heavy ion therapy. Nucl Instrum Meth A. 1993;330:296–305.
7. Eickhoff H, Harberer Th, Schlitt B, Weinrich U. The German hospital-based light ion cancer therapy project. In: Proceedings of 9th European particle accelerator conference, Lucern; 2004. p. 290–94.
8. Borloni E, Rossi S. The CNAO project and the status of the construction. In: Proceedings of NIRS-CNAO Joint Symposium on Carbon Ion Radiotherapy; 2006. p. 1–15.
9. Furukawa T, Inaniwa T, Sato S, Minohara S, Noda K, Kanai T. Design study of a raster scanning system for moving target irradiation in heavy-ion radiotherapy. Med Phys. 2007;34(3):1085–97.
10. Furukawa T, Inaniwa T, Sato S, Shirai T, Mori S, Takeshita E, Mizushima K, Himukai T, Noda K. Moving target irradiation with fast rescanning and gating in particle therapy. Med Phys. 2010;37(9):4874–9.
11. Furukawa T, Inaniwa T, Sato S, Shirai T, Takei Y, Takeshita E, Mizushima K, Iwata Y, Himukai T, Mori S, Fukuda S, Minohara S, Takada E, Murakami T, Noda K. Performance of the NIRS fast scanning system for heavy-ion radiotherapy. Med Phys. 2010b; 37(11):5672–82.
12. Lomax A. Intensity modulation methods for proton radiotherapy. Phys Med Biol. 1999;44:185–205.
13. Iwata Y, Noda K, Shirai T, Murakami T, Furukawa T, Mori S, Fujita T, Itano A, Shoda K, Mizushima K, Fujimoto T, Ogitsu T, Obana T, Amemiya N. Design of a superconducting rotating gantry for heavy-ion therapy. Phys Rev Spec Top Accel Beams. 2012;15:044701-1–044701-14 (Online Only http://prst-ab.aps.org/).
14. Hirao Y, Ogawa H, Yamada S, Sato Y, Yamada T, Sato K, Itano A, Kanazawa M, Noda K, Kawachi K, Endo M, Kanai T, Kohno T, Sudou M, Minohara S, Kitagawa A, Soga F, Takada E, Watanabe S, Endo K, Kumada M, Matsumoto S. Heavy ion synchrotron for medical use. Nucl Phys A. 1992;538:541c–50.
15. Mori S, Shibayama K, Tanimoto K, Kumagai M, Matsuzaki Y, Furukawa T, Inaniwa T, Shirai T, Noda K, Tsuji H, Kamada T. First clinical experience in carbon-ion scanning beam therapy: retrospective analysis of patient positional accuracy. J Radiat Res. 2012;53:760–8.
16. Tsujii H, et al. Research on radiation protection in the application of new technologies for proton and heavy ion radiotherapy. Igakubuturi. 2009;28:172.
17. Brenner D, et al. Second malignancies in prostate carcinoma patients after radiotherapy compared with surgery. Cancer. 2000; 88:398.
18. Hall E. Intensity-modulated radiation therapy, protons, and the risk of second cancers. Int J Radiat Oncol Biol Phys. 2006;65:1.
19. Brenner D, Hall E. Secondary neutrons in clinical proton radiotherapy: a charged issue. Radiother Oncol. 2008;86:165.
20. Tubiana M. Can we reduce the incidence of second primary malignancies occurring after radiotherapy? A critical review. Radiother Oncol. 2009;91:4.
21. Rossi S. Developments in proton and light-ion therapy. In: Proceedings of the 10th EPAC. Edinburgh: 2006. p. 3631–35.
22. Muramatsu M, Kitagawa A, Sakamoto Y, Sato S, Sato Y, Ogawa H, Yamada Y, Ogawa HY, Yoshida Y, Drentje AG. Development of a compact electron-cyclotron-resonance ion source for high-energy carbon-ion therapy. Rev Sci Instrum. 2005;76: 113304-1–6.
23. Iwata Y, Yamada S, Murakami T, Fujimoto T, Fujisawa T, Ogawa H, Miyahara, N, Yamamoto K, Hojo S, Sakamoto Y, Muramatsu M, Takeuchi T, Mitsumoto T, Tsutsui H, Watanabe T, Ueda T. Performance of a compact injector for heavy-ion medical accelerators. Nucl Instrum Meth A. 2007;572:1007–21.
24. Komori M, Furukawa T, Kanai T, Noda K. Optimization of spiral wobbler system for heavy-ion radiotherapy. Jpn J Appl Phys. 2004;43:6463–7.
25. Yonai S, Kanematsu N, Komori M, Kanai T, Takei Y, Takahashi O, Isobe Y, Tashiro M, Koikegami H, Tomita H. Evaluation of beam wobbling methods for heavy-ion radiotherapy. Med Phys. 2008; 35:927–38.
26. Noda K, Furukawa T, Fujimoto T, Fukuda S, Inaniwa T, Himukai T, Iwata Y, Kanematsu N, Katagiri K, Kitagawa A, Minohara S, Miyoshi T, Mori S, Murakami T, Sano Y, Sato S, Shirai T, Takada E, Takei Y, Takeshita E. Recent progress on new treatment research project at HIMAC. Nucl Instrum Meth B. 2011;269: 2924–27.
27. Iwata Y, Uchiyama H, Fujimoto T, Takada E, Shirai T, Furukawa T, Mizushima K, Takeshita E, Katagiri K, Sato S, Noda K, Kadowaki T, Sona Y. Multiple-energy operation with extended flattops at HIMAC. Nucl Instrum Meth A. 2010;624:33–8.
28. Inaniwa T, Furukawa T, Kanematsu N, Mori S, Mizushima K, Sato S, Toshito T, Shirai T, Noda K. Evaluation of hybrid depth scanning for carbon-ion radiotherapy. Med Phys. 2012;39:2820–5.

Part VII

Oncology Information System

Oncology Information System

13

Yutaka Ando

Abstract

A system that can manage patient treatment schedules, treatment plans, treatment delivery, treatment summaries, and results is inevitable. An oncology information system (OIS) can be used to manage these data. This OIS will encompass the information exchange between radiation therapy departments and the overall healthcare enterprise. Particle therapy departments utilize many information systems. For medical safety purposes, patient demographic information and treatment data should be shared among these systems. The OIS must be connected with other hospital information systems (HISs, e.g., electronic medical records). All HISs should share radiation treatment information. This information may be transmitted transparently by each device. Evaluating and improving the quality of radiation therapy requires complete information on cancer stage and treatment results. Hospital-based registries are a key tool. The development of information systems requires standardization for rapid development and ease of integration. Standardization also facilitates preparation and reduces the test time. For standardization there are some standards (such as Digital Imaging and Communications in Medicine-Radiotherapy (DICOM-RT) and Integrating the Healthcare Enterprise (IHE)). By using these standards we can easily share the patient data. And this interoperability will lead to improved medical safety and professional effectiveness.

Keywords

DICOM-RT • IHE • Interoperability • Standardization of data

13.1 Scope of an Oncology Information System

For particle therapy, hospitals need a system that can manage patient treatment schedules, treatment plans, treatment delivery, treatment summaries, and results; an oncology information system (OIS) [1–3] can be used to manage these data. Radiotherapy departments also need to communicate with other systems such as the hospital information system (HIS) and the picture archiving and communication systems (PACS).

The OIS is a tool that can be used to manage patient information, treatment information, and treatment delivery information in a radiation therapy department. The development of an OIS is inevitable for the safety and efficiency of particle therapy. This OIS will encompass the information exchange between radiation therapy departments and the overall healthcare enterprise. The OIS comprises systems

Y. Ando (✉)
Research Center Hospital for Charged Particle Therapy, National Institute of Radiological Sciences, 4-9-1, Anagawa, Inage, Chiba 238-8555, Japan
e-mail: ando_y@nirs.go.jp

H. Tsujii et al. (eds.), *Carbon-Ion Radiotherapy: Principles, Practices, and Treatment Planning*,
DOI 10.1007/978-4-431-54457-9_13, © Springer Japan 2014

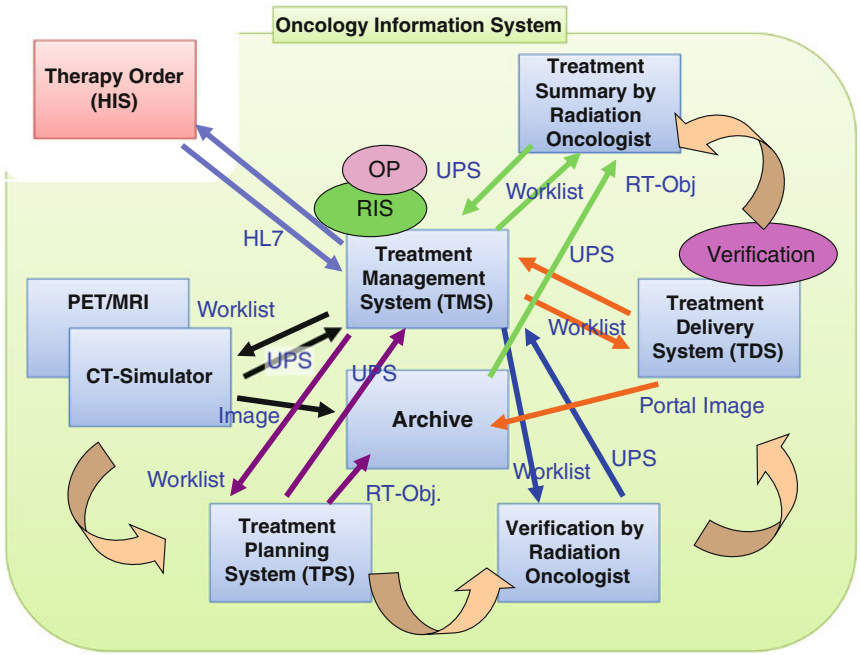

Fig. 13.1 Scope of an OIS and radiation therapy workflow. HL7, Health Level 7 [4]; UPS, Unified Worklist and Procedure Step [5]; HIS, Hospital Information System

for order entry, treatment management, treatment delivery, verification, and treatment results as well as data archiving; thus, it manages the entire scope of the radiation therapy workflow (Fig. 13.1). First, the initial radiotherapy order is issued by the HIS; this order is then transferred to the treatment management system (TMS). The order is processed in the TMS and computed tomography (CT) simulation is performed. Next, the treatment plan is developed using the treatment planning system (TPS) and approved by the radiation oncologist. Treatments are delivered according to this schedule, and each delivery is verified by the oncologist. Finally, when treatment is complete, the radiation oncologist creates the treatment summary. The OIS can handle all data related to radiation therapy and managing treatment status.

13.2 Interoperability

Information systems do not function independently. All systems should be interconnected and work in close cooperation. When linking to other systems, many department systems (e.g., the TPS, treatment delivery system, and treatment management system) require proprietary protocols and connection methods. These proprietary structures restrict selection and lead to high cost and huge effort during system upgrades and/or replacement.

Figure 13.1 illustrates the interoperability of the OIS. Patient demographic data should be exchanged between the HIS and the TMS by using the Health Level 7 (HL7) standard [4]. Worklists and the progression of radiotherapy orders should be transmitted in Digital Imaging and Communications in Medicine (DICOM) Unified Worklist and Procedure Step (UPS) [5] format. Radiation therapy dose calculation push workflow and radiation therapy pull workflow are explained in the UPS document. Treatment planning information should be stored in DICOM radiotherapy (DICOM-RT) object format and communicated using DICOM transfer protocols.

Interoperability also supports medical safety and operational efficiency. Particle therapy departments utilize many information systems. For medical safety purposes, patient demographic information and treatment data should be shared among these systems.

13.2.1 Electronic Medical Records, Electronic Healthcare Records, and Personal Health Records

The OIS must be connected with other HISs (such as electronic medical records (EMR) [6, 7], electronic healthcare records (EHR) [8, 9], and personal health records (PHR) [10, 11]) and communicate with data on basic patient information, treatment information, medical practices, and treatment results. All HISs should share radiation treatment information. This information may be transmitted transparently by each device. We have to consider the method and functionality of this cooperation. As the de facto standard, the HL7 format should be used for electronic data transfer between the EMR, EHR, and PHR and the OIS.

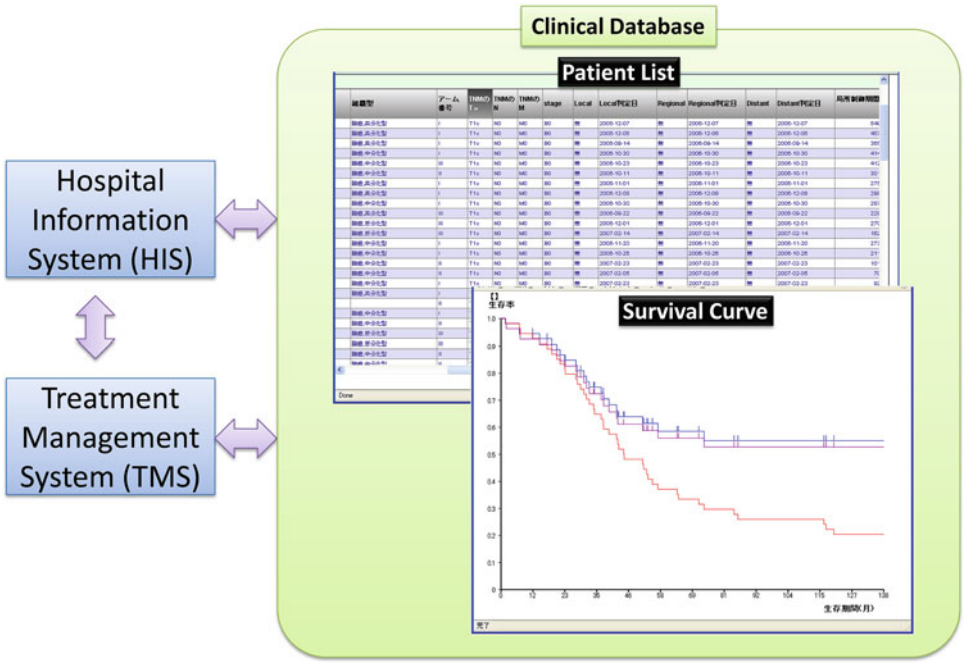

Fig. 13.2 Clinical database: the clinical database is connected to the HIS and TMS and processes patient and treatment data including results and follow-up information. The patient list and survival curves are also generated

13.2.2 Clinical Database

When particle therapy proceeds in a clinical trial, data analysis is very important. The OIS will include functions to summarize and analyze results. Treatment data processed in the EMR, TPS, and TMS will be stored in the clinical database and analyzed by calculating survival curves. The HIS and TMS are connected to the clinical database that generates patient lists specified by treatment protocols and calculates survival ratios. Figure 13.2 shows the relationship between the HIS, TMS, and clinical database.

13.3 Treatment Summary and Radiation Oncology Registry

When radiation therapy is completed, radiation oncologists evaluate treatment results and follow up with patients. Therefore, the OIS needs to store clinical data, treatment plans, delivery dosages, radiation effects, and side effects to facilitate comprehensive treatment evaluation. These treatment data should be carefully maintained and summarized within a clinical database system.

Evaluating and improving the quality of radiation therapy requires complete information on cancer stage and treatment results. Hospital-based registries are a key tool. To determine the completeness of registry data, a nationwide cancer database is expected [12, 13]. The National Radiation Oncology Registry (NROR) [14] pilot program was presented as the basis for the creation of a nationwide electronic registry in the USA. This will be supported by an innovative information technology infrastructure that will maximize efficiency through the automated collection and electronic transfer of data. The NROR is supported by the Radiation Oncology Institute and the American Society of Radiation Oncology (ASTRO). Similar nationwide registries have also been planned and established in other countries. The automated collection and electronic transfer of data is a key issue to reduce physician workload and maximize efficiency. In Japan, the Japanese Society for Therapeutic Radiology and Oncology (JASTRO) [15] is planning to develop a similar radiation oncology database.

This registry should be developed with the careful selection of items. The items registered in the database should be standardized and anonymized to protect patient privacy. Moreover, security must be considered when determining the method to link patient data between the registry and hospital identification numbers.

13.4 Standardization

In a radiation oncology system, multiple devices and subsystems are connected to each other. The transfer of information depends upon the coordination between devices. Further, the development of information systems requires standardization

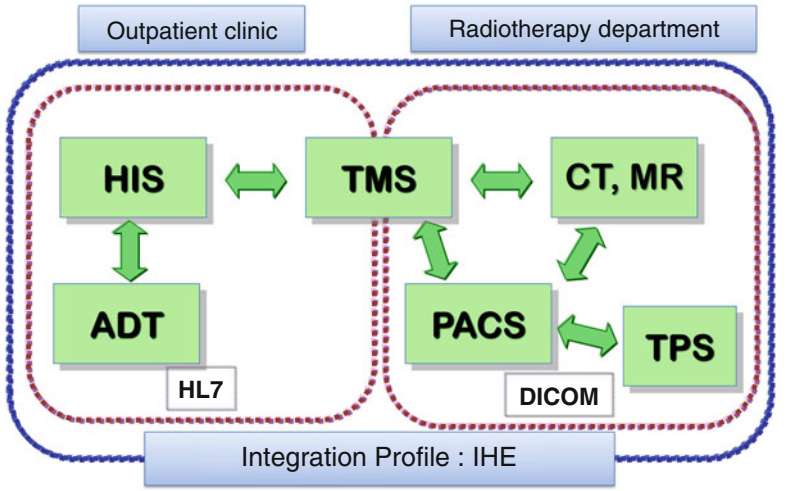

Fig. 13.3 Information exchanged between the "admission, discharge, and transfer"; HIS; and TMS is transferred in HL7 format. In radiotherapy departments, however, data are exchanged in DICOM format. The integration profile of IHE defines the workflow related to both outpatient clinics and radiotherapy departments

for rapid development and ease of integration. Standardization also facilitates preparation and reduces the test time. When standardized devices are used, it is much simpler to replace systems as needed and create request for proposal (RFP) documents.

There are several arguments in favor of standardization:

- Easy creation of RFP documents
- Shortening of preparation and test times for systems integration
- Simple replacement by standardized systems
- Increased connectivity between the HIS, PACS, and departmental systems

13.4.1 DICOM-RT

DICOM [16, 17] is widely used in the field of medical imaging and has been extended for use in various subspecialties; DICOM-RT [18, 19] was created for use with radiation therapy. DICOM-RT objects consist of radiotherapy (RT) images (digitally reconstructed radiographs, portal images, and simulation images), RT doses (dose matrix, dose points, isodoses, and dose-volume histograms), RT structure sets (VOIs, dose reference points, and observations/characterizations), RT plans (external and brachytherapy plans, tolerance tables, fractionation, schemes, and patient setup), RT treatment records (beam and brachytherapy session/summary recording information), and RT treatment summary records. DICOM-RT was originally designed for photon radiotherapy but was adopted for particle therapy by Radiotherapy Extensions for Ion Therapy [20].

13.4.2 Integrating the Healthcare Enterprise

Integrating the Healthcare Enterprise (IHE) [21, 22] is a project which initiates to improve the cooperation of medical information systems such as the HIS, PACS, TPS, and TMS. The IHE is not a simple standard but also a guideline which defines workflows and usages of established standards (DICOM and HL7). The document architecture of IHE consists of several Technical Frameworks which contain many Integration Profiles. These profiles then describe use cases, actors, and transactions. Figure 13.3 illustrates the relationship between the HL7, DICOM, and IHE definition.

13.4.2.1 Radiotherapy Planning Workflow

The radiotherapy domain of IHE defines a radiotherapy planning workflow called Basic Radiation Therapy Objects (BRTO) [23]. The BRTO involves the flow of DICOM images and treatment planning data from CT scanners through dose display for 3D conformal external beam radiation therapy. This first integration profile emphasizes reducing ambiguity and facilitating basic interoperability in the exchange of DICOM-RT objects. This profile is formally known as Normal Treatment Planning—Simple. The BRTO profile is applicable to particle therapy.

13.4.2.2 Radiotherapy Schedule Integration

This integration profile involves the exchange of schedule, order, and results information between the HIS and TMS. The emphasis of this profile is improving schedule and procedure coordination between the radiation oncology department and the rest of the clinical enterprise. These transactions

involve both workflow and the intent of radiation. This workflow is referred to as Enterprise Schedule Integration [24] by the IHE radiation oncology domain.

13.5 Conclusion

An information system for carbon ion radiotherapy is inevitable. This OIS should include all systems related to the provision and management of carbon ion therapy such as systems for order entry, treatment management, treatment planning, treatment delivery, treatment verification, treatment summary, and data archiving. Moreover, data on patient demographics, treatment planning, executed treatments, and results should be shared among these systems. Standardization of the data format and transmission protocols is also necessary for efficient data sharing. This interoperability will lead to improved medical safety and professional effectiveness.

References

1. Urda D, Ribelles N, Subirats JL, Franco L, Alba E, Jerez JM. Addressing critical issues in the development Of an oncology information system. Int J Med Inform. 2012;S1386-5056(12):00152–9. doi:10.1016/j.ijmedinf.2012.08.001.
2. Yu P, Gandhidasan S, Miller AA. Different usage of the same oncology information system in two hospitals in Sydney–lessons go beyond the initial introduction. Int J Med Inform. 2010;79(6):422–9. doi:10.1016/j.ijmedinf.2010.03.003. Epub 2010 Apr 3.
3. Yamada T, Ikeda M, Murao T, Yanagawa S, Ishigaki T, Ishiguchi T. Image storing system for radiation therapy (radiation oncology information system: ROIS) as a branch of diagnostic PACS; implementation and evaluation. Comput Med Imaging Graph. 1999; 23(2):111–7.
4. Henderson M. HL7 Messaging Second Edition, OTech Inc, 2007. http://www.hl7.org/.
5. DICOM Standards Committee, Working Group 6. DICOM Supplement 96: Unified worklist and procedure step. ftp://medical.nema.org/medical/dicom/final/sup96_ft.pdf.
6. Belletti D, Zacker C, Mullins CD. Perspectives on electronic medical records adoption: electronic medical records (EMR) in outcomes research. Patient Relat Outcome Meas. 2010;1:29–37. Epub 2010 Apr 30.
7. Grams R. The "New" America Electronic Medical Record (EMR)-design criteria and challenge. J Med Syst. 2009;33(6):409–11.
8. Cho I, Kim J, Kim JH, Kim HY, Kim Y. Design and implementation of a standards-based interoperable clinical decision support architecture in the context of the Korean EHR. Int J Med Inform. 2010;79(9):611–22. doi:10.1016/j.ijmedinf.2010.06.002.
9. Zhang J, Zhang K, Yang Y, Sun J, Ling T, Wang G, Ling Y, Peng D. Grid-based implementation of XDS-I as part of image-enabled EHR for regional healthcare in Shanghai. Int J Comput Assist Radiol Surg. 2011;6(2):273–84. doi:10.1007/s11548-010-0522-8. Epub 2010 Aug 6.
10. Kaelber D, Pan EC. The value of personal health record (PHR) systems. AMIA Annu Symp Proc. 2008;6:343–7.
11. Archer N, Fevrier-Thomas U, Lokker C, McKibbon KA, Straus SE. Personal health records: a scoping review. J Am Med Inform Assoc. 2011;18(4):515–22. doi:10.1136/amiajnl-2011-000105.
12. Mallin K, Palis BE, Watroba N. Completeness of american cancer registry treatment data: implications for quality of care research. J Am Coll Surg. 2013;216(3):428–37. doi:10.1016/j.jamcollsurg.2012.12.016. Epub 2013 Jan 26.
13. German RR, Wike JM, Bauer KR. Quality of cancer registry data: findings from CDC-NPCR's breast and prostate cancer data quality and patterns of care study. J Registry Manag. 2011;38(2): 75–86.
14. Palta JR, Efstathiou JA, Justin EB. Developing a national radiation oncology registry: from acorns to oaks. Pract Radiat Oncol. 2012; 2(1):10–7.
15. Japanese Society for Therapeutic Radiology and Oncology(JASTRO). http://www.jastro.or.jp/.
16. Bidgood Jr WD, Horii SC, Prior FW, Van Syckle DE. Understanding and using DICOM, the data interchange standard for biomedical imaging. J Am Med Inform Assoc. 1997;4(3):199–212. Review.
17. Oosterwijk H. DICOM versus HL7 for modality interfacing. J Digit Imaging. 1998;11(3 Suppl 1):39–41. Review.
18. DICOM Radiotherapy Information Objects Supplement 11. ftp://medical.nema.org/MEDICAL/Dicom/Final/sup11_ft.pdf.
19. Law MY, Liu B, Chan LW. Informatics in radiology: DICOM-RT-based electronic patient record information system for radiation therapy. Radiographics. 2009;29(4):961–72. doi:10.1148/rg.294085073. Epub 2009 May 15. Review.
20. DICOM Standards Committee, Working Group 7. DICOM Radiotherapy Extensions for Ion Therapy Supplement 102. ftp://medical.nema.org/MEDICAL/Dicom/Final/sup102_ft.pdf.
21. Cavanaugh BJ, Garland HT, Hayes BL. Upgrading legacy systems for the Integrating The Healthcare Enterprise (IHE) initiative. J Digit Imaging. 2000;13 Suppl 1:180–2. doi:10.1007/BF03167655.
22. Integrating the Healthcare Enterprise IHE. http://www.ihe.net/.
23. Integrating the Healthcare Enterprise, IHE Radiation Oncology, Technical Framework Vol 1 (RO TF-1), Revision 1.7, http://www.ihe.net/Technical_Framework/upload/IHE_RO_TF_Rev1-7_Vol1_2011-0509.pdf.
24. JASTRO, Integrating the Healthcare Enterprise. Enterprise Schedule Integration ESI, http://www.ihe-j.org/file2/comments/IHE-J_RO_TF_Volume_1_Supplement_for_Enterprise_Schedule_Integration_v0.1b.pdf.

Part VIII

Evaluation of Treatment Outcome

14 Evaluation of Treatment Outcomes Using the Heavy-Ion Medical Accelerator in Chiba (HIMAC) Approach

Tadashi Kamada

Abstract

At present, most of the patients receiving carbon ion radiotherapy (C-ion RT) at the NIRS visit the clinic seeking this specific modality, and it is difficult to obtain consent for a randomized controlled study from these patients, so it may be unnecessary to conduct a phase III trial. However, in selected tumors where a high LET benefit could be appreciated, randomized studies should be performed. In addition, studies aimed at clarifying the usefulness of carbon ion radiotherapy and elucidating any advantages from hypo-fractionation should be considered. A good quality observational study, such as a multi-institutional prospective nonrandomized concurrent phase II clinical trial, is one such new approach, and it will be proposed not only to the Japanese but also to the international community in the fields of particle therapy and radiation oncology.

Keywords

Phase II clinical trial • Randomized clinical trials (RCTs)

14.1 Introduction

The pioneering work in carbon ion radiotherapy (C-ion RT) by Japanese and European investigators has generated great enthusiasm. However, as a particle therapy center is certain to be an extremely complex and expensive medical facility, it may become a source of disagreement in the radiation oncology community.

The paradigm of drug development in medical oncology from phase I to phase II to phase III trials remains unaltered, but this is not the case in radiation oncology.

According to the presentations at the NCI "Workshop on Advanced Technologies in Radiation Oncology" in December 2006, there were only a few level I trials of new technologies in radiation oncology (http://www3.cancer.gov/rrp/workshop/2006AdvancedRadiationTech/presentations.html). For protons, the physical proof of better depth dose characteristics, virtually identical biological effects compared with X-rays, and the fact that decreased doses to normal tissues always result in decreased toxicity argue against conducting phase III trials comparing protons with X-rays [1].

Radiation oncology has not, until this decade, seen dramatic changes in technological innovations, and these give rise to new and complicated issues. For example, what kind of studies should be carried out to sort out the indications, advantages, and disadvantages of new techniques? In this chapter, the issue of evaluating the clinical results of carbon ion radiotherapy and their comparison with other modalities will be discussed.

14.2 Carbon Ion Radiotherapy Clinical Trials at the Heavy-Ion Medical Accelerator in Chiba (HIMAC)

The carbon ion radiotherapy program at the HIMAC was initiated based on the rationale of exploiting the high physical selectivity of carbon ions, as well as their high LET, with the

T. Kamada, MD., PhD (✉)
Research Center for Charged Particle Therapy, National Institute of Radiological Sciences, Anagawa 4-9-1, Inage-Ku, Chiba 263-8555, Japan
e-mail: t_kamada@nirs.go.jp

H. Tsujii et al. (eds.), *Carbon-Ion Radiotherapy: Principles, Practices, and Treatment Planning*,
DOI 10.1007/978-4-431-54457-9_14,

attendant potential radiobiological advantages for selected tumor types. From the beginning, all carbon ion radiotherapies were carried out as prospective phase I/II and II clinical trials in an attempt to identify tumor sites suitable for this treatment, including radioresistant tumors, and to determine the optimal dose fractionation, especially for hypo-fractionation, in common cancers. Our ultimate goal is to prove that C-ion RT is effective and safe for cancer treatment.

A total of 70 protocols have been conducted as of March 2013. The number of patients who have received C-ion RT has already exceeded 7,000, and in the 2012 fiscal year, more than 800 patients were treated under such protocols at the NIRS.

Clinical studies have revealed that intractable cancers such as advanced head and neck cancer, large skull base tumors, pelvic recurrence of surgically treated rectal cancer, and inoperable sarcomas can be cured, and cancers in the lungs, liver, and prostate can also be cured safely with a shorter treatment period than is required for conventional radiotherapy [2].

14.3 Should Carbon Ion Radiotherapy Be Subjected to Randomized Clinical Trials?

When comparing various therapies, the results of randomized controlled studies provide the strongest evidence. Dr. Lawrence, the Editor-in-Chief of the *Journal of Clinical Oncology*, has made the following statement about the need for phase III (randomized controlled studies) when comparing different therapies, or different types of therapeutic equipment, in the field of radiation oncology:

> In medical oncology, there is a need to compare drug treatment A to drug treatment B. It is not possible to determine which is better without carrying out a randomized trial. In radiation oncology, one can know, based on physics, that protons deliver a better dose distribution than photons, or that IMRT is superior to three-dimensional conformal therapy. If treatment planning and delivery are carried out using consistent methodology, there is no debate; this is a matter of physics. The big question is: is any observed difference clinically meaningful enough to justify the added expense? What kind of trial needs to be designed to answer this question? Would it be difficult to run a randomized trial in the United States asking whether a treatment that is superior based on physics translates into superior patient survival and/or quality of life? Would patients permit themselves to be randomly assigned to the standard but less expensive therapy [3]?

Progress in radiation oncology is inextricably linked to the development of treatment facilities; however, almost no randomized controlled study has been conducted for the purpose of the introduction of any new modality. In fact, no randomized controlled study was conducted in the shift from cobalt to linear accelerator (LINAC), but if there had been, there would have been little difference between cobalt and LINAC in the treatment results for patients with early glottic cancer. Nevertheless, cobalt irradiation has advantages in terms of both cost and equipment maintenance, and the results of LINAC may be poor unless a suitable energy is selected. Cobalt is sufficient to treat laryngeal cancer, and it may be unnecessary to introduce LINAC to achieve successful treatment for this cancer. In recent years, however, treatments with cobalt have been significantly reduced in developed countries. The distribution of the very-high-energy X-rays from the LINAC allows safer treatment of deeply situated targets, and the design of a study to determine the difference between cobalt and LINAC in patients with glottic cancer is itself a problem.

In any case, the question remains: "Should carbon ion therapy be subjected to randomized clinical trials?" In addition, what must be seen in a phase II study to justify moving to phase III? No matter how exciting the laboratory technique or how great the improvement in animal models, there must be evidence that the method is transferable to humans and that successes in the laboratory can be reproduced in humans. Further, there must be real promise of improvement in phase II studies in human tumors. There is real promise of improvement in our C-ion RT results described in this book, and the findings have been sufficient to justify the move to phase III studies, at least under the conventional program of therapeutic development.

14.4 From Phase II Clinical Trials to Randomized Clinical Trials (RCTs)

Before moving to a phase III studies, several questions must be answered. First, are there comparable phase II results in other modalities? If the answer is yes, did those modalities use the same eligibility criteria? Third, how do we recruit the patients for the phase III trial? Our patients often travel long distances to Chiba seeking carbon ion-based therapy. Finally, we charge patients more than $30,000 USD for carbon ion therapy; how do we fund such a trial? C-ion RT is effective against advanced head and neck cancer, large skull base tumors, recurrent rectal cancer, and inoperable sarcomas that are not treatable by other means. For these intractable diseases, it is clear that there are no ample data for other modalities. For these diseases, there is no clear rationale for how to conduct a phase III study and to obtain consent from patients. Hence, the answer to the question "should carbon ion therapy be subjected to randomized trials?" is "no" in the case of these intractable diseases. Promising results in the lung, liver, and prostate cancer have also been obtained with C-ion RT. A randomized controlled study might be possible in these rather common cancers. However, as described above, patients are

traveling long distances to Chiba specifically to obtain C-ion RT. It would be very hard to obtain consent from these patients for a randomized trial. Thus, our answer to the question is that it is untenable. Although RCTs provide the firmest evidence in various clinical settings, it is too difficult to conduct RCTs to assess new types of radiation therapy.

14.5 Methodologies for the Critical Assessment of New Health-Related Technologies

Radiation oncology researchers need to develop new methodologies for the critical assessment of new health-related technologies as a complement to RCTs. Possible future comparative studies of C-ion RT may include the following: (1) multi-institutional prospective clinical studies using the same protocols that can be applied to other therapies (non-randomized concurrent clinical trials), (2) matched-pair controlled studies in subjects matched to those receiving other therapies, and (3) RCTs between carbon ions and protons or other high-tech radiotherapies.

The comparative studies that are feasible at present, to further clarify the usefulness of carbon ion radiotherapy for various indications, include those in which the same protocol applied to other therapies is followed, in which the backgrounds of the subjects are matched and the treatment desired by the study participants is performed. In this case, consent from study participants can be easily obtained, the study cost is low, and an agreement among the participating facilities is relatively easily obtained, as the treatment desired by the patients is provided by the cooperating institutions.

To realize this type of comparative study, a project team has been organized to conduct a multi-institutional prospective prostate cancer study in all particle therapy facilities in operation in Japan. This study is expected to start within 1 or 2 years. This could represent a new methodology for the assessment of new radiotherapy technologies. Another method would be to determine the inclusion criteria for patients already treated and then to comparatively analyze the therapeutic results in a matched-pair study. This is feasible for common cancers if consent is obtained from the institutions that performed the treatments being compared.

References

1. Goitein M, Cox JD. Should randomized clinical trial be required for proton radiotherapy? J Clin Oncol. 2008;26:175–6.
2. Tsujii H, Mizoe J, Kamada T, et al. Clinical results of carbon ion radiotherapy at NIRS. J Radiat Res. 2007;48(Suppl A):A1–13.
3. Lawrence TS, Petrelli NJ, Li BD, Galvin JM. Think globally, act locally. J Clin Oncol. 2007;25:924–30.

Part IX

Head and Neck Tumors

Cancer of the Head and Neck

15

Azusa Hasegawa

Abstract

Carbon-ion radiotherapy, with its powerful biological effects, provides excellent therapeutic efficacy for patients with radioresistant tumors. By focusing the irradiation beam on the target lesion, this approach guarantees a low probability of damage to critical organs (e.g., the brain, spinal cord, eyes, and optic nerves) in the immediate vicinity of the target tumor. With regard to tumors in the head and neck region, carbon-ion radiotherapy is indicated for the treatment of adenoid cystic carcinomas, adenocarcinomas, and malignant mucosal melanomas in the oral and maxillofacial area. The safety and efficacy of this therapy have been established. Certain groups of radioresistant tumors are not indicated for surgical resection because of possible surgery-induced injury to critical organs, and these tumors raise a significant clinical concern because of the paucity of effective treatment options. Carbon-ion radiotherapy will represent a definitive treatment for these malignancies.

Keywords

Adenoid cystic carcinoma • Carbon ions • Head and neck cancer • Mucosal malignant melanoma • Radiotherapy

15.1 Introduction

It is often difficult to completely eradicate malignant tumors in the head and neck region by surgery alone, owing to the location of these tumors or progression. Radiotherapy is, in most cases, the first-line treatment of choice for such tumors. In the head and neck region, however, various types of non-squamous cell tumors that are not sensitive to photon radiotherapy (X- and γ-rays) develop. Dose restrictions for the critical organs located in the proximity of the target lesion (e.g., the brain, brain stem, spinal cord, eyeballs, and optic nerves) limit the administration of sufficient therapeutic radiation doses. For these reasons, a considerable proportion of cases of non-squamous cell neoplasms of the head and neck region are diagnosed as intractable, resulting in poor local control rates [1–7].

In June 1994, the National Institute of Radiological Sciences (NIRS) initiated a clinical trial on heavy charged particle therapy for malignant head and neck tumors; for these tumors, the radiation oncologist can clearly visualize reactions in the adjacent skin and mucous membrane that serve as dose-limiting factors. Carbon ions exhibit excellent dose localization attributable to their physical characteristics, commonly known as the Bragg peak, in addition to beneficial biological effectiveness [8]. Because of these features, carbon-ion radiotherapy has been expected to serve as an effective tool for the treatment of radioresistant tumors, and its safety and effectiveness have been established for tumors of various sites [9–11].

A clinical trial of carbon-ion radiotherapy for malignant head and neck tumors was conducted under the "Phase I/II Clinical Trial (Protocol 9301) on Heavy Particle Radiotherapy for Malignant Head-and-Neck Tumors," which was initiated

A. Hasegawa (✉)
Research Center Hospital for Charged Particle Therapy, National Institute of Radiological Sciences, 4-9-1 Anagawa, Inage-ku, Chiba 263-8555, Japan
e-mail: azusa@nirs.go.jp

H. Tsujii et al. (eds.), *Carbon-Ion Radiotherapy: Principles, Practices, and Treatment Planning*,
DOI 10.1007/978-4-431-54457-9_15,

in June 1994 by way of a dose escalation study using 18 fractions over 6 weeks. This trial was followed by another dose escalation study that commenced in April 1996 under the title of "Phase I/II Clinical Trial (Protocol 9504) on Heavy Particle Radiotherapy for Malignant Head-and-Neck Tumors," which used 16 fractions over 4 weeks. On the basis of the outcome of these two studies [12], the "Phase II Clinical Trial on Heavy Particle Radiotherapy for Malignant Head-and-Neck Tumors (Protocol 9602)" was initiated in April 1997, using 57.6 or 64.0 GyE in 16 fractions over 4 weeks. The dose level to be used depends on the tumor size and possibility of sparing critical organs.

15.2 Significance of Carbon-Ion Radiotherapy

Non-squamous cell, locally advanced tumors are generally considered poor candidates for photon radiotherapy and/or chemotherapy; however, carbon-ion radiotherapy (C-ion RT) showed excellent therapeutic effectiveness for these types of tumors. C-ion RT will prove beneficial as first-line local treatment for advanced tumors that are not indicated for surgery.

High-linear energy transfer charged particles such as carbon ions have excellent dose-localizing properties, and this can potentiality cause severe damage to the tumor while minimizing the effect of the treatment on normal tissue. When the tumor is located close to critical organs, the clinical target volume (CTV) is delineated, with efforts made to spare these organs.

15.3 General Management of Radiation Technique

Target contouring is performed by employing multimodality imaging and image fusions. Each patient is studied using simulation computed tomography (CT), gadolinium-enhanced magnetic resonance imaging (MRI), and 11C-methionine positron emission tomography (MET-PET). The gross tumor volume (GTV) encompasses the gadolinium-enhanced area and the area with high methionine uptake.

A shrinking-field technique is employed: the larger CTV1 receives the first 9 or 10 fractions and the reduced CTV2 receives the remaining 6 or 7 fractions. CTV1 encompasses a 10- to 15-mm uniform margin around the GTV. CTV1 can be reduced if anatomical barriers are present (e.g., for an extracranial tumor with no evidence of skull invasion, the brain is excluded from CTV1). CTV1 is usually enlarged to cover any suspected areas. In mucosal malignant melanoma (MMM), if the GTV involves part of a mucosal cavity, the entire cavity is usually included in CTV1. In adenoid cystic carcinoma (ACC), if the GTV involves part of a cranial nerve, the entire nerve is included in CTV1 up to the skull base. CTV2 encompasses a 5-mm uniform margin around GTV. It can be reduced to spare the skin, optic nerve, or other critical organs. In particular, when the eyeball or optic nerve is involved in the high-dose area, treatment planning is performed to spare the contralateral optic nerve and chiasm according to our previous dose criteria [13, 14]. Efforts are being made to decrease untoward adverse reactions by clinically applying the results of these studies.

15.3.1 Skin Reaction

Late skin reaction is an adverse effect that, depending on the severity, could significantly impair the quality of life. Extensive efforts are being made to minimize the risk of severe skin toxicity, including the use of multi-portal irradiation. A trade-off between adequate target coverage (local control) and skin sparing may be necessary, for which a 3-dimensional surface dose distribution of the skin has been used as a powerful tool to evaluate treatment plans. In our experience, marginal recurrence due to overgenerous skin sparing is a rare event (<5 %).

15.3.2 Brain Toxicity

Brain necrosis is a side effect often encountered after high-dose radiotherapy. Vascular injury, direct damage to glial cells, changes in the fibrinolytic enzyme system, and immune response are all relevant pathophysiological mechanisms, but their relative role is not yet completely clear. Radiation-induced brain necrosis is a serious complication that usually shows a progressive course, threatening the patient's life.

In C-ion RT, brain necrosis may develop in the region where the tumor was present and a high dose was administered. Necrosis is usually locally confined and asymptomatic. A cystic lesion may develop, which sometimes needs to be managed by surgical removal. Treatment planning should be performed to irradiate the smallest possible amount of normal brain tissue.

15.3.3 Optic Nerve Complications

Optic nerve irradiation can cause partial or complete visual loss, in particular when the optic nerve is involved or encased by the tumor. The tolerance dose for whole-organ irradiation with photons using conventional fractionation is well known (TD5/5 = 50 Gy; TD50/5 = 65 Gy). The tolerance of optic nerves to C-ion RT has been previously reported. Dose of 20 % volume of the optic nerve (D_{20}) has been shown to be

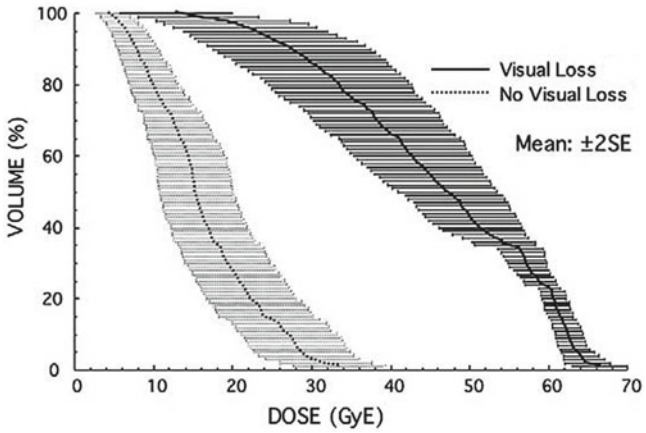

Fig. 15.1 DVH analysis was performed to compare optic nerves that did and did not develop toxicity

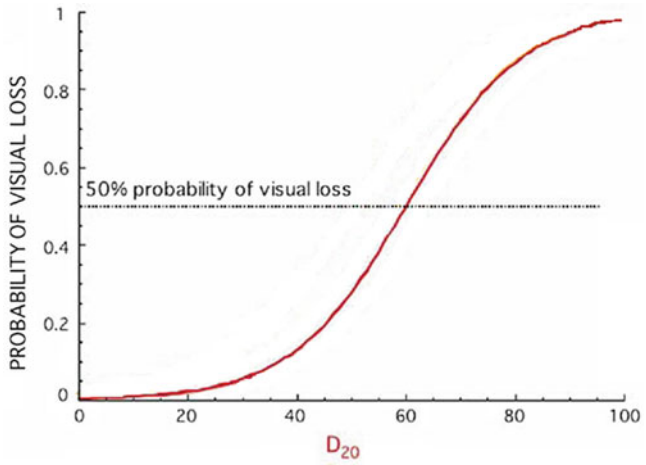

Fig. 15.2 Probability of visual loss as a function of D_{20} was calculated according to an integral logistic model

the most statistically significant predictor of toxicity. The incidence of visual loss has been 58 % when a maximum dose (D_{max}) in excess of 55 GyE and 48 % when a D_{20} in excess of 40 GyE was delivered (Figs. 15.1 and 15.2).

Every effort should be made to spare the uninvolved optic nerve so that bilateral visual acuity loss can be avoided. Dose constraints at NIRS have been previously published, in which the most relevant parameter is D_{20}. Preservation of visual acuity at a risk of <5 % can be achieved if D_{20} is maintained lower than 30 GyE. It is important to evaluate the risk on the basis of the whole nerve dose-volume histogram (DVH) and not only the specific dose or volume.

15.3.3.1 Optic Nerve Sparing

The GTV (Fig. 15.3, dark orange line) is contoured according to contrast MRI, CT, and MET-PET images, and image fusion is routinely employed. A shrinking-field technique is employed in head and neck cancer. The larger CTV1 (Fig. 15.3, light orange line) receives the first 9 fractions and the smaller CTV2 receives the last 7 fractions. Addition of uniform geometric margins around the GTV would result in CTV1 and CTV2, which were drawn similarly for avoidance of irradiation to the right optic nerves (Fig. 15.3, blue contours). Irradiation of the left optic nerve was unavoidable (Fig. 15.4).

This 76-year-old male patient with ACC was treated in December 2008. The prescribed dose was 64 GyE in 16 fractions over 4 weeks. At 37 months after C-ion RT, the patient is alive, with local control and preservation of visual acuity in both eyes.

15.3.4 Osteonecrosis

In radiation therapy, blood supply to the bone may be inhibited at the microscopic level. In particular, if the bone is destroyed by the tumor and irradiated with high-dose carbon ions or photons, the bone may undergo necrotic changes and subsequent infection may occur. Osteonecrosis caused by both tumor involvement and irradiation is extremely difficult to treat and can cause severe pain. Surgical resection of necrotic bone (sequestrectomy) may be necessary for pain control. The jawbone is also more prone to radiation-induced necrosis because of exposure to the oral bacterial load.

When the bone infiltrated by the tumor is irradiated at a high dose (for instance, in sarcoma cases), the risk of bone necrosis may be unavoidable. Oral care with weekly irrigation has the potential of lowering this risk. When bone necrosis develops, it is important to administer conservative treatment first, with systemic antibiotics, analgesics, and local antiseptic agents. Surgical resection may be necessary if the patient experiences severe pain. Close cooperation between the radiation oncologist and the oral and maxillofacial surgeon is required, and treatment planning should be optimized to allow future implant surgery (for instance, sparing zeugmatic processes whenever possible).

15.4 Results of Therapy

Between April 1997 and August 2012, a total of 438 cases were treated using 57.6 or 64.0 GyE. Histologically, 175 patients had ACC, 102 had MMM, 50 had adenocarcinoma, and the others had different diagnoses. With regard to the tumor site studied, the paranasal sinus was studied in 119 cases, the nasal cavity in 81, the major salivary gland in 59, the oral cavity in 54, the pharynx in 51, and other sites in the remaining cases. Almost all patients (74 %) had inoperable tumors.

The 5-year local control rates according to major histological types in our institution were as follows: 81 % for

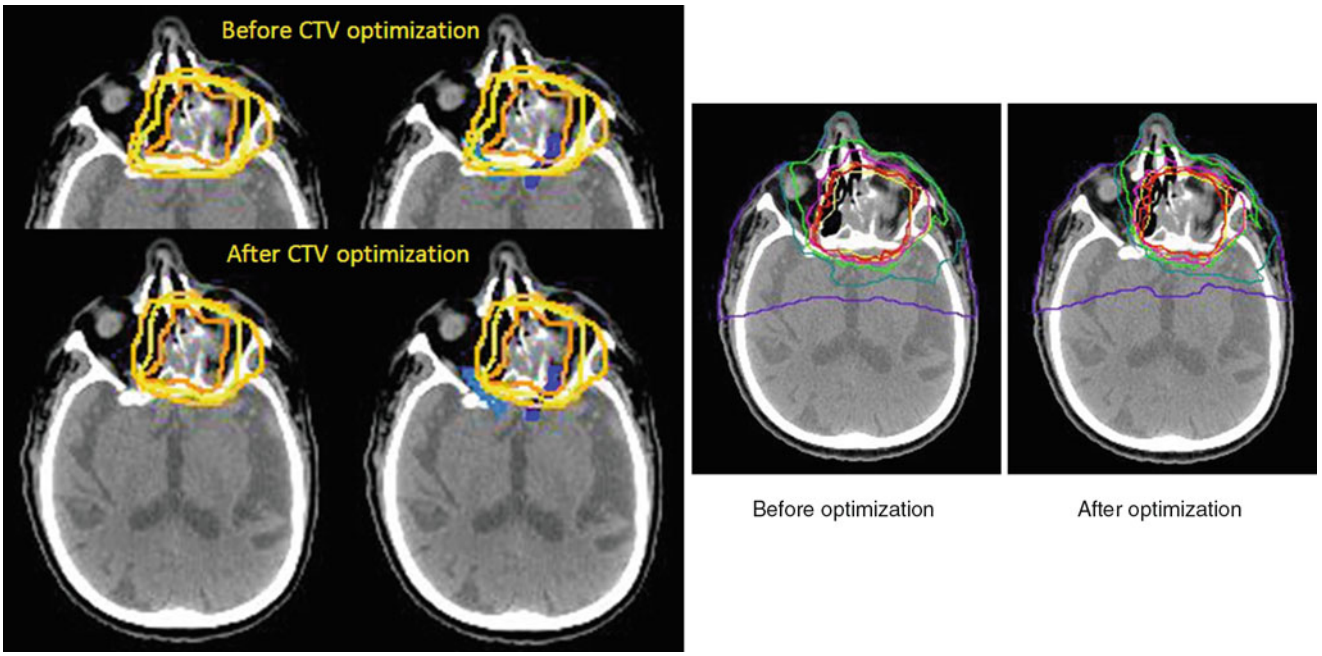

Fig. 15.3 Before CTV optimization, both optic nerves were included in the high-dose area. After CTV optimization, good sparing of the right optic nerve was achieved. Isodose level: *red* = 96 %; *orange* = 90 %; *magenta* = 70 %; *green* = 50 %; *cyan* = 30 %; *purple* = 10 %. Contour: *dark orange* = gross tumor volume, *light orange* = large clinical target volume, *yellow* = small clinical target volume

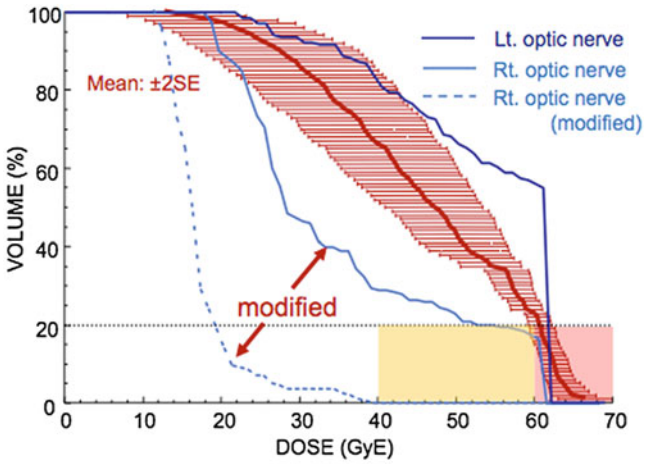

Fig. 15.4 Probability of visual loss: *red zone* 58 %, *yellow* 30 %, *pink* 50 %. Relatively small changes in CTV can produce a dramatic effect on the optic nerve DVH

adenocarcinomas, 74 % for ACCs, and 79 % for MMMs. With regard to the prescribed tumor dose, the 5-year local control rates of ACC were 81 % for the 64 GyE group and 69 % for the 57.6 GyE group. Although this rate did not differ significantly between these groups ($p = 0.0789$), the local control rate for the 64 GyE group tended to be better. However, 14 patients with bone and soft tissue sarcomas in the head and neck region (mostly osteosarcomas) had a poor 5-year local control rate, although a majority of the patients received 64 GyE. Consequently, a new treatment protocol was introduced in April 2001 to apply a total irradiation dose of 70.4 GyE in 16 fractionations over 4 weeks (see Chap. 17), a schedule similar to that used for the treatment of bone and soft tissue sarcomas of the trunk.

Additionally, the 5-year overall survival rates were 57 % for adenocarcinomas, 72 % for ACCs, and 33 % for MMMs. Although the local control facilitated by C-ion RT was promising for MMM, the survival rate was not commensurate with the favorable local control rate because of subsequent regional lymph node or distant metastases. Further to the results of preliminary analysis of this study, a new protocol was introduced in April 2001 for the purpose of prophylactic therapy against distant metastasis, the major cause of death in MMM of the head and neck region (see Chap. 16).

Regarding late radiation morbidities, almost all of the late skin and mucosal reactions were of grade 1 or lower. Less than 5 % of the patients developed grade 2 skin or mucosal reactions. The recorded tumor-related events that needed surgical treatment included encephalitis, sinusitis, otitis media, and maxillary bone necrosis. These events were documented in patients that had been informed before the start of therapy about the possibility of adverse events due to tumor infiltration. Other patients reported no unexpected serious adverse reactions.

15.5 Case Studies

15.5.1 Skin Reaction

15.5.1.1 A Case with Severe Skin Reaction

A 59-year-old man with MMM was treated with C-ion RT in July 1997. A bulky tumor invading the right nasal and paranasal cavity was observed on enhanced MRI (Fig. 15.5). The prescribed dose was 57.6 GyE in 16 fractions over 4 weeks. During the early phase of the dose escalation study, most of the tumors were treated using only two portals from the antero-posterior and lateral directions, with the safety margin being drawn equally around the GTV or CTV. Therefore, when the tumor invaded or was close to the overlying skin, it was also irradiated with the same dose as was administered to the tumor. This treatment was applied in the current case, in which the cheek skin was included for irradiation with high-dose levels, as shown in the Fig. 15.5b.

At 52 months after C-ion RT, the patient showed complete disappearance of the tumor but developed external fistula of the skin (Figs. 15.5c and 15.6-middle) corresponding to the high-dose area (Fig. 15.6-left).

In this case, only two portals were used and no specific plan for sparing the skin was considered at the time. A wide surface of the skin received the full dose. Local control was achieved, but a severe late effect developed corresponding to the high-dose area. Although this patient had received surgery for skin grafting (Fig. 15.6-right), he survived 58 months after C-ion RT and died of intercurrent diseases.

15.5.1.2 A Case with Acceptable Skin Reaction

A 63-year-old woman with MMM of the left nasal and paranasal cavity was treated with C-ion RT from January to February 2007. The prescribed dose was 64.0 GyE in 16 fractions over 4 weeks. In this case, a very tight margin toward the cheek skin was set to reduce the dose to the skin (Fig. 15.7).

Twenty-five months after C-ion RT, the patient is alive without tumor progression. No significant late toxicity is present apart from a right facial nerve deficit, which was already present at diagnosis (Fig. 15.8).

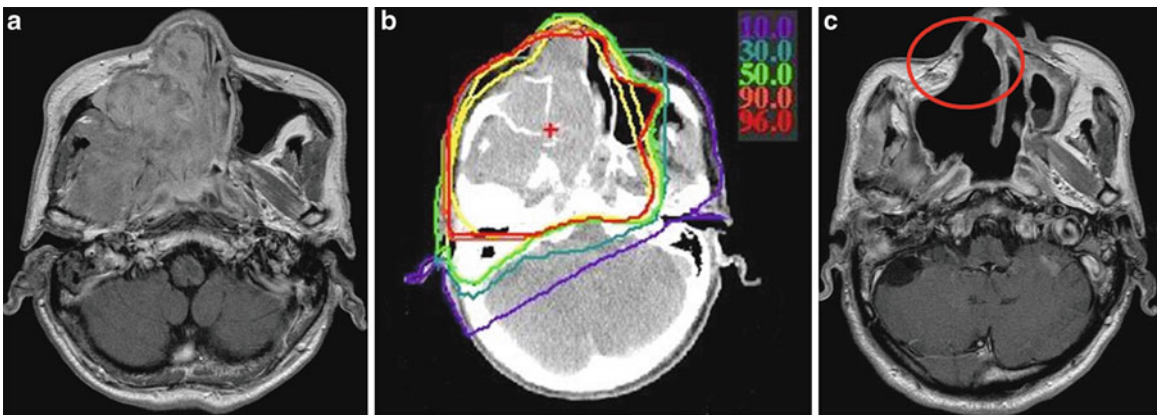

Fig. 15.5 Gadolinium-enhanced T1WI images and isodose distribution. (**a**) Before treatment, (**b**) isodose distribution, (**c**) after treatment. Isodose level: *red* = 96 %; *orange* = 90 %; *green* = 50 %; *cyan* = 30 %; *purple* = 10 %. Contour: *yellow* = clinical target volume

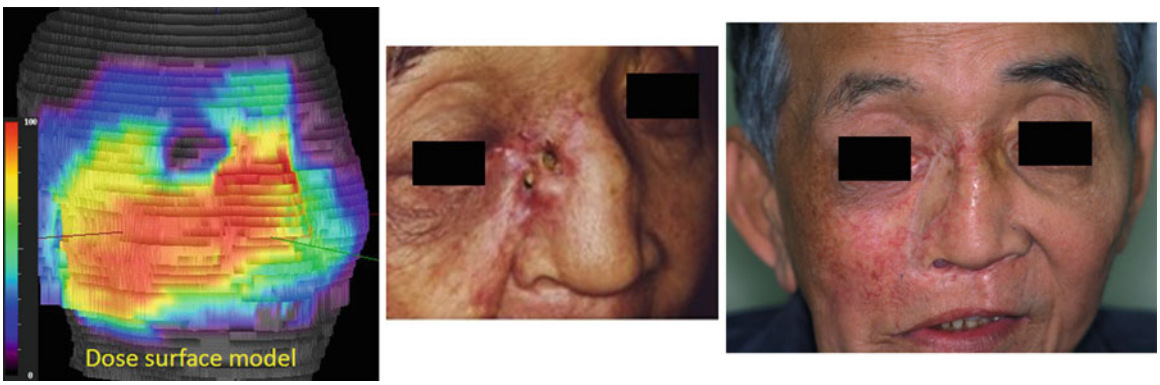

Fig. 15.6 Dose-surface model and skin reaction. The image on the right side is taken after skin grafting

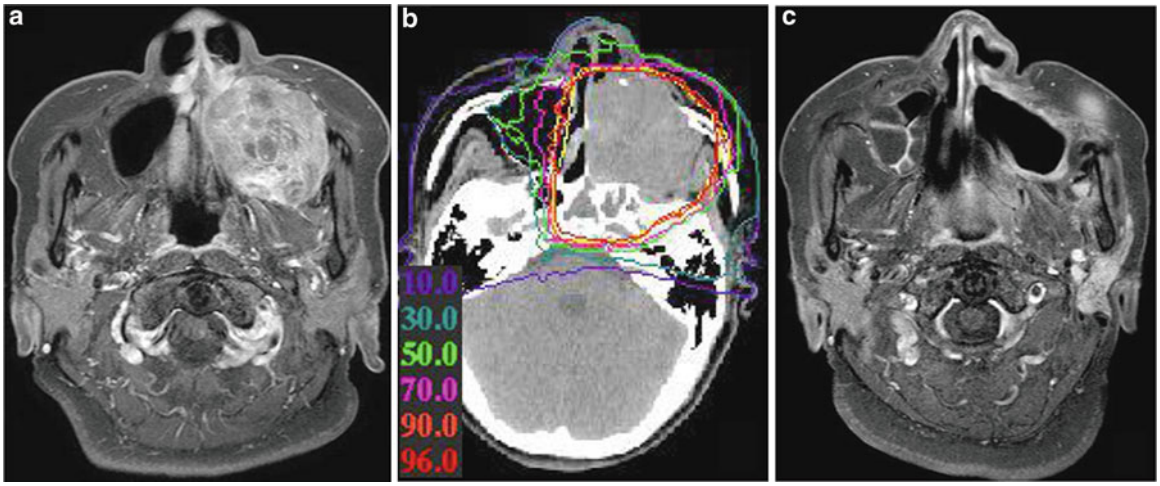

Fig. 15.7 Gadolinium-enhanced T1WI images and isodose distribution. (**a**) Before treatment, (**b**) isodose distribution, (**c**) after treatment

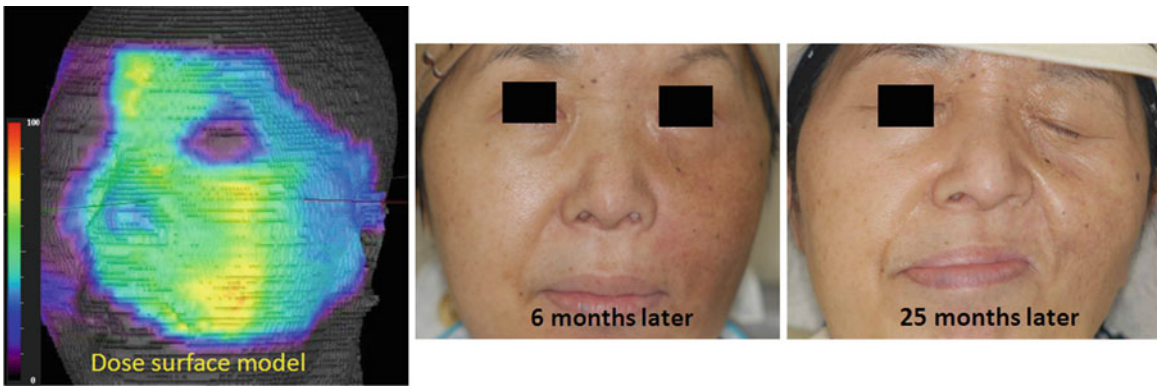

Fig. 15.8 Dose-surface model and skin reaction

15.5.2 Brain Toxicity

15.5.2.1 A Case with Late Grade 2 Reaction

A 54-year-old man with postoperative recurrence of ACC in the palate was treated with C-ion RT in April 2002. The tumor originated from the palate and extended upward to invade the brain. The dose delivered to the CTV was 57.6 GyE in 16 fractions over 4 weeks using three portals (Fig. 15.9). At 22 months after C-ion RT, grade 2 brain reaction (RTOG/EORTC, SOMA LENT) developed and was treated with steroids (Fig. 15.10). All of these lesions were found within the dose level of 70 % or greater of the prescribed dose. At 85 months after C-ion RT, there is no evidence of local recurrence and the patient is asymptomatic, requiring no medication.

15.5.2.2 A Case with Cyst Formation

A 25-year-old man with giant cell tumor was treated with C-ion RT in June 2001 (Fig. 15.11). The tumor appeared to invade the right temporal lobe. The prescribed dose was 57.6 GyE in 16 fractions over 4 weeks using three oblique portals. The brain injury was developed with cystic change in the right temporal lobe. Surgical removal of cystic lesion was performed for severe headache. This patient does not require any medication after surgery. At 8 years after C-ion RT, the patient is alive with no evidence of tumor progression.

15.5.3 Optic Nerve Complications

15.5.3.1 A Case with Visual Loss in the Involved Side

A 71-year-old man with MMM was treated with C-ion RT in November 1998. The tumor occupied the nasal cavity and ethmoidal sinus. Evidence of direct tumor invasion of the left orbit and left optic nerve was noted on enhanced MRI. The tumor was close to the right optic nerve. A total dose of 57.6 GyE was delivered in 16 fractions over 4 weeks using two portals (antero-posterior and left lateral) (Fig. 15.12). A reduced margin was employed in order to avoid irradiation

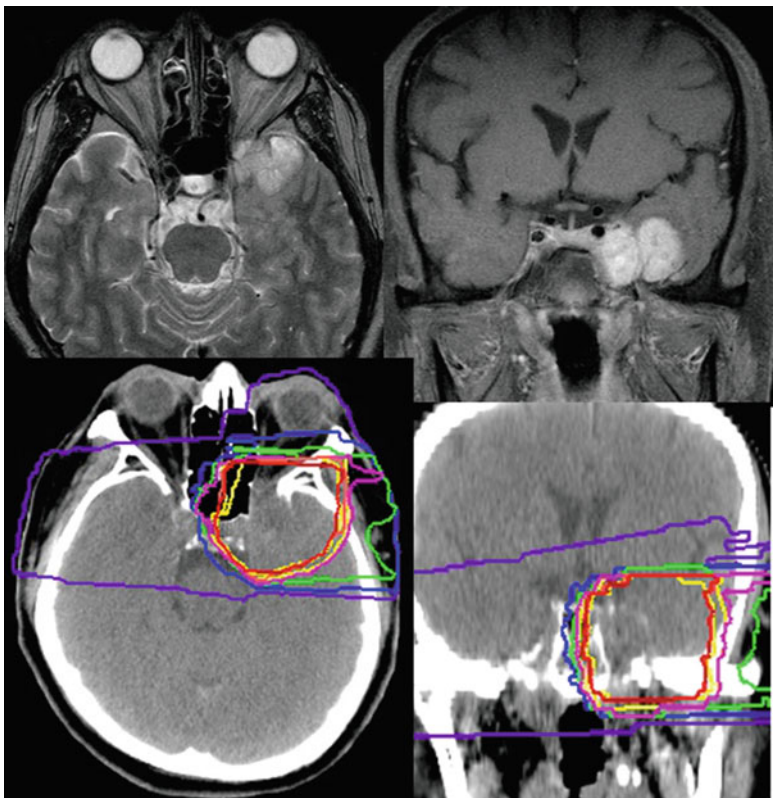

Fig. 15.9 MRIs before treatment and isodose distribution. Isodose level: *red* = 96 %; *orange* = 90 %; *magenta* = 70 %; *green* = 50 %; *cyan* = 30 %; *purple* = 10 %. Contour: *yellow* = clinical target volume

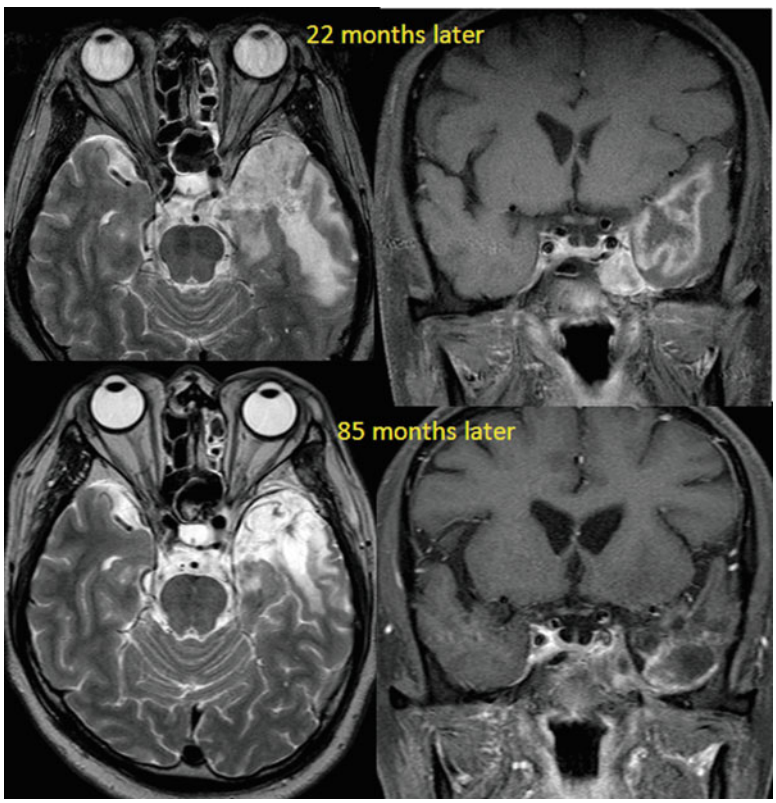

Fig. 15.10 MRIs after treatment

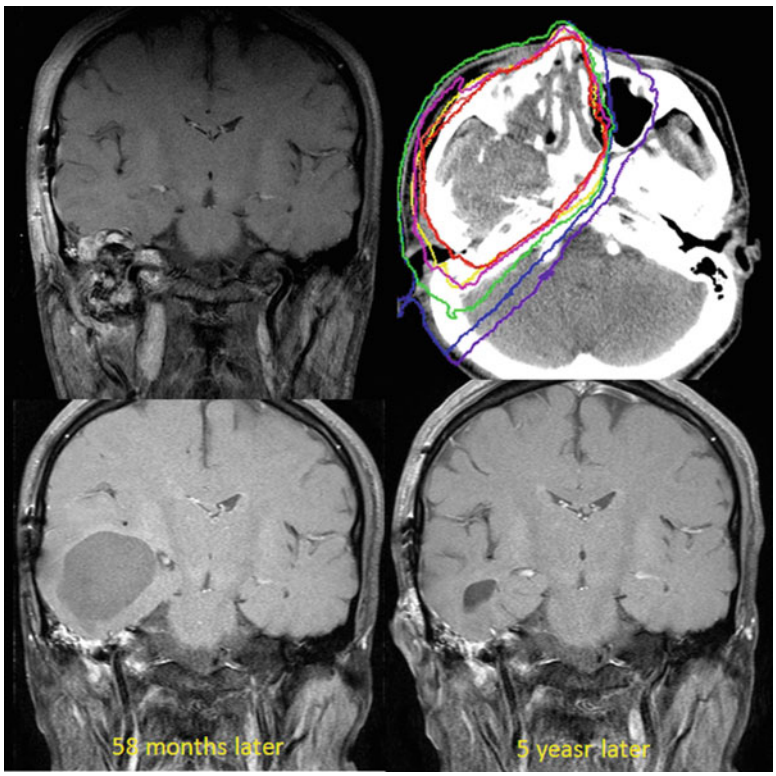

Fig. 15.11 Isodose distribution and MRIs before and after treatment. Isodose level: *red* = 96 %; *orange* = 90 %; *magenta* = 60 %; *green* = 50 %; *cyan* = 30 %; *purple* = 10 %. Contour: *yellow* = clinical target volume

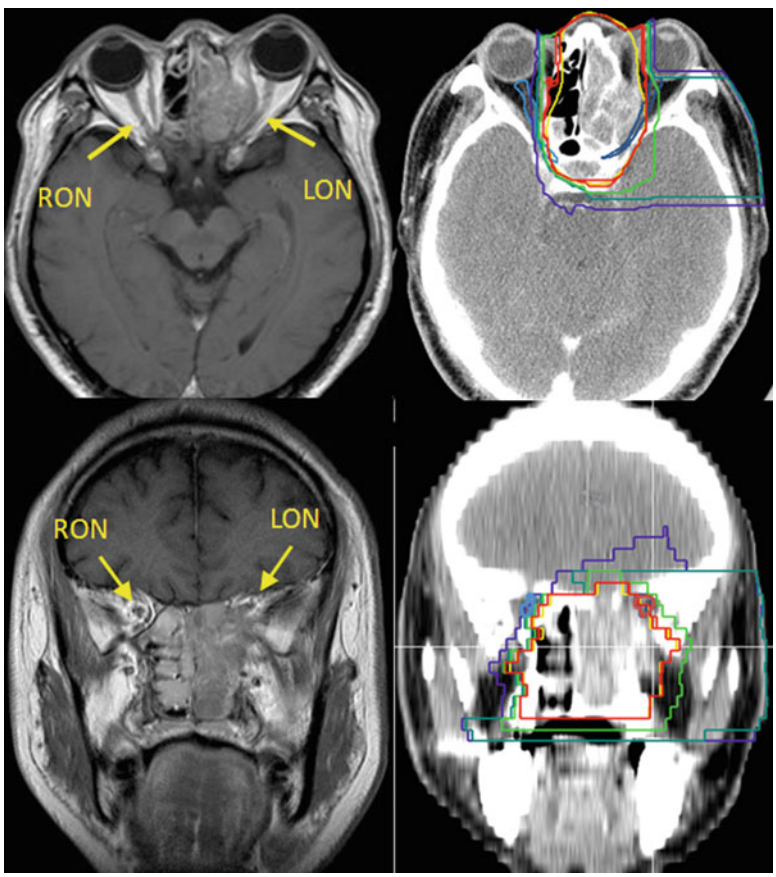

Fig. 15.12 MRIs before treatment and isodose distribution. Isodose level: *red* = 96 %; *orange* = 90 %; *green* = 50 %; *cyan* = 30 %; *purple* = 10 %. Contour: *yellow* = clinical target volume

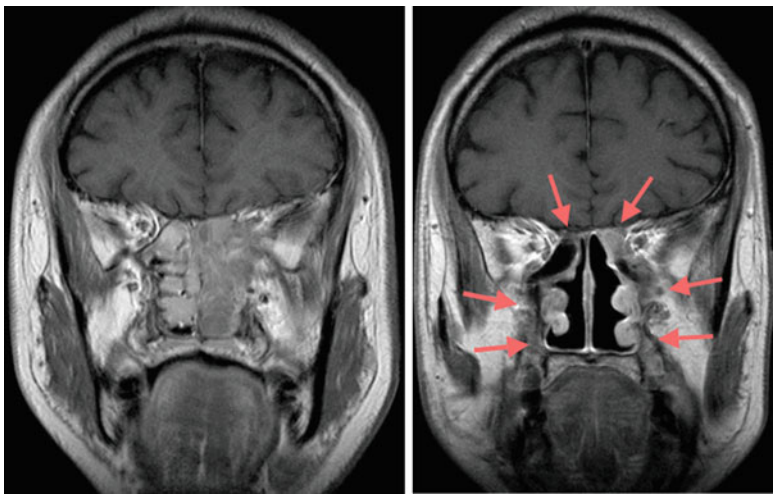

Fig. 15.13 After 22 months, MRI shows complete local response

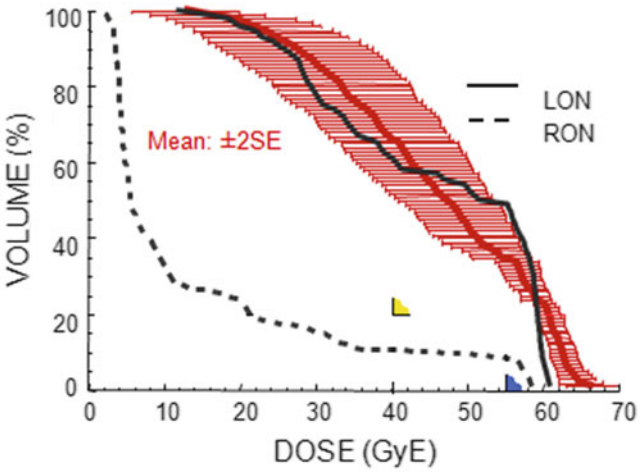

Fig. 15.14 Left optic nerve DVH (*full line*) was in the region that had resulted in visual loss in past experience at NIRS. Right optic nerve DVH (*broken line*) was within acceptable constraints for D_{20} (*yellow triangle*) but slightly above safe levels for D_{max} (*blue triangle*)

of the right optic nerve. Care was taken to avoid the patch line within the optic nerve, although the right optic nerve did receive high-dose irradiation.

The patient was alive without tumor progression for 73 months after C-ion RT (Fig. 15.13). There has been complete visual loss in the left eye, whereas the visual acuity of right eye has remained unchanged (Fig. 15.14) [13].

15.5.4 Osteonecrosis

15.5.4.1 A Case with Osteosarcoma

A 52-year-old woman with maxillary bone osteosarcoma was treated with C-ion RT in June 2004. The bone was partially destroyed by tumor as shown on MRI and CT scans (Fig. 15.15a). The prescribed dose was 70.4 GyE in 16 fractions over 4 weeks using three oblique portals (Fig. 15.15b). Nine months after C-ion RT, the patient developed well-defined bone necrosis. At 14 months after C-ion RT, since the tumor was locally controlled and the necrotic bone was locally limited, surgical resection of necrotic bone was performed for pain control. A denture and palatal prosthesis were successfully applied (Fig. 15.16). At 62 months after C-ion RT, the patient is alive with no evidence of disease.

The bone infiltrated by tumor can easily result in bone necrosis after radiotherapy. After C-ion RT, as bone necrosis is generally limited, it can be surgically resected; thereafter, a denture and palatal prosthesis can be applied in most cases.

15.5.4.2 A Case with Mucosal Malignant Melanoma

A 63-year-old woman with MMM of the left nasal and paranasal cavity was treated with C-ion RT from January 5 to February 1, 2007 (Fig. 15.17). The prescribed dose was 64.0 GyE in 16 fractions over 4 weeks. This is the same patient as in a case with acceptable skin reaction (20.6.1.2). At 25 months after C-ion RT, since the tumor was locally controlled and the necrotic bone was locally limited, surgical resection of necrotic bone was performed for pain control (Fig. 15.18). A denture and palatal prosthesis were successfully applied. At 62 months after C-ion RT, the patient is alive with no evidence of disease.

15.5.5 Recurrence Pattern and Re-Irradiation

Loco-regional recurrence of the tumor is classified as "in-field recurrence" if the lesion recurs within the high-dose volume (planning target volume, PTV), "marginal recurrence" if it recurs on the boundary of the PTV, and "regional recurrence" if the tumor recurs in the region nearby but apart from the PTV. When the shrinking technique is used, it is very difficult to distinguish in-field and marginal recurrence.

Fig. 15.15 Gadolinium-enhanced T1WI image, CT, and isodose distribution. (**a**) Before treatment, (**b**) isodose distribution. Isodose level: *red* = 96 %; *orange* = 90 %; *magenta* = 60 %; *green* = 50 %; *cyan* = 30 %; *purple* = 10 %. Contour: *yellow* = clinical target volume

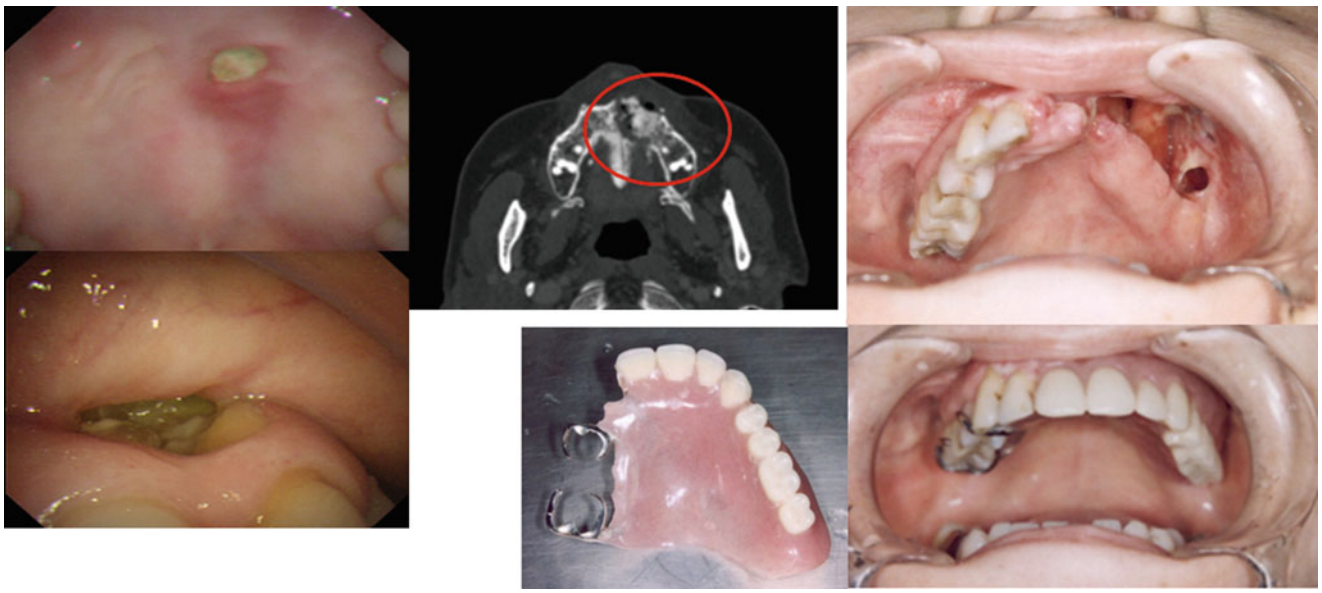

Fig. 15.16 Osteonecrosis after sequestrectomy

Fig. 15.17 Isodose distribution and CT images. (**a**) Before treatment, (**b**) after treatment. Isodose level: *red* = 96 %; *orange* = 90 %; *magenta* = 70 %; *green* = 50 %; *cyan* = 30 %; *purple* = 10 %. Contour: *yellow* = clinical target volume

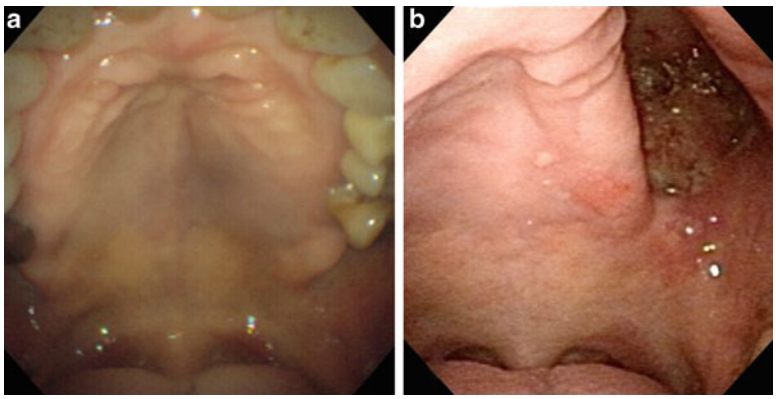

Fig. 15.18 Clinical pictures of the palate. (**a**) Before treatment, (**b**) after treatment and sequestrectomy

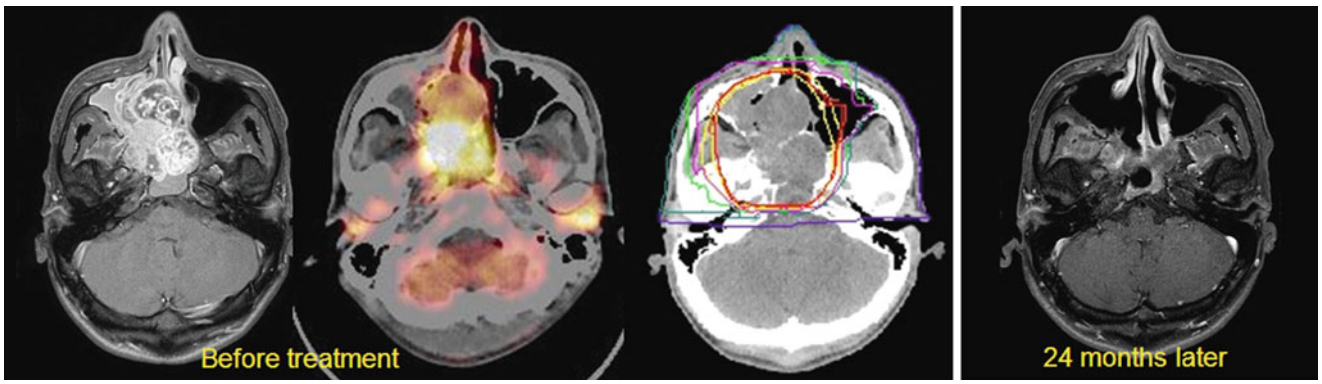

Fig. 15.19 Magnetic resonance and MET-PET images before treatment, isodose distribution, and 24 months later. Isodose level: *red* = 96 %; *orange* = 90 %; *magenta* = 60 %; *green* = 50 %; *cyan* = 30 %; *purple* = 10 %. Contour: *yellow* = clinical target volume

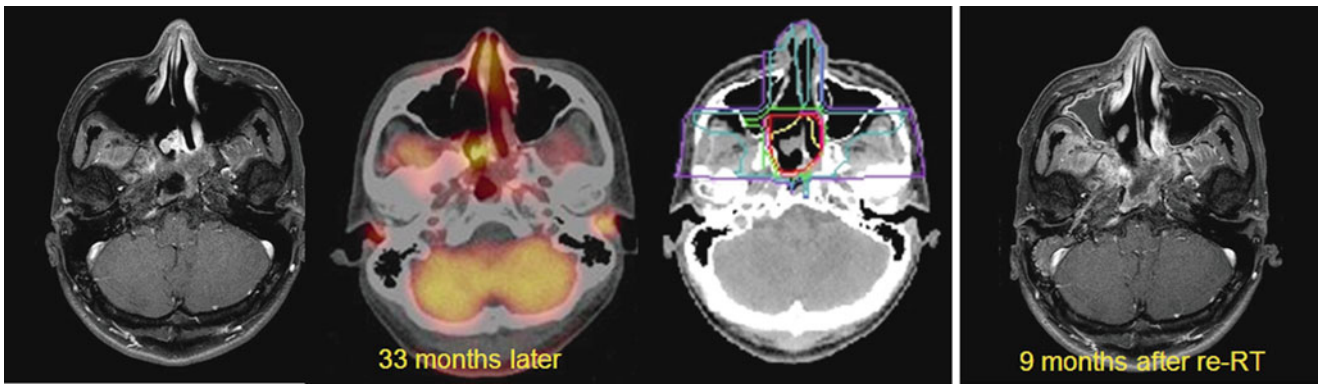

Fig. 15.20 Magnetic resonance and MET-PET images before re-irradiation, isodose distribution, and after re-irradiation. Isodose level: *red* = 96 %; *orange* = 90 %; *magenta* = 70 %; *green* = 50 %; *cyan* = 30 %; *purple* = 10 %. Contour: *yellow* = clinical target volume

Since 2008, re-irradiation to local recurrence has been performed. Because of their good physical and biological properties, carbon ions are excellent tools for re-irradiation to small recurrences. Special care must be taken to avoid toxicity of previously irradiated critical organs.

15.5.5.1 A Case with In-Field Recurrence

A 34-year-old man affected by ACC was treated with C-ion RT in January 2006. The nasal cavity and paranasal sinuses were almost entirely replaced by the tumor, which was distinctly seen on MET-PET. A total dose of 64 GyE was administered in 16 fractions over 4 weeks using three portals. At 24 months after C-ion RT, remarkable shrinkage of the tumor was observed (Fig. 15.19).

At 33 months after C-ion RT (Fig. 15.20), however, the patient developed a new lesion, seen within CTV2 on MRI and MET-PET. Biopsy indicated the same histology as the primary tumor. The lesion was judged to be an in-field recurrence, for which C-ion RT was again attempted, with 57.6 GyE in 12 fractions using three portals. At 42 months

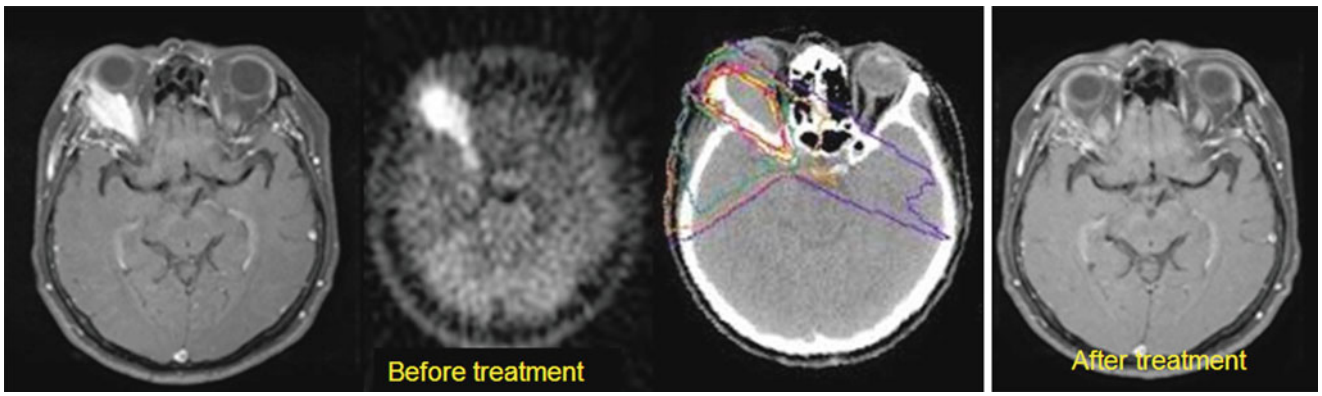

Fig. 15.21 Magnetic resonance and MET-PET images and isodose distribution. Isodose level: *red* = 96 %; *orange* = 90 %; *magenta* = 60 %; *green* = 50 %; *cyan* = 30 %; *light orange* = 20 %; *purple* = 10 %. Contour: *yellow* = clinical target volume

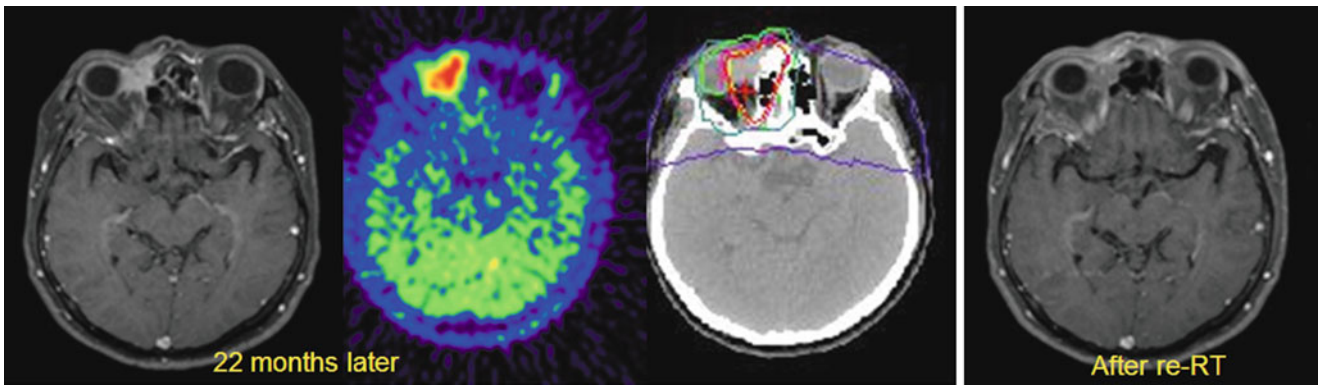

Fig. 15.22 Magnetic resonance and MET-PET images before and after re-irradiation and isodose distribution. Isodose level: *red* = 96 %; *orange* = 90 %; *magenta* = 70 %; *green* = 50 %; *cyan* = 30 %; *purple* = 10 %. Contour: *yellow* = clinical target volume

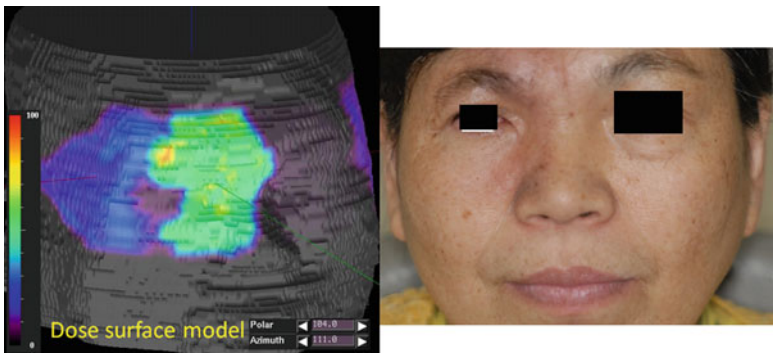

Fig. 15.23 Dose-surface model before re-irradiation and late skin reaction

after the initial C-ion RT (9 months after re-irradiation), the tumor disappeared completely without severe side effects.

15.5.5.2 A Case with Marginal Relapse

A 56-year-old woman had lacrimal gland ACC and was treated with C-ion RT in July 2005. MRI and MET- PET showed the presence of the tumor in the inner part of the orbital cavity. A total dose of 57.6 GyE was administered in 16 fractions over 4 weeks. The nasal part of the orbit was not irradiated. At 10 months after C-ion RT, complete response was achieved (Fig. 15.21).

Twenty-two months after C-ion RT (Fig. 15.22), recurrence was evident on MRI and MET-PET. The lesion originated in the nasal part of the orbit that had not received full dose and was considered as marginal recurrence within the CTV1. C-ion RT was performed again with 57.6 GyE in 12 fractions.

Four months after re-irradiation with carbon ions, a complete MET-PET and MRI response was achieved. Skin sparing is critical in re-irradiation. In this case, the use of multi-portals facilitated reduction of the high-dose area to a small spot. Skin reaction 1 week after re-irradiation was mild (G1) (Fig. 15.23).

References

1. Lengyel E, Gilde K, Remenár E, et al. Malignant mucosal melanoma of the head and neck. Pathol Oncol Res. 2003;9: 7–12.
2. Mendenhall WM, Morris CG, Amdur RJ, et al. Radiotherapy alone or combined with surgery for adenoid cystic carcinoma of the head and neck. Head Neck. 2004;26:154–62.
3. Mendenhall WM, Amdur RJ, Hinerman RW, et al. Head and neck mucosal melanoma. Am J Clin Oncol. 2005;28:626–30.
4. Bridger AG, Smee D, Baldwin, et al. Experience with mucosal melanoma of the nose and paranasal sinuses. ANZ J Surg. 2005;75:192–7.
5. Mendenhall WM, Morris CG, Amdur RJ, et al. Radiotherapy alone or combined with surgery for salivary gland carcinoma. Cancer. 2005;103:2544–50.
6. Krengli M, Masini L, Kaanders JH, et al. Radiotherapy in the treatment of mucosal melanoma of the upper aerodigestive tract; analysis of 74 cases. A Rare Cancer Network study. Int J Radiat Oncol Biol Phys. 2006;65:751–9.
7. Cheng YF, Lai CC, Ho CY, et al. Toward a better understanding of sinonasal mucosal melanoma: clinical review of 23 cases. J Chin Med Assoc. 2007;70:24–9.
8. Kanai T, Endo M, Minohara S, et al. Biophysical characteristics of HIMAC clinical irradiation system for heavy-ion radiation therapy. Int J Radiat Oncol Biol Phys. 1999;44:201–10.
9. Tsujii H, Morita S, Miyamoto T, et al. Preliminary results of phase I/II carbon-ion therapy at the National Institute of Radiological Sciences. J Brachytherapy Int. 1997;3:1–8.
10. Tsujii H, Mizoe JE, Kamada T, et al. Overview of clinical experiences on carbon ion radiotherapy at NIRS. Radiother Oncol. 2004;73:41–9.
11. Tsujii H, Mizoe J, Kamada T, et al. Clinical results of carbon ion radiotherapy at NIRS. J Radiat Res. 2007;48A:A1–13.
12. Mizoe J, Tsujii H, Kamada T, et al. Dose escalation study of carbon ion radiotherapy for locally advanced head-and-neck cancer. Int J Radiat Oncol Biol Phys. 2004;60:358–64.
13. Kanematsu N, Endo M, Futami Y, et al. Treatment planning for the layer-stacking irradiation system for three-dimensional conformal heavy-ion radiotherapy. Med Phys. 2002;29:2823–9.
14. Hasegawa A, Mizoe JE, Mizota A, et al. Outcomes of visual acuity in carbon ion radiotherapy: analysis of dose-volume histograms and prognostic factors. Int J Radiat Oncol Biol Phys. 2006;64:396–401.
15. Hirasawa N, Tsuji H, Ishikawa H, et al. Risk factors for neovascular glaucoma after carbon ion radiotherapy of choroidal melanoma using dose-volume histogram analysis. Int J Radiat Oncol Biol Phys. 2007;67:538–43.

Malignant Melanoma of the Head and Neck

16

Ryo Takagi

Abstract

Malignant mucosal melanoma (MMM) of the head and neck is rare and has a poor prognosis. Additionally, MMM has long been regarded as radioresistant. We recruited 106 patients with MMM of the head and neck who were treated with carbon ion radiotherapy (C-ion RT) and concomitant chemotherapy. The 5-year local control and overall survival rates of all patients were 80.6 and 54.0 %. The median survival time was 64.8 months. The most common acute toxicities were mucositis (grade 3, 21.7 %) and skin reactions (grade 3, 0.9 %); no reactions worse than grade 3 were observed. Furthermore, the most common adverse events associated with dacarbazine, nimustine hydrochloride, and vincristine sulfate (DAV) chemotherapy were myelotoxicity and liver dysfunction. C-ion RT is a safe and effective treatment for MMM of the head and neck because of good local control and acceptable toxicity. In addition, the overall survival rate was better than the rates associated with conventional radiation therapy and surgery with concomitant chemotherapy.

Keywords

Carbon ion radiotherapy • Chemotherapy • Head and neck • Malignant melanoma • Radioresistant

16.1 Introduction

Malignant mucosal melanoma (MMM) of the head and neck is a rare and malignant tumor type. The frequency of occurrence varies among races, with MMM accounting for than 1 % and 6–7.5 % of all melanomas in Caucasian [1, 2] and Japanese [3, 4] patients, respectively. These melanomas occur more frequently in individuals with darker complexions. In the head and neck area, the most common sites for MMM are the oral and sinonasal cavities, with the palate being the most common intraoral site [5, 6]. MMM of the head and neck has a poor prognosis; the overall 5-year survival rate is approximately 30 % or less [7–15] and patients have low local control rates and frequent distant metastases.

Surgery has been recognized as a standard approach in the medical community. Resection with a clear margin is emphasized as the most important factor for good local control and better prognosis. However, radical surgery is not possible in certain cases, since many important organs may be located near the tumor. Patients with unresectable local disease and those who refuse surgery should be considered for radiotherapy (RT) and chemotherapy as definitive management strategies.

Dacarbazine (DTIC) is the most effective chemotherapeutic agent for malignant melanomas [16]. In order to improve response rates, DTIC-based combination regimens are often administered [17, 18]. A combination of DTIC, amino methyl pyrimidinyl methyl chloroethyl nitrosourea hydrochloride (ACNU), and vincristine sulfate (VCR)

R. Takagi (✉)
Research Center for Charged Particle Therapy Hospital, National Institute of Radiological Sciences, Inage-ku, Anagawa 4-9-1, Chiba-shi, Chiba 263-8555, Japan
e-mail: rtakagi@nirs.go.jp

H. Tsujii et al. (eds.), *Carbon-Ion Radiotherapy: Principles, Practices, and Treatment Planning*,
DOI 10.1007/978-4-431-54457-9_16, © Springer Japan 2014

(DAV chemotherapy) has been used in many facilities in Japan. However, sufficient therapeutic effects have not been obtained with these treatment regimens. Additionally, in recent years, clinical trials of molecular targeted therapies for metastatic melanoma have been implemented [19, 20].

16.2 Significance of Carbon Ion Radiotherapy

Malignant melanoma has long been regarded as radioresistant because it often demonstrates poor regression after photon RT [21]. However, it was reported that the use of high doses per fraction might improve local responses [9, 22, 23]. Carbon ions have the biological characteristics of high linear energy transfer at the distal part of the spread-out Bragg peak and show good dose-localizing properties, compared with those of other heavier ions [24]. According to previous studies, carbon ion (C-ion) RT has a high therapeutic effect on radioresistant tumors such as malignant melanomas.

16.3 Clinical Futures and Diagnostic Work-Up

16.3.1 Eligibility for Carbon Ion Radiotherapy

Eligible patients were required to have histologically proven and measurable tumors in the head and neck region. All patients were required to be classified as having N0M0 disease, to have no coexistent malignant active tumors and no distant metastasis to other regions, be of an age between 15 and 75 years (increased to 80 years since April 2010), and have a prospective survival prognosis of at least 6 months. The candidates were also required to have a Karnofsky Performance Index of 60 % or more. Other criteria included the absence of prior radiotherapy for the carbon-treated area and the absence of intractable inflammatory lesions.

16.3.2 Eligibility for DAV Chemotherapy

Patients were required to have a hemoglobin (Hb) level greater than or equal to 10 g/dL, a white blood cell count greater than or equal to 4,000 mm^{-3}, and a platelet count greater than or equal to 100,000 mm^{-3} at the time of enrollment, as well as serum creatinine levels below 1.5 mg/dL, a creatinine clearance rate below 60 cc/min, a serum bilirubin level below 1.5 mg/dL, and aspartate aminotransferase and alanine aminotransferase levels below 1.5 times the upper limits of normal.

16.4 General Radiation Technique Management

16.4.1 Carbon Ion Radiotherapy

A custom-made immobilization device was used to hold patients in the same position during planning computed tomography (CT) and C-ion RT. A set of 2.5-mm-thick CT images were taken for treatment planning. During the 3-dimensional treatment planning, the gross tumor volumes (GTV) were defined on the planning CT using fusion images from magnetic resonance imaging (MRI) and ^{11}C-methinine positron emission tomography. The clinical target volume (CTV) included the GTV and was delineated with a minimum 5-mm margin. When there was a possibility of tumor invasion into the adjacent anatomical sites within the CTV1, the initial radiation dose was 36 GyE/10 fractions. Next, the CTV2, which was limited to the GTV, was irradiated until a total dose of 57.6 GyE/16 fractions was administered. Multiportal irradiation was fundamentally planned to avoid severe normal tissue reactions. When critical organs were located near the GTV, dose limitations for the normal tissues were ignored and the reactions in these organs were categorized as tumor-related reactions. The planning target volume (PTV) was extended 3 mm from the CTV on using the individual patient collimator and 6 mm on using the multi-leaf collimator, with the acceptance of fine-tuning to the PTV to consider at-risk organs. The limiting doses for critical normal tissues were the same as described in the previous chapter (Cancer of the head and neck).

16.4.2 DAV Chemotherapy

Each patient received 1–5 cycles of DAV therapy, and at least one cycle was performed during C-ion RT. According to our institutional protocol, DTIC (120 mg/m^2/day) was infused intravenously over a 2-h period from the first day to the fifth day, and ACNU (70 mg/m^2) and VCR (0.7 mg/m^2) were administered intravenously on the first day. We performed 5 cycles according to the above protocol every 5 weeks if the patient had no serious complications.

16.4.3 Follow-Up

The patients were followed up with CT or MRI every 1–2 months for the first 6 months after C-ion RT and every 3–6 months thereafter. The overall survival and local control rates were calculated from the first day of C-ion RT.

16.5 Results of Therapy

16.5.1 Patient Characteristics

Between April 2002 and August 2012, a total of 106 patients were enrolled into the C-ion RT with concurrent DAV chemotherapy protocol study. The characteristics of these 106 patients are listed in Table 16.1. All patients were able to receive the full C-ion RT dose. The follow-up duration ranged from 3.3 to 119 months. Fifty-seven patients (53.8 %) were able to complete five courses of DAV chemotherapy (Table 16.2). Reasons for aborting therapy were the emergence of metastasis, local recurrence, and side effects of chemotherapy.

16.5.2 Toxicity

No severe acute reactions were observed. Acute reactions of the normal tissue in the 106 patients included grade 3 skin reactions in one patient (0.9 %) and grade 3 mucosal reactions in 23 patients (21.7 %); no reactions worse than grade 3 were observed.

Table 16.1 Patient characteristics

Gender (M/F)	47/59
Age (year), range (median)	26–79 (63)
GTV (mL), range (median)	1.0–325.8 (28.3)
Tumor site	
Oral	12
Nasal	68
Paranasal sinus	18
Pharynx	5
Conjunctiva	3
Tumor status (UICC2002[a])	
T1	9
T2	18
T3	30
T4 (a, b)	34
Recurrence after surgery/chemotherapy	15

[a]UICC: Union for International Cancer Control

Table 16.2 DAV chemotherapy

Number of chemotherapy courses	
5 courses completed	57
1–4 courses	49
Reasons for discontinuing chemotherapy	
Recurrence and/or metastasis	16
Side effects	33

Late toxic reactions were grade 2 mucosal reactions in two patients (1.9 %), with no evidence of toxicities worse than grade 2.

The grades and incidence rates of radiation-induced side effects were similar to those in patients with head and neck tumors (previous chapter) and did not seem to be exacerbated by DAV chemotherapy.

The most common adverse events from DAV chemotherapy were myelotoxicity, liver dysfunction, transient nausea, vascular pain, and photosensitivity.

Of the 106 treated patients, 15 patients (14.2 %) had grade 3 myelotoxicity events and four patients (3.8 %) had grade 3 or 4 liver dysfunction events. The patient with grade 4 liver dysfunction was found shortly thereafter to have multiple hepatic metastases. Thus, the patient's liver function might have been affected by the metastases.

No treatment-related deaths occurred during the study.

16.5.3 Local Control and Overall Survival

The median survival time was 64.8 months. The 3- and 5-year overall survival rates for all patients were 65.8 and 54.0 %, respectively, and the 3- and 5-year local control rates for all patients were 83.1 and 80.6 %, respectively.

Since 1997, C-ion RT has been used for MMM of the head and neck. After C-ion RT, many patients developed distant metastasis, although local recurrence was not noted [25, 26]. This finding indicates that, in these patients, systemic micrometastases might have already existed at the time of treatment, and management of these events would be desirable for improved survival. On the basis of this result, we have begun to administer C-ion RT concomitantly with DAV chemotherapy. Consequently, although no difference was observed in the local control rate, the survival rate was significantly improved by DAV chemotherapy. C-ion RT with concomitant DAV chemotherapy is a safe and effective treatment for MMM of the head and neck because of good local control and acceptable toxicity.

16.6 Case Study

16.6.1 Case 1

A 61-year-old male patient presented with a growth in the palatal region and reported pain for a 2-month duration. The patient was admitted to the Oral and Maxillofacial Surgery outpatient clinic. Biopsy indicated a diagnosis of malignant melanoma. Melanosis was observed mainly in the left hard palate.

Tumors without thickness cannot be measured by MRI and CT. We devised a method with which to clarify the presence of the tumor by CT image fusion with a tumor outline that had been marked with metal wire (Fig. 16.1a, b).

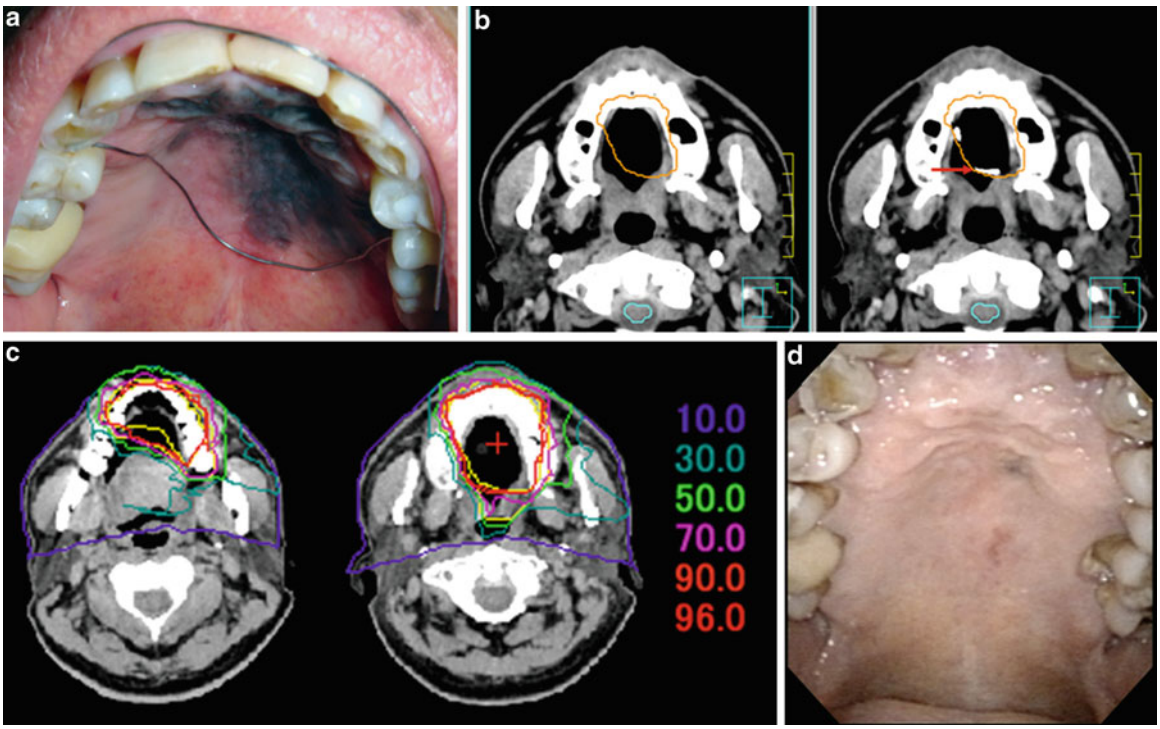

Fig. 16.1 Left palate MMM in a 61-year-old male patient. (**a**) Intraoral view of the lesion and placement of a metal wire (*arrow*) to clearly outline the tumor. (**b**) Image fusion of the planning CT (*left*) and CT with the wire (*right*). (**c**) Dose distribution of C-ion RT. (**d**) Intraoral view 2 years after C-ion RT

The patient received C-ion RT and DAV chemotherapy. A total radiation dose of 57.6 GyE in 16 equal fractions was administered over 4 weeks (Fig. 16.1c). Acute mucositis was reduced by reducing the dose to the dorsum of the tongue.

DAV chemotherapy was administered in five courses. Grade 2 leukopenia and grade 1 hepatic dysfunction were transiently experienced. However, these events were quickly resolved, with level returning to within the normal range.

The patient was followed up for 2 years after C-ion RT. Local recurrence and distant metastasis were not observed (Fig. 16.1d).

The presence of teeth in the irradiation range increases the risk of osteonecrosis. It is important that oral hygiene guidance be provided with the assistance of a dentist and dental hygienist.

16.6.2 Case 2

A 66-year-old female patient consulted the Department of Otolaryngology because of a left nasal obstruction and epistaxis. Physical examination revealed a measurable black tumor in the left nasal cavity. Imaging modalities also showed a tumor in the left nasal cavity. Biopsy indicated a diagnosis of malignant melanoma (Fig. 16.1a, b). The patient consulted our hospital in order to undergo C-ion RT.

The patient received C-ion radiotherapy and DAV chemotherapy. A total radiation dose of 57.6 GyE in 16 equal fractions was given over 4 weeks (Fig. 16.2c). Five courses of DAV chemotherapy were administered. Grade 3 leukopenia was transiently noted immediately after five courses. The white blood cell counts recovered to normal levels after granulocyte colony-stimulating factor administration for a few days. The patient was followed up for 8 years and 6 months after C-ion RT. Local recurrence and distant metastasis were not observed (Fig. 16.2d, e).

16.6.3 Case 3

A 49-year-old male patient visited the Otolaryngology outpatient clinic because of epistaxis. A right nasal septum tumor was observed. Tumor resection was performed, and the postoperative pathological diagnosis was malignant melanoma. Residual tumor was observed in the right nasal septum. The patient consulted our hospital in order to undergo C-ion RT. Physical examination revealed a

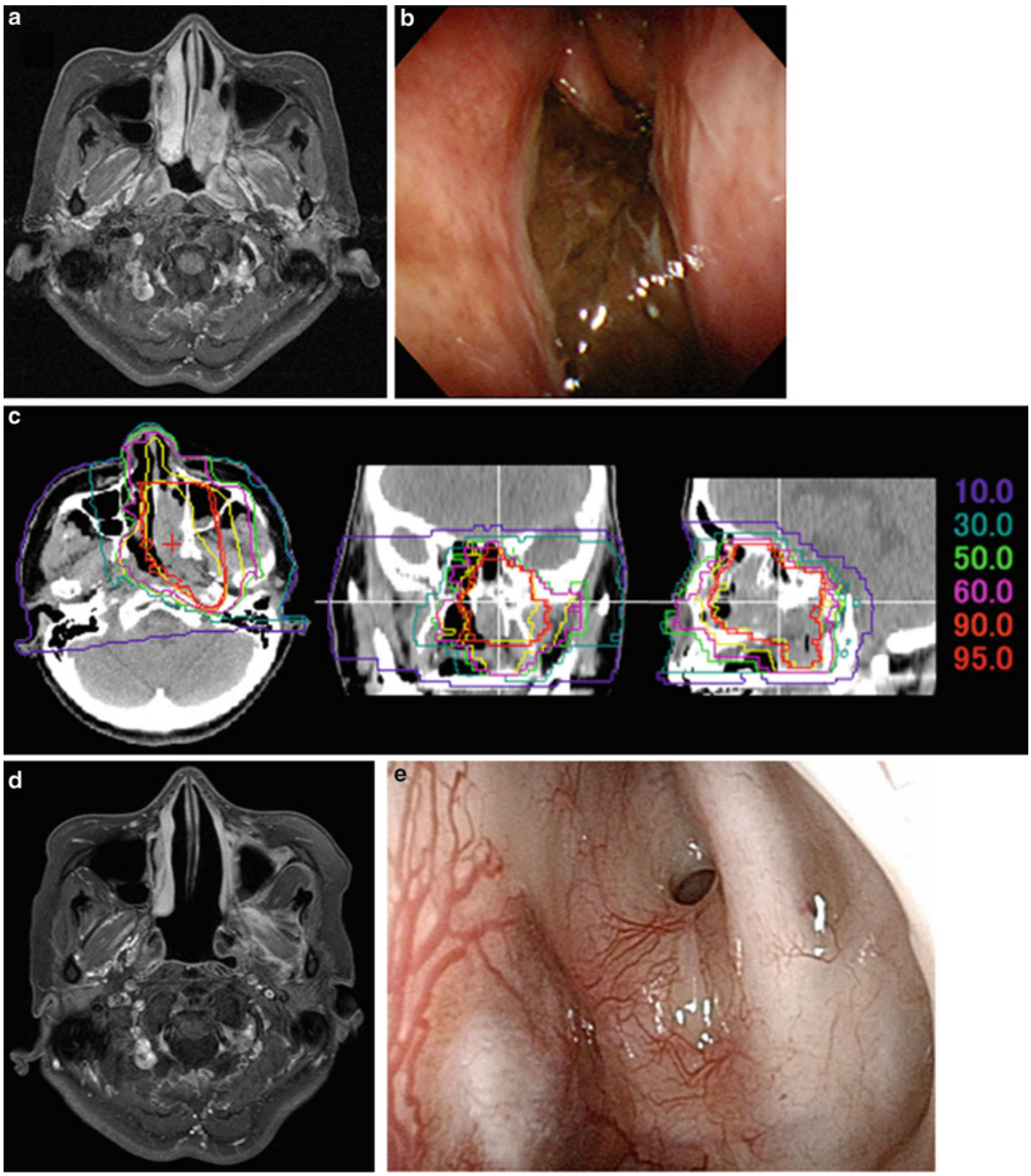

Fig. 16.2 Left nasal MMM in a 66-year-old female patient. (**a**) Transverse contrast-enhanced fat-saturated T1-weighted MRI scan (Gadolinium [Gd]-MRI) before C-ion RT. (**b**) Endoscopic image before C-ion RT. (**c**) Dose distribution of C-ion RT. (**d**) Gd-MRI 8 years and 6 months after C-ion RT. (**e**) Endoscopic image 8 years and 6 months after C-ion RT

measurable black tumor in the right nasal septum. However, the results of the imaging studies were unclear (Fig. 16.3a, b).

The patient received C-ion radiotherapy and DAV chemotherapy. A total radiation dose of 57.6 GyE in 16 equal fractions was administered over 4 weeks (Fig. 16.1c). One course of DAV chemotherapy was administered. However, this was discontinued after only 1 course because of grade 2 myelotoxicity (leukopenia).

Recurrent lesions were observed in the right ethmoid sinus (the margin of irradiation) at 3 years and 4 months after treatment (Fig. 16.3d, e).

The patient was re-treated with C-ion RT without chemotherapy. The CTV was set to a tight margin because

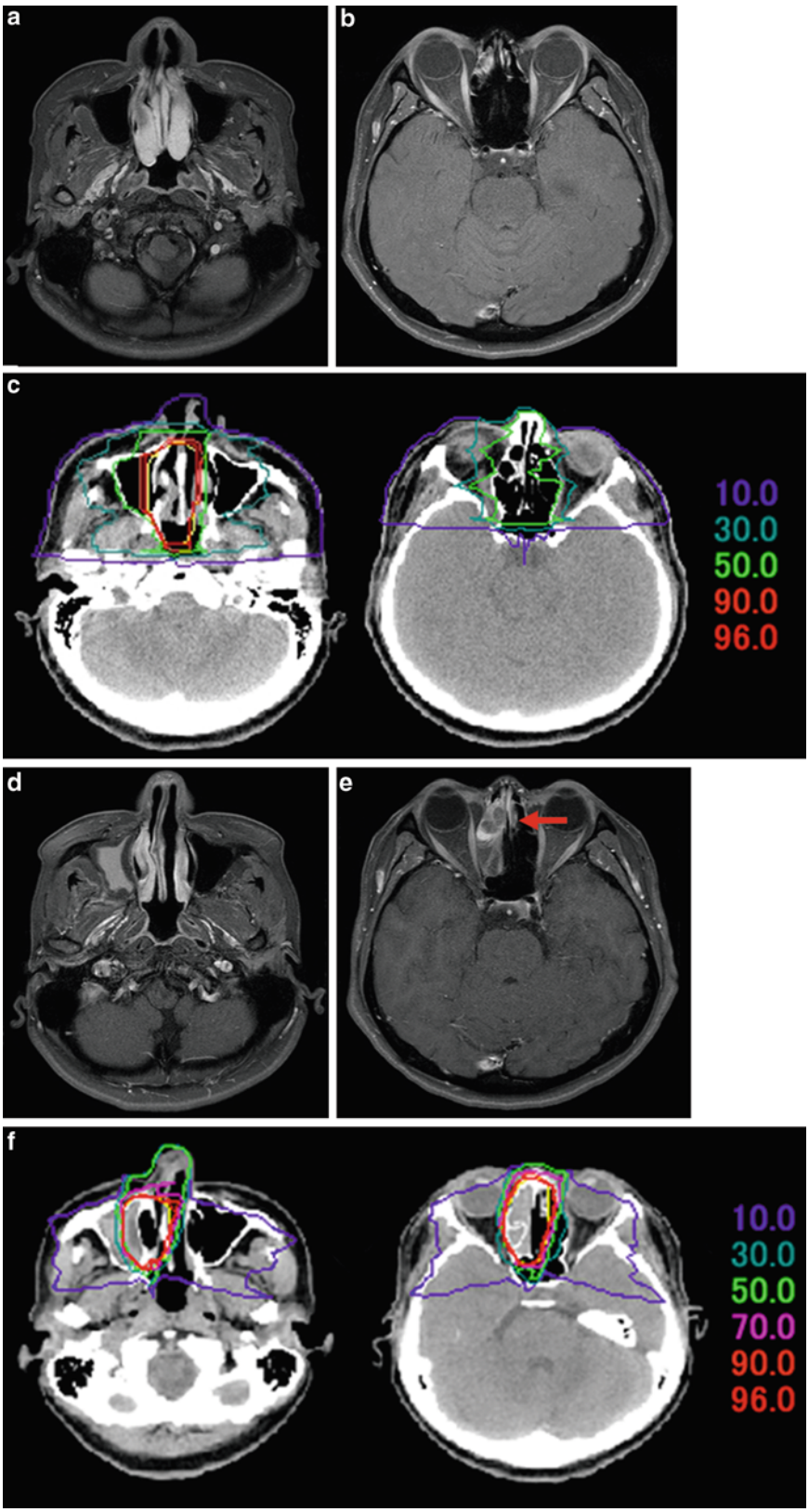

Fig. 16.3 Right nasal septum MMM in a 49-year-old female patient. (**a**) Gd-MRI of the nose before C-ion RT. (**b**) Gd-MRI of the ethmoid sinus before C-ion RT. Lesion progression was not noted. (**c**) Dose distribution of C-ion RT. (**d**, **e**) Gd-MRI 3 years and 4 months after C-ion RT. A new lesion was observed in the right ethmoid sinus (*arrow*). (**f**) Dose distribution of C-ion RT re-treatment

the region overlapped with the previously irradiated site. A total radiation dose of 57.6 GyE in 16 equal fractions was administered over 4 weeks (Fig. 16.3f).

The patient was followed up for 6 years and 4 months after the first C-ion RT course. Persistent mucositis (grade 1) was observed, and the patient showed no recurrence at the two treatment sites.

References

1. McLaughlin CC, Wu XC, Jemal A, et al. Incidence of noncutaneous melanomas in the U.S. Cancer. 2005;103(5):1000–7.
2. Chang AE, Karnell LH, Menck HR. The National Cancer Data Base report on cutaneous and noncutaneous melanoma: a summary of 84,836 cases from the past decade. The American College of Surgeons Commission on Cancer and the American Cancer Society. Cancer. 1998;83(8):1664–78.
3. Takagi M, Ishikawa G, Mori W. Primary malignant melanoma of the oral cavity in Japan. With special reference to mucosal melanosis. Cancer. 1974;34(2):358–70.
4. Ballantyne AJ. Malignant melanoma of the skin of the head and neck. An analysis of 405 cases. Am J Surg. 1970;120(4):425–31.
5. Hicks MJ, Flaitz CM. Oral mucosal melanoma: epidemiology and pathobiology. Oral Oncol. 2000;36(2):152–69.
6. Manolidis S, Donald PJ. Malignant mucosal melanoma of the head and neck: review of the literature and report of 14 patients. Cancer. 1997;80(8):1373–86.
7. Douglas CM, Malik T, Swindell R, et al. Mucosal melanoma of the head and neck: radiotherapy or surgery? J Otolaryngol Head Neck Surg. 2010;39(4):385–92.
8. Temam S, Mamelle G, Marandas P, et al. Postoperative radiotherapy for primary mucosal melanoma of the head and neck. Cancer. 2005;103(2):313–9.
9. Wada H, Nemoto K, Ogawa Y, et al. A multi-institutional retrospective analysis of external radiotherapy for mucosal melanoma of the head and neck in Northern Japan. Int J Radiat Oncol Biol Phys. 2004;59(2):495–500.
10. Owens JM, Roberts DB, Myers JN. The role of postoperative adjuvant radiation therapy in the treatment of mucosal melanomas of the head and neck region. Arch Otolaryngol Head Neck Surg. 2003;129(8):864–8.
11. Thompson LD, Wieneke JA, Miettinen M. Sinonasal tract and nasopharyngeal melanomas: a clinicopathologic study of 115 cases with a proposed staging system. Am J Surg Pathol. 2003;27(5):594–611.
12. Patel SG, Prasad ML, Escrig M, et al. Primary mucosal malignant melanoma of the head and neck. Head Neck. 2002;24(3):247–57.
13. Batsakis JG, Suarez P. Mucosal melanomas: a review. Adv Anat Pathol. 2000;7(3):167–80.
14. Lund VJ, Howard DJ, Harding L, et al. Management options and survival in malignant melanoma of the sinonasal mucosa. Laryngoscope. 1999;109:208–11.
15. Gilligan D, Slevin NJ. Radical radiotherapy for 28 cases of mucosal melanoma in the nasal cavity and sinuses. Br J Radiol. 1991;64(768):1147–50.
16. Buzaid AC, Bedikian A, Houghton AN. Systemic chemotherapy and biochemotherapy. In: Balch CM, Houghton AN, Sober AJ, editors. Cutaneous melanoma. 3rd ed. St. Louis: Quality Medical Publishing; 1998.
17. Ishihara K, Yamazaki N, Asano K. Chemotherapy of malignant melanoma. Gan To Kagaku Ryoho. 1993;20(10):1287–92. Article in Japanese.
18. Del Prete SA, Maurer LH, O'Donnell J, et al. Combination chemotherapy with cisplatin, carmustine, dacarbazine, and tamoxifen in metastatic melanoma. Cancer Treat Rep. 1984;68(11):1403–5.
19. Di Giacomo AM, Ascierto PA, Pilla L, et al. Ipilimumab and fotemustine in patients with advanced melanoma (NIBIT-M1): an open-label, single-arm phase 2 trial. Lancet Oncol. 2012;13(9):879–86. doi:10.1016/S1470-2045(12)70324-8.
20. Guo J, Si L, Kong Y, et al. Phase II, open-label, single-arm trial of imatinib mesylate in patients with metastatic melanoma harboring c-Kit mutation or amplification. J Clin Oncol. 2011;29(21):2904–9. doi:10.1200/JCO.2010.33.9275.
21. Moore ES, Martin H. Melanoma of the upper respiratory tract and oral cavity. Cancer. 1955;8(6):1167–76.
22. Overgaard J, Overgaard M, Hansen PV, et al. Some factors of importance in the radiation treatment of malignant melanoma. Radiother Oncol. 1986;5(3):183–92.
23. Trotti A, Peters LJ. Role of radiotherapy in the primary management of mucosal melanoma of the head and neck. Semin Surg Oncol. 1993;9(3):246–50.
24. Tsujii H, Kamada T, Baba M, et al. Clinical advantages of carbon-ion radiotherapy. New J Phys. 2008;10:075009. doi:10.1088/1367-2630/10/7/075009.
25. Mizoe JE, Hasegawa A, Jingu K, et al. Results of carbon ion radiotherapy for head and neck cancer. Radiother Oncol. 2012;103(1):32–7.
26. Yanagi T, Mizoe JE, Hasegawa A, et al. Mucosal malignant melanoma of the head and neck treated by carbon ion radiotherapy. Int J Radiat Oncol Biol Phys. 2009;74(1):15–20.

Soft Tissue Sarcoma of the Head and Neck

17

Masashi Koto

Abstract

Bone and soft tissue sarcomas of the head and neck account for approximately 1 % of all head and neck neoplasms. There are many histological subtypes of sarcomas, and most of them show resistance to radiotherapy. Therefore, the prognosis for local control and survival of patients with unresectable sarcomas are poor. The physical characteristics of carbon ions offer the theoretical benefit of more localized delivery of a radiation dose and greater relative biological effectiveness than that of photons. Previously, we reported the effects of carbon ion radiotherapy on 27 patients with unresectable bone and soft tissue sarcomas of the head and neck. A total dose of 70.4 Gy equivalent was administered in 16 fractions. The 3- and 5-year overall survival rates of all patients were 74.1 and 57.6 %, respectively. The 3- and 5-year local control rates were 91.8 and 80.4 %, respectively. Acute and late normal tissue reactions were within acceptable limit. Thus, carbon ion radiotherapy (C-ion RT) can be a promising treatment option for unresectable bone and soft tissue sarcomas of the head and neck.

Keywords

Carbon ion radiotherapy • Head and neck neoplasm • Soft tissue sarcoma

17.1 Introduction

Bone and soft tissue sarcomas of the head and neck are mesenchymal malignant neoplasms accounting for less than 10 % of all bone and soft tissue sarcomas and only approximately 1 % of all head and neck neoplasms. There are many histological subtypes of sarcomas, which present with a variety of clinical characteristics. Depending on the subtype and characteristics of the individual tumor, treatment may require a combination of surgery, radiotherapy, and chemotherapy. Adjuvant radiotherapy improves local tumor control, and in selected cases, it results in complete cure with acceptable adverse effects [1]. However, the prognosis for local control and survival of patients with unresectable sarcomas are poor [2, 3].

17.2 Significance of C-Ion RT

Carbon ions exhibit high linear energy transfer and exhibit good dose-localizing properties in comparison to other ion species [4, 5]. The physical characteristics of carbon ions offer the theoretical benefit of more localized delivery of a radiation dose and greater relative biological effectiveness than that of photons. The improved dose distribution can potentially be exploited either by allowing higher radiation doses to the tumor with less radiation-induced normal tissue toxicity or by reducing the adverse effects at equivalent effective doses. C-ion RT may be an effective treatment for adult patients with inoperable bone and soft tissue sarcoma of the head and neck or for those who refuse surgery.

M. Koto (✉)
Research Center for Charged Particle Therapy Hospital, National Institute of Radiological Sciences, Anagawa 4-9-1, Inage-ku, 263-8555 Chiba, Japan
e-mail: koto@nirs.go.jp

H. Tsujii et al. (eds.), *Carbon-Ion Radiotherapy: Principles, Practices, and Treatment Planning*,
DOI 10.1007/978-4-431-54457-9_17, © Springer Japan 2014

17.3 Diagnostic Work-Up

The international union against cancer (UICC) staging system for bone and soft tissue tumors is based on histologic grade, tumor size (and depth for soft tissue tumor), and the presence of distant or nodal metastases. The staging system is the same as that for sarcomas of the extremities or the trunk of the body; specific staging for head and neck sarcoma is not standardized. However, to define tumor extent and central nervous system involvement is important for planning treatment with C-ion RT. Computed tomography (CT) with contrast enhancement and magnetic resonance imaging (MRI) with gadolinium can provide useful anatomical information regarding the tumor. A chest CT scan is mandatory for staging work-up.

17.4 General Management of Radiation Technique

17.4.1 Target Delineation

Determination of gross target volume (GTV) was based on contrast-enhanced MRI. The clinical target volume (CTV) had minimum margins of 5.0 mm added around the GTV. The CTV and organs at risk (e.g., the eyeball, optic nerves, optic chiasm, and brain stem) were outlined on the planning CT images to permit dose-volume histogram analysis. The planning target volume had margins of 3.0–5.0 mm added around the CTV. The use of more than three portals was decided upon to spare the normal tissues such as the skin, eyeball, optic nerves, and brain stem.

17.4.2 Prescribed Dose

Kamada et al. reported the effects of C-ion RT performed in patients with sarcomas in the trunk of their bodies [6]. Their results indicated a rapid rise in the tumor control probability curve of sarcoma treated by carbon ion radiotherapy at approximately 70 Gy equivalent (GyE). A total dose of 70.4 GyE/16 fractions at a fraction size of 4.4 GyE is recommended for the treatment of bone and soft tissue sarcomas of the head and neck.

17.4.3 Dose Constraint of Organ at Risk

The limiting doses for critical normal tissues were decided to be 30 GyE for the spinal cord and brain stem and 40 GyE for the optic chiasm and optic nerves.

17.5 Results of Therapy

We administered C-ion RT in 27 adult patients with unresectable bone and soft tissue sarcomas of the head and neck [7]. The median observation period was 37.0 months (range, 4.1–73.0 months) for all patients and 40.0 months (range, 23.2–73.0 months) for the 18 surviving patients. The 3- and 5-year overall survival rates were 74.1 and 57.6 %, respectively. The 3- and 5-year local control rates were 91.8 and 80.4 %, respectively. The 3-year local control rate and overall survival rate for nine patients with osteosarcoma were 85.7 and 44.4 %, respectively. Acute reaction of grade 3 or more was observed in only one patient. With regard to late reactions, visual loss was observed in one patient and a grade 3 osteonecrosis of the maxillary bone was observed in four patients. Patients with osteonecrosis of the maxillary bone underwent sequestrectomy and were able to chew food using denture prosthetics.

The treatment results of unresectable bone and soft tissue sarcoma of adult head and neck are summarized in Table 17.1 [2, 3, 8–10]. In this table, we show the updated data regarding the results of C-ion RT at our institute. The local control rate with C-ion RT was much better than that of photon radiotherapy previously reported.

Table 17.1 Treatment results of unresectable bone and soft tissue sarcomas of the adult head and neck

Institute (year)	Histology	Modalities	No. of patients	5-year LC	5-year OS
RMH (1944–1988)	Soft tissue sarcoma	R, C	17	21	36
MGH (1972–1993)	Soft tissue sarcoma	R, C	14	55	63
UCSF (1961–1993)	Soft tissue sarcoma	R, C	5	0	9
NCI (1985–1996)	Osteosarcoma	R, C	71	-	22
LBL (1977–1992)	Bone and Soft tissue sarcoma	Helium ion radiotherapy	19	58	71
NIRS (2001–2012)	Bone and Soft tissue sarcoma	Carbon ion radiotherapy	42	73	53

Abbreviations: C = chemotherapy; LC = local control rate; NCI = National Cancer Institute; NIRS = National Institute of Radiological Sciences; OS = overall survival; R = radiotherapy; RMH = Royal Marsden Hospital; S = surgery; UCSF =University of California San Francisco.

17.6 Case Studies

17.6.1 Case 1

A 32-year-old woman presented with osteosarcoma of the mandible. Imaging examination revealed a tumor in the pterygopalatine fossa with intracranial invasion (Fig. 17.1a). The tumor had a maximum diameter of 66 mm. This patient was deemed inoperable and received chemotherapy. After a cycle of chemotherapy, the tumor did not show any change in size. Then, the patient was referred to our hospital for C-ion RT. Determination of the GTV was based on T1-weighted and contrast-enhanced T1-weighted and T2-weighted MRI obtained using image fusion technique. The CTV had minimum margins of 5–10 mm added to the GTV. The margin for the brain and skin was reduced as much as possible. Four portals were used mainly to avoid severe skin reaction. Because only two fixed beams (horizontal and vertical directions) were available, the patient was immobilized in a supine or oblique position to spare the critical organs. C-ion RT was administered at 70.4 GyE/16 fractions (Fig. 17.1b, c). The maximum dose to the skin was reduced to less than 80 % of the prescribed dose (Fig. 17.1d). The patient developed asymptomatic brain necrosis; however, 6 years later, she is without any disease.

17.6.2 Case 2

A 41-year-old man presented with malignant fibrous histiocytoma of the right maxillary sinus. The tumor invasion into of the sphenoid sinus, orbital space, and pterygopalatine fossa was observed (Fig. 17.2a). The maximum diameter of the tumor was 70 mm. The patient was deemed inoperable and received C-ion RT. Determination of the GTV was based on T1-weighted and contrast-enhanced T1-weighted and T2-weighted MRI obtained using image fusion technique. The CTV had minimum margins of 5–10 mm added to the GTV. It was impossible to spare the right optic nerve that was surrounded by the tumor. C-ion RT was delivered at 70.4 GyE/16 fractions using three portals. A horizontal beam from the left side of the patient was used to reduce the dose to the right cheek skin (Fig. 17.2b, c). The maximum dose to the right optic nerve was almost 70 GyE (Fig. 17.2d). The patient lost his right visual acuity, and he developed osteonecrosis of the right maxilla. However, 7 years later, this patient can maintain his personal appearance and chew his food.

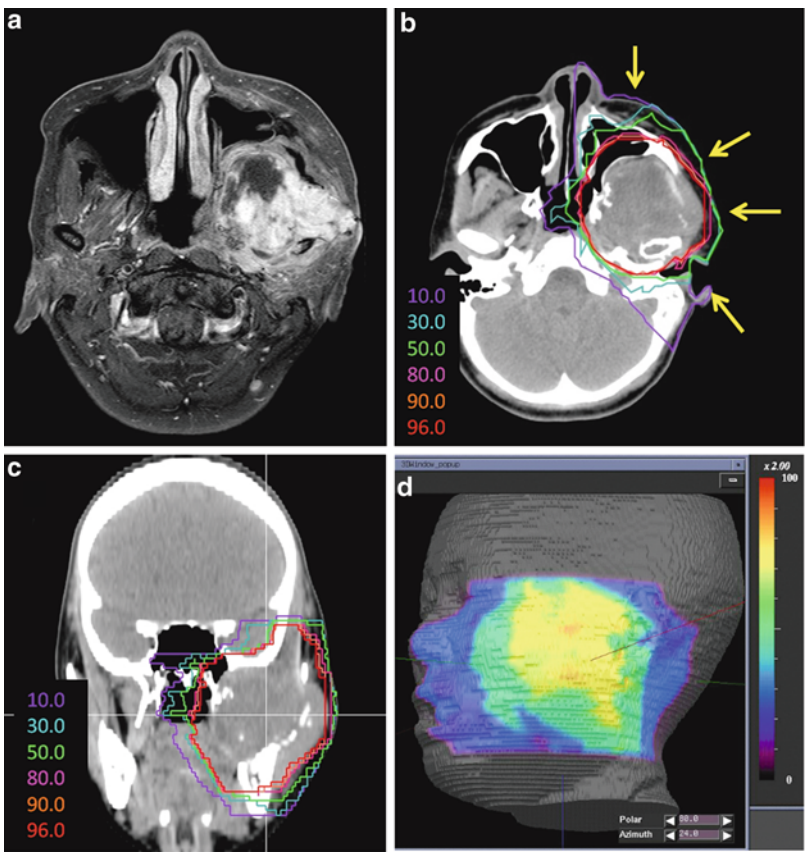

Fig. 17.1 (**a**) Contrast-enhanced T1-weighted magnetic resonance axial image obtained before carbon ion radiotherapy. (**b**) and (**c**) Representative axial and coronal isodose distributions. *Yellow arrows* indicate beam directions. (**d**) Dose to the skin surface

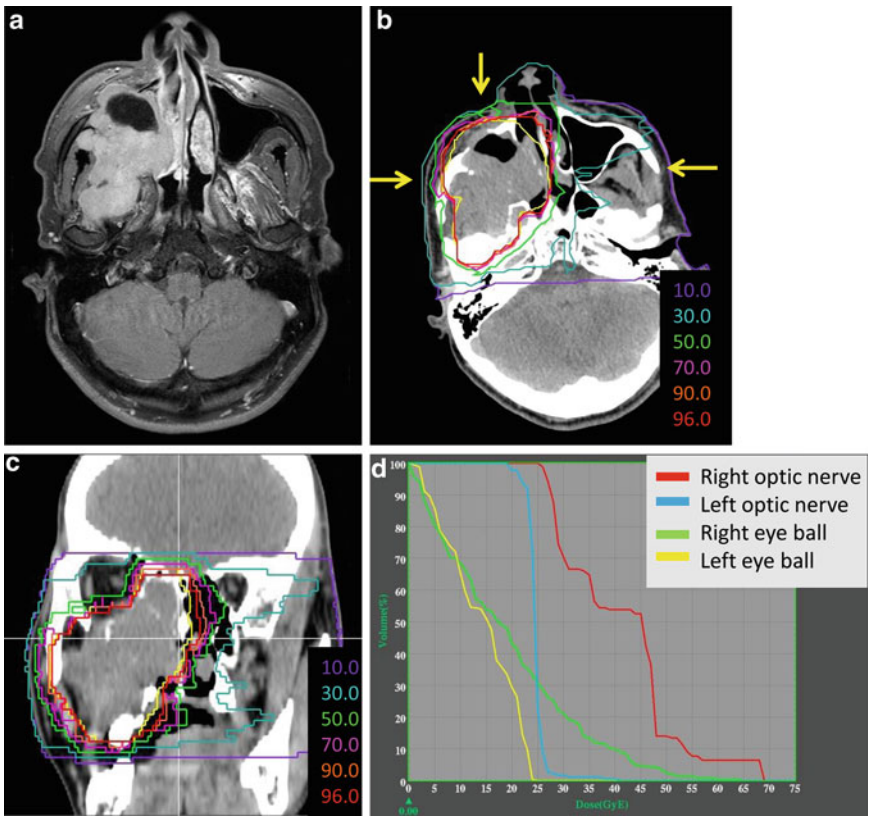

Fig. 17.2 (**a**) Contrast-enhanced T1-weighted magnetic resonance axial image obtained before carbon ion radiotherapy. (**b**) and (**c**) Representative axial and coronal isodose distributions. *Yellow arrows* indicate beam directions. (**d**) Dose-volume histogram of both optic nerves and eyeballs

References

1. Mendenhall WM, Mendenhall CM, Werning JW, Riggs CE, Mendenhall NP. Adult head and neck soft tissue sarcomas. Head Neck. 2005;27:916–22.
2. Eeles RA, Fisher C, A'Hern RP, Robinson M, Rhys-Evans P, Henk JM, Archer D, Harmer CL. Head and neck sarcomas: prognostic factors and implications for treatment. Br J Cancer. 1993;68:201–7.
3. Le QT, Fu KK, Kroll S, Fitts L, Massullo V, Ferrell L, Kaplan MJ, Phillips TL. Prognostic factors in adult soft-tissue sarcomas of the head and neck. Int J Radiat Oncol Biol Phys. 1997;37:975–84.
4. Kanai T, Endo M, Minohara S, Miyahara N, Koyama-ito H, Tomura H, Matsufuji N, Futami Y, Fukumura A, Hiraoka T, Furusawa Y, Ando K, Suzuki M, Soga F, Kawachi K. Biophysical characteristics of HIMAC clinical irradiation system for heavy-ion radiation therapy. Int J Radiat Oncol Biol Phys. 1999;44:201–10.
5. Tsujii H, Kamada T. A review of update clinical results of carbon ion radiotherapy. Jpn J Clin Oncol. 2012;42:670–85. doi:10.1093/jjco/hys104.
6. Kamada T, Tsujii H, Tsuji H, Yanagi T, Mizoe JE, Miyamoto T, Kato H, Yamada S, Morita S, Yoshikawa K, Kandatsu S, Tateishi A, Working Group for the Bone and Soft Tissue Sarcomas. Efficacy and safety of carbon ion radiotherapy in bone and soft tissue sarcomas. J Clin Oncol. 2002;20:4466–71.
7. Jingu K, Tsujii H, Mizoe JE, Hasegawa A, Bessho H, Takagi R, Morikawa T, Tonogi M, Tsuji H, Kamada T, Yamada S, Organizing Committee for the Working Group for Head-and-Neck Cancer. Carbon ion radiation therapy improves the prognosis of unresectable adult bone and soft-tissue sarcoma of the head and neck. Int J Radiat Oncol Biol Phys. 2012;82:2125–31. doi:10.1016/j.ijrobp.2010.08.043.
8. Willers H, Hug EB, Spiro IJ, Efird JT, Rosenberg AE, Wang CC. Adult soft tissue sarcomas of the head and neck treated by radiation and surgery or radiation alone: patterns of failure and prognostic factors. Int J Radiat Oncol Biol Phys. 1995;33:585–93.
9. Smith RB, Apostolakis LW, Karnell LH, Koch BB, Robinson RA, Zhen W, Menck HR, Hoffman HT. National Cancer Data Base report on osteosarcoma of the head andneck. Cancer. 2003;98:1670–80.
10. Castro JR, Linstadt DE, Bahary JP, Petti PL, Daftari I, Collier JM, Gutin PH, Gauger G, Phillips TL. Experience in charged particle irradiation of tumors of the skull base: 1977–1992. Int J Radiat Oncol Biol Phys. 1994;29:647–55.

Part X

Skull Base and Paracervical Tumors

Skull Base and Upper Cervical Spine Tumors

18

Masashi Koto

Abstract

Major types of skull base and upper cervical spine tumors include chordoma, chondrosarcoma, and olfactory neuroblastoma, for which complete resection is rarely achieved because of the vicinity to the critical organ structure. Radiotherapy is the second treatment option; however, the limiting factor for photon radiotherapy conventionally applied to skull base and upper cervical spine tumors is damage to adjacent normal tissues, owing to poor local control. On the other hand, proton radiotherapy with its superior physical spatial distribution has provided a major improvement in local control in view of possible dose escalations. However, in certain patient groups, local control with proton radiotherapy is difficult to achieve even at elevated doses. For example, the reported 5-year local control rates for skull base chordoma after proton therapy ranged from 46 to 81 %. Therefore, the high linear energy transfer of carbon ion radiotherapy (C-ion RT) has a promising potential for the treatment of skull base tumors, especially chordoma. The 5-year local control and overall survival rates for 44 chordoma patients treated with carbon ion radiotherapy were 88 and 87 %, respectively. The 5-year actuarial local control and overall survival rates for 12 chondrosarcoma patients were 86 and 63 %, respectively. Acute and late normal tissue reactions were within acceptable limit. Thus, C-ion RT can be a promising treatment option for skull base and upper cervical spine tumors.

Keywords

Carbon ion radiotherapy • Chordoma • Skull base tumor

18.1 Introduction

The management of skull base and upper cervical spine tumors is most challenging because they lie in close vicinity of critical structures such as the brain stem, spinal cord, and anterior optic pathways. These anatomic structures often limit surgical access and resectability, as well as the delivery of high-dose radiations. In addition, some tumors that originate from the skull base region are dose dependent. For example, more than 70 Gy of radiation is needed for achieving local control of chordoma, and more than 60 Gy is needed for chondrosarcoma [1]. New treatment techniques such as intensity-modulated radiotherapy and stereotactic radiotherapy have improved dose distribution and are being used for skull base tumors. However, the clinical results are still unclear.

On the other hand, proton therapy with its superior physical spatial distribution has provided a major improvement in local control with regard to possible dose escalations. Several studies reported promising results of using proton therapy for skull base tumors. Munzenrider et al. reported that the 10-year local control rate for chondrosarcoma treated with proton therapy was 94 % [2]. Wenkel et al. reported that the 10-year local control rate for meningioma

M. Koto (✉)
Research Center for Charged Particle Therapy Hospital, National Institute of Radiological Sciences, Anagawa 4-9-1, Inage-ku, 263-8555 Chiba, Japan
e-mail: koto@nirs.go.jp

H. Tsujii et al. (eds.), *Carbon-Ion Radiotherapy: Principles, Practices, and Treatment Planning*,
DOI 10.1007/978-4-431-54457-9_18, © Springer Japan 2014

treated with combined proton and photon radiotherapy was 88 % [3]. However, the reported 5-year local control rates for chordoma treated with proton therapy ranged from 46 to 81 % [2, 4–6].

18.2 Significance of C-Ion RT

In chordoma patients, local control with proton radiotherapy, even at elevated doses, is difficult to achieve. Therefore, the high linear energy transfer of C-ion RT has a promising potential in the treatment of skull base chordoma. Thus, C-ion RT should be able to achieve excellent local control in other skull base tumors such as chondrosarcoma and meningioma.

18.3 Clinical Features and Diagnostic Work-Up

The clinical symptoms of skull base tumors vary according to the location and extent of the tumor. Volpe et al. [7] reviewed the clinical features of 48 patients with chordoma and 49 patients with chondrosarcoma of the skull base. Half of these patients had ocular symptoms such as diplopia and visual impairment at initial manifestation of the disease.

In C-ion RT, it is important to define the distance between the tumor and the organs at risk, such as the brain stem, spinal cord, or cranial nerves including optic nerves, because it may be difficult to spare nerve functions when the tumor is located close to the organ at risk. Computed tomography (CT) with contrast enhancement and magnetic resonance imaging (MRI) with gadolinium are useful in evaluating tumor extension. However, specific staging for chordoma and chondrosarcoma of the skull base is not standardized.

18.4 General Management of Radiation Technique

18.4.1 Target Delineation

Determination of the gross tumor volume (GTV) was based on T1-weighted, T2-weighted, and contrast-enhanced T1-weighted MRI. The clinical target volume (CTV) had minimum margins of 5 mm added to the GTV. In case of carbon ion radiotherapy for residual tumor after surgery, the tumor bed region before surgery was included in the CTV. Furthermore, a margin of 3–5 mm was added as an internal and setup margin around the CTV to create a final planning target volume (PTV). When the tumor was located close to critical organs, such as the brain stem, spinal cord, optic nerves, or brain, the margins were reduced as necessary.

18.4.2 Dose Constraints for the Organs at Risk

The limiting doses for critical normal tissues were decided as 30 Gy equivalent (GyE) for the spinal cord and brain stem and 40 GyE for the optic chiasm and optic nerves. When the ipsilateral optic nerve was located very close to the tumor, the dose limitation for the optic nerve was ignored. The limiting dose for the brain was not provided. However, it was recommended that brain volumes receiving more than 50 GyE should be less than 5 cc to reduce the risk of developing brain necrosis.

18.4.3 Beam Direction

More than two portals were used in principle to improve dose distributions. Because two fixed beams (horizontal and vertical directions) were available, the head of the patient was occasionally immobilized with the patient in oblique or prone position to spare the critical organs.

In the case that a tumor surrounded the critical organ, patch field technique [8] was used to spare critical organs and maintain the minimum coverage dose of the tumor.

18.4.4 Treatment Schedule and Dose

A phase I/II dose escalation study for skull base and upper cervical spine tumors was initiated in April 1997. The patients were treated with a total dose of 48.0, 52.8, 57.6, or 60.8 GyE administered in 16 fractions for 4 weeks. At the level of 60.8 GyE, no dose-limiting toxicity was observed; however, tumors were well controlled. Finally, a dose of 60.8 GyE in 16 fractions was recommended for treatment of skull base tumors [9].

18.5 Results of Therapy

18.5.1 Chordoma

Previously, we reported the effects of C-ion RT on 33 patients with skull base or cervical spine chordoma [10]. Our report included the results of patients treated using the following three protocols: (1) a pilot study with a total dose of 48.0 GyE; (2) a phase I/II study with a total dose of 48.0, 52.8, 57.6, and 60.8 GyE; and (3) a phase II study with a total dose of 60.8 GyE. All the patients had a macroscopic lesion and were treated with 16 fractions over 4 weeks. The CTV ranged from 2 to 328 cc, with a median value of 32 cc. Median follow-up was 53 months (range, 8–129 months). The 5-year actuarial local control rate and overall survival rate of the 33 patients were 85.1 and 87.7 %, respectively.

Table 18.1 Clinical characteristics of reported cases of skull base chordoma

	Authors	*N*	Median dose	Median f/u (year)	Local control rate (%)		
					3-year	5-year	10-year
Photon	Catton et al. [12]	24	50	5.2		23	15
	Romero et al. [13]	18	50	3.1		17	
	Forsyth et al. [14]	39	50	8.3		39	31
	Magrini et al. [15]	12	58	6		25	25
Proton (± photon)	Munzenrider et al. [2]	169	66–83	3.4		73	54
	Noel et al. [4]	100	67	2.6	86 (2 year)	54 (4 year)	
	Igaki et al. [5]	13	72	5.8	67	46	
	Ares et al. [6]	42	73.5	3.2 (mean)		81	
Helium	Castro et al. [16]	53	65	4.3		63	
Carbon	Shults-Ertner et al. [11]	96	60	2.6 (mean)	81	70	
	NIRS	47	60.8	4.5		91	82

The 5-year actuarial local control rate and overall survival rate of the 19 patients treated with 60.8 GyE were 100 and 94.4 %, respectively. Acute reactions were classified according to the Radiation Therapy and Oncology Group (RTOG) scoring system, with a maximum reaction occurring within 3 months after initiation of C-ion RT. Late reactions were classified according to the RTOG/European Organisation for Research and Treatment of Cancer (EORTC) scoring system. One patient had grade 2 acute skin reaction and six had grade 2 acute mucosal reaction. Acute reactions of grade 3 or greater were not observed in the skin or mucosa. No acute reactions were observed in the brain or spinal cord. Regarding late reactions, no severe reactions of the skin or mucosa were noted. Only one patient developed grade 2 brain toxicity.

Schulz-Ertner et al. reported their experience of treating 96 skull base chordoma patients with C-ion RT at the Gesellschaft für Schwerionenforschung institute in Germany [11]. The median total dose was 60 cobalt Gy equivalent (CGE) (range, 60–70 CGE) delivered in 20 fractions over 3 weeks. The mean follow-up was 31 months. The mean 5-year actuarial local control rate and overall survival rate were 70.0 and 88.5 %, respectively. Optic nerve neuropathy (RTOG/EORTC grade 3) was observed in 4.1 % of patients and minor temporal lobe injury (RTOG/EORTC grade 1/2) occurred in 7.2 % of patients.

The local control rates of various radiotherapies for skull base chordoma are summarized in Table 18.1 [2–6, 11–16]. We have presented the updated data regarding the effects of C-ion RT for chordoma. The median follow-up was 54 months. The 5-year actuarial local control rate and overall survival rate of 47 chordoma patients were 91 and 92 %, respectively.

18.5.2 Chondrosarcoma

Twelve patients with chondrosarcoma were treated with C-ion RT at our institute. The 5-year actuarial local control rate and overall survival rate were 86 and 63 %, respectively. In Germany, Schulz-Ertner et al. employed C-ion RT for the treatment of 54 patients with low- and intermediate-grade chondrosarcoma of the skull base [17]. The median total dose administered was 60 CGE in 20 fractions over 3 weeks. The median follow-up was 33 months. The 4-year actuarial local control rate and 5-year overall survival rate were 89.8 and 98.2 %, respectively. Grade 3 late toxicity occurred in one patient only.

18.5.3 Other Tumors

Nine patients with olfactory neuroblastoma were treated with C-ion RT, and their 5-year actuarial local control rate and overall survival rate were 100 and 56 %, respectively. In 7 patients with skull base meningioma, the 5-year actuarial local control rate and overall survival rate were 80 and 86 %, respectively.

18.6 Case Study

18.6.1 Case 1 (Chordoma of the Skull Base)

A 61-year-old woman presented with nasal septum tumor and bilateral nasal obstructions. An incisional biopsy revealed chordoma of the skull base. MRI examination revealed a lesion in the clivus invading the nasal septum, sphenoid sinus, and anterior vertebral muscle (Fig. 18.1a). C-ion RT was delivered at 60.8 GyE/16 fractions. Determination of the GTV was based on T1-weighted and contrast-enhanced T1-weighted and T2-weighted MRI obtained using image fusion technique. The CTV had minimum margins of 8 mm added to the GTV. The margin to the brain stem was reduced to meet the dose constraint for the brain stem. Three portals, one vertical and two horizontal, were used to spare the temporal lobes. The vertical beam

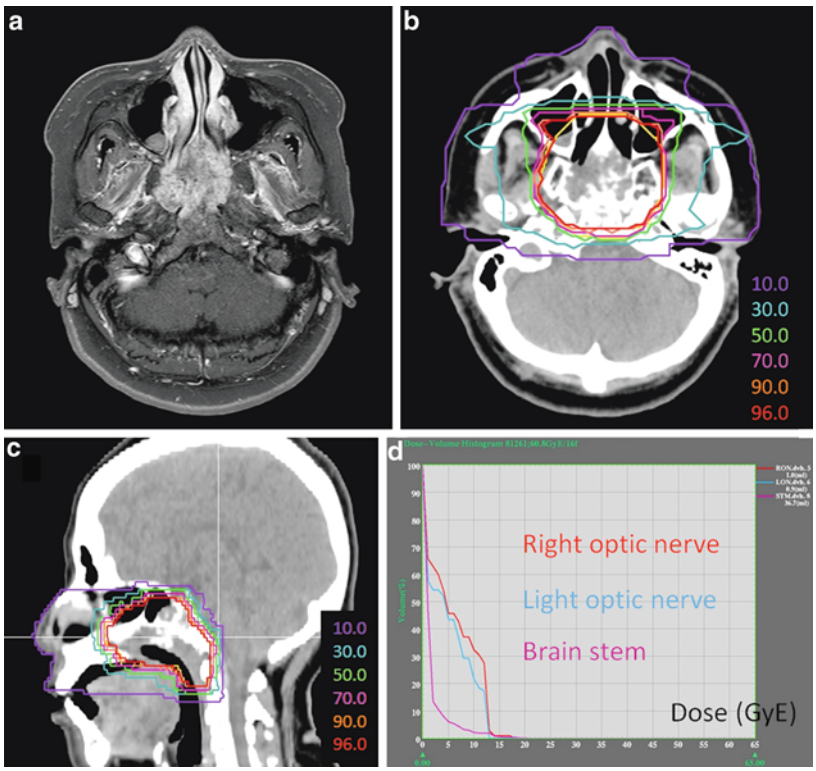

Fig. 18.1 (**a**) Contrast-enhanced T1-weighted magnetic resonance axial image obtained before carbon ion radiotherapy. (**b**) and (**c**) Representative axial and coronal isodose distributions in the clivus tumor. (**d**) Dose-volume histogram of risk organs such as the brain stem and both optic nerves

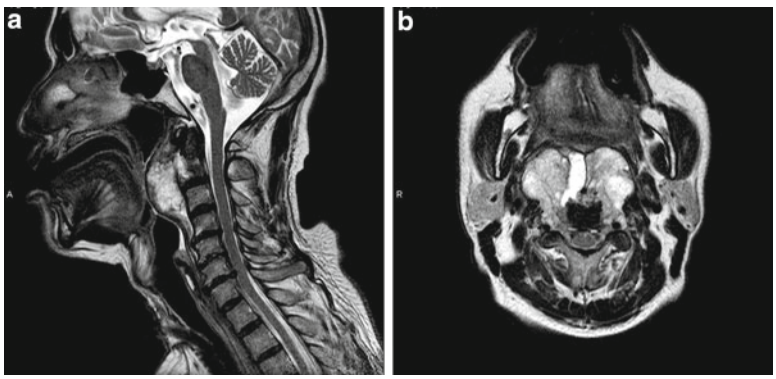

Fig. 18.2 (**a**) Axial and (**b**) sagittal T2-weighted magnetic resonance images obtained before carbon ion radiotherapy

direction should not be parallel to the nasal septum, because the beam targeted at the nasal septum may reach the brain stem, even if there is a small setup error. This patient was rotated 10° from the supine position when the vertical beam was used (Fig. 18.1b, c). The dose constraint of the optic nerves and brain stem were accomplished (Fig. 18.1d). The patient recovered well and is without any disease 2 years later.

18.6.2 Case 2 (Chordoma of the Cervical Region)

A 74-year-old man presented with neck pain and dysphagia. An incisional biopsy revealed chordoma. MRI revealed a lesion in the second cervical spine, invading the spinal canal (Fig. 18.2a, b). C-ion RT was delivered at 60.8 GyE/16 fractions. Determination of the GTV was based on T1-weighted and contrast-enhanced T1-weighted and T2-weighted MRI obtained using image fusion technique. The CTV had minimum margins of 5–10 mm added to the GTV, except for in the direction of the critical organs. The margin to the spinal cord was reduced to meet the dose constraint for the spinal cord. To optimize dose distribution within an irregular volume in close proximity to the spinal cord, the patch combination technique was used. The target volume was divided into three segments, each treated by a separate radiation field. Utilizing the sharp dose fall-off after Bragg peak, the distal edges of the vertical fields were matched with the lateral field edge of the horizontal field

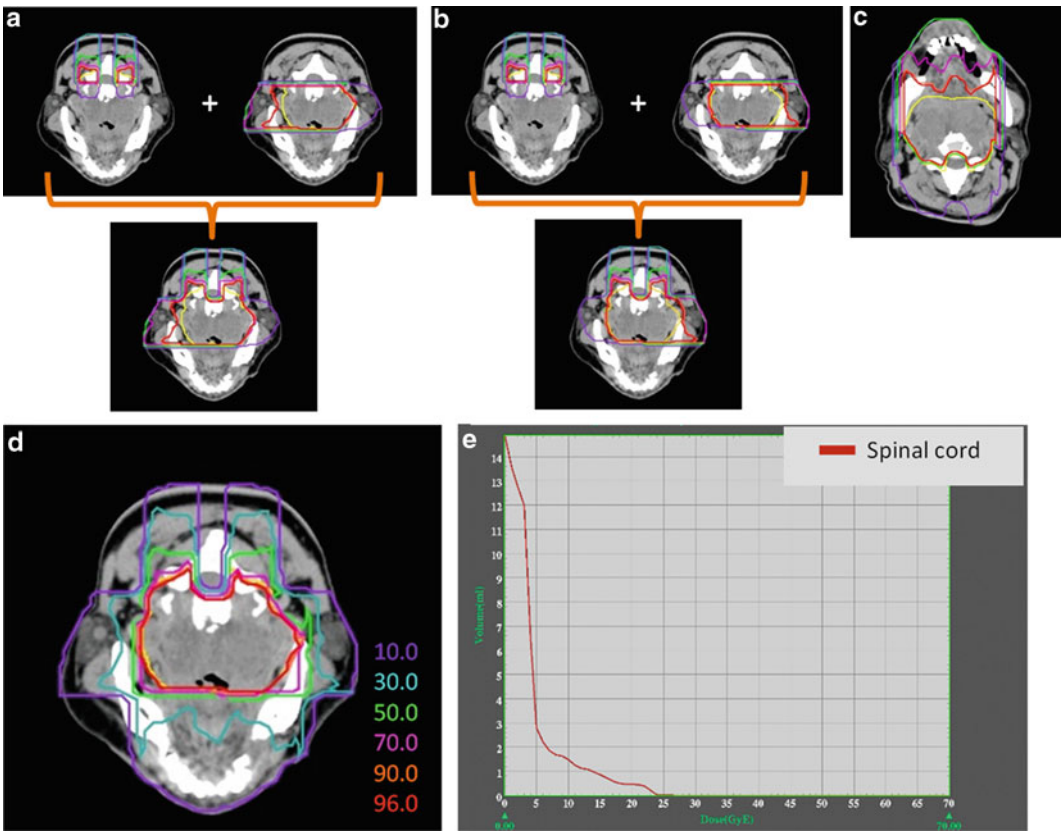

Fig. 18.3 (**a**) Port 1 consisted of two vertical beams and one horizontal beam from the right side of the patient. The patient was immobilized in the prone position. (**b**) Port 2 consisted of two vertical beams and one horizontal beam from the left side of the patient. The patient was immobilized in the prone position. (**c**) Port 3 consisted of a horizontal beam. The patient was immobilized in the supine position. (**d**) Combined dose distribution. (**e**) Dose-volume histogram of the spinal cord

(Fig. 18.3a–d). Dose constraint of the brain stem was accomplished (Fig. 18.3e). The patient recovered well and is without any disease 2 years later.

18.6.3 Case 3 (Brain Injury)

A 33-year-old woman presented with right ptosis, decreased visual acuity, and trigeminal neuralgia. She underwent partial tumor resection, and her condition was diagnosed as skull base chordoma. Four years later, tumor recurrence was detected by MRI examination. She was referred to our hospital for C-ion RT. The tumor was located in the right middle cranial fossa through right cavernous sinus and was in contact with the right temporal lobe and pons (Fig. 18.4a, b). C-ion RT was delivered at 57.6 GyE/16 fractions. Determination of the GTV was based on T1-weighted and contrast-enhanced T1-weighted and T2-weighted MRI obtained using image fusion technique. The CTV had minimum margins of 5–10 mm added to the GTV, except for in the direction of the critical organs. The margin to the brain stem was reduced to clear the dose constraint of the brain stem. The PTV margin toward the right temporal lobe was reduced as much as possible to avoid severe brain injury. The brain volume receiving more than 50 GyE radiation was 10 cc. It was difficult to abide by the dose constraints of the right optic nerve. Four portals were used (Fig. 18.4c, d). Twenty-six months after the treatment, a small enhanced lesion appeared in the right temporal lobe (Fig. 18.5a). However, the patient did not show any clinical symptom regarding brain injury. Forty-two months after the treatment, brain necrosis developed at the bottom of right temporal lobe (Fig. 18.5b). The patient experienced mild headache; however, she did not require any medication. The tumor was slightly reduced. Eleven years after the treatment, the patient is alive without any tumor recurrence. The enhanced brain lesion almost disappeared and cyst formation occurred (Fig. 18.5c). No clinical symptom of brain injury was observed.

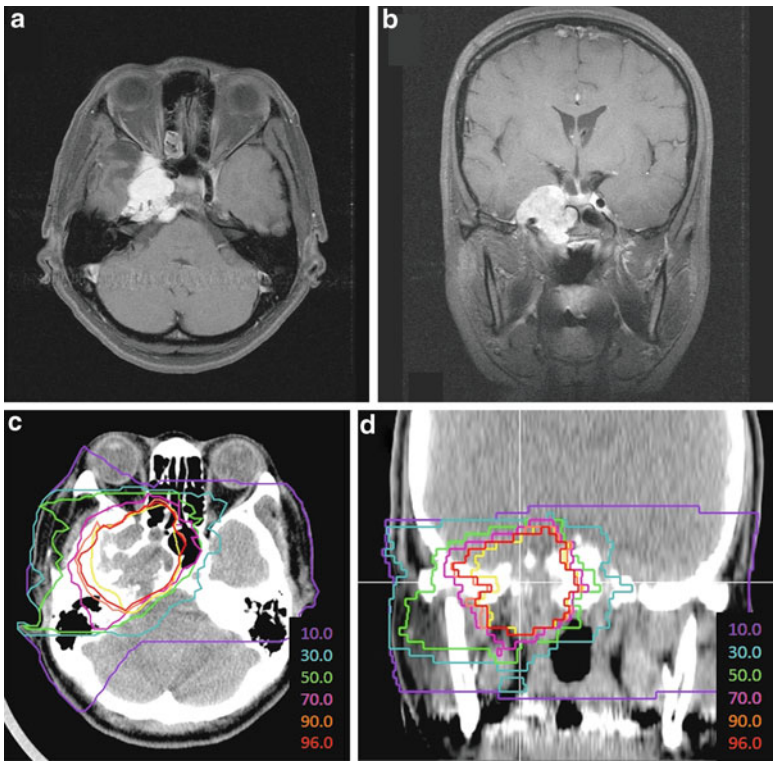

Fig. 18.4 (**a**) Axial and (**b**) sagittal contrast-enhanced T1-weighted magnetic resonance images obtained before carbon ion radiotherapy. Representative (**c**) axial and (**d**) coronal isodose distributions

Fig. 18.5 (**a**) Axial contrast-enhanced T1-weighted magnetic resonance image at the level of temporal lobe obtained 26 months after carbon ion radiotherapy. (**b**) Axial contrast-enhanced T1-weighted magnetic resonance image obtained 42 months after carbon ion radiotherapy. (**c**) Axial contrast-enhanced T1-weighted magnetic resonance image obtained 11 years after the treatment

References

1. Debus J, Schulz-Ertner D, Schad L, Essig M, Rhein B, Thillmann CO, Wannenmacher M. Stereotactic fractionated radiotherapy for chordomas and chondrosarcomas of the skull base. Int J Radiat Oncol Biol Phys. 2000;47:591–6.
2. Munzenrider JE, Liebsch NJ. Proton therapy for tumors of the skull base. Strahlenther Onkol. 1999;175:57–63.
3. Wenkel E, Thornton AF, Finkelstein D, Adams J, Lyons S, De La Monte S, Ojeman RG, Munzenrider JE. Benign meningioma: partially resected, biopsied, and recurrent intracranial tumors treated with combined proton and photon radiotherapy. Int J Radiat Oncol Biol Phys. 2000;48:1363–70.
4. Noël G, Habrand JL, Jauffret E, de Crevoisier R, Dederke S, Mammar H, Haie-Méder C, Pontvert D, Hasboun D, Ferrand R, Boisserie G, Beaudré A, Gaboriaud G, Guedea F, Petriz L, Mazeron JJ. Radiation therapy for chordoma and chondrosarcoma of the skull base and the cervical spine. Prognostic factors and patterns of failure. Strahlenther Onkol. 2003;179:241–8.
5. Igaki H, Tokuuye K, Okumura T, Sugahara S, Kagei K, Hata M, Ohara K, Hashimoto T, Tsuboi K, Takano S, Matsumura A, Akine Y. Clinical results of proton beam therapy for skull base chordoma. Int J Radiat Oncol Biol Phys. 2004;60:1120–6.
6. Ares C, Hug EB, Lomax AJ, Bolsi A, Timmermann B, Rutz HP, Schuller JC, Pedroni E, Goitein G. Effectiveness and safety of spot scanning proton radiation therapy for chordomas and chondrosarcomas of the skull base: first long-term report. Int J Radiat

Oncol Biol Phys. 2009;75:1111–8. doi:10.1016/j.ijrobp.2008.12.055.
7. Volpe NJ, Liebsch NJ, Munzenrider JE, Lessell S. Neuro-ophthalmologic findings in chordoma and chondrosarcoma of the skull base. Am J Ophthalmol. 1993;115:97–104.
8. Hug EB, Adams J, Fitzek M, De Vries A, Munzenrider JE. Fractionated, three-dimensional, planning-assisted proton-radiation therapy for orbital rhabdomyosarcoma: a novel technique. Int J Radiat Oncol Biol Phys. 2000;47:979–84.
9. Koto M, Hasegawa A, Takagi R, Fujikawa A, Morikawa T, Tsujii H, Kamada T. Carbon ion radiotherapy for skull base and paracervical tumors. In: Proceedings of NIRS-ETOILE 2nd joint symposium on carbon ion radiotherapy. Lyon: Centre ETOILE; 2011. NIRS-M-243:12–7.
10. Mizoe JE, Hasegawa A, Takagi R, Bessho H, Onda T, Tsujii H. Carbon ion radiotherapy for skull base chordoma. Skull Base. 2009;19:219–24.
11. Schulz-Ertner D, Karger CP, Feuerhake A, Nikoghosyan A, Combs SE, Jäkel O, Edler L, Scholz M, Debus J. Effectiveness of carbon ion radiotherapy in the treatment of skull-base chordomas. Int J Radiat Oncol Biol Phys. 2007;68:449–57.
12. Catton C, O'Sullivan B, Bell R, Laperriere N, Cummings B, Fornasier V, Wunder J. Chordoma: long-term follow-up after radical photon irradiation. Radiother Oncol. 1996;41:67–72.
13. Romero J, Cardenes H, la Torre A, Valcarcel F, Magallon R, Regueiro C, Aragon G. Chordoma: results of radiation therapy in eighteen patients. Radiother Oncol. 1993;29:27–32.
14. Forsyth PA, Cascino TL, Shaw EG, Scheithauer BW, O'Fallon JR, Dozier JC, Piepgras DG. Intracranial chordomas: a clinicopathological and prognostic study of 51 cases. J Neurosurg. 1993;78:741–7.
15. Magrini SM, Papi MG, Marletta F, Tomaselli S, Cellai E, Mungai V, Biti G. Chordoma-natural history, treatment and prognosis. The Florence Radiotherapy Department experience (1956–1990) and a critical review of the literature. Acta Oncol. 1992;31:847–51.
16. Castro JR, Linstadt DE, Bahary JP, Petti PL, Daftari I, Collier JM, Gutin PH, Gauger G, Phillips TL. Experience in charged particle irradiation of tumors of the skull base: 1977–1992. Int J Radiat Oncol Biol Phys. 1994;29:647–55.
17. Schulz-Ertner D, Nikoghosyan A, Hof H, Didinger B, Combs SE, Jäkel O, Karger CP, Edler L, Debus J. Carbon ion radiotherapy of skull base chondrosarcomas. Int J Radiat Oncol Biol Phys. 2007;67:171–7.

Part XI

Eye Tumors

Uveal Melanoma

19

Hiroshi Tsuji, Shingo Toyama, and Takuma Nomiya

Abstract

Proton beam therapy (PRT) for uveal melanoma was the first established treatment in the history of charged particle therapy. PRT has been used to treat the largest number of patients worldwide, and the outcomes have been quite satisfactory [1–8]. Brachytherapy using a radioactive plaque is also an established treatment option primarily for patients with a small-sized tumor [9]. Recently, stereotactic radiotherapy has also been shown to have satisfactory results in selected patients [10]. Meanwhile, carbon ion beams are able to offer even better dose conformity than proton beams based on a sharper lateral falloff (Fig. 19.1), although the differences in the dose conformity between the two methods generally depend on the depth of the target lesion. In addition, the carbon ion beam is thought to have a biological advantage relative to PRT in the treatment of relatively resistant tumors, such as malignant melanoma. Therefore, carbon ion radiotherapy (C-ion RT) for uveal melanoma was expected to result in similar or even better clinical outcomes than PRT. The clinical trial on C-ion RT for uveal melanoma was initiated at the National Institute of Radiological Sciences (NIRS) in 2001 as a phase I/II dose-escalation study [11]. As anticipated, C-ion RT was shown to be sufficiently safe and efficacious, and the study was closed in 2004. C-ion RT for uveal melanoma has been subsequently continued as an advanced treatment at NIRS and is used to treat about ten patients each year, which is almost one third to one fourth of the yearly number of patients in Japan. To date, the results have been comparable to that of PRT in western countries in both tumor control and toxicity. Additionally, the incidence of neovascular glaucoma (NVG) could potentially be decreased with 2-port C-ion RT performed in accordance with dose-volume histogram analysis. In this chapter, the treatment methods being performed at NIRS and the up-to-date outcomes are described [12, 13].

Keywords

Carbon ion radiotherapy • Choroidal melanoma • CT-based planning • Dose-volume histogram • Neovascular glaucoma

19.1 Introduction

The NIRS experience with C-ion RT for uveal melanoma has demonstrated that the carbon ion beam can provide similar or even better treatment outcomes to PRT in terms of tumor control, patient survival, and toxicity. Moreover, the NIRS experience showed that 2-port irradiation based on CT-based planning can decrease the risk of NVG [11–13].

H. Tsuji (✉) • T. Nomiya
National Institute of Radiological Sciences,
4-9-1 Anagawa, Inage-ku, Chiba, Japan
e-mail: h_tsuji@nirs.go.jp

S. Toyama
Department of Heavy Particle Therapy and Radiation Oncology,
Saga University, Saga, Japan

H. Tsujii et al. (eds.), *Carbon-Ion Radiotherapy: Principles, Practices, and Treatment Planning*,
DOI 10.1007/978-4-431-54457-9_19, © Springer Japan 2014

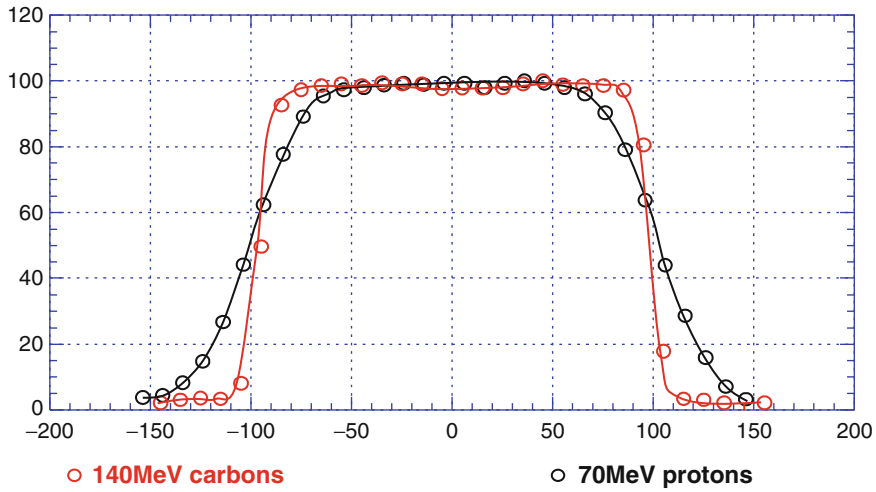

Fig. 19.1 Lateral dose distribution of 140 MeV carbon ion beam and 70 MeV proton beam. Lateral falloff of the carbon ion beam is substantially sharper than proton beam

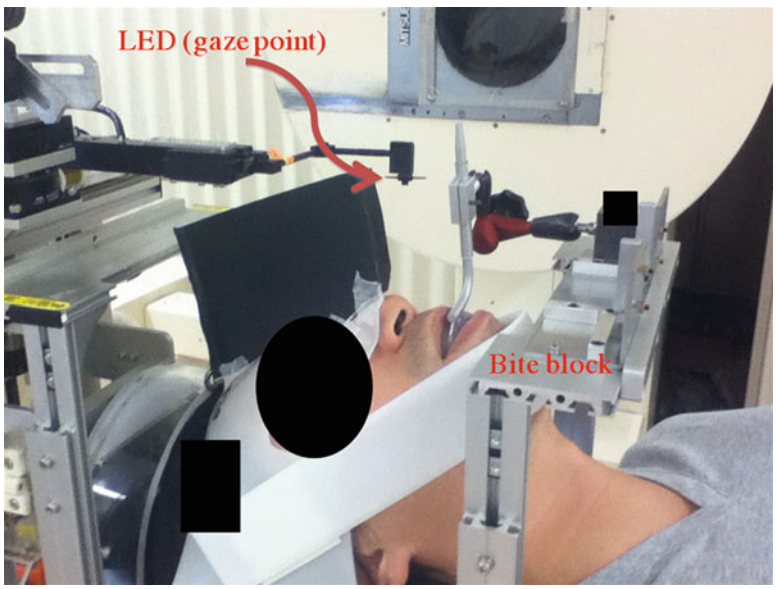

Fig. 19.2 Patient immobilization and eye fixation in the C-ion RT at the NIRS. A bite block is fixed to the bridge by strong magnet and gaze point can be set three-dimensionally with special head fixation devices

19.2 Methods of Carbon Ion Radiotherapy (C-ion RT)

In preparation for the treatment, the patient is immobilized with a low-temperature thermoplastic restraining device (Shellfitter; Kuraray, Osaka, Japan) in a supine position. Recently, a bite block has been additionally employed to fix the head more securely (Fig. 19.2). The eye is fixed by a gazing method developed at NIRS and originally used for PRT. The method of preparing the patient for treatment is similar to that at other institutes, such as the Harvard Cyclotron Laboratory [1] and the Paul Scherrer Institute [2]. Several particular differences between our institute and other institutes are that all procedures at NIRS are performed in the supine position and that the treatment planning is based on CT scans.

A set of 0.5-mm-thick CT images is obtained for the purpose of treatment planning using immobilization devices and a gazing light [11]. Titanium markers are sutured on the outer surface of the sclera for both treatment planning and field localization. Three-dimensional treatment planning had been performed using EYEPLAN software (NIRS, Chiba, Japan) until March 2005, and XiO-carbon combined with FocalPro (CMS Inc., St Louis, MO) has been used since April 2005. The contours of the target volumes and the organs at risk (e.g., lens, eyeball wall, optic disk) are drawn directly on the CT images. The gross tumor volume (GTV) is determined according to the CT images with reference to the ophthalmoscopy and MRI findings. The clinical target volume is almost the same as the GTV, with the exception that the clinical target volume has a 1.0–2.0-mm extra margin for possible tumor invasion into the sclera. Accordingly, the planning target volume (PTV) is automatically produced by the addition of an approximately ~1.0-mm margin to the CTV, but can be modified manually if necessary.

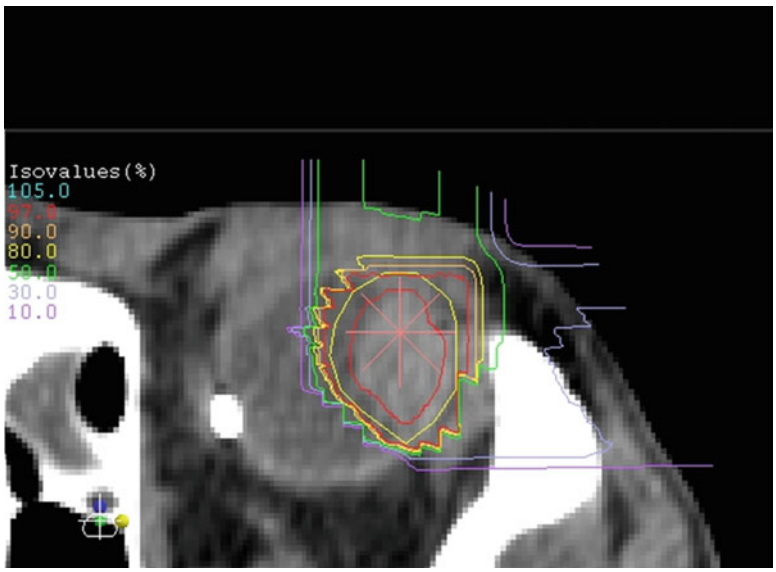

Fig. 19.3 Representative dose distribution of 2-port irradiation at the NIRS. The current prescribed dose is 70.0 GyE in 5 fractions for T3 tumor and 60.0 GyE in 5 fractions for T1/2 tumor

A compensation bolus and brass collimator are fabricated so that the PTV will be covered with greater than 95 % of the prescribed dose. In the beginning of the clinical trial, irradiation was delivered through a single anterior port; however, 2-port irradiation has been adopted for most patients since October 2005, because it seemed beneficial in reducing the risk of NVG. Indeed, the dose-volume histogram analysis using NIRS data indicated that the irradiated volume of the iris-ciliary body was related to the risk of NVG and that the V50 of the iris-ciliary body should be constrained to less than 0.1 mL [12, 13]. A typical dose distribution with 2-port irradiation is shown in Fig. 19.3.

The prescribed total dose was varied from 60 GyE/5 to 85 GyE/5 fractions in the dose-escalation study and was fixed to 70.0 GyE/5 fractions for T3 tumors and 60.0 GyE/5 fractions for T1/2 tumors in the advanced treatment since April 2004.

19.3 Up-to-Date Outcomes of the C-ion RT at NIRS

As of February 2013, 127 patients with locally advanced or unfavorably located choroidal melanoma received CT-based C-ion RT at NIRS. Of these, 122 patients were followed up at least 6 months. The 5-year overall survival and eye retention rate were 80.8 and 93.1 %, respectively (Fig. 19.4). The local control rate of the treated tumors and the intraocular recurrence-free rate were 96.4 and 92.3 %, respectively (Fig. 19.5). These results are comparable to those of PRT (Table 19.1).

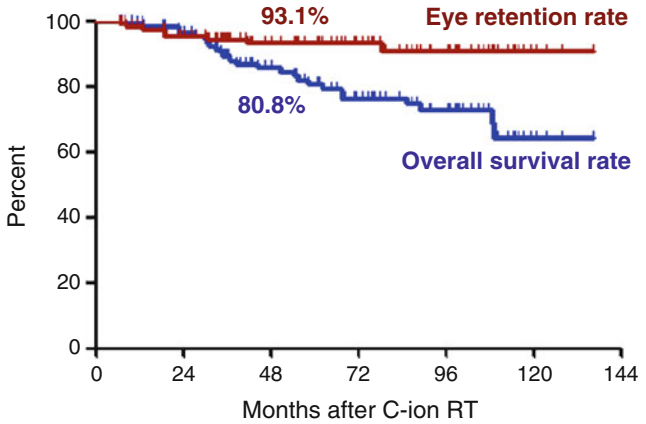

Fig. 19.4 Overall survival rate and eye retention rate of the patients treated with C-ion RT at the NIRS

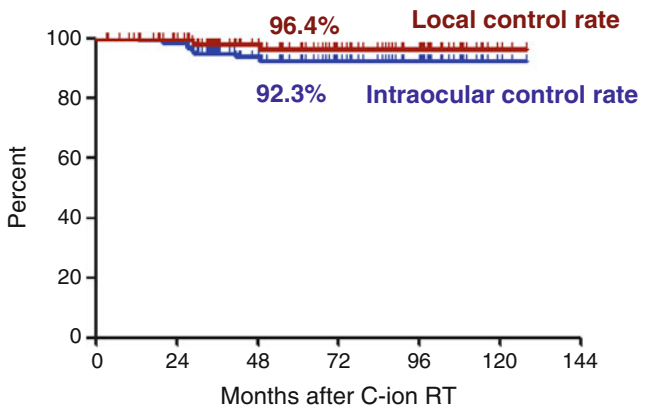

Fig. 19.5 Local control rate of the treated tumor and intraocular recurrence-free rate after C-ion RT

Table 19.1 Treatment outcomes for particle radiotherapy of uveal melanoma

Institution	Particles	Number of patients	5-year rate		
			Local control (%)	Overall survival (%)	Eye retention (%)
MGH	Proton	1,006	96.3		89.0
PSI	Proton	2,432	95.8	87.9	88.9
Nice	Proton	538	89.0	73.8	88.0
Clatterbridge	Proton	349	96.5		90.6
NIRS	Carbon	122	96.4	80.8	93.1

MGH Massachusetts General Hospital, *PSI* Paul Scherrer Institute

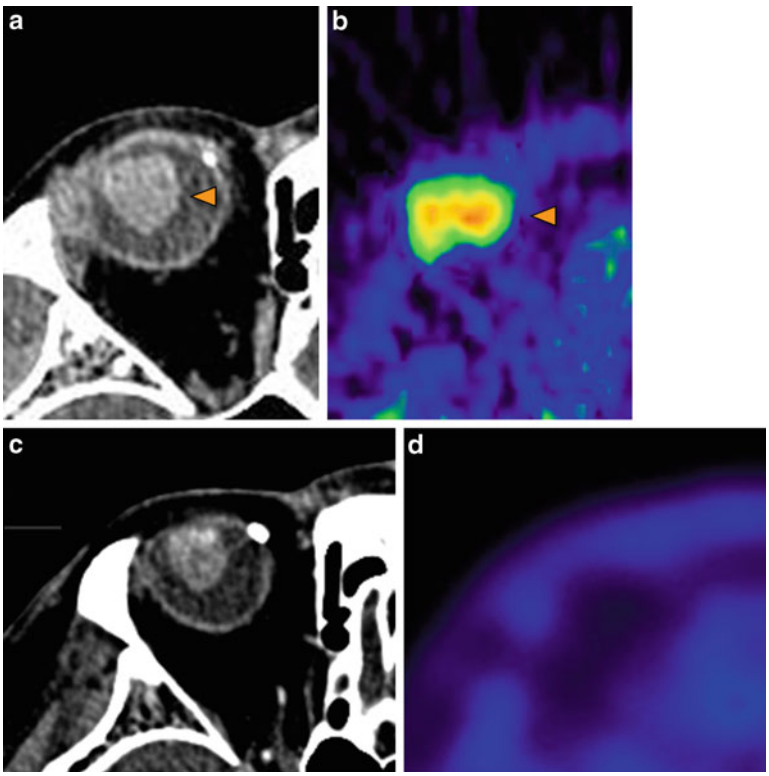

Fig. 19.6 Case study CT image before C-ion RT (**a**), methionine-PET before C-ion RT (**b**), CT image 1 year later (**c**), and methionine-PET 1 year later (**d**)

The slightly higher probability of eye retention at the NIRS likely resulted from the reduced incidence of NVG through the adoption of 2-port C-ion RT.

Based on the NIRS experience, C-ion RT with 2-port irradiation based on CT planning can provide a slightly better outcome as compared to PRT.

19.4 Case Study

A 63-year-old Japanese male was referred to the NIRS hospital with a diagnosis of T3N0M0 choroidal melanoma of his right eye. A CT image demonstrated the tumor was located on the cranial side of his right eye. The tumor was 12.0 mm in diameter and 9.0 mm in height (Fig. 19.6a). A moderate accumulation of methionine was observed in the tumor by a methionine-PET scan (Fig. 19.6b).

C-ion RT was performed with two ports in the anterior and right lateral directions; the total dose was 70.0 GyE in 5 fractions (anterior port, 3 fractions; right lateral port, 2 fractions).

One year later, a CT scan showed the size of the tumor had decreased a small amount in size (Fig. 19.6c). As revealed by methionine radioisotope accumulation on a methionine-PET scan, the tumor had disappeared completely (Fig. 19.6d). The patient is alive without any recurrence or metastasis, and the visual acuity of his right eye has been preserved at 6 years after C-ion RT.

References

1. Munzenrider JE, Verhey LJ, Gragoudas ES, et al. Conservative treatment of uveal melanoma: local recurrence after proton beam therapy. Int J Radiat Oncol Biol Phys. 1989;17:493–8.
2. Egger E, Schalenbourg A, Zografos L, et al. Maximizing local tumor control and survival after proton beam radiotherapy of uveal melanoma. Int J Radiat Oncol Biol Phys. 2001;51:138–47.
3. Egger E, Zografos L, Schalenbourg A, et al. Eye retention after proton beam radiotherapy for uveal melanoma. Int J Radiat Oncol Biol Phys. 2003;55:867–80.
4. Dendale R, Lumbroso-Le Rouic L, Noel G, et al. Proton beam radiotherapy for uveal melanoma: results of Curie Institut-Orsay proton therapy center (ICPO). Int J Radiat Oncol Biol Phys. 2006;65:780–7.
5. Caujolle JP, Mammar H, Chamorey E, et al. Proton beam radiotherapy for uveal melanomas at nice teaching hospital: 16 years' experience. Int J Radiat Oncol Biol Phys. 2010;78:98–103.
6. Damato B, Kacperek A, Chopra M, et al. Proton beam radiotherapy of choroidal melanoma: the Liverpool-Clatterbridge experience. Int J Radiat Oncol Biol Phys. 2005;62:1405–11.
7. Fuss M, Loredo LN, Blacharski PA, et al. Proton radiation therapy for medium and large choroidal melanoma: preservation of the eye and its functionality. Int J Radiat Oncol Biol Phys. 2001;49:1053–9.
8. Tran E, Ma R, Paton K, et al. Outcomes of proton radiation therapy for peripapillary choroidal melanoma at the BC Cancer Agency. Int J Radiat Oncol Biol Phys. 2012;83:1425–31.
9. Collaborative Ocular Melanoma Study Group. The COMS randomized trial of iodine 125 brachytherapy for choroidal melanoma: V. twelve-year mortality rates and prognostic factors: COMS report No. 28. Arch Ophthalmol. 2006;124:1684–93.
10. Dunavoelgyi R, Dieckmann K, Gleiss A, et al. Local tumor control, visual acuity, and survival after hypofractionated stereotactic photon radiotherapy of choroidal melanoma in 212 patients treated between 1997 and 2007. Int J Radiat Oncol Biol Phys. 2011;81:199–205.
11. Tsuji H, Ishikawa H, Yanagi T, et al. Carbon-ion radiotherapy for locally advanced or unfavorably located choroidal melanoma: a phase I/II dose-escalation study. Int J Radiat Oncol Biol Phys. 2007;67:857–62.
12. Hirasawa N, Tsuji H, Ishikawa H, et al. Risk factors for neovascular glaucoma after carbon ion radiotherapy of choroidal melanoma using dose-volume histogram analysis. Int J Radiat Oncol Biol Phys. 2007;67:538–43.
13. Toyama S, Tsuji H, Mizoguchi N, et al. Long-term results of carbon ion radiation therapy for locally advanced or unfavorably located choroidal melanoma: usefulness of CT-based 2-port orthogonal therapy for reducing the incidence of neovascular glaucoma. Int J Radiat Oncol Biol Phys. 2013;86:270–6.

Lacrimal Gland Tumors

20

Hiroshi Tsuji, Nobutaka Mizoguchi, and Takuma Nomiya

Abstract

Lacrimal gland carcinoma (LGC) is a very rare malignancy with no established treatment other than surgery [1]. If conservative surgery cannot be applied, orbital exenteration is the only treatment of choice with curative intent [2–6]. Therefore, effective and less invasive treatment methods are urgently needed. The National Institute of Radiological Sciences (NIRS) conducted a phase I/II dose-escalation study of carbon ion radiotherapy (C-ion RT) for LGC between 2002 and 2011 to establish a safe and effective treatment method using the carbon ion beam. Satisfactory results have been obtained with C-ion RT in 12 fractions over 3 weeks. An extended field was observed to be necessary for reducing the risks of marginal recurrence. In this chapter, the treatment method being performed at NIRS and up-to-date outcomes are described.

Keywords

Adenoid cystic carcinoma • Carbon ion radiotherapy • Lacrimal gland tumor

20.1 Introduction

The NIRS experience with LGC demonstrated that C-ion RT is an effective and safe treatment option for this disease; however, insufficient settings in regard to the treatment volume with the aim at preserving vision may lead to marginal recurrence.

20.2 Methods of Carbon Ion Radiotherapy

In a supine position, the patient is immobilized with a low-temperature thermoplastic restraining device (Shellfitter; Kuraray, Osaka, Japan) and a headrest made of a customized cradle. Prior to the treatment, a set of 2.5-mm-thick CT images had been acquired for treatment planning using the same immobilization devices, with 3-dimensional treatment planning subsequently performed using HIPLAN software (NIRS, Chiba, Japan) [7]. The gross tumor volume (GTV) is set with reference to both contrast-enhanced CT and contrast-enhanced MRI. The clinical target volume (CTV) is defined by adding regions of potential tumor invasion to the GTV. The initial trial at NIRS had employed a relatively small margin of around 5 mm for the CTV, with only the high-risk area around the GTV included. However, three out of the ten patients who had undergone this treatment developed marginal recurrence. Therefore, a decision was made to adopt an extended margin in 2005 even for tumors localized outside of the eyeball (Fig. 20.1). None of the subsequent 11 patients has developed marginal recurrence (Table 20.1).

CTV with extended margins includes the inner edge, which contains the lacrimal sac; the outer edge, which is represented by the frontal bone configuring the outer orbit; the upper edge of the outer malar bone, representing the outer frontal bone with the lachrymal gland; the lower edge, which is the upper maxilla bone configuring the outer

H. Tsuji (✉) • T. Nomiya
National Institute of Radiological Sciences,
4-9-1 Anagawa, Inage-ku, Chiba, Japan
e-mail: h_tsuji@nirs.go.jp

N. Mizoguchi
Department of Radiation Oncology,
Kanagawa Cancer Center, Kanagawa, Japan

H. Tsujii et al. (eds.), *Carbon-Ion Radiotherapy: Principles, Practices, and Treatment Planning*,
DOI 10.1007/978-4-431-54457-9_20,

orbit; and the outside as well as the posterior edge of the malar bone, which represents the distal optic nerve before the optic chiasma. The planning target volume (PTV) is determined as a setup margin of 3 mm around the CTV. A typical dose distribution is shown in Fig. 20.1b. The eyeball, cornea, optic nerve, optic chiasma, temporal lobe of the brain, and skin are the organs at risk in the treatment planning for LGC. Since the extended margins are employed, the visual acuity of the ipsilateral eye cannot be preserved; however, it is important to decrease the dose irradiated to the cornea, iris, and ciliary body to reduce the risk of pain from keratitis or severe glaucoma. The dose to the skin and brain should also be constrained in the same manner as in the treatments for other tumors of the head and neck region (see Chap. 15; Head and Neck Tumors). The concrete dose constraints for LGC have not yet been established; however, the aim of the planning for at least one of the three fields was to spare the temporal lobe completely, and the dose to the skin was reduced using the sharp lateral fall-off of the carbon ion beam. The irradiated dose was escalated from 48.0 to 52.8 GyE in 12 fractions for the phase I/II trial at NIRS, with 52.8 GyE/12 fractions finally chosen as the recommended dose.

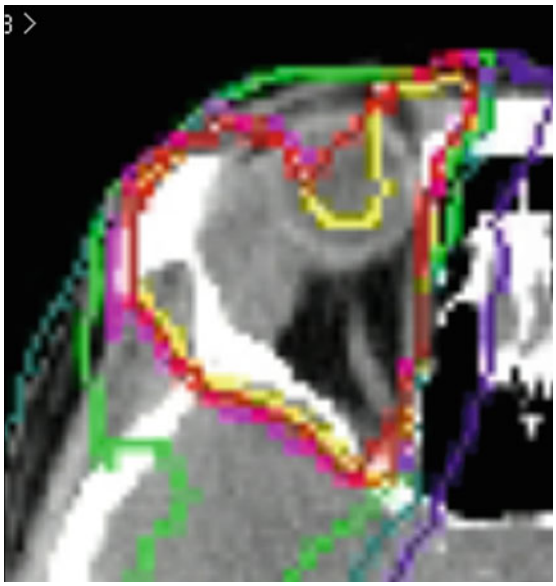

Fig. 20.1 Representative dose distribution of C-ion RT for the lacrimal gland tumor at the NIRS. The current prescribed dose is 52.8 GyE in 12 fractions

20.3 Up-to-Date Outcomes of the C-ion RT at NIRS

Between April 2002 and January 2011, a total of 21 patients with LGC were treated with C-ion RT at NIRS. Six of the patients had been untreated, while the remaining 15 patients had residual and recurrence diseases after eye-sparing surgery. The pathological diagnosis of the treated tumors was adenoid cystic carcinoma (16 patients), adenocarcinoma (3), malignant mixed tumor (1), and undifferentiated carcinoma (1). In terms of the C-ion RT dose, five patients received 48.0 GyE (4.0 GyE per fraction), while 16 patients received 52.8 GyE (4.4 GyE per fraction) (Table 20.1).

Figure 20.2 shows the Kaplan–Meier estimation of the local control rate and the patient survival rate of C-ion RT at NIRS. Local recurrence was observed in six patients. Of these, three patients developed recurrence in the irradiation field (in-field recurrence), while the remaining three patients had recurrence in the margin area of the irradiation field (marginal recurrence). The 5-year local control rate was 74.1 %, and the nonrecurrence rate in the irradiation field was 83.0 %. The cause of the marginal recurrence was believed to be an insufficient setting margin for the CTV (MM: minimal margin) in the latter three patients; therefore, the CTV margin was set to a range according to orbital exenteration (EM: extended margin). Following the adoption of treatment with EM, local recurrences did not occur (Table 20.1). No significant differences were observed in the local control rate between patients in which the tumor remained after eye-sparing surgery or those in which the tumor recurred after eye-sparing surgery before C-ion RT.

Six out of the 21 patients died, including five patients who died from the LGC. The 5-year overall survival rate with all cases was 64.0 % (Fig. 20.2)

Table 20.1 Summary of treatment outcomes in C-ion RT for lacrimal gland tumor at NIRS

	C-ion RT		Number of	Local recurrence		
Period	Dose (GyE)	Field	patients	Recurrence free	In-field recurrence	Marginal recurrence
April 2002–March 2003	48.0	Small	5	3	1	1
April 2003–June 2005	52.8	Small	5	2	1	2
July 2005–current	52.8	Extended	11	10	1	0
Total			21	15	3	3

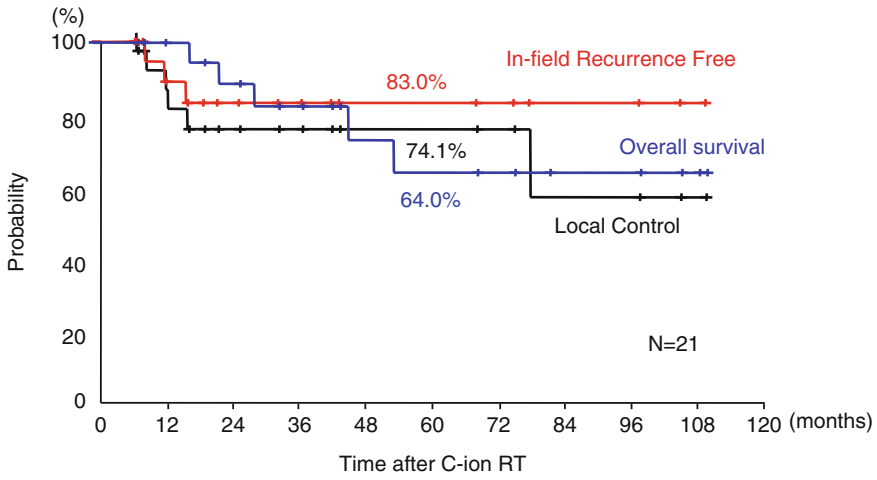

Fig. 20.2 Overall survival rate and local control rate of the patients treated with C-ion RT at the NIRS

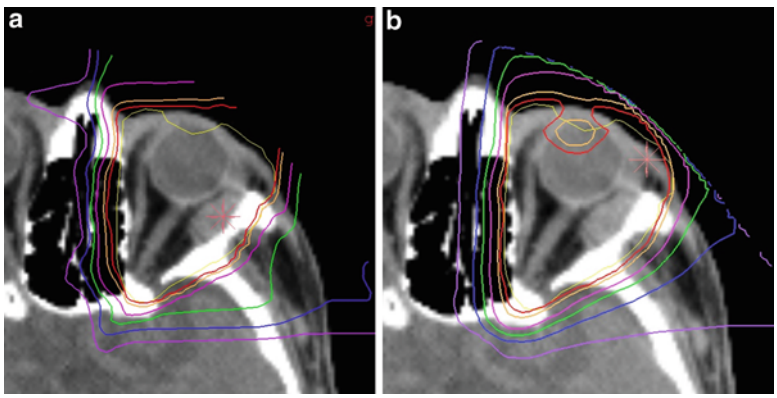

Fig. 20.3 Comparative treatment planning between passive irradiation and scanning irradiation. Even with simple two-port irradiation, the dose to the anterior structures can be reduced with scanning method. (**a**) Dose-distribution with passive delivery of carbon ion beam. (**b**) Dose-distribution with scanning delivery of carbon ion beam

Regarding toxicity following C-ion RT at NIRS, dermatitis, conjunctivitis, and retinopathy remained in grade 2, with no observations of toxicity of grade 3 or more. Neovascular glaucoma developed in four cases at 52.8 GyE/12fr; however, no patient required ophthalmectomy.

In 2011, beam delivery using spot scanning became available at NIRS. Scanning irradiation can offer even better dose distribution than the passive method in the treatment of LGC. Figure 20.3 demonstrates the dose distribution of passive irradiation (Fig. 20.3a) and scanning irradiation (Fig. 20.3b) for LGC. The plans for both types of irradiation use two ports from the anterior and left lateral directions. The scanning irradiation can reduce the dose to the lens and the surrounding normal tissues, such as the iris, ciliary body, or cornea, even with a plan involving simple 2-port irradiation. The dose-volume histogram of these normal tissues (Fig. 20.4) indicates a 5–10 % decrease in the dosage by scanning irradiation compared to passive irradiation. This difference could be meaningful in reducing the risk of severe glaucoma or keratitis.

20.4 Case Study

A 67-year-old Japanese male was referred to the NIRS hospital with the diagnosis of a postoperative recurrence of a right lacrimal gland tumor. The recurred tumor was at an initial stage (T3aN0M0), and the pathology was adenocarcinoma. MRI demonstrated the recurred tumor was located on the lateral side of his right eye (Fig. 20.5a). A moderate accumulation of methionine was seen in the tumor by a methionine-PET scan (Fig. 20.5b).

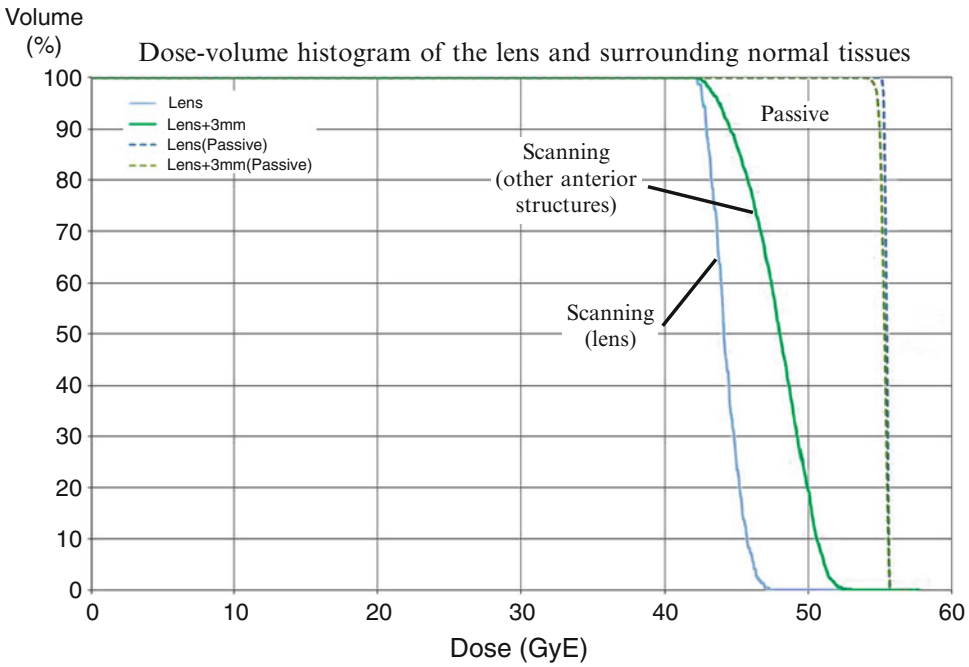

Fig. 20.4 Dose-volume histogram of the lens and other anterior structures of the eye. Five to ten percent dose reduction can be obtained by the scanning irradiation

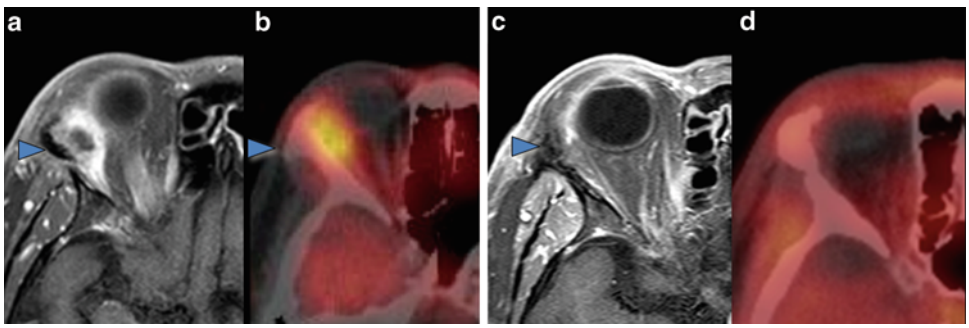

Fig. 20.5 Case study recurred tumor after conservative surgery is demonstrated in T1-weighted contrast-enhanced MRI (T1CE-MRI) before C-ion RT (**a**) and methionine-PET before C-ion RT (**b**). The tumorhas obviously decreased in size in T1CE-MRI 6 months later (**c**), and radioisotope accumulation has almost disappeared in methionine-PET 6 months later (**d**)

C-ion RT was performed with three ports in the anterior, right-lateral, and right-posterior oblique directions; the total dose was 52.8 GyE in 12 fractions. Six months later, the tumor was clearly decreased in size as demonstrated by MRI (Fig. 20.5c), and methionine accumulation had almost disappeared on a PET scan (Fig. 20.5d). The patient is alive without any recurrence or metastasis at 2 years after the C-ion RT.

References

1. Lacrimal Gland Tumor Study Group. An epidemiological survey of lacrimal fossa lesions in Japan: number of patients and their sex ratio by pathological diagnosis. Jpn J Ophthalmol. 2005;49:343–8.
2. Skinner HD, Garden AS, Rosenthal DI, et al. Outcomes of malignant tumors of the lacrimal apparatus: the University of Texas MD Anderson Cancer Center experience. Cancer. 2011;117:2801–10.
3. Ahmad SM, Esmaeli B, Williams M, et al. American Joint Committee on Cancer classification predicts outcome of patients with lacrimal gland adenoid cystic carcinoma. Ophthalmology. 2009;116:1210–5.
4. Font RL, Smith SL, Bryan RG. Malignant epithelial tumors of the lacrimal gland: a clinicopathologic study of 21 cases. Arch Ophthalmol. 1998;116:613–6.
5. Wright JE, Rose GE, Garner A. Primary malignant neoplasms of the lacrimal gland. Br J Ophthalmol. 1992;76:401–7.
6. Brada M, Henk JM. Radiotherapy for lacrimal gland tumours. Radiother Oncol. 1987;9:175–83.
7. Endo M, Koyama-Ito H, Minohara S, et al. HIPLAN: a heavy ion treatment planning system at HIMAC. J Jpn Soc Ther Radiol Oncol. 1996;8:231–8.

Part XII

Lung Tumors

Lung Cancer

21

Naoyoshi Yamamoto and Mio Nakajima

Abstract

It has been approximately two decades since we started performing carbon ion radiation therapy (C-ion RT) for non-small cell lung cancer (NSCLC). In 1994, we started conducting clinical trials using the dose-escalation method to determine the optimal dose of radiation. The additional purpose was to develop accurate, reliable, and safe irradiation techniques for C-ion RT.

In a subsequent phase II study of peripheral type stage I NSCLC, the total dose was fixed at 72 GyE in 9 fractions over 3 weeks and at 52.8 GyE for stage IA and at 60 GyE for stage 1B in 4 fractions over 1 week. In this way, the treatment period and fractionation were shortened and decreased from 18 fractions over 6 weeks to 9 fractions over 3 weeks and then further to 4 fractions over 1 week. Finally we were able to administer treatment as a single fraction.

For early-stage central- or hilar-type NSCLC, we conducted trials to identify the best way to preserve the pulmonary function with radical treatment. The prescribed dose for early central squamous cell carcinoma ranged from 54 to 61.2 GyE in nine fractions. For tumors close the hilus, we used 68.4 GyE/12 fractions, with planned target shrinking.

In addition, we also tried to treat locally advanced lung cancer, regional lymph node metastases that occurred after C-ion RT for clinical stage I cancer, and metastatic lung tumors.

This report describes the techniques and clinical trials that have been undertaken at the NIRS and describes the results of the current study. The use of C-ion RT for mediastinal or hilar lymph node metastases and metastatic lung tumors is described in Chap. 22.

Keywords

Carbon ion radiotherapy • Non-small cell lung cancer

21.1 Introduction

Non-small cell lung cancer (NSCLC) patients are classified into two groups for radiotherapy (RT). The first group comprises those with advanced lung cancer, including patients with invasion of the chest wall, mediastinum, and/or mediastinal lymph nodes. The other group includes patients with early-stage disease, i.e., peripherally localized T1 or T2 tumors without evidence of lymph node metastases. In general, only early-stage lung cancer patients are expected to have a long survival.

Surgical resection has played a pivotal role in the treatment of peripherally localized lung cancer and can provide a 5-year survival rate of 60 % and a 5-year local control rate of more than 80 % [1, 2]. As a result, the first recommended treatment for early-stage peripheral lung cancer has been

N. Yamamoto (✉) • M. Nakajima
National Institute of Radiological Sciences,
4-9-1 Anagawa, Inage-ku, Chiba, Japan
e-mail: nao_y@nirs.go.jp

H. Tsujii et al. (eds.), *Carbon-Ion Radiotherapy: Principles, Practices, and Treatment Planning*,
DOI 10.1007/978-4-431-54457-9_21, © Springer Japan 2014

surgical resection. However, this is not always feasible, and surgery may have increased morbidity due to the patients' medical conditions, such as pulmonary or cardiovascular disease. RT has played an important role as an alternative treatment for these patients. However, conventional RT provides relatively poor control of the primary tumor, thus resulting in 5-year survival rates of 30 % at best [3]. Dose escalation is essential to improve the effectiveness of RT, but this involves an increasing risk of normal tissue toxicity, especially pulmonary toxicity [4]. Since this can cause fatal reactions, it limits the applicable dose that can be given to the tumor. The goal of research on RT for lung cancer has therefore been to provide a higher dose to the target and lower doses to normal tissues, such as the lung parenchyma, esophagus, and spinal cord.

As a substitute for conventional RT, which is only a palliative treatment for medically inoperable localized NSCLC, various new modalities of RT have recently been developed, such as stereotactic body radiotherapy using photon beams (SBRT) and ion beam therapy (IBT). SBRT is now spreading worldwide, and a variety of new machines and techniques are being developed [5–9]. The radiation doses for SBRT are usually divided into multiple fractions given in multiple sessions. Hypofractionated SBRT, where few fractions of higher doses are administered, is usually applied for the treatment of peripheral stage I lung cancer [6–10]. Onishi et al. reported the results of SBRT for 257 patients with stage I NSCLC and showed lower toxicity and good local control rates (5.4 % of patients developed pulmonary complications above grade 2, and 14 % had local progression) [9]. Japan is one of the leading countries in the use of hypofractionated SBRT for the treatment of early-stage lung cancer [5].

Ion beams, with their improved dose distribution, are a novel and promising method that allows a higher dose to be applied to the tumor while minimizing the dose to the surrounding normal tissues. In particular, carbon ion radiotherapy (C-ion RT) seems to be an attractive modality due to its excellent dose distribution and increased biological effects in the Bragg peak region. Our clinical trials led us to conclude that irradiation with ion beams, notably carbon ions, offers a significant potential for improving tumor control, without increasing the risk of toxicity [11–17].

The National Institute of Radiological Sciences (NIRS) has conducted clinical trials on C-ion RT for lung cancer for almost two decades. A dose-escalation study using 18 fractions in 6 weeks was started for peripheral early-stage NSCLC in 1994. Between 1994 and 1999, a phase I/II dose-escalation study of the treatment of stage I peripheral NSCLC was conducted to determine the optimal dose and to evaluate if progression to hypofractionated C-ion RT was feasible [11]. Another purpose of these trials was to develop precise and safe irradiation techniques with maximum sparing of normal tissue.

The phase I/II study provided the following results:

1. The local control rate was dose-dependent. Local control reached more than 90 % at 90.0 GyE with a regimen of 18 fractions over 6 weeks and at 72.0 GyE with a regimen of 9 fractions over 3 weeks. Both doses were determined to be optimal for each fractionation strategy.
2. The damage to the lung was minimal; grade 3 radiation pneumonitis occurred in 2.7 % of the cases. Respiratory-gated and four-portal oblique irradiation techniques, which excluded opposed ports, proved to be successful for reducing the incidence of radiation pneumonitis.
3. Survival was significantly related to the local control and size of the primary lesion. Local failure, distant metastasis, and malignant pleurisy were associated with decreases in survival.

After the phase I/II study using this optimized schedule, a phase II clinical trial that enrolled a total of 127 patients was initiated in April 1999 and was closed in December 2003 [12, 13]. In the phase II clinical trial, the total dose was fixed at 72.0 GyE in 9 fractions within 3 weeks, at 52.8 GyE for stage IA NSCLC, and at 60.0 GyE for stage IB NSCLC in 4 fractions within 1 week. After confirming the feasibility of irradiating the tumors in four fractions, a phase I/II dose-escalation clinical trial for single-fraction irradiation for peripheral stage I NSCLC was initiated in April 2003. The initial total dose was 28.0 GyE administered in a single fraction using respiratory-gated and four-portal oblique irradiation. The total dose was escalated in increments of 2.0 GyE up to 50.0 GyE. This article describes the preliminary results of the phase I/II clinical trial and the recent results of the phase II clinical trial in terms of the local control and survival rates after C-ion RT.

For locally advanced NSCLC, a dose-escalation study using 16 fractions in 4 weeks was started in 2000. Using respiratory-gated and three- or four-portal oblique irradiation, the optimal dose was found to be 72.0 GyE.

21.2 Treatment Methodology

21.2.1 Staging

Computed tomography (CT) scans of the chest and the whole abdomen, enhanced magnetic resonance imaging (MRI) of the brain, bone scans, and bronchoscopy are routinely performed to permit staging. Enrollment in clinical trials is subject to a clear pathological diagnosis of NSCLC based on transbronchial tumor biopsy (TBB), transbronchial aspiration cytology (TBAC), or CT-guided percutaneous needle biopsy (PCNB). If regional lymph nodes are greater than 1 cm in the short axis on contrast-enhanced CT images, as well as being positive on a ^{11}C-methionine positron emission tomography (PET) scans, the regional lymph nodes are

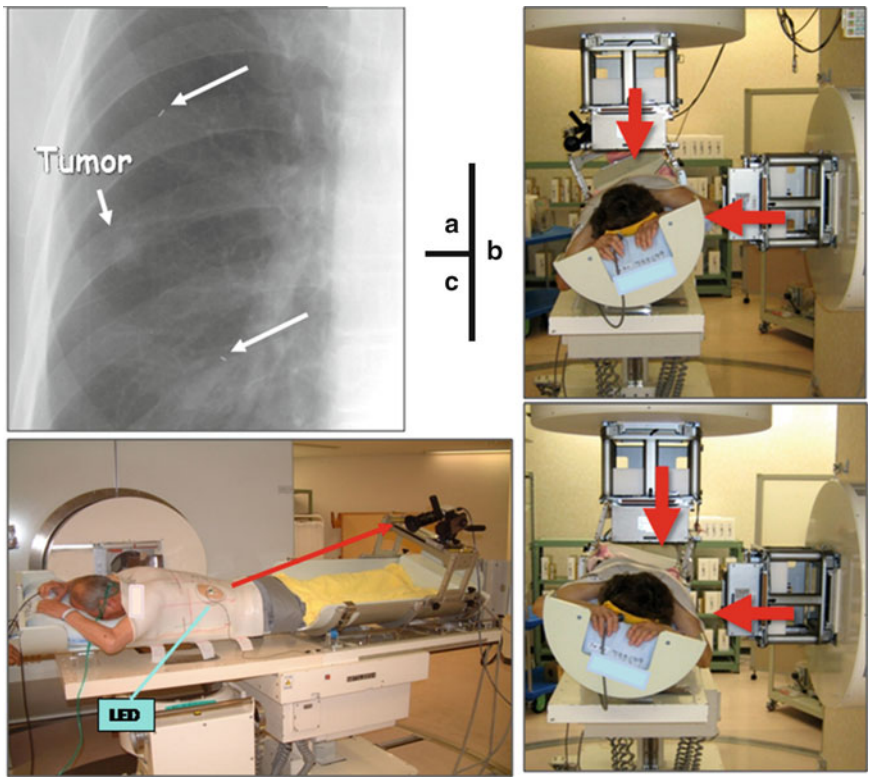

Fig. 21.1 The treatment system. (*A*) The tumor shadow and metallic markers are shown by *white arrows*. (*B*) Patients receive the carbon ion beams from four directions, as indicated by the *arrows*. (*C*) A respiratory-gated irradiation system using infrared from an LED placed on the body surface

considered to be positive for metastasis [18]. Endobronchial ultrasound-guided transbronchial needle aspiration (EBUS-TBNA) for hilar and mediastinal lymph nodes was recently introduced to provide clearer evidence of the metastatic status. Clinical staging is performed according to the UICC TNM classification [19].

21.2.2 Marker Insertion

Small iridium markers (length: 3 mm, diameter: 0.5 mm) are inserted into the lung to verify the position and direction of a patient's body during the irradiation. The markers do not interfere with the planning or implementation of the treatment. Routinely, two iridium rods are bronchoscopically placed into the patient's lung (Fig. 21.1). The markers serve as fiducial landmarks to verify the position of the tumor in the lung. In each treatment session, they are visualized by X-ray radiography.

21.2.3 Immobilization

The immobilization devices consist of polyurethane fixtures and thermoplastic plates. The fixtures and plates are personalized for each patient before CT scanning for treatment planning. The patient is usually treated in the supine position. If the tumor is in the posterior lung, the patient assumes a prone position.

Irradiation is typically administered from four directions. As the beam lines are fixed in vertical and horizontal directions, the other two directions are achieved by tilting the patient to the left or right (Fig. 21.1).

21.2.4 Respiratory Gating

CT images for treatment planning are taken in synchronization with the respiratory motion. Because the displacement of a tumor is generally lowest at the end of the expiratory phase, this timing is applied for the actual irradiation. The respiratory sensing system uses a position-sensitive detector (PSD) as a camera, along with an infrared light-emitting diode (LED). The LED is attached to the patient's body around the chest wall, and the light spot from the LED is focused on the PSD through a lens system [20]. A change in position is amplified by the zoom lens of the camera. The analog signals of the PSD are directly proportional to the spot position, without the need for a software program to calculate the position. The camera is typically mounted on the treatment couch at the feet of the patient, where it does not disturb the irradiation and does not interfere with the patient's fixation device. Setup of the respiratory sensor takes less than 30 s (Fig. 21.1). Prompt starting and stopping of the beam extraction according

to the gate signal are achieved by a special extraction method that provides an efficiency of more than 85 % of that of the standard extraction at the heavy ion medical accelerator in Chiba (HIMAC)[20, 21].

21.2.5 Irradiation

For patient positioning, fluoroscopic images are used, along with the superposition of the respiration waveform. Each treatment room of the HIMAC has a pair of orthogonal fluoroscopic devices. Fluoroscopic images of the patient in the optimal position are digitized and transferred to the positioning computer. They are displayed on the computer monitor screen, together with reference images, such as simulation images or digital reconstruction radiography, which are calculated based on the planning CT images. Fluoroscopy is performed from the beam's eye view. The patient's respiration waveform and the gate signal are also superimposed on the TV screen. The treatment couch is then moved to the matching position until the largest deviation from the field edge and the isocenter position is less than 2 mm. The whole procedure, including irradiation, takes about 20–30 min.

21.2.6 Follow-Up

Most patients underwent clinical examinations for follow-up, and CT scans of the thorax were carried out at our institute. Patients in whom follow-up testing could not be carried out until completion underwent periodic CT scanning at another institute. The clinical outcomes of all patients have been confirmed.

The first follow-up examinations were performed 4 weeks after C-ion RT and were repeated every 3–4 months. It is difficult to distinguish the changes in normal tissues due to radiation from tumor regrowth. We therefore defined transitorily enlarged densities observed after approximately 3 months as locally controlled tumors. Local recurrence was defined by an enlarging tendency of the tumor, as well as based on the findings of CT images, PET scans, tumor marker levels, and biopsy results.

21.3 Stage I Non-small Cell Lung Cancer

21.3.1 Stage I Peripheral Type Tumors

21.3.1.1 Treatment Planning

The targets are typically irradiated from four oblique directions without prophylactic elective nodal irradiation. A margin greater than 10 mm is set outside the gross target volume (GTV) to determine the clinical target volume (CTV). Spicular formations and pleural indentations are included in the CTV where possible. An internal margin (IM) is set outside the CTV in order to allow for target motion during gating. The planning target volume (PTV) is defined as the CTV plus IM. Three-dimensional treatment planning is performed using the HIPLAN software program, which was developed at the NIRS [22]. The IM is determined by extending the target margin in the head and tail directions by a width of 5 mm, which has resulted in the successful prevention of marginal recurrences caused by respiratory movement [23].

Compared with the pulmonary damage reported in stereotactic radiotherapy for stage I NSCLC [24, 25], the incidence and severity of the damage in our patients seem to be low. These mild adverse effects for the lung were achieved as a result of the small irradiated volume (V20 #9802 T1 ($n=30$) mean 5.5 % (2.3–11.6), T2 ($n=21$) mean 7.6 % (2.6–13.9), #0001 T1 ($n=41$) mean 4.8 % (1.1–13.2), T2 ($n=39$) mean 6.4 % (1.0–12.3)) achieved with the excellent dose distribution provided by the carbon ion beams due to the formation of a Bragg peak, which is in contrast to the results when X-rays are used as the permeating beam (Fig. 21.2).

21.3.1.2 A Representative Case of Single Fraction C-Ion RT

An 83-year-old Japanese male was referred to the NIRS hospital with a diagnosis of primary lung cancer, of which the initial stage was T2N0M0 and the pathology was squamous cell carcinoma. The CT scan demonstrated that the tumor was located in the upper lobe (S3) of his right lung (Fig. 21.3).

CIRT was performed with four ports in four directions, and the total dose was 46.0 GyE in a single fraction. Twelve

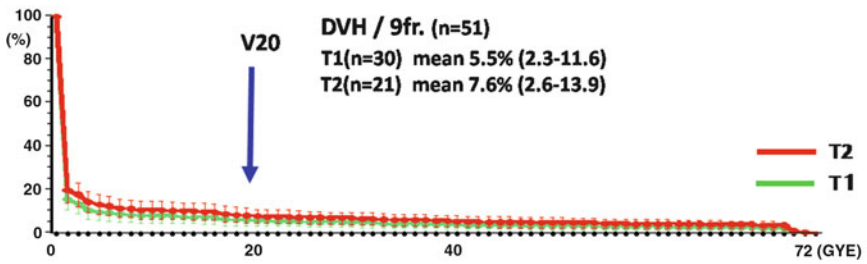

Fig. 21.2 The DVH of the phase II study (9802)

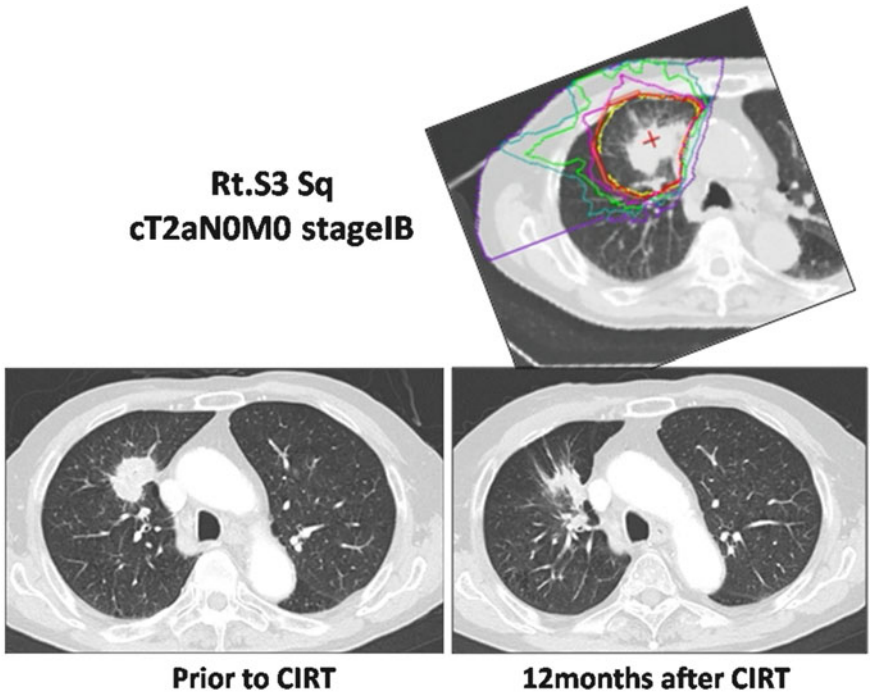

Fig. 21.3 The dose distribution of the planning CT and CT images pre- and postirradiation

months later, the tumor demonstrated by the follow-up CT was noted to have decreased in size. The patient is still alive without any recurrence or metastasis 3 years after the CIRT.

21.3.1.3 Results

The local control rate for all patients (trial #9802 and #0001) was 91.5 %, and the rates for T1 and T2 tumors were 96.3 and 84.7 %, respectively. While there was a significant difference ($p=0.0156$) in the control rates between T1 and T2 tumors, there was no significant difference ($p=0.1516$) between squamous cell carcinomas and non-squamous cell carcinomas. The 5-year cause-specific survival rate was 67.0 % (IA: 84.4 %, IB: 43.7 %), and the overall survival was 45.3 % (IA: 53.9 %, 1B: 34.2 %). No adverse effects greater than grade 2 occurred in the lung in any of the patients.

In a single fractionation trial, the 3-year local control rate for 151 patients was 83.1 %, and the control rates for T1 and T2 tumors were 88.5 and 75.0 %, respectively. The overall survival rate was 75.5 %. No adverse effects greater than grade 2 occurred in the lung in any of these patients.

21.3.2 Stage I Central-Type Tumors

21.3.2.1 Treatment Planning

When treating lesions located near the lung hilus, there are concerns about the potential for serious damage to the pulmonary function resulting from bronchial stenosis [26]. During the treatment of peripheral lung tumors in our studies, we observed very little loss of pulmonary function after the C-ion RT [27]. However, any reduction of the pulmonary function is an adverse effect that can significantly impair the quality of life. We have therefore been making an extensive effort to minimize the risk of severe bronchial toxicity during the treatment of central tumors. Adequate target coverage (local control) and the sparing of the airway (unrelated segment bronchus) are necessary. For the airway sparing, using a small CTV (cutting off the bronchus from a large CTV) is important.

21.3.2.2 Central-Type Early Squamous Cell Lung Cancer

Planning in a Representative Case

A 66-year-old male patient with central early lung cancer (squamous cell carcinoma) located from the left main bronchus to the upper lobe bronchus was treated at our hospital. Irradiation with carbon ion beams at 61.2 GyE in 9 fractions within 3 weeks was performed in November of 2001. The treatment planning is shown in Fig. 21.4. Eight years after treatment, he is still alive and well without recurrence. No severe reaction was found on the follow-up CT or bronchoscopic examination.

21.3.2.3 Early-Stage NSCLC with an Extrabronchial Tumor Near the Hilus

Planning in a Representative Case

A 64-year-old male patient with left upper lobe (S4) lung cancer (squamous cell carcinoma) that measured 34×24 mm who also had hilar lymph node metastases was diagnosed with cT2N1M0 disease. Carbon ion radiation at 68.4 GyE was performed. As of 4 years after treatment, he is still alive and well, without any recurrence (Fig. 21.5).

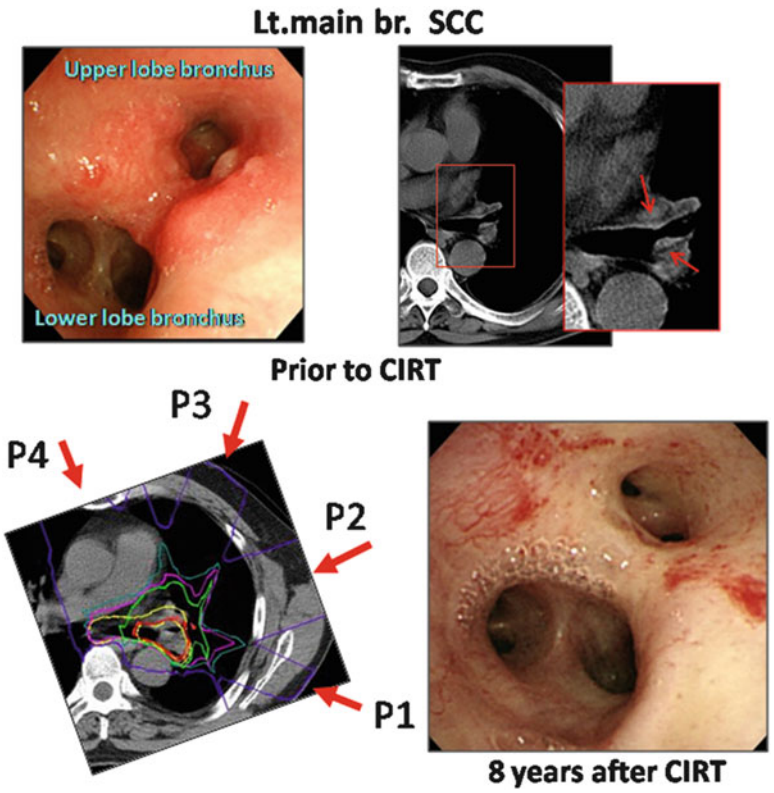

Fig. 21.4 Endoscopic findings prior to CIRT (*left upper panel*) and CT images. The tumor is shown by *arrows*. The planning CT images, where P1:P2:P3:P4 = 2:2:3:2, and P3 is a small target (*left lower panel*). An endoscopic image 8 years after CIRT (*right lower panel*)

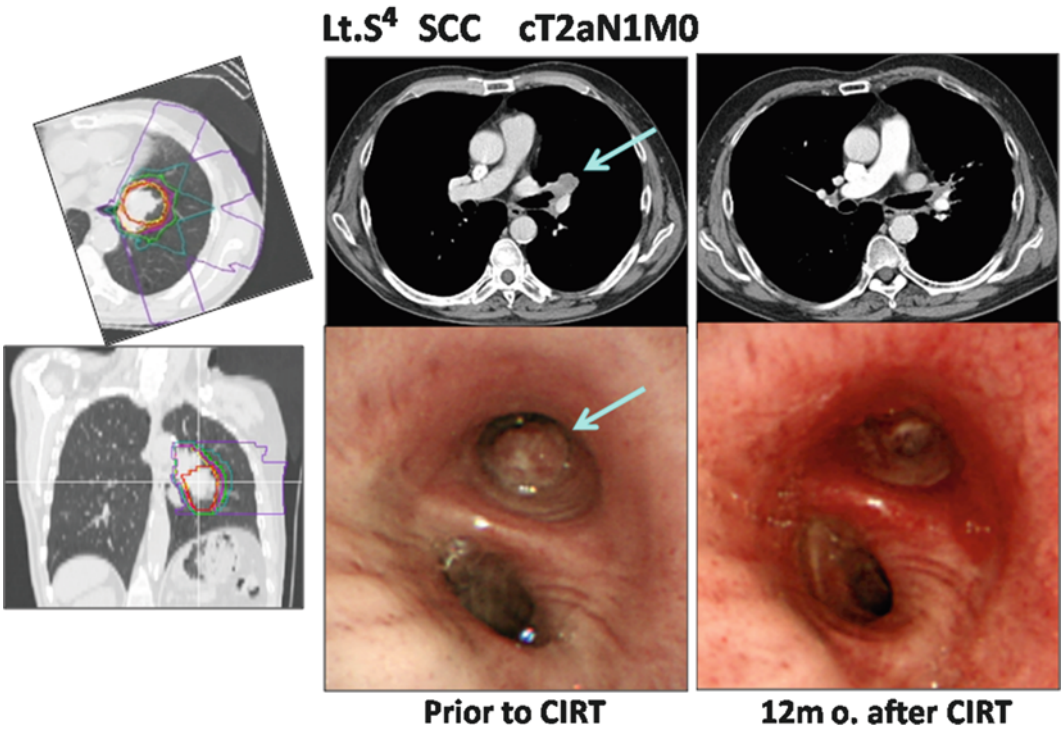

Fig. 21.5 The planning CT showing the four-portal irradiation. CT and endoscopic images taken pre- and post-therapy are shown. The *arrow* indicates the tumor

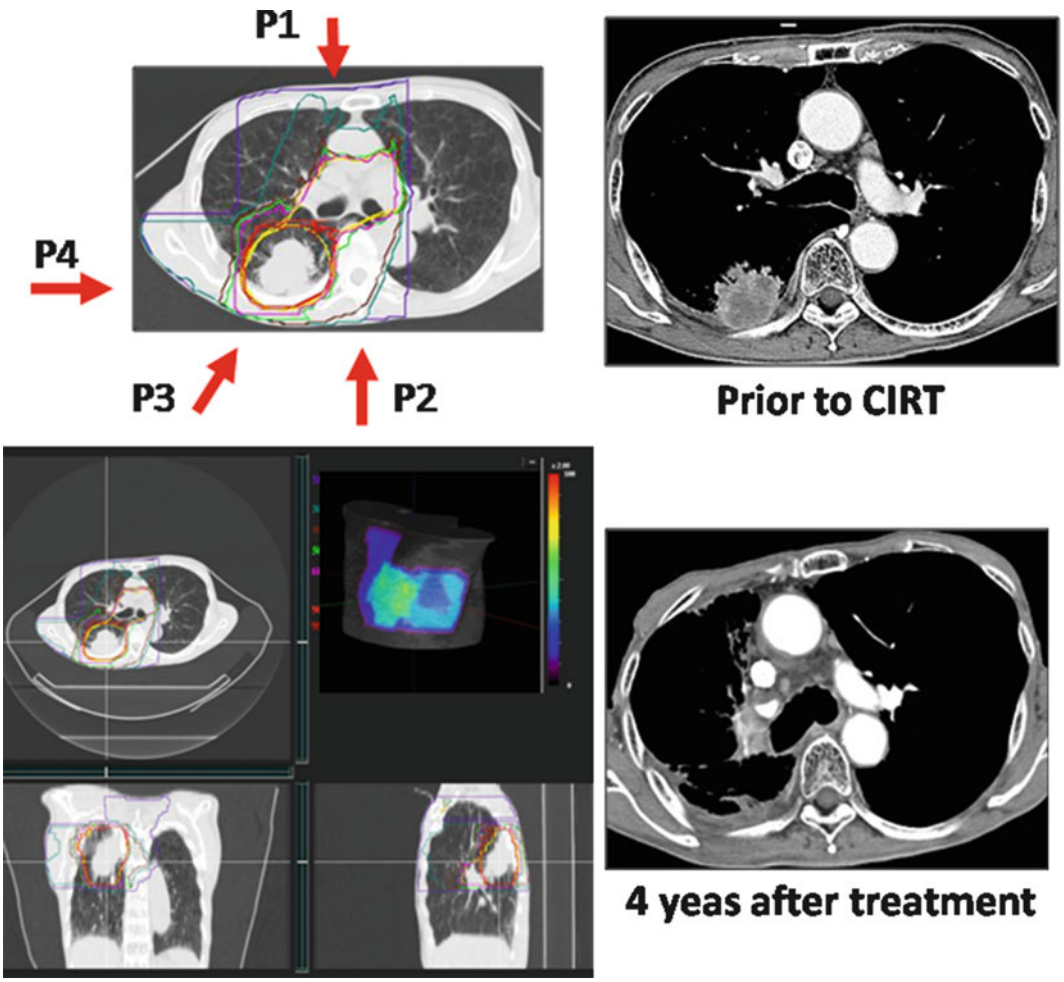

Fig. 21.6 The *left panel* shows the CTV and planning dose distribution, including 3D images and the body surface model. The irradiation times of each port were P1:P2:P3:P4 = 4:3:3:6. P4 is the small target for the primary tumor. The *right panel* shows the pre- and post-CIRT images

21.4 Locally Advanced Lung Cancer

21.4.1 Treatment Planning

Radiotherapy for advanced lung cancer is generally performed in combination with chemotherapy or surgery. During the CIRT for lung cancer, we treated some locally advanced lung cancer cases with CIRT alone. Because, these patients were unable to receive chemotherapy, or the cases of progressive disease after chemotherapy.

We have been making an extensive effort to minimize the risk of pulmonary, tracheal, and esophageal toxicity associated with the treatment. Using a small CTV for the primary lesion allows us to decrease the prescribed dose for the mediastinum. This will help improve the patients' overall status, potentially increasing the number of patients who can receive chemotherapy.

21.4.2 Planning in Representative Cases

Case 1

A 75-year-old male patient with right lower lobe (S6) lung cancer (adenocarcinoma) measuring 40×38 mm, with chest wall infiltration and nodal metastasis of the right hilum, was diagnosed to have cT3N1M0 stage IIIA disease. Carbon ion beam irradiation at 72.0 GyE in 16 fractions over 4 weeks was performed in January 2004. Figure 21.6 shows a CIRT planning image.

The entire large target, including the primary tumor, hilum, and mediastinum, was irradiated at 45.0 GyE, and then the primary tumor was irradiated to a final dose of 72.0 GyE. At 4 years after treatment, he was well without any recurrence.

Case 2

A 67-year-old male patient with left upper lobe lung cancer (adenocarcinoma) of 62×50 mm, with infiltration into the mediastinum, was diagnosed with cT4N0M0 stage

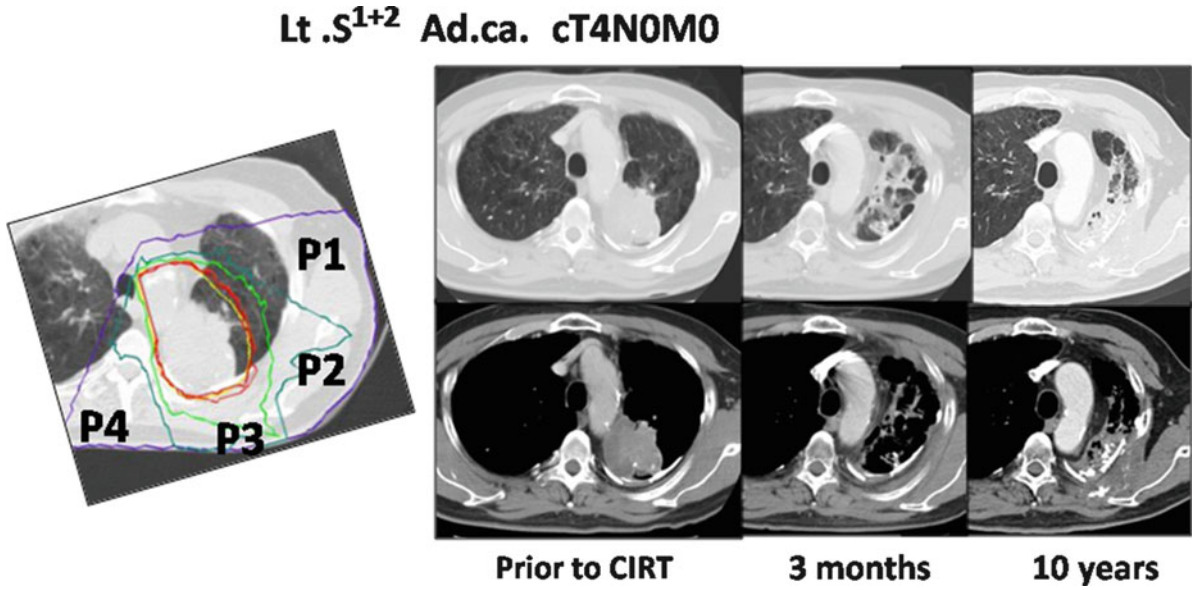

Fig. 21.7 The planning CT showing the four-portal irradiation. The irradiation times for each port were P1:P2:P3:P4 = 4:4:5:3. The CT images taken pretreatment and 3 months and 10 years after therapy are shown

IIIB disease. Irradiation with carbon ions at 72.0 GyE was performed. At 10 years after treatment, he is still alive and well without any recurrence (Fig. 21.7).

21.4.3 Results

Sixty-one patients were treated in this clinical trial between May 2000 and September 2011. The 61 primary tumors were treated by carbon ion beam irradiation alone using a total dose of 72.0 GyE in 16 fractions over 4 weeks. The mean age of the patients was 74.2 years (46–88), and the gender breakdown was 14 females and 47 males. By histological type (the cancer type was determined by biopsy), there were 27 adenocarcinomas, 31 squamous cell carcinomas, and three large cell carcinomas. Of the 61 patients, 39 were in stage II and 22 were in stage III, while there were 24 N1 cases, 13 N2 cases, and 24 N0 (T3-4N0M0) cases.

The statistical 3-year overall survival rate of the 61 patients was 41.2 %, with a median observation period of 22.8 months (range, 1.3–145.3 months). The 3-year cause-specific survival rate of 24 patients with chest wall infiltration (cT3,4N0M0) was 77.9 % with a median observation period of 37.1 months (range, 4.3–141.6 months) (Fig. 21.8).

The toxicities to the skin and lungs caused by CIRT were assessed according to the NCI-CTC (early) and RTOG/EORTC (late). No adverse events greater than grade 2 were detected among the early and late reactions.

21.5 Normal Tissue Reaction

21.5.1 Pulmonary and Skin Reactions

In the previously reported phase II study, 129 patients with 131 primary lesions were treated with C-ion RT. Fifty-one primary tumors in 50 patients were treated by carbon ion beam irradiation alone using a fixed total dose of 72 GyE in 9 fractions over 3 weeks (#9802 protocol [12]). The remaining 79 patients had 80 stage I tumors (#0001 protocol [13]). A total of 127 patients were evaluated for survival, because two patients had been treated twice, one in the first protocol #9802 and one in the second protocol #0001. The IA and IB stage tumors were treated with fixed doses of 52.8 and 60.0 GyE in 4 fractions over 1 week, respectively. The mean age of the patients was 74.5 years, and the gender breakdown was 92 males and 37 females. The tumors were 72 T1 and 59 T2 tumors. The mean tumor size was 31.5 mm in diameter. By type, there were 85 adenocarcinomas, 43 squamous cell carcinomas, two large cell carcinomas, and one adenosquamous cell carcinoma. Medical inoperability had been diagnosed in 76 % of cases.

Toxicities to the skin and lungs caused by C-ion RT were assessed according to the RTOG (early) and RTOG/EOTRC (late) guidelines, as shown in Tables 21.1 and 21.2. Early skin reactions were assessed for 131 lesions and late skin reactions for 128 lesions. Of the early reaction lesions,

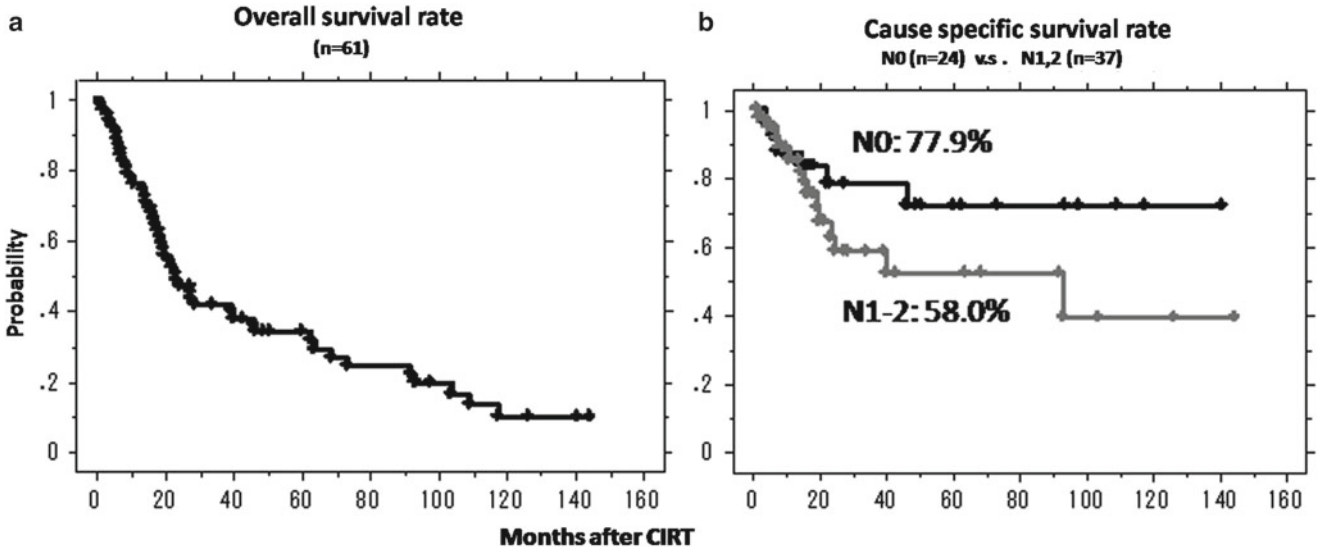

Fig. 21.8 The survival rate in 61 patients with locally advanced lung cancer. (**a**) The 3-year overall survival rate of all patients was 41.2 %. (**b**) The 3-year cause-specific survival rates based on the N factor

Table 21.1 Skin reaction

	Early reaction (RTOG)						Late reaction (RTOG/EORTC)					
		Grade						Grade				
	Lesion no.	0	1	2	3	≥4	Lesion no.	0	1	2	3	≥4
9802	51	0	50	1	0	0	51	0	49	1	1	0
0001	80	0	75	5	0	0	77[a]	0	77	0	0	0
Total	131	0	125	6	0	0	128	0	126	1	1	0

[a]Three cases were not observed due to early death

Table 21.2 Lung reaction

	Early reaction (RTOG)						Late reaction (RTOG/EORTC)					
		Grade						Grade				
	Lesion no.	0	1	2	3	≥4	Lesion no.	0	1	2	3	≥4
9802	50	49	0	1	0	0	50	0	48	2	0	0
0001	79	78	0	1	0	0	76[a]	7	68	1	0	0
Total	129	127	0	2	0	0	126	0	116	3	0	0

[a]Three cases were not observed due to early death

125 were grade 1 and six were grade 2. Among the late reaction lesions, 126 were grade 1, one was grade 2, and one was grade 3. The lung reactions were clinically assessed in 129 patients. One hundred twenty-seven had grade 0 and two had grade 2 early reactions. Late effects were followed up in 126 patients: seven patients had grade 0, 116 patients had grade 1, and three patients had grade 2 effects. No higher than a single grade 2 reaction was observed.

We also reported the pulmonary functions and pathological findings of the patients after C-ion RT [27, 28] and demonstrated that the patients in this trial suffered from less lung damage. These less extensive and severe adverse effects for the lungs were achieved as a result of the excellent dose distribution achieved with carbon ion beams due to the formation of a Bragg peak. Furthermore, in a report regarding the radiographic changes of the lungs after C-ion RT, we described that the lung damage was observed in the parenchyma and the pleura. The severity of pulmonary reactions was correlated with dose-volume factors [29].

These findings provided valuable information for the planning of C-ion RT and for the management of patients after treatment.

21.5.1.1 Planning in Representative Cases

Case 1

A 62-year-old female with a 15×15 mm adenocarcinoma located in the left lower lobe (S10) was clinically diagnosed to have cT1N0M0 stage IA disease. Irradiation with a carbon ion beam at 72.0 GyE in 9 fractions over 3 weeks was performed. Ten years after treatment, she is still alive and well without any recurrence (Fig. 21.9).

Case 2

A 60-year-old male patient with squamous cell carcinoma of 61×60 mm in size located in the right lower lobe was diagnosed with T2N0M0 disease. Carbon ion beam irradiation

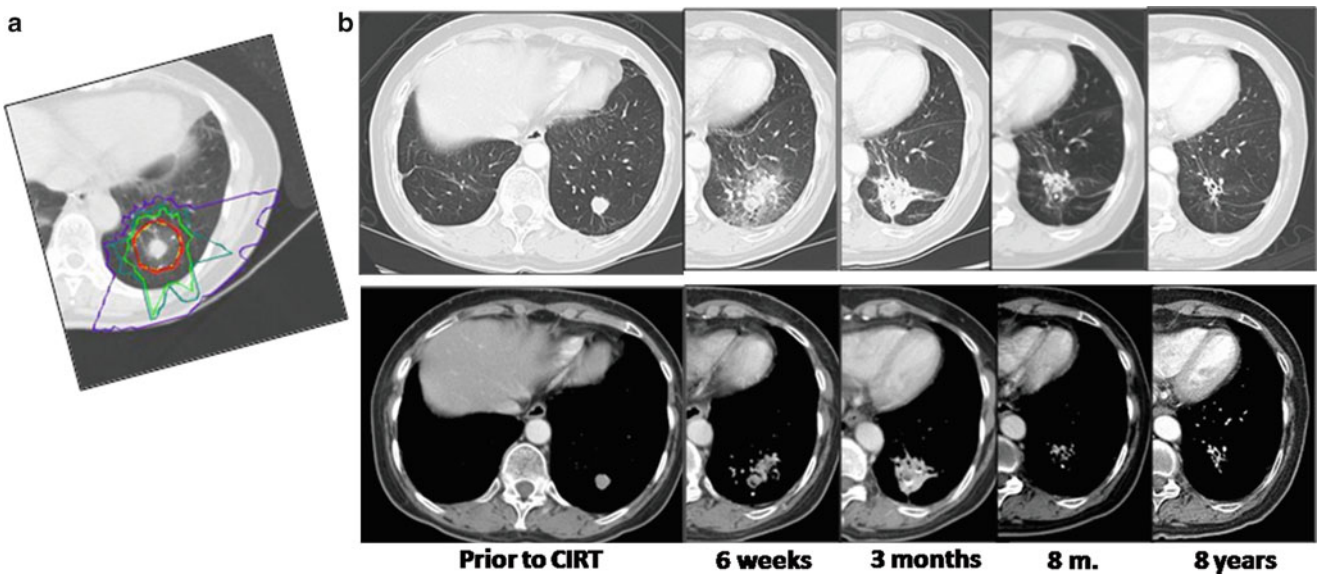

Fig. 21.9 (**a**) The dose distribution and (**b**) the changes of the tumor shadow after CIRT. The early lung reaction (RTOG) and late lung reaction (RTOG/EORTC) were both grade 1

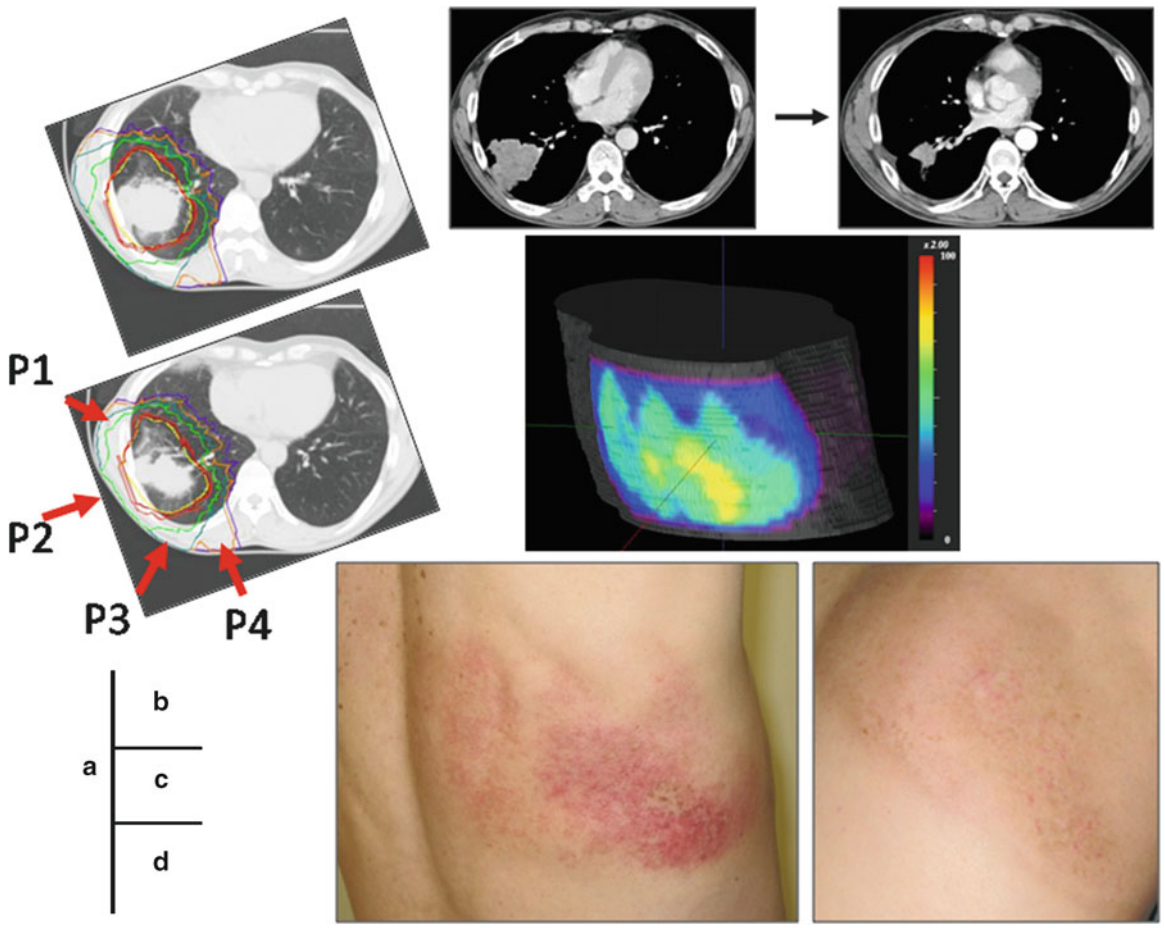

Fig. 21.10 (*A*) The Dose distribution for a tumor receiving a total carbon ion dose of 44.0 GyE from four directions. (*B*) CT images before and after treatment. Four months after the treatment, the tumor showed a partial response (PR). (*C*) The body surface model of the planning dose distribution for the patient. The *yellow area* is 75 % of the total dose for the beams from three portals that overlapped in that area. (*D*) The early skin reaction was grade 2 (2 months after irradiation, *left*), and the late reaction (4 months after CIRT, *right*) was grade 1

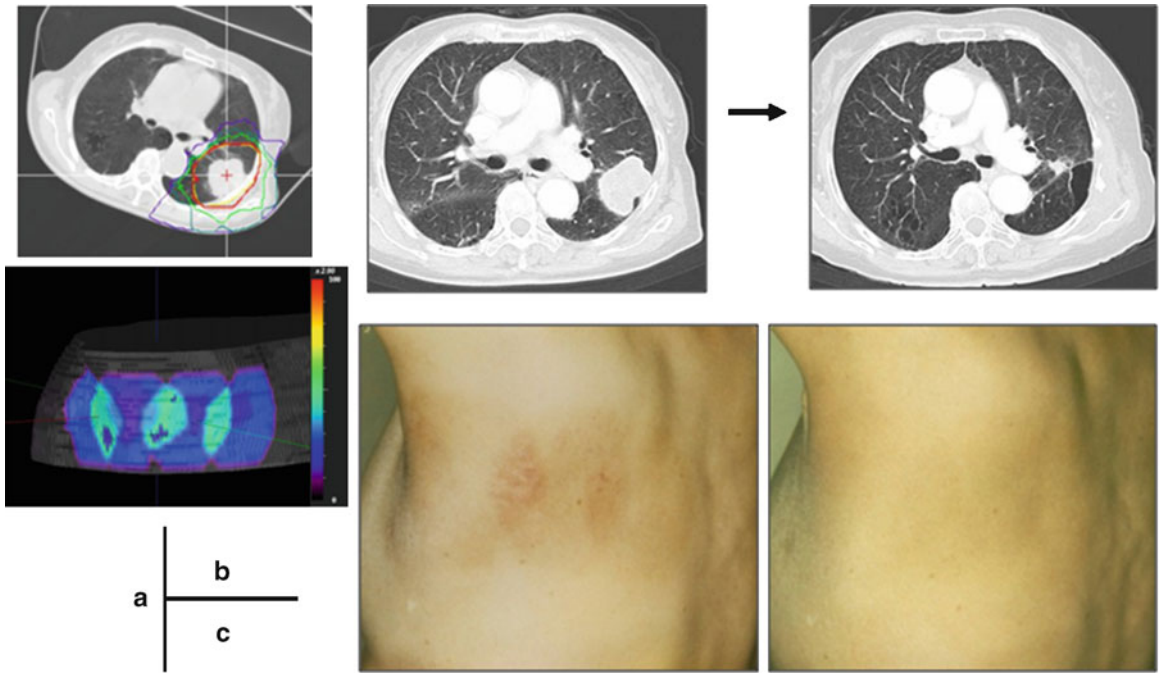

Fig. 21.11 (*A*) The dose distribution for a tumor receiving a total carbon ion dose of 40.0 GyE from four directions. The body surface model of the planning dose distribution for the patient. (*B*) CT images before and after treatment. Eighteen months after the treatment, the tumor showed a partial response. (*C*) The early skin reaction was grade 1 (5 weeks after irradiation, *left*), and the late reaction (7 months after CIRT, *right*) was grade 1

at 44.0 GyE in 1 day was performed. The treatment planning and skin reactions are shown in Fig. 21.10. We confirmed that the surface dose was not more than 75 % of the prescribed dose. It is important to minimize the risk of skin reactions (Fig. 21.10), and we believe this planning can help improve the outcome.

Case 3

A 71-year-old female with T2N0M0 squamous cell carcinoma (46×38 mm in size) was treated with CIRT (40 GyE/single fraction). At 18 months after C-ion RT, the tumor shrank without severe lung fibrosis. Figure 21.11 shows the PTV of the C-ion RT and skin reactions.

21.5.2 Chest Wall Adverse Reactions

Of 50 patients who received 72.0 GyE in nine fractions, ten patients complained of costal bone pain and tenderness around the part of the skin receiving carbon beams, which appeared at 10±2.3 months on average after the start of therapy. Slight swelling of the bone and the surrounding soft tissue was observed by inspection or CT scans and disappeared within at most 1 month after. Half of the patients needed nonsteroidal anti-inflammatory medication. Costal bone fractures were observed in two patients.

A reaction of the chest wall is an adverse effect that, depending on the severity, can significantly impair the patient's quality of life. We have been making an effort to minimize the risk of severe chest wall toxicity, and for rib sparing, by cutting off the PTV margin on the bone.

21.5.2.1 Case Study

A 69-year-old male patient with lung cancer (adenocarcinoma cT2N0M0; 37×25 mm) located in the left upper lobe (S5) was treated with carbon ion beam radiotherapy (72.0 GyE/9 fr/3 weeks). Nine months after treatment, he complained of pain around the skin that had received the carbon beams, and the pain resolved in a month. At 4 years after treatment, he was well without any recurrence (Fig. 21.12).

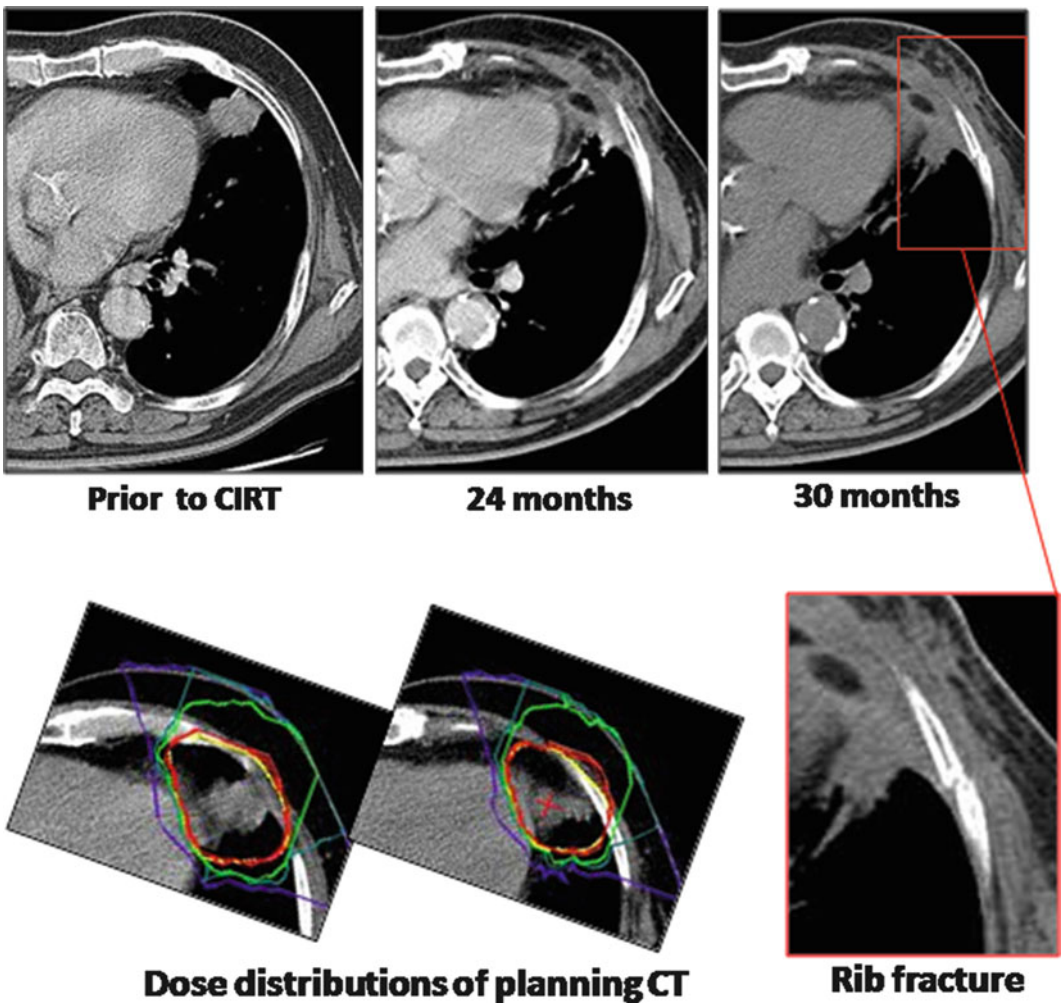

Fig. 21.12 The *upper panel* shows the CT images before and after the treatment. The costal bone fracture appeared 30 months after CIRT

References

1. Asamura H, Goya T, Koshiishi Y, et al. A Japanese Lung Cancer Registry study: prognosis of 13,010 resected lung cancers. J Thorac Oncol. 2008;3:46–52.
2. Smythe WR, American College of Chest Physicians. Treatment of stage I non-small cell lung carcinoma. Chest. 2003;123:181S–7.
3. Jeremic B, Classen J, Bamberg M. Radiotherapy alone in technically operable, medically inoperable, early-stage (I/II) non-small-cell lung cancer. Int J Radiat Oncol Biol Phys. 2002;54:119–30.
4. Zimmermann FB, Bamberg M, Molls M, et al. Radiation therapy alone in early stage non-small cell lung cancer. Semin Surg Oncol. 2003;21:91–7.
5. Nagata Y, Hiraoka M, Mizowaki T, et al. Survey of stereotactic body radiation therapy in Japan by the Japan 3-D Conformal External Beam Radiotherapy Group. Int J Radiat Oncol Biol Phys. 2009;75:343–7.
6. Zimmermann FB, Geinitz H, Schill S, et al. Stereotactic hypofractionated radiation therapy for stage I non-small cell lung cancer. Lung Cancer. 2005;48:107–14.
7. Onishi H, Araki T, Shirato H, et al. Stereotactic hypofractionated high-dose irradiation for stage I nonsmall cell lung carcinoma: clinical outcomes in 245 subjects in a Japanese multiinstitutional study. Cancer. 2004;101:1623–31.
8. Senan S, Lagerwaard F. Stereotactic radiotherapy for stage I lung cancer: current results and new developments. Cancer Radiother. 2010;14:115–8.
9. Onishi H, Shirato H, Nagata Y, et al. Hypofractionated stereotactic radiotherapy (HypoFXSRT) for stage I non-small cell lung cancer: updated results of 257 patients in a Japanese multi-institutional study. J Thorac Oncol. 2007;2 Suppl 3:S94–100.
10. Nagata Y, Takayama K, Matsuo Y, et al. Clinical outcomes of a phase I/II study of 48 Gy of stereotactic body radiotherapy in 4 fractions for primary lung cancer using a stereotactic body frame. Int J Radiat Oncol Biol Phys. 2005;63:1427–31.
11. Miyamoto T, Yamamoto N, Nishimura H, et al. Carbon ion radiotherapy for stage I non-small cell lung cancer. Radiother Oncol. 2003;66:127–40.
12. Miyamoto T, Baba M, Yamamoto N, et al. Curative treatment of stage I non-small-cell lung cancer with carbon ion beams using a hypo-fractionated regimen. Int J Radiat Oncol Biol Phys. 2007;67:750–8.
13. Miyamoto T, Baba M, Sugane T, et al. Carbon ion radiotherapy for stage I non-small cell lung cancer using a regimen of four fractions during 1 week. J Thorac Oncol. 2007;2:916–26.

14. Sugane T, Baba M, Imai R, et al. Carbon ion radiotherapy for elderly patients 80 years and older with stage I non-small cell lung cancer. Lung Cancer. 2009;64:45–50.
15. Kanai T, Endo M, Minohara S, et al. Biophysical characteristics of HIMAC clinical irradiation system for heavy-ion radiation therapy. Int J Radiat Oncol Biol Phys. 1999;44:201–10.
16. Nishimura H, Miyamoto T, Yamamoto N, et al. Radiographic pulmonary and pleural changes after carbon ion irradiation. Int J Radiat Oncol Biol Phys. 2003;55:861–6.
17. Yamamoto N, Miyamoto T, Nishimura H, et al. Preoperative carbon ion radiotherapy for non-small cell lung cancer with chest wall invasion-pathological findings concerning tumor response and radiation induced lung injury in the resected organs. Lung Cancer. 2003;42:87–95.
18. Yasukawa T, Yamaguchi Y, Aoyagi H, et al. Diagnosis of hilar and mediastinal lymph node metastasis of lung cancer by positron emission tomography using 11C-methionine. Jpn J Lung Cancer. 1996;36:919–26.
19. Sobin LH, Wittekint C, editors. TNM classification of malignant tumors. International Union Against Cancer (UICC). 6th ed. NewYork: Wiley-Liss; 2002.
20. Minohara S, Kanai T, Endo M, et al. Respiratory gated irradiation system for heavy-ion radiotherapy. Int J Radiat Oncol Biol Phys. 2000;47:1097–103.
21. Kanai T, Furusawa Y, Fukutsu K, et al. Irradiation of mixed beam and design of spread-out Bragg peak for heavy-ion radiotherapy. Radiat Res. 1997;147:78–85.
22. Endo M, Koyama-Ito H, Minohara S, et al. HIPLAN-a heavy ion treatment planning system at HIMAC. J Jpn Soc Ther Radiol Oncol. 1996;8:231–8.
23. Koto M, Miyamoto T, Yamamoto N, et al. Local control and recurrence of stage I non-small cell lung cancer after carbon ion radiotherapy. Radiother Oncol. 2004;71:147–56.
24. Nagata Y, Takayama K, Matuo Y, et al. Clinical outcomes of a phase I/II study of 48Gy of stereotactic body radiotherapy in 4 fractions for primary lung cancer using a stereotactic body frame. Int J Radiat Oncol Biol Phys. 2005;63:1427–31.
25. Onishi H, Araki T, Shirato H, et al. Stereotactic hypofractionated high-dose irradiation for stage I nonsmall cell lung carcinoma. Cancer. 2004;101:1623–31.
26. Timmerman R, MacGarry R, Yiannoutsos C, et al. Excessive toxicity when treating central tumors in a phase II study of stereotactic body rdiation therapy for medically inoperable early-stage lung cancer. J Clin oncol. 2006;24:4833–9.
27. Kadono K, Homma T, Kamahara K, et al. Ekkect of heavy – ion radiotherapy on pulmonary function in stage I Non-small cell lung cancer patients. Chest. 2002;122:1925–32.
28. Yamamoto N, Miyamoto T, Nishimura H, et al. Preoperative carbon ion radiotherapy for non-small cell lung cancer with chest wall invasion pathological findings concerning tumor response and radiation induced lung injury in the resected organs. Lung Cancer. 2003;42:87–95.
29. Nishimura H, Miyamoto T, Yamamoto N, et al. Radiographic pulmonary and pleural change after carbon ion irradiation. Int J Radiat Oncol Biol Phys. 2003;55:861–6.

Metastatic Lung Tumors and Lymph Nodes

22

Naoyoshi Yamamoto and Mio Nakajima

Abstract

The clinical results after carbon ion radiotherapy (C-ion RT) metastatic lung tumors and lymph node metastases that occurred after C-ion RT for clinical stage I non-small lung cancer (NSCLC) were evaluated and compared to surgery.

One hundred and sixteen lung metastatic lesions in 91 patients were treated with C-ion RT at our institute from April 1997 to February 2011. After a median follow-up period of 2.3 years (range, 0.3–13.1 years), the statistical overall survival rate and local control rate were 71.2 and 91.9 % at 2 years after treatment, respectively. Treatment-related side effects were not a clinical problem. When classified by the primary organ, there were 49 cases of lung cancer, 20 cases of colorectal cancer, and 22 cases of other cancers. The overall survival rate and local control rate for cases with lung metastasis from lung cancer at 2 years after treatment were 81.5 and 92.4 %, respectively, and were 65.0 and 92.0 % for lung metastasis from colorectal cancer. C-ion RT for the metastatic lung tumors is safe, and the therapeutic effect is comparable to the outcome from reported surgical resections.

With regard to the nodal metastases from lung cancer, 36 patients were treated between January 2000 and December 2010. The 36 metastatic lesions were treated by carbon ion beam irradiation alone using a total dose of 48.0 GyE in 12 fractions over 3 weeks. The statistical 3-year overall survival rate of the 36 patients was 52.9 % with a median observation period of 13.5 months (range, 2.9–114.8 m). The 3-year local control rate was 100 %. The toxicities to the skin and lungs caused by C-ion RT were assessed according to the NCI-CTC (early) and RTOG/EORTC (late). No adverse events greater than grade 2 were detected among the early and late reactions.

Keywords

Carbon ion radiotherapy • Metastatic lung tumor • Regional node metastases from lung cancer

N. Yamamoto (✉) • M. Nakajima
National Institute of Radiological Sciences,
4-9-1 Anagawa, Inage-ku, Chiba, Japan
e-mail: nao_y@nirs.go.jp

H. Tsujii et al. (eds.), *Carbon-Ion Radiotherapy: Principles, Practices, and Treatment Planning*,
DOI 10.1007/978-4-431-54457-9_22, © Springer Japan 2014

22.1 Metastatic Lung Tumors

22.1.1 Introduction

Radiotherapy is the principal treatment option for patients with early stage lung cancer and contraindications to surgery. The outcome of using conventional therapeutic techniques has been a 40–70 % 5-year local control rate, but a local control rate equivalent to surgery has been reported due to recent advances in irradiation techniques [1–4]. These irradiation techniques include stereotactic body radiation therapy (SBRT), proton beam therapy, and carbon ion radiotherapy (C-ion RT) [5, 6].

We herein report our outcomes of treating metastatic lung tumors believed to be in the state of oligo-recurrence [7] using carbon ion beams. Incidentally, the details were already described in our paper [8].

22.1.2 Patients and Methods

From April 1997 to February 2011, 116 lesions in 91 patients were treated with C-ion RT at our institute. The average age of the patient was 64.8 years (range, 10–86 years) with a male/female ratio of 57/34. The histology and diagnosis of metastasis of the tumors were determined based on the clinical course.

The conditions for applying the treatment to patients were: the primary lesion was treated with no apparent local recurrence in the primary organ at the time of lung metastasis treatment, there were no active lesions in organs other than the lungs, and there was one lesion in the lungs as a rule.

Regarding the number of lesions per patient treated with carbon ion therapy, four lesions were treated in two cases, two lesions were treated in 19 cases, and only one lesion was irradiated in 70 patients.

The prescribed dose ranged from 40 to 80 GyE, and this was divided into several fractions (range, 1–12). The fractionation regimen of 52.8 GyE in four fractions was the most commonly used, being applied for 54 tumors. This was followed by 23 lesions treated with 60.0 GyE in four fractions. In many cases, 52.8 GyE in four fractions was used for lung metastasis from lung cancer, while 60.0 GyE in four fractions was used for metastasis from colorectal cancer.

When classified by the primary organ, there were 49 cases of lung cancer, 20 cases of colorectal cancer, and 22 cases of other cancers. The breakdown of organs classified as other cancers included various types, such as bone and soft tissue tumors, cervical cancer, thymic cancer, esophageal cancer, pharyngeal cancer, ovarian cancer, pancreatic cancer, hepatic cancer, and breast cancer, with the number of cases from these organs being four or less.

22.1.3 Results

The statistical 2-year overall survival rate of 91 patients was 71.2 %, with a median observation period of 2.3 years (range, 0.3–13.1 years). The local control rate of the 116 treated lesions was 91.9 % at 2 years after therapy.

The toxicities to the skin and lung caused by C-ion RT were assessed according to the NCI-CTC (early) and RTOG/EORTC (late) recommendations. Early skin reactions were assessed for 116 lesions and late skin reactions were assessed for 114 lesions. Of the early reaction lesions, all 116 were grade 1. For the late reaction lesions, all 114 were grade 1. Lung reactions were clinically assessed in the 116 lesions of 91 patients. Only five patients had grade 2 early reactions, and no adverse events greater than grade 2 were detected.

The 2-year overall survival rate of lung metastasis cases from lung cancer was 81.5 %, and the overall survival rate of lung metastasis from other cancers was 59.3 %. The local control rates were 92.4 and 91.3 %, respectively. Furthermore, the 2-year overall survival and local control rates of 30 lesions in the 20 cases of lung metastasis from colorectal cancer were 65.0 and 92.0 %.

The effect of the tumor size on the local control was investigated. When the local control rate of 116 tumors was compared based on the length of the tumor, the local control rate was significantly superior for those shorter than 2 cm compared to those exceeding 2 cm. When lung metastasis from lung cancer was compared in the same manner, the local control rate was 100 % for tumors that were 2 cm or smaller in length.

The relationship between the tumor size and prognosis was investigated. The cause-specific survival rates were compared in 50 cases in which the maximum diameter of the treated tumor was 2 cm or smaller and 41 cases in which it exceeded 2 cm. The 2-year cause-specific survival rate was 77.5 % in the group with a tumor diameter of 2 cm or smaller, and a tendency for lower survival was observed for those exceeding 2 cm, at 67.8 %, although the difference was not significant.

One lesion was examined as a general rule, but there were cases in which multiple lesions were treated as a result of the clinical course of the disease. No difference was observed between the patients who were treated for single lesions and those treated for multiple lesions in a comparison of the survival. We were unable to determine whether the cases in which only one location was irradiated ultimately had only one metastasis or whether the cases in which multiple lesions were treated had an advantage because the treatment was successfully completed.

It is still unclear whether or not the local treatment of metastatic lung tumors is effective for improving the prognosis of patients. For metastatic lesions, surgery or radiation therapy has been carried out on some patients with varying

levels of success, but the criteria for selecting cases in which an effect may be expected are unclear [9]. We determined the eligibility criteria based on the conditions that are frequently used to select patients who would be eligible for surgical resection, that is, those in whom the primary lesion is controlled, in whom there are no lesions in places other than the lungs, and in whom there is only one lesion at the time of treatment (as a rule). Whether or not our result is superior compared to chemotherapy and the best supportive care remains to be elucidated, it was satisfactory compared to similar surgical resection cases [10] and the outcome of C-ion RT for stage I NSCLC [REFs]. There were no long-term survival cases (of 5 years or more) in cases in which local control was not achieved, although there was no significant difference between groups. However, it is believed that the prognosis will be poor. However, in order to make an accurate evaluation, a further analysis will be necessary, including an investigation of the effects of other treatments, such as chemotherapy, and the local control period.

The results of this study showed that high local control may be obtained by C-ion RT without adverse reactions and that an effect comparable to that of surgical resection may be obtained for metastatic lesions of a certain size. It is believed that an opportunity for treatment may be provided for oligo-recurrence cases, in which resection could not be carried out in the past, for reasons such as a poor pulmonary function. Furthermore, it can be argued that the indications may be expanded to cases that were not eligible for the treatment of multiple metastases in the past, because C-ion RT is a minimally invasive treatment. However, the decisions regarding treatment must be made carefully after evaluating whether or not long-term survival can be achieved.

In this report, the presence of metastatic lesions other than those of the lung and the treatment outcome of these lesions was not investigated. Therefore, the treatment course of complicated cases, for example, patients with affiliated lymph node metastasis and brain metastasis in the case of lung cancer, and local lymph node metastasis with liver metastasis in the case of colorectal cancer, must be analyzed and investigated in detail to determine the optimal indications for treatment.

22.2 Lymph Node Metastases from Primary Lung Cancer

22.2.1 Introduction

Clinical stage I lung cancers include latent nodal metastasis in about 15–20 % of cases. In our patients who received C-ion RT for stage I lung cancer, regional lymph node metastasis developed in fewer than 10 % of the patients. We treat regional node metastasis after C-ion RT with additional C-ion RT.

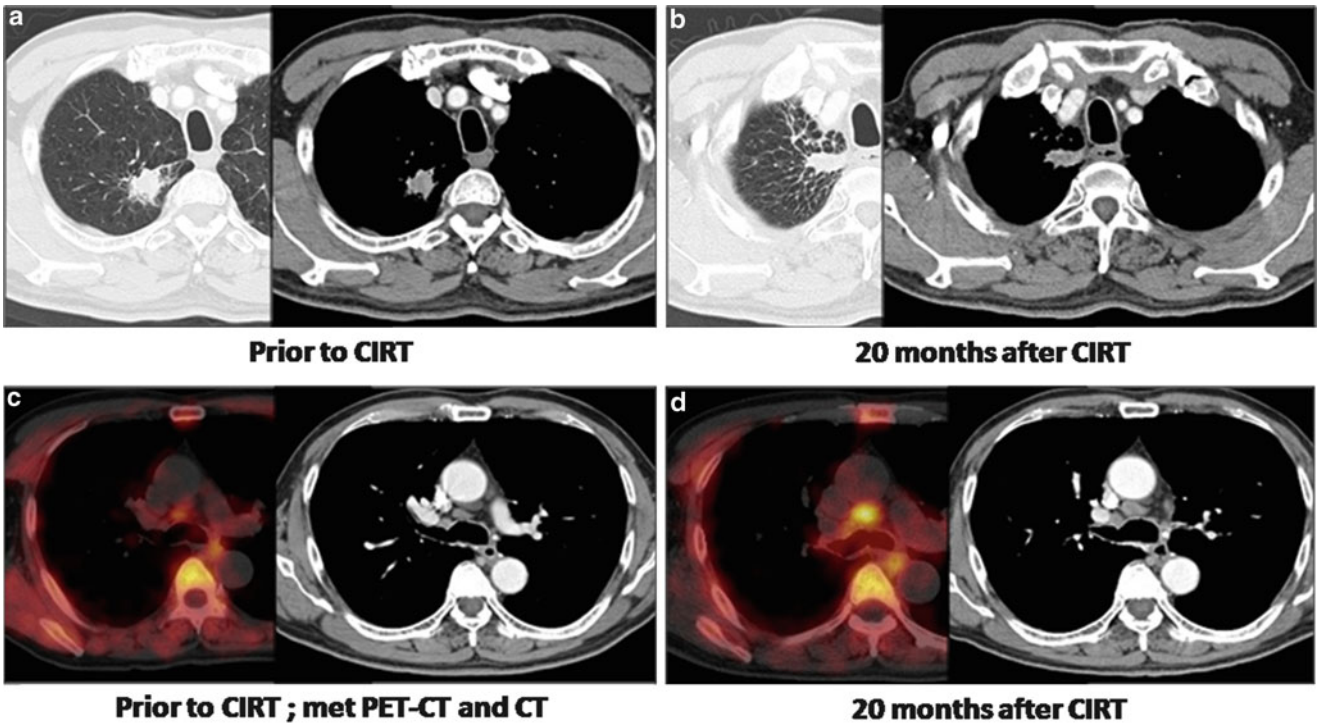

Fig. 22.1 (**a**) Prior to CIRT the CT images show the primary tumor. (**b**) Tumor shrinkage was shown 20 months after CIRT. (**c**) The CT and PET images show the pre-tracheal lymph node before CIRT. (**d**) Twenty months after CIRT, lymph node swelling and the accumulation of C^{11}-met PET appeared

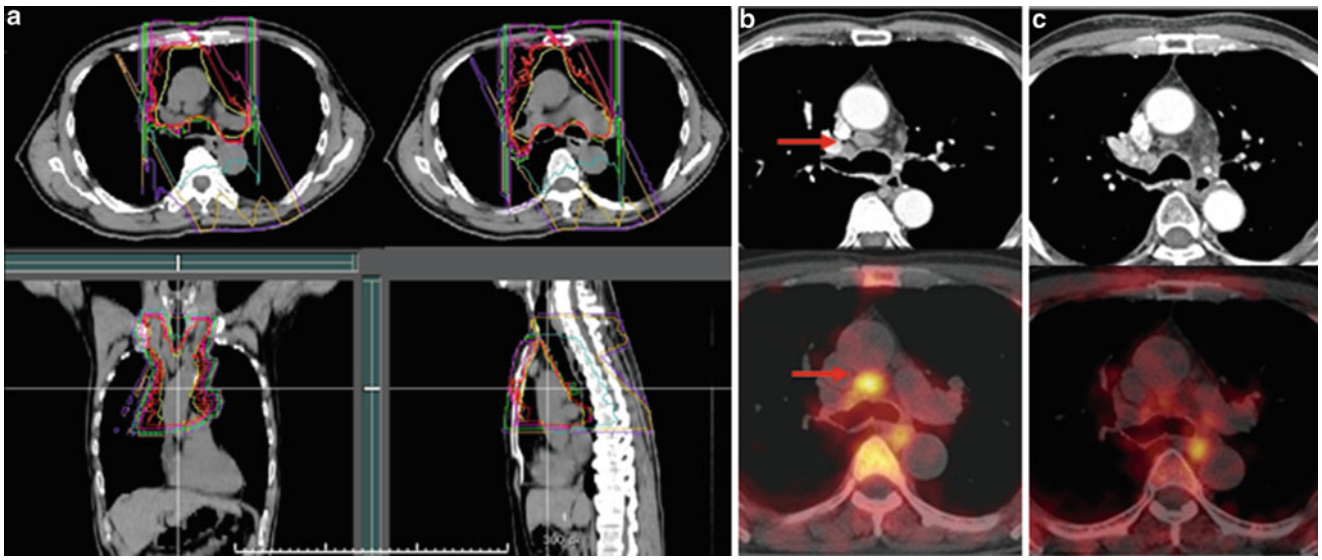

Fig. 22.2 (**a**) The planning CT for the treatment of the mediastinal and hilar lymph node metastases. (**b**) The *arrow* shows the lymph node metastasis. (**c**) CT and PET images 3 months after CIRT

We herein report on our outcomes of treating metastatic lymph nodes in patients believed to be in a state of oligo-recurrence [7].

22.2.2 Planning in a Representative Case

A 65-year-old male patient with right upper lobe S1 lung cancer (adenocarcinoma) and a tumor with a size of 38×30 mm was diagnosed to have cT2N0M0 stage IB disease. Irradiation with a carbon ion beam at 44.0 GyE in 1 day was performed in July 2008. The primary tumor did not recur, but mediastinal lymph node metastasis was suspected based on the PET and CT images 20 months after treatment (Fig. 22.1).

In this case, EBUS-TBNA was performed, and nodal metastasis was proven pathologically. The patient was also treated with C-ion RT for the nodal metastasis using 48.0 GyE in 12 fractions over 3 weeks (Fig. 22.2).

22.2.3 Results

Thirty-six patients were treated between January 2000 and December 2010. The first therapy for the primary lung cancer was surgery or C-ion RT or conventional radiotherapy, and the number of patient treated using these modalities was 10, 25, and 1, respectively.

The 36 metastatic lesions were treated by carbon ion beam irradiation alone using a total dose of 48.0 GyE in 12 fractions over 3 weeks. The mean age of the patients was 69.7 years (38–87), and the gender breakdown was 16 females and 20 males. By histological type, there were 24 adenocarcinomas, 11 squamous cell carcinomas, and 1 large cell carcinoma.

The statistical 3-year overall survival rate of the 36 patients was 52.9 %, with a median observation period of 13.5 months (range, 2.9–114.8 months). The 3-year local control rate was 100 %. The toxicities to the skin and lungs caused by C-ion RT were assessed according to the NCI-CTC (early) and RTOG/EORTC (late). No adverse events greater than grade 2 were detected among any of these reactions.

References

1. Tsujii H, Kamada T. A review of update clinical results of carbon ion radiotherapy. Jpn J Clin Oncol. 2012;42:670–85.
2. Nakayama H, Sugahara S, Tokita M, et al. Proton beam therapy for patients with medically inoperable stage I non-small cell lung cancer at the University of Tsukuba. Int J Radiat Oncol Biol Phys. 2010;78:467–71.
3. Baumann P, Nyman J, Hoyer M, et al. Outcome in a prospective phase II trial of medically inoperable stage I non-small cell lung cancer patients treated with stereotactic body radiotherapy. J Clin Oncol. 2009;27:3290–6.
4. Ricardi U, Filippi AR, Guarneri A, et al. Stereotactic body radiation therapy for early stage non-small cell lung cancer: results of a prospective trial. lung Cancer. 2010;68:72–7.
5. Miyamoto T, Baba M, Yamamoto N, et al. Curative treatment of stage I non-small cell lung cancer with carbon ion beams using a hypofractionated regimen. Int J Radiat Oncol Biol Phys. 2007;67:750–8.
6. Miyamoto T, Baba M, Sugane T, et al. Carbon ion radiotherapy for stage I non-small cell lung cancer using a regimen of four fractions during 1 week. J Thorac Oncol. 2007;2:916–26.
7. Niibe Y, Hayakawa K. Oligometastases and oligo-recurrence : the new era of cancer therapy. Jpn J Clin Oncol. 2010;40:107–11.
8. Yamamoto N, Nakajima M, Tujii T, et al. Carbon ion radiotherapy for oligo-recurrence in the lung. Pulm Med. 2013;6:219746.
9. Milano MT, Katz AW, Muhs AG, et al. A prospective pilot study of curative-intent stereotactic body radiation therapy in patients with 5 or fewer oligometastatic lesions. Cancer. 2008;112:650–8.
10. Kandioler D, Krömer E, Tüchler H, et al. Long term results after repeated surgical removal of pulmonary metastases. Ann Thorac Surg. 1998;65:909–12.

Part XIII

GI Tract Tumors

Esophageal Cancer

23

Shigeo Yasuda

Abstract

In view of the superior dose concentration, carbon-ion radiotherapy (C-ion RT) in the treatment of esophageal cancer can reduce the dose to the surrounding organs, such as heart, respiratory tract, spinal cord, and skin. In addition, C-ion RT with its high biological effect can be expected to provide high antitumor effect even without chemotherapy. In view of the above, control of tumor of the esophagus is anticipated without severe adverse events in surrounding tissues. Thus, it may be offered as a minimally invasive treatment even to elderly patients with comorbid disease who are not suitable for surgery or chemotherapy. However, because the tolerance of the esophagus to carbon-ion beams is still unknown, the therapy is always planned to be applied carefully. Thus, C-ion RT for esophageal cancer is performed as a clinical trial to confirm its therapeutic effect and safety.

Keywords

Esophageal cancer • Squamous cell carcinoma

23.1 Introduction

Esophageal carcinoma is one of the worst malignant diseases and has a poor prognosis [1]. In the world, the histological subtype of more than 90 % of esophageal cancers is squamous cell carcinoma. Most patients are elderly, over 60 years of age.

Surgical resection has been a standard treatment for resectable esophageal carcinoma. In Japan, the 5-year survival rate was 50.2 % for patients who underwent esophagectomy [2]. The poor results may be attributed to a high incidence of loco-regional recurrence as well as distant metastasis [3, 4]. To improve the results of treatment for esophageal carcinoma, various types of adjuvant therapy combined with surgery have been investigated. A recent meta-analysis provided evidence for the survival benefit of neoadjuvant chemoradiotherapy or chemotherapy compared to surgery alone [5]. Nevertheless, the treatment outcome of esophageal carcinoma remains unsatisfactory.

The standard of care for patients with inoperable esophageal carcinoma is concurrent radiation therapy and chemotherapy. A phase II study of chemoradiotherapy for patients with stage I esophageal squamous cell carcinoma demonstrated a 4-year survival rate of 80.5 % [6]. Another phase II study of chemoradiotherapy for patients with stage II/III, excluding T4, esophageal squamous cell carcinoma showed a 5-year overall survival of 45 % [7]. However, it also demonstrated that a number of patients have persistent and recurrent disease.

23.2 Clinical Features

The common symptoms of esophageal carcinoma include dysphagia, pain, and weight loss. On the other hand, the more common endoscopy examinations have become, the more early-stage esophageal carcinomas without symptoms have been detected.

S. Yasuda (✉)
National Institute of Radiological Sciences,
4-9-1 Anagawa, Inage-ku, Chiba, Japan
e-mail: yasudash@nirs.go.jp

H. Tsujii et al. (eds.), *Carbon-Ion Radiotherapy: Principles, Practices, and Treatment Planning*,
DOI 10.1007/978-4-431-54457-9_23, © Springer Japan 2014

Esophageal tumors often cause stenosis or obstruction of the esophageal lumen. Tumors may readily invade into the adjacent mediastinum, such as trachea, main bronchus, aorta, and pericardium. The rich interconnecting lymphatic network contributes to regional extension of the disease widely, from the neck to the upper abdomen. Distant metastasis is commonly seen in lung and liver.

23.3 Pretreatment Evaluation

Before the workup, medical history and a physical examination with hematologic and biochemical examinations are essential in patients with esophageal carcinoma. Staging workup includes chest X-ray, gastroesophageal endoscopy with biopsy, esophagography, endoscopic sonography, computed tomography (CT), and positron emission tomography (PET) to evaluate the extent of the disease.

23.4 Carbon-Ion Radiotherapy for Esophageal Carcinoma

In view of both the superior dose concentration and high biological effect, carbon-ion radiotherapy (C-ion RT) of esophageal cancer is highly expected to control the disease without severe adverse events in the surrounding organs, such as heart, respiratory tract, spinal cord, and skin. This means that it can be offered as a minimally invasive treatment even to the elderly patients with comorbid disease who are not suitable for surgery or chemotherapy.

However, because the tolerance of the esophagus to carbon-ion beams is still unknown, it must be applied cautiously. Thus, C-ion RT for esophageal cancer is provided in clinical trials to confirm its therapeutic effect and safety.

23.4.1 Treatment Planning

Before treatment planning, metal markers (iridium seeds, 0.5 mm in diameter and 3 mm in length) were implanted endoscopically as landmarks for tumor location in the esophageal wall close to the proximal edge of the primary tumor and, where possible, also close to the distal edge (Fig. 23.1).

Three-dimensional treatment planning with 5-mm thick CT images was performed using the HIPLAN software program [8]. Gross tumor volume (GTV) was defined as the primary tumor and pathologic lymph nodes (LNs) based on pretreatment staging examinations. The initial planning target volume (PTV) included the GTV and the node regions according to tumor location. The reduced PTV included the whole primary tumor with a 3-cm margin in the cranio-caudal direction and metastatic LNs with a minimum 1-cm margin.

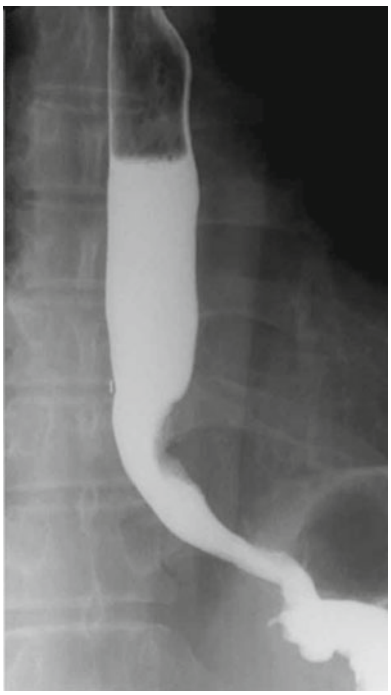

Fig. 23.1 Esophagography. Metal markers were implanted endoscopically as landmarks for tumor location in the esophageal wall close to the proximal edge of the primary tumor

A respiratory gating system was used during acquisition of the CT images and during treatment [9]. The beams were delivered in combination with anterior and posterior opposed portals (Fig. 23.2).

In terms of adverse events in some organs, special attention is required in the treatment planning. Spinal cord should not be included in the area of the dose exceeding 25 GyE to avoid nerve damage. In addition, the portion of the heart included in the high-dose area should be as small as possible to avoid severe adverse events, especially when treating tumors of the middle or lower thoracic esophagus.

23.4.2 Results of Carbon-Ion Radiotherapy for Esophageal Carcinoma

The first phase I/II clinical trial was carried out as a dose-escalation study of short-course preoperative C-ion RT for resectable esophageal carcinoma between July 2004 and June 2008. Then, the second phase I/II clinical dose-escalation study of definitive irradiation for early-stage esophageal carcinoma was started in April 2008 and is currently ongoing.

23.4.2.1 Short-Course Preoperative Carbon-Ion Radiotherapy (Protocol 0301)

Thirty-one patients with stage I–IVa, excluding T4, esophageal squamous cell carcinoma were enrolled in this study [10].

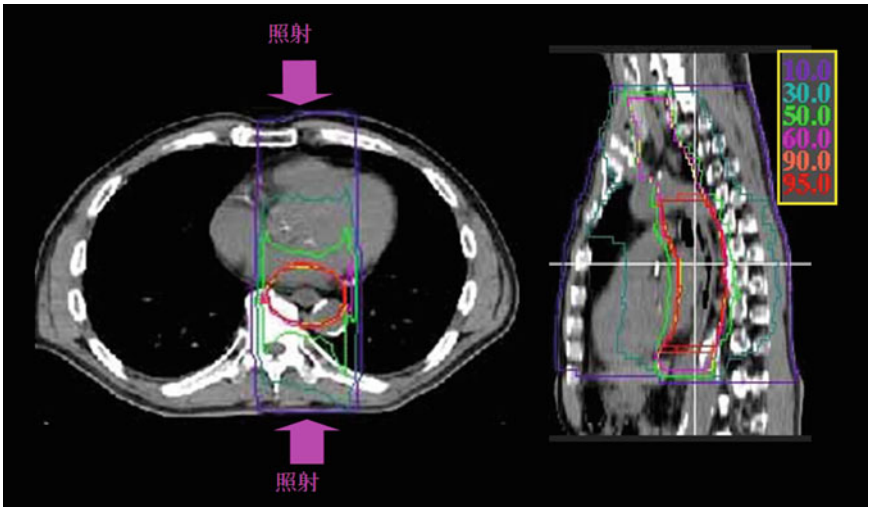

Fig. 23.2 Dose distribution. The beams were delivered in combination with anterior and posterior opposed portals. High-dose area was concentrated around the esophagus

Table 23.1 Toxicity (National Cancer Institute Common Terminology Criteria for Adverse Events version 3)

	Acute toxicity (grade)					Late toxicity (grade)				
	0	1	2	3	4	0	1	2	3	4
Esophagus	0	19	12	0	0					
Skin	4	27	0	0	0	28	0	0	0	0
Respiratory	30	0	0	1	0	28	0	0	0	0
Blood	25	4	2	0	0	28	0	0	0	0

C-ion RT was administered in 8 fractions over 2 weeks. The total radiation dose was escalated from an initial dose of 28.8 GyE in 5 % increments up to 36.8 GyE. Four to 8 weeks after the completion of C-ion RT, esophagectomy and lymph node (LN) dissection were performed. All patients were followed for 36 months or more after surgery.

Toxicity was classified in accordance with the criteria of the Common Terminology Criteria for Adverse Events version 3.0 (CTCAE v 3.0) [11]. Clinical and pathological evaluation of the primary tumor was performed according to the Japanese classification of esophageal cancer (ninth edition) [12].

Toxicities

All observed toxicities are listed in Table 23.1. None of the patients except one case (3.2 %) showed grade 3 or greater toxicities. One case (3.2 %) treated with 35.2 GyE presented grade 3 postoperative acute respiratory distress syndrome (ARDS). However, the correlation between C-ion RT and ARDS was uncertain.

Antitumor Effects

In total, 12 of the 31 patients achieved a clinically complete response (CR) (Fig. 23.3), 13 patients achieved a partial response (PR), and the overall response rate (CR + PR) was 80.6 %. According to the tumor depth, all 12 cases with T1 and all 8 cases with T2 achieved CR or PR (response rate, 100 %), while only 5 of the 11 cases with T3 disease achieved CR or PR (response rate, 45.5 %).

The pathological response in the resected primary tumor after surgery is shown in Fig. 23.4. In total, 12 patients achieved a grade 3 response (pathological CR) and 12 patients achieved a grade 2 response. The overall pathological response rate (grade 3 + grade 2) was therefore 77.4 %. The pathological response was 100 % in T1 cases and 87.5 % in T2 cases; however, it was 45.5 % in T3 cases.

In total, 11 of the 31 cases (35 %) showed recurrence after the operation (Table 23.2). All recurrences except one were seen in patients who had pathological LN metastasis at surgery. The most frequent recurrence pattern was LN recurrence, which was seen in eight of the 11 recurrence cases (73 %). Six of eight LN recurrences developed outside the radiation field.

The 5-year overall survival rates for stages I, II, and III were 61, 77, and 29 %, respectively. The 5-year cause-specific survival rate was 71 %. The cause-specific survival was better in grade 3 and grade 2 cases compared to grade 1 cases (Fig. 23.5).

23.4.2.2 Definitive Carbon-Ion Radiotherapy for Stage I Esophageal Carcinoma (Protocol 0701)

This study is currently ongoing. Up to November 2012, 16 patients had been enrolled in this study. C-ion RT was administered in 12 fractions over 3 weeks. The total radiation dose was escalated from the initial dose of 43.2 GyE in 5 % increments up to 50.4 GyE. All patients completed the prescribed treatment. Median follow-up was 36 months (range; 4–45 months). Clinical evaluation was performed according to the Japanese classification of esophageal cancer (10th edition) [13].

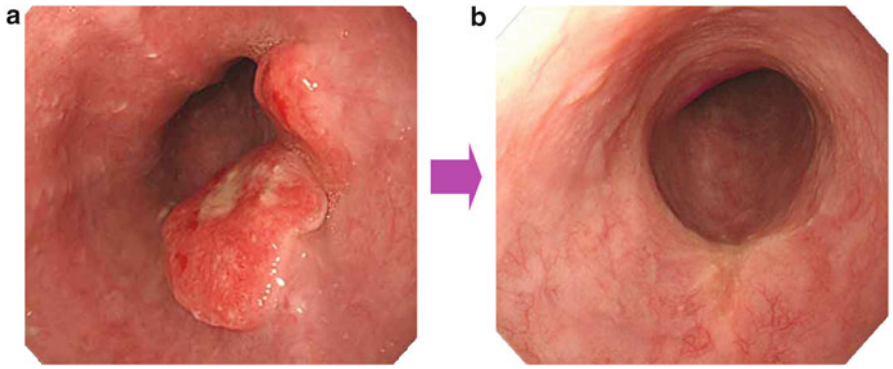

Fig. 23.3 A case with complete response to C-ion RT. The tumor also disappeared pathologically. (**a**) Before treatment. (**b**) After carbon-ion irradiation

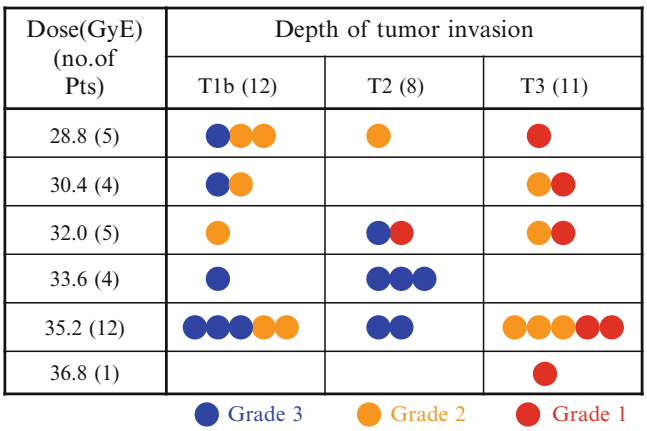

Fig. 23.4 Pathological effects of C-ion RT. Twelve (38.7 %) patients achieved grade 3 response (pathological CR) and 12 (38.7 %) patients achieved grade 2 response. The overall pathological response rate (grade 3 + grade 2) was 77.4 %

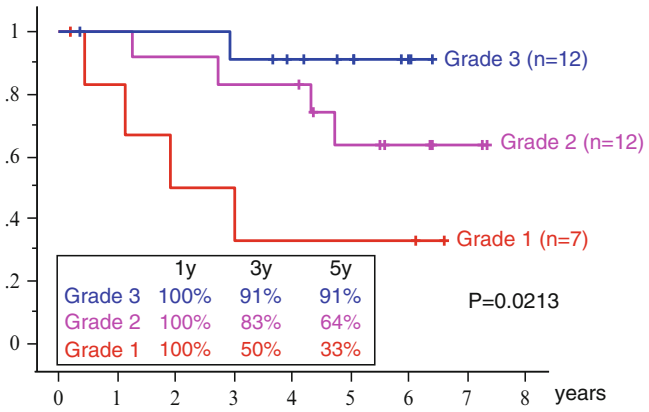

Fig. 23.5 Cause-specific survival rates by pathological effects

Table 23.2 Recurrence patterns

	Cases
Negative	20
Positive	11
Local[a,b](%)	2/11 (18)
Organ (%)	6/11 (55)
Lymph node (%)	8/11 (73)

[a] Surgical T4 (non-curative resection)
[b] Recurrence in anastomosis

Table 23.3 Toxicity (National Cancer Institute Common Terminology Criteria for Adverse Events version 3)

	Acute toxicity (grade)					Late toxicity (grade)				
	0	1	2	3	4	0	1	2	3	4
Esophagus	0	1	13	2	0	15	1	0	0	0
Skin	6	10	0	0	0	16	0	0	0	0
Respiratory	14	2	0	0	0	10	4	1	0	0
Cardiac	16	0	0	0	0	12	4	0	0	0
Blood	25	4	2	0	0	28	0	0	0	0

Toxicities

There were 2 cases of grade 3 acute esophagitis and 2 cases of grade 3 acute leucopenia (Table 23.3). No grade 3 or higher late toxicities were observed.

Antitumor Effects

Fourteen of the 16 patients (88 %) achieved CR (Fig. 23.5). Two of five patients treated with a starting total dose of 43.2 GyE did not reach CR. All patients treated with a total dose of 45.6 GyE or higher showed CR (Table 23.4).

Four patients experienced recurrence at the primary site and one at another site of the esophagus. There were no LN recurrences or distant organ metastases as a first recurrence.

The overall 3- and 4-year survival rates were 100 and 83 %, respectively (Fig. 23.6). Only one patient died of the disease.

Table 23.4 Antitumor effect

		Clinical effect		
Total dose (GyE)	Number of patients	CR	IR/SD	PD
43.2	5	3	2	0
45.6	3	3	0	0
48.0	7	7	0	0
50.4	1	1	0	0

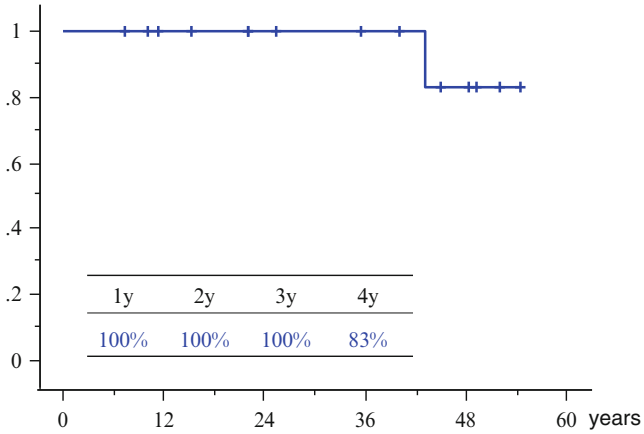

Fig. 23.6 Overall survival rates

23.4.2.3 Preoperative Carbon-Ion Radiotherapy and Concurrent Chemotherapy for Stage II and III Esophageal Carcinoma

The results of the study with preoperative C-ion RT (protocol 0301) showed that postoperative LN recurrence in regions outside the irradiated field was not uncommon in patients with advanced esophageal carcinoma. In addition, the effectiveness of C-ion RT for cases with a deeper tumor, such as T3 tumor, was found to still be unsatisfactory. To provide further improvements especially for advanced cases, additional chemotherapy should thus be considered. We are planning to start a new protocol using simultaneous chemotherapy plus C-ion RT preoperatively, which should provide a stronger antitumor effect.

References

1. Ferlay J, Shin HR, Bray F, et al. Estimates of worldwide burden of cancer in 2008: GLOBOCAN 2008. Int J Cancer. 2010;127:2893–917.
2. The Japan Esophageal Society. Comprehensive registry of esophageal cancer in Japan, 2004. The Japan Esophageal Society; 2012.
3. Baba M, Aikou T, Yoshinaka H, et al. Long-term result of subtotal esophagectomy with three-field lymphadenectomy for carcinoma of the thoracic esophagus. Ann Surg. 1994;3:310–6.
4. Matsubara T, Ueda M, Takahashi T, et al. Localization of recurrent disease after extended lymph node dissection for carcinoma of the thoracic esophagus. J Am Coll Surg. 1996;182:340–6.
5. Sjoquist KM, Burmeister BH, Smithers BM, et al. Survival after neoadjuvant chemotherapy or chemoradiotherapy for resectable oesophageal carcinoma: an updated meta-analysis. Lancet Oncol. 2011;12:681–92.
6. Kato H, Sato A, Fukuda H, et al. A phase II trial of chemoradiotherapy in patients with stage I esophageal squamous cell carcinoma: Japan Clinical Oncology Group study (JCOG 9708). Jpn J Clin Oncol. 2009;39:638–43.
7. Kato K, Muro K, Minashi K, et al. Phase II study of chemoradiotherapy with 5-fluorouracil and cisplatin for stage II–III esophageal squamous cell carcinoma: JCOG trial (JCOG 9906). Int J Radiat Oncol Biol Phys. 2011;81:684–90.
8. Endo M, Koyama-Ito H, Minohara S, et al. HIPLAN: a heavy ion treatment planning system at HIMAC. J Jpn Soc Ther Radiol Oncol. 1996;8:231–8.
9. Minohara S, Kanai T, Endo M, et al. Respiratory gated irradiation system for heavy-ion radiotherapy. Int J Radiat Oncol Biol Phys. 2000;47:1097–103.
10. Akutsu Y, Yasuda S, Nagata M, et al. A phase I/II clinical trial of preoperative short-course carbon-ion radiotherapy for patients with squamous cell carcinoma of the esophagus. J Surg Oncol. 2012;105:750–5.
11. Common Terminology Criteria for Adverse Events v3.0 (CTCAE). 2006. http://ctep.cancer.gov/protocoldevelopment/electronic_applications/docs/ctcaev3.pdf.
12. Japanese Society for Esophageal Diseases. Guide lines for the clinical and pathologic studies on carcinoma of the esophagus. 9th ed. Tokyo: Kanehara; 1999.
13. Japan Esophageal Society. Guide lines for the clinical and pathologic studies on carcinoma of the esophagus. 10th ed. Tokyo: Kanehara; 2007.

Postoperative Recurrence of Rectal Cancer

24

Shigeu Yamada, Satoshi Endo, Kohtaro Terashima, Makoto Shinoto, Shigeo Yasuda, Miho Shiomi, and Tetsuro Isozaki

Abstract

To improve long-term local control and survival of locally recurrent rectal cancer, we have initiated a radiation dose-escalation trial using carbon ion beams. The purpose of this study is to evaluate the tolerance for and effectiveness of carbon ion radiotherapy in patients with locally recurrent rectal cancer.

Between April 2001 and August 2012, 198 lesions at 189 patients were treated with C-ion RT. The dose was determined as 67.2 GyE and escalated to 70.4 GyE and 73.6 GyE. The local control rates in 197 lesions are 94 % at 3 years and 89 % at 5 years. Local control rate and survival rate at 5 years were 97 % at 73.6 GyE and 51 % at 73.6 GyE. In the literature, the reported 5-year survival rates for locally recurrent rectal cancer treated with resection were 20–40 %. Carbon ion radiotherapy seems to be a safe and effective modality in the management of locally recurrent rectal cancer, providing good local control and offering a survival advantage without acceptable morbidity.

In this chapter, the treatment methods and the up-to-date outcomes of carbon ion radiotherapy (C-ion RT) for the recurrent rectal cancer at the NIRS are introduced.

Keywords

Carbon-ion • Rectal cancer • Recurrence

24.1 Introduction

The large intestine starts at the ascending colon, which is connected to the small bowel, and ends at the rectum, which extends from the sacral promontory to the anal canal. In 2008, approximately 43,000 patients died of colorectal cancer in Japan, which is the third most common cause of cancer deaths, after lung and stomach cancers. Approximately 100,000 patients were diagnosed with colorectal cancer in 2004, thus making it the second most common type of cancer after stomach cancer. The analysis of the postoperative recurrence rates of colorectal cancer indicates a higher rate for rectal cancer than colon cancer. When compared by the site of recurrence, rectal cancer had a more than three times higher local recurrence rate than colon cancer.

With the recent advances in surgical techniques and procedures, the pelvic recurrence rate of rectal cancer has been decreasing; however, the postoperative recurrence rate is still 5–20 % today. Surgical resection is the first choice for locally recurrent rectal cancer, although total pelvic exenteration or another highly invasive procedure is often required. In many cases, locally recurrent rectal cancers are not completely resectable so generally surgical resections are not selected. The comparison of resection rates by the type of tumors shows that the resection rates were in the range of 40–50 %

S. Yamada (✉) • S. Endo • S. Yasuda • M. Shiomi • T. Isozaki
National Institute of Radiological Sciences, 4-9-1 Anagawa, Inage-ku, Chiba, Japan
e-mail: s_yamada@nirs.go.jp

K. Terashima • M. Shinoto
National Institute of Radiological Sciences, 4-9-1 Anagawa, Inage-ku, Chiba, Japan

Graduate School of Medical Sciences, Kyushu University, Fukuoka, Japan

H. Tsujii et al. (eds.), *Carbon-Ion Radiotherapy: Principles, Practices, and Treatment Planning*,
DOI 10.1007/978-4-431-54457-9_24,

Table 24.1 Resection rates and survival rates by recurrence sites

	Resc rate (%)	5-year survey (%)
Local rec	10–30	30–45
Liver meta	40–50	35–45
Lung meta	20–30	40–50

for liver metastases and 20–40 % for lung metastases, whereas the rate was 10–40 % for locally recurrent colorectal cancers (Table 24.1) [1, 2]. Curative resection of these tumors will lead to a survival rate similar to those for other types of recurrences and metastases.

24.2 Significance of C-Ion Radiotherapy

Improvements in tumor response and control have been sought through efforts to overcome the radioresistance of the hypoxic tumor cells identifiable in rectal cancers. These aspects might give high-LET particles a particular advantage, independent of whether this is due to a lower oxygen enhancement ratio (OER) or other intrinsic factors. Therefore, high-LET particle radiotherapy such as carbon ion or neutron radiotherapy may possess an advantage in the treatment of radioresistant and hypoxic, recurrent tumors. Twenty patients with recurrent rectal cancer were treated using the neutron generator in Munster by combined neutron radiotherapy [3].

The radiation schedule most often used for palliation involved giving 40 Gy photon and 10 Gy neutron doses (14 MeV). Initiation of pain relief appeared to occur faster with neutrons than with photons alone. Pain relief was achieved in 11–15 patients (73 %), and the probability for a pain-free period was 46 % at 9 months. It remains to be proven if a higher degree of pain relief, longer period of absence of pain, and length of progression-free period are improved with neutrons in comparison to photons. The incidence of acute toxicity was 30 % and late toxicity 10 %, with all reported toxicity occurring in the skin. A higher neutron dose may give better results, but its utility is potentially limited by well-recognized local radiation side effects. In contrast to neutrons, where escalation to tumoricidal doses is limited by potential normal tissue complications, carbon ion therapy offers the potential for an increase in biologically effective dose delivery in the target tissue relative to normal tissues through its superior dosimetric and radiobiological properties [4].

24.3 Clinical Trial in Recurrent Rectal Cancer at NIRS

The first clinical trial of the C-ion RT at the National Institute of Radiological Sciences (NIRS) for the recurrent rectal cancer was started in 2000. It was a phase I/II dose-searching study and the dose was escalated from the starting dose of 67.2 to 73.6 GyE in 16 fractions. A total of 38 patients were treated and the results indicated that the C-ion RT could be a sufficiently safe and effective treatment for the recurrent rectal cancer. This study was finished in 2004 and the second trial with the recommended dose determined by the first trial was initiated immediately. One hundred and fifty-two patients were treated in the second study until 2004 and the satisfactory results could be obtained as well. In November 2003 the approval of the Japanese government for the advanced medicine was given to the C-ion RT at the NIRS, and after the end of the second trial, the recurrent rectal cancer was added to the indication of the advanced medicine.

24.4 Methods of Carbon Ion Radiation Therapy at NIRS

24.4.1 Patient Immobilization

The patient needs to be immobilized for the C-ion RT as well as other tumor sites. The C-ion RT at the most heavy-ion therapy facilities is performed with fixed beam directions of vertical, horizontal, or 45-degree oblique. On the other hand, the recurrent tumor of the rectal cancer locates anywhere in the pelvis, at the presacral region, iliac lymph node, or mesenteric lymph node, and therefore the proper direction of the carbon ion beam is varied. Moreover, more than two ports are usually necessary to obtain satisfactory dose distribution in terms of avoidance of high dose to the bowels and the skin. Consequently, rather complicated immobilization is an everyday occurrence.

At the NIRS, it could be realized by using relatively thick low-temperature thermoplastic (Shellfitter; Keraray Co., Ltd., Osaka, Japan), sufficient amount of customized cradle (Moldcare; Alcare, Tokyo, Japan), and rotatable couch on the treatment bed.

Management of the respiratory motion is also essential in the most case of the recurrent rectal cancer (see Chaps. 4, 5, 6, 7, 8, and 9 Motion Management). There are plenty of methods for motion management. At the NIRS, synchronization with respiration is adopted at both CT acquisition and every session of the C-ion RT irrespective of direction of the beam. Although the influence of the respiratory motion on the session with the vertical beam is less than that with horizontal beam in the treatment of pelvic tumor, that is, mainly difference in the length of air gap, it is desirable to irradiate the tumor with similar condition to dose calculation using CT images taken at the expiratory phase.

24.4.2 Target Delineation

A set of 2.5–5.0-mm-thick CT images throughout the pelvis was taken for treatment planning, with the patient placed in immobilizing devices and with respiratory gating.

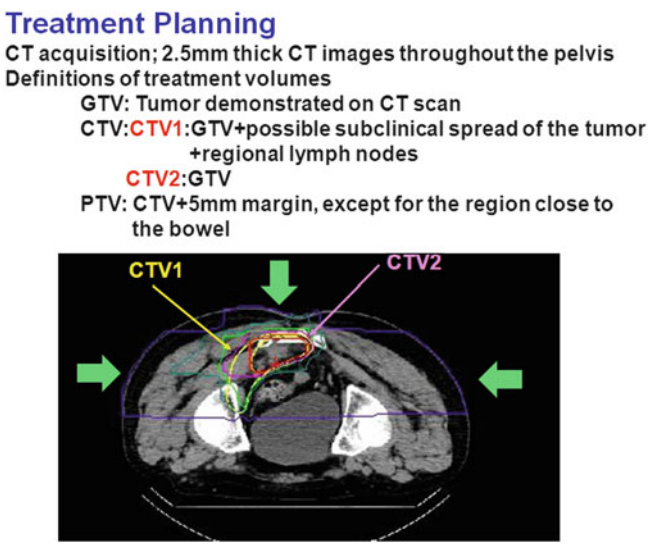

Fig. 24.1 The method of treatment planning for recurrent rectal cancer. *Yellow line* indicates the clinical target volume CTV) and *red line* indicates the planning target volume (PTV). The margins for the PTV is intentionally reduced to spare the bowels

Clinical target volume (CTV) was determined by setting the margin 5 mm outside the GTV and included the regional lymph nodes (LN). The LN areas that should be considered the target volume include the internal iliac, the external iliac, and the presacral node. The dose constraints of the maximum dose for the intestine and bladder were 30 GyE in 9 fractions and 60 GyE in16 fractions, respectively. Prophylactic nodal areas of risk are usually treated to 37.8–41.4 GyE in 9 fractions of 4.2–4.6 GyE before irradiation field is reduced in size. The target volume includes the primary tumor, adjacent lymph nodes, and presacral region. Target volumes are based on known pattern of local recurrence in locally recurrent rectal cancer. MRI and methionine PET are useful to distinguish the tumor from postoperative fibrosis and the bowels.

Planning target volume (PTV) is defined as the CTV plus at least 5 mm margin in all directions; however, the margins are modified if the critical organs, such as skin or bowels, exist near the tumor (Fig. 24.1).

24.4.3 Dose Prescription

The current recommended dose was 73.6 GyE/16 fractions as described above. One hundred percent of the prescribed dose is given at the maximum dose point of each portal. The treatment planning is performed so that the PTV is covered with at least 90 % of the prescribed dose. For this purpose, additional margins are necessary to determine the shape of collimator and compensation bolus. Figure 24.1 shows the representative dose distribution of current C-ion RT at the NIRS.

Major organs at risk (OAR) for this treatment are the bowels, sciatic nerve, urinary bladder, ureter, and skin. It is particularly important to spare the bowels from the high-dose area of the carbon ion beam. At the NIRS, dose constraints of the digestive tract are established based on the treatment results in the prostate, uterine cervical cancer, and the recurrent rectal cancer, where the maximum dose to the colon should not exceed 83 % of the prescribed dose. The sciatic nerve is also important OAR and the dose should be reduced as much as possible; however, control of the local tumor is much more important not only for the survival but also for the quality of life (QOL) of the patient. If the tumor is located close to the skin surface, the dose to the skin should also be taken into account. Selecting proper direction of the beam and using more than two ports are desirable, particularly in the treatment of big-sized lesion.

24.4.4 Field Positioning and Irradiation at NIRS

At the NIRS, the C-ion RT is carried out once a day, four fractions per week (from Tuesday to Friday). Verification of the field is carried out at every treatment session with a computer-aided online positioning system to maintain a positioning error of less than 2 mm. Fluoroscopic image is taken at the expiration phase of the patient respiration and compared with the reference images, such as the image taken at the preceded simulation or the digitally constructed radiograph (DRR). The C-ion RT is performed under respiration gating as described above, where the carbon ion beam is delivered only during the expiration phase.

24.5 Up-to-Date Results of the C-ion RT at NIRS

24.5.1 C-Ion Therapy for Patients with Pelvic Recurrence of Rectal Cancer

Between April 2001 and August 2012, 198 lesions at 189 patients were enrolled onto this study. Criteria for trial eligibility include confirmation of locally recurrent rectal cancers without distant metastases based on CT, MRI, and PET findings. The dose was determined as 67.2 GyE and escalated to 70.4 and 73.6 GyE. The predominant sites of relapse were 75 presacral, 77 lymph nodes, 28 perineal, and 9 anastomosis.

Ten patients received radiation dose at 67.2 GyE, 18(+3) at 70.4 GyE, and 161(+6) at 73.6 GyE. All toxicities in the 198 lesions at 189 patients were relatively few and mild in these patients. No grade 3–5 acute toxicity was observed. The local control rates in 197 lesions are 94 % at 3 years and 89 % at 5 years. Local control rates at 5 year were 97 % at 73.6 GyE. In terms of symptomatic response within 3 months after treatment, pain improved in 97 % of the symptomatic cases. The 3- and 5-year overall survival rates in 188 patients

Table 24.2 The results on the radiation therapy of locally recurrent rectal cancer reported by other studies

Study and reference	Year	Number	Rad dose(Gy)	Survival rate 2 years (%)	5 years (%)	Local control (%)
Lybeert et al. [5]	1992	76	6–66	61 (1 year)	3	28 (3 years)
Knol et al. [6]	1995	50	60	27	8	–
Murata [7]	1997	18	12–60	44 (1 year)	–	46 (2 years)
Hu et al. [8]	2006	23	55–66	50 (2 years)	18 (3 years)	
Kim et al. [9]	2008	23	30–51/3f	82	23	74 (5 years)
Lee et al. [10]	2011	22	54–66	66	40	56 (5 years)
NIRS	2012	136	73.6	87	45	93 (5 years)

Table 24.3 The results of the surgical treatment reported by other studies

Study and reference	Year	Number of patients	Survival rate 1 year (%)	2 years (%)	5 years (%)
Garcia-Aguilar et al. [12]	1999	42	88	62	35
Wanebo et al. [13]	1999	53	91	62	31
Salo et al. [14]	1999	71	88	75	31
Saito et al. [15]	2003	43	91	78	39
Moriya et al. [16]	2004	48	95	76	36
Melton et al. [17]	2007	29	92	65	20
NIRS	2012	136	99	87	45

were 72 % and 47 %, respectively. Survival rates at 5 years were 20 % at 67.2 GyE, 24 % at 70.4 GyE, and 51 % at 73.6 GyE. In the literature, the reported 5-year survival rates for locally recurrent rectal cancer treated with conventional radiation and with resection were 0–40 % (Table 24.2) and 20–40 % (Table 24.3), respectively. Most of our patients were inoperable, so our results seem to be better than surgery.

Carbon ion radiotherapy seems to be a safe and effective modality in the management of locally recurrent rectal cancer, providing good local control and offering a survival advantage without acceptable morbidity.

24.5.2 Indication of Spacer in the C-Ion RT for the Recurrent Rectal Cancer

Pelvic recurrent tumors are often located in close proximity to the digestive tract. Consequently, a significant proportion of patients were often judged as ineligible for carbon ion radiotherapy, because the digestive tract could not be excluded from the irradiation field. At our hospital, therefore, we adopted a surgical preparatory procedure, to place a spacer between the target tumor and the digestive tract before conducting carbon ion radiotherapy, when the tumor was located close to a sensitive organ.

The tumor locations are classified into three groups according to distance between tumor and intestine. They are penetration type, contact type, and separation type. Contact type is defined by the shorter than 5 mm distance between the tumor and intestine. Previously contact type was not eligible for carbon ion therapy. We have tried to treat these types of tumors by using spacer. To exclude the small intestine and colon from the clinical target volume (CTV) and reduce the exposure of them, we use expanded polytetrafluoroethylene (Gore-Tex soft-tissue patch, W. L. Gore & Assoc Inc, Flagstaff, Ariz) which is a strong and easy-to-use material and does not need to be removed after the conclusion of radiotherapy (Fig. 24.2). Mesenterium, muscle cutaneous flap, or omentum instead of Gore-Tex sheet is used at infectious lesion.

From 2003, 73 patients are treated with the spacer. Most of tumor sites were the sidewall or presacrum. Eight of grade 3 acute toxicities were observed. This rate is higher than without spacer. All patients completed the scheduled treatment course. Local control rate is 96 % at 2 years and 88 % at 5 years. This is almost the same as without spacer. The survival curves of patients with locally recurrent rectal cancer are similar between with and without spacer.

The case was of a 59-year-old Japanese female and referred to the NIRS hospital with a diagnosis of postoperative recurrence of the rectal cancer (Fig. 24.3). CT scan revealed a tumor mass in the sidewall of the pelvis and in contact with the intestine. After placing Gore-Tex sheet, this dose distribution revealed the dose of the surrounding intestine is extremely low. She did not experience any major toxicity. The tumor size on CT scan decreased 24 M after treatment.

24.6 Carbon Ion Radiotherapy for Locally Recurrent Rectal Cancer in Patients with Prior Pelvic Irradiation

Among gastrointestinal malignancies, many studies have shown the safety and efficacy of pelvic reirradiation for rectal cancer [10–14]. Reirradiation to the pelvis could potentially play a role in palliation of symptoms or local control. Local recurrences are located close to critical organs such as the small intestine, colon, and bladder, and in these patients reirradiation would be expected to be associated with a higher risk of acute and late toxicity at these organs than primary irradiation.

Fig. 24.2 The photograph of Gore-Tex soft-tissue patch and operative findings using it. Gore-Tex is made of expanded polytetrafluoroethylene (PTFE). It is widely applied to medical materials such as vascular grafts or hernia repair materials. This is operative finding. The spacer was fixed with the retroperitoneum and peritoneum

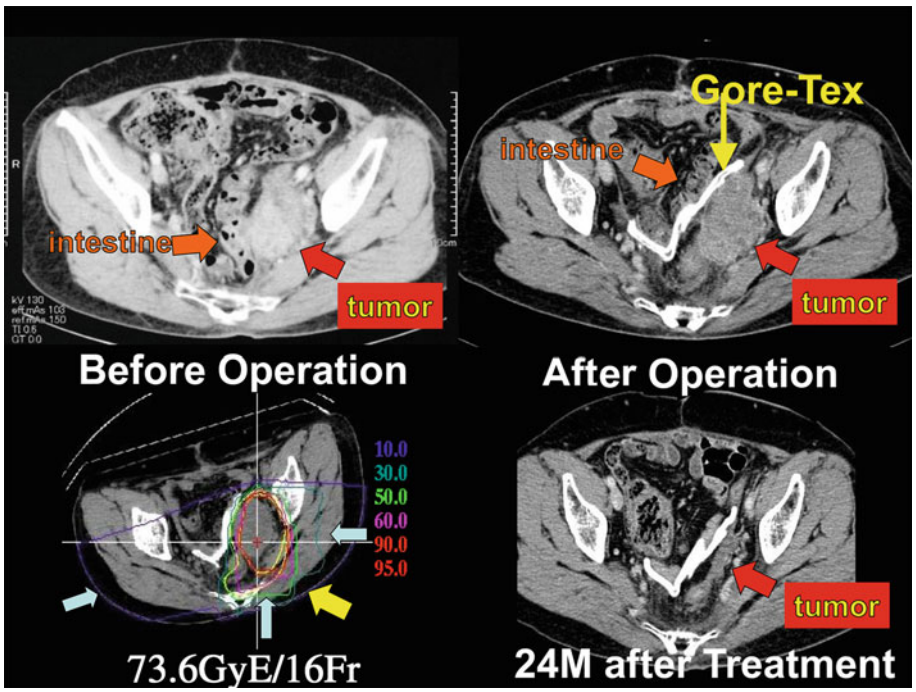

Fig. 24.3 This patient is a 59-year-old female with locally recurrent rectal cancer. CT scan revealed a tumor mass in the sidewall of the pelvis and in contact with the intestine. After placing Gore-Tex sheet, the dose distribution revealed the dose of the surrounding intestine is extremely low. The tumor size on CT scan decreased 24 M after treatment. She did not experience any major toxicity

The purpose of this study was to assess carbon ion radiation therapy performed as reirradiation in patients with locally recurrent rectal cancer. Twenty-three patients were treated with carbon ion RT as reirradiation for locally recurrent rectal cancer. Nine relapses originated in the presacral region, 8 in the pelvic sidewalls and 6 in the perineal region. The total dose range of 70.4 Gy equivalent (GyE) was administered in 16 fixed fractions over 4 weeks (4.4 GyE/fraction).

All patients completed the scheduled treatment course. Grade 3 toxicities occurred in 6 (26 %) patients. The major late toxicities were peripheral neuropathy and infection. No other severe acute reactions (grade ≥3) were observed at this study (Table 24.4).

The 1- and 3-year overall survival rates were 83 % (95 % CI, 68–98 %) and 65 % (95 % CI, 43–87 %), respectively. The 1- and 3-year disease-free survival rates were 71 % (95 % CI, 51–91 %) and 51 % (95 % CI, 27–75 %), respectively.

Carbon ion radiotherapy as reirradiation appears to be a safe and effective modality in the management of locally recurrent rectal cancer, providing good local control and offering a survival advantage without unacceptable morbidity.

24.7 Future Perspectives

24.7.1 Scanning Irradiation

In 2011, the beam delivery using spot scanning became available at the NIRS. It has been applied to the lesion without significant motion due to the respiration until April 2013. However, the spot scanning irradiation for the mobile target is being developed and will be realized in the near future. Therefore, the scanning irradiation will also be performed for the recurrent rectal cancer as well as lung cancer or liver cancer.

The scanning irradiation can offer even better dose distribution than the passive method in the treatment of various lesions because it is much more flexible. In the passive irradiation, uniform length of the spread-out Bragg peak (SOBP) must be used in each field and it often gives unnecessary high dose to the normal tissue. While, there is no unnecessary high-dose area in the dose distribution with the scanning and it is additionally possible to reduce the dose to the normal tissue even more by means of accepting the high-dose spot inside the target if desirable.

Moreover, the improvement of treatment efficiency can be obtained by the scanning. It does not require a collimator or compensation bolus, so the preparation time between CT acquisition and the start of treatment can be shortened and the cost for each treatment can be less expensive.

Furthermore, it is possible for the scanning irradiation to realize rotating gantry of the carbon ion beam. With the gantry, the patient need not be immobilized in the uncomfortable, inclined position as the current C-ion RT with passive irradiation.

Table 24.4 Comparison between maximum normal tissue damage by primary CIRT and CIRT as reirradiation

	Neuropathy					Gastrointestinal				
Toxicity	No	G0	G1	G2	G3	No	G0	G1	G2	G3
Primary CIRT	17	6	6	4	1	17	10	4	3	0
Reirradiation	23	8	7	6	2	23	17	1	2	3[a]

[a]All of the three grades were attributed to operations for spacer before treatment

24.8 Case Study

The case was of a 65-year-old Japanese male referred to the NIRS hospital with a diagnosis of postoperative recurrence of rectal cancer. He underwent the surgery 4 years before and the initial stage was IIIa. The CT scan and PET scan revealed a tumor mass in the right sidewall of the pelvis and infiltrated pelvic bone (Fig. 24.4).

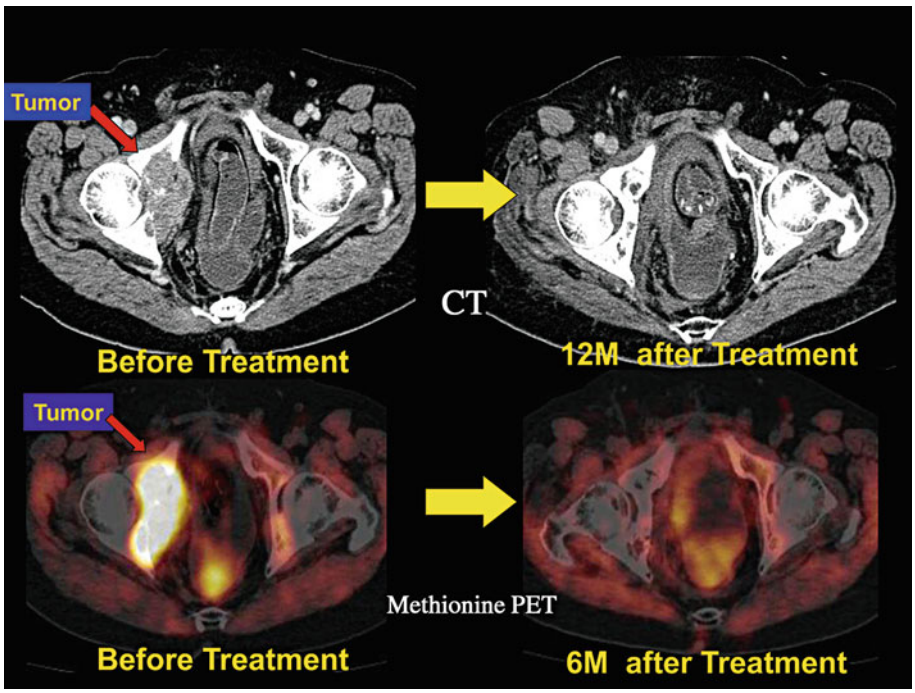

Fig. 24.4 This patient is a 65-year-old male with locally recurrent rectal cancer. A CT scan and PET scan revealed a tumor mass in the right sidewall of the pelvis and infiltrated pelvic bone

The C-ion RT was performed with three ports of left oblique lateral, right oblique lateral, and oblique posterior, and the total dose was 73.6 GyE in 16 fractions.

Twelve months later, the CT and the methionine accumulation after treatment demonstrated disappearance of the tumor and osteogenesis in the osteolytic lesion.

References

1. Kobayashi H, Hashiguchi Y, Ueno H. Follow-up for recurrent colorectal cancer. J Ppn Soci Coloproctology. 2006;59:851–6.
2. Sugihara K. Guidelines for treatment of recurrent rectal cancer. Tokyo: Nankodo Co. Ltd; 2003. p. 89–149.
3. Eising E, Potter R, Haverkamp U. Neutron therapy for recurrence of rectal cancer. Strahlenther Onkol. 1990;166:90–4.
4. Ando K, Koike S, Ohira C, et al. Accelerated reoxygenation of a murine fibrosarcoma after carbon-ion radiation. Int J Radiat Biol. 1999;75:505–12.
5. Lybeert ML, Martijn H, de Neve W, et al. Radiotherapy for locoregional relapses of rectal carcinoma after initial radical surgery: definite but limited influence on relapse-free survival and survival. Int J Radiat Oncol Biol Phys. 1992;24:241–6.
6. Knol HP, Hanssens PE, Rutten HJ, et al. Effect of radiation therapy alone or in combination with surgery and/or chemotherapy on tumor and symptom control of recurrent rectal cancer. Strahlenther Onkol. 1997;173(1):43–9.
7. Murata T, Fujii I, Yoshino M. Radiation therapy with or without chemotherapy and hyperthermia for recurrent rectal cancer. J Jpn Soc Ther Radiol Oncol. 1997;9:63–71.
8. Hu JB. Int J Radiat Oncol Biol Phys. 2006;23:241.
9. Kim MS, Choi C, Yoo S, et al. Stereotactic body radiation therapy in patients with pelvic recurrence from rectal carcinoma. Jpn J Clin Oncol. 2008;38:695–700.
10. Lee JH, Kim YS, Yang SW, et al. Radiotherapy with or without surgery for patients with idiopathic sclerosing orbital inflammation refractory or intolerant to steroid therapy. Int J Radiat Oncol Biol Phys. 2012;84:52–8.
11. Garcia-Aguilar J, Cromwell JW, Marra C, et al. Treatment of locally recurrent rectal cancer. Dis Colon Rectum. 2001;44:1743–8.
12. García-Aguilar J, Belmonte MC, Javier PJ, et al. Incontinence after lateral internal sphincterotomy: anatomic and functional evaluation. Dis Colon Rectum. 1998;41:423–7.
13. Wanebo HJ, Antoniuk P, Koness JR, et al. Pelvic resection of recurrent rectal cancer: technical considerations and outcomes. Dis Colon Rectum. 1999;42:1438–48.
14. Salo JC, Paty PB, Guillem J, et al. Surgical salvage of recurrent rectal carcinoma after curative resection: a 10-year experience. Ann Surg Oncol. 1999;6:171–7.
15. Saito N, Koda K, Takiguchi N, et al. Curative surgery for local pelvic recurrence of rectal cancer. Dig Surg. 2003;20:192–200.
16. Moriya Y, Akasu T, Fujita S, et al. Total pelvic exenteration with distal sacrectomy for fixed recurrent rectal cancer in the pelvis. Dis Colon Rectum. 2004;47:2047–54.
17. Melton GB, Paty PB, Boland PJ, et al. Sacral resection for recurrent rectal cancer: analysis of morbidity and treatment results. Dis Colon Rectum. 2006;49:1099–107.

Part XIV

Liver Tumors

Hepatocellular Carcinoma

25

Shigeo Yasuda

Abstract

Clinical trials of carbon-ion radiotherapy (C-ion RT) for hepatocellular carcinoma (HCC) were conducted at the National Institute of Radiological Sciences (NIRS) in Japan between April 1995 and August 2005. In four clinical studies, we tried to determine the optimal dose and to shorten the treatment duration with five different fractionation schedules, using 15, 12, 8, 4, and 2 fractionations. There have been no treatment-related deaths and no severe adverse events. As a result of these studies, the duration of treatment could be reduced from 5 weeks to 2 days. Two-fraction therapy is currently ongoing under the license of Highly Advanced Medical Technology. Because of the low toxicity and good local control rate, C-ion RT is a promising radical and minimally invasive therapeutic option for HCC.

Keywords

Hepatocellular carcinoma (HCC) • Radiation-induced hepatic insufficiency

25.1 Introduction

Hepatocellular carcinoma (HCC) is one of the most common malignancies worldwide and various locoregional therapies are presently available.

The standard therapies for HCC are hepatectomy, transcatheter arterial embolization (TAE), percutaneous ethanol injection (PEI), radio-frequency ablation (RFA), and liver transplantation. According to the survey and follow-up study of primary liver cancer in Japan, the relative use of these therapies in the treatment records of all patients in the 2-year period from January 1, 2004, through December 31, 2005, was: hepatectomy in 32 % of cases, TAE in 32 %, and percutaneous local therapy involving PEI, percutaneous microwave coagulation therapy (PMCT), and RFA in 31 %. Each of these procedures has merits and drawbacks. For example, while hepatectomy provides the best certainty of removing cancer cells, the procedure also results in serious stress on both the liver and the body as a whole. TAE is clinically useful and has a relatively low degree of invasiveness, but is of limited radicality. PEI and RFA, on the other hand, are simple procedures offering a high degree of radicality, but their effect is limited to comparatively small tumors (less than 3 cm in diameter).

The use of radiotherapy for HCC has been considered difficult in view of the problems associated with radiation-induced hepatic insufficiency [1, 2]. However, progress in the development of irradiation devices in recent years has made it possible to achieve highly localized irradiation, reducing the degree of toxicity [3–6]. This has spurred advances in radiotherapy research for liver cancer [7–12]. Carbon-ion beams possess the Bragg peak and have advantageous biological and physical properties that result in a higher cytocidal effect than that of photons and protons [13–16]. C-ion RT has been performed for treatment of HCC from April 1995.

S. Yasuda (✉)
National Institute of Radiological Sciences, 4-9-1 Anagawa, Inage-ku, Chiba, Japan
e-mail: yasudash@nirs.go.jp

H. Tsujii et al. (eds.), *Carbon-Ion Radiotherapy: Principles, Practices, and Treatment Planning*,
DOI 10.1007/978-4-431-54457-9_25, © Springer Japan 2014

25.2 Overview of Carbon-Ion Radiotherapy

Four clinical studies were carried out to determine the optimal dose based on a dose-escalating protocol in four different fractionation schedules, using 15, 12, 8, and 4 fractions. Most of the subjects enrolled under these protocols had been judged not to be amenable to, or as having had recurrence after, other treatments or as having no prospects of an adequate treatment effect with any of the existing therapies. Following these studies, we conducted a phase II study using a fixed total dose of 52.8 GyE in 4 fractions. This study revealed the high safety and effectiveness of the treatment. Following that, we are now offering even shorter-course radiotherapy of 2 fractions in only 2 days for patients with HCC. Thus, the duration of treatment could be safely reduced from 5 weeks to 2 days.

Two-fraction therapy is currently ongoing under the license of Highly Advanced Medical Technology.

25.3 Preparation for Treatment

Before the treatment planning, one or two metal markers (0.5×3 mm) made of iridium wire were inserted near the tumor under ultrasound imaging guidance as landmarks for target volume localization. These markers are visible not only in CT images but also in orthogonal X-ray images (Fig. 25.1). To accurately reproduce the patient position, a low-temperature thermoplastic sheet and a customized cradle were used. The supine or prone position was selected according to the location of the tumor. Patients are forbidden from eating and drinking before acquisition of the treatment planning CT images and each treatment. This is because the position of the liver would be changed depending on the volume of the stomach.

25.4 Treatment Planning

Three-dimensional treatment planning with 2.5-mm CT images was performed using the HIPLAN, which was originally developed for 3D treatment planning [17]. The planning target volume (PTV) was defined so as to include a 1 to 1.2-cm margin around the gross tumor volume. Dose-volume histogram was used to evaluate the probability of liver damage (Fig. 25.2). Double right-angled field geometry was used for irradiation in most patients. Respiratory gating was employed for CT image acquisition and irradiation stages to ensure more accurate delivery of the radiation [18]. To assess the accuracy of patient positioning and target volume localization, orthogonal fluoroscopy and radiography were used immediately prior to each treatment session.

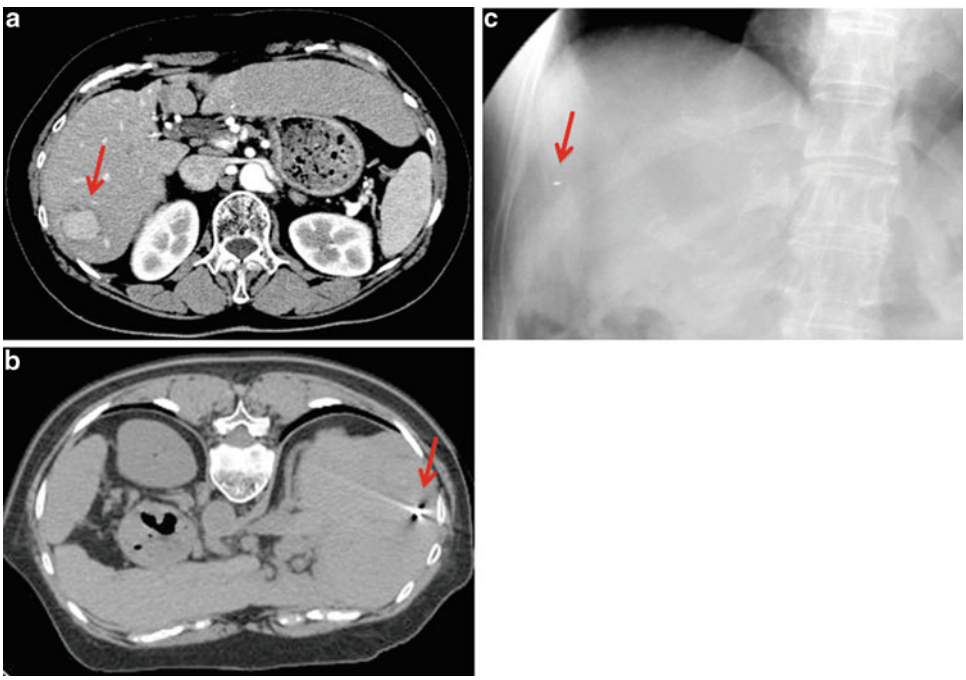

Fig. 25.1 A patient with hepatocellular carcinoma 5.5 cm in maximum diameter in the right posterior interior segment of the liver. (**a**) CT scan before the treatment. (**b**) CT image for treatment planning: the arrow shows a metal marker implanted near the tumor. (**c**) X-ray image. The metal marker can be seen (*arrow*)

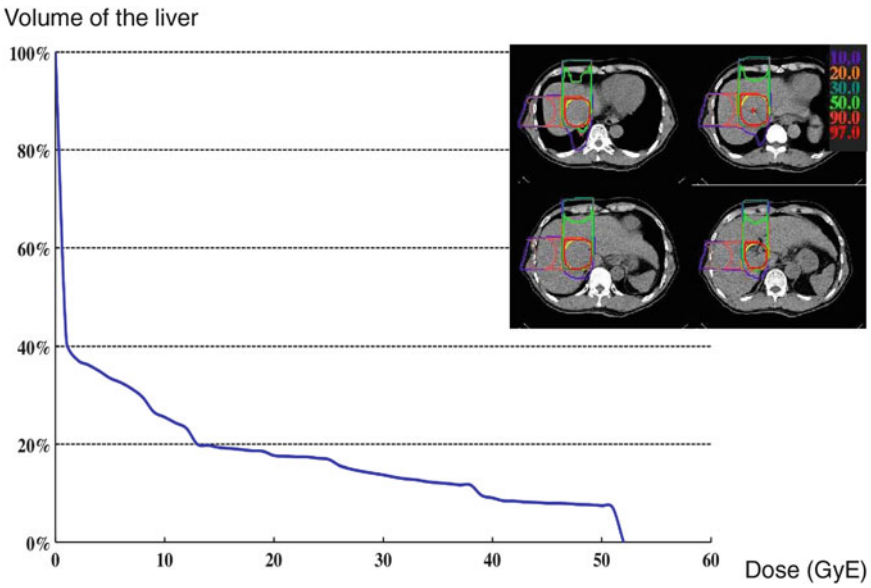

Fig. 25.2 Dose distribution and dose-volume histogram of the liver. In the treatment planning, a dose-volume histogram is used to evaluate the probability of liver damage

In order to prevent/minimize adverse events in certain organs, special attention is required in the treatment planning. To reduce rib fracture, the PTV margin should be defined so as not to include the outside of ribs in the high-dose area. Because the tumor usually does not exist on the outside of the liver surface, the PTV margin outside the liver can be set at less than that in the liver (Fig. 25.3). Skin should not be included in the area of a dose exceeding 70 % of the prescribed dose to avoid severe skin reaction. Great caution is also needed for setting the PTV margin so as not to irradiate the digestive tracts with high doses. If the gut exists near the tumor, the treatment beams should be set not to pass through the gut, if possible. If digestive tracts almost touch the tumor, high-dose irradiation is difficult because of the risk of serious gastrointestinal tract damage. In addition, the major trunk or main branch of the portal vein should not be fully included in the PTV to avoid liver failure and especially in cirrhotic liver.

25.5 Short-Course Carbon-Ion Radiotherapy

Between April 2003 and August 2012, 133 patients with HCC underwent 2-fraction C-ion RT. Background data of the patients and tumors are presented in Table 25.1. The patients consisted of 91 males and 42 females. Median age was 72 years (range, 44–87). Median maximum tumor diameter was 42 mm (range, 14–140). One hundred and twenty-three patients were classified into Child-Pugh A and ten into Child-Pugh B. All 133 patients were treated with a total dose range of 32.0–45.0 GyE.

Table 25.1 Patient and tumor characteristics in 2 fractions of C-ion RT

Characteristics	Total ($n = 133$)
Age (years)	
Median	72
Range	44–87
Sex, *n* (%)	
Male	91 (68)
Female	42 (32)
Etiology of cirrhosis, n (%)	
HCVAb positive	92 (69)
HBsAg positive	12 (9)
None	30 (23)
Both	1 (1)
Child-Pugh classification, n (%)	
A	123 (92)
B	10 (8)
UICC 5th stage, n (%)	
I	19 (14)
II	97 (73)
IIIA	15 (11)
IVA	2 (2)
Number of tumors, n (%)	
Single	118 (89)
Multiple	15 (11)
Maximum tumor diameter (mm)	
Median	42
Range	14–140
AFP (ng/mL)	
Mean ± SD	2,350.3 ± 11,891.4
PIVKA-2 (mAU/mL)	
Mean ± SD	5,256.3 ± 43,838.0

HCVAb hepatitis C virus antibody, *HBsAg* hepatitis B surface antigen, *UICC* Union for International Cancer Control, *AFP* alpha-fetoprotein, *SD* standard deviation

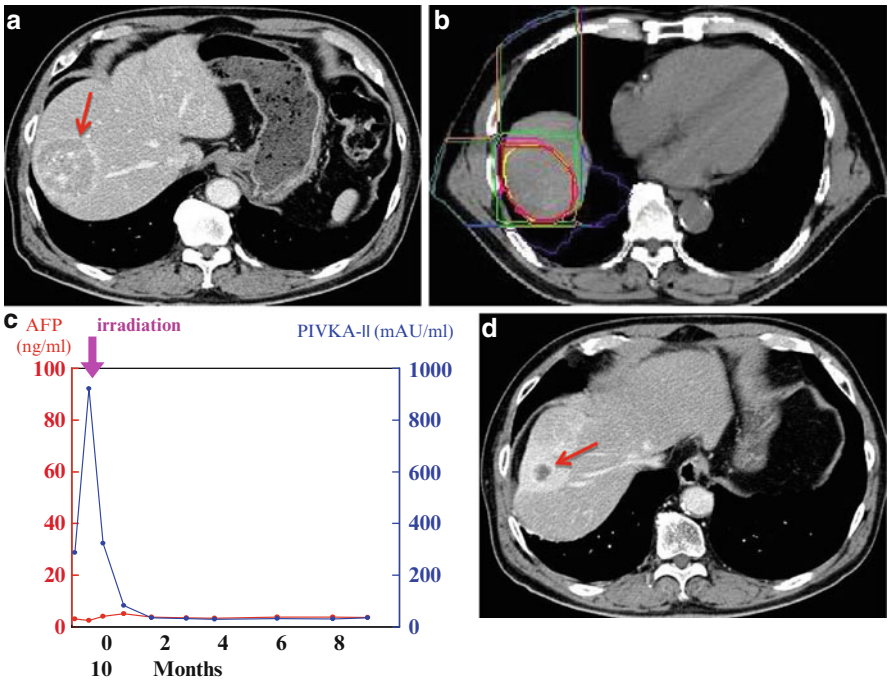

Fig. 25.3 A case with hepatocellular carcinoma 5.5 cm in maximum diameter in the right anterior superior segment of the liver. (**a**) CT scan before treatment. (**b**) Dose distribution: The beam was delivered in combination with anterior and lateral portals (dose ratio 1:1). The planning target volume was defined so as to include a 1.2-cm margin around the gross tumor volume except the right side where the margin was narrower to exclude the ribs from the high-dose area. (**c**) Change of serum tumor markers: The serum PIKA-II value promptly decreased after the treatment. (**d**) CT scan 9 months after treatment; the tumor had regressed remarkably. There were no rib fractures after the treatment

Table 25.2 Acute and late toxicities after C-ion RT

	Acute ($n=133$)					Late ($n=132$)				
	Grade					Grade				
	0	1	2	3	4	0	1	2	3	4
Skin	0	130	3	0	0	7	124	1	0	0
Liver	68	35	25	4	0	50	48	26	4	0
Gastrointestinal	133	0	0	0	0	132	0	0	0	0
Lung	104	29	1	0	0	78	53	1	0	0

No treatment-related deaths occurred in the hypofractionation trial. There were no cases of grade 4 hepatic toxicity. With regard to the Child-Pugh score, in the late phase (3 months after treatment), an increase of two points or more occurred in 6 and 3 % in the smaller-tumor group (≦5 cm) and the larger-tumor group (>5 cm), respectively. There was no significant difference between the two groups ($P=0.678$). This demonstrated that the changes in liver function remained minor after C-ion RT was performed. No serious adverse effects were noted in the digestive organs. There was no other grade 4 or higher toxicity (Table 25.2).

The local control rates were 98 and 90 % at 1 year and 83 and 76 % at 3 years in the higher-dose group (45.0 GyE) and the lower-dose group (≦42.8 GyE), respectively. There was no significant difference according to total dose ($P=0.1099$) (Fig. 25.4).

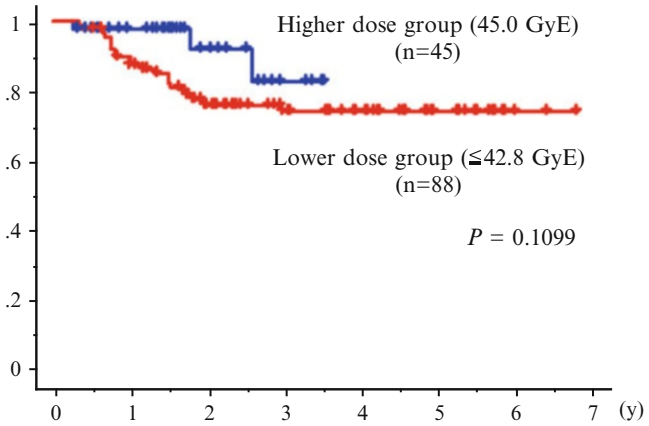

Fig. 25.4 Local control rates by total dose in 2 fractions of C-ion RT for hepatocellular carcinoma. One- and three-year local control rates were 98 and 83 % in the higher-dose group (45.0 GyE) and 90 and 76 % in the lower-dose group (≦42.8 GyE), respectively ($P=0.1099$)

In the higher-dose group, the local control rates were 97 and 100 % at 1 year and 81 and 80 % at 3 years in the smaller-tumor group (≦5 cm) and the larger-tumor group (>5 cm), respectively. Local control was not dependent on tumor size ($P=0.892$) (Fig. 25.5).

The overall survival rates were 95 and 96 % at 1 year and 71 and 59 % at 3 years in the higher-dose group (45.0 GyE)

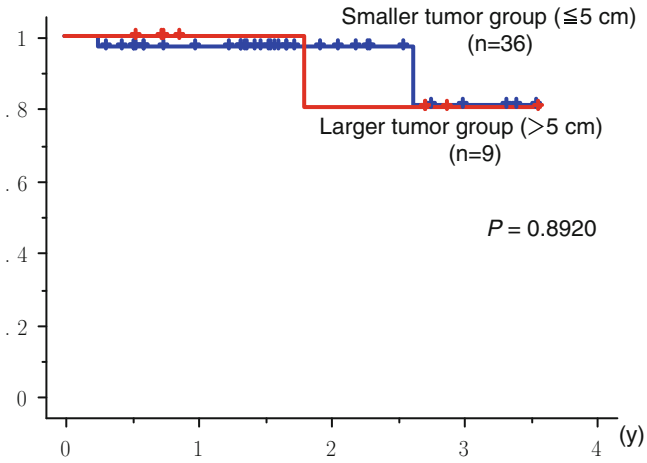

Fig. 25.5 Local control rates by tumor size in C-ion RT (45 GyE/2 fr) for hepatocellular carcinoma. 1- and 3-year local control rates were 97 and 81 % in the smaller-tumor group (≦5 cm) and 100 and 80 % in the larger-tumor group (>5 cm), respectively. Local control was not dependent on tumor size ($P=0.892$)

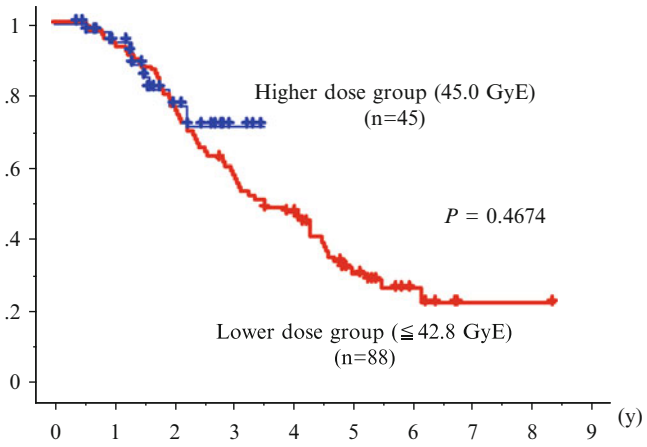

Fig. 25.6 Overall survival rates by total dose in 2 fractions of C-ion RT for hepatocellular carcinoma. One- and three-year overall survival rates were 95 and 71 % in the higher-dose group (45.0 GyE) and 96 and 59 % in the lower-dose group (≦42.8 GyE), respectively ($P=0.4674$)

and the lower-dose group (≦42.8 GyE), respectively. There was no significant difference ($P=0.4674$) (Fig. 25.6). In patients with a single lesion 5 cm or more in diameter, the overall survival rates were 88 % at 1 year, 61 % at 3 years, and 43 % at 5 years after C-ion RT. According to the report from the Liver Cancer Study Group of Japan [19], in patients with a single lesion 5–10 cm in diameter, the overall survival rates were 82 % at 1 year, 59 % at 3 years, and 44 % at 5 years after hepatic resection. Our outcomes seem to be comparable to those of hepatic resection.

Table 25.3 shows the results of proton and C-ion RT for HCC. The local control rates are similar, but C-ion RT has smaller fraction numbers.

25.6 Optimal Candidates for Carbon-Ion Radiotherapy

We have already reported that C-ion RT used for the treatment of HCC is safe and effective and that it causes only minor liver damage [16]. We investigated the reason why liver function is retained, and we found that nonirradiated lesion of the liver is considered to contribute to the retention of liver function [20]. For patients with extensive infiltration and those with multiple lesions, it is difficult to achieve radical cure with C-ion RT alone. C-ion RT is therefore indicated for patients with a level of liver function corresponding to Child-Pugh grade A or B. For small lesions 3 cm or less, however, other minimally invasive, effective, and low-cost therapies, such as PEI and RFA, are available. In contrast, lesions larger than 3 cm are difficult to treat with PEI or RFA alone, making them ideal targets for C-ion RT. Moreover, even for lesions less than 3 cm in diameter adjacent to the porta hepatis, minimally invasive treatment without complications is an important issue. We compared the efficacy and toxicity of C-ion RT of 52.8 GyE in 4 fractions for patients with HCC in terms of tumor location (adjacent to porta hepatis or not) and found that there were no significant differences in liver toxicity. Excellent local control was obtained

Table 25.3 Results of proton and C-ion RT for hepatocellular carcinoma

Type of radiation	Proton	Proton	Carbon
Facility	National Cancer Center Hospital East	University of Tsukuba	National Institute of Radiological Sciences
Number of patients	40	51	45
Maximum tumor diameter (mm)			
Median	45	28	35
Range	25–82	8–93	15–95
Total dose/fractionation	76 GyE/20 fr	66 GyE/10 fr	45 GyE/2 fr
Local control rate	2 years 96 %	3 years 94.5 %	2 years 94 %
		5 years 87.8 %	
Overall survival rate	3 years 66 %	3 years 49.2 %	3 years 73 %
		5 years 38.7 %	
References	Kawashima et al. [11]	Fukumitsu et al. [12]	

independent of the tumor location. Therefore, in certain patients with a higher risk of injury to the bile duct when undergoing RFA, C-ion RT appears to offer a promising therapeutic alternative [21].

C-ion RT is safe and effective, and it seems to be a definitive and minimally invasive radiation therapy for HCC. However, further careful follow-up is still needed to confirm its clinical efficacy in practical medicine.

References

1. Ingold DK, Reed GB, Kaplan HS, et al. Radiation hepatitis. Am J Roentgenol. 1965;93:200–8.
2. Phillips R, Murikami K. Primary neoplasms of the liver. Results of radiation therapy. Cancer. 1960;13:714–20.
3. Stillwagon GB, Order SE, Guse C, et al. 194 Hepatocellular cancers treated by radiation and chemotherapy combinations: toxicity and response: a Radiation Therapy Oncology Group study. Int J Radiat Oncol Biol Phys. 1989;17:1223–9.
4. Robertson JM, Lawrence TS, Dworzanin LM, et al. Treatment of primary hepatobiliary cancers with conformal radiation therapy and regional chemotherapy. J Clin Oncol. 1993;11:1286–93.
5. Xi M, Liu MZ, Deng XW, et al. Defining internal target volume (ITV) for hepatocellular carcinoma using four-dimensional CT. Radiother Oncol. 2007;84:272–8.
6. Sato K, Yamada H, Ogawa K, et al. Performance of HIMAC. Nucl Phys. 1995;A588:229–34.
7. Ohto M, Ebara M, Yoshikawa M, et al. Radiation therapy and percutaneous ethanol injection for the treatment of HCC. In: Okuda K, Ishak KG, editors. Neoplasm of the liver. Tokyo: Springer; 1987. p. 335–41.
8. Yasuda S, Ito H, Yoshikawa M, et al. Radiotherapy for large HCC combined with transcatheter arterial embolization and percutaneous ethanol injection therapy. Int J Oncol. 1999;15:467–73.
9. Cheng JC-H, Chuang VP, Cheng SH, et al. Local radiotherapy with or without transcatheter arterial chemoembolization for patients with unresectable HCC. Int J Radiat Oncol Biol Phys. 2000;47:435–42.
10. Guo W-J, Yu E-X. Evaluation of combined therapy with chemoembolization and irradiation for large HCC. Br J Radiol. 2000;73:1091–7.
11. Kawashima M, Furuse J, Nishio T, et al. Phase II study of radiotherapy employing proton beam for HCC. J Clin Oncol. 2005;23:1839–46.
12. Fukumitsu N, Sugahara S, Nakayama H, et al. A prospective study of hypofractionated proton beam therapy for patients with hepatocellular carcinoma. Int J Radiat Oncol Biol Phys. 2009;74:831–6.
13. Kanai T, Furusawa Y, Fukutsu K, Itsukaichi H, Eguchi-Kasai K, Ohara H. Irradiation of mixed beam and design of spread-out Bragg peak for heavy-ion radiotherapy. Radiat Res. 1997;147:78–85.
14. Kanai T, Endo M, Minohara S, et al. Biophysical characteristics of HIMAC clinical irradiation system for heavy-ion radiation therapy. Int J Radiat Oncol Biol Phys. 1999;44:201–10.
15. Tsujii H, Morita S, Miyamoto T, et al. Preliminary results of phase I/II carbon ion therapy. J Brachyther Int. 1997;13:1–8.
16. Kato H, Tsujii H, Miyamoto T, et al. Results of the first prospective study of carbon ion radiotherapy for hepatocellular carcinoma with liver cirrhosis. Int J Radiat Oncol Biol Phys. 2004;59:1468–76.
17. Endo M, Koyama-Ito H, Minohara S, et al. HIPLAN-a heavy ion treatment planning system at HIMAC. J Jpn Soc Ther Radiol Oncol. 1996;8:231–8.
18. Minohara S, Kanai T, Endo M, et al. Respiratory gated irradiation system for heavy-ion radiotherapy. Int J Radiat Oncol Biol Phys. 2000;47:1097–103.
19. Kudo M, Arii S, Ikari I, et al. Report of the 18th nationwide follow-up survey of primary liver cancer in Japan. Kanzo. 2010;51:460–84.
20. Imada H, Kato H, Yasuda S, et al. Compensatory enlargement of the liver after treatment of hepatocellular carcinoma with carbon ion radiotherapy – relation to prognosis and liver function. Radiother Oncol. 2010;96:236–42.
21. Imada H, Kato H, Yasuda S, et al. Comparison of efficacy and toxicity of short-course carbon ion radiotherapy for hepatocellular carcinoma depending on their proximity of the porta hepatis. Radiother Oncol. 2010;96:231–5.

Part XV

Pancreatic Cancer

Pancreatic Cancer

26

Shigeu Yamada, Kohtaro Terashima, Makoto Shinoto, Shigeo Yasuda, Miho Shiomi, and Tetsuro Isozaki

Abstract

Pancreatic cancer is the fifth leading cause of cancer death and is considered to be one of the most lethal cancers in Japan. Complete surgical resection is the only curative treatment. Even if curative resection is performed, the disease usually recurs, and 5-year survival rates are less than 20 %. Chemotherapy or chemoradiotherapy is selected as a standard treatment for unresectable pancreatic cancer. However, since pancreatic cancer is often resistant to chemotherapy and radiotherapy, the local control and survival rates are very low.

We conducted a phase I/II clinical trial using carbon ion radiotherapy (C-ion RT) for patients with operable and locally advanced pancreatic cancer. This was delivered preoperatively in 8 fractions over 2 weeks, was well tolerated, and resulted in excellent local control and survival rates. C-ion RT for patients with locally advanced pancreatic cancer was also well tolerated, even when concomitantly administered with the highest dose of gemcitabine (1,000 mg/m^2), and likewise resulted in a good survival rate.

In this chapter, we discuss current treatment methods and the results of C-ion RT for pancreatic cancer at the National Institute of Radiological Sciences.

Keywords

Carbon-ion • Pancreatic cancer • Radiation

26.1 Introduction

More than 26,000 people die of pancreatic cancer in Japan each year, and this number continues to increase [1]. Pancreatic cancer is also the fifth leading cause of cancer death and is considered to be one of the most lethal cancers in Japan. Complete surgical resection is the only curative treatment. However, only a small percentage of patients (10–20 %) are candidates for surgical resection because of local progression or metastatic spread at the time of diagnosis [2]. Even if a curative resection is performed, the disease usually recurs and 5-year survival rates are less than 20 % [3]. In cases where the cancer cannot be resected, chemotherapy and chemoradiotherapy are the standard treatments [4]. However, since pancreatic cancer is often resistant to both these treatments, the local control rate is very low. Recently, along with the development of new anticancer agents, more advanced radiotherapy techniques have also been introduced [5, 6]. However, these therapies still fail to provide a satisfactory outcome in most cases, and the median survival is still only approximately 10 months.

S. Yamada (✉) • S. Yasuda • M. Shiomi • T. Isozaki
National Institute of Radiological Sciences,
4-9-1 Anagawa, Inage-ku, Chiba, Japan
e-mail: s_yamada@nirs.go.jp

K. Terashima • M. Shinoto
National Institute of Radiological Sciences,
4-9-1 Anagawa, Inage-ku, Chiba, Japan

Graduate School of Medical Sciences, Kyushu University,
Fukuoka, Japan

H. Tsujii et al. (eds.), *Carbon-Ion Radiotherapy: Principles, Practices, and Treatment Planning*,
DOI 10.1007/978-4-431-54457-9_26,

26.2 Carbon Ion Radiotherapy

Koong measured the oxygen concentration in seven pancreatic tumors intraoperatively using the Eppendorf polarographic needle electrode system [8]. All seven of these tumors were revealed to have significant hypoxia, in contrast to the adjacent normal pancreas that had a normal oxygen concentration [7].

Hypoxic cells are 2–3 times more resistant than cancer cells exposed to normal oxygen levels [8]. Tumor hypoxia has been shown to be a major biological cause of local treatment failure after radiation therapy. However, when using carbon ion radiotherapy (C-ion RT), the radiosensitivities of hypoxic cells and normoxic cells are almost the same. Carbon ions are more effective at killing hypoxic cells. Furthermore, although pancreatic cancer stem cells have been shown to be resistant to conventional chemotherapy and radiation [9], carbon ion beams have greater efficacy for killing this cell type. This may be due to the prolonged induction of DNA damage caused by C-ion RT compared to X-rays [10].

Carbon ion beams are also safer than conventional radiological approaches. There are complicated neuroplexus structures around the main arteries of the pancreas, and these are the site of most local recurrences. These sites therefore need to be irradiated, even though they are close to radiosensitive organs such as the stomach, duodenum, and spinal cord. Heavy-ion beams exhibit unique depth-dose curves that offer the potential advantage of safely delivering a biological effective dose to the tumor whilst sparing these organs.

Figure 26.1 shows the dose distribution for a cancer of the pancreatic head. The patient received a 48 GyE carbon ion beam dose. A sufficient dose can be delivered to the tumor and neuroplexus without increasing the dose to surrounding organs such as the stomach and duodenum.

26.3 The Pancreatic Cancer Trial at National Institute of Radiological Sciences

We started a phase I/II clinical trial for preoperative C-ion RT delivered in 16 fractions over 4 weeks for resectable pancreatic cancer in 2000 (Fig. 26.2).

The purpose of this treatment was to reduce the risk of postoperative local recurrence, which accounts for approximately 50 % of all recurrences. We established the tolerance and effectiveness of preoperative C-ion RT and performed an additional clinical trial aimed at reducing the number of fractions to 8, delivered over 2 weeks beginning in 2003 (protocol 0203). In addition, we started a phase I/II clinical trial for patients with locally advanced pancreatic cancer and showed that the treatment was safe and provided excellent local control rates. As a result, we are currently performing a clinical trial using C-ion RT combined with gemcitabine (protocol 0513).

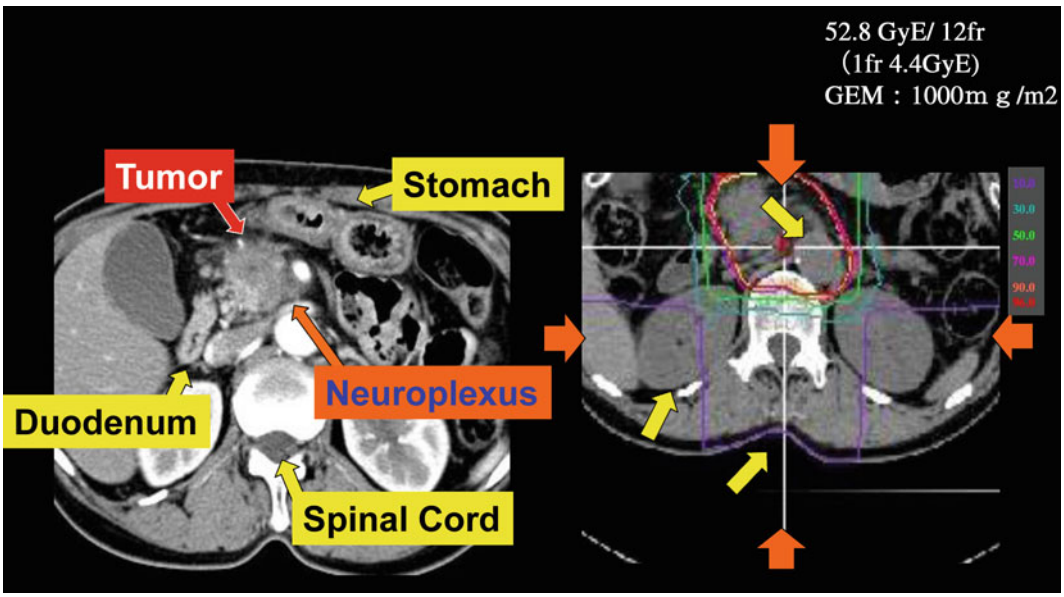

Fig. 26.1 Typical dose distribution for pancreatic cancer. The image is from a case of a 75-year-old man with cancer in the head of the pancreas that received 52.8 GyE/12 fr. It is possible to deliver a high dose to the tumor and neuroplexus whilst minimizing the dose to the surrounding organs such as the stomach or duodenum

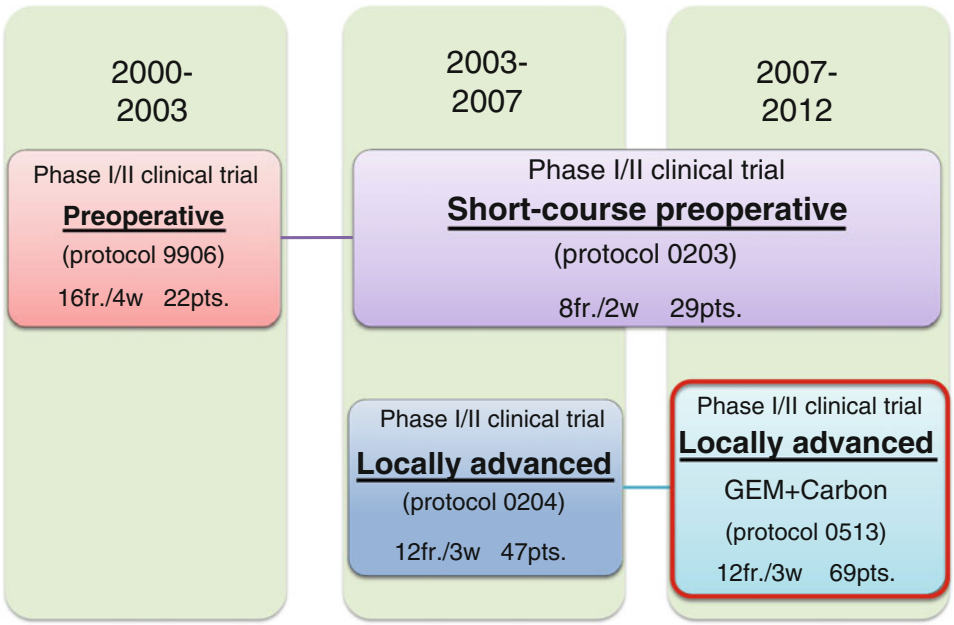

Fig. 26.2 The clinical trial pathway for C-ion RT in pancreatic cancer

26.4 Carbon Ion Radiotherapy Methodology at National Institute of Radiological Sciences

The key features of the accelerator and the carbon ion beam have been described previously [11].

26.4.1 Patient Immobilization

The patient needs to be immobilized during C-ion RT for pancreatic cancer as is the case for other tumor sites. C-ion RT at facilities with the most powerful heavy-ion beams is performed with fixed beam directions that are vertical, horizontal, or at a 45-degree oblique angle to the target. However, recurrent rectal tumors can be located anywhere in the pelvis, including the presacral region and iliac and mesenteric lymph nodes, and therefore, the direction of the carbon ion beam needs to be varied. Furthermore, it is usually necessary to use more than two ports in order to obtain a dose distribution that avoids the bowels and the skin. Consequently, complex immobilization is frequently required.

At the National Institute of Radiological Sciences (NIRS), this was achieved using relatively thick, low-temperature thermoplastic (Shellfitter; Keraray Co., Ltd., Osaka, Japan), a sufficiently large customized cradle (Moldcare; Alcare, Tokyo, Japan), and a rotatable couch on the treatment bed.

Management of respiratory motion is also essential in most cases of recurrent rectal cancer (see Chap. 9, Motion Management). There are many different methods for motion management. At the NIRS, synchronization with respiration is adopted during both computed tomography (CT) image acquisition and during every C-ion RT session, irrespective of the direction of the beam. The effect of respiratory motion when using a vertical beam is less than that when using a horizontal beam for a pelvic tumor. However, this is mainly due to differences in the length of the air gap, and it is desirable to irradiate the tumor using similar conditions to those established by dose calculations using CT images taken during the expiratory phase.

26.4.2 Target Delineation

A set of 2.5-mm-thick CT images along the whole abdomen were taken for treatment planning, with the patient placed in immobilizing devices and with respiratory gating.

Field arrangements were generally designed using a 3- or 4-field plan. The gross tumor volume (GTV) was established using CT images and margins for possible subclinical tumor spread, and magnetic resonance imaging (MRI) and fludeoxyglucose (FDG)-positron emission tomography were used to diagnose tumor spread. The clinical target volume (CTV) was defined as the gross volume plus 0.5 or 0 cm (in contact with the duodenum or stomach). The CTV included the GTV, neuroplexus, and regional lymph nodes.

The latter consisted of the celiac, superior mesenteric, common hepatic, and peri-pancreatic lymph nodes (Fig. 26.1). At least 50 % of the functioning renal parenchyma received a dose of 15 GyE or less, and the spinal cord dose was limited to 30 GyE or less. Planning target volume (PTV) is defined as the CTV with a margin of at least 5 mm in all directions, although these margins are modified if critical organs, such as the skin or bowels, are close to the tumor.

26.4.3 Dose Prescription

The current recommended dose is 55.2 GyE delivered in 12 fractions for locally advanced pancreatic cancer and 35.2 GyE delivered in 8 factions for resectable pancreatic cancer. The whole of the prescribed dose is given at the maximum dose point of each portal, and treatment planning is performed so that the PTV is covered with at least 90 % of the prescribed dose. For this purpose, additional margins are necessary to determine the shape of the collimator and compensation bolus. Figure 26.1 shows a representative dose distribution for C-ion RT as it is currently used at the NIRS.

Major organs at risk during this treatment are the stomach, duodenum, intestine, kidney, and spinal cord. It is particularly important to spare the bowels from the high-dose area of the carbon ion beam. At the NIRS, dose constraints for the digestive tract are established on the basis of the treatment results for prostate, uterine, cervical, and recurrent rectal cancers, where the maximum dose to the colon should not exceed 83 % of the prescribed dose.

26.4.4 Field Positioning and Irradiation at National Institute of Radiological Sciences

At the NIRS, C-ion RT is performed once a day and in 4 fractions per week (from Tuesday until Friday). The field is verified at every treatment session using a computer-aided online positioning system to prevent the positioning error exceeding 2 mm. A fluoroscopic image is taken during the expiration phase of respiration and compared with the reference images, including the image taken during the previous simulation or the digitally constructed radiograph. C-ion RT is performed with respiration gating as described above, where the carbon ion beam is delivered only during the expiration phase.

26.5 Results of Carbon Ion Radiotherapy Used at the National Institute of Radiological Sciences

26.5.1 Preoperative Carbon Ion Radiotherapy for Patients with Resectable Pancreatic Cancer

The purpose of this study was to evaluate the safety and efficacy of C-ion RT as preoperative treatment and to determine the optimum dose needed to reduce the risk of postoperative local recurrence without causing unacceptable damage to normal tissue.

The eligibility criteria for this study were that the pancreatic cancer was judged radically resectable and that it did not involve the celiac trunk or superior mesenteric artery. We performed C-ion RT with 8 fractions over 2 weeks, followed by resection 2–4 weeks later (Fig. 26.2). The first dose was 30 GyE over 8 fractions, and this was then increased in 5 % increments.

Twenty-six patients were enrolled between April 2003 and December 2010, and the initial dose of 30 GyE was ultimately escalated to 36.8 GyE.

We administered C-ion RT to all patients as scheduled. The clinical stage according to the UICC was IIA in 15 cases and IIB in 11 cases. Twenty-one out of 26 patients received curative resection (resection rate 81 %), although the remaining five patients did not undergo surgery due to liver metastases or refusal of treatment. Although grade 3/4 toxicities were noted in 2 patients (liver abscess in one and PV thrombus in the other), neither were directly related to C-ion RT. No other serious adverse effects were observed. In the 21 surgical cases, the 5-year local control and overall survival rates were 100 and 52 %, respectively (Fig. 26.3). In the literature, the reported 5-year survival rates for pancreatic cancer treated with resection were 20–30 % (Table 26.1).

26.5.2 Carbon Ion Radiotherapy for Patients with Locally Advanced Pancreatic Cancer

The phase I/II trial of C-ion RT (12 fractions/3 weeks) for locally advanced pancreatic cancer was performed in order to evaluate its safety and efficacy and to determine the optimum dose.

Between April 2003 and February 2007, 47 patients with stage IVa or IVb cancer but without distant metastases, as

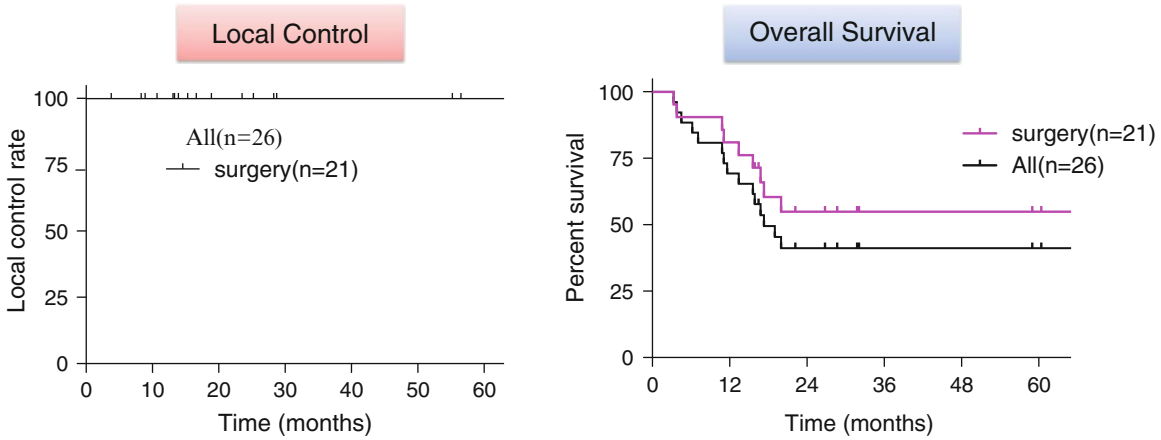

Fig. 26.3 Local control and overall survival. The local control rate in all patients was 100 %. There were no cases of recurrence within the irradiated lesion. The 5-year OS rate among patients who underwent resection was 55 %

Table 26.1 Results of preoperative chemoradiotherapy

	Year	*n*	Treatment	Local recurrence (%)	Survival	
					1 year (%)	5 years (%)
Moutardier [1]	2004	40	CRT + surgery	–	80	30
CONKO-001 [2]	2007	161	Surgery only	41	73	12
		133	Surgery + GEM	34	73	23
Varadhachary [3]	2008	52	CRT + surgery	25	98	32
Le Scodan et al. [4]	2009	26	CRT + surgery	–	48	25
NIRS		21	CIRT + surgery	0	81	55

defined by the staging criteria of the Japanese Committee on Cancer (corresponding to stage III based on the TNM classification), were enrolled into this trial. One patient was excluded because he received chemotherapy before treatment, and thus, a total of 46 patients were eligible for this analysis. Patients eligible for study entry had histologically or cytologically confirmed locally advanced and unresectable pancreatic ductal carcinoma. The basis on which the tumor was judged to not be resectable was a CT finding of tumor encasement of the celiac trunk and/or superior mesenteric artery. C-ion RT was administered once daily, 4 days a week to give a total of 12 fractions in 3 weeks. The dose was set at 38.4 GyE and escalated to 52.8 GyE at 5 % increments.

All patients completed the scheduled treatment course. One grade 3 late toxicity and seven grade 3 acute toxicities were observed. Six of the seven grade 3 acute toxicities were anorexia and the other was cholangitis. Tumor response was evaluated in 46 lesions. A CR was achieved in 1 lesion, a PR in 7, SD in 37, and PD in a single lesion. The 1-year overall local control rate and the 1-year control rate for patients receiving at least 45.6 GyE were 76 and 95 %, respectively. The 1-year overall survival estimate for the 46 analyzed patients was 43 %.

The maximum grade 3 acute reaction occurred in two-thirds of the patients (67 %) receiving 52.8 GyE. From these results, we concluded that the maximum tolerated dose of carbon ions is 52.8 GyE/12 fractions/3 weeks.

On the basis of previous studies of drugs that can sensitize tumors to heavy-particle beam radiation, further studies were scheduled in an effort to find even more effective treatment modalities based on a combination of chemotherapy and radiotherapy. We started a phase I/II clinical trial of gemcitabine combined with carbon ion radiotherapy (C-ion RT) for patients with local advanced pancreatic cancer from April 2007.

26.5.3 Gemcitabine Combined with Carbon Ion Radiotherapy for Patients with Locally Advanced Pancreatic Cancer

The purpose of this trial was to establish the optimum dose of gemcitabine (a standard anticancer agent for advanced pancreatic cancer) and C-ion RT and to evaluate the safety and efficacy of this combination.

The eligibility requirement for this study was that patients should have locally advanced pancreatic cancer

involving the celiac trunk or superior mesenteric artery without distant metastasis. All patients had histologically or cytologically proven pancreatic adenocarcinoma or adenosquamous carcinoma. The radiation fractions were fixed at 12 fractions over 3 weeks, and the dose of gemcitabine and radiation was gradually increased. The radiation dose was fixed at 43.2 GyE/8 fractions and the initial gemcitabine dose was 400 mg/m^2, which was increased to 700 and then to 1,000 mg/m^2. Subsequently, the gemcitabine dose was kept at 1,000 mg/m^2 and the radiation dose was increased in 5 % increments. Gemcitabine was administered once a week for three consecutive weeks. The irradiation field was set to include the primary tumor, perineural lesions, and a prophylactic regional lymph node area.

Sixty patients were enrolled from April 2007 through February 2011. Patients were treated with C-ion RT at five dose levels together with concurrent weekly gemcitabine over three dose levels.

Their clinical stage based on the UICC was III in 54 cases and IV in 6 cases. Dose-limiting toxicity developed as an early adverse event in only three of these 60 patients. One patient treated at the 50.4 GyE dose level suffered a grade 3 gastric ulcer 10 months after C-ion RT, but subsequently recovered with conservative management. No other serious side effects were noted. Treatment combinations that included full-dose gemcitabine (1,000 mg/m^2) did not result in any increased incidence of adverse effects with dose escalation. The 2-year local control rate and 2-year overall survival rate were 26 and 32 %, respectively, and the median

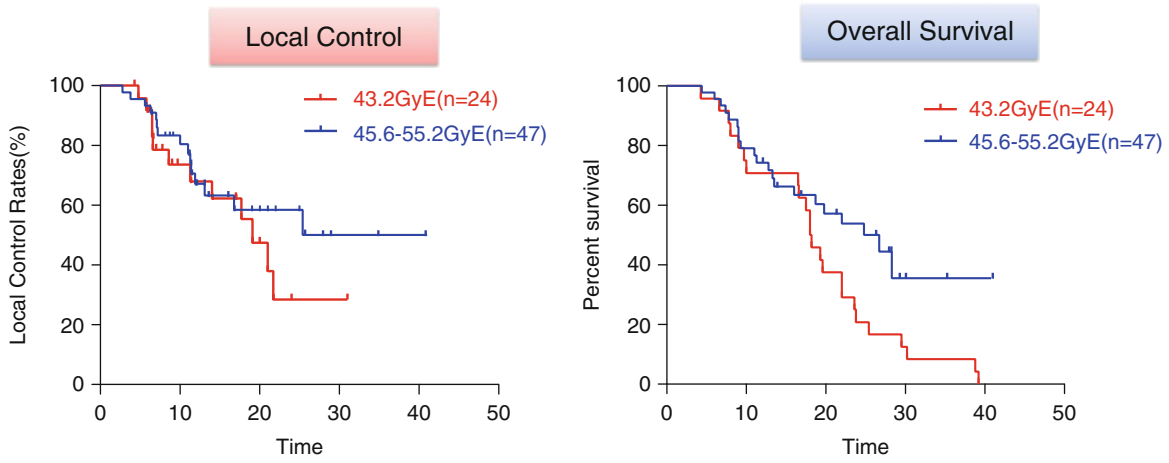

Fig. 26.4 Local control and overall survival by total dose. For doses greater than 45.6 GyE, the 2-year local control rate was 58 % and the overall survival rate was 54 %, both of which are higher than in the low-dose group

Table 26.2 Results of chemoradiotherapy for locally advanced pancreatic cancer reported by other studies

					Survival	
	Year	*n*	Treatment	Dose	1 year (%)	2 years (%)
ECOG	2008	34	GEM + RT	50.4 Gy	50	12
		37	GEM	–	32	4
Ishii	2010	50	GEM	–	64	14
Sudo	2011	34	S-1 + RT	50.4 Gy	71	25
Small	2011	28	GEM + BZ[a] + RT	36 Gy/15 fr	45	17
Schellenberg	2011	20	GEM + SBRT	25 Gy/1 fr	50	20
NIRS		47	GEM + CIRT	45.6–55.2 GyE	74	54

[a]Bevacizumab

survival time was 19.3 months. The local control and overall survival increased with increasing C-ion RT dose. In the high-dose group, in which patients were irradiated with at least 45.6 GyE, the 2-year local control and 2-year overall survival rates were 58 and 54 %, respectively (Fig. 26.4). In the literature, the reported 2-year survival rates for locally advanced pancreatic cancer were 10–25 % (Table 26.2).

26.6 Future Perspectives

26.6.1 Scanning Irradiation

In 2011, beam delivery using spot scanning became available at the NIRS. It continues to be used to target lesions without significant respiratory movement at the time of writing (April 2013). However, spot-scanning irradiation for mobile targets is currently under development and will be realized in the near future. Further improvements in the long-term outcome of treatment are expected with further dose escalation.

Scanning irradiation can provide even better dose distribution than the passive method in the treatment of a number of tumor types because it is much more flexible. When using passive irradiation, a uniform length of the spread-out Bragg peak must be used in each field, but this often gives rise to an unnecessarily high dose to the surrounding normal tissue. The use of scanning irradiation avoids this and it is in fact possible to reduce the dose to the normal tissue even more by accepting the high-dose spot inside the target, if desirable.

Figure 26.5 shows the dose distribution using both broad and scanning beams; the latter results in a lower dose to the spinal cord and kidney. A further advantage of broad-beam irradiation is the lack of any requirement for collimator or compensation bolus, reducing the preparation time between CT acquisition and the start of treatment and reducing the total cost of the procedure. In addition, a rotating gantry can be used with the carbon ion beam. As a result, patients need not be immobilized in an uncomfortable, inclined position, as they do currently when C-ion RT with passive irradiation is used.

26.7 Case Study

The case was a 66-year-old Japanese man who was referred to the NIRS with a diagnosis of pancreatic cancer (Fig. 26.6).

The C-ion RT was performed with four anterior-posterior (A-P), P-A, and bilateral ports and the total dose was 50.4 GyE in 12 fractions. The CT at 40 months post treatment and the FDG accumulation at 6 months post treatment both demonstrated the disappearance of the tumor. The patient remains disease free 70 months after treatment and currently does not require medication.

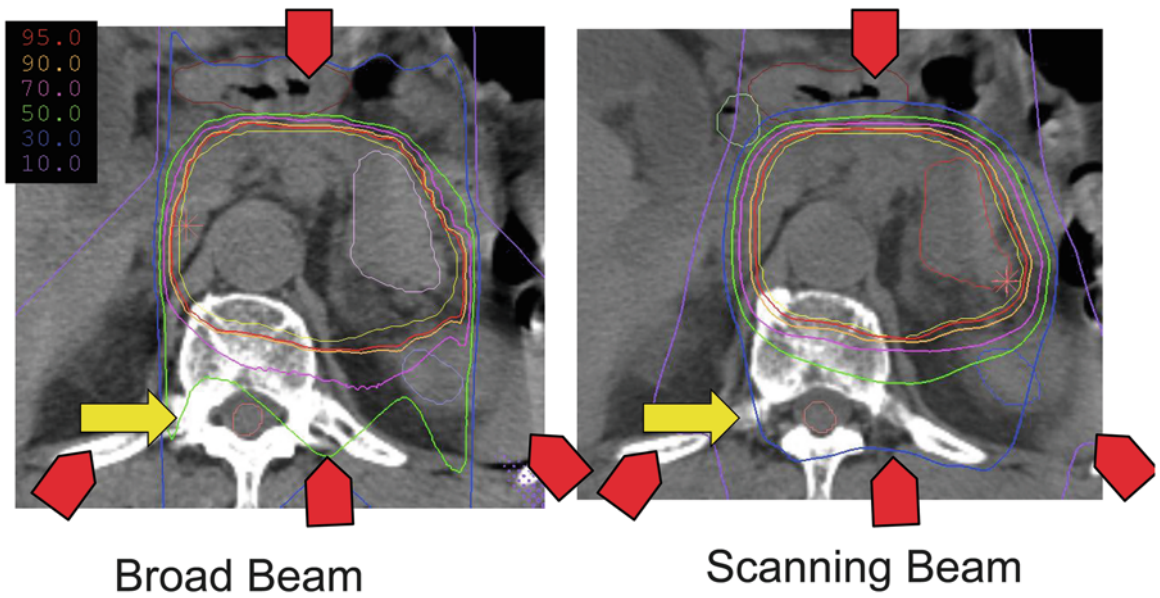

Fig. 26.5 The difference between broad-beam and scanning beam irradiation. The *left* and *right panels* show the dose distribution by broad-beam and scanning beam irradiation, respectively. Broad-beam delivery results in a lower dose to the spinal cord and the kidney

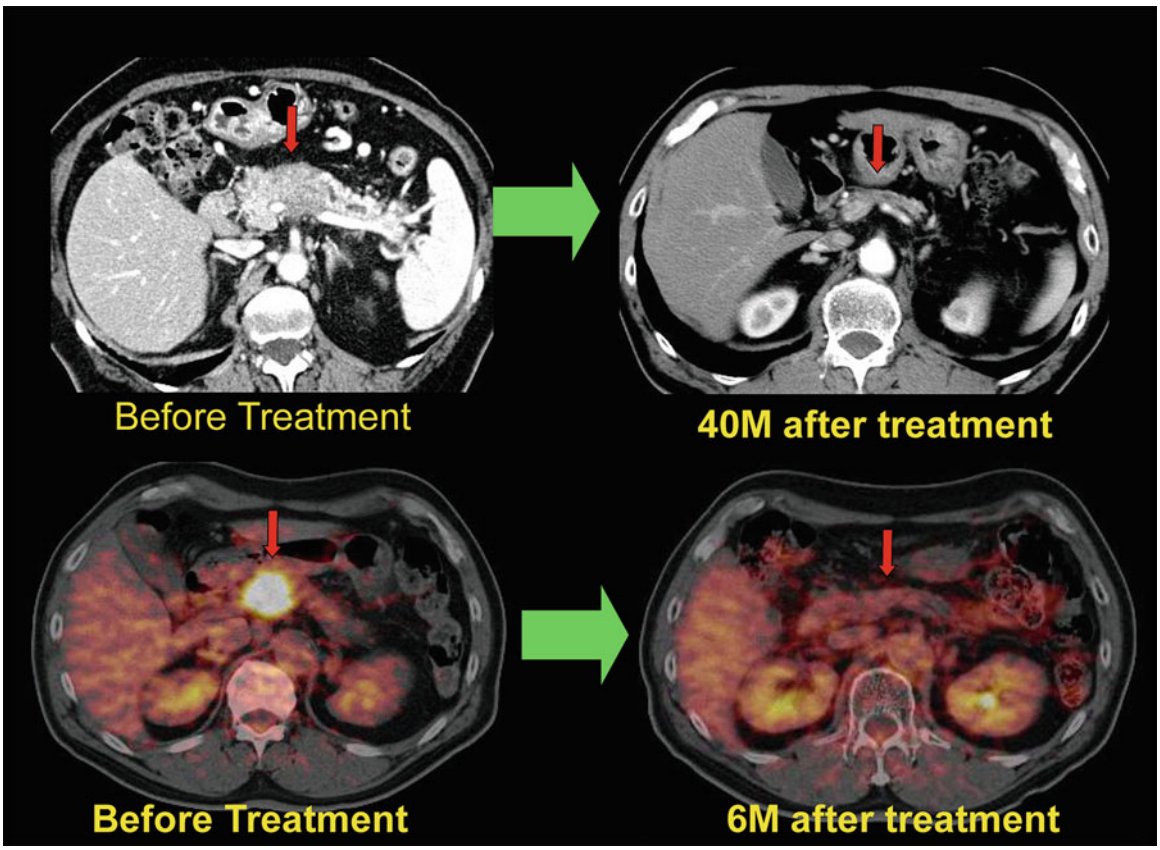

Fig. 26.6 This patient was a 66-year-old man with pancreatic cancer. He received a total dose of 50.4 GyE via carbon ion beams in 12 fractions. Both the CT at 40 months and the FDG accumulation at 6 months post treatment demonstrated the disappearance of the pancreatic tumor

References

1. Registration committee of pancreatic cancer. Annual report of nationwide survey of pancreatic cancer. J Jpn Panc Surg. 2003;18:1–169.
2. Lillemoe KD, Cameron JL, Hardacre JM, et al. Is prophylactic gastrojejunostomy indicated for unresectable periampullary cancer? Ann Surg. 1999;230:22–330.
3. Griffin JF, Smalley SR, Jewell W, et al. Patterns of failure after curative resection of pancreatic carcinoma. Cancer. 1990;66:56–61.
4. Lillemoe KD, Cameron JL, Hardacre JM, et al. Is prophylactic gastrojejunostomy indicated for unresectable periampullary cancer? Ann Surg. 1999;230:322–30.
5. Roldan GE, Gunderson LL, Nagorney DM, et al. External beam versus intraoperative and external beam irradiation for locally advanced pancreatic cancer. Cancer. 1988;61:1110–6.
6. Moertel CG, Gundeson LL, Mailliard JA, et al. Early evaluation of combined fluorouracil and leucovorin as a radiation enhancer for locally unresectable, residual, or recurrent gastrointestinal carcinoma. J Clin Oncol. 1994;12:21–7.
7. Koong AC, Mehta VK, Le QT. Pancreatic tumors show high levels of hypoxia. Int J Radiat Oncol Biol Phys. 2000;48:919–22.
8. Ando K, Koike S, Ohira C, et al. Accelerated reoxygenation of a murine fibrosarcoma after carbon-ion radiation. Int J Radiat Biol. 1999;75:505–12.
9. Lee CJ, Dosch J, Simeone M. Pancreatic cancer stem cells. J Clin Oncol. 2008;26:2806–12.
10. Oonishi K, Cui X, Hirakawa H. Different effects of carbon ion beams and X-rays on clonogenic survival and DNA repair in human pancreatic cancer stem-like cells. Radiother Oncol. 2012;103:32–7.
11. Kamada T, Tsujii H, Tsuji H, et al. Efficacy and safety of carbon ion radiotherapy in bone and soft tissue sarcomas. J Clin Oncol. 2002;20:4466–71.

Part XVI

Genitourinary Tumors

Prostate Cancer

27

Hiroshi Tsuji, Hitoshi Ishikawa, and Takuma Nomiya

Abstract

Localized prostate cancer, particularly locally advanced cancer, is a good indication for carbon-ion therapy. The carbon-ion beam can offer the most concentrated dose distribution among the various types of state-of-the-art radiation therapies, including intensity-modulated radiotherapy (IMRT), stereotactic body radiotherapy (SBRT), and proton radiotherapy. Furthermore, an improvement of the therapeutic ratio can also be expected with the higher biological effect of the carbon-ion beam [1, 2]. To evaluate these possible advantages of the carbon-ion beam in the treatment of prostate cancer, the National Institute of Radiological Sciences (NIRS) conducted clinical trials of carbon-ion radiotherapy (C-ion RT), and favorable outcomes have been obtained with a hypofractionated regimen. The trials were started in 1995, and two consecutive phase I/II dose-escalation studies with a fractionation of 20 fractions over 5 weeks were conducted to establish techniques using the carbon-ion beam and to determine the optimal dose fractionations. Consequently, a phase II study was performed to validate the feasibility and efficacy of C-ion RT delivered in 20 fractions and was successfully completed in 2003 [3–6]. Thereafter, hypofractionated C-ion RT delivered in 16 fractions over 4 weeks was also performed, by which more favorable results in terms of late radiation toxicity were achieved, without increases in recurrence [7]. Currently, even more hypofractionated radiotherapy with 12 fractions in 3 weeks is being evaluated in clinical practice.

In this chapter, the treatment method established by the clinical studies and the up-to-date outcomes based on the experience of more than 1,700 patients at NIRS are described. In addition, our recent challenges and future directions will also be discussed.

Keywords

Androgen deprivation therapy • Carbon-ion radiation therapy • Hypofractionation • Prostate cancer • Survival rate

H. Tsuji (✉) • T. Nomiya
National Institute of Radiological Sciences,
4-9-1 Anagawa, Inage-ku, Chiba, Japan
e-mail: h_tsuji@nirs.go.jp

H. Ishikawa
Proton Medical Research Center, Tsukuba University,
Tsukuba, Japan

H. Tsujii et al. (eds.), *Carbon-Ion Radiotherapy: Principles, Practices, and Treatment Planning*,
DOI 10.1007/978-4-431-54457-9_27, © Springer Japan 2014

27.1 Introduction

27.1.1 Features of Carbon-Ion Radiotherapy

According to a structural survey conducted by the Japanese Society for Therapeutic Radiology and Oncology [8], the number of prostate cancer patients treated with RT has been increasing annually in Japan which is similar to the situation in Western countries. The major reason why RT has been playing a more significant role in the curative treatment for prostate cancer is that the modern 3-dimensional RT can deliver a sufficient dose to the tumor and allow the sparing of surrounding normal tissues. Indeed, state-of-the-art RT, such as brachytherapy, intensity-modulated radiotherapy (IMRT), stereotactic body radiotherapy (SBRT), and charged particle therapy, has achieved considerably better tumor control with minimum morbidity when compared to conventional RT [9–11]. Among these advanced modalities, C-ion RT has theoretical advantages in terms of both a physical and biological perspective.

A well-known physical property of a charged particle beam as based on the Bragg peak in the depth-dose curve is indeed advantageous in cancer therapy [12, 13]. In addition, carbon ions having less scattering in the body can offer a more concentrated dose deposition, allowing the irradiated volume of the rectum to be minimized. Moreover, the carbon-ion beam has additional advantages in biological effects [14], as confirmed in the treatment of radioresistant tumors such as bone and soft-tissue sarcomas and non-squamous cell cancer in the head and neck region [1, 15, 16]. Although the radiobiological benefits of C-ion RT may remain controversial in the treatment of prostate cancer, the experience at NIRS has apparently demonstrated the benefit of high-linear-energy-transfer (LET) radiation in the treatment of prostate cancer with hypofractionated C-ion RT.

27.1.2 The Benefit of Hypofractionated RT for Prostate Cancer

Hypofractionated RT for prostate cancer has recently attracted much attention because of the relatively low value of the α/β ratio for prostate cancer when compared with those of other cancers and the surrounding normal tissues, including the rectum, bladder, and urethra [17]. Based on the linear quadratic (LQ) model [18], hypofractionated RT therefore has benefits in view of both improving local tumor control and reducing the risk of gastrointestinal and genitourinary morbidities [19–21]. Indeed, IMRT and high-dose-rate (HDR) brachytherapy with hypofractionation have yielded favorable outcomes for prostate cancer, with morbidity rates comparable to those of high-precision three-dimensional conformal RT (3D-CRT) with conventional fractionation [9, 22]. Kupelian et al. [23] reported that the long-term outcomes of hypofractionated IMRT with a total dose of 70 Gy in 28 fractions with a fractional dose of 2.5 Gy were at least equivalent to those with 81 Gy given in 45 fractions as reported by Zelefsky et al. [10]. In the study by Kupelian et al., grade 2 or severe late rectal toxicity was observed only in 5 % of patients at the last follow-up. Therefore, these results may support that the use of modern RT modalities, such as IMRT, HDR, and charged particle RT, which can provide a well-localized dose to the target, can minimize rectal toxicity even when a hypofractionated regimen was applied. Clinical trials (two phase I/II and one phase II trials) at NIRS were also performed with a hypofractionated schedule [3–6], and favorable results were obtained. Moreover, with an advance in hypofractionation from 20 fractions to 16 fractions, an improvement of outcomes was achieved, particularly with respect to toxicities [7]. Based on these favorable outcomes with the hypofractionated RT, a new clinical trial on C-ion RT delivered in 12 fractions over 3 weeks was started in 2010.

27.2 Clinical Trials at NIRS

Between July 1995 and December 1997, the first dose-escalation study of C-ion RT for prostate cancer was carried out at NIRS to determine the optimum dose level for C-ion RT, and the second phase I/II study was started in January 1998 for both early and advanced prostate cancer (Table 27.1). The second study was successfully completed in March 2000 with no grade 3 or worse late complications [3–5]. After these results were taken into consideration, a phase II clinical study was designed to further confirm the effectiveness of C-ion RT using a fixed dose fractionation schedule of 66 GyE in 20 fractions over 5 weeks [6]. This clinical trial was conducted between April 2000 and October 2003. At the end of the study, the approval of the Japanese government for advanced medicine was given to C-ion RT at NIRS, and a further move in the direction toward a more hypofractionated regimen of 16 fractions over 4 weeks was started. A total dose of 57.6 GyE in 16 fractions was adopted, and the effectiveness and safety of C-ion RT with this dose fractionation was confirmed [7]. Furthermore, a new clinical trial of C-ion RT with 12 fractions over 3 weeks was carried out in 2010 to establish a more hypofractionated regimen for C-ion RT in 2010. Forty-six patients were enrolled, and none of the patients has developed grade 2 or worse toxicity or biochemical recurrence. Although the observation period was still short to evaluate the efficacy of this new fractionation, the incidence of toxicity was sufficiently low, and therefore NIRS decided to apply this fractionation to all cases of prostate cancer from April 2013.

Table 27.1 Clinical trials for prostate cancer at NIRS

Protocol ID	Study design	Dose fractionation (GyE/fractions/weeks)	Materials	Period	Number of patients (~13.3)
9402	Dose escalation	54.0–72.0/20/5	T2b–T3N0M0	95.6–97.12	35
9703	Dose escalation	60.0–66.0/20/5	T1–T3N0M0	98.1–00.2	61
9904 (1)	Phase II	66.0/20/5	T1–T3N0M0	00.4–03.11	175
9904 (2)	AM*	66.0, 63.0/20/5	T1–T3N0M0	03.12–07.8	291
9904 (3)	AM	57.6/16/4	T1–T3N0M0	07.9	1,107
1002	Dose escalation	51.6/12/3	T1–T3N0M0	10.7–12.2	64
Total				95.6	1,733

*Advanced Medicine

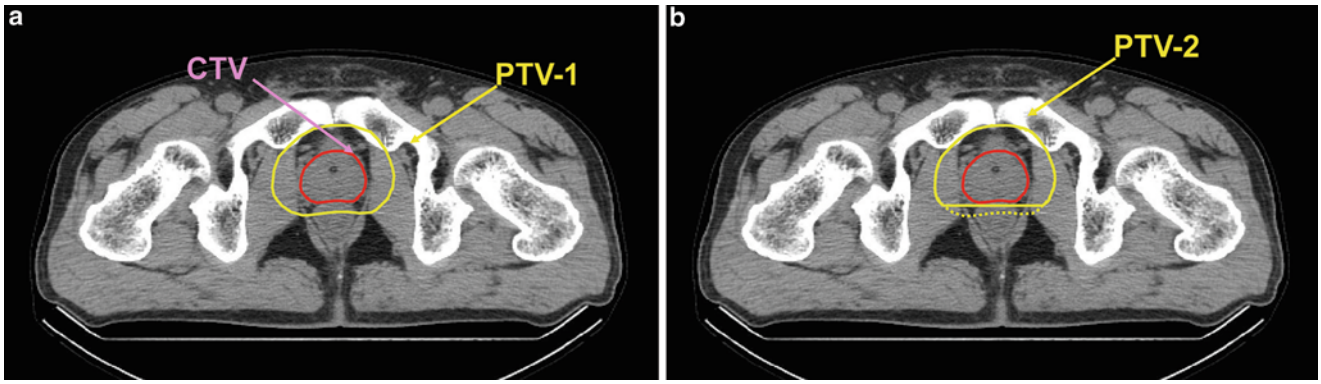

Fig. 27.1 (**a**) Clinical target volume is the prostate and seminal vesicle in principle, but the whole seminal vesicle is not always included, mainly depending on clinical stage. The initial planning target volume, PTV-1, is defined as the CTV plus 10-mm margins in all directions except for posterior margins of 5 mm. (**b**) For the latter half of the treatment at the NIRS, the posterior margin is reduced to the anterior boundary of the rectum to form the secondary planning target volume, PTV-2, for reducing the risk of rectal toxicity

27.3 Methods of C-Ion RT at NIRS

27.3.1 Patient Immobilization

For patient immobilization, the patient is placed in a supine position and devices for immobilizing the feet and pelvis are fabricated. First, using customized cradles (Moldcare; Alcare, Tokyo, Japan), the feet are immobilized to avoid inter-fractional variation in the position and angle of the feet and toes. Next, the pelvis is tightly immobilized with a low-temperature thermoplastic (Shellfitter; Keraray Co., Ltd., Osaka, Japan). The effects of respiration on prostate motion were evaluated based on the analysis of 4-dimensional CT images [5, 24]. It was confirmed that, with these immobilization devices, the prostate movement with respiration was almost negligible so that we decided not to employ respiratory-gated irradiation in C-ion RT of prostate cancer at NIRS.

When the irradiation is applied from the anterior direction, the bladder is filled with a known volume (e.g., 100 mL) of sterilized water both at the time of CT acquisition and at each treatment session. However, when only the lateral fields are used (e.g., a treatment of 12 fractions with scanning irradiation at NIRS), it is not needed to fill the bladder with sterilized water, and the bladder volume is just measured with planning CT images.

A rectal balloon is not used. Instead, the patients are instructed to empty the rectum in his/her daily effort and to use a laxative or enema, if necessary.

27.3.2 Target Delineation

With the patient lying in the immobilization devices, a set of 2.5-mm-thick CT images is taken for treatment planning. The clinical target volume (CTV) is defined as comprising the prostate and seminal vesicle (SV), as demonstrated on CT images, irrespective of T-stage and risk factors (Fig. 27.1a). However, the whole SV is not always included in the CTV for patients with a low risk. For example, the CTV of patients staged T1 or T2a does not cover the SV tips. Furthermore, anterior and lateral safety margins of 10 mm and a posterior margin of 5 mm are added to the CTV to create the initial planning target volume (PTV1). For reducing the dose to the anterior rectal wall, a rectum-sparing target volume (PTV2) is used for the latter half of the C-ion RT, with the posterior margin reduced to the anterior boundary of the rectum (Fig. 27.1b). A compensation bolus is fabricated for each patient to make the distal configuration of the SOBP similar to the PTV. The collimator defines the outline of the PTV.

27.3.3 Dose Prescription at NIRS

For passive beam irradiation at NIRS, C-ion RT was performed with five irregularly shaped ports: (1) one anterior-posterior port, (2) a pair of lateral ports for the PTV1, and (3) a pair of lateral ports for the PTV2. One port was used at each treatment session. One hundred percent of the prescribed dose was given at the maximum dose point of each portal. The PTV2 was covered with at least 90 % of the prescribed dose. The minimum dose of the PTV1 was more than 50 % of the maximum dose and depended on the volume spared by PTV2. Figure 27.2 shows the representative dose distribution of the passive beam delivery.

A dose-volume histogram (DVH) is calculated to evaluate the planned dose distribution, particularly for the rectum [25]. A reference DVH of the rectum has been obtained from the initial toxicity study on C-ion RT at NIRS, which is the average DVH of patients with grade 1 or less rectal toxicity in the first and second dose-escalation trials (Fig. 27.3). A plan for a new patient is then compared with the reference DVH to avoid the rectal DVH from exceeding the reference DVH, especially at the high-dose level.

From the experience of treating pelvic tumors, including prostate cancer, gynecological cancer, and recurrent rectal cancer, at the NIRS, the dose constraints of the digestive tract in the C-ion RT were established (Table 27.2). According to these constraints, the percent rectal volume receiving 56.0 GyE in 16 fractions should not exceed 5 %, and this agrees well with the constraint using the DVH (Fig. 27.3).

27.3.4 Field Positioning

At NIRS, the C-ion RT is carried out once a day, with four fractions per week (from Tuesday to Friday). When the treatment is given from the anterior port, the bladder is filled with the sterilized water each time just before the patient setup. Verification of the field is carried out at every treatment

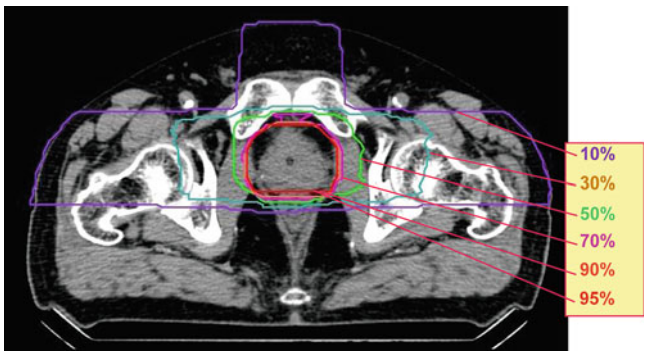

Fig. 27.2 Representative dose distribution of passive irradiation at the NIRS. Prescribed dose is a 66 or 63 GyE at the isocenter for the treatment of 20 fractions and 57.6 GyE for 16 fractions

Table 27.2 Dose constraints of digestive tract in carbon-ion radiotherapy

	Dose limits		
	20 Fractions	16 Fractions	ED[a] in 2 GyE/f
Rectum			
D_{max}(GyE)	66.0	60.8	83.2
$D_{5\%}$(GyE)	60.0	56.0	72.0
$D_{10\%}$(GyE)	50.0	46.4	55.0
$D_{20\%}$(GyE)	30.0	28.8	27.0
Small intestine			
D_{max}(GyE)	50.0	48.0	52.0

[a]*ED*, equivalent dose

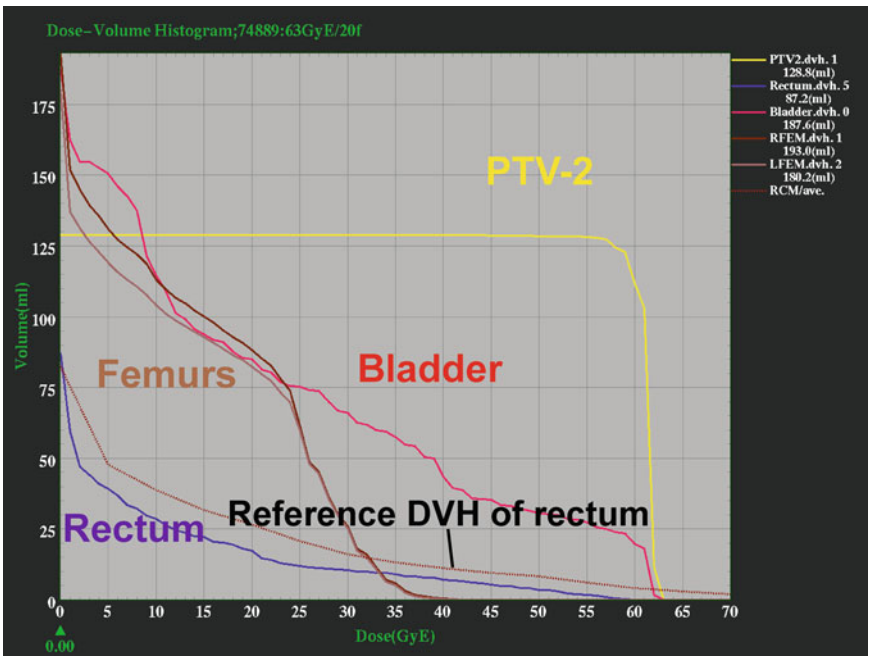

Fig. 27.3 Dose constraints at the NIRS by using a dose-volume histogram. The reference DVH, brown *dotted line* in the graph, is an average DVH of the patients with grade 0 or 1 rectal complication in the early dose-escalation studies. A new plan is made in order that the rectal DVH is below the reference line particularly at high-dose level

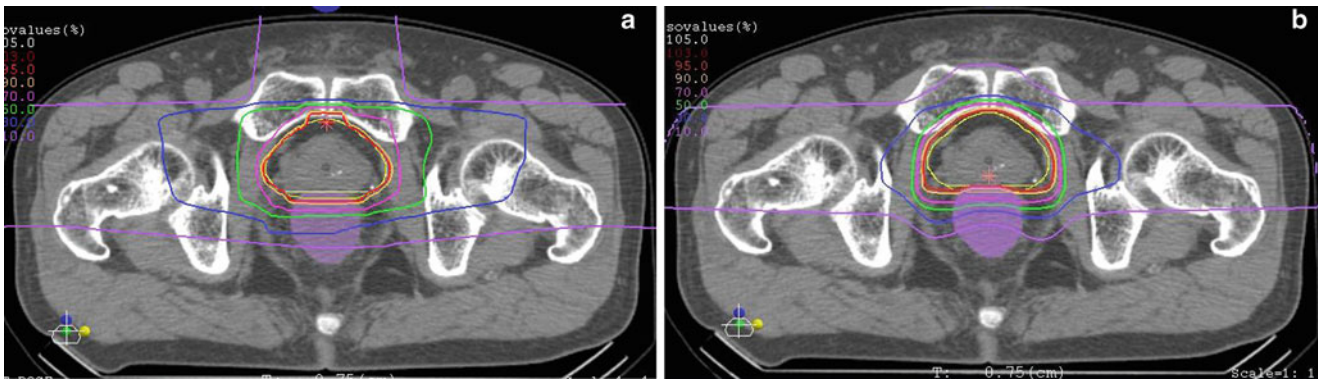

Fig. 27.4 (**a**) Dose distribution of the passive irradiation with three ports. (**b**) Dose distribution of the scanning irradiation with two ports. Dose to the hip joint can be reduced with scanning technique of two ports compared to 3-port passive irradiation

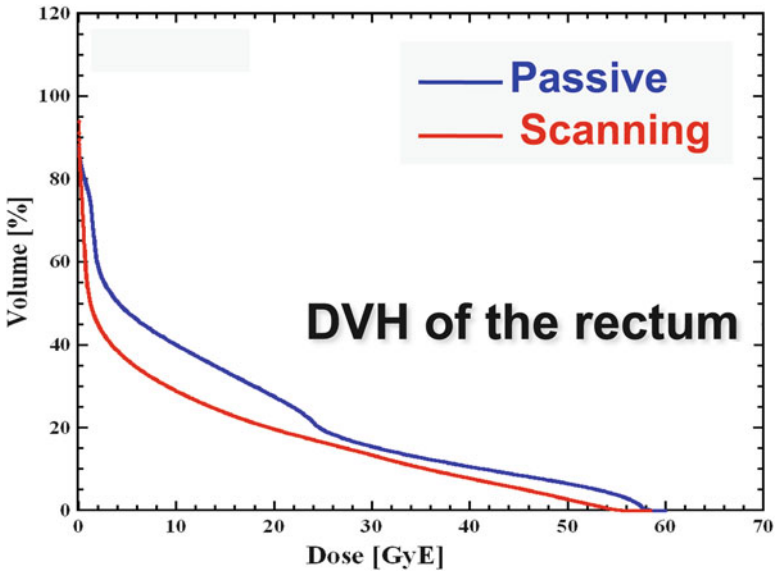

Fig. 27.5 Comparison between dose-volume histograms of the rectum by beam delivery method. Irradiated volume of the rectum is slightly smaller with scanning than passive

session with a computer-aided online positioning system to maintain a positioning error within less than 2 mm [5, 6]. A rectal balloon and respiratory-gated irradiation were not used in this treatment.

27.3.5 Scanning Irradiation and Passive Irradiation in Prostate Cancer

At NIRS, beam delivery with spot scanning became available in 2011. Currently, almost all of the patients with prostate cancer are treated with this spot scanning method. This is based on our judgment that spot scanning could provide an even better dose distribution than the passive beam method in the treatment of prostate cancer. Figure 27.4 shows the dose distributions of passive beam (a) and scanning beam (b). The plan using passive beam irradiation is calculated for the anterior and two lateral directions. The plans for scanning beam irradiation are made using only two lateral beams. The dose to the hip joint is apparently reduced in the plan for scanning beam irradiation with two ports when compared to the one using passive beam irradiation with three ports.

In addition, the irradiated volume of the rectum can be a little smaller in the plan using scanning irradiation than the one using passive irradiation, as demonstrated by the DVH (Fig. 27.5). Filling the bladder with sterilized water is needed for irradiation from the anterior port, while the treatment using only the lateral ports is more comfortable for the patient. From this point of view, it is important that the two lateral ports of scanning irradiation do not deliver a higher dose to the rectum and the hip joint as compared to the three ports of passive irradiation.

Since the intra-treatment motion of the prostate immobilized using the method at NIRS was confirmed to be very small [24], scanning irradiation can be safely applied to prostate cancer.

27.3.6 Androgen Deprivation Therapy (ADT)

The use of ADT combined with RT is still controversial. ADT consisting of medical or surgical castration with or without antiandrogen is administered according to the risk group for prostate cancer at NIRS. Before the start of C-ion

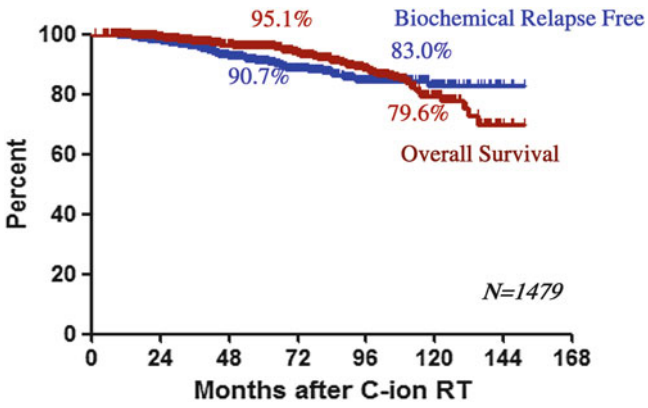

Fig. 27.6 Overall survival rate and biochemical relapse-free rate of the patients treated with C-ion RT at the NIRS. Biochemical relapse is judged according to the Phoenix criteria

Table 27.3 Significance of prognostic factors on biochemical control and overall survival rates

		5-year rate (%), log-rank test				
		Number of patients	bNED[a]	*p* value	OS[b]	*p* value
All		1,144	91.0		95.7	
T-stage	T1/2	836	93.1	0.0004	97.9	0.0026
	T3	308	85.5		90.6	
PSA	<20	829	92.1	N.s.	97.1	0.0025
	≥20	315	88.6		92.8	
GS[c]	≤6	265	92.5	0.0001[d]	97.6	0.0010[d]
	7	558	93.5	0.0001[d]	96.5	0.0026[d]
	≥8	321	85.4		92.8	

[a]bNED; 5-year rate of biochemically no evidence of disease
[b]OS; Overall survival rate
[c]GS; Gleason's score
[d]*p* values against probabilities in Gleason score ≥8

RT, neoadjuvant ADT is given to patients in the intermediate and high-risk groups for 2–6 months. Adjuvant ADT is continued for a duration of 6 months for intermediate-risk patients and for 2 years for high-risk patients. Neither neoadjuvant nor adjuvant ADT is given to patients in the low-risk group [5, 6, 26].

27.4 Up-to-Date Results of C-Ion RT at NIRS

As of February 2013, 1,733 patients have received C-ion RT for prostate cancer at NIRS (Table 27.1). Of them, 1,479 patients were treated during or after the phase II trial started in 2000 and were followed up for at least 6 months. The overall survival rate of this entire group was 95.1 % at 5 years and 79.6 % at 10 years by a Kaplan-Meier estimation (Fig. 27.6). Notably, out of the 87 patients who died, only 18 died of primary prostate cancer. One hundred and eleven patients have met the criteria of biochemical failure according to the Phoenix criteria—that is, the PSA rising over the nadir + 2.0 was judged as a failure. The 5-year and 10-year biochemical relapse-free rates were 90.7 and 83.0 %, respectively (Fig. 27.6). Out of 1,479 patients, 773 (52.3 %) belonged to the high-risk group, and therefore these outcomes for the tumor control are quite satisfactory. Based on the data available for 1,144 patients, the T-stage and Gleason score were found to have a significant influence on the biochemical relapse-free rate (Table 27.3). Further, the T-stage, initial PSA, and Gleason score influenced patient survival.

Concerning the influence of the dose fractionation of C-ion RT on biochemical control, no difference was observed between the biochemical relapse-free rate of the 20-fraction group and the 16-fraction group (Fig. 27.7) [7]. Although the observation period for the 12-fraction group has been very

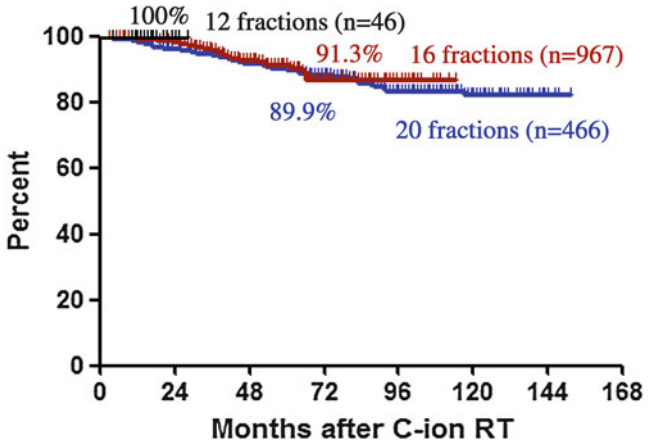

Fig. 27.7 Biochemical relapse-free rate as a function of dose fractionation of C-ion RT. No statistical difference is observed

short and the patient number too small, none of the patients has developed biochemical relapse to date.

Regarding late radiation toxicities, the incidence of late gastrointestinal (GI) and genitourinary (GU) morbidities and of grade 2 or worse morbidities in the 63.0 GyE/20 Fr and 57.6 GyE/16 Fr groups were 2.3 and 0.4 % at the rectum, respectively, and those at the GU system were 6.1 and 2.4 %, respectively. Table 27.4 shows grade 2 or worse GI and GU morbidity rates after treatment for prostate cancer using modern RT techniques with conventional fractionation or hypofractionation. C-ion RT showed a lower risk for these morbidities, especially of developing rectal bleeding, compared with other RT methods [11, 23, 27–30]. These results confirm the feasibility of further hypofractionated C-ion RT delivered in 16 fractions. Moreover, these results reveal that our assumption of the relative biological effectiveness of carbon ions and the equivalent dose calculated by the LQ model may be reasonable, even in the case of C-ion RT for prostate cancer.

Table 27.4 Comparison in incidence of late radiation toxicity

Institutes	RTx	Dose (Gy/f)	Number of patients	Toxicity ≥ grade2	
				GI (%)	GU (%)
Christie H	IMRT	60.0/20	60	9.5	4.0
Princess M. H	IMRT	60.0/20	92	6.3	10.0
Cleveland CF	IMRT	70.0/28	770	4.4	5.2
Stanford U	SRT	36.25/5	41	15.0	29.0
RTOG9406	3DCRT	78.0/39	118	25–26	23–28
Loma Linda U	Proton	75.0/39	901	3.5	5.4
NIRS	Carbon	63.0/20	216	2.3	6.1
		57.6/16	967	0.4	2.4

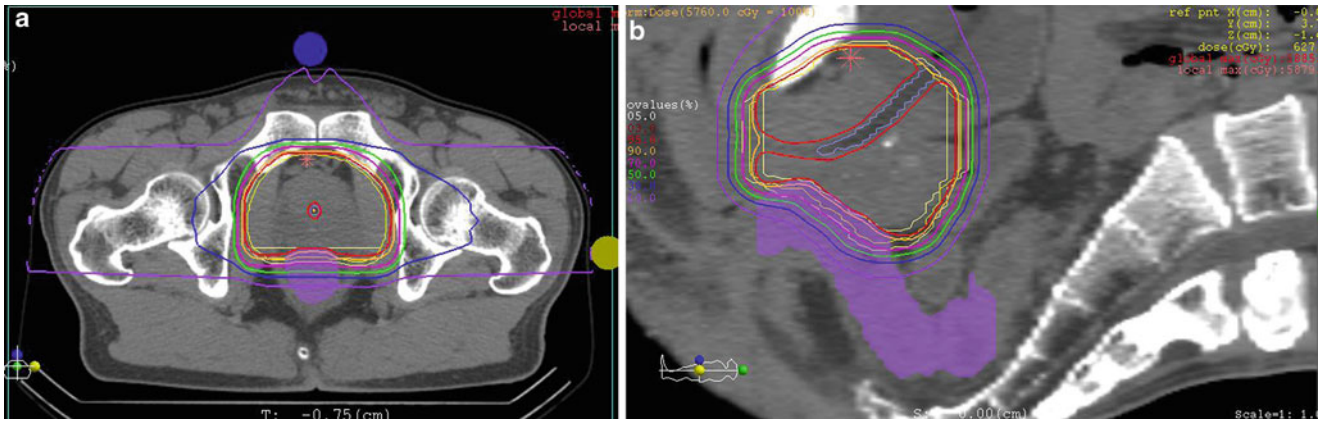

Fig. 27.8 Dose calculation using intentional dose reduction around the urethra using scanning irradiation of carbon-ion beam. (**a**) Axial view, Fig. 27.8. (**b**) Sagittal view

27.5 Future Perspectives

27.5.1 A New Trial of Further Hypofractionated RT

In view of cost-effectiveness and patient convenience, as well as the benefit of the treatment effectiveness based on the LQ model, further hypofractionated RT could be promising in the treatment of prostate cancer. The use of hypofractionated RT in IMRT, SBRT, or CyberKnife with a fraction dose of more than 3 Gy has been investigated, but some of the patients developed severe morbidities (Table 27.4) [11, 27, 28]. In contrast, C-ion RT with a hypofractionated regimen at NIRS has been successfully applied without any incidences of severe morbidities. Based on these experiences, a new trial of C-ion RT at a total dose of 51.2 GyE in 12 fractions over 3 weeks with a fractional dose of 4.3 GyE has been carried out at NIRS (Table 27.1). Although the follow-up period is still short, no patient to date has developed grade 2 or worse late toxicity or biochemical relapse.

27.5.2 *Scanning Beam Irradiation*

Scanning beam irradiation became available at the NIRS and has been mostly applied to prostate cancer. With this novel beam delivery method, not only a better dose distribution but also an improvement in efficiency has been obtained. Scanning beam irradiation does not require a collimator or compensator. Thereby, the preparation time between CT acquisition and the start of treatment can be substantially shortened. In addition, injection of water into the bladder is unnecessary, and the setup time at each treatment session can be shortened as well. However, the largest merit of scanning beam irradiation is a better and much more flexible dose distribution than that of the passive beam irradiation. In contrast to passive beam irradiation with its uniform biological dose within a spread-out Bragg peak, the dose distribution can be made arbitrarily. Even if the dose calculation is made by optimization for each port where the dose of the PTV with every single port is uniform, similar to passive beam irradiation, the dose concentration of the scanning irradiation is even better than that of passive irradiation (Figs. 27.4 and 27.5). Furthermore, it is possible for the scanning irradiation device to calculate and actually deliver the dose according to the optimization of multi-ports (IMPT; intensity modulated particle therapy), where the dose to the PTV with each port does not need to be uniform. In fact, IMRT using X-rays uses these methods to calculate and deliver the dose, and the dose distribution can be further improved by using the carbon-ion beam rather than X-rays. Figure 27.8 shows one possible idea for treatment with a nonuniform dose distribution in the PTV. In this case, the

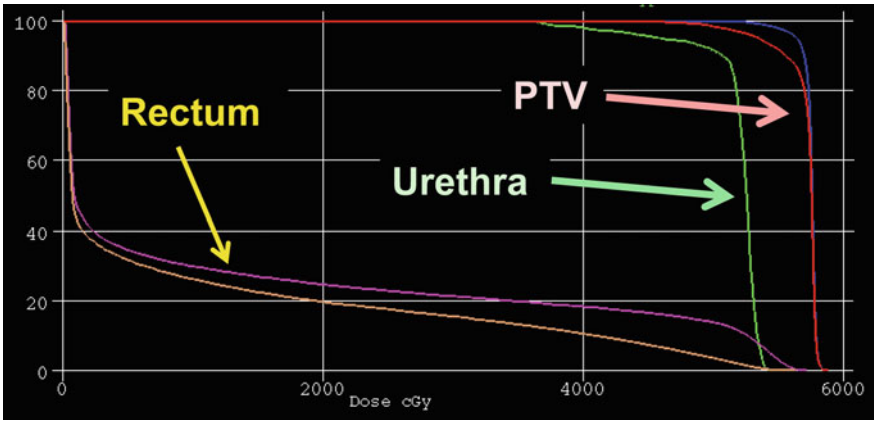

Fig. 27.9 Dose-volume histogram of the plan using intentional dose reduction around the urethra. The dose to the urethra can be reduced to 90 % of the target (PTV) dose without deterioration of the dose coverage of the PTV

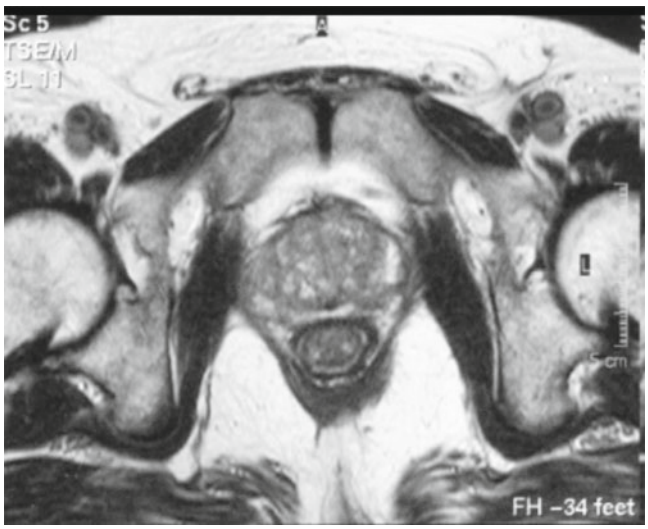

Fig. 27.10 Pretreatment T2-weighted MRI. The prostate size was slightly enlarged and the signal intensity inside was rather heterogeneous, but the apparent findings of the tumor were not seen

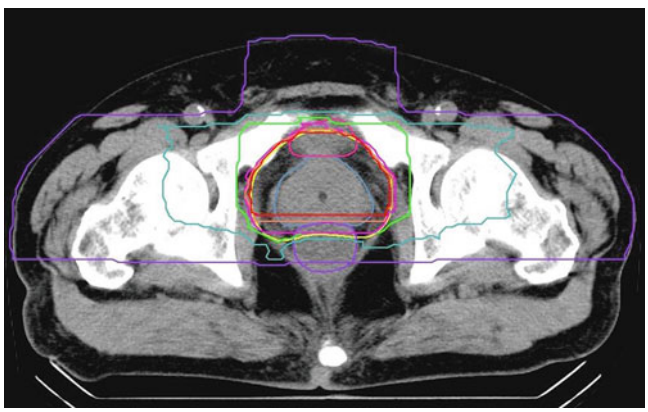

Fig. 27.11 Dose distribution of the C-ion RT for the case. Three directions of the beam, anterior and bilateral, were used

dose to the urethra can be intentionally reduced to less than 90 % of the prescribed dose, but the dose coverage of the tumor-bearing area within PTV is not very deteriorated. This can be achieved because of the quite sharp lateral falloff of the carbon-ion beam. This treatment, however, would require image guidance at each treatment session, with catheterization into the urethra. A further decrease in the number of fractions is also being examined by the SBRT group (Fig. 27.9).

27.6 Case Study

A 76-year-old Japanese male was referred to us with a diagnosis of prostate cancer (T2aN0M0). The initial PSA was 5.7 ng/mL, and the pathology was adenocarcinoma. His tumor was not detected by any imaging modalities. The MRI demonstrated only slight enlargement of prostate gland without apparent finding of a tumor (Fig. 27.10). The Gleason score as diagnosed by the central pathologist was 3+3=6. He was categorized into the low-risk group and therefore underwent only C-ion RT without ADT. The dose of C-ion RT was 57.6 GyE in 16 fractions delivered by passive irradiation (Fig. 27.11). The rectal DVH was below the reference line at any dose point.

The patient is alive without any recurrence or toxicity more than 5 years after C-ion RT.

References

1. Tsujii H, Mizoe JE, Kamada T, et al. Overview of clinical experiences on carbon ion radiotherapy at NIRS. Radiother Oncol. 2004; 73:S41–9.
2. Okada T, Kamada T, Tsuji H, et al. Carbon ion radiotherapy: clinical experiences at National Institute of Radiological Science (NIRS). J Radiat Res. 2010;51:355–64.
3. Ishikawa H, Tsuji H, Kamada T, et al. Carbon-ion radiation therapy for prostate cancer. Int J Urol. 2012;19:296–305.
4. Akakura K, Tsujii H, Morita S, et al. Phase I/II clinical trials of carbon ion therapy for prostate cancer. Prostate. 2004;58:252–8.
5. Tsuji H, Yanagi T, Ishikawa H, et al. Hypofractionated radiotherapy with carbon ion beams for prostate cancer. Int J Radiat Oncol Biol Phys. 2005;63:1153–60.

6. Ishikawa H, Tsuji H, Kamada T, et al. Carbon ion radiation therapy for prostate cancer: results of a prospective phase II study. Radiother Oncol. 2006;81:57–64.
7. Okada T, Tsuji H, Kamada T, et al. Carbon ion radiotherapy in advanced hypofractionated regimens for prostate cancer: from 20 to 16 fractions. Int J Radiat Oncol Biol Phys. 2012;84:968–72.
8. Shibuya H, Tsujii H. The structural characteristics of radiation oncology in Japan in 2003. Int J Radiat Oncol Biol Phys. 2005;62:1472–6.
9. Aström L, Pedersen D, Mercke C, et al. Long-term outcome of high dose rate brachytherapy in radiotherapy of localised prostate cancer. Radiother Oncol. 2005;74:157–61.
10. Zelefsky MJ, Fuks Z, Hunt M, et al. High-dose intensity modulated radiation therapy for prostate cancer: early toxicity and biochemical outcome in 772 patients. Int J Radiat Oncol Biol Phys. 2002; 53:1111–6.
11. King CR, Brooks JD, Gill H, et al. Stereotactic body radiotherapy for localized prostate cancer: interim results of a prospective phase II clinical trial. Int J Radiat Oncol Biol Phys. 2009;73:1043–8.
12. Wilson RR. Radiological use of fast protons. Radiology. 1946; 47:487–91.
13. Kanai T, Endo M, Minohara S. Biophysical characteristics of HIMAC clinical irradiation system for heavy-ion radiation therapy. Int J Radiat Oncol Biol Phys. 1999;44:201–10.
14. Koike S, Ando K, Uzawa A, et al. Significance of fractionated irradiation for the biological therapeutic gain of carbon ions. Radiat Prot Dosimetry. 2002;99:405–8.
15. Kamada T, Tsujii H, Tsuji H, et al. Efficacy and safety of carbon ion radiotherapy in bone and soft tissue sarcomas. J Clin Oncol. 2002; 20:4466–71.
16. Mizoe JE, Tsujii H, Kamada T, et al. Dose escalation study of carbon ion radiotherapy for locally advanced head-and-neck cancer. Int J Radiat Oncol Biol Phys. 2004;60:358–64.
17. Fowler JF, Ritter MA, Chappell RJ, et al. What hypofractionated protocols should be tested for prostate cancer? Int J Radiat Oncol Biol Phys. 2003;256:1093–104.
18. Fowler JF. Total doses in fractionated radiotherapy implications of new radiobiological data. Int J Radiat Biol. 1984;46:103–20.
19. Macías V, Biete A. Hypofractionated radiotherapy for localised prostate cancer. Review of clinical trials. Clin Transl Oncol. 2009; 11:437–45.
20. Arcangeli G, Saracino B, Gomellini S, et al. A prospective phase III randomized trial of hypofractionation versus conventional fractionation in patients with high-risk prostate cancer. Int J Radiat Oncol Biol Phys. 2010;78:11–8.
21. Livsey JE, Cowan RA, Wylie JP, et al. Hypofractionated conformal radiotherapy in carcinoma of the prostate: Five-year outcome analysis. Int J Radiat Oncol Biol Phys. 2003;57:1254–9.
22. Vicini FA, Vargas C, Edmundson G, et al. The role of high-dose rate brachytherapy in locally advanced prostate cancer. Semin Radiat Oncol. 2003;13:98–108.
23. Kupelian PA, Thakkar VV, Khuntia D, et al. Hypofractionated intensity-modulated radiotherapy (70 gy at 2.5 Gy per fraction) for localized prostate cancer: long-term outcomes. Int J Radiat Oncol Biol Phys. 2005;63:1463–8.
24. Kumagai M, Okada T, Mori S, et al. Evaluation of the dose variation for prostate heavy charged particle therapy using four-dimensional computed tomography. J Radiat Res. 2013;54:357–66.
25. Ishikawa H, Tsuji H, Kamada T, et al. Risk factors of late rectal bleeding after carbon ion therapy for prostate cancer. Int J Radiat Oncol Biol Phys. 2006;66:1084–91.
26. Ishikawa H, Tsuji H, Kamada T, et al. Adverse effects of androgen deprivation therapy on persistent genitourinary complications after carbon ion radiotherapy for prostate cancer. Int J Radiat Oncol Biol Phys. 2008;72:78–84.
27. Coote JH, Wylie JP, Cowan RA, et al. Hypofractionated intensity-modulated radiotherapy for carcinoma of the prostate: analysis of toxicity. Int J Radiat Oncol Biol Phys. 2009;74: 1121–7.
28. Martin JM, Rosewall T, Bayley A, et al. Phase II trial of hypofractionated image-guided intensity-modulated radiotherapy for localized prostate adenocarcinoma. Int J Radiat Oncol Biol. 2007;69: 1084–9.
29. Michalski JM, Bae K, Roach M, et al. Long-term toxicity following 3D conformal radiation therapy for prostate cancer from the RTOG 9406 phase I/II dose escalation study. Int J Radiat Oncol Biol Phys. 2010;76:14–22.
30. Schulte RW, Slater JD, Rossi Jr CJ, et al. Value and perspectives of proton radiation therapy for limited stage prostate cancer. Strahlenther Onkol. 2000;176:3–8.

Renal Cell Carcinoma

28

Takuma Nomiya and Hiroshi Tsuji

Abstract

Renal cell carcinoma (RCC) accounts for the vast majority of solid renal neoplasms. Standard treatment for localized RCC is partial/radical nephrectomy. RCC has always been considered to be highly radioresistant and thus few studies on definitive radiotherapy have been found for RCC. From 1997 to 2007, ten patients with primary RCC were treated with carbon ion therapy at our institution. The median maximum tumor diameter was 4.3 cm (2.4–12.0 cm), and the median total dose was 72 GyE in 16 fractions. All tumors but one have been controlled with a median follow-up for surviving patients of 86 months. Of four patients who died, one patient died of cancer and the other three patients of intercurrent disease. The tumor response to carbon ion therapy was very distinctive; almost all tumors had been shrinking for years without progression. Although the number of patients was small, initial clinical experience of carbon ion radiotherapy (C-ion RT) at our institution showed favorable outcomes. A formal phase II clinical trial of definitive carbon ion therapy for patients with primary RCC has begun. C-ion RT is expected to be one of the standard treatment options for patients with localized RCC.

Keywords

Carbon ion therapy • Renal cell carcinoma • Tumor response

28.1 Introduction

28.1.1 Epidemiology

Kidney cancer accounts for approximately 2 % of all malignant tumors in the world. The annual incidence is approximately 273,000 and annual deaths throughout the world approximately 116,000 (2008) [1]. In men, kidney cancer accounts for approximately 3 % of all malignancies, with an annual incidence of approximately 169,000 and annual deaths of approximately 72,000. In women, kidney cancer accounts for approximately 3 % of all malignancies. The annual incidence in women is approximately 104,000 and annual deaths approximately 44,000. The male to female ratio is approximately 3:2, and the mortality rate of kidney cancer with respect to cancer-specific mortality rate is not included in the top ten [1]. Compared with statistics from 2002, there is a tendency for increased morbidity in both men and women [2].

Renal cell carcinoma (RCC) accounts for more than 80 % of malignant kidney tumors; the remainder is mainly renal pelvic carcinomas. Racial differences are seen in the incidence of RCC, and the cancer is more frequent in North America and Europe and less frequent in Asia and Africa. The incidence of RCC in Western European men (11/100,000 people) is five times more frequent than that in Southeastern Asian men (2/100,000) [2]. The incidence of RCC in Japanese men (6/100,000) is approximately halfway between them.

T. Nomiya (✉) • H. Tsuji
National Institute of Radiological Sciences,
Research Center Hospital for Charged Particle Therapy,
4-9-1, Anagawa, Inage-ku, Chiba, 263-8555, Japan
e-mail: t_nomiya@nirs.go.jp

H. Tsujii et al. (eds.), *Carbon-Ion Radiotherapy: Principles, Practices, and Treatment Planning*,
DOI 10.1007/978-4-431-54457-9_28, © Springer Japan 2014

The annual incidence and the annual deaths from kidney cancer in the USA have been reported as being 65,000 and 13,700, respectively, and the male to female ratio is approximately 5:3 [3]. In the same region (i.e., USA), the incidence rate of kidney cancer tends to be higher in the black than in the white population [4]. The reason for differences observed in the incidence rate of kidney tumors across geographic areas seems to be more related to differences in the prevalence rate of imaging modalities (CT, computed tomography; US, ultrasonography; MRI, magnetic resonance imaging; etc.) and in the frequency of examinations. These backgrounds are considered to be one of the reasons for a higher incidence rate in the developed countries of Europe and North America, other than a reason for racial genetic differences.

As the reported rate of incidental RCC is 15–35 %, there are many reports that suggest an increase in the frequency of incidental RCC in recent years [5–9]. The characteristics of incidental RCC are as follows: (1) significantly more patients with early-stage tumors; (2) significantly lower histological grade; (3) significantly smaller tumor size; and (4) significantly more favorable prognosis [5–9]. On the other hand, the characteristics of symptomatic RCC are as follows: (1) more frequent advanced-stage RCC; (2) higher histological grade; and (3) associated with unfavorable prognosis. A study reported that the 5-year overall survival rates (OS) of incidental RCC and symptomatic RCC were 85 % and 40–50 %, respectively, and the prognosis of incidental RCC is significantly more favorable than that of symptomatic RCC [8]. Another study suggests that the rate of incidental RCC is significantly higher in women than in men and that the prognosis of women patients is significantly more favorable than that of men [9]. However, it is not mentioned in relation to the cause.

28.1.2 Etiology

Smoking has been suggested as one of the causes of RCC [10, 11]. A long-term cohort study spanning more than 25 years revealed that the incidence of RCC was significantly higher in smoking patients. A clear correlation between the number of cigarettes smoked per day and the incidence of RCC has been observed, and the incidence risk of RCC is increased by 2.06 times in heavy smokers (more than 40 cigarettes per day). Thus, smoking is considered to be a major risk factor for RCC.

Obesity and hypertension are also considered as risk factors for RCC [12]. Chow et al. analyzed 360,000 Swedish men classified into eight groups according to body mass index (BMI). The results of the analysis showed a significantly higher incidence risk of RCC (1.7–1.9) in the two groups with the highest BMI, and a statistically significant difference in incidence risk was seen in the whole group analysis ($P<0.001$).

In an analysis of blood pressure (BP) in which patients were classified into six groups according to systolic/diastolic BP, the incidence risk of RCC was 1.4–2.3 times higher in the higher BP groups than in the lower BP groups ($P=0.007$, $P<0.001$, respectively) [12]. On the other hand, BMI, systolic BP, and diastolic BP are not considered significant incidence risk factors of renal pelvic cancer ($P=0.25$, 0.74, 0.91, respectively) [12].

Some genetic analyses revealed that the loss of function of von Hippel–Lindau (VHL) protein (a tumor suppressor protein) may be responsible for a greater incidence of RCC [13]. VHL protein is associated with the degradation of hypoxia-inducible factor 1 alpha (HIF-1α); thus, a loss of function of VHL protein is believed to induce overexpression of HIF-1α. Overexpression of HIF-1α leads to increased transcription of HIF-1-regulated genes, such as transforming growth factor alpha (TGF-α), platelet-derived growth factor (PDGF), and vascular endothelial growth factor (VEGF), and these transcripts promote developing cancer and tumor growth.

28.2 Significance of Carbon Ion Radiotherapy

28.2.1 Treatment: Radical Surgery

Except in cases of small renal masses, which can be managed with active surveillance, the standard treatment for localized RCC is radical surgery. Complete surgical excision by partial nephrectomy is considered to be a standard treatment for patients with T1aN0 RCC [14]. Radical nephrectomy is considered to be a standard treatment for patients with stage II/III RCC. The utilization of the less invasive partial nephrectomy (nephron-sparing surgery) has recently been expanded [15–19]. One of the benefits of these minimal invasive procedures is to preserve ipsilateral renal function and to reduce renal dysfunction after surgery. Many studies report very good outcomes of more than 90 % in disease-specific survival with this procedure [15–19]. However, the treatment outcomes are worse in patients with T2 or larger tumor; hence, nephron-sparing surgery should be considered carefully in such patients.

28.2.2 Treatments Other Than Surgery

Radiofrequency ablation (RFA) and cryoablation are considered as topical therapies and provide an alternative to surgery for patients with RCC. A meta-analysis suggested good outcomes are associated with cryoablation with a local progression rate of approximately 5 % [20]. In contrast, outcomes

associated with RFA are significantly more unfavorable than those of both cryoablation and partial nephrectomy, with a local progression rate of approximately 13 %. However, cryoablation is performed laparoscopically and is thus a more invasive procedure. Thus, RFA should be considered for limited patients with inoperable status.

Because RCC is believed to be highly radioresistant, conventional fractionation radiotherapy has not been performed as definitive treatment for primary RCC, and almost all papers on radiotherapy for RCC discuss the procedure as palliative treatment [21, 22]. But studies on definitive radiotherapy for primary RCC have recently been reported [23, 24]. Conventional irradiation of 1.8–2.0 Gy/fraction (fr) is less effective due to the radioresistance of RCC. A larger dose/fraction of 8–15 Gy/fr is used for definitive stereotactic radiotherapy in RCC, and a good treatment outcome with a 4-year local control rate of approximately 80 % has been reported. Although challenging studies are increasing these days, definitive radiotherapy for primary RCC is yet to be established. Under these circumstances, the favorable outcomes associated with carbon ion therapy, as will be described later, may change the concept of radiotherapy as a treatment option for primary RCC.

28.3 Clinical Features and Diagnostic Work-Up

28.3.1 Pathology of RCC

The World Health Organization (WHO) published a new classification of renal tumors in 2004 [25]. In that publication, malignant renal tumors are classified as follows: clear cell RCC, papillary RCC, chromophobe RCC, carcinoma of the collecting ducts of Bellini, renal medullary carcinoma, Xp11 translocation carcinomas, neuroblastoma-associated carcinoma, mucinous tubular, and spindle cell carcinoma. Approximately 90 % of the solid renal tumors are RCC and include all benign and malignant renal tumors [26]. The vast majority of RCCs is clear cell RCC which accounts for approximately 85 % of RCCs, papillary RCC accounts for approximately 10 %, chromophobe RCC accounts for approximately 2–5 %, and other types of RCCs are rare [27, 28]. In a comparison of prognosis according to histologic types, the prognosis of clear cell RCC is unfavorable, while the prognosis of papillary RCC and chromophobe RCC is more favorable than that of the clear cell type [27, 28]. In North America, an analysis demonstrated an association between histologic subtype and decade of life. The proportions of clear cell RCC ($P=0.008$) decreased while the proportion of papillary RCC ($P=0.005$) increased with increasing decade of life [29]; however, the significance of these changes has not been clearly defined.

28.3.2 Natural History of RCC

Recently, active surveillance has been positively considered for incidental RCC or small renal tumors. According to a review of more than 60 small renal masses with average follow-up time of 22.5–39 months by Volpe et al., average tumor growth was 1–5 mm/year in diameter [30]. The rate of eventual surgical removal was 14–100 %, and the rates differ according to the reports; the rate of histologically confirmed RCC was 80–100 %. Sowery et al. reported that 2 of 22 incidental renal tumors were surgically removed due to rapid growth, and the other 20 tumors showed slow growth with an average growth of 8 mm/year in diameter over a median follow-up period of 26 months [31].

Although primary treatment for RCC is surgery as a general rule, watchful waiting should be considered for incidental RCC or in cases of slow-growing RCC as mentioned above [32].

28.3.3 Diagnosis and TNM Staging

TNM staging was defined by AJCC (American Joint Committee on Cancer) [33]. RCC is clinically diagnosed with imaging modalities such as CT, US, or MRI. As mentioned above, more than 90 % of solid renal tumors are RCC, so diagnosis by imaging modalities without biopsy is acceptable. And therefore, the significance of a routine biopsy is controversial due to the risk of tumor implantation and the low impact on treatment strategy [34].

28.4 General Management of Radiation Technique

28.4.1 Carbon Ion Therapy Planning

Resinous shells for immobilization are individually made for all patients, and the patients are immobilized during CT for treatment planning and during irradiation. All patients undergo diagtreatment, and nonenhanced CT with a slice thickness of 3–5 mm is used for treatment planning. Figure 28.1 shows typical planning and dose distribution for treatment of RCC. Radiotherapy (RT) planning of two ports with a vertical port and a horizontal port is commonly used for the treatment of RCC. However, in case a high-dose area reaches the body surface, changing the direction of the ports or providing an additional port should be considered in order to avoid skin ulcers. In cases with no definitive lymph node metastasis, the target is limited to the tumor, and a regional lymph node area is not included in the irradiation field.

The clinical target volume (CTV) should include a margin of 0–5 mm around the macroscopic tumor (gross target volume: GTV), ITV (internal margin) should include a margin of

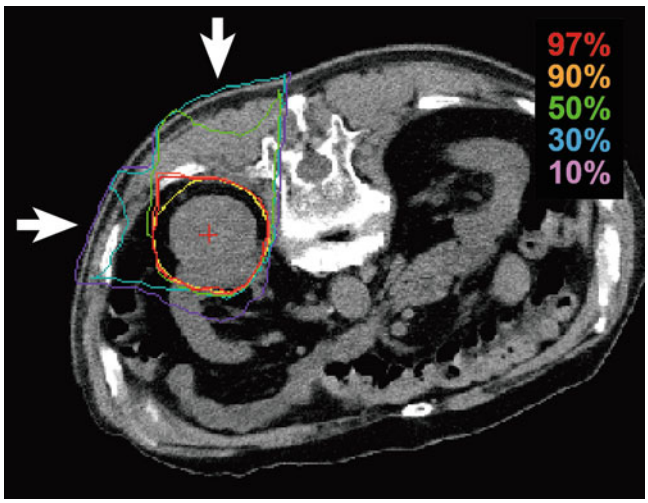

Fig. 28.1 Dose distribution of the carbon ion therapy

5–10 mm (depends on the accuracy of respiratory gating) in the craniocaudal direction around the CTV, and the planning target volume should include 5–10 mm around ITV. The whole kidney is not required to be included in the irradiation field. An optimum ridge filter is used for adjustment of the spread-out Bragg peak (SOBP), a resinous bolus is manufactured for adjustment of depth and shape of irradiation field, and a multi-leaf collimator or metallic collimator is used for shaping the irradiation field. Irradiation is delivered once per day and 4 times per week (Tuesday to Friday) at the present institution.

Due to respiratory organ motion, respiration-synchronized irradiation using a respiration sensing system is essential for treatment. Because the location of the kidney (or tumor) is hard to identify with X-ray imaging, the implantation of one or more metallic markers (1–3 mm in length) under local anesthesia in the ipsilateral renal cortex around the tumor as target markers is required. Metallic markers should not be implanted in the tumor so that there is no influence on dose distribution and also no induction of tumor seeding. Two or three markers are desirable due to the risk of migration of the markers after implantation. All irradiations are performed identifying these permanent markers by X-ray radiography.

A total dose of 64–80 GyE/16 fr was used in past treatments, and favorable outcomes were obtained. Local recurrence occurred in one patient treated with 72 GyE/16 fr; however, it is not clear whether 72 GyE/16 fr is sufficient because of the marginal recurrence. A total dose of 66 GyE in 12 fractions is used in a phase II clinical trial in the present institution.

28.4.2 Organs at Risk

28.4.2.1 Gastrointestinal Tract

The most important organ at risk during RT for renal tumors is the gastrointestinal tract. It is difficult to treat when the ascending or descending colon is in contact with renal tumor. When it comes to a tumor located in the superior and anterior region of the kidney, attention to the duodenum, small intestine, and stomach should be required.

28.4.2.2 Liver

A part of the liver will be irradiated in case the tumor is in the cranial region of the right kidney. But there is less possibility to cause severe toxicity other than transient mild liver dysfunction.

28.4.2.3 Kidney/Renal Pelvis

It is possible to avoid renal function loss by preserving the ipsilateral normal kidney. Because atrophy of the renal pelvis leads to dysfunction of the upstream renal cortex, renal pelvis must be preserved as much as possible.

28.4.2.4 Adrenal Gland

Because it is on the bilateral side, there is less possibility of symptomatic adrenal insufficiency by ipsilateral adrenal dysfunction. Prior explanation would be essential when a patient has existing adrenal dysfunction.

28.4.2.5 Skin/Muscle

Body surface dose should be limited as follows: 60 GyE $\leq$ 20 cm^2 to avoid $\geq$grade 3 late skin toxicity [35]. Muscle is less likely to be affected by radiation, but high-dose irradiation sometimes causes long-lasting dull pain.

28.4.2.6 Spinal Cord

It usually is not in close proximity to a renal tumor; however, in case the spinal cord is in contact with a tumor (T4 or massive tumor), high-dose irradiation to the spinal cord should be avoided.

28.5 Results of Therapy

28.5.1 Outcome of Carbon Ion Therapy

We previously reported the initial use of carbon ion therapy for primary RCC [36]. Patient characteristics are listed in Table 28.1. Nine patients had histologically proven RCC, including eight patients with clear cell carcinoma and one patient with mixed type; in addition, RCC was diagnosed in one patient without a biopsy. There were seven patients with clinical stage I (T1a N0: 5, T1b N0: 2) and three patients with stage IV (T4 N0: 2, T3a N2: 1) carcinoma. The median maximum diameter of the tumor was 4.3 cm (range, 2.4–12 cm), and the median initial tumor volume was 38.4 cc (range, 5.8–508.7 cc). The median follow-up for surviving patients was 86.2 months (8.1–137.8). Local recurrence was defined as definite regrowth of the tumor except for transient enlargement of the tumor after irradiation.

Table 28.1 Patient characteristics

No.	Age	Gender	Histology	TNM (UICC)	Total dose/ fraction (GyE/16 fr)	Max diameter (cm)	Tumor volume (cc)	Local failure	Distant metastasis	Late toxicity	Follow-up period (months)	Dead or alive
1	67	Male	RCC	T1bN0M0	72	5	52.33	(–)	(–)	(–)	118	DID
2	70	Male	RCC	T1aN0M0	72	3.2	11.32	(–)	(–)	(–)	42.4	DID
3	59	Male	RCC	T4N0M0	80	6.5	120.21	(–)	(–)	(+)	72.3	NED
4	55	Male	RCC	T1aN0M0	80	2.4	5.8	(–)	(–)	(–)	137.8	NED
5	71	Male	RCC	T1aN0M0	80	3	6.28	(–)	(–)	(–)	126.8	NED
6	69	Male	RCC	T4N0M0	72	12	508.68	(–)	(+)	(–)	74.4	DOD
7	82	Male	RCC	T1aN0M0	72	3	12.31	(–)	(–)	(–)	8.1	DID
8	55	Male	–	T1aN0M0	72	3.6	24.42	(–)	(–)	(–)	89.5	NED
9	61	Male	RCC	T1bN0M0	72	5	62.8	(+)	(+)	(–)	82.9	AWD
10	52	Female	RCC	T3aN2M0	64	6.5	137.2	(–)	(+)	(–)	75.7	AWD

NED alive with no evidence of disease, *DID* died of intercurrent disease, *DOD* died of disease, *AWD* alive with disease

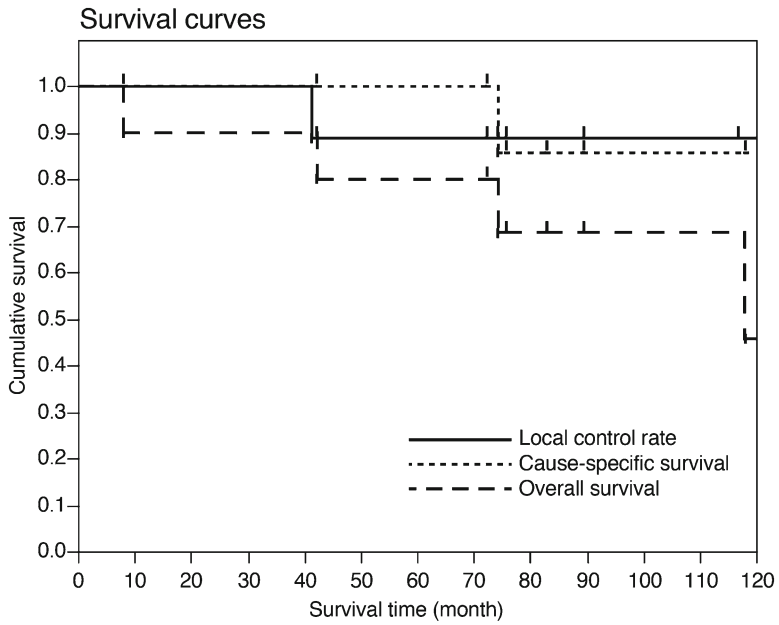

Fig. 28.2 Outcomes of carbon ion therapy for the patients with RCC

The 5-year local control rate, cause-specific survival, and overall survival were 89, 100, and 80 %, respectively (Fig. 28.2). Of four patients who died, one patient died of RCC and the other three patients died of intercurrent disease (pneumonia, 2; acute myocardial infarction, 1). Although there were residual tumors in three patients with intercurrent death, it was confirmed that there were neither local recurrence nor distant metastases of RCC. Distant metastases were seen in three patients, and the first site of metastases was the lung in all three patients. One patient showed local recurrence at 41 months after carbon ion therapy. Local recurrence was determined by a definitely growing tumor with contrast enhancement in the periphery of the irradiated tumor on MRI. Multiple lung metastases were detected at the same time; therefore, interferon therapy was initiated, and subsequently interleukin therapy and molecular target therapy were initiated. Because of these treatments, this patient is alive with disease at final follow-up date.

28.5.2 Time Course of Tumor Volume

The time course of tumor volume is shown in Fig. 28.3. The response of RCC to carbon ion therapy is distinctive. As shown in the figure, almost all tumors do not disappear within 2 years. Tumor response within a year after irradiation is classified into three patterns as follows: “shrinkage,” “no change,” and “transient enlargement.” However, tumors in all groups eventually begin to shrink; thus, these acute tumor responses do not predict prognosis. Transient enlargement of the tumor is often experienced clinically in other

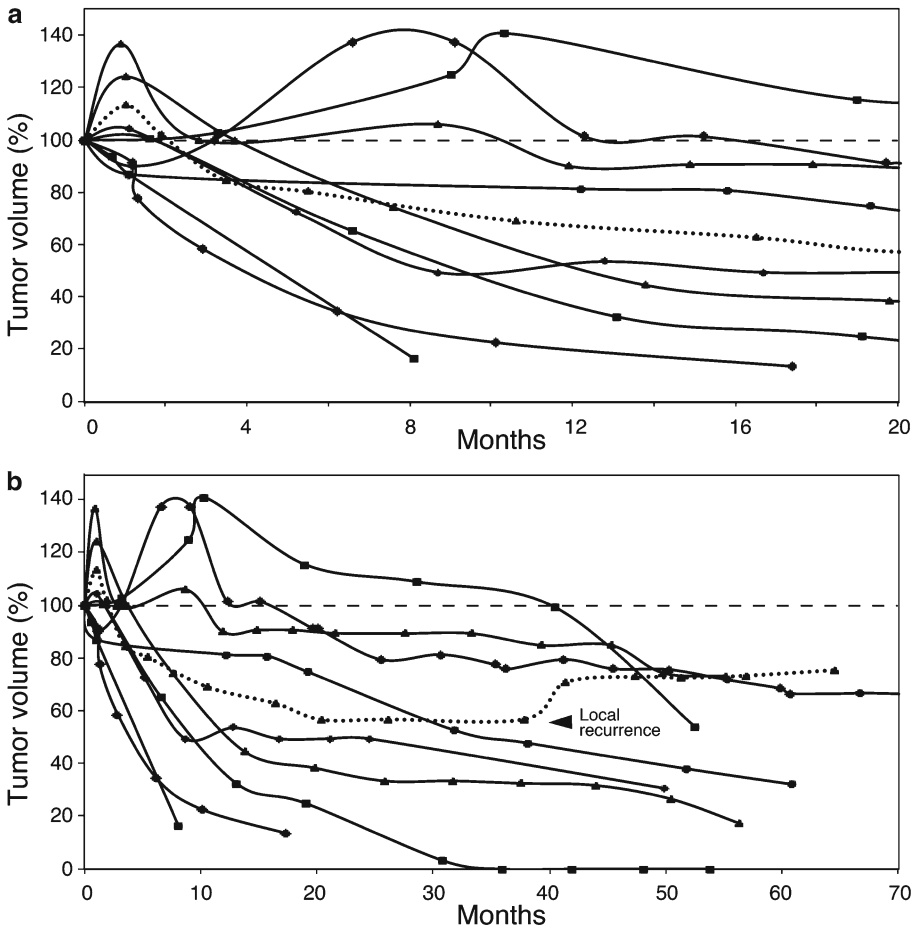

Fig. 28.3 (**a**) Time course of tumor volume over a short period. (**b**) Time course of tumor volume over a long period. The latest tumor volume before carbon ion radiotherapy was defined as 100 %. In the short-term observation, the tumors are classified approximately according to "transient enlargement," "no change," and "shrinkage." In the long-term observation, however, all tumors began to shrink. One patient showed obvious regrowth of the tumor, and it was decided as local recurrence (*dashed line*)

malignancies, particularly in squamous cell carcinomas, but this is generally observed within 1–2 months after treatment. In contrast, transient enlargement had been lasting for 6–12 months after treatment in several patients, so one must be careful not to mistake this for progressive disease (PD). There was no definite tumor enlargement except in one patient with definite local recurrence, as mentioned above (dashed line in Fig. 28.3).

28.5.3 Toxicity of Carbon Ion Therapy

The severe toxicity associated with carbon ion therapy was grade 4 skin toxicity in only one patient who had a huge T4 tumor with iliocostalis muscular invasion. In reviewing RT planning, a part of skin was included in the high-dose area in the radiotherapy planning to include the whole tumor with margins in the irradiation field. This patient was treated with a dose of 80 GyE/5 fr in 1998, and the skin dose had exceeded the abovementioned dose limitation (dose limitation had not been defined at that time). And the technical experience of sparing skin in carbon ion therapy appeared to be insufficient at that time. We believe that toxicity would not occur if the same patient were treated at the present time with sufficient experience and knowledge. This patient underwent skin transplantation and is alive with no evidence of disease. No other toxicity of grade 2 or more was observed.

Although RCC is generally believed to be radioresistant, the outcome of carbon ion therapy for RCC, which is only ten cases, appeared to be favorable.

28.5.4 Tumor Response Criteria RCC After Radiotherapy

Evaluation of tumor response after carbon ion therapy (radiotherapy) should be carefully performed. The natural

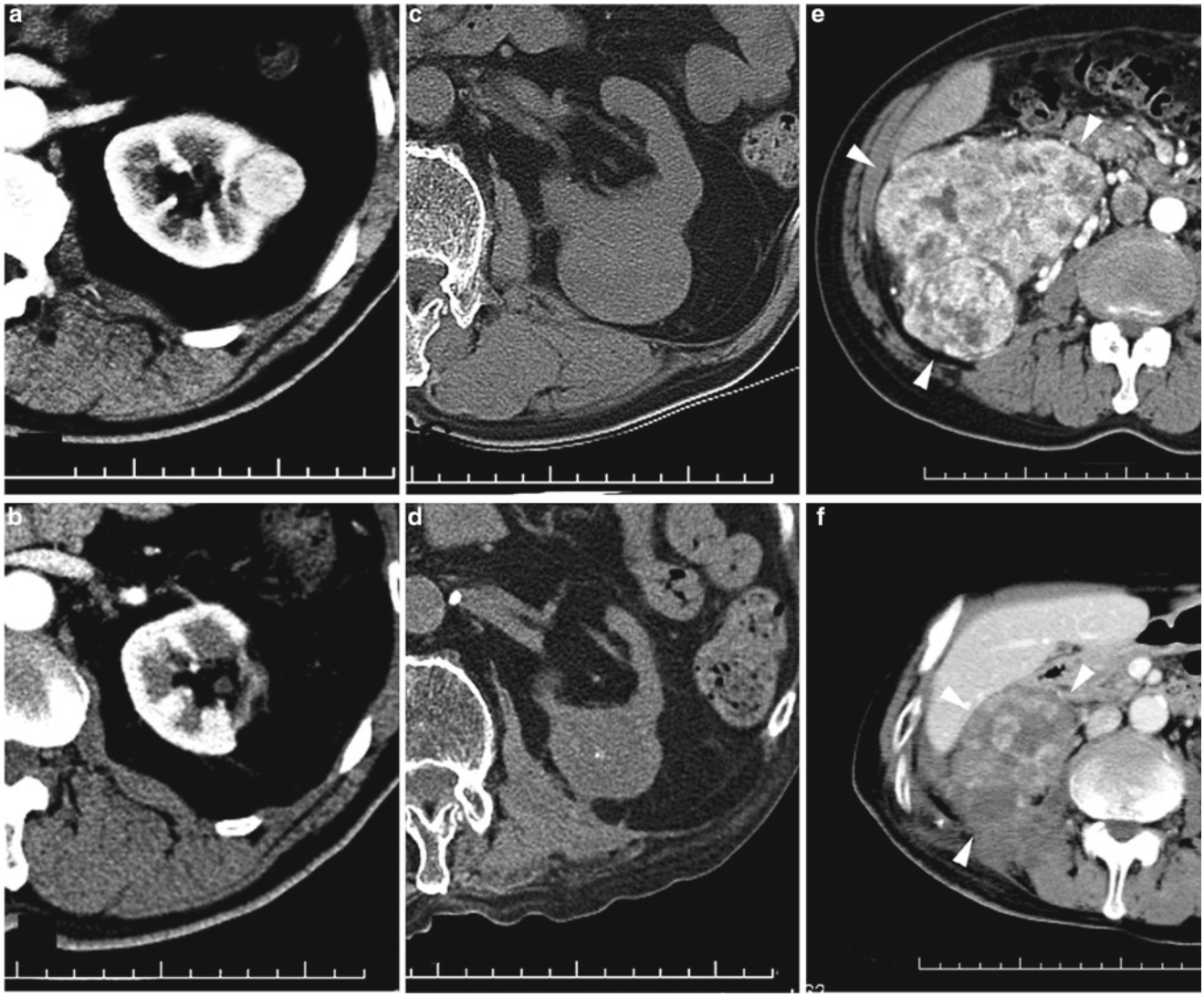

Fig. 28.4 CT images before carbon ion radiotherapy (CIRT) (**a**) and 5 years after CIRT (**b**). CT images before CIRT (**c**) and 9 years after CIRT (**d**) in another patient, showing that the tumor had been shrinking. Nonenhanced CT was performed because of diabetic nephropathy. CT images before CIRT (**e**) and 4 years after CIRT (**f**). This tumor, although large (*white arrowheads*), had been shrinking without metastasis

course of RCC after carbon ion therapy is distinctive, in that it exists for many years without progression or metastasis. As almost all treated RCCs shrink very slowly for many years, this course is considered as a response to carbon ion irradiation because there is no shrinkage in the natural history of untreated RCCs [30–32]. Based on these characteristics, the tumor response criteria for RCC after carbon ion therapy (radiotherapy) should include the following concepts: (1) a tumor should be considered as "controlled" even if the tumor exists for years without regrowth, and (2) "local recurrence" should be defined as "definite regrowth of the tumor except in cases of transient enlargement after treatment."

28.6 Case Study

As shown in Fig. 28.3, all tumors except one recurrent tumor have undergone very slow shrinkage. There was a case of residual tumor that existed more than 9 years that was associated with very slow shrinkage (Fig. 28.4c, d). Small tumors tend to shrink rapidly and tend to disappear in a short period of time. The autopsy specimen of RCC without recurrence after treatment from a case with intercurrent disease could be obtained (Fig. 28.5). There was remarkable shrinkage of the tumor, and it remained 8 months after treatment; however, neither recurrence nor distant metastases had been proven by autopsy (Fig. 28.6). Figures show microscopic findings of the residual renal tumor.

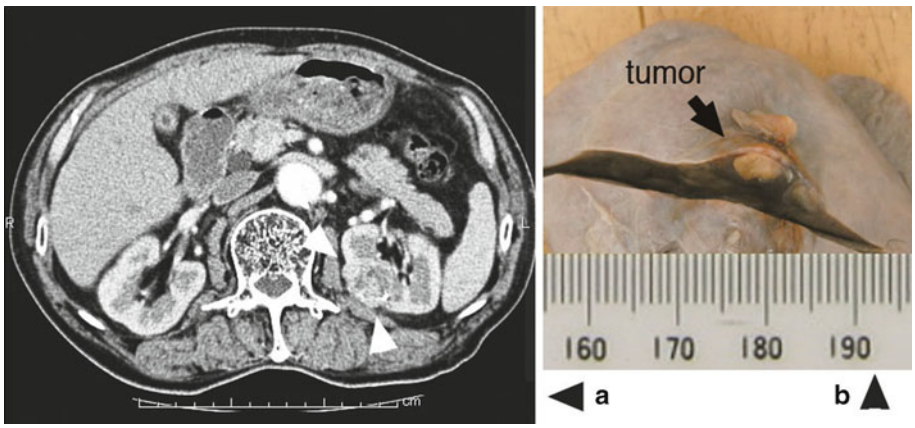

Fig. 28.5 Findings of a patient who died of intercurrent disease. (**a**) CT just before the treatment for RCC. Initial maximal diameter of the tumor was 3 cm. (**b**) Macroscopic findings of the tumor at the autopsy (8 months after the carbon ion therapy)

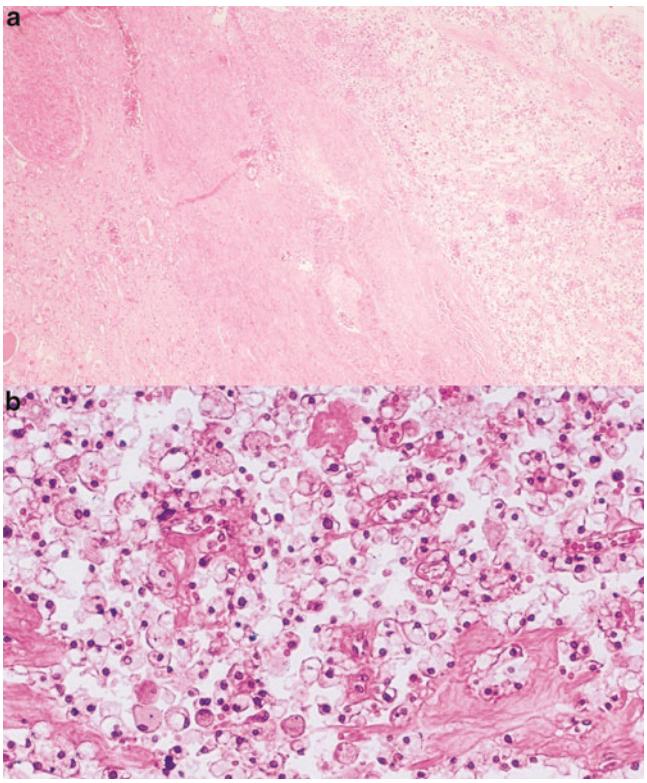

Fig. 28.6 (**a**) Specimen of the RCC 8 months after carbon ion therapy, at low magnification (×40). (**b**) Specimen of the RCC at high magnification (×200). The specimen of treated RCC shows degenerative cancer cells with clear cytoplasm, loss of nucleus, hyaline degeneration, macrophage/lymphatic invasion, and vascular invasion

The specimen showed degenerative cancer cells with clear cytoplasm, loss of nucleus, hyaline degeneration, macrophage/lymphatic invasion, and vascular invasion. These findings suggest that the tumor tissue was in the process of degeneration.

28.7 Conclusion

Historically, RCC is a tumor that has been thought to be a typically radioresistant neoplasm. So opportunities for curative radiotherapy are rarely performed for patients with RCC, except in cases of inoperable status or under special circumstances. Thus, there are few studies that have examined definitive radiotherapy for primary RCC. However, the initial clinical experience of carbon ion therapy for RCC in our institution resulted in unexpectedly favorable outcomes. The advantages of this treatment were its minimally invasive nature and it is an effective therapy for small and large tumors exceeding 10 cm in diameter. A formal phase II clinical trial of carbon ion therapy for primary RCC has begun at our institution, and patient registration began for this study in 2012. Long-term outcomes of this clinical trial are expected.

References

1. Ferlay J, Shin HR, Bray F, et al. GLOBOCAN 2008 v2.0, Cancer incidence and mortality worldwide: IARC CancerBase No. 10 [Internet]. Lyon: International Agency for Research on Cancer; 2010. http://globocan.iarc.fr, accessed on day/month/year.
2. Parkin DM, Bray F, Ferlay J, et al. Global cancer statistics, 2002. CA Cancer J Clin. 2005;55(2):74–108.
3. DeSantis C, Naishadham D, Jemal A. Cancer statistics for African Americans. CA Cancer J Clin. 2013;63(3):151–66. doi:10.3322/caac.21173.
4. Vaishampayan UN, Do H, Hussain M, et al. Racial disparity in incidence patterns and outcome of kidney cancer. Urology. 2003;62(6):1012–7.
5. Sánchez-Martín FM, Millán-Rodríguez F, Urdaneta-Pignalosa G, et al. Small renal masses: incidental diagnosis, clinical symptoms, and prognostic factors. Adv Urol. 2008:310694. doi:10.1155/2008/310694. Epub 2009 Jan 21.

6. Tsui KH, Shvarts O, Smith RB, et al. Renal cell carcinoma: prognostic significance of incidentally detected tumors. J Urol. 2000;163(2):426–30.
7. Lightfoot N, Conlon M, Kreiger N, et al. Impact of noninvasive imaging on increased incidental detection of renal cell carcinoma. Eur Urol. 2000;37(5):521–7.
8. Homma Y, Kawabe K, Kitamura T, et al. Increased incidental detection and reduced mortality in renal cancer–recent retrospective analysis at eight institutions. Int J Urol. 1995;2(2):77–80.
9. Beisland C, Medby PC, Beisland HO. Renal cell carcinoma: gender difference in incidental detection and cancer-specific survival. Scand J Urol Nephrol. 2002;36(6):414–8.
10. Vineis P, Alavanja M, Buffler P, et al. Tobacco and cancer: recent epidemiological evidence. J Natl Cancer Inst. 2004;96(2):99–106.
11. McLaughlin JK, Hrubec Z, Heineman EF, et al. Renal cancer and cigarette smoking in a 26-year followup of U.S. veterans. Public Health Rep. 1990;105(5):535–7.
12. Chow WH, Gridley G, Fraumeni Jr JF, et al. Obesity, hypertension, and the risk of kidney cancer in men. N Engl J Med. 2000;343(18):1305–11.
13. Zagzag D, Krishnamachary B, Yee H, et al. Stromal cell-derived factor-1alpha and CXCR4 expression in hemangioblastoma and clear cell-renal cell carcinoma: von Hippel-Lindau loss-of-function induces expression of a ligand and its receptor. Cancer Res. 2005;65(14):6178–88.
14. Campbell SC, Novick AC, Belldegrun A, et al. Practice Guidelines Committee of the American Urological Association. Guideline for management of the clinical T1 renal mass. J Urol. 2009;182(4):1271–9.
15. Novick AC. Laparoscopic and partial nephrectomy. Clin Cancer Res. 2004;10(18 Pt 2):6322S–7.
16. Hafez KS, Fergany AF, Novick AC. Nephron sparing surgery for localized renal cell carcinoma: impact of tumor size on patient survival, tumor recurrence and TNM staging. J Urol. 1999;162(6):1930–3.
17. Belldegrun A, Tsui KH, deKernion JB, et al. Efficacy of nephron-sparing surgery for renal cell carcinoma: analysis based on the new 1997 tumor-node-metastasis staging system. J Clin Oncol. 1999;17(9):2868–75.
18. Lerner SE, Hawkins CA, Blute ML, et al. Disease outcome in patients with low stage renal cell carcinoma treated with nephron sparing or radical surgery. J Urol. 1996;155(6):1868–73.
19. Moll V, Becht E, Ziegler M. Kidney preserving surgery in renal cell tumors: indications, techniques and results in 152 patients. J Urol. 1993;150(2 Pt 1):319–23.
20. Kunkle DA, Uzzo RG. Cryoablation or radiofrequency ablation of the small renal mass: a meta-analysis. Cancer. 2008;113(10):2671–80.
21. Onufrey V, Mohiuddin M. Radiation therapy in the treatment of metastatic renal cell carcinoma. Int J Radiat Oncol Biol Phys. 1985;11(11):2007–9.
22. DiBiase SJ, Valicenti RK, Schultz D, et al. Palliative irradiation for focally symptomatic metastatic renal cell carcinoma: support for dose escalation based on a biological model. J Urol. 1997;158(3 Pt 1):746–9.
23. Wersäll PJ, Blomgren H, Lax I, et al. Extracranial stereotactic radiotherapy for primary and metastatic renal cell carcinoma. Radiother Oncol. 2005;77(1):88–95.
24. Svedman C, Sandström P, Pisa P, et al. A prospective phase II trial of using extracranial stereotactic radiotherapy in primary and metastatic renal cell carcinoma. Acta Oncol. 2006;45(7):870–5.
25. Lopez-Beltran A, Scarpelli M, Montironi R, et al. 2004 WHO classification of the renal tumors of the adults. Eur Urol. 2006;49(5):798–805.
26. Steinbach F, Stockle M, Muller SC, et al. Conservative surgery of renal cell tumors in 140 patients: 21 years of experience. J Urol. 1992;148(1):24–9.
27. Cheville JC, Lohse CM, Zincke H, et al. Comparisons of outcome and prognostic features among histologic subtypes of renal cell carcinoma. Am J Surg Pathol. 2003;27(5):612–24.
28. Patard JJ, Leray E, Rioux-Leclercq N, et al. Prognostic value of histologic subtypes in renal cell carcinoma: a multicenter experience. J Clin Oncol. 2005;23(12):2763–71.
29. Skolarus TA, Serrano MF, Berger DA, et al. The distribution of histological subtypes of renal tumors by decade of life using the 2004 WHO classification. J Urol. 2008;179(2):439–43.
30. Volpe A, Jewett MA. The natural history of small renal masses. Nat Clin Pract Urol. 2005;2(8):384–90.
31. Sowery RD, Siemens DR. Growth characteristics of renal cortical tumors in patients managed by watchful waiting. Can J Urol. 2004;11(5):2407–10.
32. Kouba E, Smith A, McRackan D, et al. Watchful waiting for solid renal masses: insight into the natural history and results of delayed intervention. J Urol. 2007;177(2):466–70.
33. Edge SB, Byrd DR, Compton CC, Fritz AG, Greene FL, Trotti A, editors. AJCC cancer staging manual. 7th ed. New York: Springer; 2010.
34. Herts BR, Baker ME. The current role of percutaneous biopsy in the evaluation of renal masses. Semin Urol Oncol. 1995;13(4):254–61.
35. Yanagi T, Kamada T, Tsuji H, et al. Dose-volume histogram and dose-surface histogram analysis for skin reactions to carbon ion radiotherapy for bone and soft tissue sarcoma. Radiother Oncol. 2010;95(1):60–5.
36. Nomiya T, Tsuji H, Hirasawa N, et al. Carbon ion radiation therapy for primary renal cell carcinoma: initial clinical experience. Int J Radiat Oncol Biol Phys. 2008;72(3):828–33.

Part XVII

Gynecologic Tumors

Uterine Cancer

29

Masaru Wakatsuki

Abstract

Carbon-ion beams offer improved dose distribution, resulting in the concentration of a sufficient dose within a target volume while minimizing the dose in surrounding normal tissues. Moreover, carbon ions possess a biological advantage due to their high relative biological effectiveness (RBE) in the Bragg peak. A number of reports have demonstrated the favorable results of carbon-ion radiotherapy (C-ion RT) in the treatment of several malignant tumors. As for clinical trials of C-ion RT for locally advanced cervical cancer, five have already been completed, and two are still ongoing.

Between June 1995 and March 2013, 197 patients with locally advanced cervical cancer in seven protocols were treated with C-ion RT. C-ion RT has been established as a safe short-term treatment for locally advanced uterine cervical cancer. Although the patient population in these trials was small, it was shown that C-ion RT has the potential to improve the treatment for locally advanced bulky squamous cell carcinoma or adenocarcinoma of the uterine cervix, with the results supporting the view that investigations should be continued to confirm the therapeutic efficacy. In addition, we are now conducting a new clinical trial of C-ion RT with concurrent chemotherapy.

Keywords

Carbon-ion radiotherapy • Locally advanced uterine cervical cancer • Particle therapy • Uterine adenocarcinoma • Uterine cervical cancer

29.1 Introduction

Uterine cervical cancer is the second most common cancer after breast cancer in women in most developing countries. The majority of the patients have squamous histology, but there has also been an increasing trend in the incidence of adenocarcinoma and adenosquamous carcinoma of the uterine cervix in the past 40 years, especially among younger women.

In the early stage of the disease, cervical cancer is highly curable by surgery or radiotherapy alone [1]. In the case of locally advanced disease, however, the treatment results have been unsatisfactory. Several randomized phase III clinical trials in the 1990s and a meta-analysis demonstrated that the improvement of survival and local control was achieved by cisplatin-based concurrent chemoradiation therapy (CCRT) [2–4]. From the results of these clinical trials, CCRT has apparently become the standard treatment for this disease. Nevertheless, a 5-year local failure rate of 30 % or higher has still been observed, especially in patients with stage III or IVA disease, with the pelvis being the major site of failure. In addition, adenocarcinoma of the uterine cervix is more radioresistant than squamous cell carcinoma and has been shown as a predictive factor after radiation therapy.

Hence, further treatment strategies should be explored with the aim of obtaining better outcomes for locally advanced bulky squamous cell carcinoma and locally advanced adenocarcinoma.

M. Wakatsuki (✉)
National Institute of Radiological Sciences, Chiba, Japan
e-mail: waka@nirs.go.jp

H. Tsujii et al. (eds.), *Carbon-Ion Radiotherapy: Principles, Practices, and Treatment Planning*,
DOI 10.1007/978-4-431-54457-9_29, © Springer Japan 2014

29.2 Significance of C-Ion RT

Standard therapy for locally advanced cervical carcinoma is concurrent chemoradiation therapy. Recently, many researchers have reported clinical trials for locally advanced cervical carcinoma, and cisplatin-based CCRT has become the standard therapy. However, analysis of failure patterns following CCRT in locally advanced disease has shown locoregional recurrence of 20–30 % of the patients treated, and higher incidence with increasing tumor size. Toita et al. reported 2-year locoregional control rates for CCRT in patients with tumors <50, 50–70, and >70 mm of 85, 72 and 54 %, respectively [5]. Parker et al. reported 5-year local control rates for <50 and >50 mm of 73 and 56 %, respectively [6].

In most clinical trials, the majority of the patients had squamous cell carcinoma and approximately 10 % had adenocarcinomas. As for the results of radiation therapy, adenocarcinoma of the uterine cervix appeared more radioresistant than squamous cell carcinoma, and local control was poor after radiation therapy with or without chemotherapy for locally advanced adenocarcinoma of the uterine cervix. Grigsby et al. reported a 5-year local control rate of 33 % for stage III adenocarcinoma of the uterine cervix by RT alone [7]. Niibe et al. reported local control of 36 % for stage IIIB by RT alone or CCRT [8]. Huang et al. reported 58 % for stage III and 48 % for stage IB–IIA bulky (>4 cm) by RT alone or CCRT [9]. Radiation therapy with or without chemotherapy for adenocarcinoma of the uterine cervix is still unsatisfactory.

Thus, these results have illustrated that even more effective therapy is required for locally advanced bulky cervical cancer or adenocarcinoma. One of the approaches for improving treatment results is to use other drugs as radiosensitizing chemotherapy, and another is the use of particle therapy. Since 1995, National Institute of Radiological Sciences (NIRS) has been conducting a series of clinical trials for locally advanced squamous cell carcinoma and adenocarcinoma of the cervix.

29.3 Clinical Features and Diagnostic Workup

At NIRS, we have so far performed seven clinical trials (five completed two ongoing) for locally advanced squamous cell carcinoma and adenocarcinoma of the uterine cervix (Fig. 29.1). The eligibility criteria for enrollment in these studies were: (1) histologically proven squamous cell carcinoma, adenocarcinoma, or adenosquamous cell carcinoma, (2) International Federation of Gynecology and Obstetrics (FIGO 1994) stage IIB, III, or IVA disease (> 4 cm in diameter for squamous cell carcinoma) without rectal invasion, (3) no prior treatment, and (4) expected survival of longer than 6 months. Patients were also excluded if they had severe pelvic infection, severe psychological illness, or active double cancer. Pretreatment evaluation consisted of an assessment of the patient's history, physical and pelvic examinations by gynecologists and radiation oncologists, cervical biopsy, routine blood cell counts, chemistry profile, chest X-ray, cystoscopy, and rectoscopy. Bladder or rectal involvement was assessed by endoscopy. CT scans of the abdomen and pelvis, magnetic resonance imaging (MRI) of the pelvis, and positron emission tomography (PET) scans were also performed for all patients. Patients were staged according to the FIGO staging system, but patients with para-aortic lymph nodes > 1 cm in minimum diameter on CT images were excluded from the studies, although patients with only enlarged pelvic lymph nodes were included. Tumor size was assessed by both pelvic examination and MRI, and tumor dimensions were measured according to T2-weighted MRI images. Staging laparotomy was not performed, and no histologic confirmation of CT-positive pelvic lymph nodes was obtained. No patient underwent lymph node resection. PET scans were supplementarily used for detecting distant metastases. Working group pathologists reviewed the tumor specimens. The treatment protocols for these clinical studies were reviewed and approved by the NIRS Ethics Committee of Human Clinical Research, and all patients signed an informed consent form before the initiation of therapy.

29.4 General Management of Radiation Technique

Carbon-ion RT was given daily at 4 days per week (Tuesday to Friday). At every treatment session, the patient was positioned on the treatment couch while wearing the immobilization devices, and the patient's position was verified with a computer-aided, online positioning system. To minimize internal target positional uncertainty, 100–150 mL of normal saline was infused into the bladder. Patients were also encouraged to use laxatives, if necessary, to prevent constipation throughout the treatment period. The radiation dose was calculated for the target volume and surrounding normal structures and was expressed in GyE, defined as the carbon physical dose (Gy) multiplied by a relative biological effectiveness value of 3.0.

The treatment consisted of prophylactic whole pelvic or extended-field irradiation and local boost. Planning computed tomography (CT) scan is basically performed three times during the course of the treatment, and the clinical target volume (CTV) of local boost is reduced twice in accordance with tumor shrinkage. The clinical target volume of whole pelvic irradiation (CTV-1) includes CTV for primary disease and prophylactic area of lymph nodes, which are all

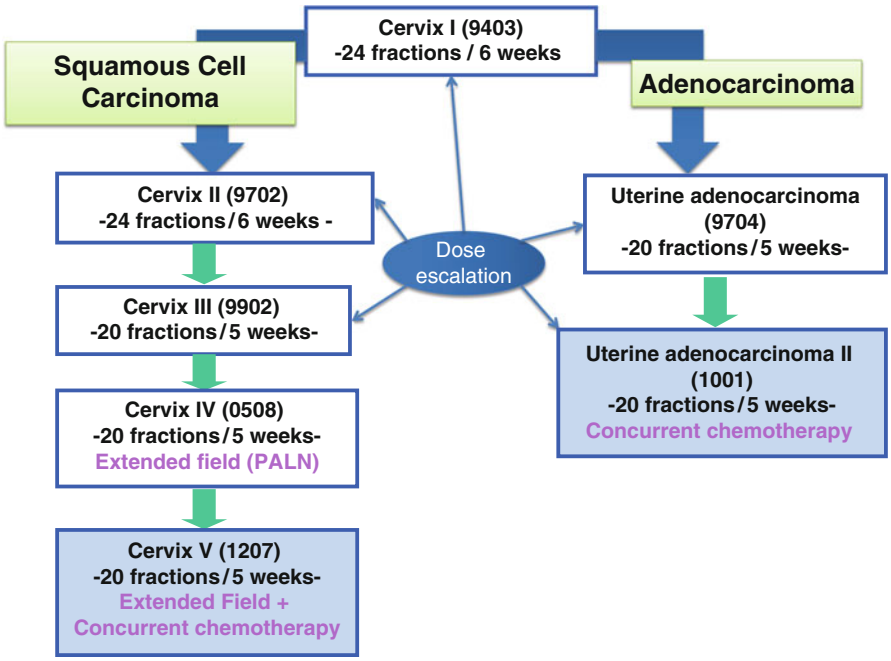

Fig. 29.1 History of clinical trials for uterine cervical cancer

areas of gross and potentially microscopic disease. The clinical target volumes for primary disease and lymph nodes are similar to those for photon irradiation [10–14]. The clinical target volume for primary disease consists of the tumor, uterus, ovaries, parametrium, and at least the upper half of the vagina [10]. The clinical target volume for pelvic lymph nodes consists of the area of common iliac, internal iliac, external iliac, obturator, and presacral lymph nodes and that for extended-field consists of the pelvic lymph node area and para-aortic lymph node area (Fig. 29.2a–c) [14].

The planning target volume (PTV-1) includes CTV-1 plus a 5-mm safety margin for positioning uncertainty and the uterus plus a 1.5-cm safety margin for intra- and inter-movement. CTV-1 is covered by at least 90 % of the prescribed dose (Fig. 29.2d). After completing CTV-1 irradiation, first reduction of CTV includes the gross tumor volume (GTV) and uterine cervix, uterine corpus, parametrium, upper half of the vagina, and ovaries (=CTV-2). A 5-mm margin was added to PTV-2 (Fig. 29.2e). Finally, CTV is shrunk to GTV only (CTV-3), and no margin was added to PTV-3 (Fig. 29.2f). Normal tissue structures, such as the rectum, sigmoid colon, bladder, and the small bowel in the pelvis, were excluded from PTV as much as possible.

In the first two clinical trials of C-ion RT (9403 and 9702) for squamous cell carcinoma of the uterine cervix, 18 % of the patients developed major gastrointestinal (GI) complications [15]. Therefore the treatment technique was revised after 2000. The dose to the GI tracts was limited to <60 GyE according to DVH analysis, and this limitation had higher priority than the prescription to PTV-3 as final boost irradiation [15]. In addition, vaginal packing for spacer between tumor of uterine cervix and rectum has been placed at the time of C-ion RT since 2002 (Fig. 29.3).

The treatment schedule for locally advanced squamous cell carcinoma of the uterus consisted of irradiation of PTV-1, PTV-2, and PTV-3 in 13, 5, and 2 fractions, respectively. The first three clinical trials (protocols 9403, 9702, and 9902) were dose-escalation trials, and the fourth (protocol 0508) included extended-field irradiation. In protocol 9902, based on DVH analysis of protocols 9403 and 9702, the doses to PTV-1 and PTV-2 were fixed at 39.0 GyE in 13 fractions and 15.0 GyE in 5 fractions (3.0 GyE per fraction), respectively. With regard to local boost, a dose-escalation study was planned with an initial dose of 10 GyE in 2 fractions to PTV-3. The dose to all GI tracts was strictly limited to <60 GyE to prevent major late toxicities. The initial dose was determined based on the results of protocols 9403 and 9702, in which 18 % of patients developed major late GI complications, and dose escalation to 18 GyE in 2 fractions was performed after careful observation of late toxicity according to discussions of the Working Group of the Gynecological Tumor on a semiannual basis. Total dose to the cervical tumor was 64.0–72.0 GyE in 20 fractions. In protocol 0508, CTV-1 is CTV of whole pelvic irradiation with para-aortic lymph node area. The doses to PTV-1, PTV-2, and PTV-3 in 0508 were fixed at 39.0 GyE in 13 fractions, 15.0 GyE in 5 fractions, and 18 GyE in 2 fractions, respectively (Fig. 29.4).

In the treatment schedule for locally advanced adenocarcinoma of the uterus (protocol 9704), PTV-1, PTV-2, and PTV-3 were irradiated with 12, 4, and 4 fractions, respec-

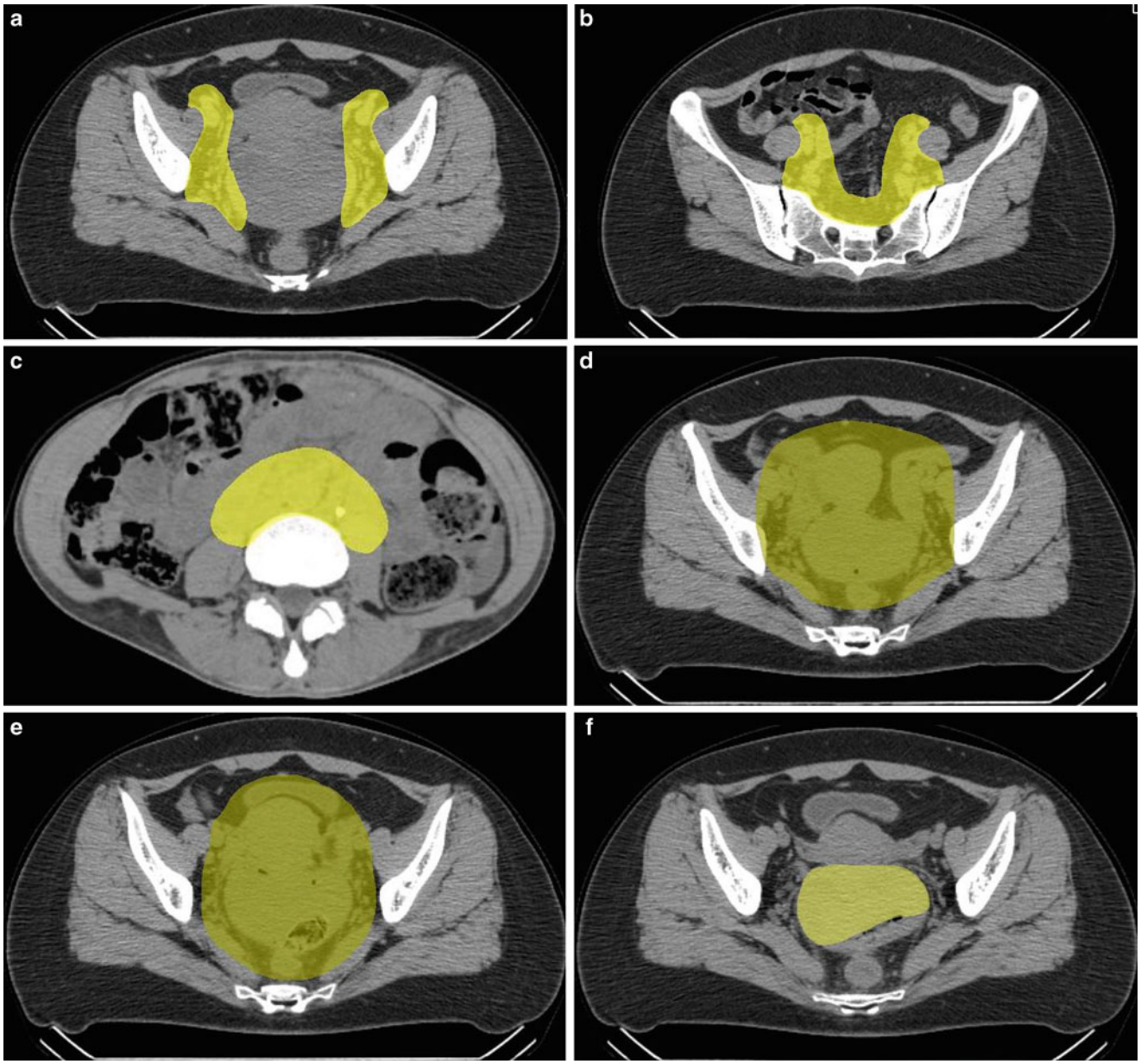

Fig. 29.2 (**a**, **b**) Clinical target volume for pelvic lymph nodes. (**c**) Clinical target volume for para-aortic lymph nodes. (**d**) Clinical target volume 1. (**e**) Clinical target volume 2. (**f**) Clinical target volume 3

tively (Fig. 29.5). This clinical trial was a dose-escalation trial. Based on the results of a previous study (protocol 9403), the dose to PTV-1 was fixed at 36.0 GyE in 12 fractions (3.0 GyE per fraction) in this protocol. With regard to local boost, a dose-escalation study was planned with an initial dose of 26.4 GyE in 8 fractions, then gradually increasing up to 38.4 GyE in 8 fractions by 2.4 or 3.6 GyE increments. Dose escalation was performed after careful observation of acute normal tissue responses according to discussion twice per year of the Working Group of the Gynecological Tumor. Total dose to the cervical tumor was 62.4–74.4 GyE over 20 fractions.

29.5 Results of Therapy

29.5.1 Locally Advanced Squamous Cell Carcinoma of the Uterus (9702, 9902, and 0508)

Between December 1997 and January 2011, 62 patients with locally advanced squamous cell carcinoma of the uterine cervix were treated with C-ion RT. Patients with histories of prior chemotherapy or pelvic radiotherapy were excluded from the studies. Patient characteristics are summarized in Table 29.1. Overall treatment time (OTT) ranged from 32 to

48 days, with a median of 36 days. The median follow-up durations for all patients and surviving patients were 29 and 49 months, respectively.

All of the observed acute and late toxicities are listed in Table 29.2. Although 28 patients (45.2 %) developed acute GI toxicity (G1–G2) and 15 patients (24.2 %) had acute GU toxicity (G1–G2), all patients completed the scheduled therapy. No patient developed grade 3 or higher acute toxicity. As for late toxicities, 20 patients developed GI complications (G1–G4). Among them, 18 patients had mild or intermediate bleeding of the rectum or sigmoid colon. Only one patient had rectal complication of G4, which was surgically salvaged, and the other had severe rectal bleeding. These cases were treated before revision of the treatment technique. Fifteen patients had grade 1 or 2 late GU toxicities, and no patient developed grade 3 or higher toxicity.

The 5-year overall survival rate and local control rate were 74.1 and 53.2 %, respectively (Fig. 29.6). The 5-year overall survival rate was still unsatisfactory, most likely because the patients frequently developed distant metastases. The high rate of distant metastasis can be ascribed to the advanced stage of the tumors, including the bulky tumors and high rate of pelvic lymph node metastasis.

In order to improve the survival rate as well as the local control rate, the use of chemotherapy in combination with C-ion RT has been explored. Currently, we are conducting a new clinical trial of C-ion RT combined with concurrent chemotherapy for locally advanced squamous cell carcinoma of the uterus.

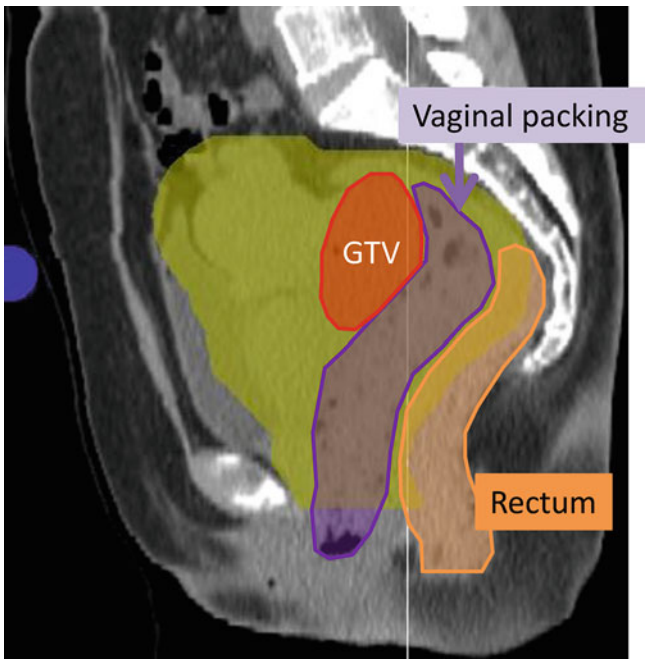

Fig. 29.3 Vaginal packing (*purple area*) for spacer between tumor of uterine cervix (*red*) and rectum (*orange*)

29.5.2 Locally Advanced Adenocarcinoma of the Uterus (9704)

Between April 1998 and February 2010, 55 patients with locally advanced adenocarcinoma of the uterus were treated with C-ion RT. Patient characteristics are summarized in Table 29.3. OTT ranged from 32 to 40 days, with a median of 35 days. Median follow-up for all patients and surviving patients was 38 months (range, 7–141 months), and 66 months (range, 27–141 months), respectively.

All of the observed acute and late toxicities are listed in Table 29.4. Although 23 patients (41.8 %) developed acute GI toxicity (G1–G2) and 11 patients (12.7 %) had acute GU toxicity (G1), all patients completed the scheduled therapy. No patient developed grade 3 or higher acute toxicity. As for late toxicities, 19 patients developed late GI complications. Among them, 18 patients had mild or intermediate bleeding of the rectum or sigmoid colon. Only one patient had rectal complication of G4, which was surgically salvaged. This case was treated before revision of the treatment technique. Thirteen patients had grade 1 or 2 late GU toxicities, and no patient developed grade 3 or higher toxicity.

The 5-year local control rate, local control rate including salvage surgery, and overall survival rate in all cases were 54.5, 68.2, and 38.1 %, respectively (Fig. 29.7a). The overall survival rate, however, was not satisfactory in this study, even though favorable local control was

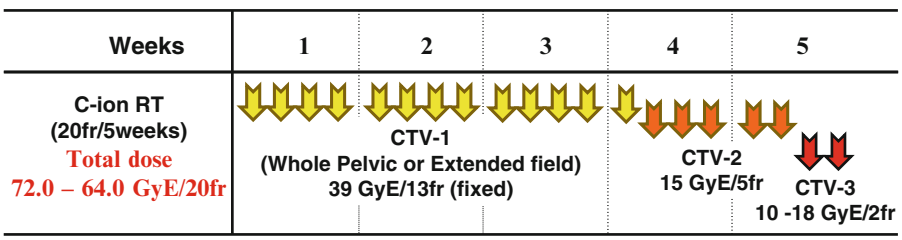

Fig. 29.4 Treatment schedule of protocols 0508 and 9902

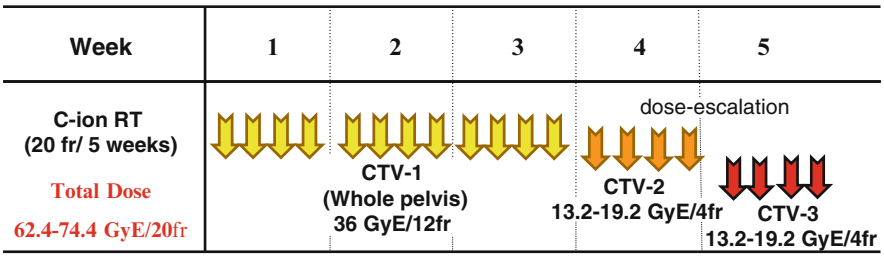

Fig. 29.5 Treatment schedule of protocol 9704

Table 29.1 Patient characteristics (9702, 9902, 0508, squamous cell carcinoma)

Number of patients	62
Follow-up, range (median) (month)	8–168 (29)
Age, range (mean) (year)	31–80 (59)
Performance status	
0–1	21
2	1
Stage	
IIB	14
IIIB	38
IVA	10
Lymph node status	
Negative	24
Positive	38
Tumor size (cm) (range (median))	4.0–12.0 (6.4)
<5.0	10
5.0–6.9	30
≥7.0	22

Table 29.2 Toxicity (9702, 9902, 0508)

		Acute (CTCAE ver 3.0)					
	N	G0	G1	G2	G3	G4	G5
GI tract	62	34	23	5	0	0	0
GU tract	62	47	13	2	0	0	0
Skin	62	37	25	0	0	0	0
	N	Late (RTOG/EORTC)					
		G0	G1	G2	G3	G4	
GI tract	62	42	14	4	1	1	
GU tract	62	49	7	6	0	0	
Skin	62	61	1	0	0	0	

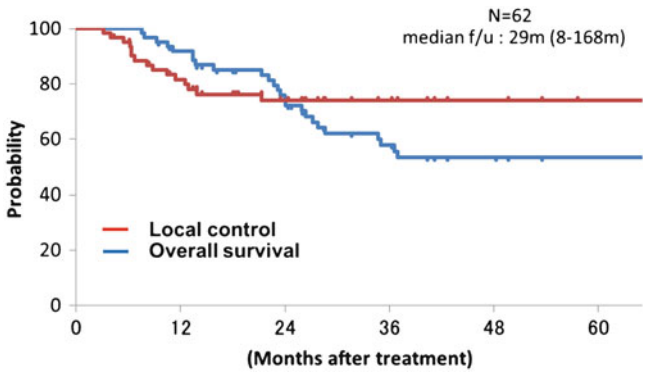

Fig. 29.6 Overall survival and local control curves in protocols 9702, 9902, and 0508 (Sq.C.C.): *Blue line* is overall survival curve; *red line* is local control curve

Table 29.3 Patient characteristics (9704, cervical adenocarcinoma)

Cases of uterine cervix	55
Age (median)	28–85 years (59 years)
Histology	
Adenocarcinoma	42
Adenosquamous cell carcinoma	13
Stage	
IIB	20
IIIB	33
IVA	2
Tumor size (median)	3.0–11.8 cm (5.5 cm)
Pelvic lymph node	
Negative	31
Positive	24
Dose (C-ion RT)	
62.4 GyE/20 fr	3
64.8 GyE/20 fr	4
68.0 GyE/20 fr	10
71.2 GyE/20 fr	21
74.4 GyE/20 fr	17

Table 29.4 Toxicities (9704, cervical adenocarcinoma)

		Acute (CTCAE ver 3.0)					
	N	G0	G1	G2	G3	G4	G5
GI tract	55	32	20	3	0	0	0
GU tract	55	51	11	0	0	0	0
Skin	55	30	8	0	0	0	0
		Late (RTOG/EORTC)					
		G0	G1	G2	G3	G4	
GI tract	55	43	10	2	0	1	
GU tract	55	45	5	5	0	0	
Skin	55	57	1	0	0	0	

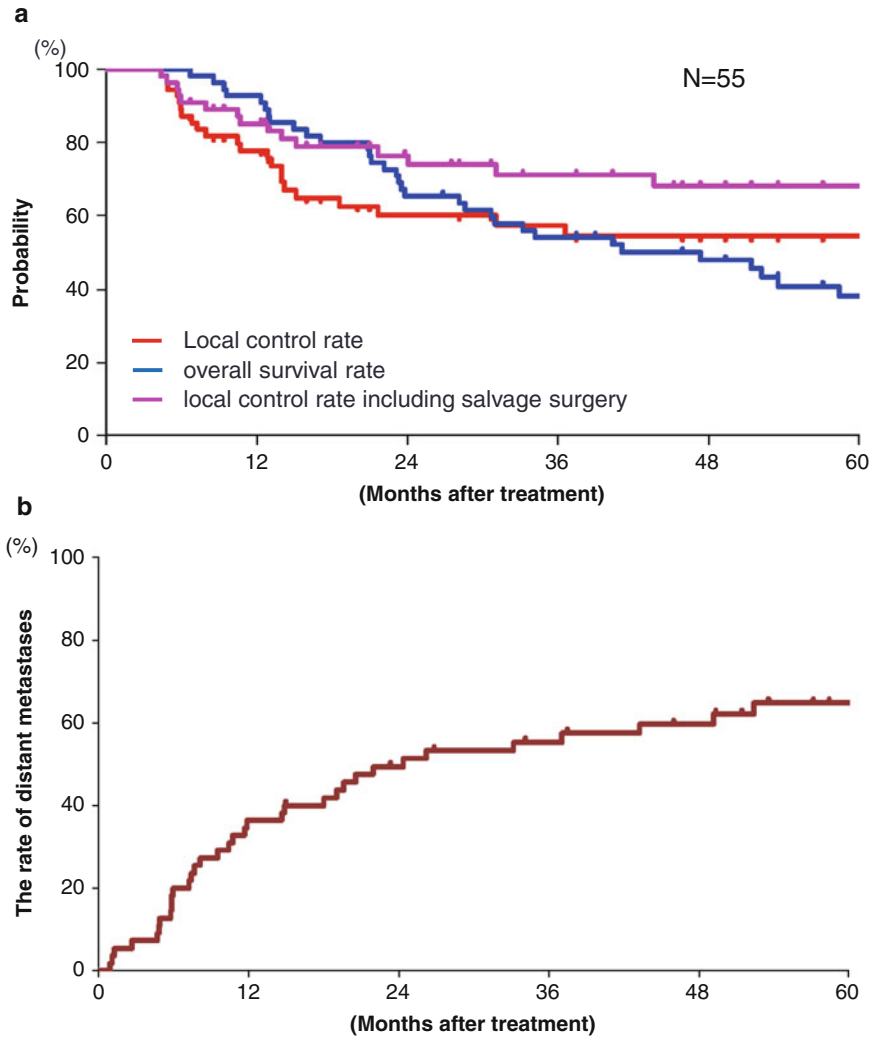

Fig. 29.7 (**a**) Local control rate, local control rate including salvage surgery, and overall survival rate in protocol 9704(cervical adenocarcinoma): *Blue line* is overall survival curve, *red line* is local control curve, and *pink line* is local control curve including salvage surgery. (**b**) Cumulative distant metastasis rate

obtained in bulky tumors. It has been shown that the prognosis of locally advanced adenocarcinoma of the uterine cervix is poor, and the 5-year survival rates were only 25–29 % [7–9, 16]. This could be attributed to poor local control as well as frequent distant metastases. In the present study, 2- and 5-year distant metastasis rates were 49.1 and 64.8 %, respectively (Fig. 29.7b). These rates were higher than those in the other studies, possibly because the patients in the present study did not receive concurrent chemotherapy, tumor size was larger than in the other studies, and the overall survival rate was higher than in the other studies. Thus, to improve the survival rate as well as the reduction of distant failures and local control rate, the use of chemotherapy in combination with C-ion RT should be further explored.

29.6 Case Study

The case of a 32-year-old Japanese female was referred to us with a diagnosis of FIGO stage IIB squamous cell carcinoma of the uterine cervix. MRI images detected a cervical mass measuring 76×80×56 mm (Fig. 29.8a) and bilateral external iliac lymph node enlargements (Fig. 29.8b). The higher accumulation of methionine to the tumor was seen on the methionine-PET scan images (Fig. 29.8a). The tumor invaded to the parametrium but did not extend to the pelvic sidewall.

The C-ion RT was performed with 39.0 GyE in 13 fractions for prophylactic extended-field irradiation, 15.0 GyE in 5 fractions for CTV of primary disease and swelling lymph nodes, and 18.0 GyE in 2 fractions for tumors. The total dose was 72.0 GyE in 20 fractions (Fig. 29.8c).

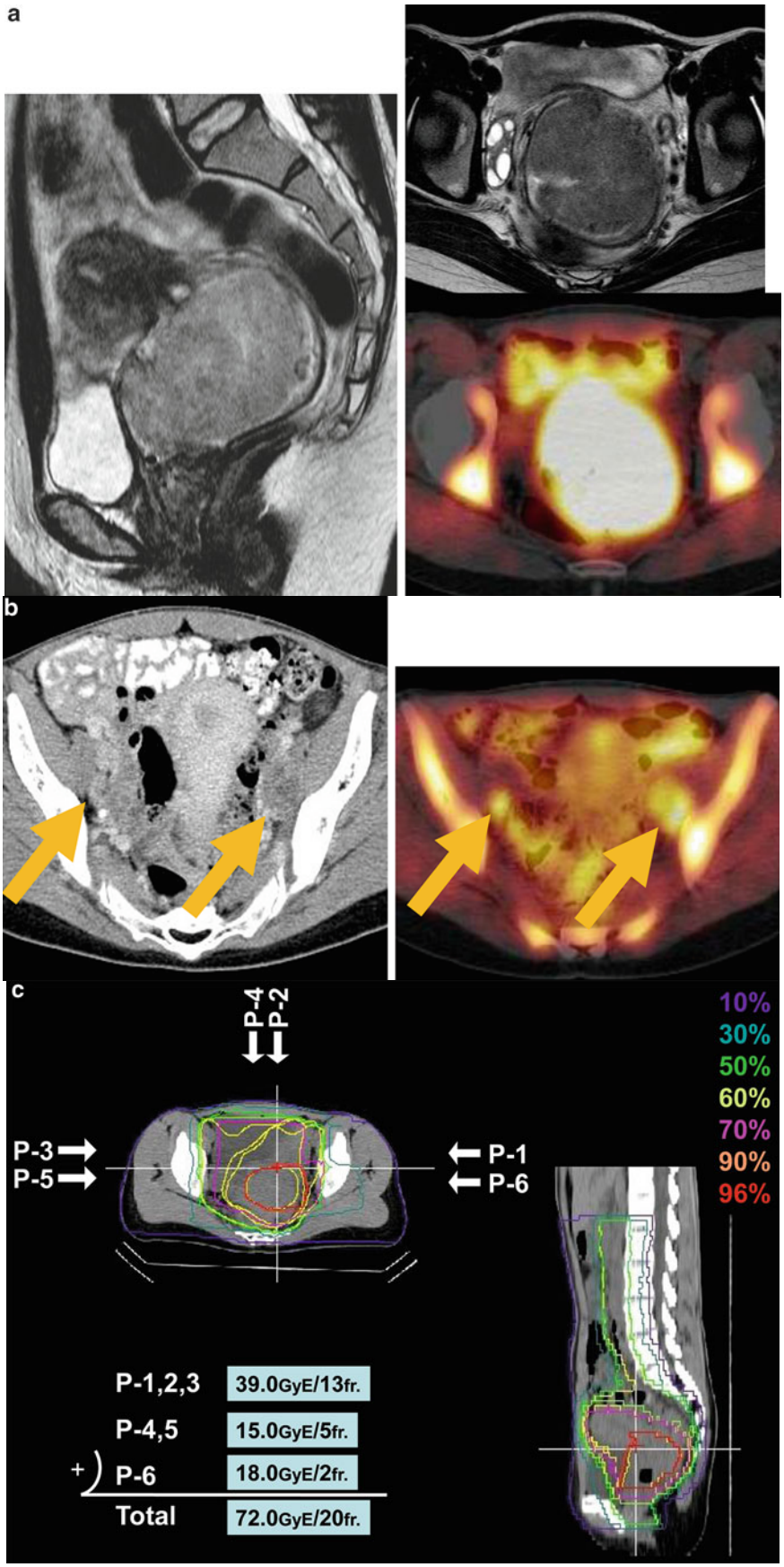

Fig. 29.8 (**a**) MRI and the methionine-PET scan images of uterine cervix before treatment. (**b**) CT and the methionine-PET scan images of pelvic lymph node before treatment. (**c**) Dose distribution of C-ion RT. (**d**) MRI images 6 months after C-ion RT

Fig. 29.8 (continued)

Six months later, the tumor demonstrated by the MRI completely disappeared (Fig. 29.8d). The patient is alive without any recurrence or metastasis at 3 years after the C-ion RT.

29.7 Summary

Carbon-ion RT has been established as safety treatment for locally advanced uterine cervical cancer. These results suggested that C-ion RT has the potential to improve the treatment for locally advanced bulky squamous cell carcinoma or adenocarcinoma of the uterine cervix, with the results supporting the view that investigations should be continued to confirm the therapeutic efficacy. In addition, we are now conducting a new clinical trial of C-ion RT with concurrent chemotherapy.

References

1. Nakano T, et al. Long-term results of high-dose rate intracavitary brachytherapy for squamous cell carcinoma of the uterine cervix. Cancer. 2005;103(1):92–101.
2. Rose PG, et al. Long-term follow-up of a randomized trial comparing concurrent single agent cisplatin, cisplatin-based combination chemotherapy, or hydroxyurea during pelvic irradiation for locally advanced cervical cancer: a Gynecologic Oncology Group Study. J Clin Oncol. 2007;25(19):2804–10.
3. Eifel PJ, et al. Pelvic irradiation with concurrent chemotherapy versus pelvic and para-aortic irradiation for high-risk cervical cancer: an update of radiation therapy oncology group trial (RTOG) 90-01. J Clin Oncol. 2004;22(5):872–80.
4. Chemoradiotherapy for Cervical Cancer Meta-Analysis, C. Reducing uncertainties about the effects of chemoradiotherapy for cervical cancer: a systematic review and meta-analysis of individual patient data from 18 randomized trials. J Clin Oncol. 2008;26(35):5802–12.
5. Toita T, et al. Phase II study of concurrent chemoradiotherapy with high-dose-rate intracavitary brachytherapy in patients with locally advanced uterine cervical cancer: efficacy and toxicity of a low cumulative radiation dose schedule. Gynecol Oncol. 2012; 126(2):211–6.
6. Parker K, et al. Five years' experience treating locally advanced cervical cancer with concurrent chemoradiotherapy and high-dose-rate brachytherapy: results from a single institution. Int J Radiat Oncol Biol Phys. 2009;74(1):140–6.
7. Grigsby PW, et al. Adenocarcinoma of the uterine cervix: lack of evidence for a poor prognosis. Radiother Oncol. 1988;12(4): 289–96.
8. Niibe Y, et al. High-dose-rate intracavitary brachytherapy combined with external beam radiotherapy for stage IIIb adenocarcinoma of the uterine cervix in Japan: a multi-institutional study of Japanese Society of Therapeutic Radiology and Oncology 2006–2007 (study of JASTRO 2006–2007). Jpn J Clin Oncol. 2010;40(8):795–9.
9. Huang YT, et al. Long-term outcome and prognostic factors for adenocarcinoma/adenosquamous carcinoma of cervix after definitive radiotherapy. Int J Radiat Oncol Biol Phys. 2011;80(2): 429–36.
10. Toita T, et al. A consensus-based guideline defining clinical target volume for primary disease in external beam radiotherapy for intact uterine cervical cancer. Jpn J Clin Oncol. 2011;41(9):1119–26.
11. Taylor A, et al. Mapping pelvic lymph nodes: guidelines for delineation in intensity-modulated radiotherapy. Int J Radiat Oncol Biol Phys. 2005;63(5):1604–12.
12. Small Jr W, et al. Consensus guidelines for delineation of clinical target volume for intensity-modulated pelvic radiotherapy in postoperative treatment of endometrial and cervical cancer. Int J Radiat Oncol Biol Phys. 2008;71(2):428–34.
13. Lim K, et al. Consensus guidelines for delineation of clinical target volume for intensity-modulated pelvic radiotherapy for the definitive treatment of cervix cancer. Int J Radiat Oncol Biol Phys. 2011;79(2):348–55.
14. Japan Clinical Oncology Group, et al. A consensus-based guideline defining the clinical target volume for pelvic lymph nodes in external beam radiotherapy for uterine cervical cancer. Jpn J Clin Oncol. 2010;40(5):456–63.
15. Kato S, et al. Dose escalation study of carbon ion radiotherapy for locally advanced carcinoma of the uterine cervix. Int J Radiat Oncol Biol Phys. 2006;65(2):388–97.
16. Eifel PJ, et al. Adenocarcinoma of the uterine cervix. Prognosis and patterns of failure in 367 cases. Cancer. 1990;65(11):2507–14.

Gynecological Melanoma

30

Kumiko Karasawa

Abstract

Primary malignant melanoma (MM) of the gynecological organs is extremely rare. Surgical resection has been performed as the best modality for this tumor, although all patients are not necessarily suitable candidates for surgery because of tumor extension, age, or physical condition. Based on the promising local control obtained with carbon-ion radiotherapy (C-ion RT) in mucosal MM of the head and neck as well as choroidal MM at the National Institute of Radiological Sciences (NIRS), we also started to treat gynecological MM with carbon ions in 2004. The small pelvic space was prophylactically irradiated with up to a total dose of 36 GyE in 10 fractions via three portals, followed by primary tumor and palpable lymph nodes irradiation with up to a total dose of 57.6 GyE in 16 fractions via two or three portals. From April 2011, tumors of more than 60 mL were irradiated with a larger dose of 64.0 GyE in 16 fractions. Limiting dose for critical normal tissues was 60 GyE for bowels. The overall 3-year local control rate for 23 cases was 50 %. C-ion RT may represent a potential noninvasive alternative to surgery.

Keywords

Malignant melanoma • Vaginal melanoma • Vulvar melanoma

30.1 Introduction

Primary MM of the gynecological organs including the vulva, vagina, uterus, and ovary is extremely rare. Gynecological melanoma is reported to occupy only 1–3 % of all melanomas. The incidence of MM in primary malignancies in vulva is 2–4 %, in vagina 3 %, in uterine cervix less than 1 %, and in ovary less than 1 % [1–4].

Surgical resection has been performed as a suitable modality for MM. En bloc excision with some safety margins has been most frequently chosen for primary treatment, although not all patients are suitable candidates for surgery, depending on tumor extension, age, and physical condition. Furthermore, even when total resection of the tumor has been performed, the outcome in terms of local tumor control and long-term survival has not been satisfactory, with postoperative physical and functional disabilities. Systemic therapy, such as dacarbazine monotherapy and DAVFeron (dacarbazine, nimustine, vincristine, and interferon-β) therapy, has been used in advanced or recurrent disease, and currently, molecular-target drugs such as vemurafenib and ipilimumab are being introduced. It is reported that local control and survival rates are mostly related to tumor thickness and the 5-year survival rate for tumors thicker than 4 mm was approximately 25 %. Because of the rarity of gynecological MM, it has not yet been possible to develop an optimal treatment modality, and treatment results have been unsatisfactory. As for disease staging, various classifications such as invasion depth of Breslow, Clark's level, and Chung's level have been

K. Karasawa (✉)
Research Center Hospital for Charged Particle Therapy, National Institute of Radiological Sciences, 4-9-1 Anagawa, Inage-ku, Chiba 263-8555, Japan
e-mail: kkarasaw@nirs.go.jp

H. Tsujii et al. (eds.), *Carbon-Ion Radiotherapy: Principles, Practices, and Treatment Planning*,
DOI 10.1007/978-4-431-54457-9_30,

employed, and the UICC classification of the skin reflects prognosis better than the UICC classification of each gynecological site.

30.2 Significance of C-Ion Radiotherapy

MM has been regarded as a radioresistant tumor, resulting in unsatisfactory local control by photon radiotherapy. However, the use of a high dose per fraction improves local response, with a 3-year local control rate of 30–60 % [2–4]. One of the significant features of C-ion RT is its high relative biological effectiveness, which benefits the treatment of radioresistant tumors. The favorable local control of C-ion RT to MM of head and neck and choroidal MM at NIRS suggests high effectiveness. C-ion RT could be a definitive noninvasive treatment modality for gynecological MM.

30.3 Clinical Features and Diagnostic Work-Up

Tumor extension is determined by CT, MRI, and PET. A candidate for C-ion RT is MM of genital mucosa without extension to the skin. Lymph node metastasis also should not extend beyond inguinal lymph nodes and the pelvic region. In C-ion RT, the tumor and normal structures such as the bowel and bladder should be separated by more than 5 mm.

30.4 General Management of Radiation Techniques

For patient immobilization, the pelvic cast (Moldcare; Alcare, Tokyo, Japan) and the fixation body shell (Shellfitter; Keraray Co., Ltd., Osaka, Japan) were applied in the supine position. Clinical target volume (CTV1) was defined as a small pelvic space including GTV (gross tumor volume) and metastatic lymph nodes in positive cases with a minimum margin of 5 mm, which was irradiated with 36 GyE in 10 fractions via three portals. Then CTV2, confined to GTV and metastatic lymph nodes in positive cases with a minimum margin of 5 mm, was irradiated with up to a total dose of 57.6 GyE in 16 fractions via 2–3 portals. In a previous study, large-volume tumors had a tendency to have poor control. From April 2011, therefore, we irradiated with a total dose of 64.0 GyE in 16 fractions to tumors of more than 60 mL. Limiting dose for critical normal tissue was 60 GyE for the bowel. Figure 30.1 shows a typical RT field and dose distribution.

30.5 Results of Therapy

A total of 23 patients were treated with C-ion RT. Acute grade 3 reactions of the skin, bowl, and bladder were observed in one patient. The overall 3-year local control, regional control, and distant metastasis-free rates were 50, 76, and 40 %, respectively. These values are comparable to surgical treatment results [5–12]. Figures 30.2 and 30.3 show pictures before and after treatment in patients with vulvar and vaginal MM.

30.6 Case Study

Case 1
An 80-year-old female had T2N0M0 vaginal MM. Her gynecologist consulted us due to her old age. She was treated with C-ion RT. A total of 57.6 GyE was delivered in 16 fractions at 4.4 GyE per fraction (Fig. 30.1).
Case 2
A 76-year-old female with vulvar melanotic macules was diagnosed as T1N0M0 MM. Her dermatologist consulted us for treating her by C-ion RT after sentinel lymph node biopsy. She received 57.6 GyE in 16 fractions of C-ion RT by scanning method (Fig. 30.4).

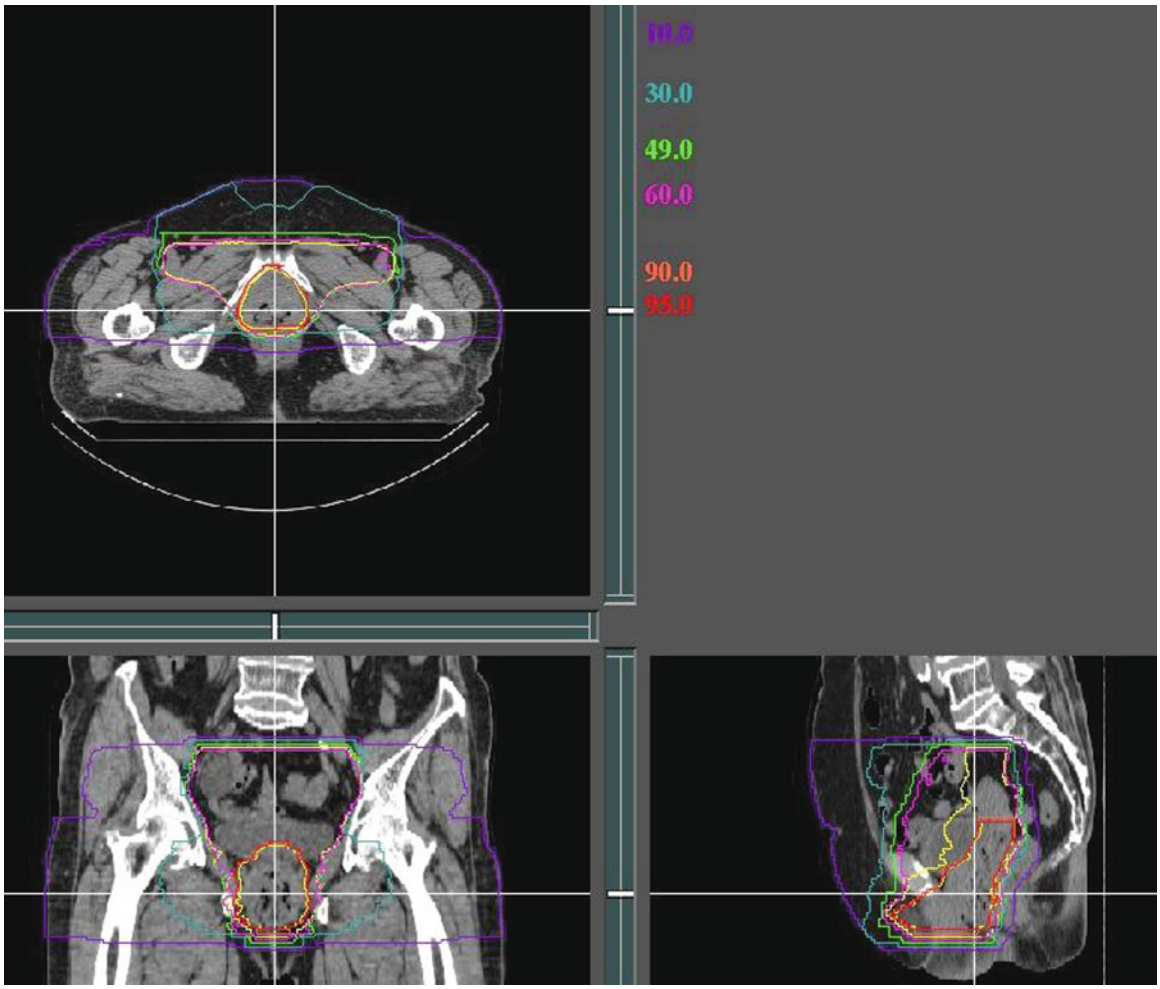

Fig. 30.1 A typical RT field with dose distribution of gynecological MM. A case with T1N0M0 vaginal MM

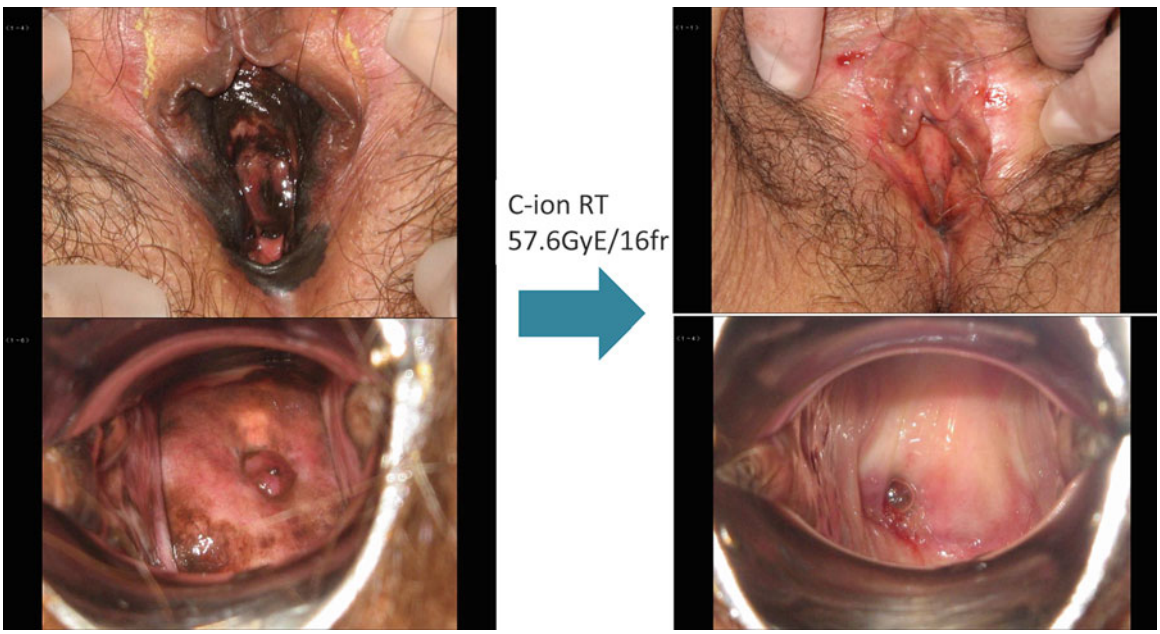

Fig. 30.2 A case of T4N0M0 vulvar MM treated with C-ion RT. Images before and after treatment

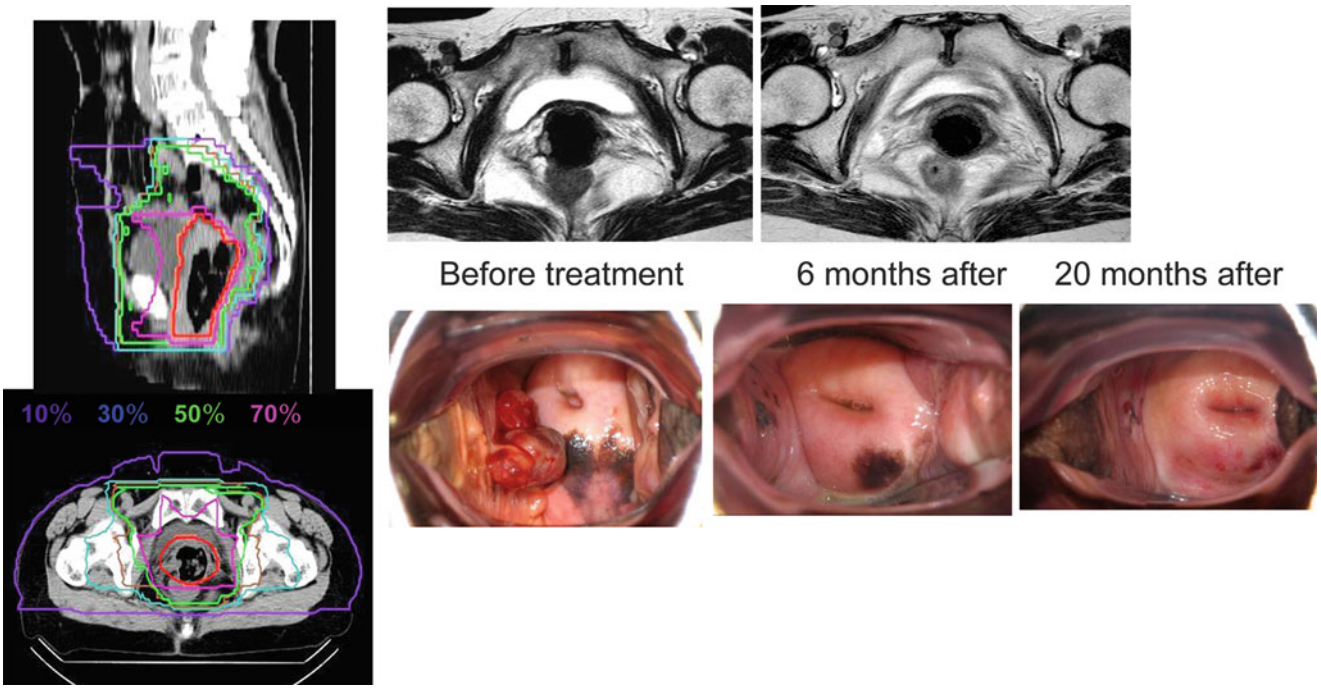

Fig. 30.3 A case of T4N0M0 vaginal MM treated with C-ion RT. Images before and after treatment

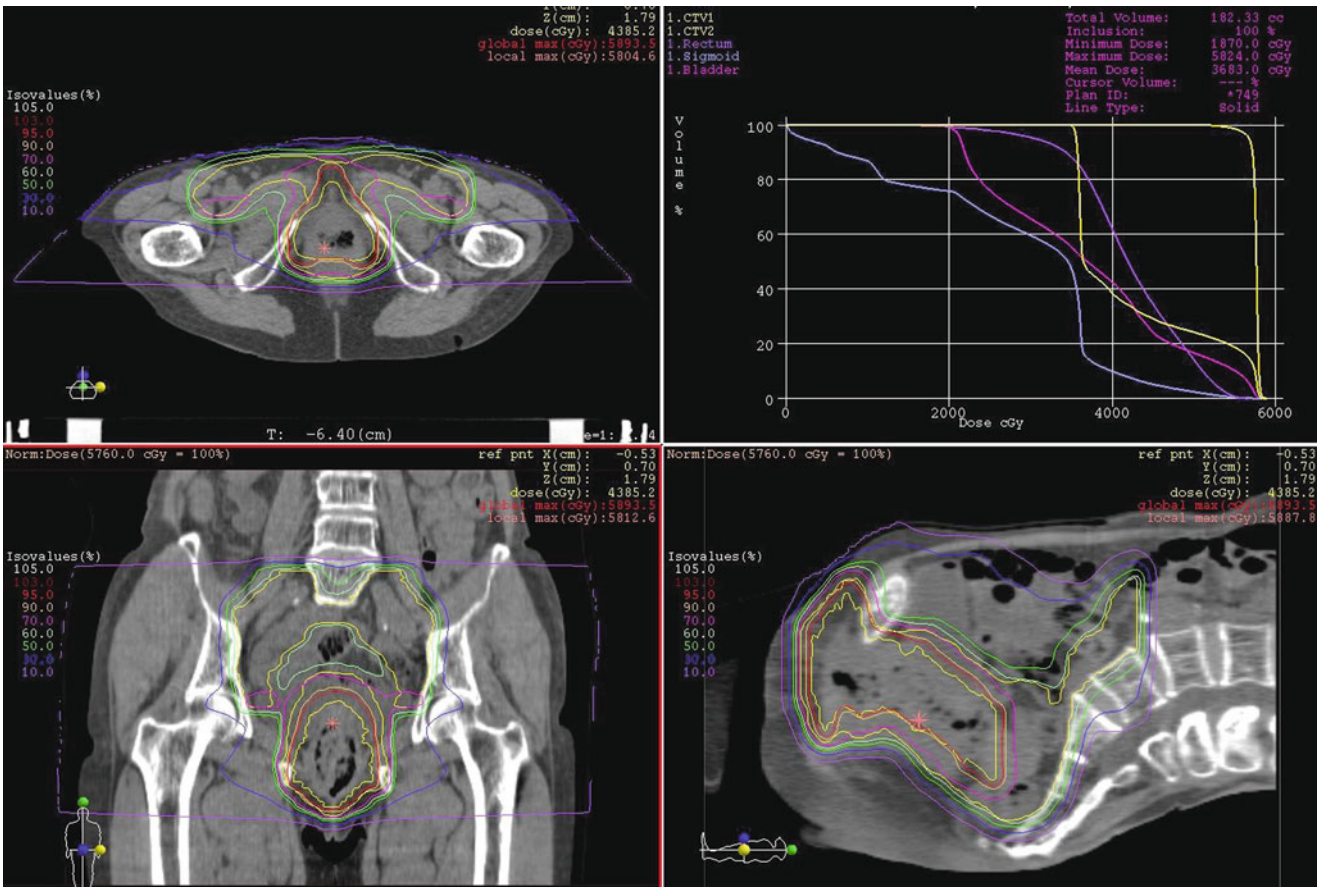

Fig. 30.4 A case of T1N0M0 vulvar melanoma treated with C-ion RT by scanning beam

References

1. Slingluff CL, Flaherty K, Posenberg SA, Read PW. Cutaneous melanoma. In: DeVita VT, Lawrence TS, Rosenberg SA, editors. Cancer principle & practice of oncology. 9th ed. Philadelphia: Lippincott Williams & Wilkins; 2011. p. 1643–91.
2. Tewari KS, Monk BJ. Malignant melanoma. In: Stehman FB, Schilder JM, editors. Invasive cervical cancer, Clinical gynecologic oncology. 7th ed. Philadelphia: Elsevier; 2012. p. 102.
3. Tewari KS, Monk BJ. Melanoma. In: Slomovitz BM, Coleman RL, editors. Invasive cancer of vulva, Clinical gynecologic oncology. 7th ed. Philadelphia: Elsevier; 2012. p. 239–43.
4. Tewari KS, Monk BJ. Malignant melanoma. In: Di Saia P, Creasman WT, editors. Invasive cancer of the vagina, Clinical gynecologic oncology. 7th ed. Philadelphia: Elsevier; 2012. p. 257–8.
5. Frumovitz M, Etchepareborda M, Sun CC, et al. Primary malignant melanoma of the vagina. Obstet Gynecol. 2010;116:1358–65.
6. Verschraegen CF, Benjapibal M, Supakarapongkul W, et al. Vulvar melanoma at the M. D. Anderson Cancer Center: 25 years later. Int J Gynecol Cancer. 2001;11:359–64.
7. Creasman WT, Phillips JL, Mench HR. A survey of hospital management practice for vulvar melanoma. J Am Coll Surg. 1999;188:670–5.
8. Ragnarsson-Olding BK, Kanter-Lewensohn LR, Lagerlof B, et al. Malignant melanoma of the vulva in a nationwide, 25-year study of 219 Swedish females. Cancer. 1999;86:1273–84.
9. DeMatos P, Tyler D, Seigler HF. Mucosal melanoma of the female genitalia: a clinicopathologic study of forty-three cases at Duke University Medical Center. Surgery. 1998;124:38–48.
10. Look KY, Roth LM, Sutton GP. Vulvar melanoma reconsidered. Cancer. 1993;72:143–6.
11. Trimble EL, Lewis Jr JL, Williams LL, et al. Management of vulvar melanoma. Gynecol Oncol. 1992;45:254–8.
12. Bradgate MG, Rollason TP, McConkey CC, et al. Malignant melanoma of the vulva: a clinicopathological study of 50 women. Br J Obstet Gynaecol. 1990;97:124–33.

Part XVIII

Bone and Soft Tissue Sarcomas

Bone and Soft-Tissue Sarcomas

31

Reiko Imai

Abstract

A dose-escalation clinical trial was first initiated in 1996 to evaluate the safety and efficacy of carbon ion radiotherapy (C-ion RT) for inoperable bone and soft-tissue sarcomas. The dose-escalation trial and a subsequent fixed-dose trial on patients with non-metastatic sarcomas revealed that carbon ion radiotherapy provided good local control and offered a survival advantage with acceptable levels of morbidity. Ninety-five percent of the patients enrolled in the trials had axial sarcomas. The 3- and 5-year local control rates of the entire study population in the fixed-dose trial were 79 and 71 %, respectively, with the corresponding 3- and 5-year overall survival rates being 71 and 59 %. As of March 2013, over 900 patients were treated with carbon ion radiotherapy for bone and soft-tissue sarcomas in several trials. The most commonly treated sarcoma was sacral chordoma, followed by axial high-grade bone and soft-tissue sarcomas. This chapter deals with C-ion RT for unresectable sarcomas below C2.

Keywords

Carbon ion radiotherapy • Charged particle therapy • Sarcoma • Sarcoma of the trunk

31.1 Introduction

Sarcomas have a much lower incidence than other cancers. In Japan, approximately 500 and 2,000 patients are diagnosed every year with malignant tumors originating from the bone and soft tissue, respectively [1, 2]. Sarcomas involve a wide variety of histological types (e.g., osteosarcoma, chondrosarcoma, and liposarcoma) and can develop in any part of the body. Depending on both the histological type and the original site of the tumor, the same treatment protocol can lead to different outcomes [3]. The mainstay of treatment for bone and soft-tissue sarcomas is inevitably surgery. Multidisciplinary approaches, including surgery, chemotherapy, and radiotherapy, have been successful in the treatment of some types of bone and soft-tissue sarcomas during the last three decades. In addition, dramatic advances in surgical techniques and prosthetics technology have markedly increased the limb salvage rate. However, some tumors aren't resectable depending on their location, size, and/or depth of invasion. Tumors in the extremities can often be curatively resected, whereas those involving the spine, pelvis, and other axial parts of the body are not always amenable to surgery, especially in advanced cases [4].

Until recently, unresectable sarcomas were sometimes treated with external radiation therapy and/or brachytherapy combined with chemotherapy. However, chemotherapy is effective for several types of sarcomas, and conventional radiotherapy affords good results only for some sarcomas. Therefore, unresectable sarcomas had a very poor prognosis due to the lack of any effective local treatment [5]. At National Institute of Radiological Sciences (NIRS), Chiba, Japan NIRS, a dose-escalation clinical trial was initiated in 1996 to evaluate the safety and efficacy of carbon ion radiotherapy for inoperable bone and soft-tissue sarcomas [6].

R. Imai (✉)
National Institute of Radiological Sciences, 4-9-1 Anagawa, Inage-ku, Chiba, Japan
e-mail: r_imai@nirs.go.jp

H. Tsujii et al. (eds.), *Carbon-Ion Radiotherapy: Principles, Practices, and Treatment Planning*,
DOI 10.1007/978-4-431-54457-9_31, © Springer Japan 2014

This trial and a subsequent fixed-dose trial for patients with non-metastatic sarcomas revealed that C-ion RT provided good local control and offered a survival advantage with acceptable levels of morbidity. Of the patients enrolled in the trials, 95 % had axial sarcomas. The 3- and 5-year local control rates of the entire study population in the fixed-dose trial were 79 and 71 %, respectively, and the corresponding 3- and 5-year overall survival rates were 71 and 59 %. As of March 2013, over 900 patients with bone and soft-tissue sarcomas had been treated with carbon ion radiotherapy in a series of trials.

31.2 Carbon Ion Radiotherapy

Three-dimensional treatment planning was performed using the HIPLAN software program specifically designed at NIRS for planning C-ion RT. The standard protocol for the treatment of bone and soft-tissue sarcomas consists of 16 irradiation sessions delivered over 4 weeks, once daily, 4 times per week, from Tuesday to Friday. A dose of 52.8–73.6 GyE was administered in the dose-escalation and the subsequent fixed-dose trials. In both trials, 70.4 GyE was administered as the standard total dose for sarcomas; 64.0 GyE, for spinal tumors; and 67.2 GyE, for sacral chordomas, in 16 fractions over 4 weeks. Energies of 350, 400, and 430 MeV/n were primarily used for the treatment of axial sarcomas.

Images of thin-slice computed tomography (CT) (3–5 mm) using contrast medium are essential for target delineation. Magnetic resonance imaging (MRI) using contrast medium is useful to evaluate the extent of bone invasion and tumors spreading in the soft tissue. Positron emission tomography–CT is sometimes useful to evaluate residual tumor areas after chemotherapy. The clinical target volume (CTV) included the gross tumor volume (GTV) plus at least a 5-mm margin for potential microscopic invasion, irrespective of the histological findings. CTV encompassed enhanced area on the images of CT and MRI as well. Larger margins were maintained for high-grade sarcomas invading the surrounding tissues and tumors recurring after resection. The planning target volume (PTV) included the CTV plus a 5-mm safety margin to account for positioning errors. If the tumor was located close to or abutting critical organs (e.g., the intestine, skin, and spinal cord), the margin was reduced.

The patients were usually treated with more than three ports to avoid severe reactions in the normal tissue. C-ion RT does not use the rotating gantry and its effect depends on the irradiated angle; therefore, immobilization devices are used to maintain positions, such as supine, prone, and oblique supine, to obtain the best irradiation paths. One port is used during each session. During irradiation, patients are placed in either the supine or prone position on the treatment couch using tailor-made immobilization devices for 20–30 min, in the treatment room. Irradiation with the carbon ion beams is applied for a few minutes.

With regard to toxicity, skin/soft-tissue late toxicity of grades 3 and 4 was observed in 2 % of the cases. The magnitude of the total dose applied to the skin was the major cause of the reaction. Yanagi et al. found that the values of $V_{64} > 100$ mL for the dose–volume histogram and $S_{60} > 20$ cm^2 for the dose–surface histogram could be used for predicting late skin reactions [7]. In addition, the appearance of late skin reactions suggested the involvement of other risk factors thought to include the following: (1) subcutaneous tumor invasion, (2) a large tumor volume, (3) sacrococcygeal involvement, (4) previous surgery, (5) additional chemotherapy, and (6) irradiation using two ports. Skin reactions by irradiation could be prevented by using over three ports, which reduces the dose administered to the skin surface. The incidence of late skin reactions of grade 3 or higher in patients receiving a total dose of 70.4 GyE with over three ports has remained within the acceptable level for the past several years.

31.3 Major Sarcomas Treated with C-Ion RT

31.3.1 Chordoma

Sacral chordoma is the most common bone and soft-tissue sarcoma treated with C-ion RT at our hospital. Sacral chordoma is a rare tumor. Although surgery is the first choice for the treatment of this tumor, it is not always possible. Since sacral chordomas usually develop gradually, they are often left undetected until they cause pain and other symptoms. Many patients referred to our hospital presented with sacral chordomas over 10 cm in diameter. Curative surgery for sacral chordoma (sacrectomy) is one of the most invasive surgeries. The sacrum houses the sacral nerves, which are involved in excretory function and ambulation. Depending on the level of tumor involvement of the sacral bone, excision of these nerves causes disabilities of gait, urinary function, and bowel movement and impairs the patients' quality of life. Sacrectomy is a challenging surgery. Sacral chordomas frequently occur among the elderly population, who are also often unfit for surgery because of comorbidities and old age.

Ninety-five patients with sacral chordoma underwent C-ion RT between 1996 and 2007 at NIRS [8]. The median age of the 95 patients was 66 years. Eighty-four patients had not been treated previously, whereas the remaining 11 experienced local recurrence of a previously resected tumor. The median tumor diameter was 9 cm. The carbon ion dose ranged from 52.8 to 73.6 GyE, and the median total dose was

70.4 GyE administered in 16 fractions over 4 weeks. The 5-year local control rate was 88 %, and the median time to local failure was 35 months (13–60 months). The 5-year overall survival rate was 86 %, with a median follow-up period of 42 months (13–112 months). Of the 95 patients, 91 % remained ambulatory with or without a supportive device. Two patients experienced severe skin and soft-tissue reactions requiring a skin graft. Fifteen patients experienced severe sciatic nerve complications, which required continued medication and affected their daily activities. After C-ion RT, the volume of the chordoma gradually reduced [9]. As of March 2012, 204 patients with chordomas at various sites had been treated with C-ion RT. As mentioned above, patients with chordomas were usually elderly. Currently, C-ion RT is being applied not only for unresectable tumors but also for resectable tumors in the elderly as an alternative to surgery [10, 11].

31.3.2 Osteosarcoma

Osteosarcoma of the trunk constituted the next largest group, and patients with this tumor were younger than those with chordoma. For osteosarcomas of the extremity, a combination of surgery and chemotherapy has been well established as the effective treatment strategy, and C-ion RT is unlikely to outweigh its advantages. C-ion RT is indicated in axial osteosarcomas not suited for surgery, such as lesions originating in the pelvis or the spinal and paraspinal areas. In our series, the 5-year local control and the 5-year overall survival rates for the 78 patients with unresectable osteosarcoma of the trunk were 62 and 33 %, respectively [12]. The median age at the time of initial referral was 41 years (range, 11–83 years). The tumor was located in the pelvis in 61 patients, in the spinal or paraspinal region in 15 patients, and in other regions in two patients (mediastinum and chest wall). The median diameter of the tumors was 10 cm. The median follow-up duration was 24 months (range, 2–166 months) for all 78 patients. Except for three patients who experienced severe skin/soft-tissue complications requiring skin grafts, no other severe toxicities were observed. Of the nine patients, including five teenagers who had been disease free for over 5 years, eight were able to walk with or without the help of a cane and six acquired freedom from the use of pain killers.

As reported in the literature, the survival rate for cases of unresectable osteosarcoma is 10 % or less [13]. Therefore, C-ion RT appears to provide a survival benefit for cases of unresectable disease. In our series, tumor volume was a prognostic factor for both survival and local control. Thirty-eight patients with a tumor volume of less than 500 cc had a 5-year local control rate of 88 %; this percentage was 31 % for 40 patients with a tumor volume of more than 500 cc. The 5-year overall survival rate of the 38 patients with smaller tumors was 46 %, whereas that in the larger tumor group was 19 % [12].

31.3.3 Chondrosarcoma

Chondrosarcoma is the second most frequent primary malignant bone tumor among bone sarcomas. Definitive en bloc resection of the tumor is mandatory for long-term disease-free survival. Chemotherapy and radiotherapy are not effective [14]. Chondrosarcomas of the trunk constituted the third largest group in our study. We evaluated 75 patients treated with C-ion RT for 78 chondrosarcomas, including two limbs. None of the patients had metastasis at the time of referral to our hospital, and the tumors were deemed unresectable by the referring surgeons. The median patient age was 56 years. Of the 78 lesions, 85 % were of a histological grade greater than 2. The median irradiated total dose was 70.4 GyE administered in 16 fractions over 4 weeks. The CTV ranged between 25 and 2,900 cm^3 (median, 496 cm^3). The median follow-up time was 41 months (range, 3–117 months) for all patients, and all living patients were followed up for more than 2 years. At 5 years, the actuarial local control and overall survival rates were 55 and 57 %, respectively. Four patients experienced skin/soft-tissue late reactions of grade 3 or 4. Among 16 patients aged more than 70 years, ten survived over a 3-year follow-up period and remained ambulatory [15].

31.4 Major Sites Treated with C-Ion RT

31.4.1 Sacral Sarcoma

Sacrectomy is one of the most challenging interventions among orthopedic surgeons and can sometimes cause severe neurological impairment in an attempt to maintain an adequate surgical margin. Resection of the sciatic nerves on both sides above S3 causes severe bowel and urological impairment. Resection of both the S1 nerves may damage the ambulatory function of patients. In cases of a large tumor involving the iliac bone over the sacroiliac joint or huge mass spreading to the buttock, surgery is not always performed. The choice of surgery is based on a comprehensive assessment of the case. Patients with unresectable tumors are candidates for C-ion RT.

Sacral sarcomas were the commonest tumors treated in our study, and the most common sarcoma was sacral chordoma.

When applying C-ion RT to sacral tumors, the following precautions need to be taken. First, exposure of the bowels, especially the rectum, to irradiation should be

avoided/minimized. If the tumor pushes the rectum, rendering the entire rectum flat, it is sometimes better to perform colostomy before carbon ion radiotherapy. If the tumor protrudes into the intestines, spacer placement to separate the tumor and intestines before the radiotherapy is recommended. Second, exposure of the skin to radiation should be minimized. This can be achieved by using more than three ports to disperse the radiation dose to the skin and by using a horizontal port effectively to direct the beams off the skin surface. Third, exposure of the sciatic nerves to radiation should be minimized. In our study, the severity of sciatic nerve injury depended on the DVH of the sciatic nerves. In the case of sciatic nerves, the higher the dose of radiation and the greater the target volume, the more severe are the resultant complications. As a tentative guide, a dose of 70.4 GyE in 16 fractions administered to a volume of 10 cm^3 appears to be related to severe symptoms such as paralysis. However, it is impossible to minimize the DVH when the tumor extensively involves the sciatic nerves. In our study, we did not set a specific dose constraint for the sciatic nerve. For sacral chordoma a dose of 67.2 GyE in 16 fractions is administered.

31.4.2 Pelvic Sarcoma

Surgical resection has been the mainstay in the treatment of pelvic sarcomas, and extensive surgery with adequate surgical margins affords good local control and survival. Similar to the case with sacral sarcomas, surgery in cases of pelvic sarcomas is decided on the basis of a comprehensive evaluation of the anatomical location of the tumors. In particular, acetabular sarcomas, wherein the tumor originates from the acetabular bone or invades the acetabulum, account for two-thirds of all pelvic sarcomas, excluding sacral lesions, treated with C-ion RT. When C-ion RT is administered to pelvic tumors, the following precautions should be taken. First, exposure of the bowels to radiation, by measures such as spacer placement to separate the tumor from the bowels, should be minimized. Second, irradiation of the skin, by measures such as using more than three ports to disperse the irradiation dose administered to the skin, should be minimized. Finally, irradiation to the acetabular bone and femoral head should be minimized. The destruction of the acetabular bone and the femoral head is sometimes noted a few years after C-ion RT (Fig. 31.7). In some cases in which the beam passed through the femoral neck, femoral neck fracture was noted. However, it is impossible to avoid exposure of the acetabular bone and the femoral head to radiation when the tumor originates or involves those bones. In 2011, beam delivery using the spot-scanning method became available at the NIRS. Scanning irradiation can offer better dose distribution than the passive method in the treatment of acetabular sarcomas and thereby reduce the dose administered to the femoral head and neck. This strategy may be useful to preclude the destruction of the femoral head and neck (Fig. 31.12).

31.4.3 Spinal and Paraspinal Sarcoma

Treatment of spinal and paraspinal tumors makes the best use of the characteristics of the charged particle beam. The treatment of such tumors is complicated by the proximity of lesions to the spinal cord. The radiation tolerance limit using photon beams to the spinal cord is generally quoted at 40–46 Gy in 20–25 fractions.

A “patch combination technique” is used in patients to optimize the dose distribution within tumors of an irregular volume and lying close to the spinal cord. The target volume is divided into two segments, and each segment is treated by a separate radiation field—an anterior/posterior field and a lateral field. By utilizing the sharp dose falloff after the Bragg peak, the distal edge of one field is matched with the lateral edge of the second field. The combination of the two fields and match lines are utilized on alternating days to smear out the potential dose inhomogeneities where the lateral edge of one portal abuts the distal end of the stopping beam [16, 17]. The dose constraint of the carbon ion beams directed to the cross sections involving the spinal cord is 30 GyE administered in 16 fractions; however, radiation-induced myelopathy was quite rare especially in limited experience of C-ion RT; more accumulation of cases and further analysis are needed in the future. The irradiated dose to the spinal cord should be minimized. In our study, as of 2012, C-ion RT was employed in 100 cases with spinal and paraspinal sarcomas, excluding sacral lesions. The patient age ranged from 12 to 84 years (median, 53 years). In principal, a total dose of 64 GyE in 16 fractions and 70.4 GyE in 16 fractions was applied for spinal and paraspinal sarcomas, respectively. The median follow-up duration was 31 months for all patients. At 5 years, the actuarial overall local control rate and overall survival rates were 75 and 51 %, respectively. Two patients in this series developed grade 3 late reactions of the spinal cord. Matsumoto et al. also reported the impact of C-ion RT for 48 spinal sarcomas [18].

31.4.4 Retroperitoneal Sarcoma

Radiotherapy for soft-tissue sarcomas, including retroperitoneal sarcoma, has played an auxiliary role to surgery [19]. C-ion RT has been used in locally advanced unresectable cases; however, the prevalent anatomical conditions may

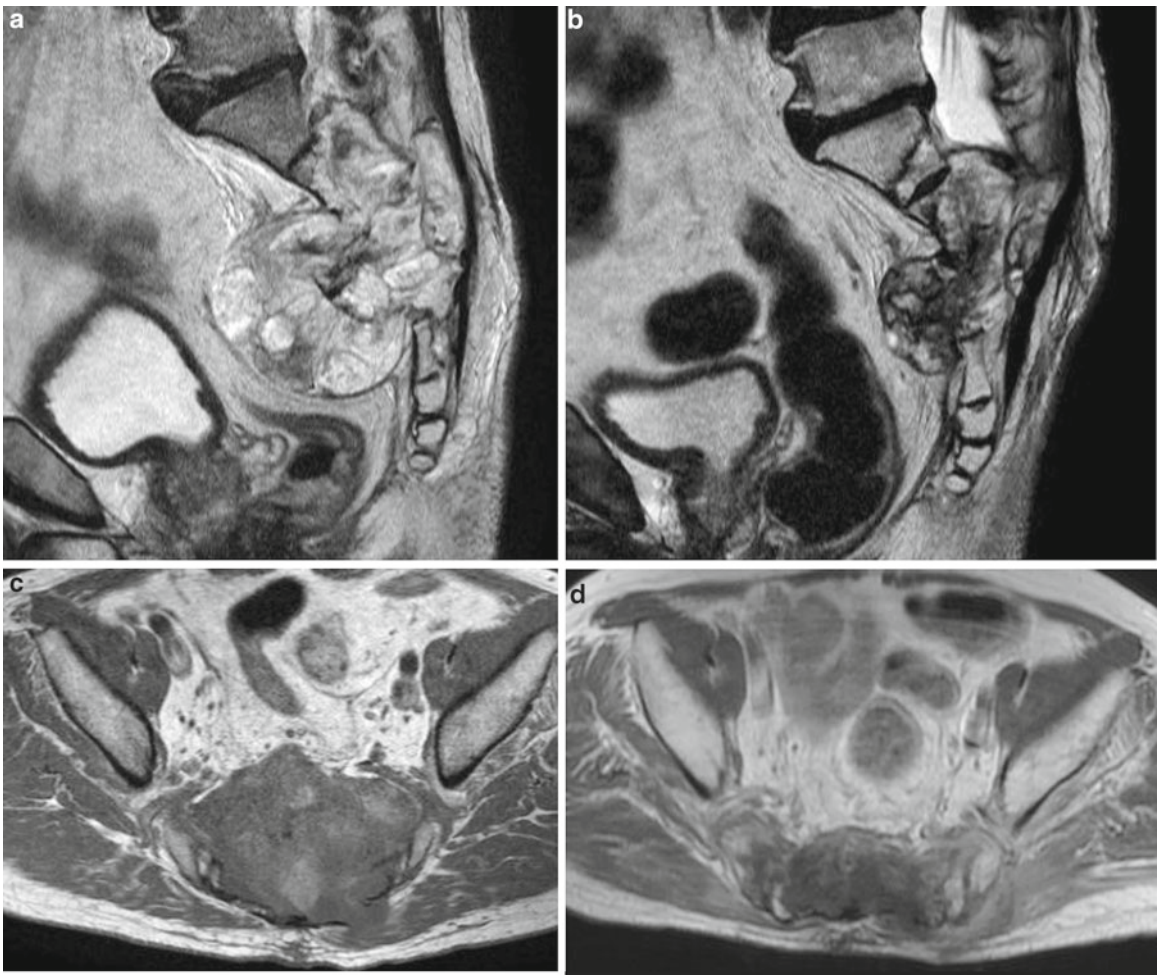

Fig. 31.1 (**a**) T2-weighted sagittal MRI before carbon ion radiotherapy. (**b**) T2-weighted sagittal MRI 4 years after carbon ion radiotherapy. (**c**) T1-weighted axial MRI with a contrast medium before carbon ion radiotherapy. (**d**) T1-weighted axial MRI with a contrast medium 4 years after carbon ion radiotherapy

cause technical difficulties. C-ion RT in patients with tumors abutting the small intestine, kidney, and spinal canal is highly risky. In the case of tumors adjacent to the small intestine, placement of surgical spacers made of sheets with minimal foreign body response and less extensive vascularization before C-ion RT is sometimes adopted. The sheets help to separate the intestine from the irradiation field and ensure an adequate margin.

Between May 1997 and February 2006, 24 patients (17 males and 7 females) with unresectable retroperitoneal sarcomas treated with C-ion RT were analyzed [20]. Patient age ranged from 16 to 77 years (median, 48.4 years). Both patients with primary tumors and recurrent tumors were included. Twelve of the patients had undergone chemotherapy for more than 4 weeks prior to radiotherapy. The total dose delivered in most of the cases was 70.4 GyE in 16 fractions. CTVs ranged from 57 cm^3 to 1,194 cm^3 (median, 525 cm^3). At 2 and 5 years, the actuarial overall survival rates were 75 and 50 %, respectively. At 2 and 5 years, the actuarial local control rates were 77 and 69 %, respectively. Grade 3 toxicity was not observed in any case during the follow-up period.

31.4.5 Extremity Sarcomas

C-ion RT for extremity sarcomas is considered in rare cases, such as for tumors in the thigh extending to the proximal and inguinal areas or when the patient is too old to undergo surgery or has comorbidities. C-ion RT might also be considered for the treatment of soft-tissue sarcoma in very elderly patients, such as those in their 80s. Between April 2000 and May 2010, 17 patients with localized primary sarcoma of the extremities underwent C-ion RT. The median patient age was

53 years. Nine patients had primary disease and eight had recurrent disease. Of the 17 patients, eight refused amputation. Tumors were located in the upper limbs in 4 patients and in the lower limbs in 13. Four patients had bone sarcomas and 13 had soft-tissue sarcomas. In 13 of 17 cases, the prescribed dose was 70.4 GyE administered in 16 fractions over 4 weeks. The median follow-up period was 37 months (range, 11–97 months). The radiological response rate was 65 %, whereas the local control rate at 5 years was 76 %. The overall survival rate at 5 years was 56 %. At the end of the follow-up period, 10 of the 17 patients survived without disease progression. Four patients had local recurrence: one patient survived after repeated C-ion RT and the other three died due to systemic diseases. Distant failure was observed in six patients. One patient with femoral chondrosarcoma had a femoral fracture and underwent surgical fixation for 27 months after C-ion RT. No other severe reactions were observed [21].

31.5 Case Study

Case 1: Sacral Sarcoma
A 67-year-old man presented with lumbar pain. MRI revealed a sacral tumor. Needle biopsy was performed, and the tumor was diagnosed as a chordoma. The tumor was deemed unresectable (Figs. 31.1 and 31.2).

Case 2: Sacral Sarcoma
A 25-year-old man presented with left leg pain. A sacral tumor was detected on MRI. Needle biopsy was performed, and the tumor was diagnosed as osteosarcoma. The patient received two cycles of chemotherapy, and the response was no change. The tumor was judged unresectable (Figs. 31.3 and 31.4).

Case 3: Acetabular Sarcoma
A 44-year-old man presented with pain in the left hip. MRI indicated an acetabular tumor. Needle biopsy was performed, and the tumor was diagnosed as chondrosarcoma (grade 2). The patient refused surgery (Figs. 31.5, 31.6, and 31.7).

Case 4: Retroperitoneal Sarcoma
A 71-year-old man presented with a large mass in the left major psoas muscle. He had undergone partial colostomy of the transverse colon 10 months earlier, and the histological diagnosis at that time was established as malignant fibrous histiocytoma (MFH). Needle biopsy was performed, and the tumor was diagnosed as metastatic MFH. The tumor was judged unresectable (Figs. 31.8 and 31.9).

Case 5: Spinal Sarcoma
A 59-year-old woman presented with neck pain. MRI indicated a cervical spine tumor. Needle biopsy was performed, and the tumor was diagnosed as an epithelioid hemangioendothelioma. The tumor was judged unresectable (Figs. 31.11 and 31.12).

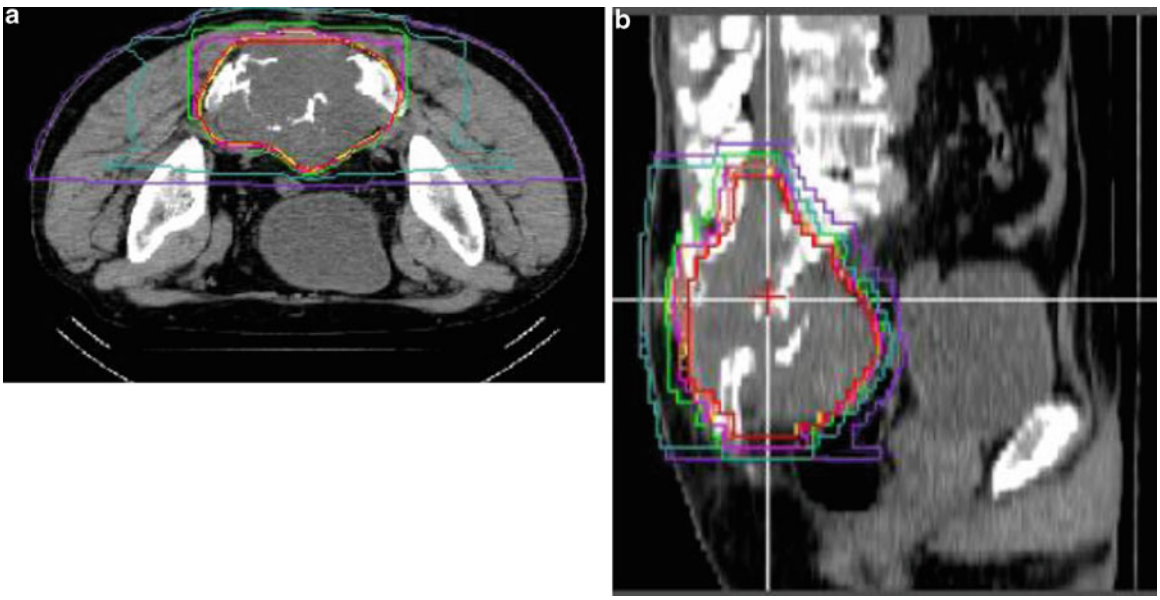

Fig. 31.2 Dose distribution for the patient with sacral chordoma: (**a**, **b**) 70.4 GyE in 16 fractions over 4 weeks

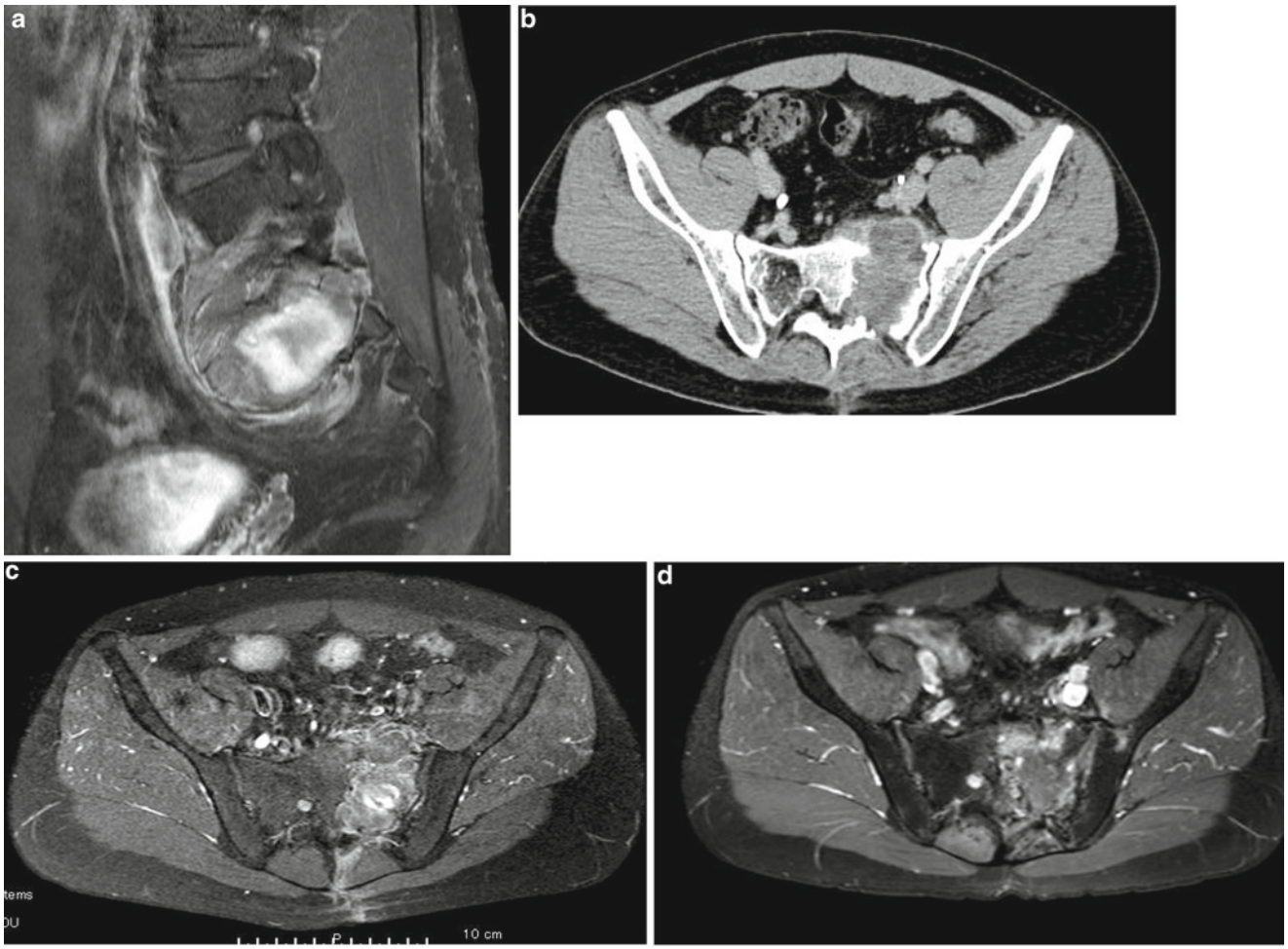

Fig. 31.3 (**a**) T1-weighted sagittal MRI with a contrast medium before carbon ion radiotherapy. (**b**) CT image with a contrast medium before carbon ion radiotherapy. (**c**) T1-weighted axial MRI with a contrast medium before carbon ion radiotherapy. (**d**) T1-weighted axial MRI with a contrast medium 5 years after carbon ion radiotherapy

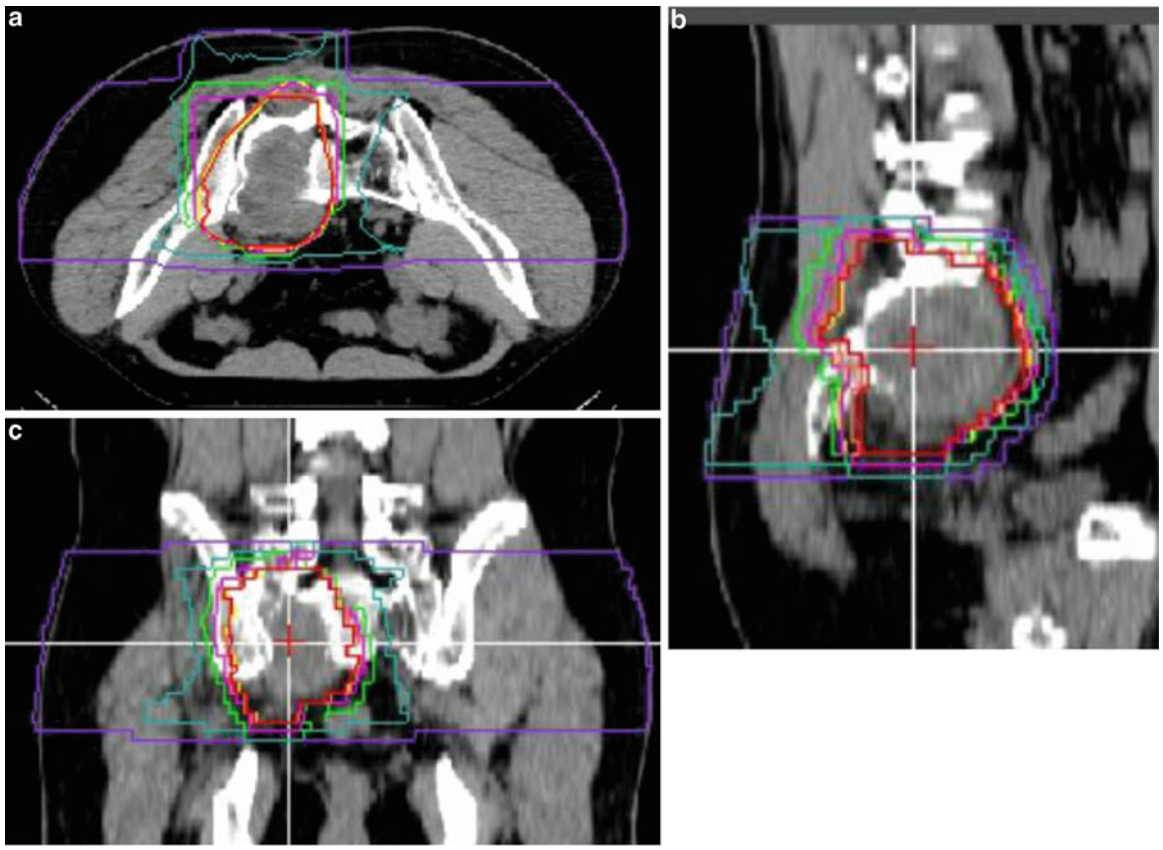

Fig. 31.4 Dose distribution for the patient with sacral osteosarcoma: (**a**–**c**) 70.4 GyE in 16 fractions over 4 weeks

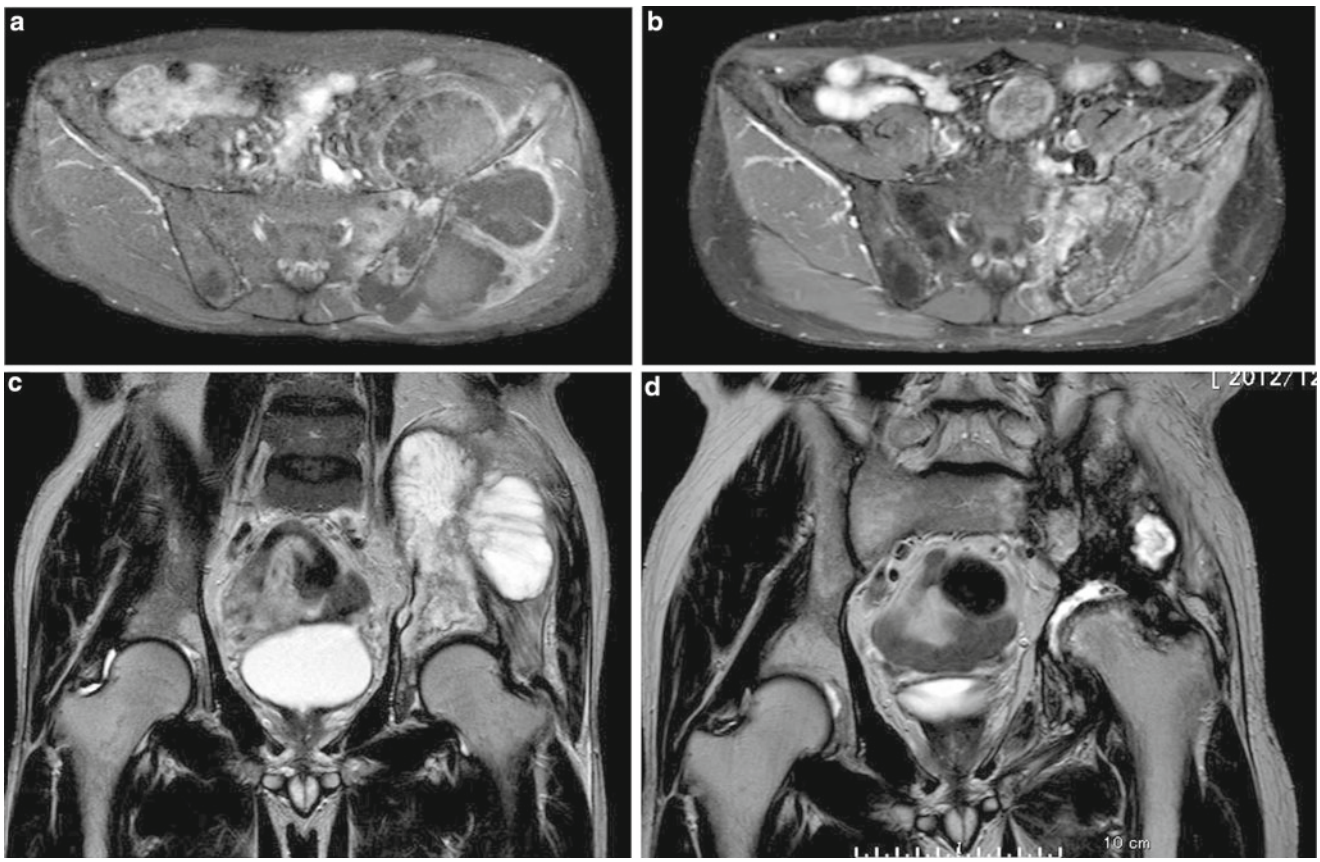

Fig. 31.5 (**a**) T1-weighted axial MRI with a contrast medium before carbon ion radiotherapy. (**b**) T1-weighted axial MRI with a contrast medium 3.5 years after carbon ion radiotherapy. (**c**) T2-weighted coronal MRI before carbon ion radiotherapy. (**d**) T2-weighted coronal MRI 3.5 years after carbon ion radiotherapy

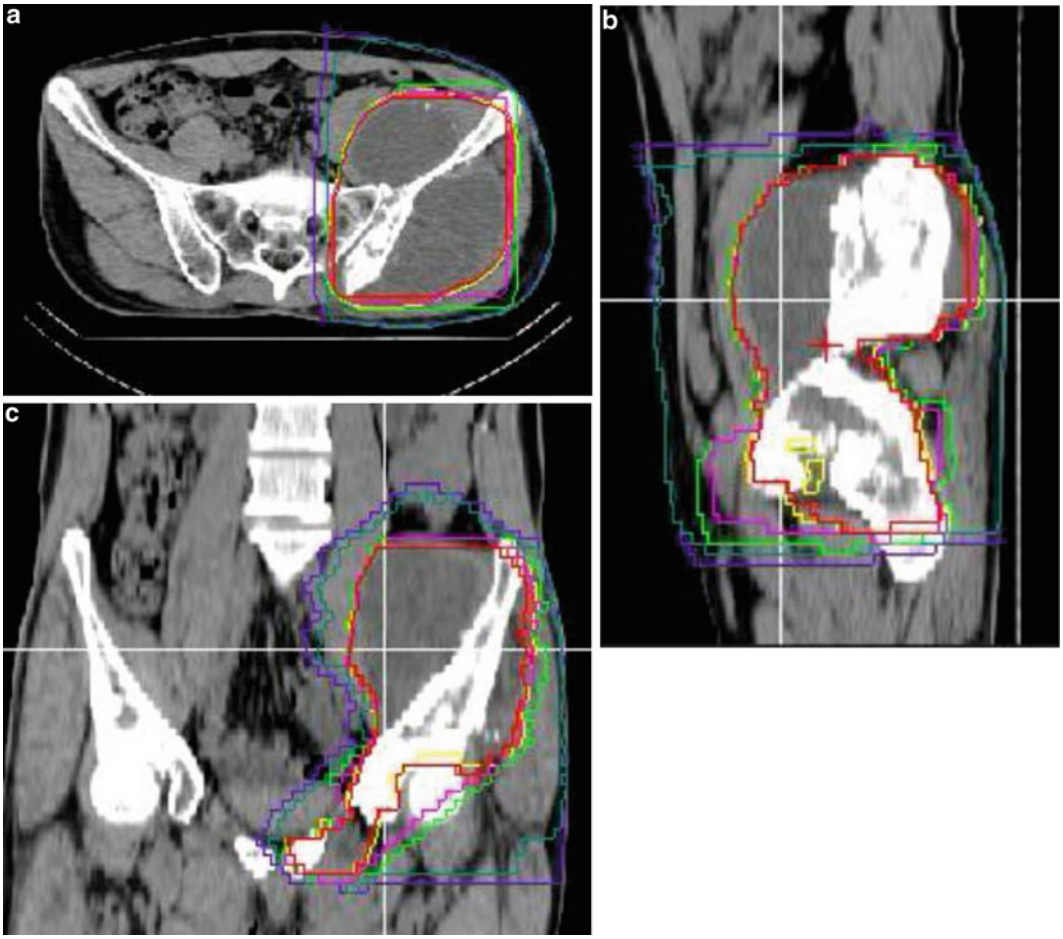

Fig. 31.6 Dose distribution for the patient with acetabular chondrosarcoma: (**a**–**c**) 70.4 GyE in 16 fractions over 4 weeks. The irradiation to the femoral head was not avoided completely

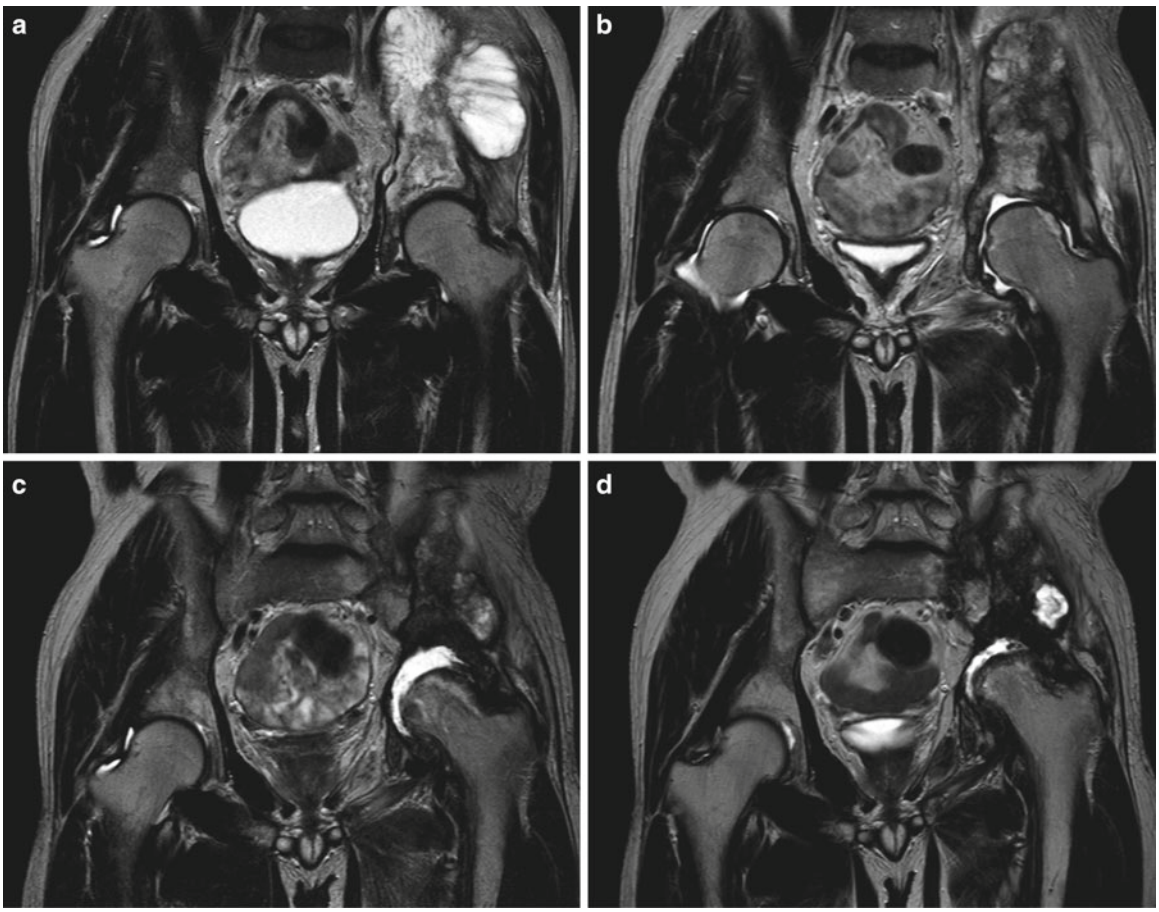

Fig. 31.7 Destruction of the acetabulum and the femoral head over time, after carbon ion radiotherapy. (**a**) T2-weighted coronal MRI before carbon ion radiotherapy (**b**) T2-weighted coronal MRI 1 year later. (**c**) T2-weighted coronal MRI 2 years later. The left femoral head appeared to be presenting deeper in the iliac bone than the right one due to the acetabular bone degeneration. (**d**) T2-weighted coronal MRI 3.5 years later

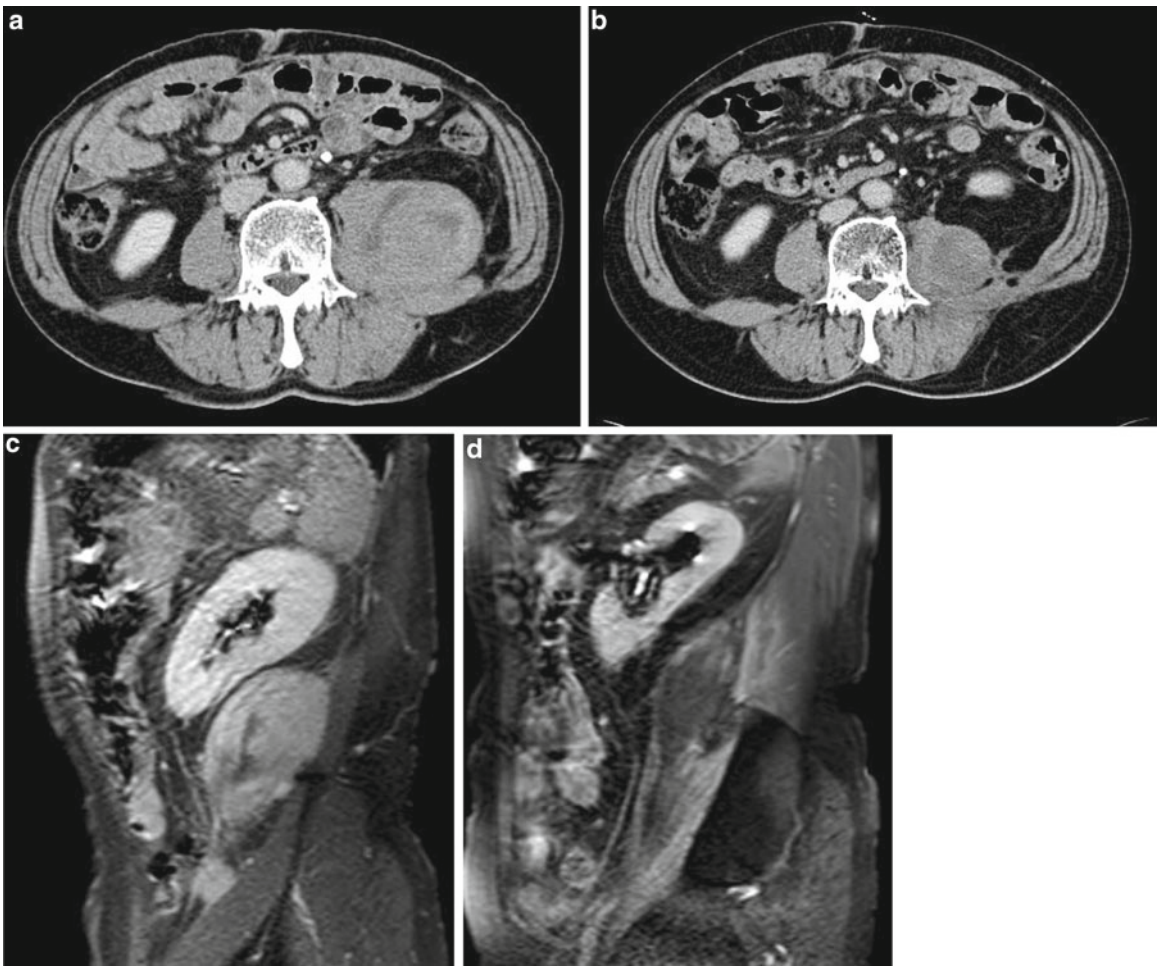

Fig. 31.8 (**a**) CT image with a contrast medium before carbon ion radiotherapy. (**b**) CT image with a contrast medium 3 years later carbon ion radiotherapy. (**c**) T1-weighted sagittal MRI with a contrast medium before carbon ion radiotherapy. (**d**) T1-weighted sagittal MRI with a contrast medium 3 years later after carbon ion radiotherapy

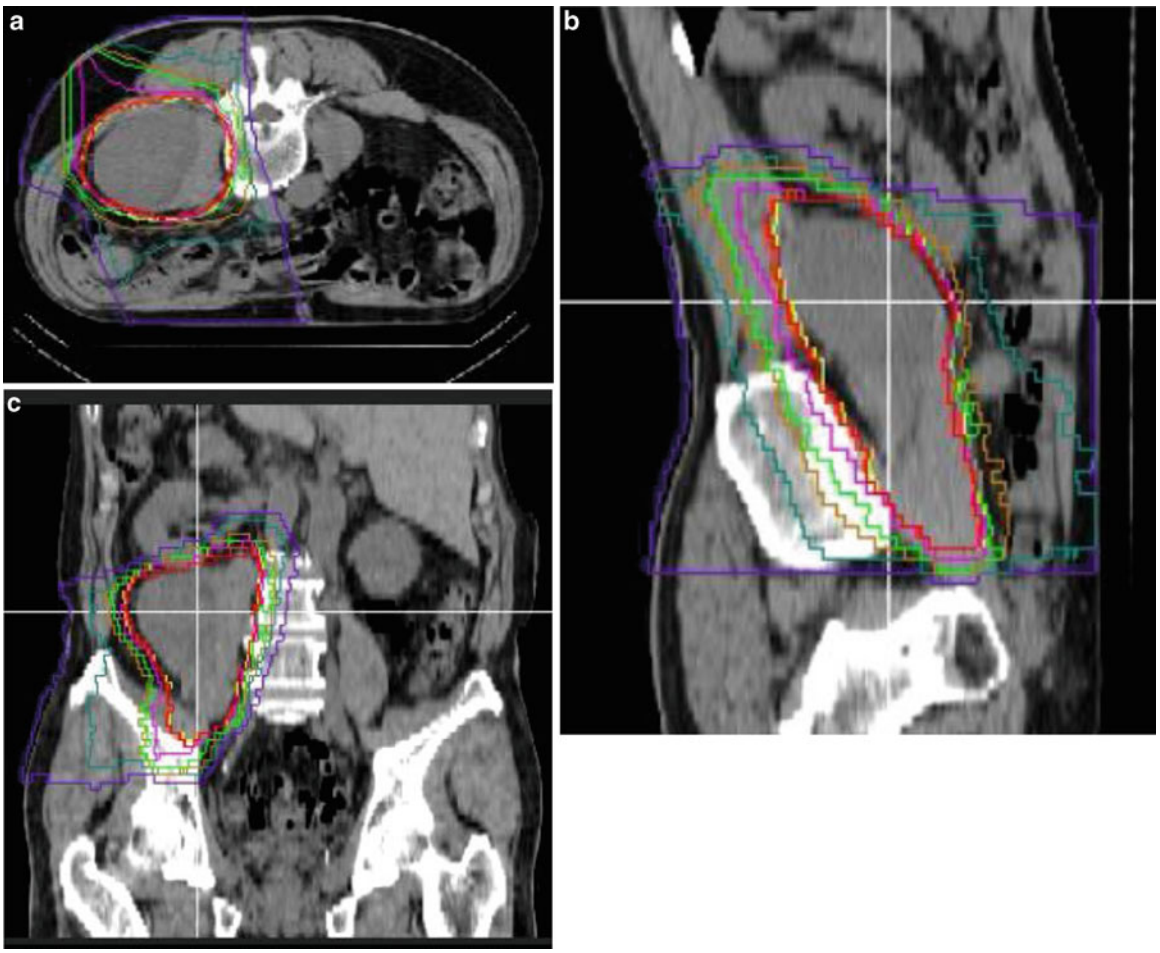

Fig. 31.9 Dose distribution for the patient with retroperitoneal MFH: (**a**–**c**) 70.4 GyE in 16 fractions over 4 weeks

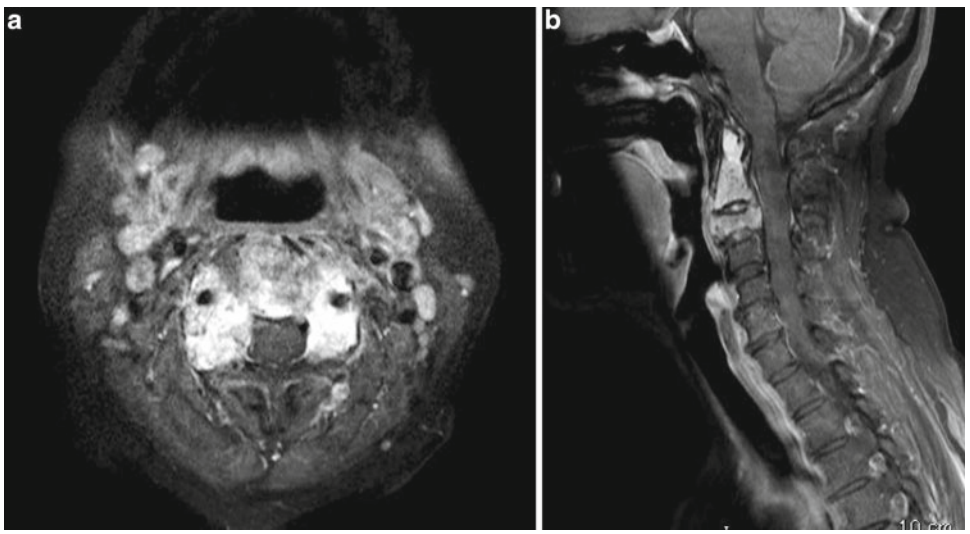

Fig. 31.10 (**a**) T1-weighted axial MRI with a contrast medium before carbon ion radiotherapy. (**b**) T1-weighted sagittal MRI with a contrast medium before carbon ion radiotherapy

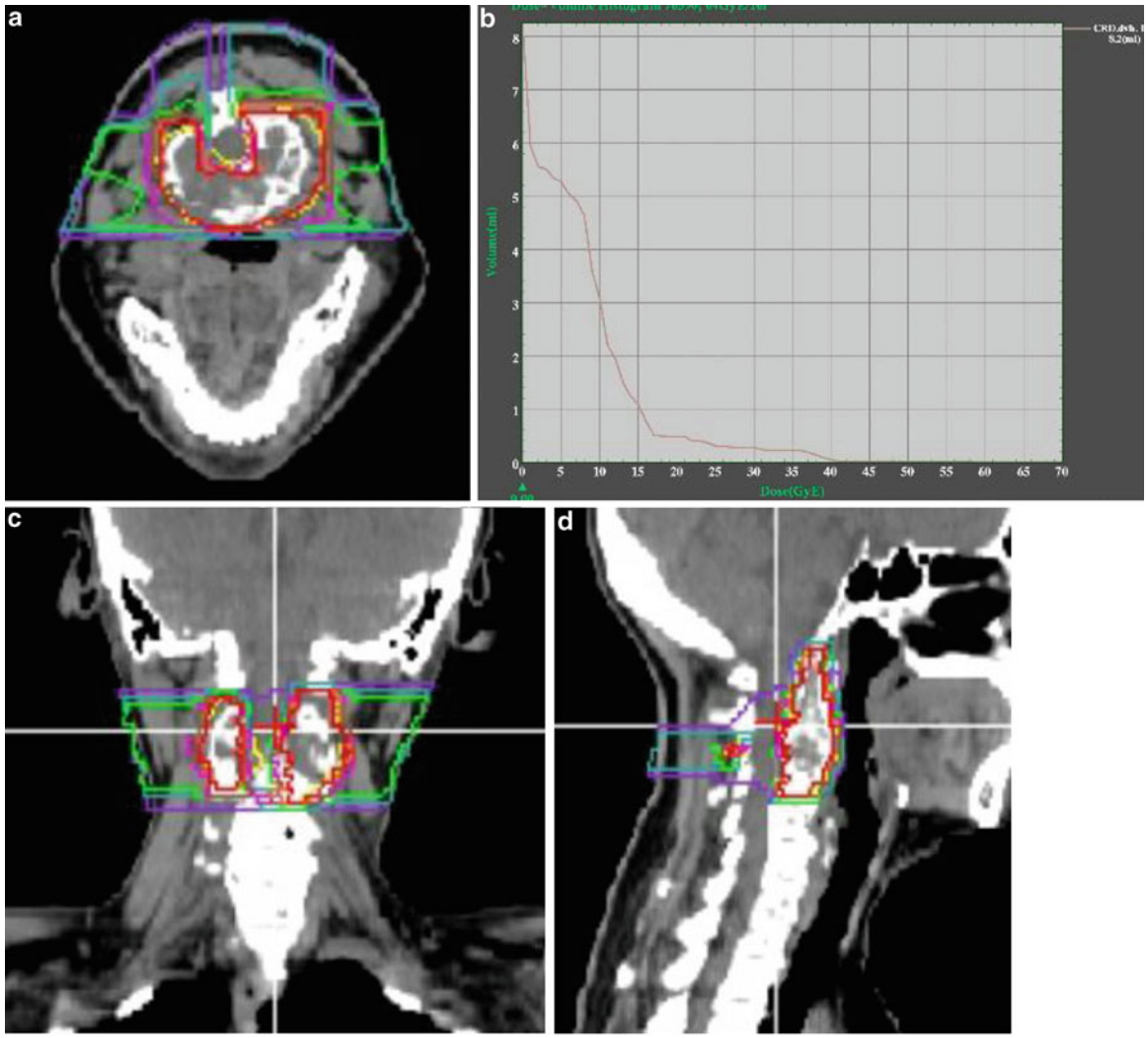

Fig. 31.11 Dose distribution for the patient with cervical epithelioid hemangioendothelioma treated with 64.0 GyE in 16 fractions over 4 weeks (**a**, **c**, **d**), using the patch technique. The dose–volume histogram of the spinal cord is shown (**b**)

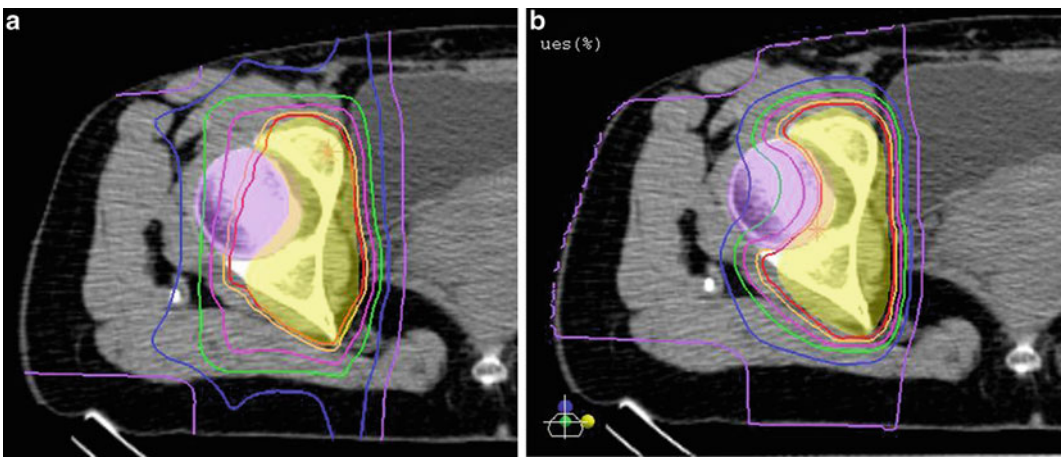

Fig. 31.12 (**a**) Dose distribution of passive beam irradiation for acetabular sarcoma. (**b**) Dose distribution of scanning beam irradiation. Both plans involved three ports from the anterior, posterior, and left lateral directions. The *red*, *pink*, *green*, and *blue lines* show 96, 70, 50, and 30 % of total dose, respectively. It is obvious that the high-dose area of the femoral head using scanning beam irradiation is smaller than that using passive beam irradiation

References

1. The JOA committee of tumors. General rules for clinical and pathological studies on malignant bone tumors. 3rd ed. Tokyo: Kanehara; 2000.
2. The JOA committee of tumors. General rules for clinical and pathological studies on malignant soft tissue tumors. 3rd ed. Tokyo: Kanehara; 2000.
3. Jaffe N. Osteosarcoma: review of the past, impact on the future. The American experience. Cancer Treat Res. 2009;152:239–62.
4. Ozaki T, Flege S, Kevric M, et al. Osteosarcoma of the pelvis: experience of the Cooperative Osteosarcoma Study Group. J Clin Oncol. 2003;21:334–41.
5. Fernández-Trigo V, Sugarbaker PH. Sarcomas involving the abdominal and pelvic cavity. Tumori. 1993;79:77–91.
6. Kamada T, Tsujii H, Tsuji H, et al. Efficacy and safety of carbon ion radiotherapy in bone and soft tissue sarcomas. J Clin Oncol. 2002;20:4466–71.
7. Yanagi T, Kamada T, Tsuji H, et al. Dose-volume histogram and dose-surface histogram analysis for skin reactions to carbon ion radiotherapy for bone and soft tissue sarcoma. Radiother Oncol. 2010;95:60–5.
8. Imai R, Kamada T, Sugahara S, et al. Carbon ion radiotherapy for sacral chordoma. Br J Radiol. 2011;84:S48–54.
9. Serizawa I, Imai R, Kamada T, et al. Changes in tumor volume of sacral chordoma after carbon ion radiotherapy. J Comput Assist Tomogr. 2009;33:795–8.
10. Imai R, Kamada T, Tsuji H, et al. Effect of carbon ion radiotherapy for sacral chordoma: results of phase I-II and phase II clinical trials. Int J Radiat Oncol Biol Phys. 2010;77:1470–6.
11. Imai R, Kamada T, Tsuji H, et al. Carbon ion radiotherapy for unresectable sacral chordomas. Clin Cancer Res. 2004;10:5741–6.
12. Matsunobu A, Imai R, Kamada T, et al. Impact of carbon ion radiotherapy for unresectable osteosarcoma of the trunk. Cancer. 2012;118:4555–63.
13. Kawai A, Huvos AG, Meyers PA, et al. Osteosarcoma of the pelvis-oncologic results of 40 patients. Clin Orthop Relat Res. 1998; 348:196–207.
14. Pring ME, Weber KL, Unni KK, et al. Chondrosarcoma of the pelvis. A review of sixty-four cases. J Bone Joint Surg Am. 2001;83:1630–42.
15. Maruyama K, Imai R, Kamada T, et al. Carbon ion radiation therapy for chondrosarcoma. Int J Radiat Oncol Biol Phys. 2012; 84:S139.
16. Hug EB, Adams J, Fitzek M, et al. Fractionated, three-dimensional, planning-assisted proton-radiation therapy for orbital rhabdomyosarcoma: a novel technique. Int J Radiat Oncol Biol Phys. 2000; 47:979–84.
17. Imai R, Kamada T, Tsuji H, et al. Cervical spine osteosarcoma treated with carbon-ion radiotherapy. lancet Oncol. 2006;7: 1034–5.
18. Matsumoto K, Imai R, Kamada T, et al. Impact of carbon ion radiotherapy for primary spinal sarcoma. Cancer. 2013;119:3496–503.
19. Heslin MJ, Lewis JJ, Nadler E, et al. Prognostic factors associated with long-term survival for retroperitoneal sarcoma: implications for management. J Clin Oncol. 1997;15:2832–9.
20. Serizawa I, Kagei K, Kamada T, et al. Carbon ion radiotherapy for unresectable retroperitoneal sarcomas. Int J Radiat Oncol Biol Phys. 2009;75:1105–10.
21. Sugahara S, Kamada T, Imai R, et al. Carbon ion radiotherapy for localized primary sarcoma of the extremities: results of a phase I/II trial. Radiother Oncol. 2012;105:226–31.

Part XIX

Other Tumors

Previously Irradiated Tumors

32

Masashi Koto

Abstract

Carbon ion radiotherapy (C-ion RT) has characteristics of high physical selectivity and high biological effects, permitting a delivery of sufficient dose to the tumor while sparing the normal tissues. It therefore has a possibility to control a radioresistant tumor, even such tumors which developed in the previously irradiated area. In this chapter, general principles of treatment for locally recurrent tumor are discussed, showing examples of patients who were reirradiated with carbon ions to their previously irradiated tumors.

Keywords

Carbon ion radiotherapy • Reirradiation

32.1 Introduction

Therapeutic options are generally limited for those patients who present with locally recurrent disease or a second primary tumor in a previously irradiated field. Surgical salvage with a curative intent has been a preferred option, which however can be applied only to those with limited-volume disease. Reirradiation is an alternative for patients who are not candidates for surgical salvage, but indications of reirradiation have been limited to selected patients because the radiation tolerance of the normal tissues is significantly reduced as compared with the primary treatment.

Reirradiation has been often used for palliative intent but only occasionally for curative intent. Despite development of modern radiotherapeutic techniques such as intensity-modulated radiotherapy and stereotactic radiotherapy, treatment results for these patients have not been satisfactory [1]. In this regard, C-ion RT may have a capability of controlling these patients. In addition, by using magnetic resonance imaging (MRI) and positron emission tomography (PET) in treatment planning, sophisticated techniques such as respiratory-gated irradiation and image-guided radiotherapy have made it easier to provide more precise irradiation. Accordingly, sufficient doses can be safely applied to the recurrence tumor with C-ions while sparing normal tissues. Reirradiation with C-ions can be a curative approach in selected patients.

32.2 Significance of Carbon Ion Radiotherapy

C-ions have a higher physical selectivity because they have a finite range in tissue; thereby C-ion RT permits superior dose conformity as compared with photon radiotherapy. They also have a biological advantage because they have higher linear energy transfer (LET) components in the Bragg peak when compared to photons [2]. Therefore, C-ion RT has a possibility to control the radioresistant tumor, which developed in the previously irradiated area.

M. Koto (✉)
Research Center Hospital for Charged Particle Therapy, National Institute of Radiological Sciences, 4-9-1 Anagawa, Inage-ku, Chiba 263-8555, Japan
e-mail: koto@nirs.go.jp

H. Tsujii et al. (eds.), *Carbon-Ion Radiotherapy: Principles, Practices, and Treatment Planning*,
DOI 10.1007/978-4-431-54457-9_32,

32.3 Clinical Features and Diagnostic Work-Up

Before reirradiation, the previous radiation planning must be referred to confirm the dose distribution as well as the prescribed dose and the dose of the normal tissues. Computed tomography and MRI are useful to identify the location of the recurrent tumor relative to critical organs. For tumor delineation, PET is often useful.

32.4 General Management of Radiation Technique

In reirradiation, attention should be paid to the remaining tolerance of the normal tissues. The loss of repair capacity of normal tissues may be the major concern for reirradiation, where the risk of late toxicity is significantly increased compared with the primary radiotherapy [3]. Therefore, a high dose should not be irradiated to the critical organs, especially serial organs such as the intestine, skin, or central nerve system. Cases that were reirradiated using C-ions were shown in the next section.

32.5 Case Studies

32.5.1 Case 1 (Rectal Cancer)

A 69-year-old man with rectal cancer underwent abdominoperineal rectal resection. Three years later, he developed local recurrence in front of the sacrum. Photon radiotherapy with 60 Gy in 30 fractions and chemotherapy were administered; however, the recurrent tumor revealed regrowth 2 years after photon radiotherapy. He was referred to our hospital for C-ion RT. The tumor located at presacral area had a maximum diameter of 33 mm (Fig. 32.1a). He was immobilized in the prone position and irradiated using three portals. C-ion RT was delivered at 70.4 Gy equivalent (GyE) in16 fractions. The critical organs such as the small intestine and skin were spared (Fig. 32.1b). Four years later, the patient was disease-free without any severe complication (Fig. 32.1c, d).

32.5.2 Case 2 (Sacral Chordoma)

A 33-year-old man with sacral chordoma underwent surgical resection followed by postoperative radiotherapy

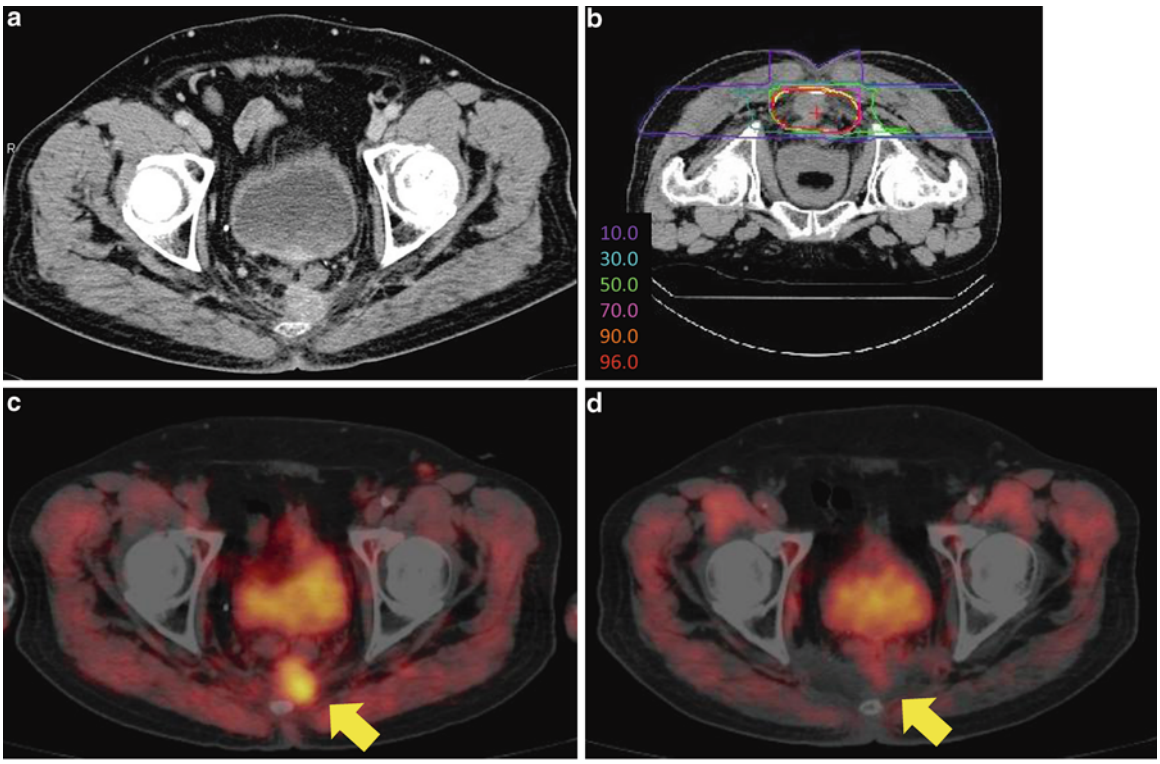

Fig. 32.1 (**a**) Axial computed tomography before carbon ion radiotherapy. (**b**) Representative axial isodose distributions. 11C-labeled methionine positron emission tomography images (**c**) before carbon ion radiotherapy and (**d**) 40 months after treatment

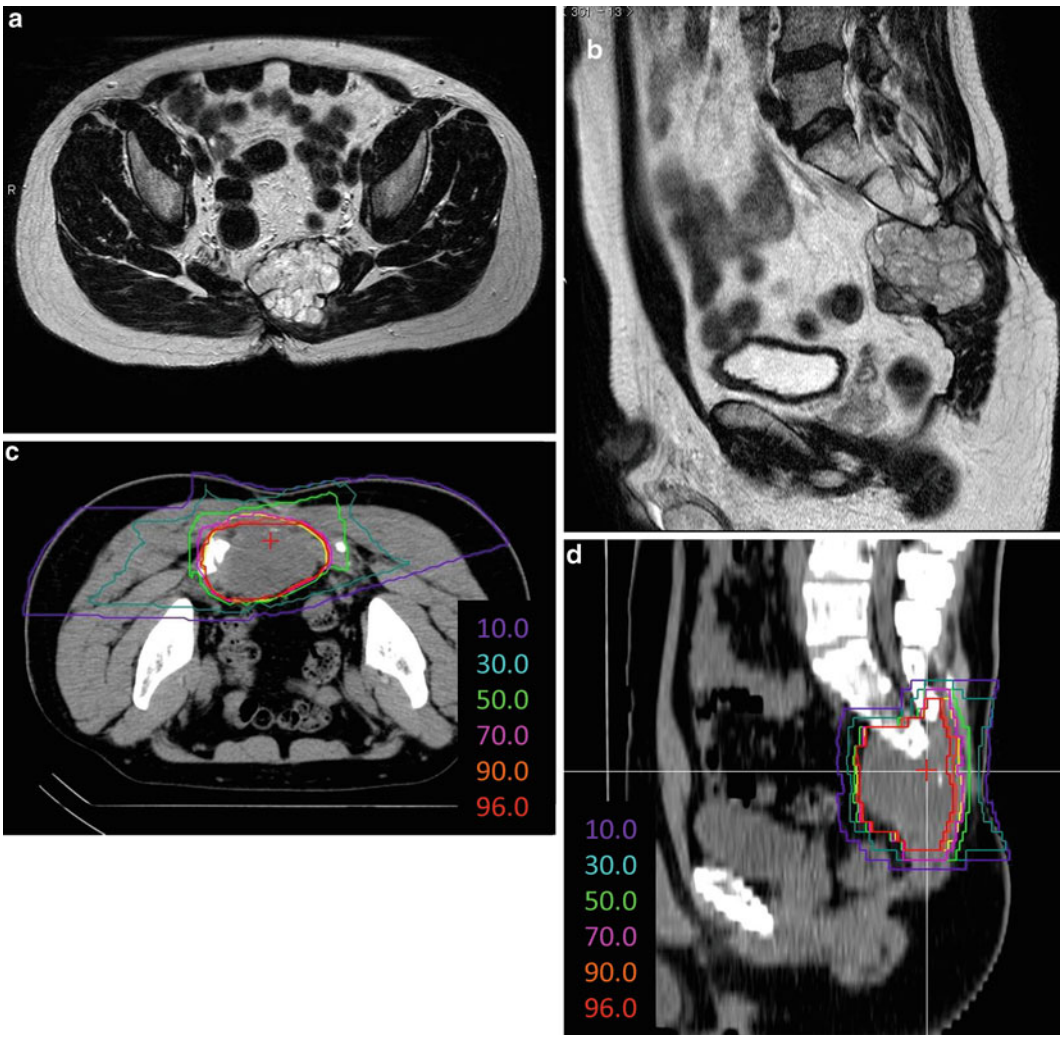

Fig. 32.2 (**a**) Axial and (**b**) sagittal T2-weighted magnetic resonance images obtained before carbon ion radiotherapy. Representative (**c**) axial and (**d**) sagittal isodose distributions

administered at 50 Gy in 25 fractions. Twenty years later, he developed local recurrence, which was confirmed by biopsy. He was referred to our hospital for C-ion RT. The tumor located at the edge of the residual sacrum had a maximum diameter of 60 mm (Fig. 32.2a, b). He was immobilized in the prone position and irradiated using three portals. C-ion RT was delivered at 64.0 GyE in16 fractions. The critical organs such as the colon and skin were spared (Fig. 32.2c, d). In addition, the bilateral sciatic nerves could be spared. Seven years later, the patient was disease-free and could walk without an aid.

32.5.3 Case 3 (Myxoid Liposarcoma in the Left Buttock)

A 46-year-old man with myxoid liposarcoma in the left buttock underwent preoperative radiotherapy with 30 Gy in 15 fractions and surgical resection. Two years later, he developed local recurrence and underwent another surgery. He developed local recurrence 6 months after the second surgery and was referred to our hospital for C-ion RT. MRI examination revealed a tumor in front of the left piriformis muscle, involving left sciatic nerve (Fig. 32.3a, b). He was

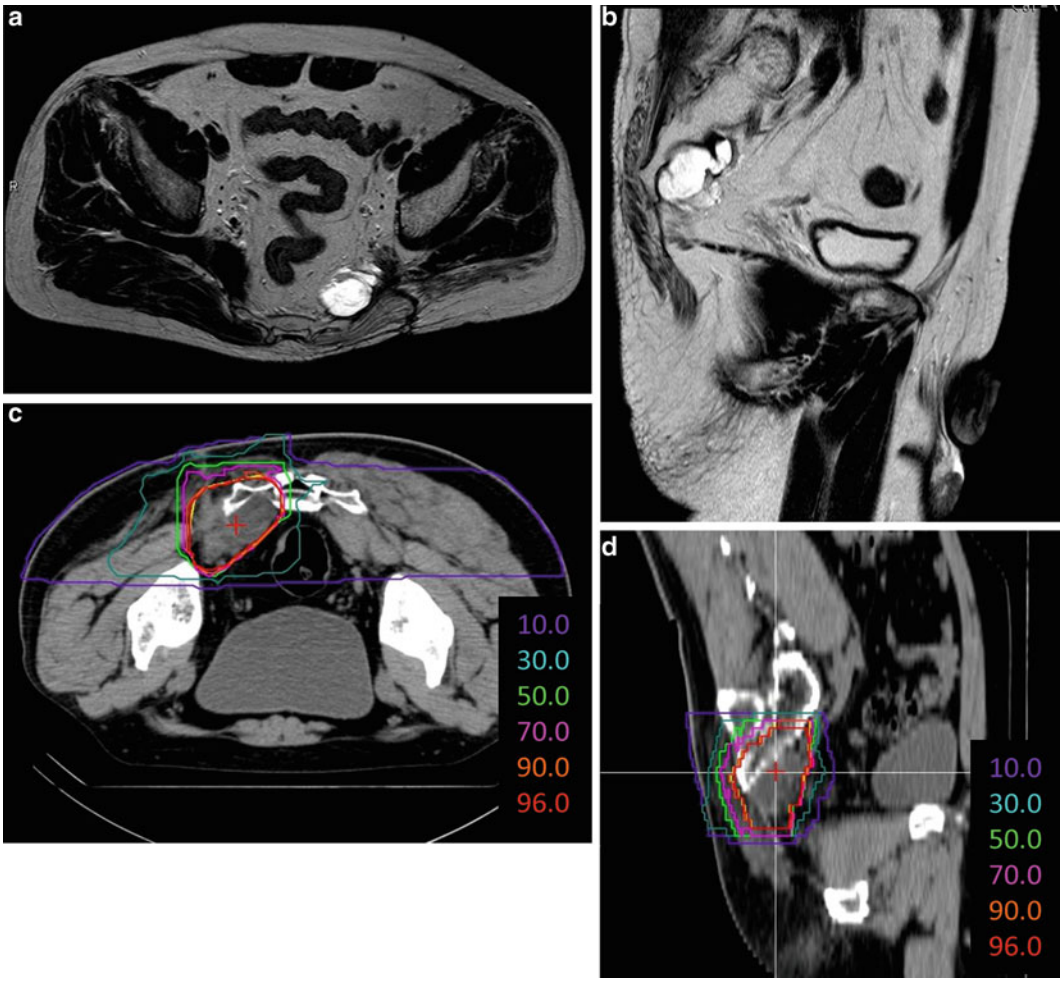

Fig. 32.3 (**a**) Axial and (**b**) sagittal T2-weighted magnetic resonance images obtained before carbon ion radiotherapy. Representative (**c**) axial and (**d**) sagittal isodose distributions

immobilized in the prone position and irradiated using three portals. C-ion RT was delivered at 64.0 GyE/16 fractions. The doses for the rectum and skin were adequately reduced; however, it was difficult to spare the left sciatic nerve (Fig. 32.3c, d). He developed left sciatic nerve palsy 2 years after treatment and uses an aid for walking. Although the patient is alive without recurrence 6 years after C-ion RT.

32.5.4 Case 4 (Basal Cell Adenocarcinoma in the Parotid Gland)

A 36-year-old man with basal cell adenocarcinoma in the left parotid gland was treated with surgery followed by hyperfractionated radiation at 60 Gy in 50 fractions. Ten years later, he presented with facial numbness and was found

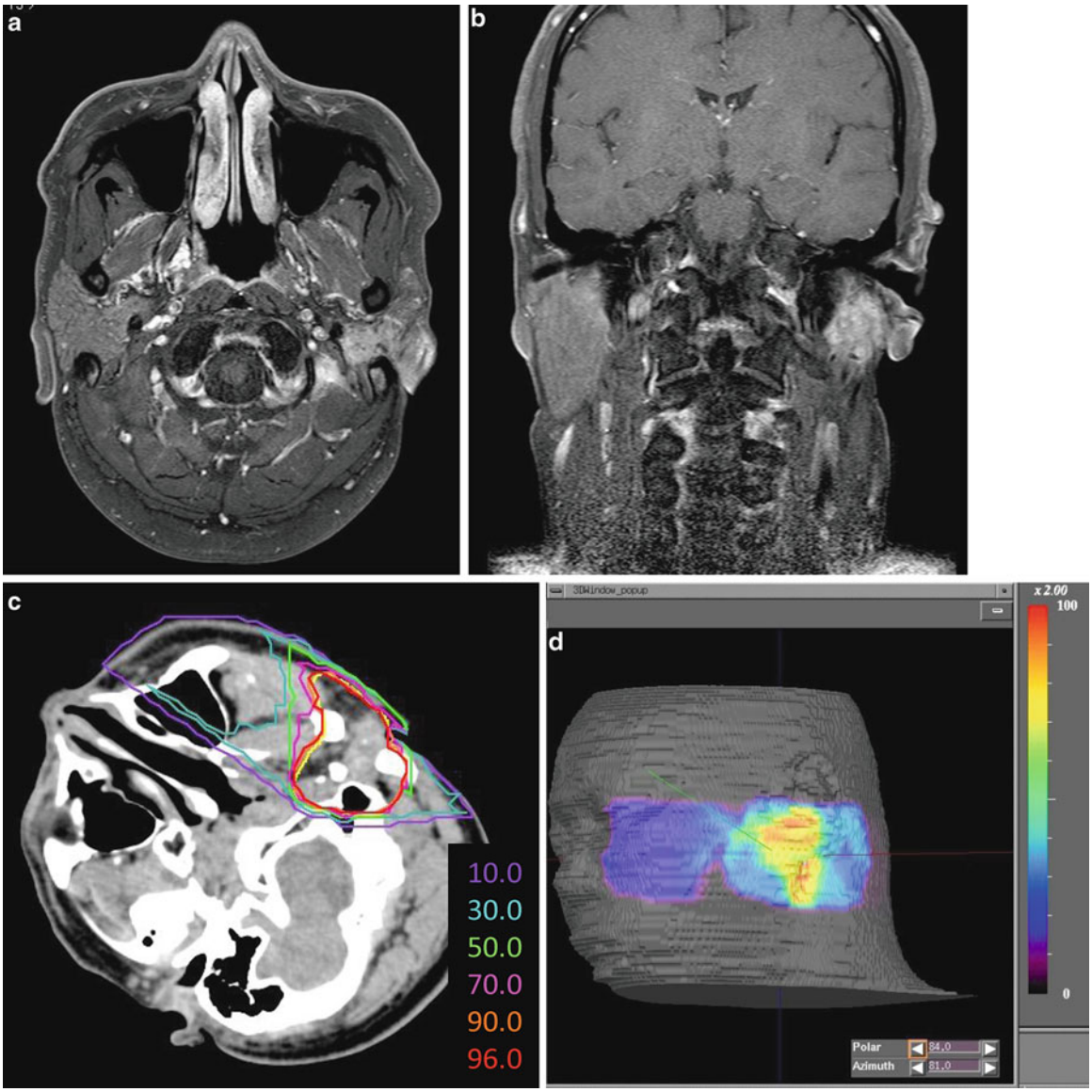

Fig. 32.4 (**a**) Axial and (**b**) coronal contrast-enhanced T1-weighted magnetic resonance images obtained before carbon ion radiotherapy. (**c**) Representative axial isodose distributions. (**d**) Dose of the skin surface

to have mass in the bed of the left parotid gland. MRI examination revealed a tumor in the bed of the left parotid gland, invading the skull base along the facial nerve (Fig. 32.4a, b). The patient was considered inoperable and underwent C-ion RT at 57.6 GyE/12 fractions. Three portals were used to avoid severe skin reactions (Fig. 32.4c, d). No recurrence or severe reaction was observed 2 years after the treatment.

References

1. Cardinale RM, Benedict SH, Wu Q, Zwicker RD, Gaballa HE, Mohan R. A comparison of three stereotactic radiotherapy techniques: ARCS vs. noncoplanar fixed fields vs. intensity modulation. Int J Radiat Oncol Biol Phys. 1998;42:431–6.
2. Kanai T, Endo M, Minohara S, Miyahara N, Koyama-ito H, Tomura H, Matsufuji N, Futami Y, Fukumura A, Hiraoka T, Fu-rusawa Y, Ando K, Suzuki M, Soga F, Kawachi K. Bio-physical characteristics of HIMAC clinical irradiation system for heavy-ion radiation therapy. Int J Radiat Oncol Biol Phys. 1999;44:201–10.
3. Okayasu R. Repair of DNA damage induced by accelerated heavy ions–a mini review. Int J Cancer. 2012;130:991–1000. doi:10.1002/ijc.26445.

Metastatic Tumors

33

Kumiko Karasawa

Abstract

Metastatic tumor without systemic extension, so-called oligometastasis, is a good candidate for carbon ion radiotherapy (C-ion RT). Careful patient selection must be needed before starting C-ion RT. The fractionation schedule is variously dependent on the tumor site, size, extension, radiosensitivity, and previously irradiated site or not. In principle, 48 GyE in 12 fractions for lymph node is used. Tumor progressions at irradiated sites were 8 %, whereas at distant sites 55 %. C-ion RT for lymph node recurrence from various malignancies might be promising to have favorable local control with acceptable toxicities, although not affecting to reduce distant metastases.

Keywords

Bone metastasis • Lymph node metastasis • Solitary metastasis

33.1 Introduction

Cancer metastasis is thought to be a part of a systemic disease, usually treated with systemic therapies, although solitary lymph node metastasis or distant metastasis without systemic extension, so-called oligometastasis, could be a candidate for C-ion RT. Most of patients with recurrence are treated with systemic chemotherapy before consulting C-ion RT and some are treated with chemo-radiotherapy. Careful patient selection must be needed for C-ion RT to avoid patients with systemic metastases during or just after RT.

33.2 Significance of C-Ion RT

C-ion RT for metastatic tumor is suitable for localized tumor without other tumor extension, resulting in long-term survival for patients. Because of high biological effectiveness and high dose conformity, C-ion provides a higher local control than photons. Therefore C-ion RT has a potential to control previously irradiated areas (see Chap. 29).

33.3 Clinical Futures and Diagnostic Work-Up

The cases with solitary or small regional lymph node metastasis and solitary lung, liver, and bone metastases with at least a 5-mm gap between the recurrent lesion and radiosensitive organs, including gastrointestinal tract, skin, spinal cord, and bladder, could be a candidate.

The diagnostic work-up including PET/CT could be considered.

33.4 General Management of Radiation Technique

The treatment system needs at least a 5-mm gap between the recurrent lesion and radiosensitive organs, including gastrointestinal tract and bladder, and irradiated field not exceeding 15 cm. In some cases, Gore-Tex-made spacer had been

K. Karasawa (✉)
Research Center Hospital for Charged Particle Therapy,
National Institute of Radiological Sciences, 4-9-1 Anagawa,
Inage-ku, Chiba 263-8555, Japan
e-mail: kkarasaw@nirs.go.jp

H. Tsujii et al. (eds.), *Carbon-Ion Radiotherapy: Principles, Practices, and Treatment Planning*,
DOI 10.1007/978-4-431-54457-9_33,

inserted surgically before carbon ion radiotherapy to make a gap between surrounding radiosensitive tissues. As a radiation technique, all sites were irradiated using 3-D conformal planning system with 2–4 portals, with respiratory gating if necessary. In target delineation, the involved node was defined as GTV, prophylactic lymph node area was defined as CTV, and CTV + 5 mm (excluding GI) was defined as PTV. Treatment was performed four times a week, up to a total dose of 48 GyE in 12 fractions for 3 weeks in principle.

33.5 Results of Therapy

We treated 189 cases with 233 sites of metastatic lymph node from 1996 to February 2012. No acute grade 3 or higher adverse toxicities have been observed. Late adverse events were observed in one case, who developed duodenum bleeding at re-irradiated site. Tumor progressions were recognized at irradiated sites in 8 % and regional in 15 %, whereas distant sites in 55 %. The overall survival rates of the entire group were 77 % in 1 year, 53 % in 2 years, 43 % in 3 years, and 29 % in 4 years, respectively (median survival time, 2 years and 2 months).

33.6 Case Study

Case 1

A 54-year-old male presented a rib tumor and needle biopsy revealed that the tumor originated from thyroid cancer. It was judged unresectable by his orthopedic surgeon and he was referred to our hospital (Fig. 33.1 by courtesy of Dr. Reiko Imai).

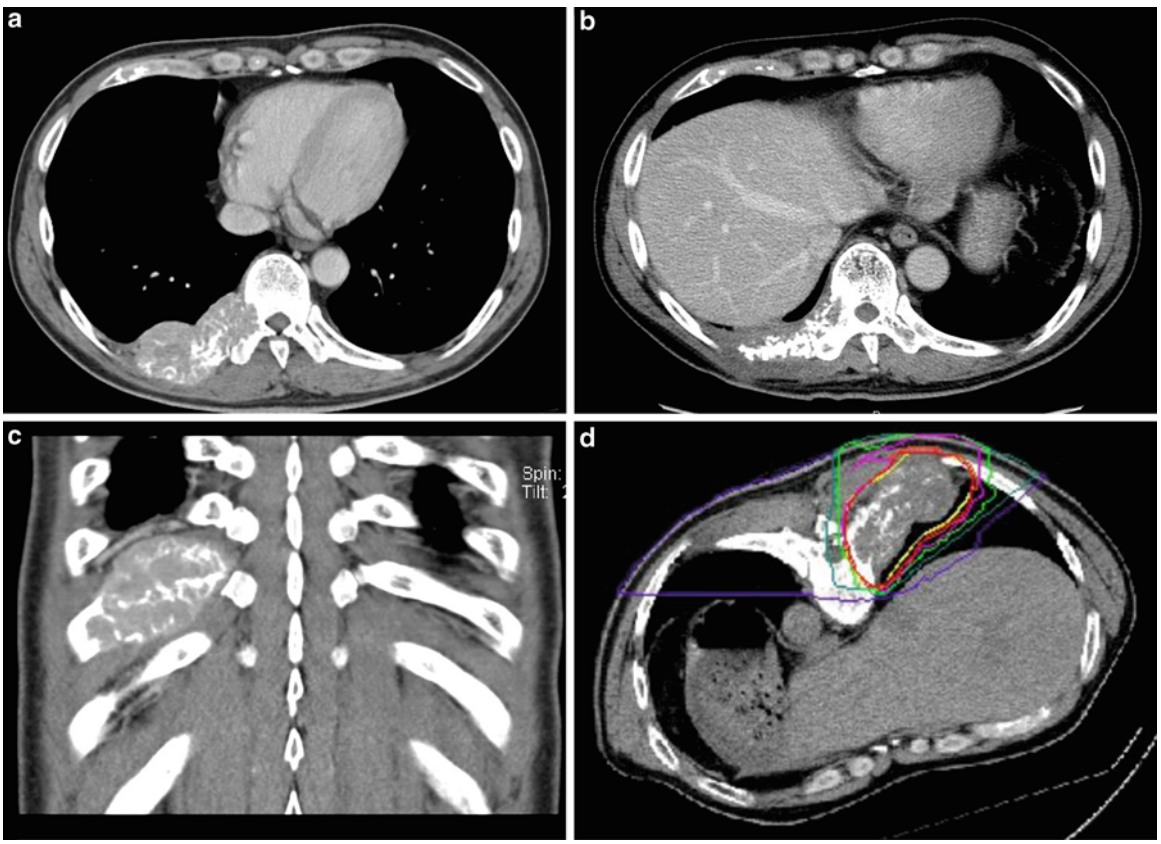

Fig. 33.1 (**a**) CT image with a contrast medium before carbon ion radiotherapy. The tumor is located in the right tenth rib and he complained of back pain. (**b**) CT image with a contrast medium 8 years after carbon ion radiotherapy. The tumor shrank and partially calcified. He had no complain. (**c**) CT image with a contrast medium before C-ion RT. (**d**) Dose distribution for the patient: 70.4 GyE in 16 fractions over 4 weeks (Courtesy of Dr. Reiko Imai)

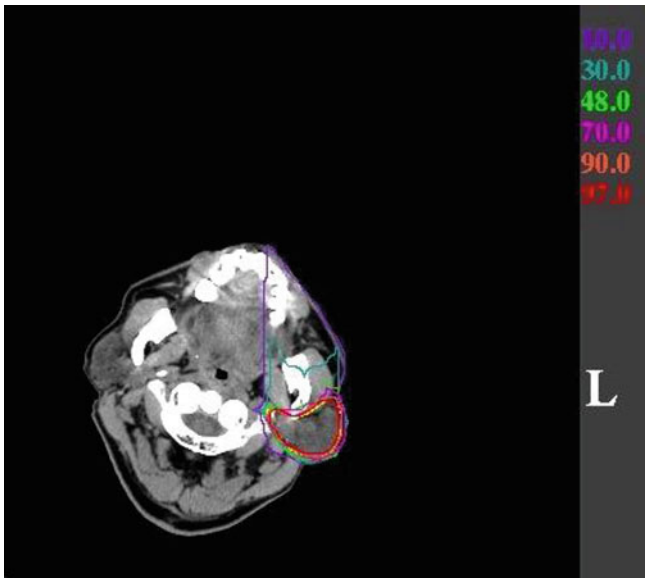

Fig. 33.2 Dose distribution for a case of parotid gland lymph node metastasis from orbital squamous cell carcinoma

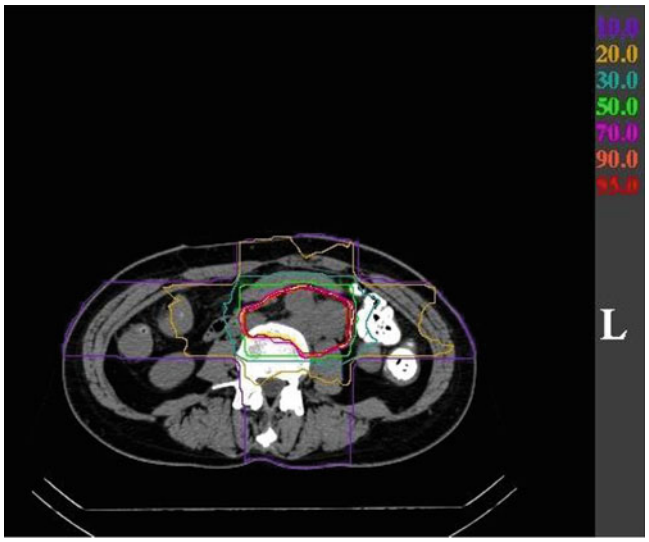

Fig. 33.3 Dose distribution for a case of para-aortic lymph node metastases from ovarian cancer

Case 2

A 65-year-old male with orbital squamous cell carcinoma was successfully treated with carbon ion. However, unfortunately, he had recurred at parotid lymph node. He received 52.8 GyE in 12 fraction by carbon ion radiotherapy and has been living without late adverse effect for 4 years (Fig. 33.2).

Case 3

A 57-year-old female with recurrent ovarian cancer (adenocarcinoma) was treated with carbon ion. She had recurred multiple para-aortic lymph nodes and received chemotherapy, although the effect was SD. She irradiated 52.8 GyE in 12 fractions and has been living well without late adverse effect for 6 years (Fig. 33.3).

Brain Tumors

34

Masashi Koto

Abstract

Glioblastoma multiforme (GBM) is the most common and aggressive tumor of the brain and is associated with a high rate of mortality. Radiotherapy is a part of the combined therapy for GBM. However, the rate of the cumulative infield recurrence has been reported to be more than 80 %. Carbon ions owing to their greater biological effectiveness have a potential efficacy in terms of improvement of the local control and overall survival. This chapter reports the result of the first clinical trial conducted using carbon ions for GBM.

Keywords

Carbon ion radiotherapy • Glioblastoma

34.1 Introduction

GBM is the most common and aggressive tumor of the brain and is associated with a high rate of mortality [1]. Despite combined therapeutic efforts of surgery, chemotherapy, and radiotherapy, GBM remains poor for tumor control and long-term survival [2]. The median survival time (MST) of patients with GBM is only approximately 1 year. Several studies have demonstrated the pattern of recurrence of GBM after treatment. The rate of the cumulative infield recurrence has been reported to be more than 80 % [3]. Temozolomide-based chemoradiation was shown to improve the survival rate of GBM patients, especially the ones with O^6-methylguanine-DNA methyltransferase promoter methylation [4]. However, infield recurrence was the most common recurrence pattern after temozolomide-based chemoradiation [5].

34.2 Significance of Carbon Ion Radiotherapy

In the treatment of GBM, carbon ions possessing high linear energy transfer (LET) components may have advantageous effects on GBM because of better dose localization in the tumor and greater relative biological effectiveness (RBE). Combs et al. reported that carbon ion radiotherapy (C-ion RT) exerts a stronger cytotoxic effect on glioblastoma cells compared to photon radiotherapy [6]. C-ion RT can potentially increase the infield tumor control rate of GBM and prolong the survival period.

34.3 Clinical Features and Diagnostic Work-Up

Patients with GBM experience headache, nausea, seizure, unilateral weakness, or mental changes.

The standard methods used for the diagnosis and treatment planning of patients with GBM are computed tomography (CT) and magnetic resonance imaging (MRI). High-grade gliomas are characterized by a disrupted blood-brain barrier and increased water content compared with a normal brain tissue; hence, the tumor can be visualized using

M. Koto (✉)
Research Center Hospital for Charged Particle Therapy,
National Institute of Radiological Sciences,
4-9-1 Anagawa, Inage-ku, Chiba 263-8555, Japan
e-mail: koto@nirs.go.jp

H. Tsujii et al. (eds.), *Carbon-Ion Radiotherapy: Principles, Practices, and Treatment Planning*,
DOI 10.1007/978-4-431-54457-9_34,

contrast-enhanced MRI and CT. T1-weighted MRI are more suited for visualizing the anatomy and areas of contrast enhancement, while T2-weighted MRI are more sensitive for detecting edema. Positron emission tomography (PET) images can provide information on the metabolic and blood-brain barrier functions. One of the radiolabeled amino acids used in the diagnosis of gliomas is 11C-labeled methionine (MET). Radiolabeled amino acids are taken up avidly by glioma cells independent of blood-brain barrier disturbance, whereas only low uptake occurs in the normal cerebral tissue. Thus, MET-PET is more accurate than either CT or MRI in defining the extent of gliomas [7]. Previously, we reported that for patients with high-grade gliomas, MET-PET may serve as a predictor of the outcomes of C-ion RT [8]. Direct use of MET-PET fused to treatment planning CT has been useful for the definite target delineation.

34.4 General Management and Radiation Techniques

The phase I/II clinical study for patients with high-grade gliomas was performed between 1994 and 2002 [9]. Patients were treated with surgery in conjunction with chemoradiotherapy at 50 Gy in 25 fractions, followed by C-ion RT. The target volume of the conventional radiotherapy was preferably based on MRI and included the resection cavity and presumed infiltrative volume characterized by T2 abnormality with a minimum of a 5-mm margin (Fig. 34.1a). Photon radiotherapy consisted of two lateral opposing fields or two rectangular wedge-pair fields, and all portals were used during each treatment session. Nimustine hydrochloride (ACNU) was administrated on the first and fourth or fifth weeks of photon radiotherapy at a dose of 100 mg/m^2. After photon radiotherapy and ACNU, C-ion RT was administered 4 day/week for 8 fractions over 2 weeks. The total dose of C-ion RT was escalated from 16.8 Gy equivalent (GyE) to 24.8 GyE in every 10 % increment (16.8, 18.4, 20.0, 22.4, and 24.8 GyE) after careful observation of normal tissue morbidity. The target volume of C-ion RT was based on MRI and included the contrast-enhancing volume with a minimum of a 5-mm margin (Fig. 34.1b).

34.5 Results of Therapy

At National Institute of Radiological Sciences (NIRS), a total of 48 patients including 32 GBM and 16 anaplastic astrocytoma were treated in the phase I/II dose escalation study [9] C-ion RT followed by photon radiotherapy was accomplished via dose escalation up to the fifth level (16.8, 18.4, 20.0, 22.4, and 24.8 GyE), with all patients receiving treatment as scheduled.

The median survival time (MST) for the 32 GBM patients was 17 months. The patients were subdivided into three groups according to the carbon ion dose: the low-dose group (16.8 GyE), the middle-dose group (18.4–22.4 GyE), and the high-dose group (24.8 GyE). In the 32 patients with GBM, the MST was 7, 19, and 26 months for the low-dose, moderate-dose, and high-dose groups, respectively. Univariate analysis of the 32 patients with GBM revealed that only the carbon ion dose showed statistical significance. Non-hematological severe adverse effects were few. Maximum acute reaction of the skin was grade 2 and that of the brain was grade 1. In late morbidity of the brain, four patients had grade 2 reaction, requiring steroid administration. However, no grade 3/4 reactions occurred.

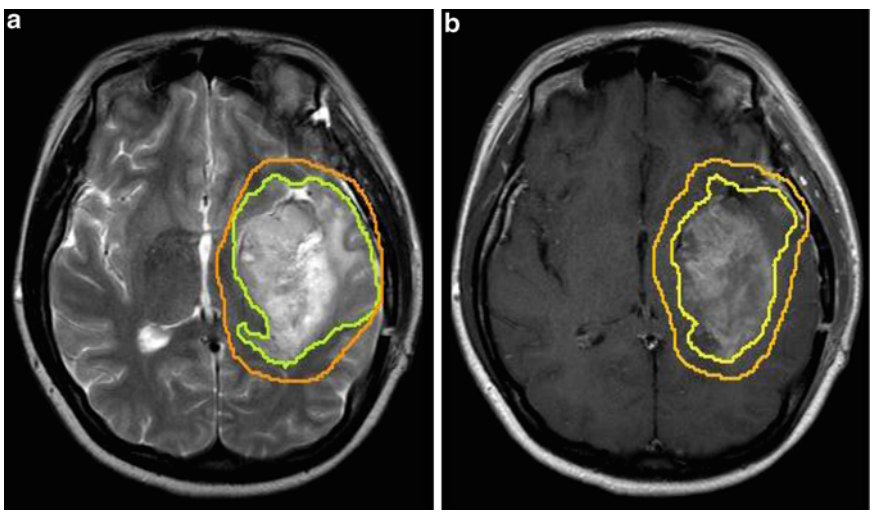

Fig. 34.1 Target delineation in photon radiotherapy and carbon ion radiotherapy (C-ion RT). (**a**) The *light green contour* shows the high-intensity area on the T2-weighted magnetic resonance image (MRI), while the *orange contour* shows the final target for photon radiotherapy. (**b**) The *yellow contour* shows the gadolinium-enhanced area on the T1-weighted MRI, while the *orange contour* shows the final target for C-ion RT

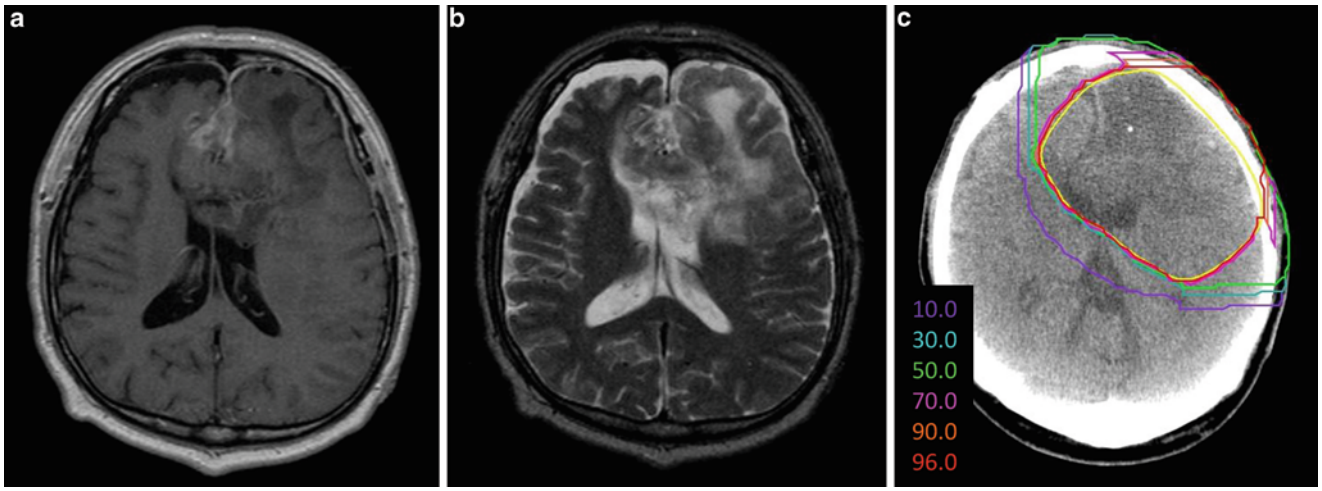

Fig. 34.2 (**a**) T2-weighted MRI and (**b**) gadolinium-enhanced T1-weighted MRI obtained before C-ion RT. (**c**) Representative axial isodose distributions at the level of lateral ventricle

34.6 Case Study

A 47-year-old man presented with gait disturbance. MRI examination revealed a tumor involving the bilateral frontal lobes. He underwent subtotal resection and his disease was diagnosed as GBM (Fig. 34.2a, b). He was referred to our hospital for radiation therapy. Photon radiotherapy at 50 Gy in 25 fractions and administration of ACNU was started 30 days after surgery. After the chemoradiation, the boost treatment using C-ion RT with 18.4 GyE/8 fractions was administered (Fig. 34.2c). He developed marginal recurrence 1 year after the combined therapy and received a stereotactic radiotherapy at 40 Gy in 10 fractions. Sixteen years later, the patient is alive without any disease.

References

1. Behin A, Hoang-Xuan K, Carpentier AF, Delattre JY. Primary brain tumours in adults. Lancet. 2003;361:323–31.
2. Laperriere N, Zuraw L, Cairncross G, Cancer Care Ontario Practice Guidelines Initiative Neuro-Oncology Disease Site Group. Radiotherapy for newly diagnosed malignant glioma in adults: a systematic review. Radiother Oncol. 2002;64:259–73.
3. Hegi ME, Diserens AC, Gorlia T, Hamou MF, de Tribolet N, Weller M, Kros JM, Hainfellner JA, Mason W, Mariani L, Bromberg JE, Hau P, Mirimanoff RO, Cairncross JG, Janzer RC, Stupp R. MGMT gene silencing and benefit from temozolomide in glioblastoma. N Engl J Med. 2005;352:997–1003.
4. Stupp R, Hegi ME, Mason WP, van den Bent MJ, Taphoorn MJ, Janzer RC, Ludwin SK, Allgeier A, Fisher B, Belanger K, Hau P, Brandes AA, Gijtenbeek J, Marosi C, Vecht CJ, Mokhtari K, Wesseling P, Villa S, Eisenhauer E, Gorlia T, Weller M, Lacombe D, Cairncross JG, Mirimanoff RO; European Organisation for Research and Treatment of Cancer Brain Tumour and Radiation Oncology Groups; National Cancer Institute of Canada Clinical Trials Group. Effects of radiotherapy with concomitant and adjuvant temozolomide versus radiotherapy alone on survival in glioblastoma in a randomised phase III study: 5-year analysis of the EORTC-NCIC trial. Lancet Oncol. 2009;10:459–66. doi:10.1016/S1470-2045(09)70025-7.
5. Milano MT, Okunieff P, Donatello RS, Mohile NA, Sul J, Walter KA, Korones DN. Patterns and timing of recurrence after temozolomide-based chemoradiation for glioblastoma. Int J Radiat Oncol Biol Phys. 2010;78:1147–55. doi:10.1016/j.ijrobp.2009.09.018.
6. Combs SE, Zipp L, Rieken S, Habermehl D, Brons S, Winter M, Haberer T, Debus J, Weber KJ. In vitro evaluation of photon and carbon ion radiotherapy in combination with chemotherapy in glioblastoma cells. Radiat Oncol. 2012;27(7):9. doi:10.1186/1748-717X-7-9.
7. Ogawa T, Shishido F, Kanno I, Inugami A, Fujita H, Murakami M, Shimosegawa E, Ito H, Hatazawa J, Okudera T, et al. Cerebral glioma: evaluation with methionine PET. Radiology. 1993;186:45–53.
8. Mahasittiwat P, Mizoe JE, Hasegawa A, Ishikawa H, Yoshikawa K, Mizuno H, Yanagi T, Takagi R, Pattaranutaporn P, Tsujii H. l-[METHYL-(11)C] methionine positron emission tomography for target delineation in malignant gliomas: impact on results of carbon ion radiotherapy. Int J Radiat Oncol Biol Phys. 2008;70:515–22.
9. Mizoe JE, Tsujii H, Hasegawa A, Yanagi T, Takagi R, Kamada T, Tsuji H, Takakura K; Organizing Committee of the Central Nervous System Tumor Working Group. Phase I/II clinical trial of carbon ion radiotherapy for malignant gliomas: combined X-ray radiotherapy, chemotherapy, and carbon ion radiotherapy. Int J Radiat Oncol Biol Phys. 2007;69:390–6.

Breast Cancer

35

Kumiko Karasawa

Abstract

Breast cancer is a major health problem for women all over the world. In recent years, about half of the cases detected in Japan were below stage I. The standard care for early-stage breast cancer is breast-conserving therapy, which consists of conservative surgery and fractionated whole breast irradiation. Breast surgery followed by more than 5 weeks of radiotherapy causing adverse skin reactions is still a burden to patients. Accelerated partial breast irradiation (APBI) is an alternative to whole breast irradiation in patients with low-risk tumor, based on four randomized trials and more than 40 prospective trials. In this sense, carbon-ion radiotherapy (C-ion RT) is suitable as an effective local therapy and could be even more effective than standard radical radiotherapy. Our institute started a clinical trial of radical C-ion RT for patients with low-risk T1N0M0 invasive ductal carcinoma in 2013. The idea was to develop a short-course C-ion RT to be finished in 1 week, which we believe could replace surgery and more than 5 weeks of radiotherapy. Furthermore, it is assumed that C-ion RT may play a role in preventing regional lymph node recurrence and solitary distant metastasis.

Keywords

Early breast cancer • Low-grade breast cancer • Partial breast irradiation • Regional lymph node recurrence

35.1 Introduction

Breast cancer is one of the most common cancers in women in most areas of the world. According to breast cancer statistics of the Japanese Breast Cancer Society in 2010, clinical stages 0 to II were 92 %, of which 88.9 % of the histological types were common-type invasive ductal carcinoma (http://www.jbcs.gr.jp/Member/tourokusyukei.html). The standard care for early-stage breast cancer is breast-conserving therapy consisting of conservative surgery and fractionated whole breast irradiation. However, the question is whether it is really necessary to irradiate the whole breast in all early cancer. Whole breast irradiation takes over 5 weeks and causes adverse skin reaction with breast atrophy. Several articles report that 90 % of intra-breast recurrences developed around the surgical margin and 96 % of intra-breast tumor recurrences developed in the same quadrant, especially in low-grade tumor [1].

It has been acknowledged that in breast cancer both tumor control and quality of life (QOL) during and after treatment should be considered, and whole breast irradiation could be overtreatment for early low-grade breast cancer. Accelerated partial breast irradiation (APBI) is an alternative to whole breast irradiation in patients with low-risk tumor. Four randomized trial and more than 40 prospective trials certified the usefulness of APBI. In 2009, the American Society of Radiation Oncology presented a guideline regarding the use of APBI (Table 35.1) [1].

K. Karasawa (✉)
Research Center Hospital for Charged Particle Therapy, National Institute of Radiological Sciences, 4-9-1 Anagawa, Inage-ku, Chiba 263-8555, Japan
e-mail: kkarasaw@nirs.go.jp

H. Tsujii et al. (eds.), *Carbon-Ion Radiotherapy: Principles, Practices, and Treatment Planning*,
DOI 10.1007/978-4-431-54457-9_35,

Table 35.1 ASTRO consensus statement for APBI (2009)

Factor	Suitable	Cautionary	Unsuitable
Age	>60 years	50–59 years	<50 years
BRCA 1/2 mutation	Not present	–	Present
Tumor size	>2 cm	2 cm<, 2 cm, <3 cm	3 cm, 3 cm<
T stage	T1	T0, T2	T3, T4
LVSI	No	Limited/focal	Present
ER status	Positive	Negative	–
Multicentricity	Unicentric only	–	Present
Multifocality	<2 cm	2.1–3 cm	>3 cm
Histology	Invasive ductal or other favorable	Invasive lobular	
Pure DCIS	Not allowed	<3 cm	If >3 cm
EIC	Not allowed	<3 cm	If >3 cm
N stage	pN0	–	pN1,2,3
Nodal surgery	SLN Bx, ALND	–	Not performed

In this guideline, not only an APBI-suitable group but also an APBI-cautionary group and an APBI-unsuitable group are shown. Accordingly, age 60 and over, negative BRCA1/2 variation, 2 cm or less tumor (T1), lymph vascular space invasion negative, estrogen receptor (ER) positive, unicentric tumor, invasive ductal or other favorable histology, without extensive intraductal component (EIC), pN0 are suitable for local treatment alone. C-ion RT is suitable for localized treatment and could be effective enough for radical radiotherapy of localized breast cancer. Preparations have been ongoing at the National Institute of Radiological Sciences (NIRS) for the treatment of breast cancer with carbon ions since 2011. We have just started a clinical trial of radical C-ion RT for patients with low-risk T1N0M0 invasive ductal carcinoma from 2013.

35.2 Significance of C-Ion RT

C-ion RT has a benefit in terms of dose distribution, which is even better than stereotactic body irradiation (SBRT) and intensity-modulated radiation therapy (IMRT) using high-energy X-rays. In addition, C-ion RT has higher biological effectiveness as well, resulting in higher local tumor control and a lesser degree of adverse effects to normal tissues. Although more than 7,000 patients have been treated with C-ion RT at NIRS in the last 19 years, a breast cancer study protocol has not been performed until now. Clinical trials with C-ion RT have two major purposes, one being the treatment of advanced tumors that are hard to cure with conventional treatment and the other the treatment of common cancers with the aim of improving survival and QOL of patients. The reason we did not treat breast cancer is that cases treatable by partial irradiation were difficult to identify.

Breast cancer is the most common cancer of Japanese women and more than 50,000 patients are newly diagnosed every year. It is also a disease with a favorable prognosis in Japan, with a 5-year survival rate of 82 % (http://www.jbcs.gr.jp/Member/tourokusyukei.html). Median age of the patients is 59 years, and patients 80 years or older are more than 2,000 every year, with some of them unable to undergo surgery due to associated diseases. Therefore, the development of lesser-invasive treatment for those not suited for guideline treatment is important in an aging society.

C-ion RT considered suitable for meeting the aim of lessening the treatment burden in early cancer by taking advantage of the better dose distribution and biological effectiveness of carbon ions compared to photons and protons [2–4].

35.3 Clinical Features and Diagnostic Work-Up

A candidate of C-ion RT for breast tumor is T1N0M0, ER positive, HER2 negative, invasive ductal carcinoma, or other favorable type, without EIC, without lymph vascular space invasion, tumor located more than 5 mm from the skin. Tumor extension including ductal spread has to be evaluated by enhanced MRI before treatment decision [5].

35.4 General Management and Radiation Techniques

35.4.1 Placement of Fiducial Markers

Two fiducial markers (Visicoil™; IBA) are implanted before treatment 5 mm apart from the upper and lower border of ductal spread (Fig. 35.1).

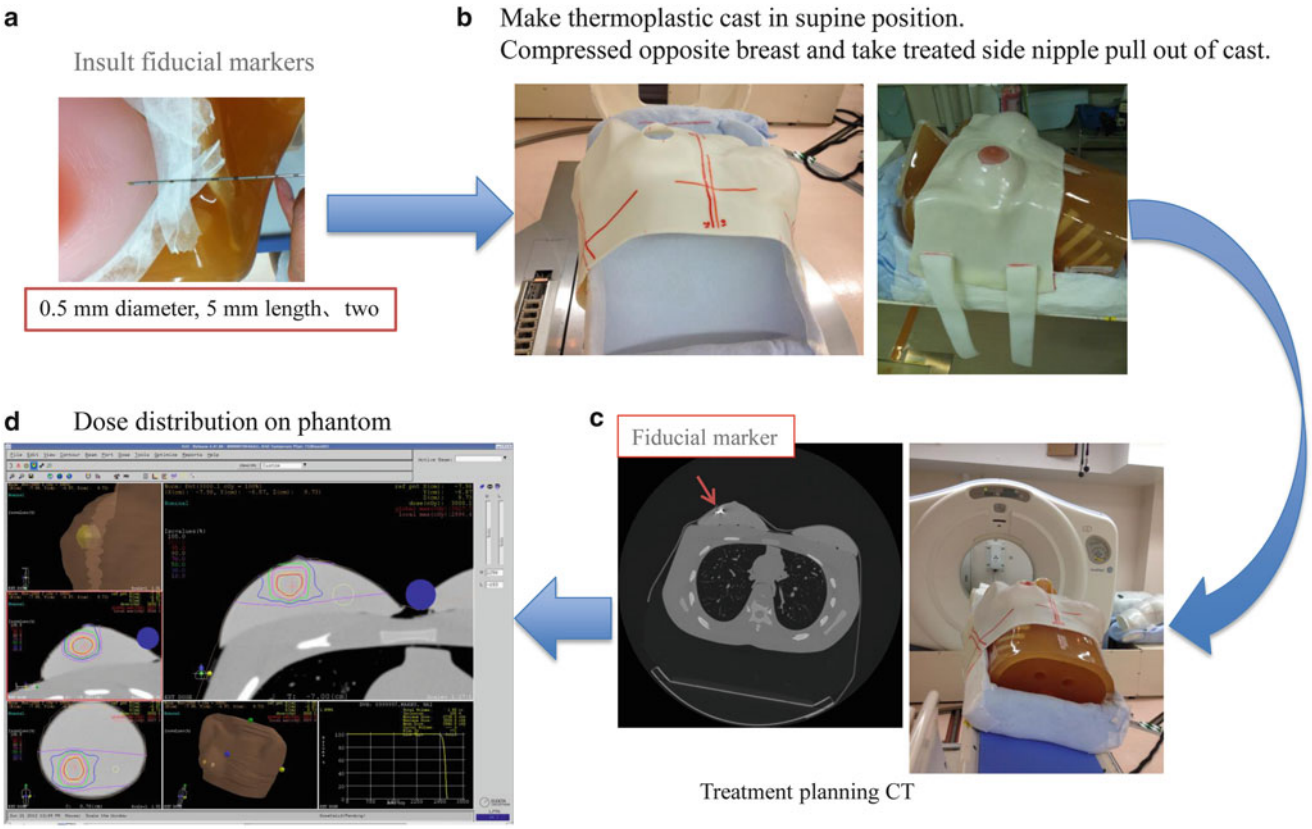

Fig. 35.1 Simulation planning on phantom. (**a**) Insult fiducial markers. (**b**) Making thermoplastic cast in supine position. Compressing opposite breast and taking affected side nipple out of cast. (**c**) Treatment planning CT. (**d**) Dose distribution on phantom

35.4.2 Treatment Position and Immobilization

Treatment posture is supine in principle. Immobilization of the involved breast must be one of the key points in this treatment. The cast (Moldcare; Alcare, Tokyo, Japan) is made at the supine position with head up slightly to lower both upper limbs. The fixation body shell (Shellfitter; Keraray Co., Ltd., Osaka, Japan) is made of three parts: neck, breast, and abdomen. As for the breast shell, a hole is opened for the circumference of the nipple of the involved side, and the nipple is guided through the hole and fixed. The opposite side does not have the hole opened but is pressed by the shell.

35.4.3 Target Delineation and Risk Organs

A set of 2.5-mm-thick planning CT using the patient immobilization devices is applied for treatment planning with dynamic MRI fusion. Clinical target volume (CTV) is defined as the gross tumor and intraductal component detected by MRI images. Safety margins of 5 mm and an anterior margin of 5 mm are added to CTV to create the initial planning target volume (PTV). If the tumor is located less than 5 mm from the skin surface, a tight margin is set toward the skin.

35.4.4 Dose Prescription

A dose escalation study is designed for C-ion RT for breast cancer. The total dose is 48.0, 52.8, and 60.0 GyE in 4 fractions within 1 week at fraction sizes of 12, 13.2, and 15 GyE, respectively. These dose levels were chosen on the basis of our experience of treating lung metastases from breast cancer.

35.4.5 Daily Treatment

Position collation is guided by two fiducial markers, marks written on the shell and skin, calcification within the breast,

and bony structure. Irradiation is performed using respiratory gating. Treatment duration is 1 week, daily from Tuesday to Friday (Fig. 35.2).

35.4.6 Results of Therapy

We have just started a clinical trial for breast tumor, and no data has been available from any other institute to demonstrate the radiosensitivity of primary breast cancer. However, our limited experience with C-ion RT for metastases from breast cancer may provide a clue for estimating optimal dose fractionation for control of primary breast cancer.

Between 1997 and 2013, four cases with solitary lung metastases, two cases of parasternal lymph node metastasis, and one case of solitary liver metastasis were treated with C-ion RT. The patient with 6-cm metastatic liver tumor was treated by a single fraction of 36 GyE, and he has survived for more than 5 years with local control. The patients with lung metastases were treated with 60.0 GyE in 4 fractions. One case of 13-cm lung metastasis could not be controlled with 57.6 GyE in 16 fractions, although the other cases could be controlled.

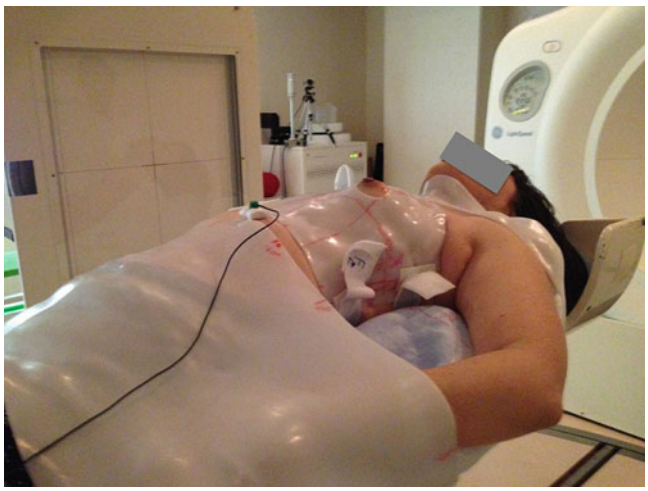

Fig. 35.2 Patient setup of breast tumor irradiation

35.5 Case Study

Case 1

A 50-year-old female with a 2-cm left breast tumor was diagnosed as T1N0M0 invasive ductal breast cancer. She refused any type of surgery since having severe adverse effects from previous surgery for Cushing syndrome. She was treated with C-ion RT, 4 fractions of 13.2 GyE, up to a total dose of 52.8 GyE (Fig. 35.3). For the moment, the tumor is controlled.

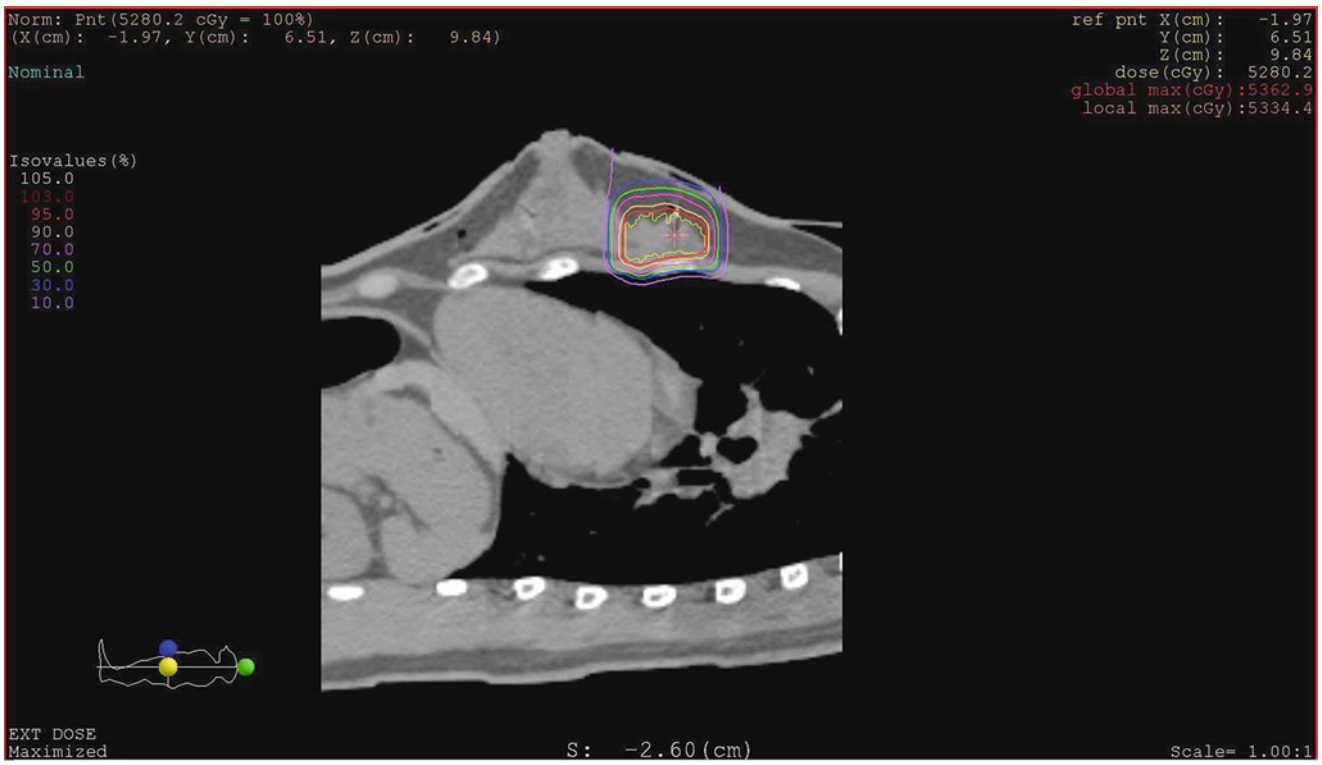

Fig. 35.3 Dose distribution of a case of T1N0M0 breast cancer

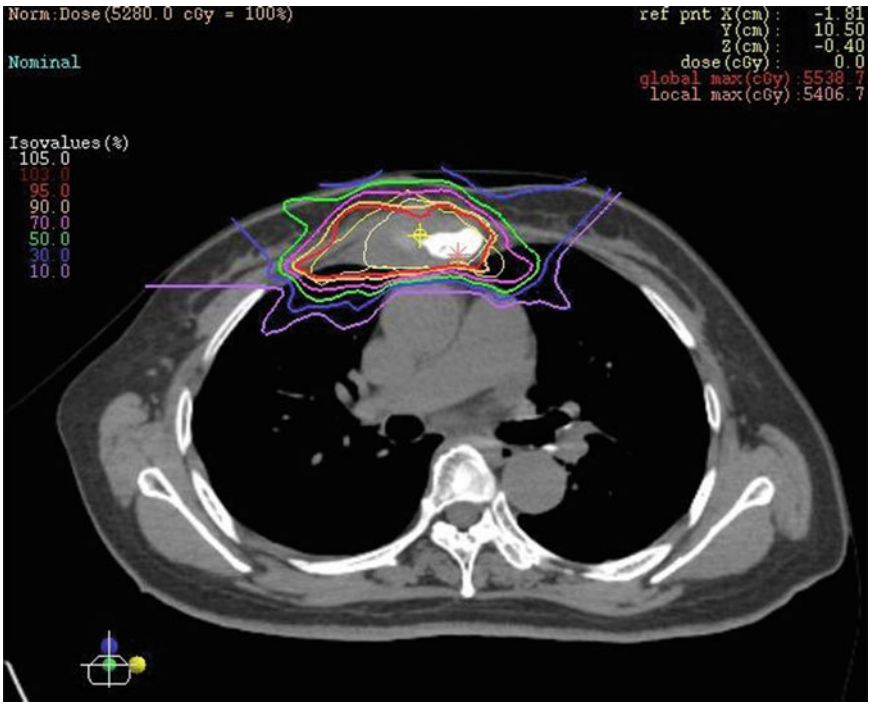

Fig. 35.4 Dose distribution of a case of parasternal lymph node recurrence

Case 2

A 73-year-old female with right parasternal lymph node recurrence. She was treated with bilateral breast-conserving therapy including bilateral whole breast irradiation. After recurrence of right parasternal lymph nodes, she had been treated with some systemic chemotherapies, although the result was progressive disease. She was treated with C-ion RT, 12 fractions of 4.4 GyE, up to a total dose of 52.8 GyE (Fig. 35.4). For the moment, there are no signs of a recurrence.

References

1. Smith BD, Arthur DW, Buchholz TA, et al. Accelerated partial breast irradiation consensus statement from the American Society for Radiation Oncology (ASTRO). Int J Radiat Oncol Biol Phys. 2009;74:987–1001.
2. Hepel JT, Tokita M, MacAusland SG, et al. Toxicity of three-dimensional conformal radiotherapy for accelerated partial breast irradiation. Int J Radiat Oncol Biol Phys. 2009;75(5):1290–6.
3. Kozak KR, Smith BL, Adams J, et al. Accelerated partial-breast irradiation using proton beams: initial clinical experience. Int J Radiat Oncol Biol Phys. 2006;66(3):691–8.
4. Bush DA, Slater JD, Garberoglio C, et al. Partial breast irradiation delivered with proton beam: results of a phase II trial. Clin Breast Cancer. 2011;11(4):241–5.
5. Vicini FA, Kestin LL, Goldstein NS. Defining the clinical target volume for patients with early-stage breast cancer treated with lumpectomy and accelerated partial breast irradiation: a pathologic analysis. Int J Radiat Oncol Biol Phys. 2004;60(3):722–30.

Index

H. Tsujii et al. (eds.), *Carbon-Ion Radiotherapy: Principles, Practices, and Treatment Planning*,
DOI 10.1007/978-4-431-54457-9, © Springer Japan 2014